Expedient Synthesis of High-Value Organoboronates Through Catalytic Enantioselective Alkene Functionalization:

Author: Jaehee Lee

Boston College Electronic Thesis or Dissertation, 2017

Boston College

The Graduate School of Arts and Sciences

Department of Chemistry

EXPEDIENT SYNTHESIS OF HIGH-VALUE ORGANOBORONATES THROUGH CATALYTIC ENANTIOSELECTIVE ALKENE FUNCTIONALIZATION

A Dissertation

By

JAEHEE LEE

Submitted in partial fulfillment of the requirements

For the degree of

Doctor of Philosophy

December 2017

Dedication

To Sujin Kim, my companion, reason of my life, my everything and my best friend.

To Byoungsook Bae and Keunyong Lee, my parents, my origin and my life sponsors.

To Hyunje Seong and Woosung Kim, my parents-in-law and my great supporters.

I love you forever and ever.

사랑합니다.

Acknowledgements

I am honored to be a member of the Hoveyda Research Group working with one of the greatest scientists in the world. To me, Professor Amir H. Hoveyda is a hero and father of science. His sense of understanding chemistry, teaching, writing, presentation, and art has had a profound impact on me. Thank you for your great patience, leadership, and advise.

I really appreciate to my friend Dr. Miho Kaneko who is the most successful woman I ever met. Without her assistance and encouragement, I could not step in to the science field.

I was the luckiest graduate student ever since I met Dr. Byunghyuck Jung and Dr. Suttipol (Benz) Radomkit who were fantastic mentors to teach me fundamental organic chemistry and great techniques. Without talented people like Dr. Suttipol (Benz) Radomkit, Dr. Sebastian Torker, and Dr. Juan del Pozo del Valle, it was not possible to solve and understand mechanistic problems of our complicated projects.

I am also deeply grateful to my wonderful friends from the Hoveyda research group and Boston College chemistry department. Hwanjong Jang, KyungA Lee, Ming Joo Koh, Thack Nguyen, Ying Shi, and Farid van der Mei gave me a lot of lessons, helpful advices, and creative ideas for my projects and life. I will miss our Saturday lunch meeting a lot.

Most importantly, everything was impossible without endless love and patience of my wife Sujin Kim. The chemistry with her love is the best reaction I have ever set, and I can see that this reaction creates tremendous happiness. Thank you and Love you SUJIN.

EXPEDIENT SYNTHESIS OF HIGH-VALUE ORGANOBORONATES THROUGH CATALYTIC ENANTIOSELECTIVE ALKENE FUNCTIONALIZATION

JAEHEE LEE

Thesis Advisor: Professor Amir. H. Hoveyda

Abstract

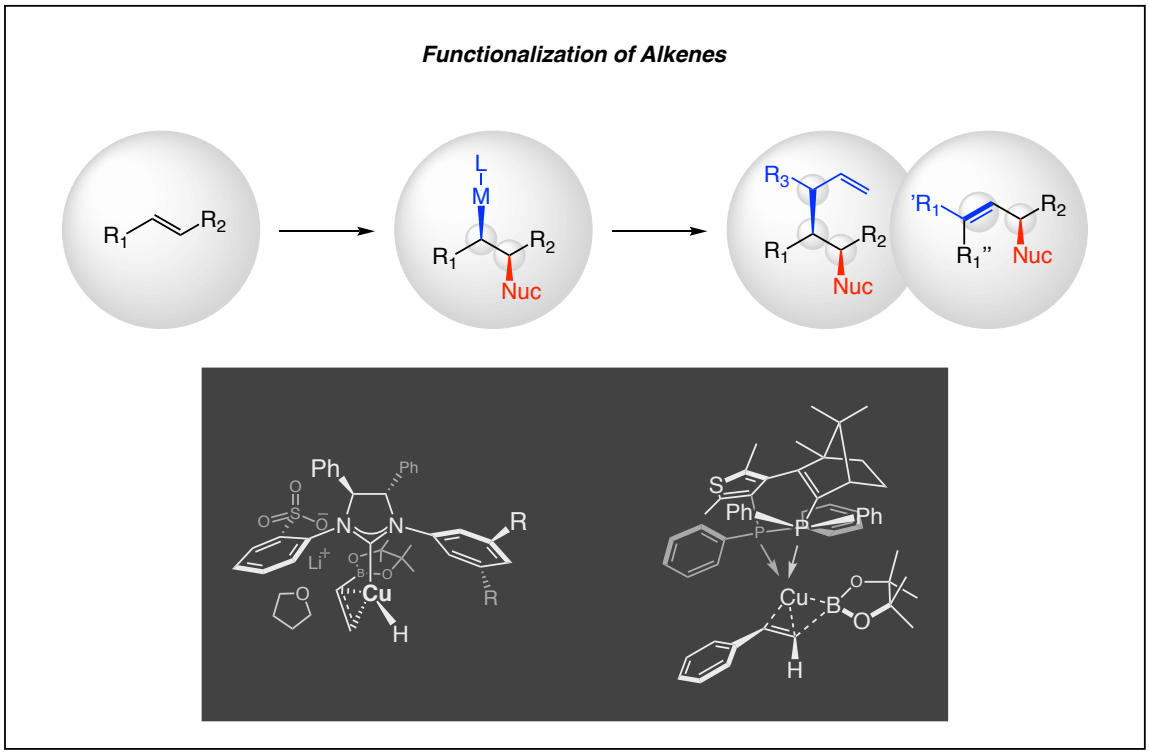

■ **Chapter 1**

Mechanism-Based Enhancement of Scope and Enantioselectivity for Reactions Involving a Copper-Substituted Stereogenic Carbon Center: Organoborons are important building blocks of complex natural products, functional materials, and pharmaceutically relevant compounds due to their prevalent utility in C–C and C–hetero atom bond transformations. Using a readily accessible copper catalyst, we have developed highly site- and enantioselective allylic substitution by way of a three-component, single-vessel, and sustainable catalytic protocol. Detailed mechanistic studies revealed valuable insights which led us to develop copper–boron and copper–hydride additions to olefins with broader substrate scope, higher efficiency, and higher enantioselectivity. In addition, the method can be applied to the synthesis of biologically active molecules such as preclamol and heliespirone A and C.

Publication: Lee, J.; Radomkit, S.; Torker, S.; del Pozo, J.; Hoveyda, A. H. *Nat. Chem.* **2018,** *10,* 99–108.

■ **Chapter 2**

Versatile Homoallylic Boronates by Chemo-, S_N2'-, Diastereo- and Enantioselective Catalytic Sequence of Cu–H Addition to Vinyl-B(pin)/Allylic Substitution: To achieve an efficient multicomponent reaction, high chemoselectivity between a starting material and a reagent must be accomplished during the first catalytic transformation to generate an intermediate which then selectively reacts with another substrate to furnish the product in a site-, and/or stereoselective fashion. Development and application of efficient multicomponent reactions involving allylic substitution can provide alternative solutions for difficult

synthetic problems in organic chemistry. Our group has developed a sulfonate-containing chiral NHC–Cu catalyzed chemo-, S_N2'-, diastereo-, and enantioselective multicomponent reaction through Cu–H addition to readily available vinyl–B(pin) followed by allylic substitution to deliver homoallylic boronates. The derived homoallylic alcohols can be used as building blocks of biologically active molecules.

Publication: Lee, J.; Torker, S.; Hoveyda, A. H. *Angew. Chem. Int. Ed.* **2017,** *56,* 821–826.

■ **Chapter 3**

Enantioenriched Halogen-Substituted Alkenes through NHC–Cu-Catalyzed Borylation/Dehalogenation and Their Applications: Because of their unique properties, mono- and difluoroalkenes have received attention as an important class of compounds as building blocks for fluorine-containing monomers for functional polymers and biologically active molecules in medicine and agriculture. However, reported methods to prepare enantioenriched difluoroalkenes are scarce and often require undesirable amounts of precious transition metals and very high/low temperatures. To solve these challenges, we have developed a highly efficient, regio-, and enantioselective boron allylic substitution to CF_3-alkenes and other halogen-substituted olefins by using an abundant copper-based catalyst.

Work in Progress: Lee, J.; Lee. K.; Koh, M.; Hoveyda, A. H.

Table of Contents

Ligand Index

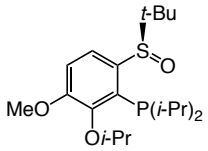

L1

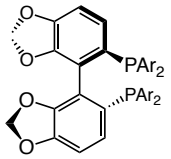

L2
Ar = 4-OMe-3,5-*t*-BuC_6H_2

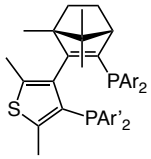

L3a Ar = Ph, Ar' = Ph
L3b Ar = 3,5-$(Me)_2C_6H_3$, Ar' = Ph
L3c Ar = Ph, Ar' = 3,5-$(Me)_2C_6H_3$

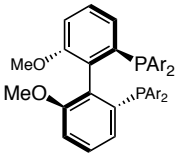

L4
Ar = 3,5-*t*-BuC_6H_3

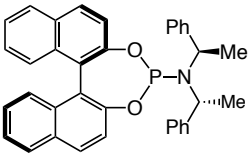

L5

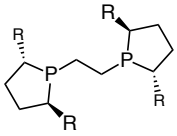

L6 R = Me, **L7** R = Ph

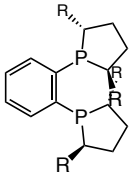

L8 R = Me, **L9** R = *i*-Pr

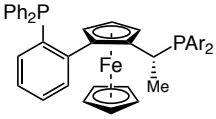

L10
Ar = 3,5-$(CF_3)_2C_6H_3$

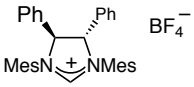

NHC-1

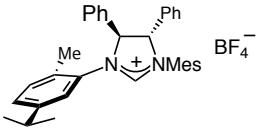

NHC-2

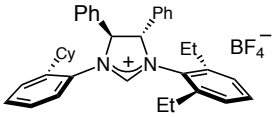

NHC-3

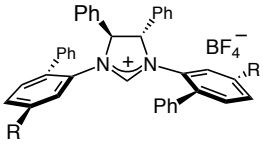

NHC-4 R = H, **NHC-5** R = *t*-Bu

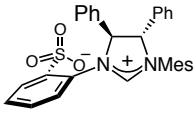

NHC-6

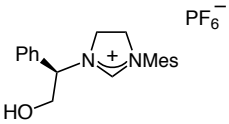

NHC-7

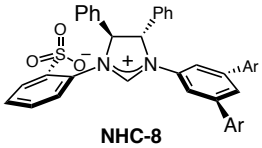

NHC-8
Ar = 2,4,6,-(*i*-Pr)$_3C_6H_2$

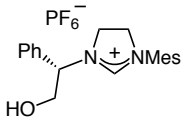

NHC-9

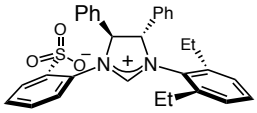

NHC-10

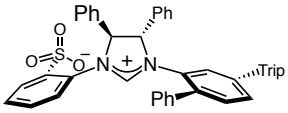

NHC-11

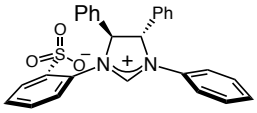

NHC-12

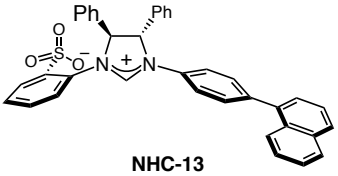

NHC-13

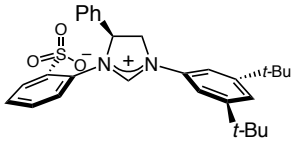

NHC-14

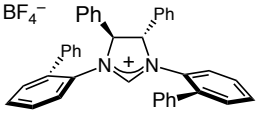

NHC-15

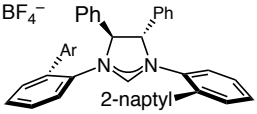

NHC-16

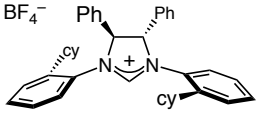

NHC-17

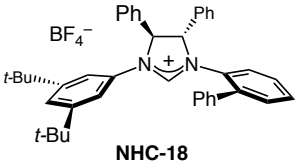

NHC-18

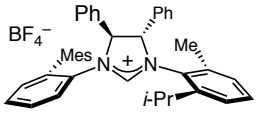

NHC-19

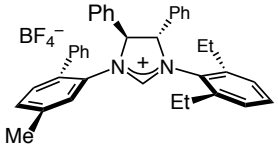

NHC-20

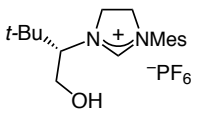

NHC-21

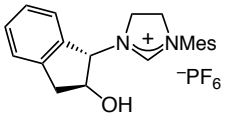

NHC-22

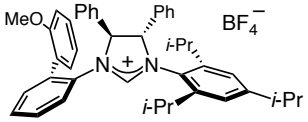

NHC-23

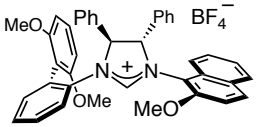

NHC-24

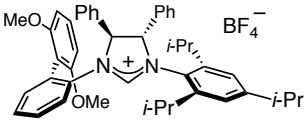

NHC-25

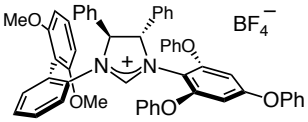

NHC-26

CHAPTER 1

Mechanism-Based Enhancement of Scope and Enantioselectivity for Reactions Involving a Copper-Substituted Stereogenic Carbon Center

1.1 Introduction

In chemical synthesis, development of highly efficient and stereoselective C–C bond formations is in high demand and, in this regard, allylic substitution reactions have proven to be a powerful approach.[1] Since multicomponent reaction strategies have contributed to stereoselective construction of complex natural products,[2] an enantioselective allylic substitution reaction through a multicomponent approach is fundamentally important and synthetically very interesting. To achieve high selectivities in multicomponent reactions, high chemoselectivity between a starting material and a reagent must occur during the first catalytic transformation. Moreover, the first reaction intermediate has to selectively react with a second substrate to generate site, and/or stereoselective complex products (Scheme 1.1). Through the utilization of a multicomponent approach in stereoselective allylic substitution, we aim to provide

---

(1) For reviews of catalytic enantioselective allylic substitution (EAS) reactions with "hard" organometallic nucleophiles see: (a) Hoveyda, A. H.; Hird, A. W.; Kacprzynski, M. A. *Chem. Commun.* **2004**, *16*, 1779–1785. (b) Yorimitsu, H.; Oshima, K. *Angew. Chem. Int. Ed.* **2005**, *44*, 4435–4439. (c) Alexakis, A.; Bäckvall, J. -E.; Krause, N.; Pàmies, O.; Diéguez, M. *Chem. Rev.* **2008**. *108*, 2796–2823.

(2) For a review on multicomponent catalytic reactions see: Touré, B. B.; Hall, D. G. *Chem Rev.* **2009**, *109*, 4439–4486.

alternative solutions for difficult synthetic problems in organic chemistry. Herein, we

Scheme 1.1. Challenge of Multicomponent Reaction with Readily Available Substrates

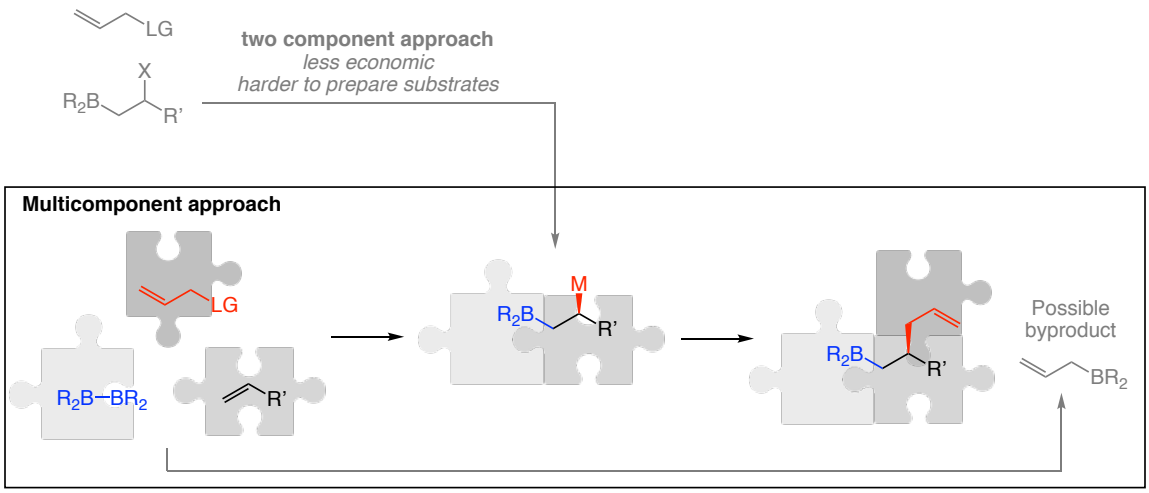

X, halogen; LG, leaving group; M, transition metal; R, alkoxy; R' aryl and heteroaryl

report the development of a highly site- and enantioselective allylic substitution by way of a three-component, single-vessel, and sustainable catalytic protocol.

1.2 Background

In organic synthesis, organoborons are important building blocks for complex natural products, functional materials, and pharmaceutically important compounds because of their significant utility in C–C and C–heteroatom bond forming reactions.[3] Recent studies of copper catalyzed stereoselective catalytic proto- and hydroboration reactions with $B_2(pin)_2$[4] and HB(pin)[5] (pin, pinacolato) opened the gate to surpass the limitations of previous synthetic methods and achieve new creative disconnections. However, a number of problems still remained until we understood the mechanistic details of Cu–H and/or Cu–B(pin) addition to alkenes followed by addition to various

(3) For reviews on functionalizations of organoboron compounds see: (a) Brown, H. C.; Singaram, B. *Pure & Appl. Chem.* **1987**, *59*, 879–894. (b) Brown, H. C.; Singaram, B. *Acc. Chem. Res.* **1988**, *21*, 287–293. (c) Miyaura, N.; Suzuki, A. *Chem. Rev.* **1995**, *95*, 2457–2483. (d) Miyaura, N. *Bull. Chem. Soc. Jpn.* **2008**, *81*, 1535–1553.

(4) Lee, Y.; Hoveyda, A. H. *J. Am. Chem. Soc.* **2009**, *131*, 3160–3161.

(5) Noh, D.; Chea, H.; Ju, J.; Yun, J. *Angew. Chem. Int. Ed.* **2009,** *48,* 6062–6064.

electrophiles.

1.2.1 Initial Study of Enantioselective Cu–B(pin) Addition to Alkene

In 2006, Sadighi and coworkers reported the first copper–boron addition to styrene with stoichiometric amounts of NHC–Cu–B(pin) complex **1.1** (Scheme 1.2).[6] The high regioselectivity of the reaction comes from the electronic match between styrene and the copper complex. The electron-rich benzylic carbon readily adds to the Lewis acidic

Scheme 1.2. First Examples of Cu–B(pin) Addition to Alkene

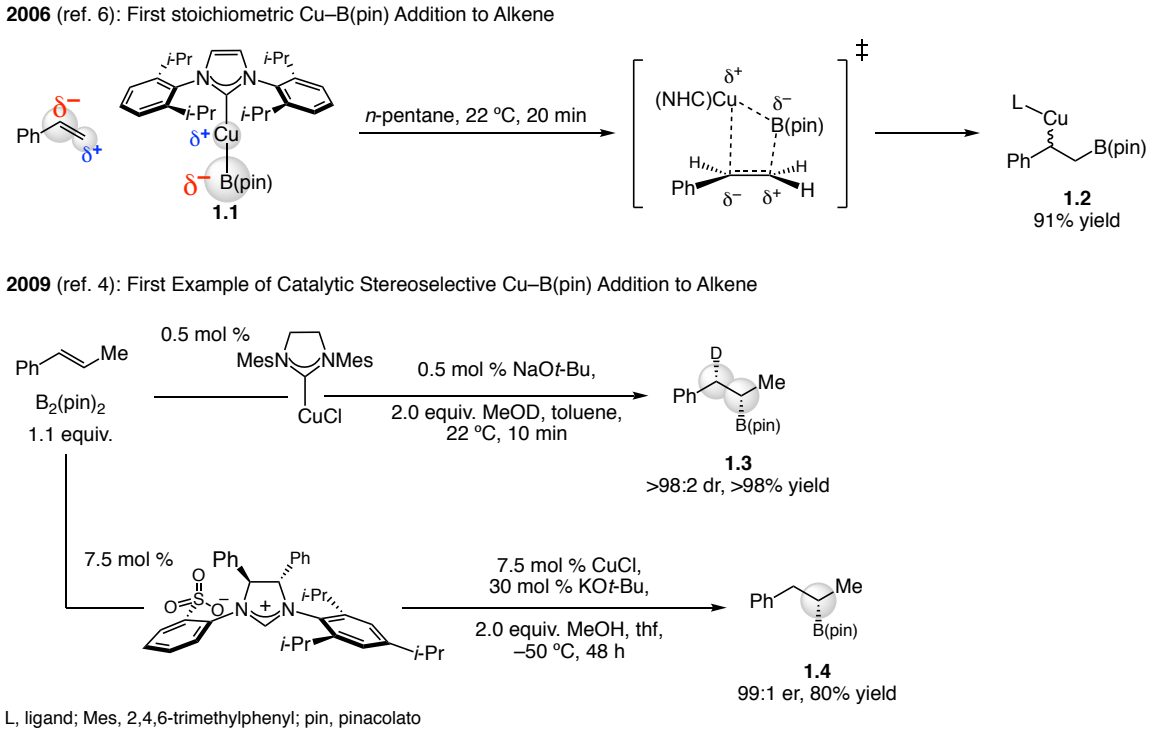

copper, and the electron-rich boron adds to the electron-deficient homobenzylic carbon. Two years later, our group reported the first catalytic, diastereo-, and enantioselective protoboration with chiral sulfonate-containing NHC ligands.[4] In the presence of MeOH, the nucleophilic organocopper complex can readily add to the proton electrophile to generate the desired product. The notable study with deuterated methanol (MeOD) has

(6) Laitar, D. S.; Tsui, E. Y.; Sadighi, J. P. *Organometallics* **2006,** *25,* 2405–2408.

shown that the copper–boron addition step is exclusively *syn*-selective (**1.3**, >98:2 dr, Scheme 1.2) which means that the high diastereo- and enantioselectivity comes from the initial copper–carbon stereochemistry after copper–boron addition to alkenes. Another

Scheme 1.3. Rate of Catalytic Cycle with Electron Deficient and Rich Aryl Olefins

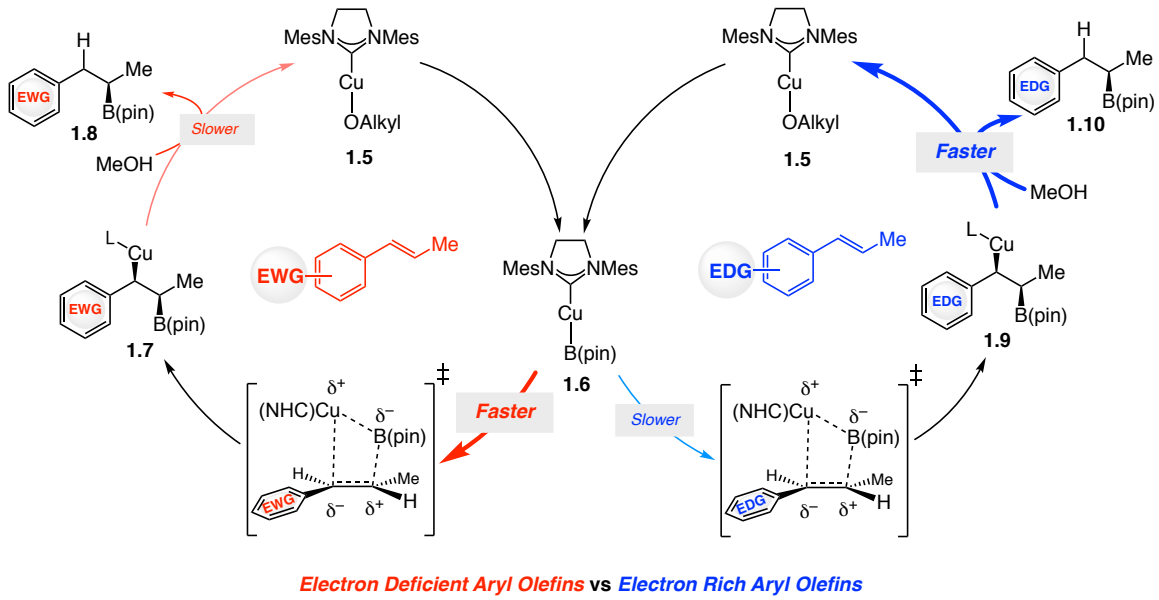

EWG, electron withdrawing group; EDG electron donating group; L, ligand; pin, pinacolato

mechanistically interesting point in this reaction is that the rate of the reaction depends on the electrophilicity of substrate and the nucleophilicity of the generated organocopper species (Scheme 1.3). Since the NHC–copper–boron complex **1.6** is a nucleophilic species, generation of the organocopper complex would be much faster with more electrophilic substrate (e.g., **1.6** → **1.7** is much faster than **1.6** → **1.9**). However, the subsequent protonation of complex **1.7** would be much slower since it is less nucleophilic compared to complex **1.9**. During this process, the final enantiomeric ratio depends on how stereoselectively the organocopper species (**1.7** or **1.9**) is formed and by what mechanism the addition to the electrophile occurs.

1.2.2 Multicomponent Reactions with Copper–Boron/Hydride Complexes and Their Limitations

After the first catalytic, diastereo-, and enantioselective protoboration was developed,[4] a large number of studies with copper-substituted stereogenic carbon centers were rapidly carried out. Although there are numerous reports and notable advances were made, a lot of fundamentally important problems remained to unsolved. In 2015, a dual-catalyst protocol for net allyl-boron addition to aryl alkenes was developed by Liao and coworkers.[7] Although high enantioselectivity was achieved with electronically neutral aryl olefins, several key cases were not reported with electron-rich aryl olefins and

Scheme 1.4. Enantioselective Cu–B Adiition to Alkenes/Allylic Substitution

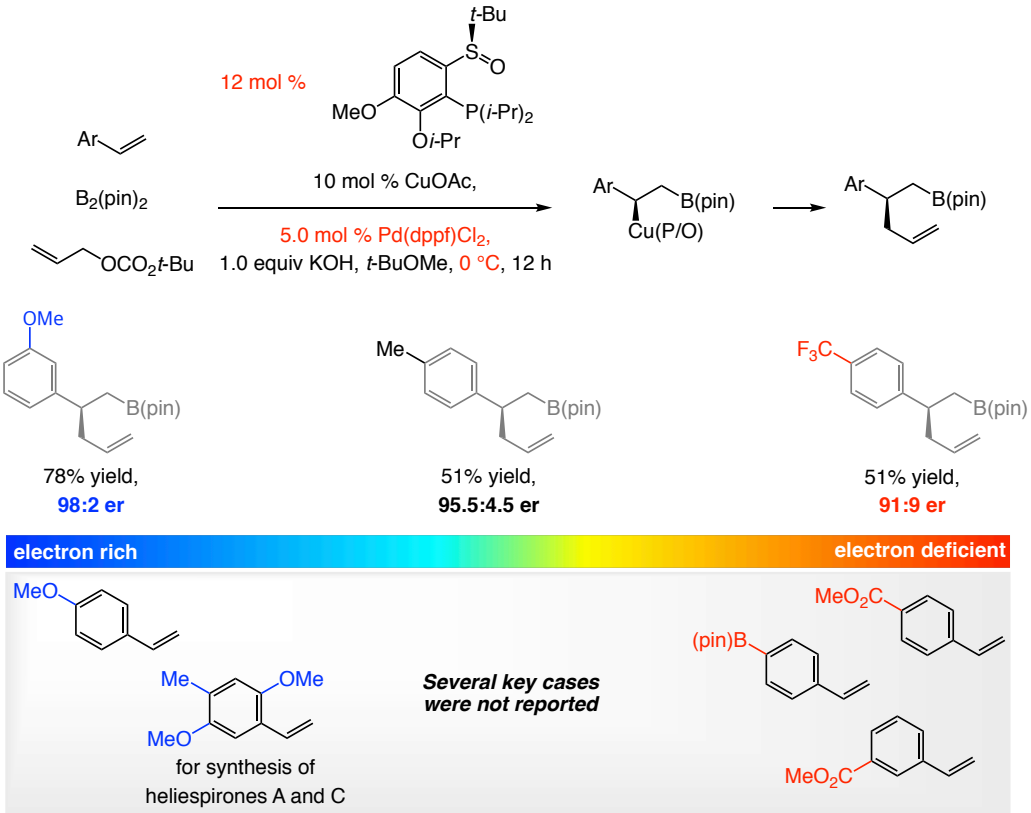

dppf, 1,1′-bis(diphenylphosphino)ferrocene; pin, pinacolato

electron-deficient aryl olefins besides *para*-CF_3 styrene (Scheme 1.4). In addition,

(7) Jia, T.; Cao, P.; Wang, B.; Lou, Y.; Yin, X.; Wang, M.; Liao, J. *J. Am. Chem. Soc.* **2015**, *137*, 13760–13763.

hindered electrophiles such as 2-substituted allyl carbonates, which are known to react slowly in the alkylation step, were also not examined in this study. We also found that a number of different enantioselective copper–boron or copper–hydride additions to electron-deficient aryl olefins (for example, halo-, trifluoromethyl-, or ester-substituted) are either not mentioned[5,8] or provide less stereoselective[9] products. Until the detailed

Scheme 1.5. Enantioselectivity Fluctuation by Changing Electrophile

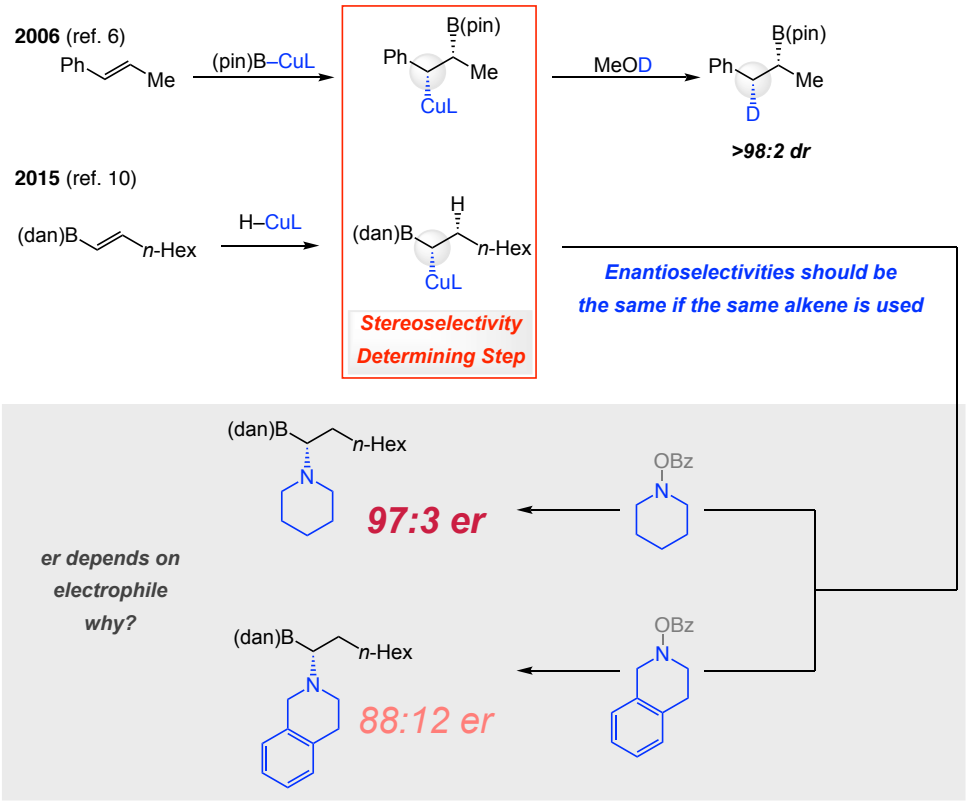

L, ligand; pin, pinacolato; dan,1,8-diaminonaphthalene; Bz, benzoyl

mechanistic studies of Cu–B(pin) and Cu–H complexes from the Hoveyda laboratory, it

(8) (a) Matsuda, N.; Hirano, K.; Satoh, T.; Miura, M. *J. Am. Chem. Soc.* **2013,** *135,* 4934–4937. (b) Zhu, S.; Niljianskul, N.; Buchwald, S. L. *J. Am. Chem. Soc.* **2013,** *135,* 15746–15749. (c) Shi, S. L.; Buchwald, S. L *Nat. Chem.* **2015,** *7,* 38–44. (d) Ascic, E.; Buchwald, S. L. *J. Am. Chem. Soc.* **2015,** *137,* 4666–4669. (e) Logan, K. M.; Brown, M. K. *Angew. Chem. Int. Ed.* **2017,** *56,* 851–855. (f) Jia, T.; Cao, P.; Wang, D.; Lou, Y.; Liao, J. *Chem. Eur. J.* **2015,** *21,* 4918–4922.

(9) (a) Zhong, C.; Kunii, S.; Kosaka, Y.; Sawamura, M.; Ito, H. *J. Am. Chem. Soc.* **2010,** *132,* 11440–11442. (b) Gribble, M. W.; Pirnot, M. T.; Bandar, J. S.; Liu, R. Y.; Buchwald, S. L. *J. Am. Chem. Soc.* **2017,** *139,* 2192–2195. (c) Bandar, J. S.; Pirnot, M. T.; Buchwald, S. L. *J. Am. Chem. Soc.* **2015,** *137,* 14812–14818. (d) Friis, S. D.; Pirnot, M. T.; Buchwald, S. L. *J. Am. Chem. Soc.* **2016,** *138,* 8372–8375. (e) Bandar, J. S.; Ascic, E.; Buchwald, S. L. *J. Am. Chem. Soc.* **2016,** *138,* 5821–5824.

was not certain why enantioselectivity is lower with some alkenes. It was also not clear why enantioselectivity depends on the electrophile, despite the fact that the Cu–B(pin)/Cu–H addition step is stereochemistry-determining (97:3 vs 88:12 er, Scheme 1.5).[10] A recent Cu–H addition to alkene study surmised[9b] that some kinetic enantioselectivity might be lost if an organocopper intermediate were to react slowly, whereas rapid trapping, for example with higher electrophile concentration, could improve enantioselectivity. However, the lack of examples with strongly electron-rich and electron-deficient alkenes still stimulated our curiosities, and the study of enantiomeric purity variations when utiliing different electrophiles was also required.

1.3 Catalytic Enantioselective Boron-Allyl Additions to Aryl and Heteroaryl Olefins

The main goal of the enantioselective allyl-boron addition that our laboratory intended to develop was avoiding the use of a precious metal, low temperatures, and high ligand loading (e.g., Pd, 0 ºC, and 12 mol % ligand). In addition, we aimed to

Scheme 1.6. Key Questions Regarding Multicomponent Catalytic Processes Involving a Cu-Substituted Stereogenic Center

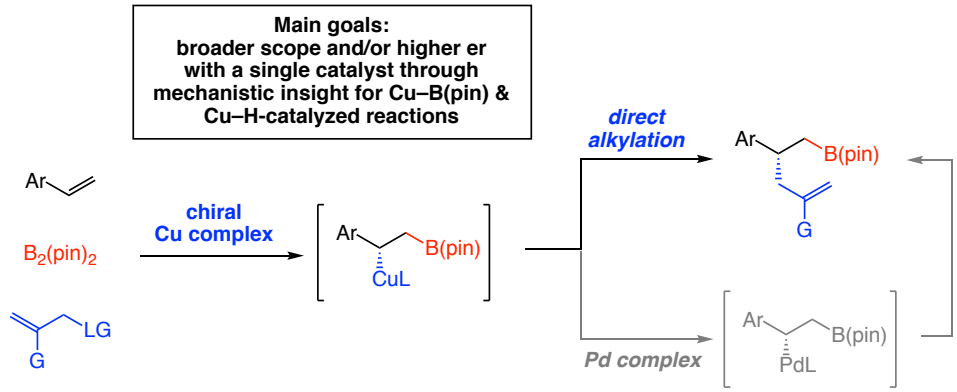

LG, leaving group; L, ligand; G, functional group; pin, pinacolato

minimize enantioselectivity fluctuations by using a single Cu-based complex with larger functional group compatibility (Scheme 1.6).

(10) Nishikawa, D.; Hirano, K.; Miura, M. *J. Am. Chem. Soc.* **2015,** *137,* 15620–15623.

1.3.1 Identification of an Effective Enantioselective Cu-Based Catalyst

To identify an appropriate chiral catalyst, we used the transformation shown in

Table 1.1. Examination of Different Types of Cu Complexes[a]

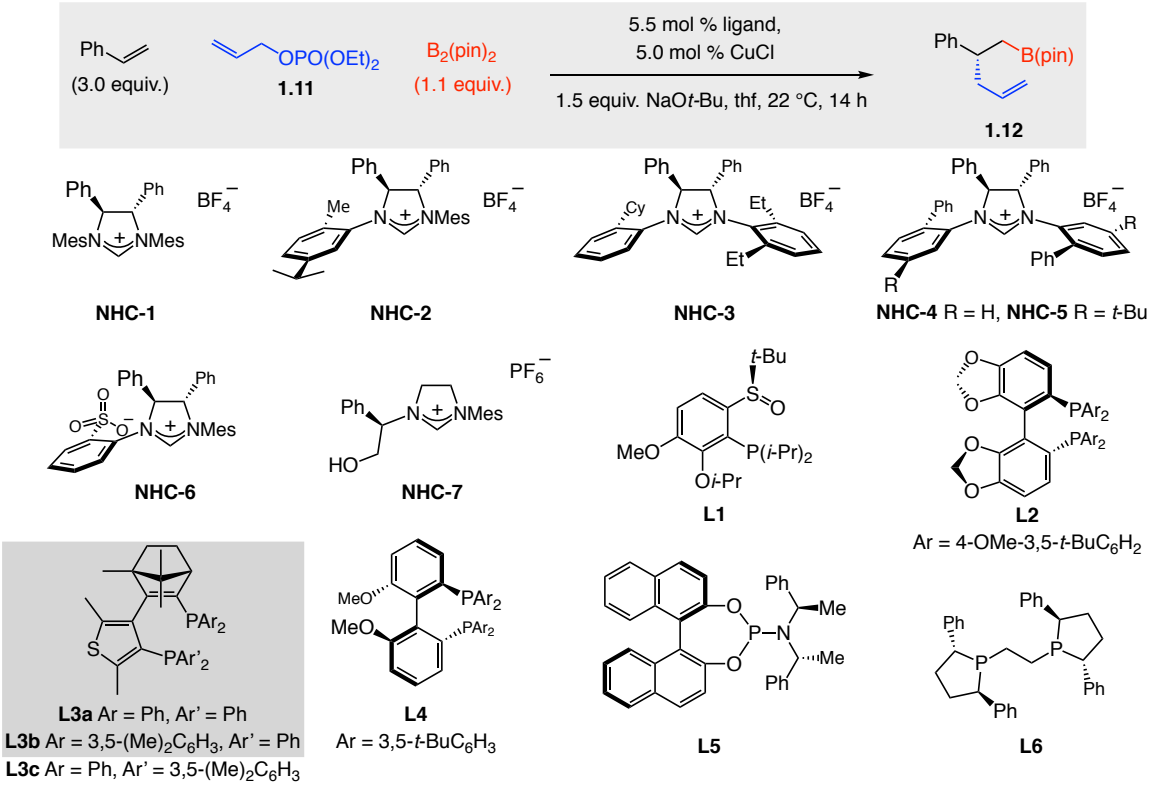

Entry	Ligand	Conv. (%)§	Yield (%)§§	er†
1	**NHC-1**	94	41	56:44
2	**NHC-2**	40	25	58:42
3	**NHC-3**	>98	78	56:44
4	**NHC-4**	80	71	61:39
5	**NHC-5**	35	25	17:83
6	**NHC-6**	44	<2 [only allyl–B(pin)]	NA
7	**NHC-7**	>98	<2 [only allyl–B(pin)]	NA
8	**L1**	15	6	9:91
9	**L2**	66	<2 [only allyl–B(pin)]	NA
10	**L3a**	>98	67	95:5
11	**L3b**	94	51	94:6
12	**L3c**	>98	62	20:80
13	**L4**	86	11	51:49
14	**L5**	39	11	55:45
15	**L6**	>98	22	55:45

a Reactions were perfomed under N_2 atmosphere. § Conversion (conv.) was based on the disappearance of the limiting reagent (1.11) and determined by analysis of the ^{1}H NMR spectra of the unpurified mixtures; the variance of values is estimated to be <±2%. §§ Yield of isolated and purified product; the variance of values is estimated to be <±5%. † Enantiomeric ratios were determined by HPLC analysis; the variance of values is estimated to be <±1%. See the Experimental section for details. NA, not applicable; Mes, 2,4,6-trimethylphenyl; pin, pinacolato.

Table 1.1. NHC ligands and most phosphines were ineffective and nonselective (e.g., entry 1–9 and 13–15, Table 1.1). The exceptions were **L3a** and **L3b**,[11] the use of which led to the formation of **1.12** in 95:5 and 94:6 er, respectively. Although, in this particular instance the er was slightly lower compared to when the Cu/Pd system[7] was used (95:5 compared to 97.5:2.5 er), ligand loading was lower (5.5 mol % as opposed to 17 mol %) and room temperature sufficed (rather than 0 ºC). In addition, our main goal was to expand the scope of the method through improved knowledge of the mechanistic details.

1.3.2 Electronic Properties of Alkenes and Their Effect on Enantioselectivity

In general, highly selective organoboron products were obtained with electron neutral and rich aryl olefins (≥55% yield and 90:10 er). However, substrates which react slowly in the alkylation step due to stabilization of the alkyl-copper intermediate, also lower enantioselectivity as we expected. *meta*-Carboxylic ester **1.24** and *ortho*-trifluoromethyl **1.25** products were formed in 82:18 and 83:17 er, respectively, and *para*-ester- and trifluoromethyl-substituted **1.26** and **1.27** were generated in 51:49 and 58:42 er, respectively. The same trend was found in the reported Cu/Pd protocol, but no rationale was provided. In the case of alkenes that are clearly electron-deficient, the enantiomerically less pure product was likely formed under bimetallic conditions (91:9 er vs 98:2 er, Scheme 1.4). *para*-Methoxy-substituted **1.21** (not reported in the Cu/Pd system) was obtained in 97:3 er and 28% yield. The lower yield is probably because reaction of a Cu–B(pin) complex to a more electron-rich substrate is slower (Scheme1.3),

---

(11) Kadyrov, R.; Iladinoc, I. Z.; Almena, J.; Monsees, A.; Roermeier, T. H. *Tetrahedron Lett.* **2005,** *46,* 7397–7400.

thus addition to allylic phosphate [to give allyl–B(pin)][12] becomes the major pathway (Scheme 1.1).

Scheme 1.7. Representative Products of Bis-Phosphine–Cu-Catalyzed Reactions (3:1 Alkene:Allylphosphate ratio)[a]

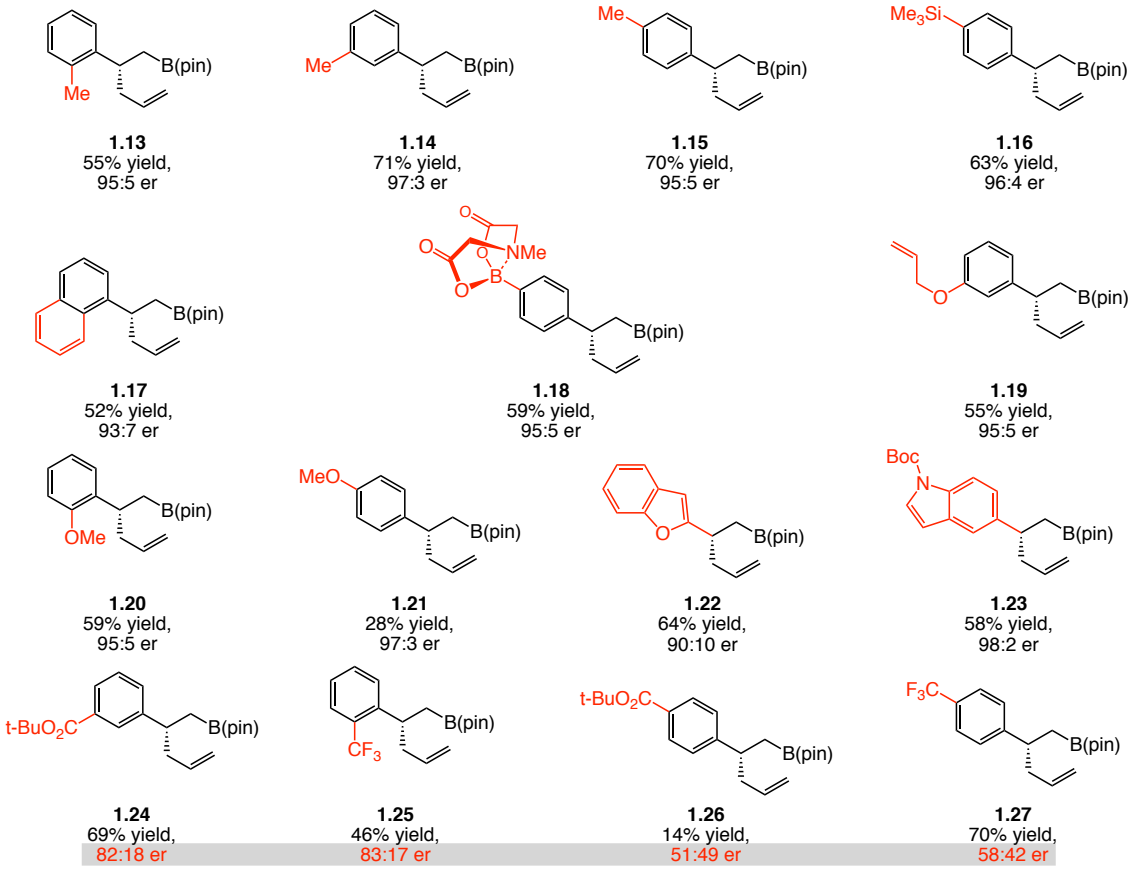

a Reactions were perfomed under N_2 atmosphere. Yield of isolated and purified product; the variance of values is estimated to be <±5%. Enantiomeric ratios were determined by HPLC analysis; the variance of values is estimated to be <±1%. Experiments were performed at least in triplicate. See the Experimental section for details. Boc, *tert*-butoxycarbonyl; pin, pinacolato.

1.3.3 Alkene:Electrophile Ratio and Its Effect on Enantioselectivity

Fluctuations in enantioselectivity possibly arise from a difference in kinetic selectivity during the initial Cu–B(pin) addition step. Or, erosion of stereochemistry could occur prior to C–C bond formation by epimerization. This could be especially noticeable with electron-deficient alkenes (**1.24–1.27,** Scheme 1.7) since less nucleophilic Cu–alkyl species derived from electron-deficient alkenes would react less

(12) (a) Guzman-Martinez, A.; Hoveyda, A. H. *J. Am. Chem. Soc.* **2010,** *132,* 10634–10637. (b) Ito, H., Ito, S.; Sasaki, Y.; Matsuura, K.; Sawamura, M. *J. Am. Chem. Soc.* **2007,** *129,* 14856–14857.

readily (Scheme 1.3). In the latter case, higher electrophile concentration should lead to faster alkylation, minimizing the erosion of enantioselectivity due to epimerization.[9b] Indeed, whereas **1.24** was formed in 82:18 er with a 3:1 aryl olefin:allylphosphate ratio, when the ratio was reversed, the enantioselectivity improved to 95:5 er (Scheme 1.8). *para*-B(pin)-substituted **1.28** (92:8 compared to 82:18 er, Scheme 1.8), *meta*-B(pin)-substituted **1.29** (96.5:3.5 compared to 83:17 er, Scheme 1.8), and 2-naphthyl-substituted **1.30** (96:4 compared to 89:11 er, Scheme 1.8) were also generated with notably higher

Scheme 1.8. Effect of Aryl Olefin:Allyl Phosphate Ratio and Size of Electrophile on Enantioselectivity[a]

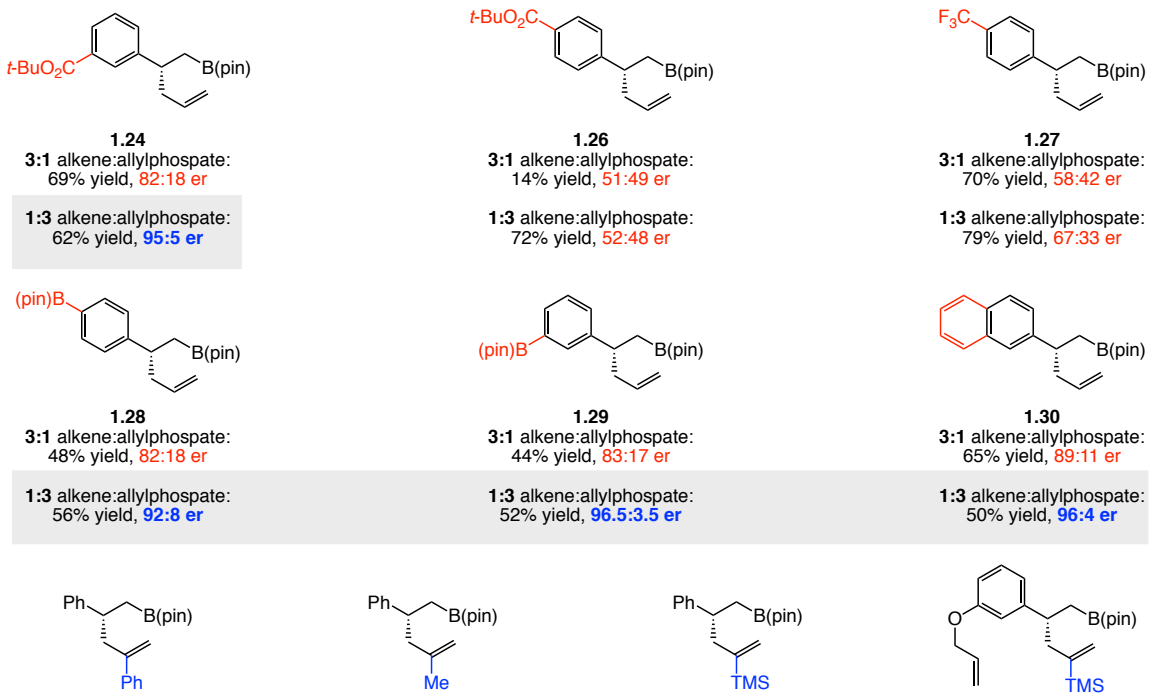

a Reactions were perfomed under N_2 atmosphere. Yield of isolated and purified product; the variance of values is estimated to be <±5%. Enantiomeric ratios were determined by HPLC analysis; the variance of values is estimated to be <±1%. Experiments were performed at least in triplicate. See the Experimental section for details. TMS, trimethylsilyl; pin, pinacolato.

enantioselectivities. Therefore, differences in kinetic selectivity in the initial Cu–B(pin) addition step are not the reason for the enantiomeric ratio variations. However, we soon discovered that matters are more complex. In several cases, increasing the allylphosphate

concentration did not improve er. For example, although the yield for **1.26** was much higher when increasing allylphosphate concentration (72% compare to 14%, Scheme 1.8), there was little impact on the enantioselectivity of its formation. Similar results were seen with *para*-trifluoromethyl-substituted **1.27**. There was no improvement in enantioselectivity when reversing the substrate ratio for *para*-methoxy-substituted **1.21** (Scheme 1.7) which was generated through an exceedingly nucleophilic Cu–alkyl intermediate. With hindered 2-substituted allylphosphates (**1.31**–**1.34**), which were also not included in the disclosure on the Cu/Pd system[7] (in addition to **1.24**, **1.28,** and **1.29**, Scheme 1.8), Cu-alkyl trapping should be slower and enantioselectivity would be expected to suffer. Indeed, transformations leading to **1.31** and **1.32**, which contain 2-substituted alkenes, were more enantioselective when additional amounts of electrophile was present (96:4 compared to 90:10 er and 95:5 compared to 90:10 er). With alkenylsilane **1.33** and **1.34**, the same alteration was less consequential (Scheme 1.8).

1.3.4 Higher Enantioselectivity with a Less Reactive Electrophile

Faster Cu–alkyl trapping is not the only way to obtain high enantioselectivity. Regardless of the alkene:electrophile ratio, use of allylphenyl carbonate **1.35**, shown to be less reactive than allylphosphate[13] (Scheme 1.9), generally led to higher er (96:4 to 98:8 er, Scheme 1.10). However, larger amounts of this electrophile were required with the more electron withdrawing aryl olefins **1.25** and **1.27** (less nucleophilic copper–alkyl intermediates) because of its lower reactivity of **1.35**. With electron-neutral or electron-rich olefins, the use of allylphosphate was often preferred due to better yields as opposed to higher er.

---

(13) (a) Zhong, C.; Kunii, S., Kosaka, Y.; Sawamura, M.; Ito, H. *J. Am. Chem. Soc.* **2010,** *132,* 11440–11442. (b) Bayer, A.; Kazmaier, U. *Chem. Eur. J.* **2014,** *20,* 10484–10491.

Scheme 1.9. Relative Reactivity of Allylphosphate and Allylphenyl Carbonate[a]

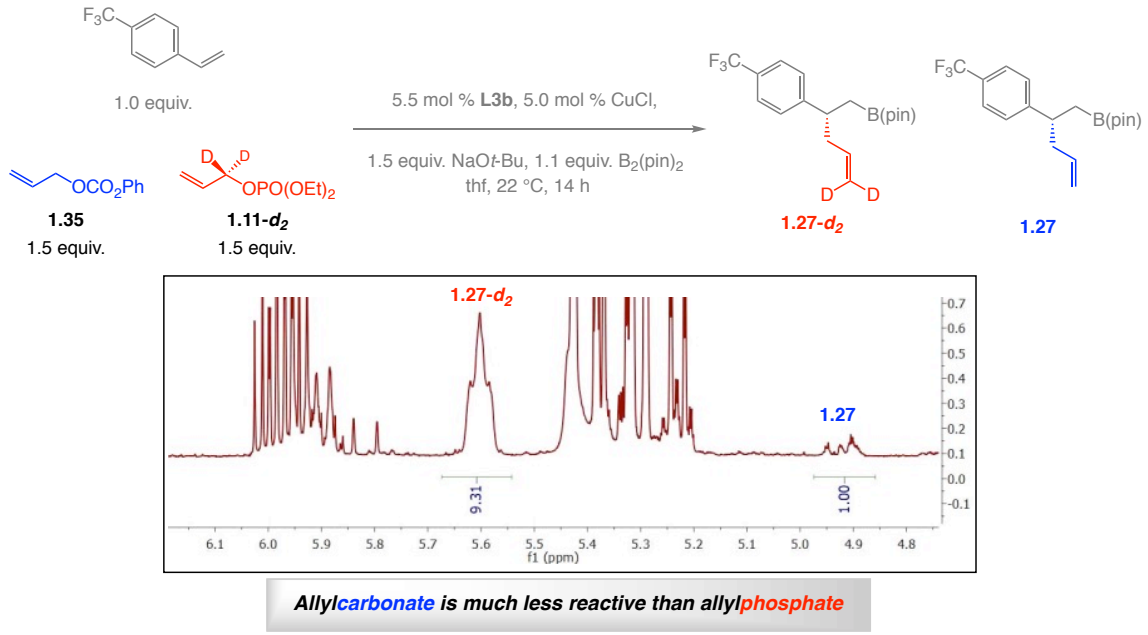

Allylcarbonate is much less reactive than allylphosphate

a See the Experimental section for a detailed spectroscopic analysis. pin, pinacolato.

Scheme 1.10. Higher er with a Less Reactive Electrophile[a]

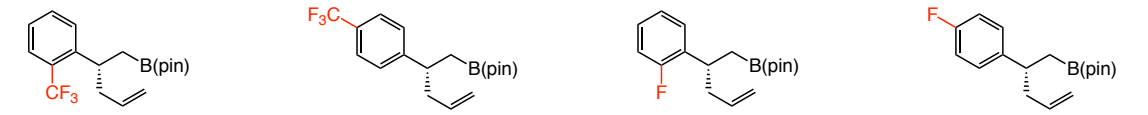

1.25	**1.27**	**1.36**	**1.37**
3:1 alkene:allylphospate: 46% yield, 83:17 er	**3:1** alkene:allylphospate: 70% yield, 58:42 er	**3:1** alkene:allylphospate: 54% yield, 89:11 er	**3:1** alkene:allylphospate: 66% yield, 92:8 er
1:3 alkene:allylcarbonate: 50% yield, 96:4 er	**1:3** alkene:allylcarbonate: 68% yield, 96:4 er	**3:1** alkene:allylcarbonate: 64% yield, 96:4 er	**3:1** alkene:allylcarbonate: 65% yield, 98:2 er

a Reactions were perfomed under N_2 atmosphere. Yield of isolated and purified product; the variance of values is estimated to be <±5%. Enantiomeric ratios were determined by HPLC analysis; the variance of values is estimated to be <±1%. Experiments were performed at least in triplicate. See the Experimental section for details. pin, pinacolato.

1.3.5 Mechanism: Epimerization

Reactions with (*E*)- and (*Z*)-β-deuterio-para-*tert*-butyl-ester substituted styrenes afforded **1.26-*d*** in low dr (Scheme 1.11), indicating that the Cu–C bond can epimerize after *syn*-Cu–B(pin) addition[4] (Scheme 1.2 and Scheme 1.3). The same outcome was found with the Cu/Pd system (Scheme 1.11). The radical clock experiments do not support that the epimerization proceeds through a radical-based pathway, but that there is heterolytic cleavage/re-formation of Cu–C bond (Scheme 1.12). Changes in catalyst

Scheme 1.11. Loss of Kinetic Enantioselectivity Due to Epimerization[a]

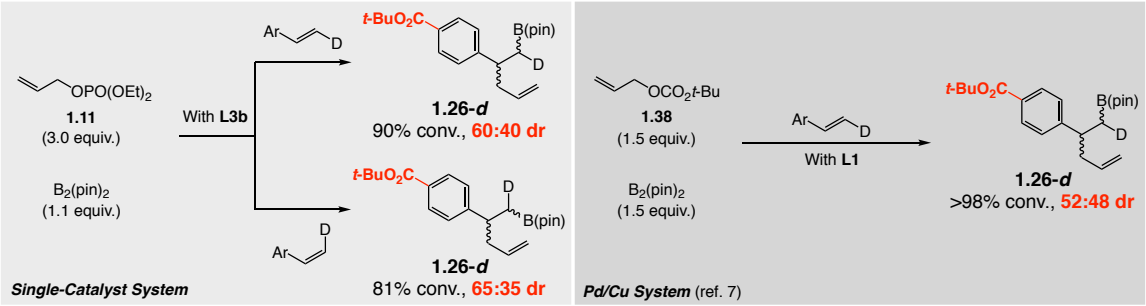

a Reactions were perfomed under N_2 atmosphere. Conversion (conv.) was based on the disappearance of the limiting reagent and determined by analysis of the ^{1}H NMR spectra of the unpurified mixtures. Diastereomeric ratios were determined by NMR analysis; the variance of values is estimated to be <±2%. Experiments were performed at least in triplicate. See the Experimental section for details. pin, pinacolato.

concentration did not impact er, showing that epimerization does not proceed via a bimetallic pathway.[14] The highly electron-deficient aryl unit probably stabilizes electron density at the benzylic site, facilitating heterolytic cleavage/re-formation of the Cu–C bond through epimerization via metal-enolate **1.46**. A para-ester-substituted aryl olefin was the only case where increasing electrophile concentration (Scheme 1.8) or the use of

Scheme 1.12. Radical Colck Experiments and Cu–C Bond Epimerization[a]

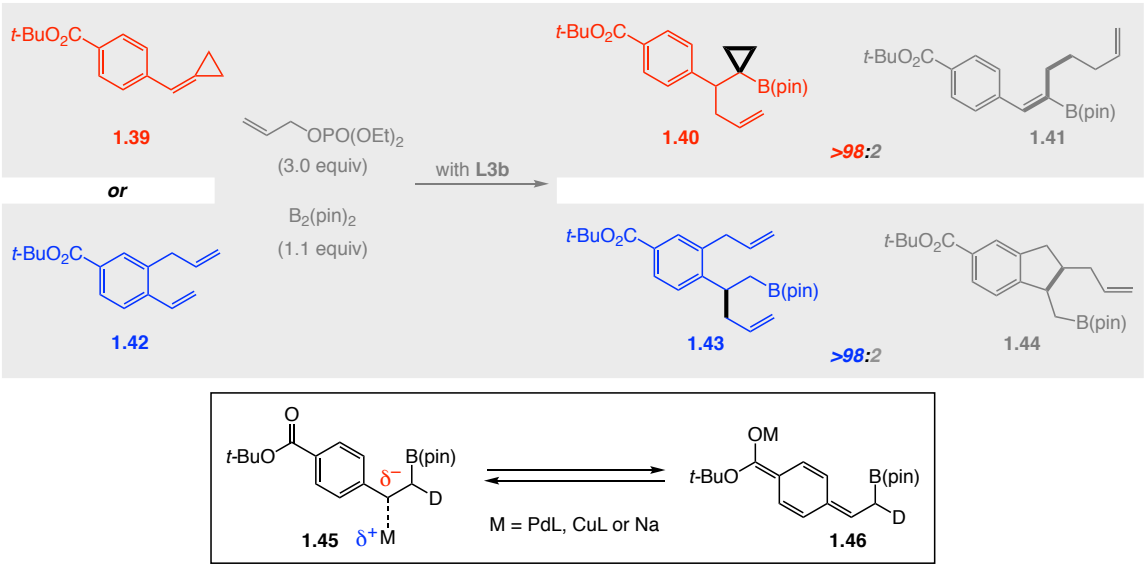

a Reactions were perfomed under N_2 atmosphere. Product ratios were determined by NMR analysis; the variance of values is estimated to be <±2%. Experiments were performed at least in triplicate. See the Experimental section for details. L, ligand; pin, pinacolato.

allylphenyl carbonate did not enhance er. Loss of enantioselectivity is too facile in this particular case.

(14) Suess, A. M.; Uehling, M. R.; Kaminsky, W.; Lalic, G. *J. Am. Chem. Soc.* **2015,** *137,* 7747–7753.

1.3.6 Mechanism: Temporary Ligand Loss at the Cu–Alkoxide Stage

Reactions with other deuterated alkenes, such as those in Scheme 1.13, were completely diastereospecific (>98% ds). Again, similar results were obtained under Cu/Pd conditions.[7] Thus, in most cases, diminution in er does not arise from Cu–alkyl trapping with inversion of stereochemistry[15] or Cu–C bond rupture,[16] as, otherwise, dr would be lower when labelled alkenes were used. Except *para*-ester-substituted **1.26**

Scheme 1.13. Study of the Possibility of Epimerization through Isotopic Labeling[a]

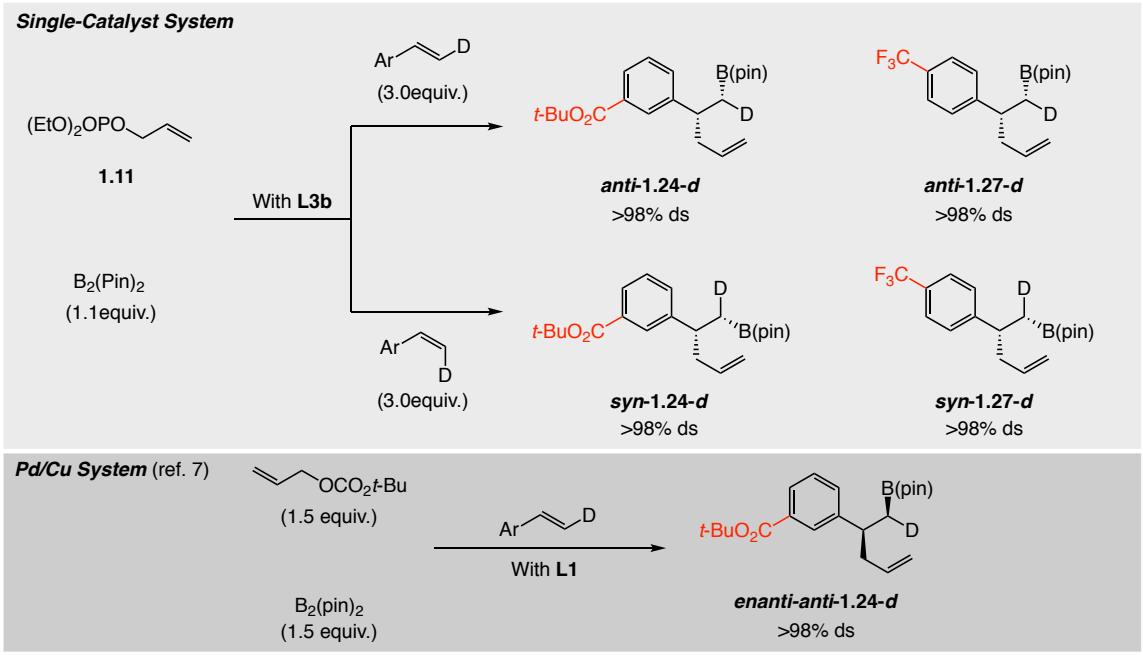

a Reactions were perfomed under N_2 atmosphere. Diastereomeric ratios were determined by NMR analysis; the variance of values is estimated to be <±2%. Experiments were performed at least in triplicate. See the Experimental section for details. pin, pinacolato.

case, what is the detailed mechanism behind the loss of enantioselectivity? What is the specific role for the excess amount of electrophile? Could it be that in some cases, er improves (for example, **1.24,** Scheme 1.8) by reversal of the alkene:electrophile ratio because the alkene concentration is reduced and not because of higher electrophile concentration? The most likely enantioselective pathway is shown in Scheme 1.14a.

(15) Yang, Y.; Perry, I. B.; Buchwald, S. L. *J. Am. Chem. Soc.* **2016,** *138,* 9787–9790.
(16) Whitesides, G. M.; Panek, E. J.; Stedronsky, E. R. *J. Am. Chem. Soc.* **1972,** *94,* 232–239.

After the formation of Cu–alkyl complex **1.49** from the chiral Cu–B(pin) complex **1.48** which is generated through transmetalation with $B_2(pin)_2$ and Cu–alkoxide complex **1.47**. Complex **1.49** would then readily react with the electrophile (**1.11** or **1.35**) to deliver **1.51** via transition state structure **1.50**, which in turn affords the final product **1.52**. Spectroscopic studies show that the chiral ligand dissociates from the metal center of the Cu–O*t*-Bu complex. Subjection of Cu–O*t*-Bu to 1.1 equivalents of **L3c** (spectrum A,

Scheme 1.14. The Catalytic Cycle and Temporary Dissociation of the Chiral Ligand

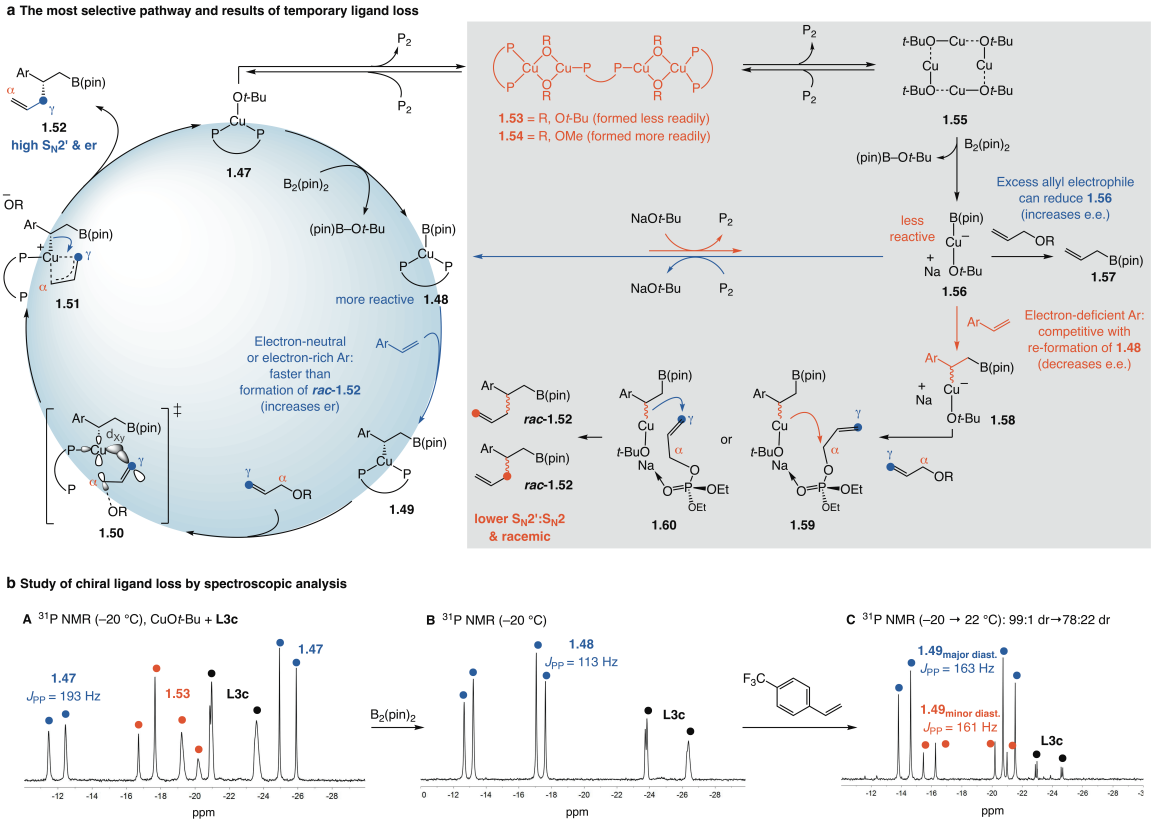

Scheme 1.14b) generated mixtures of complex **1.47**, ~30 mol % of unbound chiral ligand **L3c**, and the derived aggregates (for example, **1.53**) which could readily transform to the well-defined copper-alkoxide[17] **1.55** (Scheme 1.14a). Addition of $B_2(pin)_2$ yielded **L3c**–Cu–B(pin) complex **1.48**, which was stable enough for analysis at –20 °C (spectrum B,

(17) Greiser, T.; Weiss, E. *Chem. Ber.* **1976,** *109,* 3142–3146.

Scheme 1.14b). There was still ~30% unbound bis-phosphine ligand at this point which indicates that there is no chiral ligand re-association after Cu–B bond formation. This suggests that there is a significant amount of achiral Cu–B(pin) complex available to react (see the Experimental section for a detailed spectroscopic analysis). Addition of *para*-CF_3-styrene at –20 °C initially afforded **1.49** in 99:1 dr (~75% conv.). When the mixture was allowed to warm to 22 °C (spectrum C, Scheme 1.14b) there was complete conversion and diastereoselectivity was reduced to 72:28 with ~10% of unbound **L3c** remaining, which is due to the excess 0.1 equivalents used initially. The oxygen atom of a Cu–alkoxide species can form a bridge with another Cu–alkoxide unit facilitating aggregation,[18] ligand dissociation and generation of achiral Cu–B(pin) species **1.56**. Under the catalytic reaction condition with 1.5 equivalents of NaO*t*-Bu, ligand dissociation would be more problematic since there is only 5.5 mol % of ligand. Spectroscopic studies confirm that when excess chiral ligand is employed, the equilibrium shifts towards the bis-phosphine–Cu complex (Scheme 1.15). The achiral

Scheme 1.15. Aggregates Derived from Bis-Phosphine–Cu Complexes and Related Equilibria

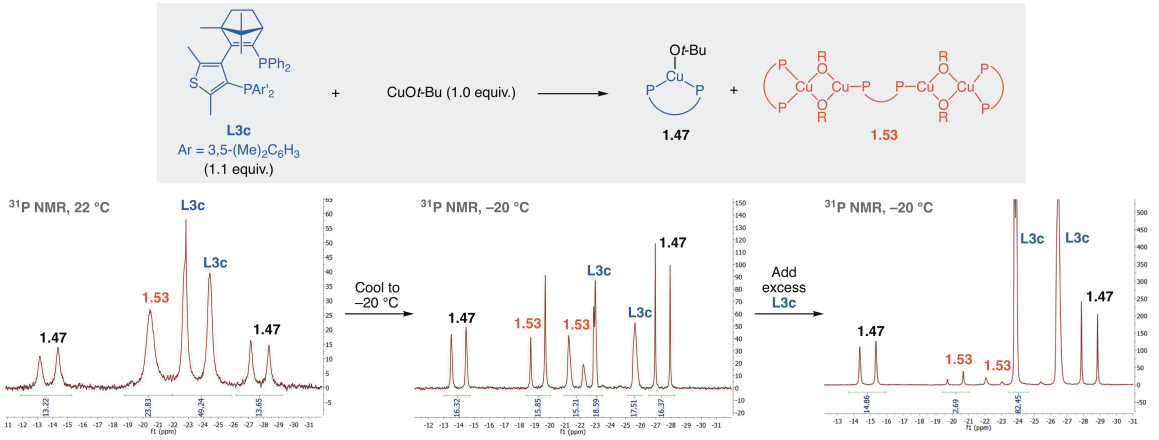

(18) (a) Lemmen, T. H.; Goeden, G. V.; Huffman, J. C.; Geerts, R. L.; Caulton, K. G. *Inorg. Chem.* **1990,** *29,* 3680–3685. (b) Dubinina, G. G.; Furutachi, H.; Vicic, D. A. *J. Am. Chem. Soc.* **2008,** *130,* 8600–8601. (c) Bradley, D. C.; Mehrotra, R. C.; Rothwell, I. P.; Singh, A. Alkoxo and Aryloxo Metal Derivatives *Elsevier,* **2001,** 329–332.

Cu–B(pin) species **1.56** lacks the Lewis basic phosphine ligand, causing the complex to be less nucleophilic. Thus, the complex cannot readily react with an electron-rich alkene (**1.56** → **1.58**). Density functional theory (DFT) calculations show that reaction between an achiral Cu–B(pin) and an electron-poor olefin is more favorable and can be problematic compared to an electron-rich olefin (Scheme 1.16; for full system calculations see the Experimental section). Faster Cu–B(pin) addition to an electron-poor alkene suggests that the aryl olefin concentration must be kept low for higher er, otherwise rate of the achiral alkyl-copper complex **1.58** formation would be faster. The

Scheme 1.16. Selected Energy Barriers Obtained through DFT Studies with Model System[a]

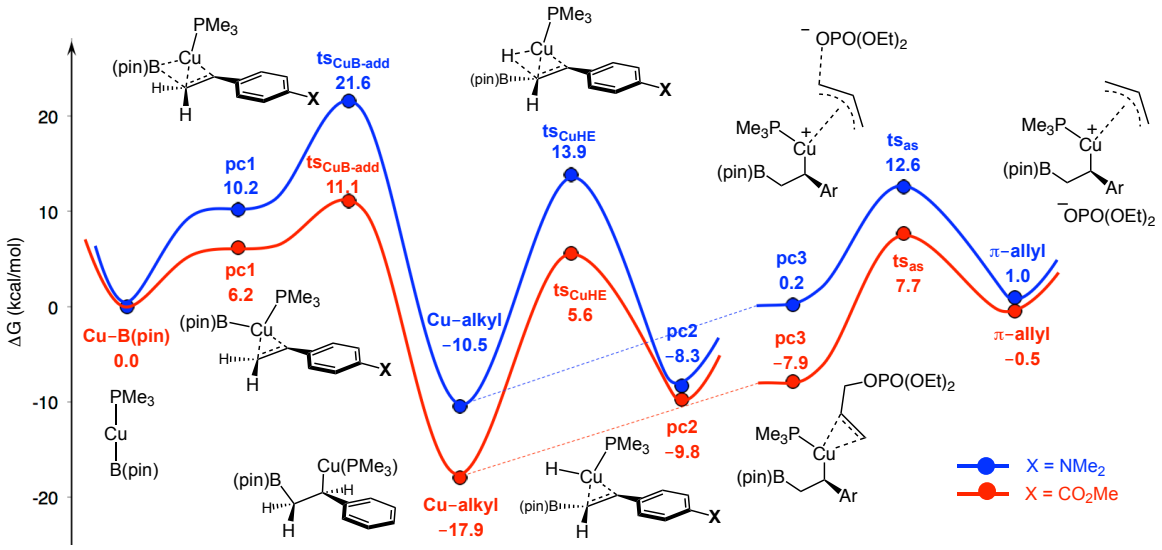

a DFT calculations were performed at the MN12SX/Def2TZVPP//ωB97XD/Def2SVP level in THF (SMD: solvation model based on density)

lower concentration of electron-poor olefin would allow faster ligand re-association (**1.56** → **1.48**) to occur before the Cu–B(pin) reacts with an alkene (**1.56** → **1.58**, Scheme 1.14). This is less likely when an electron-neutral or electron-rich olefin is used, where altering the aryl olefin concentration is largely inconsequential and increasing the amount of electrophile significantly impacts enantioselectivity. In the cases with electron-neutral or electron-rich olefins, formation of achiral alkyl-copper complex **1.58** would be much slower. However, increasing the amount of allylic phosphate facilitates conversion of the

achiral Cu–B(pin) complex to allyl–B(pin) side product (**1.56** → **1.57**, Scheme 1.14).[12] Thus, as a result of forming more **1.57**, there would be much less opportunity, for **1.56** to go on to form ***rac*-1.52**. The following observations offer more clarification. A systematic study of the effect of substrate concentration on selectivity (changing only one substrate concentration at a time; Scheme 1.17, more examples in the Experimental section) indicated that although increasing the amount of electrophile can lead to higher er with

Scheme 1.17. Effect of Aryl Olefin or Allyl Electrophile Concentration on Enantioselectivity

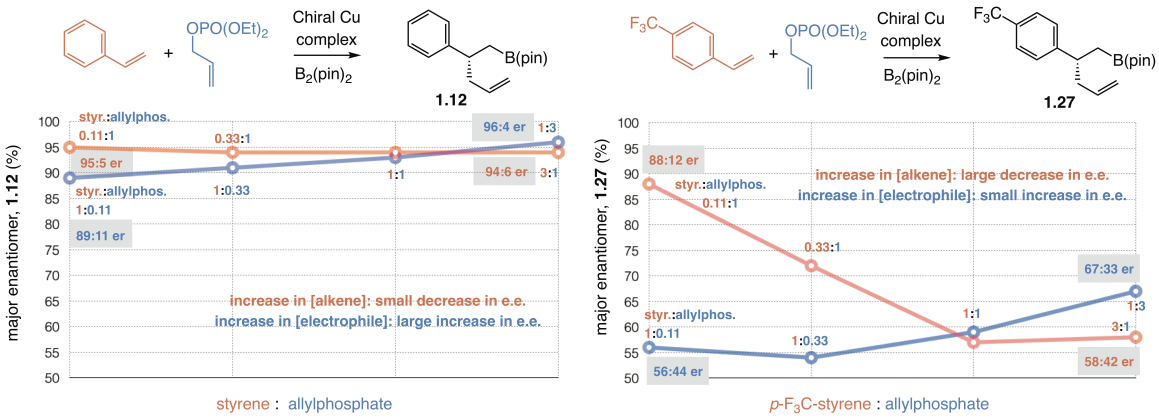

styrene, variations in olefin concentration have a stronger influence on enantioselectivity with electron-deficient olefins (95:5 to 94:6 er for **1.12** compared to 88:12 to 58:42 er for **1.27**; shown in red). With excess alkene, addition of achiral Cu–B(pin) to the more reactive electron-deficient π bond (**1.56** → **1.58**, Scheme 1.14) is faster than its association with the chiral ligand (**1.56** → **1.48**, Scheme 1.14) decreasing the enantioselectivity by generating ***rac*-1.52**. Alkene concentration is a very important factor in improving selectivity, but the enantiomeric ratio does not change beyond a certain olefin concentration (1:1–3:1 alkene:allylphosphate, shown in red, Scheme 1.17). The proposed scenario is also supported by the following additional experiments. First, higher eanantioselectivity was obtained with greater amounts of chiral ligand (95:5 er at 20 mol % **L3b** compared to 86:14 er at 5.5 mol % **L3b**, Scheme 1.18a). Second, with the smaller

Scheme 1.18. Effect of Ligand Concentration on er and S_N2' selectivity[a]

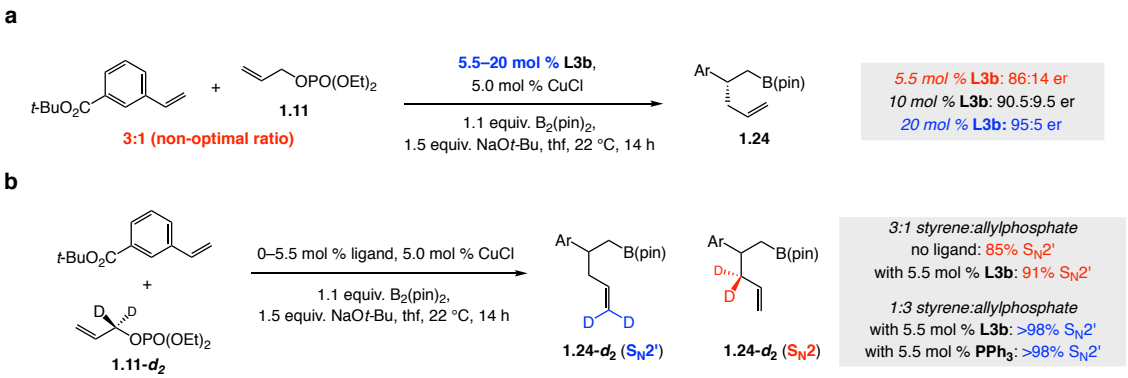

a Reactions were perfomed under N_2 atmosphere. Ratios of S_N2' and S_N2 products were determined by NMR analysis; the variance of values is estimated to be <±2%. Experiments were performed at least in triplicate. See the Experimental section for details. pin, pinacolato.

NaOMe (versus NaO*t*-Bu), expected to bridge Cu centers and cause ligand dissociation more efficiently (**1.53** versus **1.54**, Scheme 1.14), enantioselectivity was lower (77:33 er with NaOMe compare to 86:14 er with NaO*t*-Bu and 5.5 mol % **L3b**). The experiments with deuterated electrophile (**1.11-*d*$_2$**, Scheme 1.18b) describe the matter in more detail. A bis-phosphine–Cu complex delivers high S_N2' selectivity due to the HOMO (highest occupied molecular orbital) of the copper species being on the d_{xy} orbital, while the LUMO (lowest unoccupied molecular orbital) of the allyl phosphate besides on the C_γ, as shown in **1.50** (Shceme 1.14).[19] The Cu–alkyl bond in square planar **1.51** is thus *syn* to the newly formed Cu–C_γ bond, furnishing the S_N2' addition (**1.52**) product after the C–C bond formation. With the achiral alkyl–Cu complexes (**1.59** and **1.60**, Scheme 1.14), S_N2' selectivity is lower due to the sodium ion being able to bridge the Cu–alkoxide oxygen[20] and phosphate moiety. These scenarios are also supported by DFT calculations (see the Experimental section). In the reaction with *meta-tert*-butyl-ester-substituted styrene and **1.11-*d*$_2$** (non-optimal conditions, 3:1 alkene:electrophile) without a ligand and with **L3b** present, the S_N2':S_N2 ratios were 85:15 and 91:9, respectively (Scheme 1.18). In contrast,

(19) Yoshikai, N.; Nakamura, E. *Chem. Rev.* **2012,** *112,* 2339–2372.
(20) Konovalov, A. I.; Benet-Buchholz, J., Martin, E.; Grushin, V. V. *Angew. Chem. Int. Ed.* **2013,** *52,* 11637–11641.

with an optimal alkene:electrophile ratio (1:3) and a chiral bis-phosphine present, the S_N2':S_N2 ratio was >98:2. As long as the alkene concentration was kept low, regardless of the ligand identity (**L3b** or PPh_3), the S_N2 product was not detected. This finding shows that lowering the alkene concentration and/or increasing ligand loading is more effective especially for electron-deficient aryl olefins, to prevent the undesired reactivity of achiral Cu-B(pin) complexes from occurring. There was a much smaller increase in enantioselectivity at higher electrophile concentration for products derived from electron-poor alkenes, such as **1.27** (Scheme 1.17) because the formation of **1.58** was still too facile in these cases (compared electron-neutral alkenes).

1.3.7 Mechanism: Low Enantioselectivity Due to Cu–H Elimination

Through computational studies (Scheme 1.16) we found that, especially with electron-deficient alkene as substrates (red versus blue), Cu–H elimination is able to compete with allylic substitution (Cu–alkyl → ts_{CuHE} → pc2 versus Cu–alkyl → pc3 → ts_{as} → π-allyl). Indeed, additional mechanistic studies with (*E*)- and (*Z*)-β-deuterio-aryl olefins indicated that Cu–H elimination was involved in the fluctuation on enantioselectivity. The data in Scheme 1.19a shows that Cu–H elimination could be one of the reasons why enantioselectivity is lower if Cu–alkyl trapping is slow (for example, when excess aryl olefin is used). With unlabeled aryl olefins or (*E*)-β-deuterio-styrenes there was only a small change in er. However, notably higher selectivities were obtained with (*Z*)-β-deuterio-styrene compared to when unlabeled styrene was used (***syn*-1.31-*d*** and ***syn*-1.27-*d***, Scheme 1.19a). Thus, while reaction with the *Z* isomers involve a slower Cu–D elimination (primary isotope effect) or Cu–H elimination via a sterically hindered intermediate [eclipsing Ar and B(pin)], *β*-hydride elimination can proceed more readily

with the *E* isomer (Scheme 1.19a). Spectroscopic studies provide additional insight to verify re-addition of Cu–H to the alkenyl B(pin) compounds (**1.63**, Scheme 1.19b). Treatment of a sample of Cu-alkyl complex **1.62** (82:18 dr) to *para*-trifluoromethyl alkenyl–B(pin) **1.63** afforded ~20% alkenyl–B(pin) **1.64** and isomeric species **1.65** (22 °C, 2 h; see the Experimental section for a detailed spectroscopic analysis). Hence, Cu–H

Scheme 1.19. Low er due to Cu–H Elimination[a]

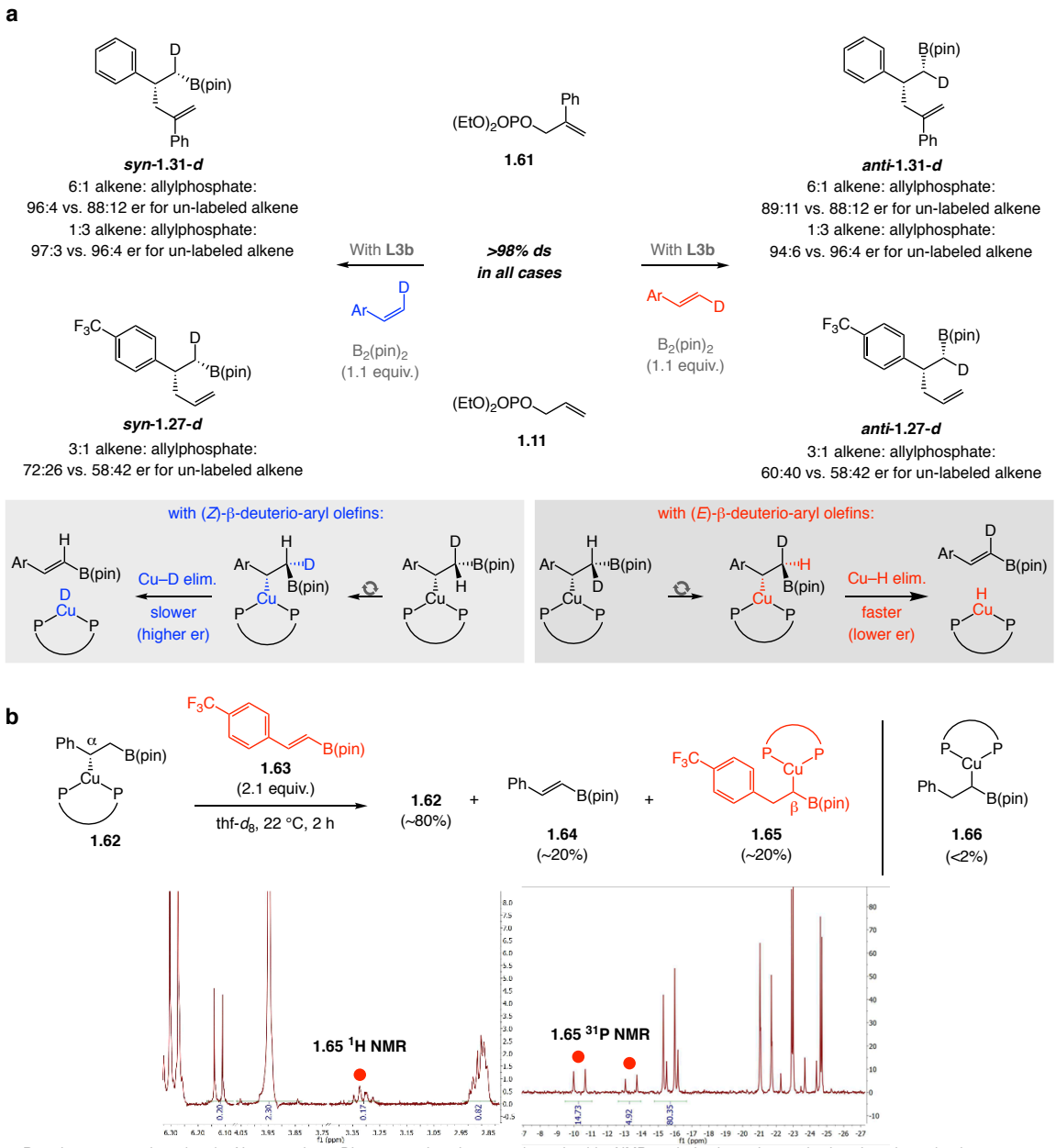

a Reactions were perfomed under N_2 atmosphere. Diastereomeric ratios were determined by NMR analysis; the variance of values is estimated to be <±2%. Enantiomeric ratios were determined by HPLC analysis; the variance of values is estimated to be <±1%. Experiments were performed at least in triplicate. See the Experimentals section for all details. pin, pinacolato.

elimination converts **1.62** to **1.64** and the generated metal–hydride complex adds preferentially to the more electrophilic alkene (**1.65** versus **1.66**). The data shows that under unoptimal conditions (excess alkene versus allyl electrophile), low enantioselectivity does not originate from Cu–H elimination/re-addition since Cu–H re-addition yields the regioisomer as shown in **1.65** due to the polarity reversal of the olefin in alkenyl–B(pin)[6] **1.63**. Instead, diminished enantioselectivity might be attributed to the major Cu-alkyl diastereomer undergoing faster Cu–H elimination. At higher electrophile concentration, Cu-alkyl trapping can compete better with diastereoselective Cu–H elimination, resulting in improved enantioselectivity. It would be difficult to anticipate to what extent and how much faster one isomer might undergo Cu–H elimination.

1.3.8 Mechanism: High Enantioselectivity Due to Cu–H Elimination

Although counterintuitive, use of the less reactive allylphenyl carbonate gives rise to higher selectivity due to Cu–H elimination. One piece of evidence to which support this hypothesis was the larger amounts of alkenyl–B(pin) formed in reactions with allylphenyl carbonate (~10% versus ~2% with allylphosphate under catalytic enantioselective conditions). This means that there is minimal trapping of the achiral Cu–B(pin) species with allylphenyl carbonate (**1.58**, Scheme 1.20) when compared to allylic

Scheme 1.20. High er due to Cu–H Elimination

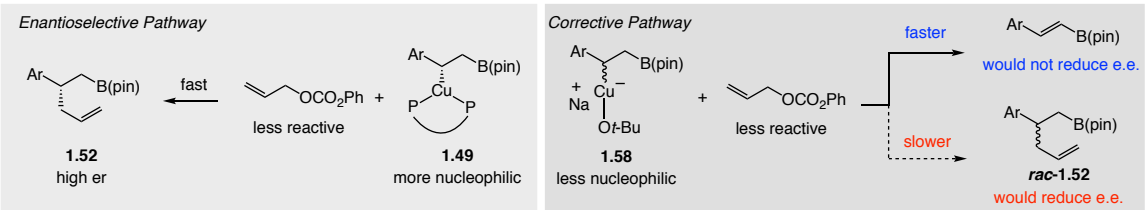

phosphate. The racemic pathway may thus be corrected by chemoselective Cu–H elimination of the achiral Cu-alkyl intermediate (cf. the derived bis-phosphine complex)

rather than allylic substitution to furnish ***rac*-1.52**. This is for two reasons: (1) bis-phosphine–Cu-alkyl species are less prone to undergo Cu–H elimination compared to the ligand-free achiral complex[21]; and (2) with the less reactive allylcarbonate and under more dilute catalytic conditions, intramolecular Cu–H elimination in **1.58** (Scheme 1.20) is likely faster than intermolecular allylic substitution (to give ***rac*-1.52**), or chiral ligand reassociation (**1.58** → ***rac*-1.49**). Therefore, especially for **1.27** and **1.36**, enantioselectivity is high only when carbonate **1.35** is used (Scheme 1.10). The adverse effect of Cu–H elimination when Cu–alkyl trapping is slow would be applicable here, since the major Cu-alkyl diastereomer decomposes faster (Scheme 1.19b). However, the ability of Cu–H elimination to prevent racemic product generation from achiral Cu-alkyl complexes (**1.58**) appears to be the dominant factor.

1.3.9 Advantage of the Single-Catalyst Method

Under the Cu/Pd conditions,[7] where higher electrophile concentration means increasing the amount of electrophile as well as the co-catalyst, enantioselectivity could

Scheme 1.21. Influence of Variations in Elctrophile/Co-Catalyst Concentration on Enantioselectivity[a]

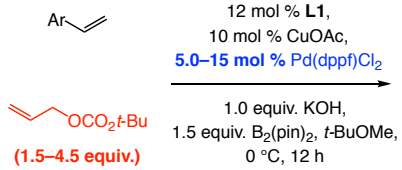

	Change [E⁺] conc. with 5.0 mol% [Pd]	Change [Pd] conc. with 1.5 equiv. of E⁺
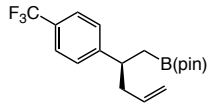 ***enant*-1.27**	alkene:E^+ 1:4.5 >98% conv, 66% yield, **82:18 er** alkene:E^+ 1:1.5 >98% conv, 88% yield **83:17 er**	15 mol % $Pd(dppf)Cl_2$ >98% conv, 93% yield, **81:19 er** 5.0 mol % $Pd(dppf)Cl_2$ >98% conv, 88% yield, **83:17 er**
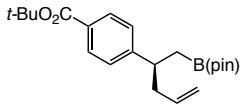 ***enant*-1.26**	alkene:E^+ 1:4.5 >98% conv, 86% yield, **70:30 er** alkene:E^+ 1:1.5 >98% conv, 56% yield **67:33 er**	15 mol % $Pd(dppf)Cl_2$ 80% conv, 64% yield, **66:34 er** 5.0 mol % $Pd(dppf)Cl_2$ >98% conv, 56% yield, **67:33 er**

a Reactions were perfomed under N_2 atmosphere; Conversion (conv.) was based on the disappearance of the limiting reagent and determined by analysis of the ^{1}H NMR spectra of the unpurified mixtures; the variance of values is estimated to be <±2%; Yield of isolated and purified product; the variance of values is estimated to be <±5%; Enantiomeric ratios were determined by HPLC analysis; the variance of values is estimated to be <±1%; E^+, electrophile, pin, pinacolato; dppf, 1,1′-bis(diphenylphosphino)ferrocene.

(21) Miyashita, A.; Yamamoto, T.; Yamamoto, A. *Bull. Chem. Soc. Jpn.* **1977,** *50,* 1109–1117.

not be improved by adjusting the electrophile and co-catalyst concentrations (Scheme 1.21). This might be because the presence of achiral bis-phosphine Pd species allows for an achiral Cu–B(pin) complex to be generated through ligand exchange.[22] The resulting non-enantioselective pathways offset any benefits that might result from a change in conditions. One advantage of the single catalyst system is that it can be used as a reasonable platform to achieve broader applicability. The cases in Scheme 1.22a are illustrative; except for **1.27**, none were previously reported under the two-catalyst conditions (Scheme 1.4). With relatively electron-rich substrates (for example, **1.21** or **1.67**), where Cu–alkyl formation is more sluggish, higher alkene concentration led to high yield and enantioselectivity. The positive effect of utilizing a less reactive

Scheme 1.22. Broader Scope and Utility[a]

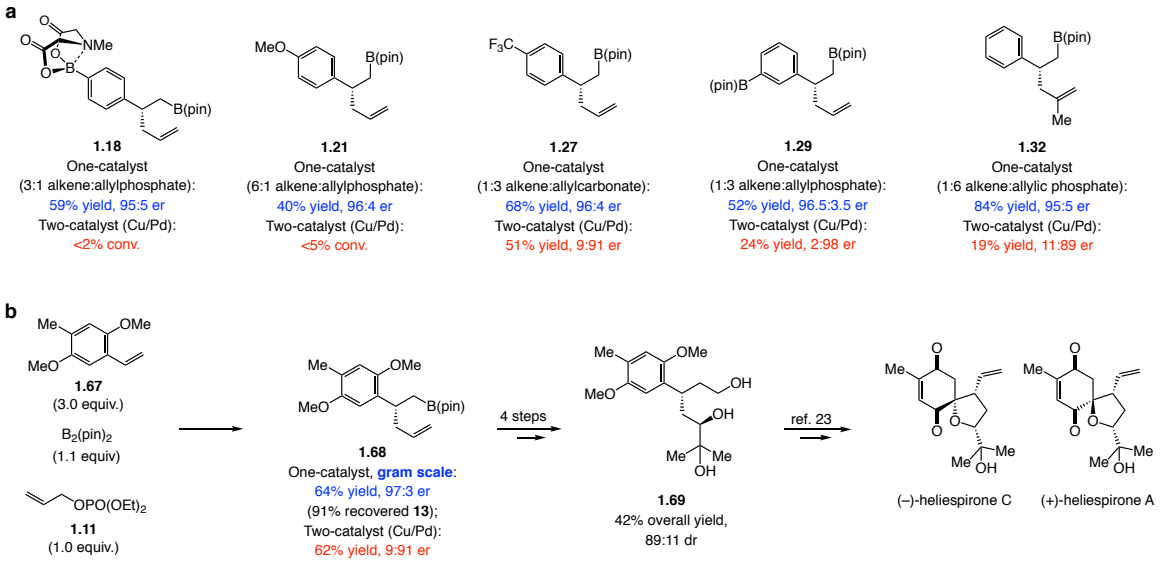

a Reactions were perfomed under N_2 atmosphere. Conversion (conv.) was based on the disappearance of the limiting reagent (1.11 or 1.39) and determined by analysis of the ^{1}H NMR spectra of the unpurified mixtures; the variance of values is estimated to be <±2%.Yield of isolated and purified product; the variance of values is estimated to be <±5%. Enantiomeric ratios were determined by HPLC analysis; the variance of values is estimated to be <±1%. See the Experimental section for details. pin, pinacolato

electrophile in reactions with a strongly electron-deficient alkene is underscored by the improved yield and enantioselectivity for **1.27**. When electronically-neutral styrene was used (for example, **1.32**), larger amounts of allylic phosphate reduced the possibility of

(22) DelPozo, J.; Casares, J. A.; Espinet, P. *Chem. Commun.* **2013,** *49,* 7246–7248.

diastereoselective Cu–H elimination and lower the concentration of achiral Cu–B(pin), resulting in higher er (see Scheme 1.14 and Scheme 1.19a for details). Gram-scale synthesis of **1.68** proceeded in higher enantioselectivity (97:3 er compared to 9:91 er with the two-catalyst method). Diol **1.69**, applicable to synthesis of heliespirones A and C,[23] was prepared from **1.68** in four steps and 42% overall yield (89:11 dr; see the Experimental section for details). Unreacted **1.67** was easily recovered (91% yield). Compounds **1.68** or **1.69** cannot be accessed through enantioselective hydroboration[24] or conjugate addition of an aryl or a prenyl group to an enoate[25].

1.3.10 Relevance to Cu–H-Catalyzed Processes

Reactions with electronically-neutral dihydronaphthalene and electron-deficient alkenyl–B(dan) were investigated to see if the aforementioned principles apply to Cu–H additions as well (Scheme 1.23). With dihydronaphthalene,[8b] increasing the hydroxyamine concentration led to improvement in enantioselectivity (**1.70** from 90:10 to 93:7 er); similarly, in reactions with alkenyl–B(dan)[10] there was a significant increase in er when larger amounts of electrophile were utilized (88:12 to 96:4 er). However, based on the above studies, with the more electron-deficient alkenyl–B(dan), er variations are probably caused by adventitious reaction by an achiral Cu–H complex. This is supported by the distinct way through which increased ligand loading impacts these reactions: with electron-richer dihydronaphthalene, there was no change in er when 2.0 or 8.0 mol % **L2**

---

(23) (a) Huang, C.; Liu, B. *Chem. Commun.* **2010,** *46,* 5280–5282. (b) Bai, W.-J.; Green, J. C.; Pettus, T. R. R. *J. Org. Chem.* **2012,** *77,* 379–387.

(24) (a) Gonzalez, A. Z.; Román, J. G.; Gonzalez, E.; Martinez, J.; Medina, J. R.; Matos, K.; Soderquist, J. A. *J. Am. Chem. Soc.* **2008,** *130,* 9218–9219. (b) Thomas, S. P.; Aggarwal, V. K. *Angew. Chem. Int. Ed.* **2009,** *48,* 1896–1898. (c) Zhang, L.; Zuo, Z., Wan, X.; Huang, Z. *J. Am. Chem. Soc.* **2014,** *136,* 15501–15504. (d) Mazet, C.; Gérard, D. *Chem. Commun.* **2011,** *47,* 298–300. (e) Corberán, R.; Mszar, N. W.; Hoveyda, A. H. *Angew. Chem. Int. Ed.* **2011,** *50,* 7079–7082.

(25) Alexakis, A.; Krause, N.; Woodward, S. Copper-Catalyzed Asymmetric Synthesis, *VCH–Wiley* **2014,** 33–68.

was used. However, **1.71** was generated in 97:3 er when higher catalyst loading was used

Scheme 1.23. Improve Selectivity in Cu–H Systems[a]

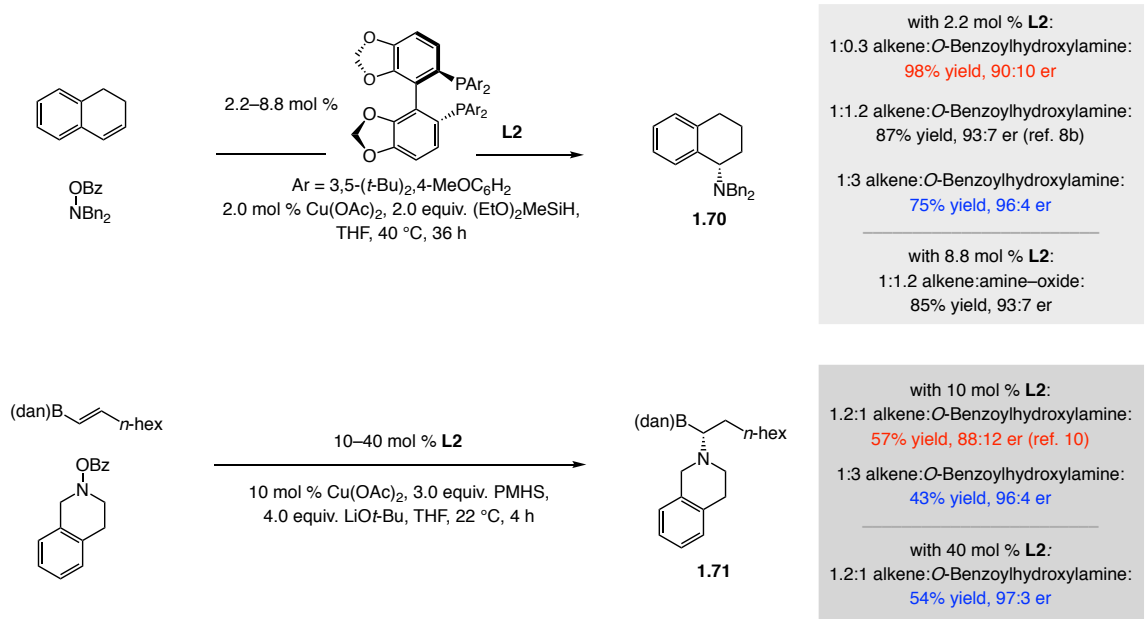

a Reactions were perfomed under N_2 atmosphere. Yield of isolated and purified product; the variance of values is estimated to be <±5%. Enantiomeric ratios were determined by HPLC analysis; the variance of values is estimated to be <±1%. See the Experimentals sections for all details. Bz, benzoyl; Bn, benzyl; dan, 1,8-diaminonaphthalene; PMHS, polymethylhydrosiloxane.

(compared to 88:12 er with fourfold lower ligand loading). Only in the latter instance is competitive addition by an achiral Cu–H complex an issue and a shift in equilibrium away from the achiral Cu–H complex becomes consequential.

1.4 Conclusions

The detailed mechanistic studies and investigations from our laboratory shed light on several factors that directly impact the efficiency and enantioselectivity of a rapidly developing class of transformations using copper–boron and copper–hydride complexes. Our study shows that enantioselectivity can increase with higher electrophile concentration due to the minimization of diastereoselective Cu–H elimination in the major chiral Cu–alkyl intermediate (Scheme 1.8). In addition, prevention of achiral Cu–B(pin) or Cu–H complex generation through ligand loss can inhibit racemate formation but maintain initial selectivity (**1.56** → **1.48** vs **1.56** → **1.58**, Scheme 1.14). Other

important consequences from this study are that lower alkene concentration can lead to enhanced enantioselectivity when electron-deficient alkenes are involved (Scheme 1.17), and Cu–H elimination can elevate enantioselectivity by rerouting racemic pathways towards the formation of other by-products (Scheme 1.20). Very interestingly, this corrective pathway was achieved when a less reactive electrophile was employed. This goes against the general idea that faster Cu–alkyl trapping can increase selectivity. As highlighted by the representative applications in Cu–H-catalyzed processes (Scheme 1.23), the newly acquired understanding and its strategic implications are likely to be instrumental in the success of future endeavors in this area.

1.5 Experimentals

1.5.1 General

Infrared (IR) spectra were recorded on a Bruker FT-IR Alpha (ATR mode) spectrophotometer, ν_{max} in cm^{-1}. Bands are characterized as broad (br), strong (s), medium (m), and weak (w). ^{1}H NMR spectra were recorded on Varian Unity INOVA 400 (400 MHz), 500 (500 MHz), or 600 (600 MHz) spectrometers. Chemical shifts are reported in ppm from tetramethylsilane with the solvent resonance as the internal standard ($CDCl_3$: δ 7.26 ppm). Data are reported as follows: chemical shift, integration, multiplicity (s = singlet, d = doublet, t = triplet, q = quartet, pent = pentet, m = multiplet, br = broad, app = apparent), and coupling constants (Hz). ^{13}C NMR spectra were recorded on Varian Unity INOVA 400 (100 MHz), 500 (125 MHz), or 600 (150 MHz) spectrometers with complete proton decoupling. Chemical shifts are reported in ppm from tetramethylsilane with the solvent resonance as the internal standard ($CDCl_3$: δ 77.16 ppm). High-resolution mass spectrometry was performed on a JEOL AccuTOF DART (positive mode) at the Mass Spectrometry Facility, Boston College. Enantiomeric ratios were determined by HPLC analysis (high-performance liquid chromatography) with a Shimadzu chromatograph [Chiral Technologies Chiralcel AZ-H (4.6 x 250 mm), Chiral Technologies Chiralcel OC-H (4.6 x 250 mm), Chiral Technologies Chiralcel OD-H (4.6 x 250 mm), Chiral Technologies Chiralcel OJ-H (4.6 x 250 mm), Chiral Technologies Chiralcel OZ-H (4.6 x 250 mm), or Chiral Technologies Chiralpak AD-H (4.6 x 250 mm)] in comparison with authentic racemic materials. Specific rotations were measured on a Rudolph Research Analytical Autopol IV Polarimeter. Melting points were measured on a Thomas Hoover capillary melting point apparatus and are

uncorrected. X-ray structures were obtained, as described in the cif file, with a Microfocus sealed Cu tube from Incote. It is well established that that aforementioned detector allows for the determination of absolute configuration of molecules that do not have a heavy atom.

Unless otherwise noted, reactions were carried out with distilled and degassed solvents under an atmosphere of dry N_2 in oven- (135 ºC) or flame-dried glassware with standard dry box or vacuum-line techniques. Hexanes was purified under a positive pressure of dry argon by a modified Innovative Technologies purification system through a copper oxide and alumina column. Tetrahydrofuran (thf; Aldrich Chemical Co.) was purified by distillation from sodium benzophenone ketyl immediately prior to use. All work-up and purification procedures were carried out with reagent grade solvents (purchased from Fisher Scientific) under air.

1.5.2 Reagents

Allyl phenyl carbonate (1.35): purchased from Aldrich and used as received.

Allyl *tert*-butyl carbonate: prepared according to a previously reported procedure.[26]

Bis(pinacolato)diboron [$B_2(pin)_2$]: purchased from Frontier Scientific, Inc., recrystallized from pentane and dried under vacuum prior to use.

***n*-Butyllithium (1.6 M in hexanes):** purchased from Aldrich and used as received.

Chlorotrimethylsilane: purchased from Acros and used as received.

Copper(I) chloride: purchased from Strem and used as received.

Deuterium oxide (D_2O): purchased from Cambridge Isotope Laboratories and used as received.

---

(26) Zhang, P.; Brozek, L. A.; Morken, J. P. *J. Am. Chem. Soc.* **2010,** *132,* 10686–10688.

Diethyl allyl phosphate (1.11): purchased from Aldrich and used as received.

Diisobutylaluminum hydride (dibal-H): purchased neat from Aldrich and used as received.

Di-*tert*-butyl-dicarbonate (Boc_2O): purchased from Advanced ChemTech and used as received.

Hoveyda-Grubbs catalyst 2nd generation: purchased from Aldrich and used as received.

Hydrogen peroxide (30 wt % in H_2O): purchased from Aldrich and used as received.

Imidazolinium salt NHC-1, 2, 3, 4, and 5: prepared according to a previously reported procedure.[27]

Imidazolinium salt NHC-6: prepared according to a previously reported procedure.[28]

Imidazolinium salt NHC-7: prepared according to a previously reported procedure.[29]

2-Isopropoxy-4,4,5,5-tetramethyl-1,3,2-dioxaborolane [*i*-PrOB(pin)]: purchased from Aldrich and used as received.

Oxone®, monopersulfate compound: purchased from Aldrich and used as received.

Phosphine L1: prepared according to a previously reported procedure.[30]

Phosphine ligands (L2, 3a–c, 4, 5, and 6): purchased from Strem and used as received.

Pyridinium dichromate (PDC): purchased from Aldrich and used as received.

---

(27) Lee, K-s.; Hoveyda, A. H. *J. Org. Chem.* **2009,** *74,* 4455–4462.
(28) (a) Brown, M. K.; May, T. L.; Baxter, C. A.; Hoveyda, A. H. *Angew. Chem. Int. Ed.* **2007,** *46,* 1097–1100. (b) May, T. L.; Brown, M. K.; Hoveyda, A. H. *Angew. Chem. Int. Ed.* **2008,** *47,* 7468–7472.
(29) Clavier, H.; Coutable, L.; Toupet, L.; Guillemin, J.-C.; Mauduit, M. *J. Organomet. Chem.* **2005,** *690,* 5237–5254.
(30) Jia, T.; Cao, P.; Wang, B.; Lou, Y.; Yin, X.; Wang, M.; Liao, J. *J. Am. Chem. Soc.* **2015,** *137,* 13760–13763.

Sodium *tert*-butoxide: purchased from Strem and used as received.

Sodium hydroxide (2 M): prepared from NaOH purchased from Fisher (used as received) and deionized water.

Sulfuric acid: purchased from Fisher and used as received.

Tetrabutylammonium fluoride (tbaf, 1.0 M in thf): purchased from Oakwood and used as received.

Preparation of aryl or heteroaryl olefins: unless otherwise noted, olefins were purchased from Acros, Aldrich, Alfa Aesar, Combi-Blocks, Matrix Scientific, or TCI, and distilled over CaH_2 under reduced pressure prior to use.

The following olefins were synthesized from the corresponding aldehydes by Wittig olefination.[31]

1,4-Dimethoxy-2-methyl-5-vinylbenzene (1.67): Melting point: 41–42°C. IR (neat): 2995 (w), 2935 (w), 2830 (w), 1623 (w), 1501 (s), 1464 (m), 1416 (m), 1399 (m), 1207 (s), 1182 (m), 1042 (s), 996 (m), 902 (m) cm^{-1}; ^1H NMR (400 MHz, $CDCl_3$): δ 7.02 (1H, dd, *J* = 18.0, 11.2 Hz), 6.95 (1H, s), 6.70 (1H, s), 5.68 (1H, dd, *J* = 17.8, 1.4 Hz), 5.22 (1H, dd, *J* = 11.2, 1.2 Hz), 3.82 (3H, s), 3.80 (3H, s), 2.23 (3H, s); ^{13}C NMR (100 MHz, $CDCl_3$): δ 152.0, 150.8, 131.7, 127.5, 124.5, 114.7, 113.3, 108.2, 56.4, 55.9, 16.4; HRMS (DART): Calcd for $C_{11}H_{15}O_2$ $[M+H]^+$: 179.1072, Found: 179.1069.

1-(Allyloxy)-3-vinylbenzene (substrate for 1.19 and 1.34): The spectroscopic data match those reported previously.[32] ^1H NMR (400 MHz, $CDCl_3$): δ 7.24 (1H, t, *J* = 8.0

---

(31) Cho, S. J.; Jensen, N. H.; Kurome, T.; Kadari, S.; Manzano, M. L.; Malberg, J. E.; Caldarone, B.; Roth, B. L.; Kozikowski, A. P. *J. Med. Chem.* **2009,** *52,* 1885–1902.

(32) Paul, C. E.; Rajagopalan, A.; Lavandera, I.; Gotor-Fernández, V.; Kroutil, W.; Gotor V. *Chem. Commun*. **2012,** *48,* 3303–3305.

Hz), 7.03–6.96 (2H, m), 6.83 (1H, ddd, *J* = 8.2, 2.6, 0.9 Hz), 6.68 (1H, dd, *J* = 17.6, 10.8 Hz), 6.07 (1H, ddt, *J* = 17.3, 10.6, 5.3 Hz), 5.73 (1H, dd, *J* = 17.6, 0.9 Hz), 5.43 (1H, dq, *J* = 17.3, 1.6 Hz), 5.29 (1H, dq, *J* = 10.5, 1.4 Hz), 5.25 (1H, dd, *J* = 10.9, 0.9 Hz), 4.56 (2H, dt, *J* = 5.3, 1.5 Hz).

2-Vinylbenzofuran (substrate for 1.22): The spectroscopic data match those reported previously.[33] ^{1}H NMR (400 MHz, $CDCl_3$): δ 7.52 (1H, ddd, *J* = 7.6, 1.4, 0.7 Hz), 7.45 (1H, dq, *J* =8.2, 0.9 Hz), 7.30–7.24 (2H, m), 6.64 (1H, dd, *J* = 17.5, 11.2 Hz), 6.60 (1H, s), 5.96 (1H, ddd, *J* = 17.4, 1.3, 0.6 Hz), 5.41 (1H, dd, *J* = 11.2, 1.2 Hz).

***tert*-Butyl 5-vinyl-1*H*-indole-1-carboxylate (substrate for 1.23):** The spectroscopic data match those reported previously.[34] ^{1}H NMR (400 MHz, $CDCl_3$): δ 8.08 (1H, d, *J*= 8.0 Hz), 7.58–7.57 (2H, m), 7.41 (1H, dd, *J* = 8.4, 1.2 Hz), 6.81 (1H, dd, *J* = 17.6, 10.8 Hz), 6.55–6.54 (1H, m), 5.75 (1H, dd, *J* = 17.2, 1.2 Hz), 5.21 (1H, dd, *J* = 10.4, 0.8 Hz), 1.68 (9H, s).

The following olefins were synthesized from the corresponding aryl bromides by a two-step lithium halogen exchange/addition to TMSCl or *i*-PrOB(pin). To a flame-dried round bottom flask equipped with a stir bar was added 4-bromostyrene (0.71 mL, 5.5 mmol) and thf (30 mL) under N_2. The resulting solution was allowed to cool to –78 ºC (dry ice/acetone) and *n*-butyllithium (1.6 M in hexanes, 3.8 mL, 6.0 mmol) was added dropwise into the solution through syringe. The resulting light yellow solution was allowed to stir for 1 h at –78 ºC and then TMSCl (0.84 mL, 6.6 mmol) was added dropwise by syringe. The mixture was allowed to slowly warm up to 22 ºC. After 16 h,

---

(33) (a) Brewer, J. D.; Elix, J. A. *Aust. J. Chem.* **1975,** *28,* 1059–1081. (b) Aitken, R. A.; Burns, G. *J. Chem. Soc., Perkin Trans.* **1994,** *1*, 2455–2460.
(34) Molander, G. A.; Brown, A. R. *J. Org. Chem.* **2006,** ***71,*** 9681–9686.

the reaction was quenched by the addition of H_2O (10 mL) and a saturated solution of aqueous NH_4Cl (10 mL). The layers were separated and the aqueous layer was washed with Et_2O (3 x 20 mL). The combined organic layers were dried over $MgSO_4$ and concentrated under reduced pressure. The resulting yellow oil was purified by silica gel chromatography (100% hexanes) to afford **trimethyl(4-vinylphenyl)silane (substrate for 1.16)** as colorless oil (876 mg, 5.0 mmol, 91%): IR (neat): 3063 (w), 3008 (w), 2956 (m), 1629 (w), 1389 (m), 1248 (m), 1105 (m), 989 (m), 906 (m), 826 (s), 761 (m), 730 (m), 692 (m), 642 (m) cm^{-1}; ^1H NMR ($CDCl_3$, 400 MHz): δ 7.51 (2H, d, *J* = 7.6 Hz), 7.43 (2H, d, *J* = 8.0 Hz), 6.74 (1H, dd, *J* = 17.6, 10.9, Hz), 5.80 (1H, d, *J* = 17.6 Hz), 5.27 (1H, d, *J* = 10.9 Hz), 0.29 (9H, s); ^{13}C NMR ($CDCl_3$, 100 MHz): δ 140.3, 138.1, 137.0, 133.7, 125.7, 114.2, –1.0; HRMS (DART): Calcd for $C_{11}H_{17}Si$ $[M+H]^+$: 177.1100, Found: 177.1101.

4,4,5,5-Tetramethyl-2-(4-vinylphenyl)-1,3,2-dioxaborolane (substrate for 1.28): Following the above procedure except *i*-PrOB(pin) was used instead of TMSCl, the product was obtained as colorless oil [purified by silica gel chromatography (hexanes:Et_2O = 25:1)] (1.0 g, 4.5 mmol, 82%). IR (neat): 2978 (m), 2930 (w), 1629 (m), 1552 (w), 1397 (m), 1356 (s), 1322 (s), 1269 (m), 1213 (w), 1142 (s), 1088 (s), 1018 (m), 990 (m), 962 (m), 830 (m), 758 (w), 682 (m) cm^{-1}; ^1H NMR ($CDCl_3$, 400 MHz): δ 7.82 (2H, d, *J* = 8.0 Hz), 7.44 (2H, d, *J* = 8.0 Hz), 6.76 (1H, dd, *J* = 17.6, 10.8 Hz), 5.84 (1H, dd, *J* = 17.6, 1.2 Hz), 5.32 (1H, dd, *J* = 10.8, 0.8 Hz), 1.38 (12H, s); ^{13}C NMR ($CDCl_3$, 100 MHz): δ 140.3, 137.0, 135.1, 125.6, 114.9, 83.8, 25.0, 24.9; HRMS (DART): Calcd for $C_{14}H_{20}BO_2$ $[M+H]^+$: 231.1556; Found: 231.1563.

4,4,5,5-Tetramethyl-2-(3-vinylphenyl)-1,3,2-dioxaborolane (substrate for 1.29): Following the above except 3-bromostyrene and *i*-PrOB(pin) were used instead of 4-bromostyrene and TMSCl, respectively, the product was obtained as colorless oil [purified by silica gel chromatography (hexanes:Et_2O = 25:1)] (1.1 g, 4.7 mmol, 85%). IR (neat): 2978 (w), 2929 (m), 1380 (m), 1353 (s), 1319 (s), 1141 (s), 1079 (s), 990 (m), 963 (m), 908 (m), 831 (m), 710 (w), 699 (s), 681 (m) cm^{-1}; ^1H NMR ($CDCl_3$, 400 MHz): δ 7.87 (1H, s), 7.73 (1H, d, *J* = 7.3 Hz), 7.53 (1H, dt, *J* = 7.8, 1.6 Hz), 7.35 (1H, t, *J* = 7.5 Hz), 6.75 (1H, dd, 17.6, 10.9 Hz), 5.81 (1H, dd, *J* = 17.6, 0.9 Hz), 5.26 (1H, dd, *J* = 10.9, 0.9 Hz), 1.37 (12H, s); ^{13}C NMR ($CDCl_3$, 100 MHz): δ 137.0, 136.9, 134.3, 132.9, 129.0, 128.0, 114.0, 83.9, 25.0, 24.9; HRMS (DART): Calcd for $C_{14}H_{20}BO_2$ $[M+H]^+$: 231.1556, Found: 231.1567.

***tert*-Butyl 3-vinylbenzoate (substrate for 1.24)**: Prepared according to the reported procedure.[35] IR (neat): 2978 (w), 2932 (w), 1711 (s), 1367 (m), 1294 (s), 1271 (m), 1256 (m), 1158 (s), 1113 (m), 1086 (m), 909 (m), 763 (s) cm^{-1}; ^1H NMR (400 MHz, $CDCl_3$): δ 8.03 (1H, dd, *J* = 2.2, 1.0 Hz), 7.88 (1H, dt, *J* = 7.6, 1.2 Hz), 7.57–7.55 (1H, m), 7.37 (1H, t, *J* = 7.8 Hz), 6.75 (1H, dd, *J* = 17.6, 10.8 Hz), 5.82 (1H, dd, *J* = 17.6, 0.4 Hz), 5.31 (1H, dd, *J* = 11.0, 0.6 Hz), 1.61 (9H, s); ^{13}C NMR (100 MHz, $CDCl_3$): δ 165.8, 137.8, 136.2, 132.4, 130.1, 128.8, 128.5, 127.3, 115.0, 81.2, 28.3, ; HRMS (DART): Calcd for $C_{13}H_{17}O_2$ $[M+H]^+$: 205.1229, Found: 205.1235.

---

(35) Miller, W. H.; Seefeld, M. A.; Newlander, K. A.; Uzinskas, I. N.; Burgess, W. J.; Heerding, D. A.; Yuan, C. C. K.; Head, M. S.; Payne, D. J.; Rittenhouse, S. F.; Moore, T. D.; Pearson, S. C.; Berry, V.; DeWolf, Jr., W. E.; Keller, P. M.; Polizzi, B. J.; Qiu, X.; Janson, C. A.; Huffman, W. F. *J. Med. Chem.* **2000,** *45,* 3246–3256.

***tert*-Butyl 4-vinylbenzoate (substrate for 1.26)**: Prepared according to the reported procedure.[10] The spectroscopic data match those reported previously.[36] ^{1}H NMR (400 MHz, $CDCl_3$): δ 7.94 (2H, d, *J*= 8.0 Hz), 7.44 (2H, d, *J* = 8.0 Hz), 6.75 (1H, dd, *J* = 17.6, 10.8 Hz), 5.84 (1H, dd, *J* = 17.6, 1.2 Hz), 5.36 (1H, dd, *J* = 11.0, 0.2 Hz), 1.60 (9H, s).

Preparation of allylic phosphates (substrates for 1.31, 1.33–1.34): Allylic alcohols were synthesized from the corresponding alkenyl bromides (purchased from Aldrich and used as received) by a two-step lithium halogen exchange/addition to formaldehyde sequence.[37] Subsequently, allylic alcohols were converted to the corresponding allylic phosphates based on an established method.[38]

Diethyl (2-phenylallyl) phosphate (substrates for 1.31): IR (neat): 2983 (w), 2908 (w), 1444 (w), 1262 (m), 1165 (w), 1016 (s), 975 (s), 778 (m), 707 (m) cm^{-1}; ^{1}H NMR (400 MHz, $CDCl_3$): δ 7.43–7.46 (2H, m), 7.28–7.37 (3H, m), 5.57 (1H, s), 5.44 (1H, s), 4.93 (2H, d, *J* = 7.2 Hz), 4.11–4.03 (4H, m), 1.31–1.28 (6H, m); ^{13}C NMR (100 MHz, $CDCl_3$): δ 142.9 (d, *J* = 7.5 Hz), 137.7, 128.6, 128.2, 126.2, 115.4, 68.7 (d, *J* = 5.3 Hz), 63.9 (d, *J* = 5.3 Hz), 16.2 (d, *J* = 6.8 Hz); HRMS (DART): Calcd for $C_{13}H_{20}O_4P_1$ $[M+H]^+$: 271.1099, Found: 271.1087.

Diethyl (2-(trimethylsilyl)allyl) phosphate (substrate for 1.33–1.34): IR (neat): 2982 (w), 2957 (w), 2908 (m), 1394 (w), 1250 (m), 1167 (w), 1024 (s), 976 (m), 840 (s) cm^{-1}; ^{1}H NMR (400 MHz, $CDCl_3$): δ 5.85 (1H, s), 5.45 (1H, s), 4.65 (2H, d, *J* = 6.0 Hz), 4.15–4.08 (4H, m), 1.33 (6H, t, *J* = 7.0 Hz), 0.13 (9H, s); ^{13}C NMR (100 MHz, $CDCl_3$): δ

---

(36) Mäsing, F.; Mardyukov, A.; Doerenkamp, C.; Eckert, H.; Malkus, U.; Nüsse, H.; Klingauf, J.; Studer, A. *Angew. Chem. Int. Ed.* **2015,** *54,* 12612–12617.
(37) Amat, M.; Arioli, F.; Pérez, M.; Molins, E.; Bosch, J. *Org. Lett.* **2013,** *15,* 2470–2473.
(38) Kacprzynski, M. A.; May, T. L.; Kazane, S. A.; Hoveyda, A. H. *Angew. Chem. Int. Ed.* **2007,** *46,* 4554–4558.

146.8 (d, *J* = 7.6 Hz), 125.1, 70.7 (d, *J* = 6.0 Hz), 63.9 (d, *J* = 6.1 Hz), 16.3 (d, *J* = 6.9 Hz), –1.5; HRMS (DART): Calcd for $C_{10}H_{24}O_4P_1Si_1$ $[M+H]^+$: 267.1182, Found: 267.1177.

Preparation of an allylic phosphate for 1.32: 2-Methyl-2-propen-1-ol (purchased from Aldrich and used as received) was converted to the corresponding allylic phosphate based on a previously disclosed method.[38]

Diethyl (2-methylallyl) phosphate (substrate for 1.32): IR (neat): 2983 (w), 2911 (w), 1447 (w), 1264 (m), 1166 (w), 1008 (s), 973 (s) cm^{-1}; ^1H NMR (400 MHz, $CDCl_3$): δ 4.94 (1H, s), 4.83 (1H, s), 4.32 (2H, d, *J* = 7.2 Hz), 4.05–3.98 (4H, m), 1.67 (3H, s), 1.26–1.21 (6H, m); ^{13}C NMR (100 MHz, $CDCl_3$): δ 140.0 (d, *J* = 6.8 Hz), 113.0, 70.5 (d, *J* = 6.1 Hz), 63.7 (d, *J* = 6.1 Hz), 18.9, 16.0 (d, *J* = 6.8 Hz); HRMS (DART): Calcd for $C_8H_{18}O_4P_1$ $[M+H]^+$: 209.0943, Found: 209.0944.

Preparation of allyl-1,1-*d*$_2$-diethyl phosphate (1.11-*d*$_2$): Allylic alcohol was synthesized from the reported procedure.[39] Subsequently, allylic alcohol was converted to the corresponding allylic phosphates based on an established method.[13] IR (neat): 2984 (w), 2934 (w), 1265 (m), 1017(s), 976 (s), 801 (m) cm^{-1}; ^1H NMR (400 MHz, $CDCl_3$): δ 5.91 (1H, dd, *J* = 17.2, 10.4 Hz), 5.33 (1H, dt, *J* = 17.2, 1.5 Hz), 5.21 (1H, dt, *J* = 10.0, 1.4 Hz), 4.12–4.04 (4H, m), 1.32–1.28 (6H, m); ^{13}C NMR (100 MHz, CDCl3): δ 135.6 (d, *J* = 6.8 Hz), 118.3, 63.8 (d, *J* = 6.1 Hz), 16.2 (d, *J* = 6.8 Hz); HRMS (DART): Calcd for $C_7H_{14}D_2O_4P_1$ [M+H]+: 197.0912, Found: 197.0920.

1.5.3 Representative Procedure for the Catalytic Enantioselective Boron-Allyl Addition to Aryl Alkenes

---

(39) Schuetz, R. D.; Millard, F. W. *J. Org. Chem.* **1959,** *24,* 297–300.

In an N_2-filled glove box, an oven-dried 1 dram vial equipped with a stir bar was charged with bisphosphine **L3a** (3.4 mg, 0.0055 mmol), NaO*t*-Bu (14 mg, 0.15 mmol), and CuCl (0.50 mg, 0.0050 mmol), and thf (1.0 mL). The mixture was allowed to stir for 1 h under N_2 at 22 °C; during this time the solution turned light yellow. Bis(pinacolato)diboron (28 mg, 0.11 mmol) was added to the mixture, causing the solution to turn dark brown immediately. Styrene (31 mg, 0.30 mmol), allylphosphate (**1.11**) (19 mg, 0.10 mmol), and thf (0.50 mL) were added. The vial was sealed with a cap and electrical tape before removal from the glove box. The resulting mixture was allowed to stir at 22 °C for 14 h. The mixture was then passed through a short plug of silica gel (4 x 1 cm) and eluted with Et_2O. The organic layer was concentrated under reduced pressure, affording yellow oil, which was purified by silica gel chromatography (100% hexanes→hexanes:Et_2O = 10:1) to afford **1.12** as colorless oil (18 mg, 0.067 mmol, 67% yield).

(*R*)-4,4,5,5-Tetramethyl-2-(2-phenylpent-4-en-1-yl)-1,3,2-dioxaborolane (1.12): 44% yield was obtained with 3:1 alkene:carbonate (**1.35**). IR (neat): 3027 (w), 2977 (m), 2925 (w), 1452 (m), 1367 (s), 1319 (s), 1270 (w), 12134(w), 1164 (m), 1143 (s), 968 (m), 911 (m), 847 (m), 756 (m), 699 (s) cm^{-1}; ^1H NMR ($CDCl_3$, 400 MHz): δ 7.25–7.09 (5H, m), 5.68 (1H, ddt, *J* =17.2, 10.0, 7.2 Hz), 4.96–4.88 (2H, m), 2.96–2.88 (1H, m), 2.40–2.27 (2H, m), 1.23 (1H, dd, *J* =15.4, 6.6 Hz), 1.14–1.08 (1H, m), 1.10 (6H, s), 1.09 (6H, s); ^{13}C NMR ($CDCl_3$, 100 MHz): δ 146.9, 137.3, 128.2, 127.6, 126.0, 116.1, 83.1, 43.9, 41.5, 24.83, 24.78; HRMS (DART): Calcd for $C_{17}H_{26}B_1O_2$ $[M+H]^+$: 273.2026, Found: 273.2015. Specific rotation: $[\alpha]_D^{20}$ +6.7 (*c* 0.30, $CHCl_3$) for an enantiomerically enriched sample of 95:5 er Enantiomeric purity was determined by HPLC analysis in comparison

with authentic racemic material (95:5 er shown; Chiralcel OD–H column, 100% hexanes, 0.3 mL/min, 220 nm).

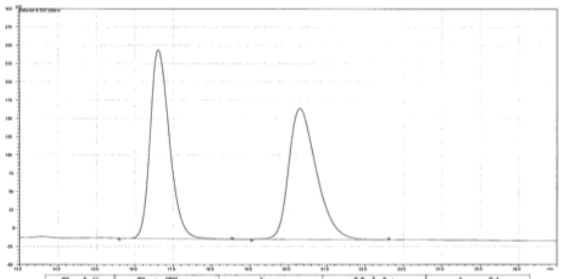

Peak#	Ret. Time	Area	Height	Area %
1	16.604	8995664	258220	50.067
2	20.296	8971612	179187	49.933
Total		17967275	437407	100.000

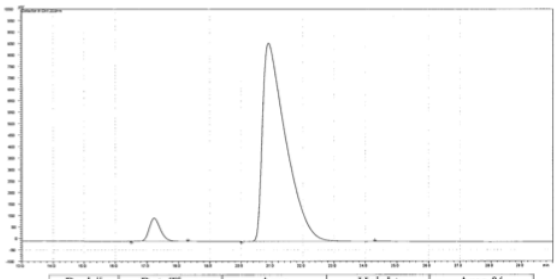

Peak#	Ret. Time	Area	Height	Area %
1	17.223	2468299	100781	5.239
2	20.890	44643911	865166	94.761
Total		47112211	965948	100.000

Peak #	Time (min)	Area (%)	Peak #	Time (min)	Area (%)
1	16.604	50.067	1	17.223	5.239
2	20.296	49.933	2	20.890	94.761

(*R*)-4,4,5,5-Tetramethyl-2-(2-(*o*-tolyl)pent-4-en-1-yl)-1,3,2-dioxaborolane (1.13): IR (neat): 2977 (w), 2928 (w), 1365 (s), 1317 (s), 1144 (s), 968 (m), 911 (m), 846 (m), 758 (m), 726 (m) cm^{-1}; ^{1}H NMR ($CDCl_3$, 400 MHz): δ 7.20 (1H, d, *J* = 8.0 Hz), 7.14 (1H, t, *J* = 7.2 Hz), 7.09–7.01 (2H, m), 5.74–5.63 (1H, m), 4.99–4.91 (2H, m), 3.23 (1H, app pent, *J* = 7.3 Hz), 2.38–2.24 (2H, m), 2.36 (3H, s), 1.23 (1H, dd, *J* = 14.6, 7.8 Hz), 1.12 (1H, dd, *J* = 16.0, 8.0 Hz), 1.05 (s, 6H), 1.03 (6H, s); ^{13}C NMR ($CDCl_3$, 100 MHz): δ 145.1, 137.3, 135.7, 130.0, 126.1, 125.6, 116.1, 83.0, 43.6, 36.0, 24.7, 20.0; HRMS (DART): Calcd for $C_{18}H_{28}B_1O_2$ $[M+H]^+$: 287.2182, Found: 287.2177; Specific Rotation: $[\alpha]_D^{20}$ +8.8 (*c* 1.32, $CHCl_3$) for an enantiomerically enriched sample of 95:5 er Enantiomeric purity was determined by HPLC analysis in comparison with authentic racemic material (95:5 er shown; Chiralcel OD–H column, 100% hexanes, 0.3 mL/min, 220 nm).

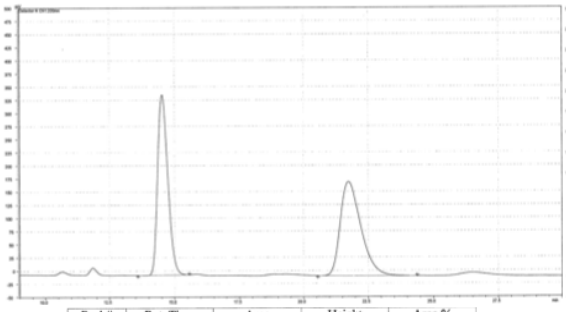

Peak#	Ret. Time	Area	Height	Area %
1	14.521	9382886	342961	48.770
2	21.736	9856116	178644	51.230
Total		19239002	521605	100.000

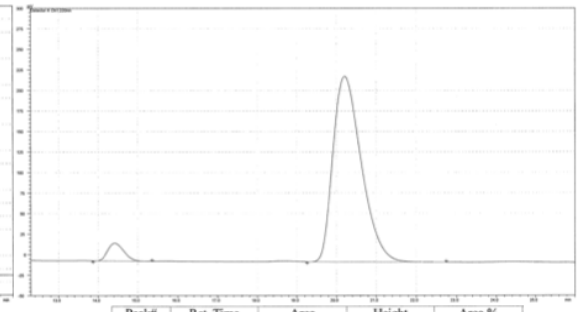

Peak#	Ret. Time	Area	Height	Area %
1	14.419	614971	21643	5.191
2	20.205	11232070	226080	94.809
Total		11847041	247723	100.000

Peak #	Time (min)	Area (%)	Peak #	Time (min)	Area (%)
1	14.521	48.770	1	14.419	5.191
2	21.736	51.230	2	20.205	94.809

(*R*)-4,4,5,5-Tetramethyl-2-(2-(*m*-tolyl)pent-4-en-1-yl)-1,3,2-dioxaborolane (1.14): IR (neat): 2977 (w), 2922 (w), 1366 (s), 1319 (s), 1144 (s), 968 (m), 847 (m), 704 (m) cm^{-1}; ^{1}H NMR ($CDCl_3$, 400 MHz): δ 7.15 (1H, dd, *J* = 9.0, 6.2 Hz), 7.00 (1H, s), 6.97–6.93 (2H, m), 5.72–5.62 (1H, m), 4.98–4.89 (2H, m), 2.89 (1H, app pent, *J* = 7.6 Hz), 2.40–2.26 (5H, m), 1.25–1.18 (1H, m), 1.11–1.03 (13H, m); ^{13}C NMR ($CDCl_3$, 100 MHz): δ 146.9, 137.5, 137.46, 128.4, 128.1, 126.7, 124.5, 116.0, 83.1, 43.7, 41.4, 24.82, 24.79, 21.6; HRMS (DART): Calcd for $C_{18}H_{28}B_1O_2$ $[M+H]^+$: 287.2182, Found: 287.2188; Specific Rotation: $[\alpha]_D^{20}$ +16.9 (*c* 0.98, $CHCl_3$) for an enantiomerically enriched sample of 97:3 er Enantiomeric purity was determined by HPLC analysis in comparison with authentic racemic material (97:3 er shown; Chiralcel OD–H column, 100% hexanes, 0.3 mL/min, 220 nm).

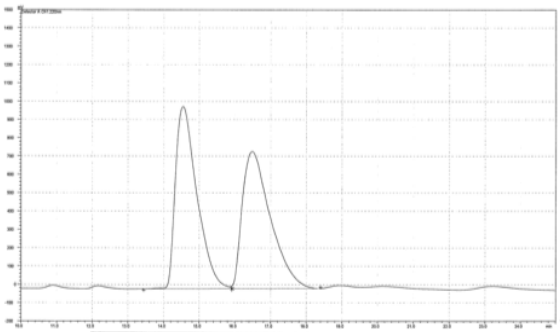

Peak#	Ret. Time	Area	Height	Area %
1	14.537	41844216	994508	50.572
2	16.483	40897888	747456	49.428
Total		82742104	1741964	100.000

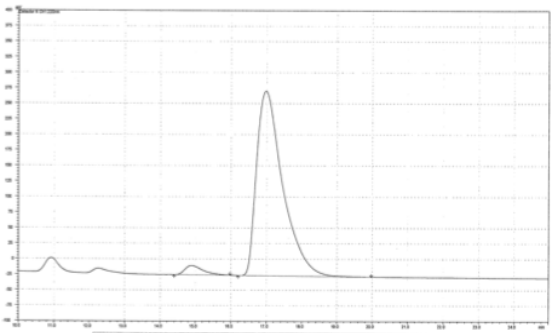

Peak#	Ret. Time	Area	Height	Area %
1	14.887	520079	14680	3.297
2	16.975	15256111	297016	96.703
Total		15776189	311696	100.000

Peak #	Time (min)	Area (%)	Peak #	Time (min)	Area (%)
1	14.537	50.572	1	14.887	3.297
2	16.483	49.428	2	16.975	96.703

(*R*)-4,4,5,5-Tetramethyl-2-(2-(*p*-tolyl)pent-4-en-1-yl)-1,3,2-dioxaborolane (1.15): IR (neat): 2977 (m), 2924 (m), 1514 (w), 1368 (s), 1322 (s), 1145 (s), 968 (m), 911 (m), 846 (m), 813 (m) cm^{-1}; ^{1}H NMR ($CDCl_3$, 600 MHz): δ 7.09 (2H, d, *J* = 5.2 Hz), 7.06 (2H, d, *J* = 5.6 Hz), 5.71–5.64 (1H, m), 4.97–4.90 (2H, m), 2.91 (1H, app pent, *J* = 5.0 Hz), 2.39–2.30 (5H, m), 1.21 (1H, dd, *J* = 9.8, 4.2 Hz), 1.12–1.06 (13H, m); ^{13}C NMR ($CDCl_3$, 150 MHz): δ 143.9, 137.5, 135.3, 128.9, 127.4, 116.0, 83.1, 43.8, 41.0, 24.84, 24.81, 21.1; HRMS (DART): Calcd for $C_{18}H_{28}B_1O_2$ $[M+H]^+$: 287.2182, Found: 287.2184; Specific Rotation: $[\alpha]_D^{20}$ +8.6 (*c* 1.00, $CHCl_3$) for an enantiomerically enriched sample of 95:5 er Enantiomeric purity was determined by HPLC analysis in comparison with authentic racemic material (95:5 er shown; Chiralcel OD–H column, 100% hexanes, 0.3 mL/min, 220 nm).

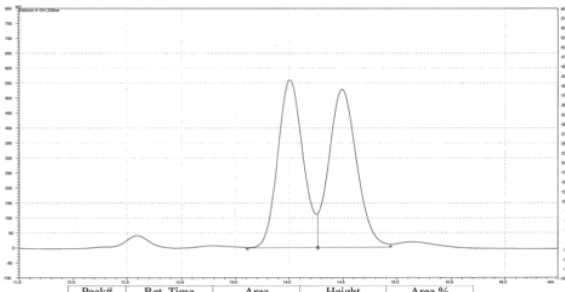

Peak#	Ret. Time	Area	Height	Area %
1	14.002	9188277	560090	49.406
2	14.488	9409294	528116	50.594
Total		18597571	1088206	100.000

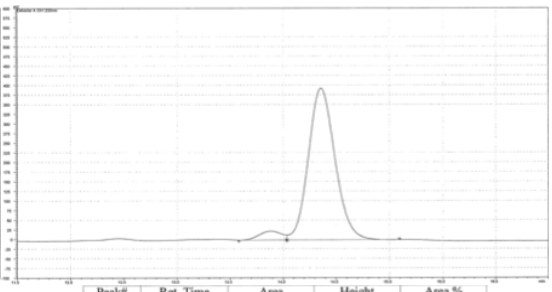

Peak#	Ret. Time	Area	Height	Area %
1	13.876	340454	23048	4.731
2	14.354	6855113	393961	95.269
Total		7195567	417009	100.000

Peak #	Time (min)	Area (%)	Peak #	Time (min)	Area (%)
1	14.002	49.406	1	13.876	4.731
2	14.488	50.594	2	14.354	95.269

(*R*)-Trimethyl(4-(1-(4,4,5,5-tetramethyl-1,3,2-dioxaborolan-2-yl)pent-4-en-2-yl)phenyl)silane (1.16): IR (neat): 3068 (w), 2977 (m), 2955 (m), 2926 (w), 1640 (w), 1599 (w), 1365 (s), 1322 (s), 1164 (m), 1144 (s), 1110 (m), 997 (m), 968 (m), 911 (m), 837 (s), 757 (m), 725 (m) cm^{-1}; ^{1}H NMR ($CDCl_3$, 400 MHz): δ 7.41 (2H, d, *J* = 8.1 Hz), 7.23–7.17 (2H, m), 5.70 (1H, dddd, *J* = 16.8, 10.1, 7.6, 6.5 Hz), 4.98 (1H, ddt, *J* = 17.2, 2.5, 1.4 Hz), 4.93 (1H, ddt, *J* = 10.1, 2.1, 1.0 Hz), 2.99–2.88 (1H, m), 2.46–2.26 (2H, m), 1.29–1.20 (2H, m), 1.09 (6H, s), 1.08 (6H, s), 0.23 (9H, s); ^{13}C NMR ($CDCl_3$, 100 MHz): δ147.6, 137.5, 137.3, 133.2, 127.0, 116.1, 83.0, 43.5, 41.4, 24.8, 24.7, –0.8, –0.9; HRMS (DART): Calcd for $C_{20}H_{34}BO_2Si$ $[M+H]^+$: 345.2421, Found: 345.2431; Specific Rotation: $[\alpha]_D^{20}$ +8.2 (*c* 0.85, $CHCl_3$) for an enantiomerically enriched sample of 96:4 er Enantiomeric purity was determined by HPLC analysis of the alcohol product after oxidation in comparison with authentic racemic material (96:4 er shown; Chiralcel AZ–H column, 99% hexanes, 1% *i*-PrOH, 0.3 mL/min, 220 nm).

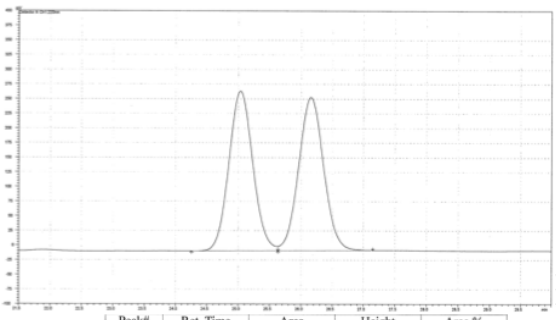

Peak#	Ret. Time	Area	Height	Area %
1	25.030	7233091	272759	49.887
2	26.150	7266002	261783	50.113
Total		14499093	534542	100.000

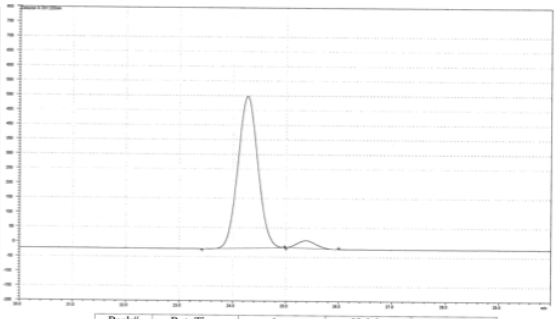

Peak#	Ret. Time	Area	Height	Area %
1	24.263	13449364	517639	95.727
2	25.372	600312	25247	4.273
Total		14049676	542886	100.000

Peak #	Time (min)	Area (%)	Peak #	Time (min)	Area (%)
1	25.030	49.887	1	24.263	95.727
2	26.150	50.113	2	25.372	4.273

(*R*)-4,4,5,5-Tetramethyl-2-(2-(naphthalen-1-yl)pent-4-enyl)-1,3,2-dioxaborolane (1.17): IR (neat): 2976 (w), 2975 (w), 1367 (s), 1312 (s), 1251 (w), 1142 (s), 967 (m), 846 (m), 792 (s) cm^{-1}; ^{1}H NMR ($CDCl_3$, 400 MHz): δ 8.22 (1H, d, *J* = 8.1 Hz), 7.83 (1H, dd, *J* = 7.9, 1.6 Hz), 7.68 (1H, dd, *J* = 6.9, 2.5 Hz), 7.56–7.37 (4H, m), 5.75 (1H, ddt, *J* =17.2, 10.1, 7.0 Hz), 5.06–4.91 (2H, m), 3.90 (1H, app pent, *J* = 7.3 Hz), 2.66–2.53 (1H, m), 2.50–2.38 (1H, m), 1.47–1.35 (1H, m), 1.35–1.23 (1H, m), 1.04 (6H, s), 0.96 (6H, s); ^{13}C NMR ($CDCl_3$, 100 MHz): δ 143.2, 137.2, 134.0, 131.8, 128.8, 126.4, 125.6, 125.6, 125.3, 123.9, 123.4, 116.4, 83.1, 43.3, 35.0, 24.7; HRMS (DART): Calcd for $C_{21}H_{28}B_1O_2$ $[M+H]^+$: 323.2182, Found: 323.2185; Specific Rotation: $[\alpha]_D^{20}$ +5.6 (*c* 1.08, $CHCl_3$) for an enantiomerically enriched sample of 93:7 er Enantiomeric purity was determined by HPLC analysis in comparison with authentic racemic material (93:7 er shown; Chiralcel OJ–H column, 100% hexanes, 0.3 mL/min, 220 nm).

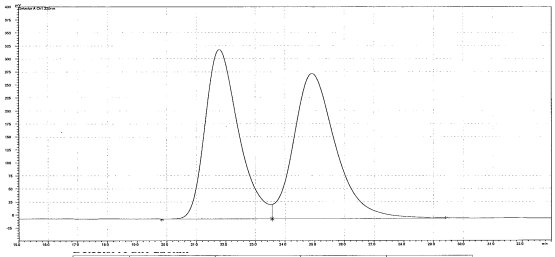

Peak#	Ret. Time	Area	Height	Area %
1	21.777	25778878	325680	48.483
2	24.906	27392466	279410	51.517
Total		53171343	605090	100.000

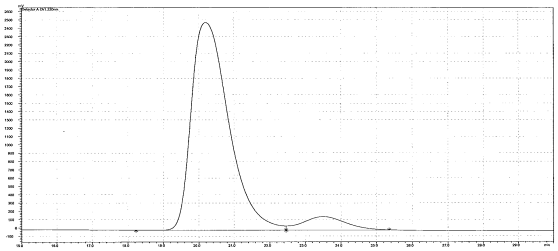

Peak#	Ret. Time	Area	Height	Area %
1	20.183	183585831	2496092	93.067
2	23.495	13676947	162887	6.933
Total		197262778	2658979	100.000

Peak #	Time (min)	Area (%)	Peak #	Time (min)	Area (%)
1	21.777	48.483	1	20.183	93.067
2	24.906	51.517	2	23.495	6.933

(*R*)-6-Methyl-2-(4-(1-(4,4,5,5-tetramethyl-1,3,2-dioxaborolan-2-yl)pent-4-en-2-yl)phenyl)-1,3,6,2-dioxazaborocane-4,8-dione (1.18): IR (neat): 2977 (w), 2927 (w), 1765 (s), 1457 (w), 1370 (m), 1334 (m), 1293 (m), 1235 (m), 1145 (m), 1040 (m), 993 (m) cm^{-1}; ^{1}H NMR (400 MHz, $CDCl_3$): δ 7.40 (2H, d, *J* = 7.6 Hz), 7.23 (2H, d, *J* = 8.0 Hz), 5.69–5.59 (1H, m), 4.96–4.88 (2H, m), 3.93 (2H, d, *J* = 16.4 Hz), 3.75 (2H, d, *J* = 16.0 Hz), 2.95 (1H, app pent, *J* = 7.5 Hz), 2.51 (3H, s), 2.38–2.32 (2H, m), 1.23 (1H, dd, *J* = 15.2, 7.2 Hz), 1.12–1.06 (13H, m); ^{13}C NMR (100 MHz, $CDCl_3$): δ 167.5, 149.0, 137.1, 132.2, 127.7, 116.3, 83.1, 61.8, 47.5, 43.6, 41.4, 24.9, 24.8; HRMS (DART): Calcd for $C_{22}H_{35}B_2N_2O_6$ $[M+NH_4]^+$: 445.2681, Found: 445.2689. Specific Rotation: $[\alpha]_D^{20}$ +6.4 (*c* 0.87, $CHCl_3$) for an enantiomerically enriched sample of 95:5 er Enantiomeric purity was determined by HPLC analysis of the product from oxidation/acetylation in comparison with authentic racemic material (95:5 er shown; Chiralcel OC–H column, 98% hexanes, 2% *i*-PrOH, 0.3 mL/min, 220 nm).

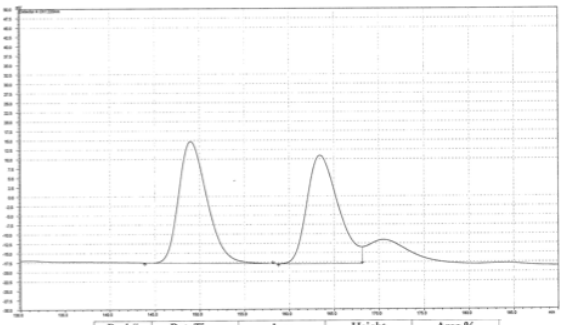

Peak#	Ret. Time	Area	Height	Area %
1	148.992	7103125	32385	50.354
2	163.447	7003134	28830	49.646
Total		14106259	61216	100.000

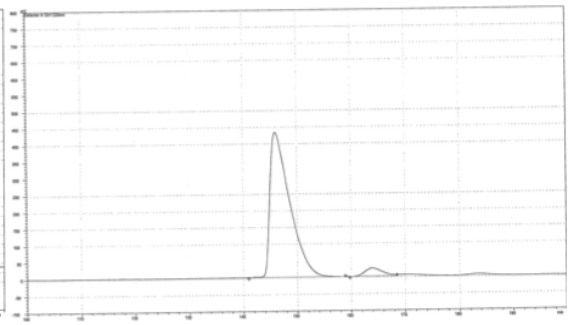

Peak#	Ret. Time	Area	Height	Area %
1	145.989	110364232	433639	95.214
2	163.902	5546930	24090	4.786
Total		115911162	457729	100.000

Peak #	Time (min)	Area (%)	Peak #	Time (min)	Area (%)
1	148.992	50.354	1	145.989	95.214
2	163.447	49.646	2	163.902	4.786

(*R*)-2-(2-(3-(Allyloxy)phenyl)pent-4-enyl)-4,4,5,5-tetramethyl-1,3,2-dioxaborolane (1.19): IR (neat): 3076 (w), 2977 (w), 2925 (w), 1600 (m), 1583 (m), 1422 (s), 1366 (s), 1265 (m), 1142 (s), 1034 (w), 913 (m), 846 (m), 776 (m), 699 (m) cm^{-1}; ^{1}H NMR ($CDCl_3$, 400 MHz): δ 7.16 (1H, t, *J* = 7.9 Hz), 6.84–6.76 (2H, m), 6.71 (1H, ddd, *J* = 8.2, 2.6, 0.9 Hz), 6.06 (1H, ddt *J* = 17.3, 10.6, 5.3 Hz), 5.67 (1H, dddd, *J* = 16.9, 10.1, 7.5, 6.6 Hz), 5.40 (1H, dd, *J* = 17.3, 1.6 Hz), 5.27 (1H, dd, *J* = 10.5, 1.5 Hz), 5.00–4.87 (2H, m), 4.52 (2H, dt, *J* = 5.3, 1.5 Hz), 3.04–2.82 (1H, m), 2.43–2.26 (2H, m), 1.29–1.16 (2H, m), 1.12 (6H, s), 1.11 (6H, s); ^{13}C NMR ($CDCl_3$, 100 MHz): δ 158.6 148.7, 137.3, 133.7, 129.1, 120.2, 117.6, 116.2, 114.2, 112.2, 83.1, 68.8, 43.7, 41.5, 24.85, 24.82; HRMS (DART): Calcd for $C_{20}H_{30}B_1O_3$ $[M+H]^+$: 329.2288, Found: 329.2295; Specific Rotation: $[\alpha]_D^{20}$ +6.4 (*c* 1.17, $CHCl_3$) for an enantiomerically enriched sample of 95:5 er Enantiomeric purity was determined by HPLC analysis in comparison with authentic racemic material (95:5 er shown; Chiralcel OD–H column, 100% hexanes, 0.3 mL/min, 220 nm).

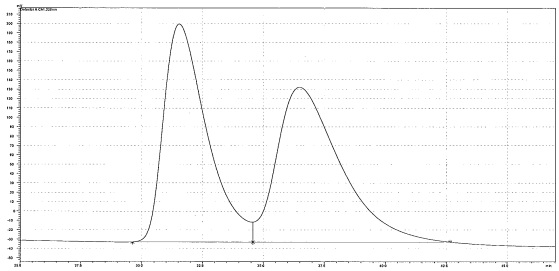

Peak#	Ret. Time	Area	Height	Area %
1	31.532	28645850	232498	49.049
2	36.476	29756939	165229	50.951
Total		58402788	397727	100.000

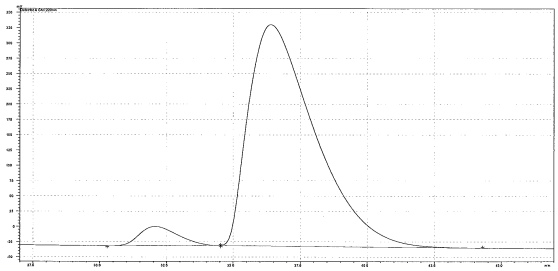

Peak#	Ret. Time	Area	Height	Area %
1	32.064	3105696	31399	4.765
2	36.398	62073723	362214	95.235
Total		65179419	393613	100.000

Peak #	Time (min)	Area (%)	Peak #	Time (min)	Area (%)
1	31.532	49.049	1	32.064	4.765
2	36.476	50.951	2	36.398	95.235

(*R*)-2-(2-(2-Methoxyphenyl)pent-4-enyl)-4,4,5,5-tetramethyl-1,3,2-dioxaborolane (1.20): IR (neat): 2976 (w), 2929 (w), 2836 (w), 1599 (w), 1585 (w), 1491 (m), 1464 (w), 1438 (w), 1368 (s), 1318 (s), 1215 (s), 1143 (s), 1101 (s), 1031 (m), 968 (m), 909 (m), 885 (w), 749 (s) cm^{-1}; ^{1}H NMR ($CDCl_3$, 400 MHz): δ 7.17–7.10 (2H, m), 6.88 (1H, t, *J* = 7.4 Hz), 6.81 (1H, d, *J* = 8.4 Hz), 5.75–5.65 (1H, m), 4.96–4.88 (2H, m), 3.81 (3H, s), 3.42 (1H, app pent, *J* = 7.5 Hz), 2.44–2.26 (2H, m), 1.26–1.19 (1H, m), 1.16–1.08 (1H, m), 1.11 (6H, s), 1.08 (6H, s); ^{13}C NMR ($CDCl_3$, 100 MHz): δ 157.2, 137.8, 135.1, 127.8, 126.7, 120.4, 115.7, 110.6, 82.9, 55.5, 42.3, 33.9, 24.80, 24.77; HRMS (DART): Calcd for $C_{18}H_{28}B_1O_3$ $[M+H]^+$: 303.2132, Found: 303.2128; Specific Rotation: $[\alpha]_D^{20}$ +13.9 (*c* 1.61, $CHCl_3$) for an enantiomerically enriched sample of 95:5 er Enantiomeric purity was determined by HPLC analysis in comparison with authentic racemic material (95:5 er shown; Chiralcel OZ–H column, 100% hexanes, 0.3 mL/min, 220 nm).

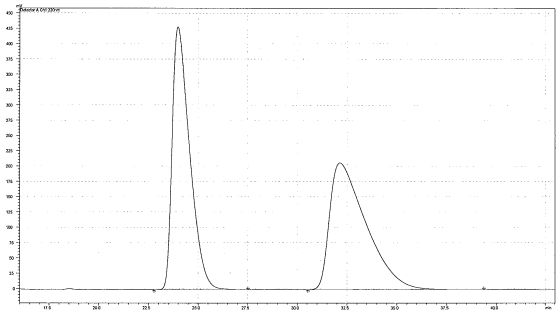

Peak#	Ret. Time	Area	Height	Area %
1	23.978	26303630	429169	50.115
2	32.136	26182411	207068	49.885
Total		52486041	636237	100.000

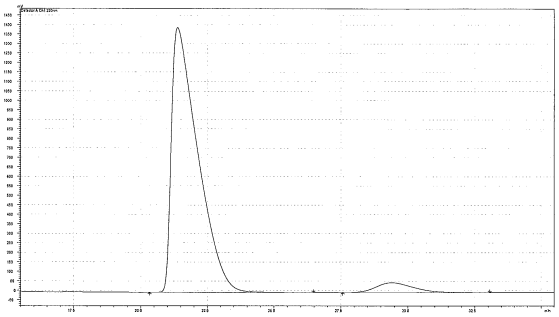

Peak#	Ret. Time	Area	Height	Area %
1	21.378	95311996	1394885	95.065
2	29.394	4947535	51312	4.935
Total		100259531	1446197	100.000

Peak #	Time (min)	Area (%)	Peak #	Time (min)	Area (%)
1	23.978	50.115	1	21.378	95.065
2	32.136	49.885	2	29.394	4.935

(*R*)-2-(2-(4-Methoxyphenyl)pent-4-enyl)-4,4,5,5-tetramethyl-1,3,2-dioxaborolane (1.21): 40% yield was obtained with 6:1 (0.6 mmol: 0.1 mmol) alkene:phosphate (**1.11**). IR (neat): 2976 (w), 2926 (w), 2834 (w), 1610 (w), 1511 (s), 1366 (s), 1319 (m), 1244 (s), 1214 (w), 1177 (m), 1165 (s), 1143 (w), 1104 (m), 1037 (m), 967 (m), 910 (w), 885 (w), 846 (m), 828 (m), 806 (w) cm^{-1}; ^{1}H NMR ($CDCl_3$, 400 MHz): δ 7.12 (2H, dd, J = 6.4, 2.0 Hz), 6.80 (2H, dd, J = 6.4, 2.0 Hz), 5.67 (1H, ddt, J = 17.2, 9.6, 7.2 Hz), 4.97–4.90 (2H, m) 3.77 (3H, s), 2.94–2.86 (1H, m), 2.38–2.26 (2H, m), 1.25–1.18 (1H, m), 1.11–1.04 (13H, m). ^{13}C NMR ($CDCl_3$, 100 MHz): δ 157.9, 139.1, 137.4, 128.4, 116.0, 113.6, 83.1, 55.4, 44.1, 40.7, 24.9, 24.8; HRMS (DART): Calcd for $C_{18}H_{28}BO_3$ $[M+H]^+$: 303.2132, Found: 303.2126; Specific Rotation: $[\alpha]_D^{20}$ +9.8 (c 0.76, $CHCl_3$) for an enantiomerically enriched sample of 97:3 er Enantiomeric purity was determined by HPLC analysis in comparison with authentic racemic material (97:3 er shown; Chiralcel OD–H column, 100% hexanes, 0.3 mL/min, 220 nm).

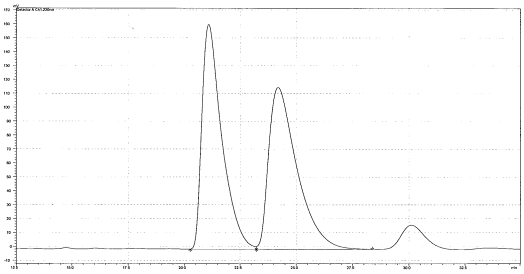

Peak#	Ret. Time	Area	Height	Area %
1	21.084	10063076	161641	49.788
2	24.175	10148737	116341	50.212
Total		20211813	277981	100.000

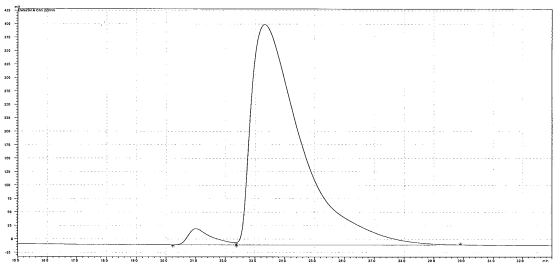

Peak#	Ret. Time	Area	Height	Area %
1	20.993	1662337	30072	3.369
2	23.315	47674508	409729	96.631
Total		49336845	439801	100.000

Peak #	Time (min)	Area (%)	Peak #	Time (min)	Area (%)
1	21.084	49.788	1	20.993	3.369
2	24.175	50.212	2	23.315	96.631

(*R*)-2-(2-(Benzofuran-2-yl)pent-4-enyl)-4,4,5,5-tetramethyl-1,3,2-dioxaborolane (1.22) : IR (neat): 2977 (w), 2928 (w), 1584 (w), 1455 (m), 1370 (s), 1321 (s), 1253(w), 1142 (s), 1006 (m), 912 (m), 846 (m), 796 (m), 749 (s), 738 (s), 671 (w) cm^{-1}; ^{1}H NMR ($CDCl_3$, 400 MHz): δ 7.49–7.44 (1H, m), 7.42–7.38 (1H, m), 7.22–7.13 (2H, m), 6.38 (1H, s), 5.76 (1H, ddt, *J* = 17.2, 10.1, 7.1 Hz), 5.08–4.96 (2H, m), 3.26–3.16 (1H, m), 2.63–2.53 (1H, m), 2.49–2.38 (1H, m), 1.23 (2H, d, *J* = 7.7 Hz), 1.20 (6H, s), 1.18 (6H, s); ^{13}C NMR ($CDCl_3$, 100 MHz): δ 163.3, 154.7, 136.3, 129.0, 123.1, 122.4, 120.4, 117.0, 110.9, 101.4, 83.3, 40.3, 35.0, 24.94, 24.88; HRMS (DART): Calcd for $C_{19}H_{26}BO_3$ $[M+H]^+$: 313.1975, Found: 313.1987; Specific Rotation: $[\alpha]_D^{20}$ +17.2 (*c* 1.67, $CHCl_3$) for an enantiomerically enriched sample of 90:10 er Enantiomeric purity was determined by HPLC analysis in comparison with authentic racemic material (90:10 er shown; Chiralcel OZ–H column, 100% hexanes, 0.3 mL/min, 220 nm).

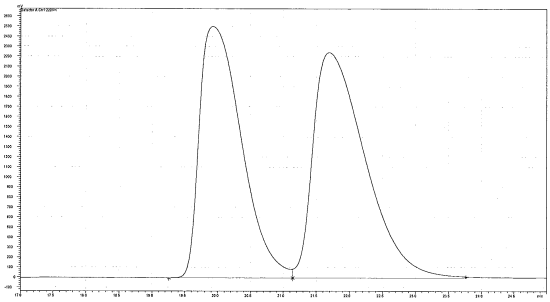

Peak#	Ret. Time	Area	Height	Area %
1	19.923	111510728	2504369	47.625
2	21.690	122634341	2245527	52.375
Total		234145069	4749896	100.000

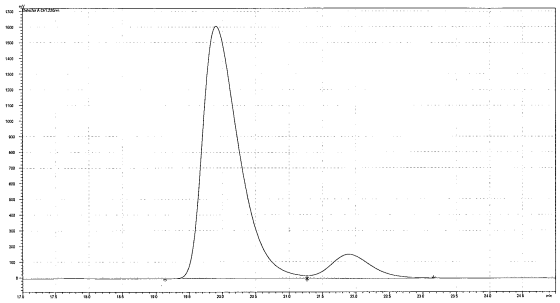

Peak#	Ret. Time	Area	Height	Area %
1	19.900	61004630	1610521	90.179
2	21.888	6644064	153966	9.821
Total		67648694	1764486	100.000

Peak #	Time (min)	Area (%)	Peak #	Time (min)	Area (%)
1	19.923	47.625	1	19.900	90.179
2	21.690	52.375	2	21.888	9.821

***tert*-Butyl (*R*)-5-(1-(4,4,5,5-tetramethyl-1,3,2-dioxaborolan-2-yl)pent-4-en-2-yl)-1*H*-indole-1-carboxylate (1.23)**: Following the representative procedure except for 6:1 (0.6 mmol: 0.1 mmol) alkene:phosphate (**1.11**) used. IR (neat): 2977 (m), 2927 (w), 1731 (s), 1469 (m), 1441 (w), 1352 (s), 1318 (s), 1253 (m), 1162 (s), 1141 (s), 1081 (m), 1022 (m), 968 (w), 846 (w), 766 (m), 725 (m) cm^{-1}; ^{1}H NMR (400 MHz, $CDCl_3$): δ 8.00 (1H, d, J = 8 Hz), 7.54 (1H, d, J = 3.6 Hz), 7.38 (1H, d, J = 1.6 Hz), 7.17 (1H, dd, J = 8.8, 2.0 Hz), 6.50 (1H, d, J = 3.6 Hz), 5.68 (1H, ddt, J = 17, 10.4, 6.4 Hz), 4.98–4.88 (2H, m), 3.04 (1H, app pent, J = 7.0 Hz), 2.46–2.34 (2H, m), 1.66 (9H, s), 1.30–1.25 (1H, m), 1.19–1.13 (1H, m), 1.09 (6H, s), 1.08 (6H, s); ^{13}C NMR (100 MHz, $CDCl_3$): δ 150.1, 141.4, 137.5, 133.8, 130.7, 125.9, 124.1, 119.5, 116.0, 114.8, 107.5, 83.5, 83.1, 44.2, 41.4, 28.4, 24.9, 24.8; HRMS (DART): Calcd for $C_{24}H_{35}B_1N_1O_4$ $[M+H]^+$: 412.2659, Found: 412.2653; Specific Rotation: $[\alpha]_D^{20}$ +17.1 (c 0.43, $CHCl_3$) for an enantiomerically enriched sample of 98:2 er Enantiomeric purity was determined by HPLC analysis in

comparison with authentic racemic material (98:2 er shown; Chiralcel AD–H column, 100% hexanes, 0.3 mL/min, 220 nm).

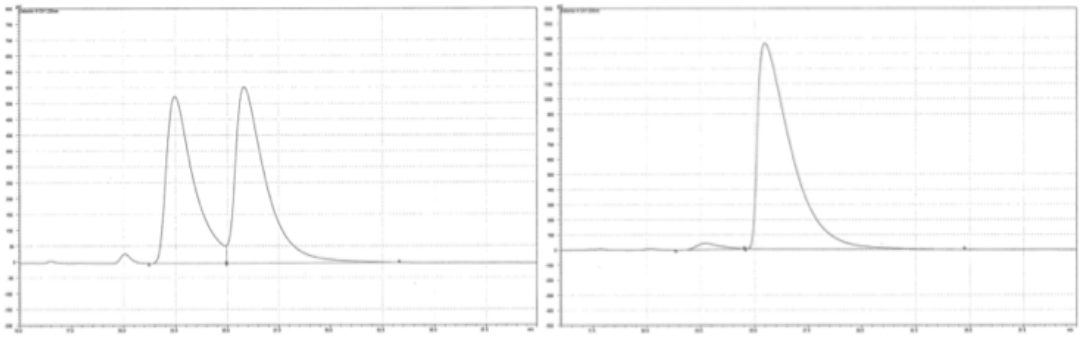

Peak#	Ret. Time	Area	Height	Area %
1	22.469	48390167	527379	46.056
2	25.810	56677153	556188	53.944
Total		105067320	1083567	100.000

Peak#	Ret. Time	Area	Height	Area %
1	22.708	2977277	40960	1.990
2	25.481	146670197	1361804	98.010
Total		149647473	1402765	100.000

Peak #	Time (min)	Area (%)	Peak #	Time (min)	Area (%)
1	22.469	46.056	1	22.708	1.990
2	25.810	53.944	2	25.481	98.010

***tert*-Butyl (*R*)-3-(1-(4,4,5,5-tetramethyl-1,3,2-dioxaborolan-2-yl)pent-4-en-2-yl)benzoate (1.24):** Following the representative procedure except for 1:3 (0.1 mmol: 0.3 mmol) alkene:phosphate (**1.11**) used. IR (neat): 2977 (w), 2929 (w), 1713 (s), 1440 (w), 1390 (w), 1367 (s), 1320 (m), 1294 (s), 1161 (s), 1144 (s), 1110 (m) cm^{-1}; ^{1}H NMR (400 MHz, $CDCl_3$): δ 7.83 (1H, dd, *J* = 1.6, 1.2 Hz), 7.78 (1H, ddd, *J* = 7.7, 2.3, 1.1 Hz), 7.37 (1H, dd, *J* = 7.6, 1.6 Hz), 7.30 (1H, t, *J* = 7.4 Hz), 5.66 (1H, ddt, *J* = 17.2, 10.0, 7.2 Hz), 4.98–4.91 (2H, m), 3.04–2.96 (1H, m), 2.44–2.32 (2H, m), 1.59 (9H, s), 1.25 (1H, dd, *J* = 15.8, 7.0 Hz), 1.20–1.06 (13H, m); ^{13}C NMR (100 MHz, $CDCl_3$): δ 166.2, 147.1, 137.0, 131.9, 131.6, 128.8, 128.1, 127.2, 116.5, 83.2, 80.9, 43.4, 41.4, 28.4, 24.9, 24.8; HRMS (DART): Calcd for $C_{22}H_{34}B_1O_4$ $[M+H]^+$: 373.2550, Found: 373.2565; Specific Rotation: $[\alpha]_D^{20}$ +4.9 (*c* 1.05, $CHCl_3$) for an enantiomerically enriched sample of 95:5 er Enantiomeric purity was determined by HPLC analysis in comparison with authentic

racemic material (95:5 er shown; Chiralcel OZ–H column, 100% hexanes, 0.3 mL/min, 220 nm).

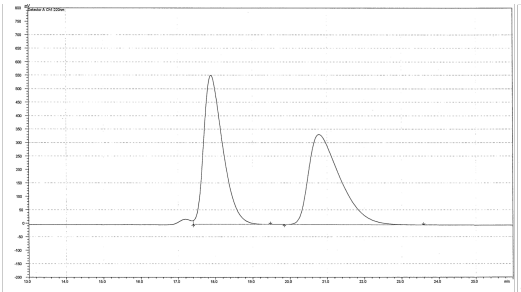

PeakTable

Detector A Ch1 220nm

Peak#	Ret. Time	Area	Height	Area %	Height %
1	17.885	19631455	553324	50.079	62.322
2	20.783	19569298	334519	49.921	37.678
Total		39200753	887842	100.000	100.000

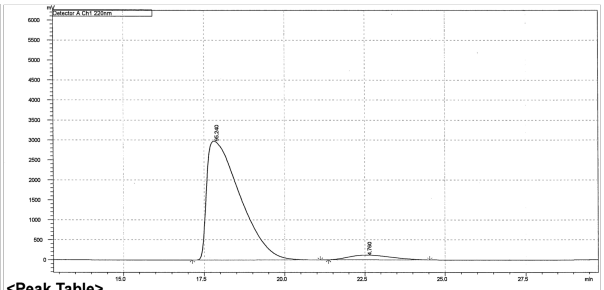

<Peak Table>

Detector A Channel 1 220nm

Peak#	Ret. Time	Area	Height	Conc.	Area%
1	17.799	211784035	2977196	95.240	95.240
2	22.547	10584480	116111	4.760	4.760
Total		222368516	3093307		100.000

Peak #	Time (min)	Area (%)	Peak #	Time (min)	Area (%)
1	17.885	50.079	1	17.799	95.240
2	20.783	49.921	2	22.547	4.760

***tert*-Butyl (*R*)-3-(1-(4,4,5,5-tetramethyl-1,3,2-dioxaborolan-2-yl)pent-4-en-2-yl-5,5-d_2)benzoate [1.24-d_2 (S_N2')]:** Following the representative procedure except **1.11-d_2** and **L3b** was used. IR (neat): 2977 (w), 2929 (w), 1713 (s), 1367 (s), 1320 (m), 1295 (s), 1162 (s), 1145 (s), 1111 (m), 968 (m), 848 (m) cm^{-1}; ^{1}H NMR (400 MHz, $CDCl_3$): δ 7.83 (1H, t, *J* = 1.6 Hz), 7.78 (1H, dt, *J* = 7.6, 1.6 Hz), 7.37 (1H, dt, *J* = 7.2, 1.6 Hz), 7.30 (1H, t, *J* = 7.8 Hz), 5.65 (1H, t, *J* = 7.0 Hz, 3.04–2.96 (1H, m), 2.44–2.32 (2H, m), 1.59 (9H, s), 1.25 (1H, dd, *J* = 15.2, 6.0 Hz) 1.11 (6H, s), 1.10 (6H, s), 1.12–1.06 (1H, m); ^{13}C NMR (100 MHz, $CDCl_3$): δ 166.2, 147.1, 136.8, 131.9, 131.6, 128.8, 128.1, 127.2, 83.2, 80.9, 43.3, 41.4, 28.4, 24.9, 24.8; HRMS (DART): Calcd for $C_{22}H_{35}D_2B_1N_1O_4$ $[M+NH_4]^+$: 392.2941, Found: 392.2954.

(*R*)-4,4,5,5-Tetramethyl-2-(2-(2-(trifluoromethyl)phenyl)pent-4-en-1-yl)-1,3,2-dioxaborolane (1.25): Following the representative procedure except except for 1:3 (0.1

mmol: 0.3 mmol) alkene:carbonate (**1.35**) used. IR (neat): 2979 (w), 2928 (w), 1363 (m), 1312 (s), 1145 (s), 1124 (s), 1036 (m), 768 (m) cm^{-1}; ^1H NMR (400 MHz, $CDCl_3$): δ 7.58 (1H, d, *J* = 8.0 Hz), 7.50–7.43 (2H, m), 7.26–7.22 (1H, m), 5.70 (1H, ddt, *J* = 18.0, 10.0, 7.2 Hz), 4.99–4.92 (2H, m), 3.42 (1H, app pent, *J* = 7.4 Hz), 2.45–2.25 (2H, m), 1.26 (1H, dd, *J* = 15.4, 7.0 Hz), 1.14 (1H, dd, *J* = 15.6, 8.4 Hz), 1.08 (6H, s), 1.05 (6H, s); ^{13}C NMR (100 MHz, $CDCl_3$): δ 146.5, 136.7, 131.8, 128.2 (q, *J* = 29.0 Hz), 128.18, 125.7, 125.6, 124.7 (q, *J* = 272.5 Hz), 116.6, 83.1, 43.9, 36.0, 24.7, 18.6 (br, C–B); HRMS (DART): Calcd for $C_{18}H_{25}B_1F_3O_2$ $[M+H]^+$: 341.1900, Found: 341.1903; Specific Rotation: $[\alpha]_D^{20}$ +11.9 (*c* 1.20, $CHCl_3$) for an enantiomerically enriched sample of 88:12 er Enantiomeric purity was determined by HPLC analysis in comparison with authentic racemic material (96:4 er shown; Chiralcel OZ–H column, 100% hexanes, 0.3 mL/min, 220 nm).

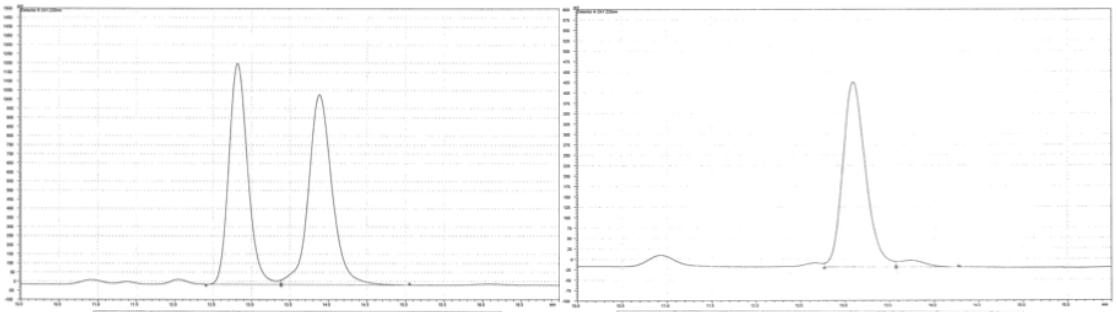

Peak#	Ret. Time	Area	Height	Area %
1	12.811	20832986	1213915	48.449
2	13.878	22166706	1044726	51.551
Total		42999693	2258641	100.000

Peak#	Ret. Time	Area	Height	Area %
1	13.090	7952410	444664	96.273
2	13.739	307821	15826	3.727
Total		8260231	460490	100.000

Peak #	Time (min)	Area (%)	Peak #	Time (min)	Area (%)
1	12.811	48.449	1	13.090	96.273
2	13.878	51.551	2	13.739	3.727

***tert*-Butyl (*R*)-4-(1-(4,4,5,5-tetramethyl-1,3,2-dioxaborolan-2-yl)pent-4-en-2-yl)benzoate (1.26):** IR (neat): 2978 (m), 2930 (w), 1712 (s), 1609 (w), 1367 (s), 1312 (m), 1290 (s), 1166 (s), 1145 (s), 1116 (s), 848 (m) cm^{-1}; ^1H NMR (400 MHz, $CDCl_3$): δ

7.88 (2H, d, J = 8.0 Hz), 7.24 (2H, d, J = 8.0 Hz), 5.68–5.58 (1H, m), 4.96–4.90 (2H, m), 3.00 (1H, app pent, J = 7.5 Hz), 2.35 (2H, t, J = 7.2 Hz), 1.58 (9H, s), 1.27–1.21 (1H, m), 1.14–1.08, (1H, m) 1.12 (6H, s), 1.11 (6H, s); ^{13}C NMR (100 MHz, $CDCl_3$): δ 166.1, 152.0, 136.8, 129.9, 129.5, 127.4, 116.5, 83.2, 80.8, 43.5, 41.5, 28.4, 24.9, 24.8; HRMS (DART): Calcd for $C_{22}H_{34}B_1O_4$ $[M+H]^+$: 373.2550, Found: 373.2534; Specific Rotation: $[\alpha]_D^{20}$ –3.0 (c 1.00, $CHCl_3$) for an enantiomerically enriched sample of 67:33 er Enantiomeric purity was determined by HPLC analysis in comparison with authentic racemic material (52:48 er shown; Chiralcel OD–H column, 100% hexanes, 0.3 mL/min, 220 nm).

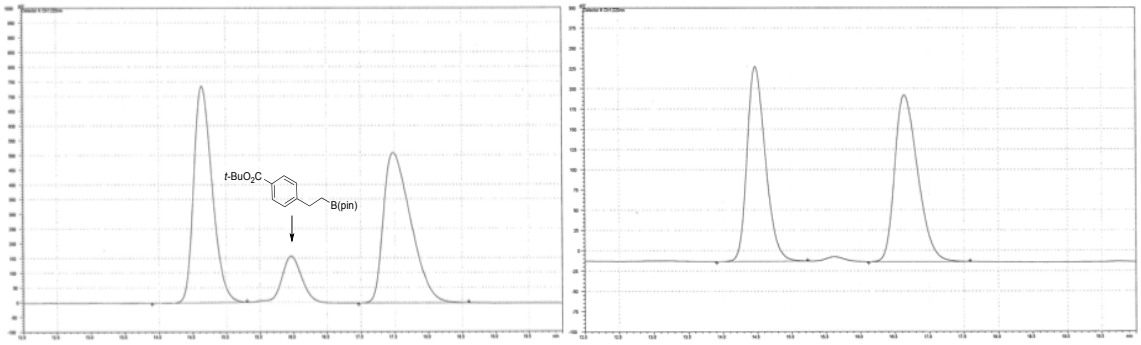

Peak#	Ret. Time	Area	Height	Area %
1	14.638	14061810	735507	49.374
2	17.479	14418511	510741	50.626
Total		28480320	1246248	100.000

Peak#	Ret. Time	Area	Height	Area %
1	14.474	4480291	240810	48.271
2	16.639	4801309	206218	51.729
Total		9281600	447028	100.000

Peak #	Time (min)	Area (%)	Peak #	Time (min)	Area (%)
1	14.638	49.374	1	14.474	48.271
2	17.479	50.626	2	16.639	51.729

(*R*)-4,4,5,5-Tetramethyl-2-(2-(4-(trifluoromethyl)phenyl)pent-4-en-1-yl)-1,3,2-dioxaborolane (1.27): Following the representative procedure except for 1:3 (0.1 mmol: 0.3 mmol) alkene:carbonate (**1.35**) used. The spectroscopic data match those reported previously.[5] ^{1}H NMR (400 MHz, $CDCl_3$): δ 7.58 (1H, d, J = 8.0 Hz), 7.50–7.43 (2H, m), 7.26–7.22 (1H, m), 5.70 (1H, ddt, J = 18.0, 10.0, 7.2 Hz), 4.99–4.92 (2H, m), 3.42 (1H,

app pent, J = 7.4 Hz), 2.45–2.25 (2H, m), 1.26 (1H, dd, J = 15.4, 7.0 Hz), 1.14 (1H, dd, J = 15.6, 8.4 Hz), 1.08 (6H, s), 1.05 (6H, s). Specific Rotation: $[\alpha]_D^{20}$ +6.1 (c 0.45, $CHCl_3$) for an enantiomerically enriched sample of 96:4 er Enantiomeric purity was determined by HPLC analysis of the alcohol product after oxidation in comparison with authentic racemic material (96:4 er shown; Chiralcel OZ–H column, 99% hexanes, 0.3 mL/min, 220 nm).

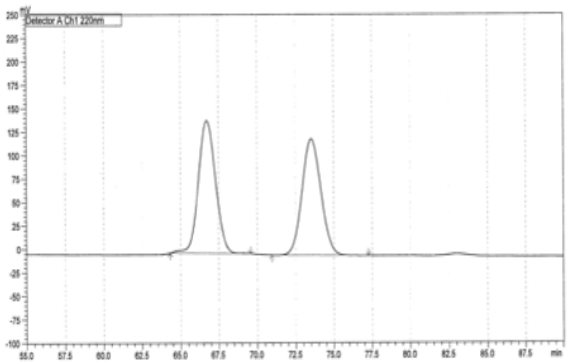

Peak#	Ret. Time	Area	Height	Area%
1	66.741	11143770	141643	50.949
2	73.532	10728683	124323	49.051
Total		21872454	265966	100.000

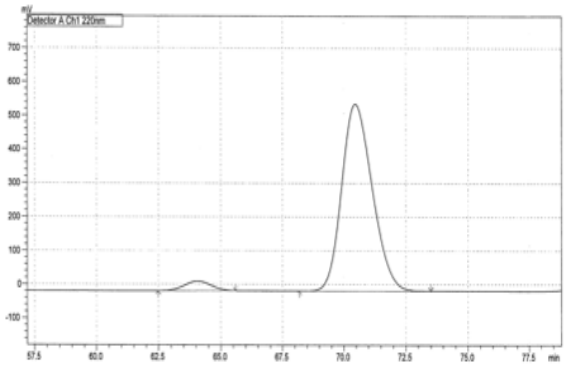

Peak#	Ret. Time	Area	Height	Area%
1	64.054	2108669	28141	4.220
2	70.462	47865409	554084	95.780
Total		49974079	582225	100.000

Peak #	Time (min)	Area (%)	Peak #	Time (min)	Area (%)
1	66.741	50.949	1	64.054	4.220
2	73.532	49.051	2	70.462	95.780

(*R*)-4,4,5,5-Tetramethyl-2-(4-(1-(4,4,5,5-tetramethyl-1,3,2-dioxaborolan-2-yl)pent-4-en-2-yl)phenyl)-1,3,2-dioxaborolane (1.28): Following the representative procedure except for 1:3 (0.1 mmol: 0.3 mmol) alkene:phosphate (**1.11**) used. IR (neat): 2977 (m), 2925 (m), 2041 (w), 2034 (w), 2024 (w), 1611 (m), 1399 (m), 1360 (s), 1319 (m), 1271 (w), 1144 (m), 1090 (s), 964 (w), 860 (w), 830 (w), 660 (m)cm^{-1}; ^1H NMR ($CDCl_3$, 400 MHz): δ 7.70 (2H, d, J= 8.0 Hz), 7.21 (2H, d, J = 8.0 Hz), 5.73–5.57 (1H, m), 4.97–4.88 (2H, m), 3.01–2.90 (1H, m), 2.43–2.28 (2H, m), 1.33 (12H, s), 1.28–1.16 (2H, m), 1.12

(6H, s), 1.11 (6H, s); ^{13}C NMR ($CDCl_3$, 100 MHz): δ 150.4, 137.2, 134.8, 127.0, 116.2, 83.6, 83.1, 43.5, 41.6, 25.0, 24.8; HRMS (DART): Calcd for $C_{23}H_{40}B_2N_1O_4$ $[M+NH_4]^+$: 416.3143, Found: 416.3158; Specific Rotation: $[\alpha]_D^{20}$ +9.1 (*c* 1.02, $CHCl_3$) for an enantiomerically enriched sample of 92:8 er Enantiomeric purity was determined by HPLC analysis in comparison with authentic racemic material (92:8 er shown; Chiralcel AZ–H column, 99% hexanes, 1% *i*-PrOH, 0.3 mL/min, 220 nm).

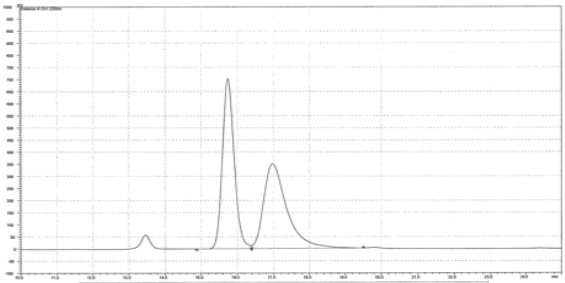

Peak#	Ret. Time	Area	Height	Area %
1	15.733	15938425	701950	50.363
2	16.969	15708809	350049	49.637
Total		31647234	1051999	100.000

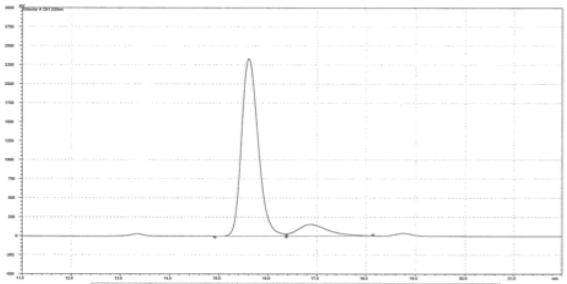

Peak#	Ret. Time	Area	Height	Area %
1	15.594	53721818	2323030	92.237
2	16.862	4521581	126537	7.763
Total		58243399	2449567	100.000

Peak #	Time (min)	Area (%)	Peak #	Time (min)	Area (%)
1	15.733	50.363	1	15.594	92.237
2	16.969	49.637	2	16.862	7.763

(*R*)-4,4,5,5-Tetramethyl-2-(3-(1-(4,4,5,5-tetramethyl-1,3,2-dioxaborolan-2-yl)pent-4-en-2-yl)phenyl)-1,3,2-dioxaborolane (1.29): Following the representative procedure except for 1:3 (0.1 mmol: 0.3 mmol) alkene:phosphate (**1.11**) used. IR (neat): 2977 (m), 2926 (w), 2035 (w), 1611 (w), 1457 (w), 1399 (m), 1360 (s), 1320 (m), 1271 (w), 1214 (w), 1144 (s), 1090 (m), 964 (w), 860 (w), 829 (w), 659 (w) cm^{-1}; ^{1}H NMR ($CDCl_3$, 400 MHz): δ 7.66 (1H, s), 7.60 (1H, d, *J* = 7.1 Hz), 7.34–7.23 (2H, m), 5.68 (1H, ddt, *J* = 17.1, 10.1, 7.0 Hz), 4.97 (1H, dd, *J* = 17.2, 1.9 Hz), 4.94–4.89 (1H, m), 3.03–2.91 (1H, m), 2.49–2.29 (2H, m), 1.34 (6H, s), 1.33 (6H, s), 1.27–1.17 (2H, m), 1.10 (12H, s);^{13}C NMR ($CDCl_3$, 100 MHz): δ 146.2, 137.5, 134.2, 132.5, 130.3, 127.6, 116.0, 83.7, 83.0, 43.3,

41.4, 25.0, 24.9, 24.8; HRMS (DART): Calcd for $C_{23}H_{37}B_2O_4$ $[M+H]^+$: 399.2878, Found: 399.2887; Specific rotation: $[\alpha]_D^{20}$ +5.8 (*c* 0.43, $CHCl_3$) for an enantiomerically enriched sample of 96.5:3.5 er Enantiomeric purity was determined by HPLC analysis in comparison with authentic racemic material (96.5:3.5 er shown; Chiralcel OD–H column, 98% hexanes, 2% *i*-PrOH, 0.3 mL/min, 220 nm).

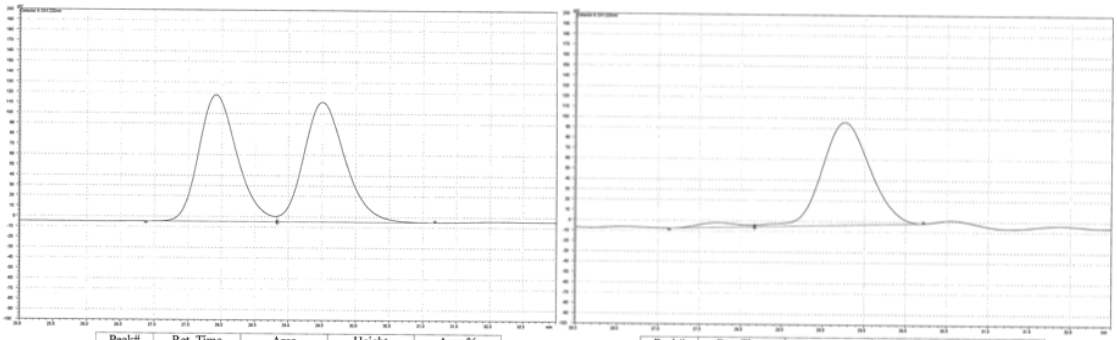

Peak#	Ret. Time	Area	Height	Area %
1	27.908	4860456	122631	49.566
2	29.493	4945478	116002	50.434
Total		9805934	238632	100.000

Peak#	Ret. Time	Area	Height	Area %
1	27.717	146707	4498	3.516
2	29.249	4025925	99634	96.484
Total		4172632	104132	100.000

Peak #	Time (min)	Area (%)	Peak #	Time (min)	Area (%)
1	27.908	49.566	1	27.717	3.516
2	29.493	50.434	2	29.249	96.484

(*R*)-4,4,5,5-Tetramethyl-2-(2-(naphthalen-2-yl)pent-4-en-1-yl)-1,3,2-dioxaborolane (1.30): Following the representative procedure except for 1:3 (0.1 mmol: 0.3 mmol) alkene:phosphate (**1.11**) used. IR (neat): 2976 (w), 2923 (s), 2853 (m), 1639 (w), 1362 (s), 1315 (s), 1143 (s), 968 (m), 911 (m), 847 (s), 814 (s), 744 (s), 476 (s) cm^{-1}; ^1H NMR ($CDCl_3$, 400 MHz): δ 7.81–7.73 (3H, m), 7.65–7.62 (1H, m), 7.46–7.35 (3H, m), 5.76–5.64 (1H, m), 5.01–4.89 (2H, m), 3.19–3.08 (1H, m), 2.55–2.37 (2H, m), 1.28–1.17(2H, m), 1.06 (6H, s), 1.07 (6H, s); ^{13}C NMR ($CDCl_3$, 100 MHz): δ 144.5, 137.2, 133.6, 132.3, 127.82, 127.78, 127.74, 127.68, 126.3, 125.81, 125.79, 125.1, 116.3, 83.1, 43.6, 41.6, 24.85, 24.77; HRMS (DART): Calcd for $C_{21}H_{28}B_1O_2$ $[M+H]^+$: 323.2182, Found:

323.2194; Specific Rotation: $[\alpha]_D^{20}$ +16.4 (*c* 0.72, $CHCl_3$) for an enantiomerically enriched sample of 96:4 er Enantiomeric purity was determined by HPLC analysis in comparison with authentic racemic material (96:4 er shown; Chiralcel OZ–H column, 100% hexanes, 0.3 mL/min, 254 nm).

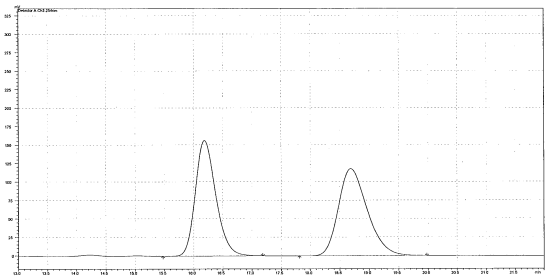

Peak#	Ret. Time	Area	Height	Area %
1	16.181	3853441	156647	48.876
2	18.684	4030671	117933	51.124
Total		7884112	274580	100.000

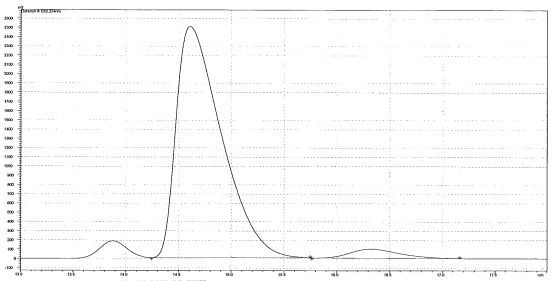

Peak#	Ret. Time	Area	Height	Area %
1	14.602	74811271	2504237	96.000
2	16.317	3116821	98231	4.000
Total		77928092	2602467	100.000

Peak #	Time (min)	Area (%)	Peak #	Time (min)	Area (%)
1	16.181	48.876	1	14.602	96.000
2	18.684	51.124	2	16.317	4.000

(*R*)-2-(2,4-Diphenylpent-4-en-1-yl)-4,4,5,5-tetramethyl-1,3,2-dioxaborolane (1.31): Following the representative procedure except for 1:3 (0.1 mmol: 0.3 mmol) alkene:phosphate (**1.11**) used. IR (neat): 3027 (w), 2977 (w), 2929 (w), 1494 (m), 1452 (w), 1369 (s), 1320 (s), 1145 (s), 699 (s) cm^{-1}; ^1H NMR (400 MHz, $CDCl_3$): δ 7.39–7.36 (2H, m), 7.33–7.19 (5H, m), 7.14–7.09 (3H, m), 5.15 (1H, d, *J* = 2.0 Hz), 4.83 (1H, d, *J* = 1.2 Hz), 2.96 (1H, app pent, *J* = 7.7 Hz), 2.87 (1H, dd, *J* = 13.8, 7.0 Hz), 2.73 (1H, dd, *J* = 13.6, 8.0 Hz), 1.26 (1H, dd, *J* = 15.6, 6.8 Hz), 1.13 (1H, dd, *J* = 15.6, 9.2 Hz), 1.07 (6H, s), 1.05 (6H, s); ^{13}C NMR (100 MHz, $CDCl_3$): δ 146.9, 146.8, 141.2, 128.4, 128.1, 127.6, 127.4, 126.6, 125.9, 114.5, 83.1, 45.7, 39.9, 24.8, 24.7; HRMS (DART): Calcd for $C_{23}H_{30}B_1O_2$ $[M+H]^+$: 349.2339, Found: 349.2347; Specific Rotation: $[\alpha]_{20}^D$ –11.9 (c 0.50, $CHCl_3$) for an enantiomerically enriched sample of 88:12 er Enantiomeric purity was

determined by HPLC analysis of the alcohol product after oxidation in comparison with authentic racemic material (96:4 er shown; Chiralcel OD–H column, 99% hexanes, 1% *i*-PrOH, 0.3 mL/min, 220 nm).

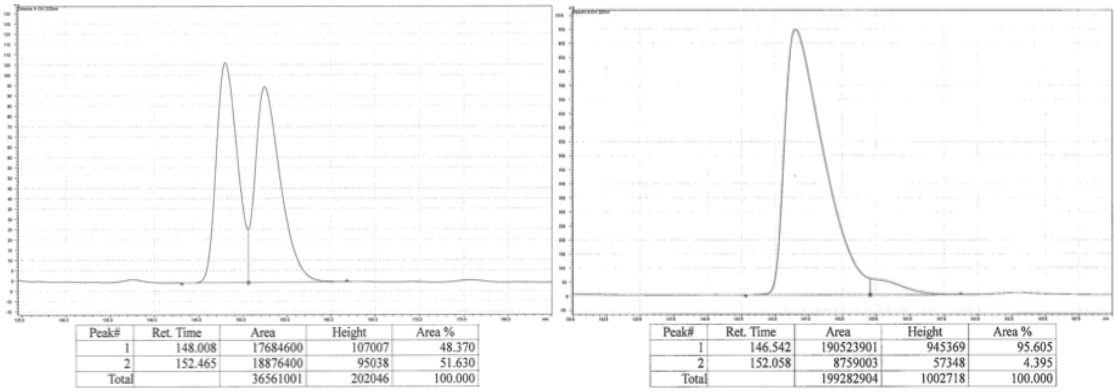

Peak #	Time (min)	Area (%)	Peak #	Time (min)	Area (%)
1	148.008	48.370	1	146.542	95.605
2	152.465	51.630	2	152.058	4.395

(*R*)-4,4,5,5-Tetramethyl-2-(4-methyl-2-phenylpent-4-en-1-yl)-1,3,2-dioxaborolane (1.32): Following the representative procedure except for 1:6 (0.1 mmol: 0.6 mmol) alkene:phosphate (**1.11**) used. IR (neat): 3028 (w), 2978 (m), 2929 (m), 1453 (w), 1369 (s), 1320 (m), 1145 (s), 968 (w), 888 (w), 699 (m) cm^{-1}; ^{1}H NMR (400 MHz, $CDCl_3$): δ 7.24–7.18 (4H, m), 7.13–7.10 (1H, m), 4.64 (1H, s), 4.56 (1H, s), 3.03 (1H, app pent, J = 7.7 Hz), 2.29 (2H, d, J = 7.6 Hz), 1.65 (3H, s), 1.24–1.16 (1H, m), 1.09–1.03 (13H, m); ^{13}C NMR (100 MHz, $CDCl_3$): δ 147.2, 144.3, 128.1, 127.5, 125.9, 112.4, 83.0, 48.3, 39.8, 24.83, 24.75, 22.5; HRMS (DART): Calcd for $C_{18}H_{28}B_1O_2$ $[M+H]^+$: 287.2182, Found: 287.2189; Specific Rotation: $[\alpha]_D^{20}$ +5.7 (c 0.33, $CHCl_3$) for an enantiomerically enriched sample of 90:10 er Enantiomeric purity was determined by HPLC analysis of the alcohol

product after oxidation in comparison with authentic racemic material (95:5 er shown; Chiralpak AD–H column, 99% hexanes, 1% *i*-PrOH, 0.3 mL/min, 220 nm).

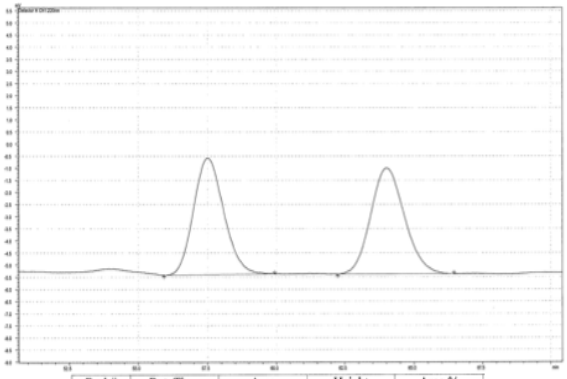

Peak#	Ret. Time	Area	Height	Area %
1	57.500	366961	4812	49.676
2	64.003	371750	4379	50.324
Total		738711	9191	100.000

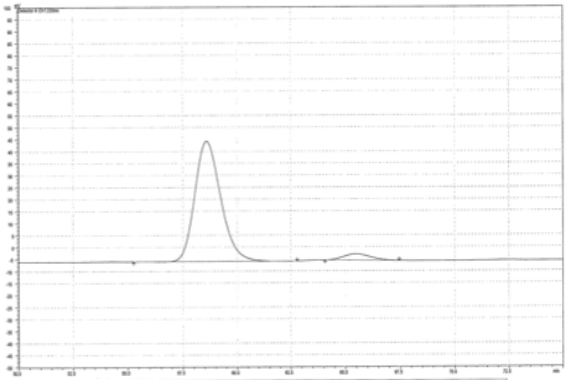

Peak#	Ret. Time	Area	Height	Area %
1	58.582	4158680	50182	94.890
2	65.442	223953	2661	5.110
Total		4382633	52843	100.000

Peak #	Time (min)	Area (%)	Peak #	Time (min)	Area (%)
1	57.500	49.676	1	58.582	94.890
2	64.003	50.324	2	65.442	5.110

(*R*)-Trimethyl(4-phenyl-5-(4,4,5,5-tetramethyl-1,3,2-dioxaborolan-2-yl)pent-1-en-2-yl)silane (1.33): IR (neat): 2978 (w), 2955 (w), 1368 (s), 1319 (m), 1247 (m), 1145 (s), 968 (w), 836 (s), 757 (m), 699 (m) cm^{-1}; ^{1}H NMR (400 MHz, $CDCl_3$): δ 7.25–7.18 (4H, m), 7.15–7.10 (1H, m), 5.45–5.44 (1H, m), 5.31 (1H, d, J = 3.2 Hz), 3.06–2.98 (1H, m), 2.49–2.35 (1H, m), 1.26–1.20 (1H, m), 1.09–1.01 (13H, m), 0.07 (9H, m); ^{13}C NMR (100 MHz, $CDCl_3$): δ 150.3, 147.4, 128.1, 127.7, 126.5, 125.8, 83.0, 45.9, 40.7, 24.9, 24.8, –1.2; HRMS (DART): Calcd for $C_{20}H_{34}B_1O_2Si_1$ $[M+H]^+$: 345.2421, Found: 345.2424. Specific Rotation: $[\alpha]_D^{20}$ +7.9 (*c* 0.33, $CHCl_3$) for an enantiomerically enriched sample of 95:5 er Enantiomeric purity was determined by HPLC analysis in comparison with authentic racemic material (96:4 er shown; Chiralcel OD–H column, 100% hexanes, 0.3 mL/min, 220 nm).

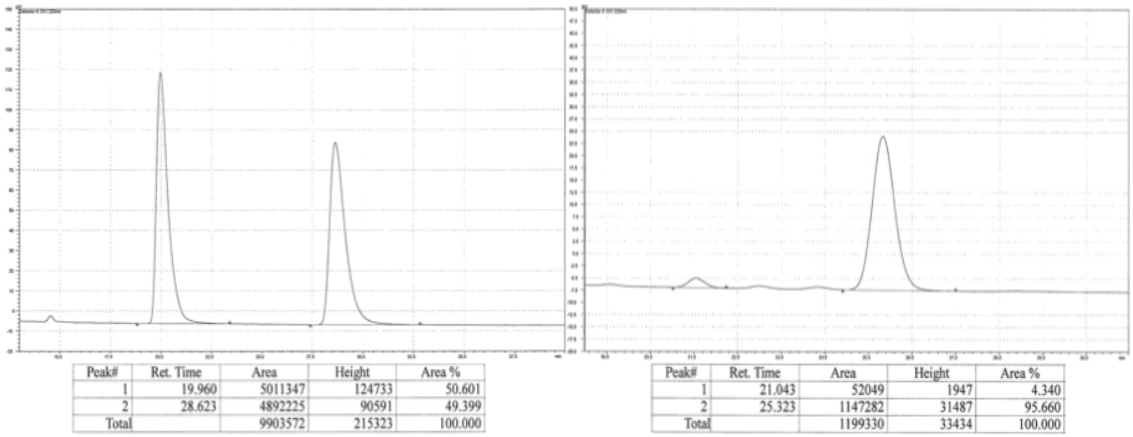

Peak #	Time (min)	Area (%)	Peak #	Time (min)	Area (%)
1	19.960	50.601	1	21.043	4.340
2	28.623	49.399	2	25.323	95.660

(*R*)-(4-(3-(Allyloxy)phenyl)-5-(4,4,5,5-tetramethyl-1,3,2-dioxaborolan-2-yl)pent-1-en-2-yl)trimethylsilane (1.34): IR (neat): 2977 (w), 2954 (w), 1600 (w), 1584 (w), 1366 (m), 1317 (m), 1247 (m), 1144 (s), 924 (m), 836 (s) cm^{-1}; ^{1}H NMR (500 MHz, $CDCl_3$): δ 7.14 (1H, t, *J* = 6.2 Hz), 6.80–6.77 (2H, m), 6.69 (1H, dd, *J* = 6.4, 2.0 Hz), 6.10–6.02 (1H, m), 5.45–5.38 (2H, m), 5.32–5.26 (2H, m), 4.52–4.51 (2H, m), 2.99 (1H, app pent, *J* = 6.1 Hz), 2.45 (1H, dd, *J* = 11.2, 6.0 Hz), 2.38 (1H, dd, *J* = 11.2, 6.0 Hz), 1.21 (1H, dd, *J* = 14.0, 3.6 Hz), 1.11 (6H, s), 1.09 (6H, s), 1.02 (1H, dd, *J* = 12.2, 7.0 Hz), 0.07 (9H, s); ^{13}C NMR (125 MHz, $CDCl_3$): δ 158.5, 150.3, 149.3, 133.8, 129.0, 126.5, 120.4, 117.5, 114.3, 112.1, 83.0, 68.8, 45.7, 40.7, 24.9, 24.8, –1.2; HRMS (DART): Calcd for $C_{23}H_{38}B_1O_3Si_1$ $[M+H]^+$: 401.2683, Found: 401.2695; Specific Rotation: $[\alpha]_D^{20}$ +4.7 (*c* 0.88, $CHCl_3$) for an enantiomerically enriched sample of 95:5 er Enantiomeric purity was determined by HPLC analysis in comparison with authentic racemic material (96:4 er shown; Chiralcel OD–H column, 100% hexanes, 0.3 mL/min, 220 nm).

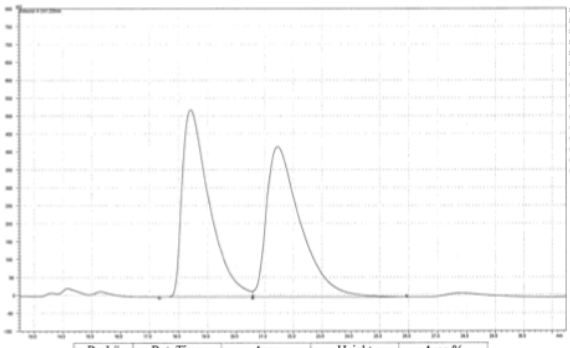

Peak#	Ret. Time	Area	Height	Area %
1	18.411	34022079	522332	49.710
2	21.443	34419427	419076	50.290
Total		68441506	941408	100.000

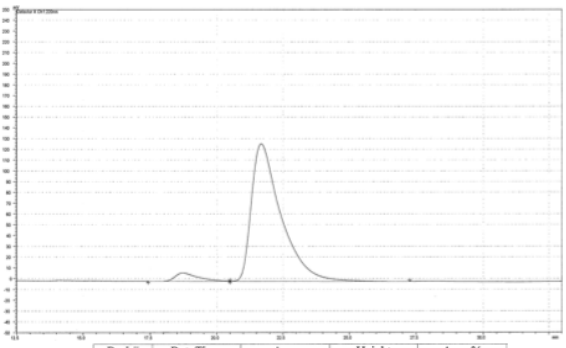

Peak#	Ret. Time	Area	Height	Area %
1	18.713	401900	7376	3.920
2	21.668	9850379	127553	96.080
Total		10252279	134930	100.000

Peak #	Time (min)	Area (%)	Peak #	Time (min)	Area (%)
1	18.411	49.710	1	18.713	3.920
2	21.443	50.290	2	21.668	96.080

(*R*)-2-(2-(2-Fluorophenyl)pent-4-en-1-yl)-4,4,5,5-tetramethyl-1,3,2-dioxaborolane (1.36): Following the representative procedure except **135** was used. IR (neat): 2978 (w), 2931 (w), 1765 (s), 1490 (m), 1401 (s), 1369 (s), 1223 (m), 1144 (s), 968 (m), 913 (m), 846 (m), 754 (s) cm^{-1}; ^{1}H NMR (400 MHz, $CDCl_3$): δ 7.21 (1H, td, *J* = 7.6, 1.6 Hz), 7.13–7.10 (1H, m), 7.09–7.02 (1H, m), 6.98–6.94 (1H, m), 5.68 (1H, ddt, *J* = 16.8, 10.4, 6.8 Hz), 4.97–4.90 (2H, m), 3.35–3.27 (1H, m), 2.43–2.32 (2H, m), 1.28–1.22 (1H, m), 1.19–1.08 (1H, m), 1.11 (6H, s), 1.08 (6H, s); ^{13}C NMR (100 MHz, $CDCl_3$): δ 160.9 (d, *J* = 243.7 Hz), 136.9, 133.5 (d, *J* = 14.4 Hz), 128.8 (d, *J* = 5.3 Hz), 127.3 (d, *J* = 8.4 Hz), 123.9 (d, *J* = 3.8 Hz), 116.4, 115.3 (d, *J* = 22.8 Hz), 83.1, 42.5, 34.3, 24.8, 24.7; HRMS (DART): Calcd for $C_{17}H_{25}B_1F_1O_2$ $[M+H]^+$: 291.1932, Found: 291.1937; Specific Rotation: $[\alpha]_D^{20}$ +14.2 (*c* 0.87, $CHCl_3$) for an enantiomerically enriched sample of 96:4 er Enantiomeric purity was determined by HPLC analysis in comparison with authentic racemic material (96:4 er shown; Chiralcel OD–H column, 100% hexanes, 0.3 mL/min, 220 nm).

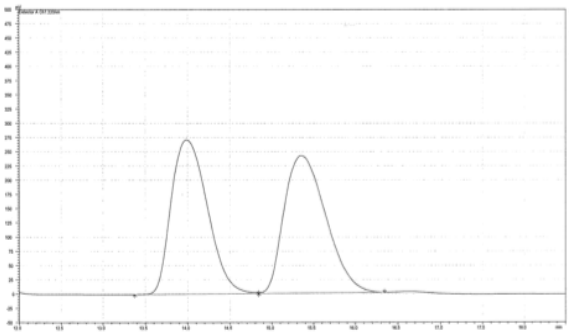

Peak#	Ret. Time	Area	Height	Area %
1	13.984	8054086	270865	48.955
2	15.351	8397818	241482	51.045
Total		16451904	512347	100.000

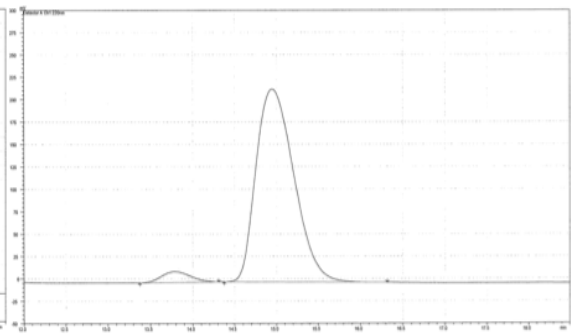

Peak#	Ret. Time	Area	Height	Area %
1	13.782	289017	12096	4.082
2	14.947	6790935	215149	95.918
Total		7079952	227246	100.000

Peak #	Time (min)	Area (%)	Peak #	Time (min)	Area (%)
1	13.984	48.955	1	13.782	4.082
2	15.351	51.045	2	14.947	95.918

***(R)*-2-(2-(4-Fluorophenyl)pent-4-en-1-yl)-4,4,5,5-tetramethyl-1,3,2-dioxaborolane (1.37):** Following the representative procedure except **1.35** was used. IR (neat): 2978 (w), 2925 (w), 2855 (w), 1604 (w), 1509 (s), 1369 (s), 1322 (m), 1223 (m), 1144 (s), 968 (w), 912 (w), 832 (m) cm^{-1}; ^{1}H NMR (400 MHz, $CDCl_3$): δ 7.17–7.13 (2H, m), 6.98–6.91 (2H, m), 5.65 (1H, ddt, *J* = 17.2, 10.0, 7.2 Hz), 4.96–4.91 (2H, m), 2.97–2.89 (1H, m), 2.36–2.27 (2H, m), 1.26–1.16 (1H, m), 1.09–1.04 (13H, m); ^{13}C NMR (100 MHz, $CDCl_3$): δ 161.4 (d, *J* = 241.3 Hz), 142.5 (d, *J* = 3.0 Hz), 137.0, 128.9 (d, *J* = 7.6 Hz), 116.4, 114.9 (d, *J* = 20.5 Hz), 83.2, 44.0, 40.8, 24.8, 24.7; HRMS (DART): Calcd for $C_{17}H_{25}B_1F_1O_2$ $[M+H]^+$: 291.1932, Found: 291.1939; Specific Rotation: $[\alpha]_D^{20}$ +14.9 (*c* 1.20, $CHCl_3$) for an enantiomerically enriched sample of 92:8 er Enantiomeric purity was determined by HPLC analysis in comparison with authentic racemic material (98:2 er shown; Chiralcel OZ–H column, 100% hexanes, 0.3 mL/min, 220 nm).

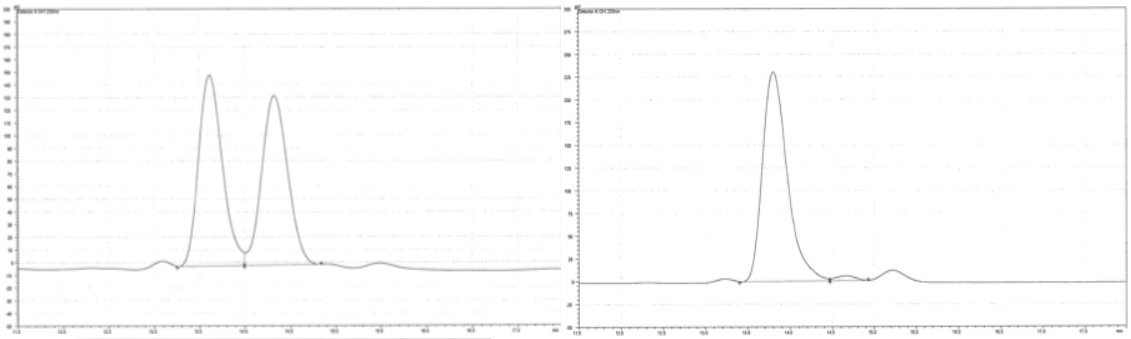

Peak#	Ret. Time	Area	Height	Area %
1	13.603	2742136	150222	50.944
2	14.313	2640469	133432	49.056
Total		5382605	283655	100.000

Peak#	Ret. Time	Area	Height	Area %
1	13.798	4698854	230536	98.211
2	14.657	85578	5325	1.789
Total		4784432	235861	100.000

Peak #	Time (min)	Area (%)	Peak #	Time (min)	Area (%)
1	13.603	50.944	1	13.798	98.211
2	14.313	49.056	2	14.657	1.789

1.5.4 Additional Examples of Single-Catalyzed Multicomponent Reaction

Scheme 1.24 Additional Substrates Scope

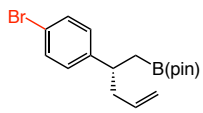

1.72
62% yield,
90:10 e.r.

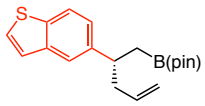

1.73
61% yield,
95:5 e.r.

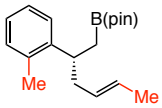

1.74
50 yield, >98% S_N2',
92:8 e.r. (*E* & *Z*)

(*R*)-2-(2-(4-Bromophenyl)pent-4-en-1-yl)-4,4,5,5-tetramethyl-1,3,2-dioxaborolane (1.72): Following the representative procedure except for 1:3 (0.1 mmol: 0.3 mmol) alkene:phosphate (**1.11**) used. IR (neat): 2977 (w), 2926 (w), 1488 (w), 1368 (s), 1320 (s), 1143 (s), 1073 (m), 1010 (m), 968 (m), 913 (m), 846 (m), 820 (m) cm^{-1}; ^1H NMR (400 MHz, $CDCl_3$): δ 7.37 (2H, d, J = 6.4, Hz), 7.07 (2H, d, J = 7.6 Hz), 5.63 (1H, ddt, 17.2, 10.0, 7.2 Hz), 4.97–4.91 (2H, m), 2.94–2.87 (1H, m), 2.32 (2H, t, J = 7.0 Hz), 1.21 (1H, dd, J = 15.4, 6.6 Hz), 1.12 (6H, s), 1.10 (6H, s), 1.09–1.03 (1H, m); ^{13}C NMR (100 MHz, $CDCl_3$): δ 145.9, 136.8, 131.2, 129.4, 119.6, 116.5, 83.2, 43.6, 41.0, 24.9, 24.8; HRMS

(DART): Calcd for $C_{17}H_{25}B_1Br_1O_2$ $[M+H]^+$: 351.1131, Found: 351.1141; Specific Rotation: $[\alpha]_D^{20}$ +4.1 (*c* 0.85, $CHCl_3$) for an enantiomerically enriched sample of 90:10 er Enantiomeric purity was determined by HPLC analysis in comparison with authentic racemic material (90:10 er shown; Chiralcel OZ–H column, 100% hexanes, 0.3 mL/min, 220 nm).

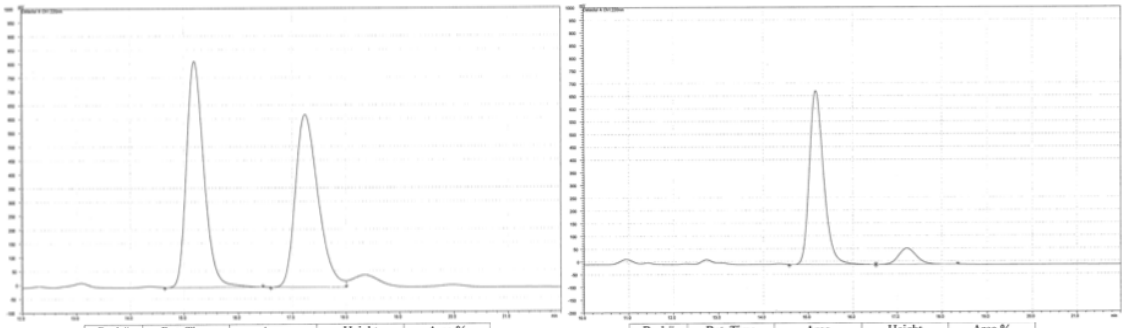

Peak#	Ret. Time	Area	Height	Area %
1	15.188	18344370	817276	49.869
2	17.236	18440831	624668	50.131
Total		36785201	1441944	100.000

Peak#	Ret. Time	Area	Height	Area %
1	15.166	15139095	683458	89.619
2	17.215	1753578	63872	10.381
Total		16892673	747330	100.000

Peak #	Time (min)	Area (%)	Peak #	Time (min)	Area (%)
1	15.188	49.869	1	15.166	89.619
2	17.236	50.131	2	17.215	10.381

(*R*)-2-(2-(Benzo[b]thiophen-5-yl)pent-4-en-1-yl)-4,4,5,5-tetramethyl-1,3,2-dioxaborolane (1.73): Following the representative procedure except for 1:3 (0.1 mmol: 0.3 mmol) alkene:phosphate (**1.11**) used. IR (neat): 3073 (w), 2976 (w), 2924 (w), 1365 (s), 1319 (s), 11142 (s), 846 (m), 820 (m), 699 (s) cm^{-1}; ^1H NMR ($CDCl_3$, 400 MHz): δ 7.76 (1H, d, *J* = 8.4 Hz), 7.65 (1H, s), 7.38 (1H, dd, *J* = 5.4, 0.6 Hz), 7.27 (1H, d, *J* = 5.2 Hz), 7.22 (1H, d, *J* = 8.4 Hz), 5.74–5.64 (1H, m), 4.97 (1H, d, *J* = 17.2 Hz), 4.92 (1H, dd *J* = 10.4, 0.8 Hz), 3.08 (1H, app pent, *J* = 7.5 Hz), 2.48–2.36 (2H, m), 1.30 (1H, dd, *J* = 15.8, 7.0 Hz), 1.17 (1H, dd, *J* = 15.4, 9.0 Hz), 1.07 (12H, s); ^{13}C NMR ($CDCl_3$, 100 MHz): δ 152.3, 140.0, 139.2, 136.4, 124.0, 123.4, 122.9, 122.3, 119.8, 116.9, 83.4, 43.8,

37.6, 24.9, 24.8; HRMS (DART): Calcd for $C_{19}H_{26}B_1O_2S_1$ $[M+H]^+$: 329.1747, Found: 329.1744; Specific Rotation: $[\alpha]_D^{20}$ +18.0 (*c* 1.23, $CHCl_3$) for an enantiomerically enriched sample of 95:5 er Enantiomeric purity was determined by HPLC analysis in comparison with authentic racemic material (95:5 er shown; Chiralcel OZ–H column, 100% hexanes, 0.3 mL/min, 220 nm).

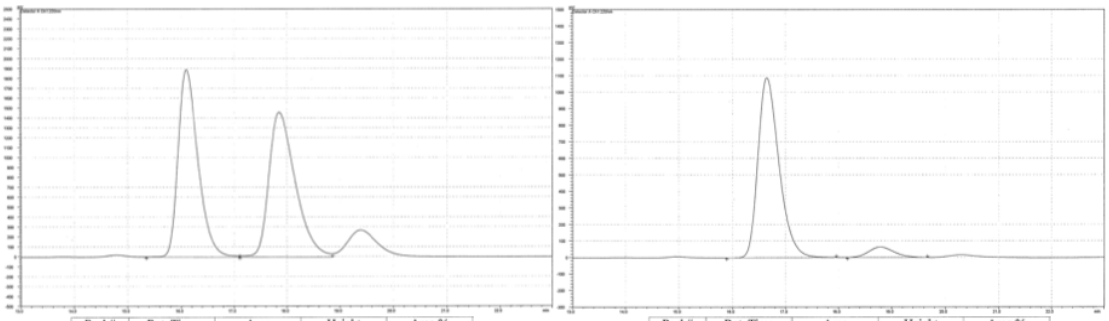

Peak#	Ret. Time	Area	Height	Area %
1	16.094	49552908	1892349	49.409
2	17.848	50738265	1463677	50.591
Total		100291173	3356026	100.000

Peak#	Ret. Time	Area	Height	Area %
1	16.643	30009118	1088972	94.738
2	18.783	1666797	56629	5.262
Total		31675915	1145601	100.000

Peak #	Time (min)	Area (%)	Peak #	Time (min)	Area (%)
1	16.094	49.409	1	16.643	94.738
2	17.848	50.591	2	18.783	5.262

(*R*)-4,4,5,5-Tetramethyl-2-(2-(*o*-tolyl)hex-4-en-1-yl)-1,3,2-dioxaborolane (1.74): Following the representative procedure except **L3b** was used. The spectroscopic data match those reported previously.[5] ^{1}H NMR (400 MHz, $CDCl_3$): δ 7.26–7.01 (8H, m, *E*/*Z*), 5.46–5.28 (4H, m, *E*/*Z*), 3.24–3.13 (2H, m, *E*/*Z*), 2.36 (3H, s, *E*) 2.35 (3H, s, *Z*), 2.32–2.13 (4H, m, *E*/*Z*), 1.59 (3H, d, *J* = 5.6 Hz, *E*), 1.54 (3H, d, *J* = 6 Hz, *Z*), 1.23–1.10 (4H, m, *E*/*Z*), 1.053 (6H, s, *E*), 1.045 (6H, s, *E*), 1.03 (6H, s, *Z*), 1.02 (6H, s, *Z*) Specific Rotation: $[\alpha]_D^{20}$ +6.1 (*c* 0.45, $CHCl_3$) for an enantiomerically enriched sample of 92:8 er Enantiomeric purity was determined by HPLC analysis of the alcohol product after oxidation in comparison with authentic racemic material prepared according to the

procedure reported previously obtaining ***rac-E*-1.74**.[30] (92:8 er shown for *E* and *Z*; Chiralcel OJ–H column, 98% hexanes, 0.3 mL/min, 220 nm).

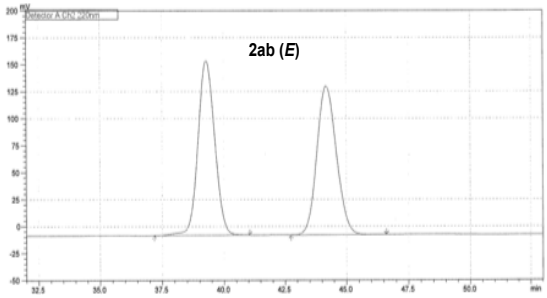

Peak#	Ret. Time	Area	Height	Area%
1	39.289	7684209	162000	50.239
2	44.190	7611006	137735	49.761
Total		15295214	299735	100.000

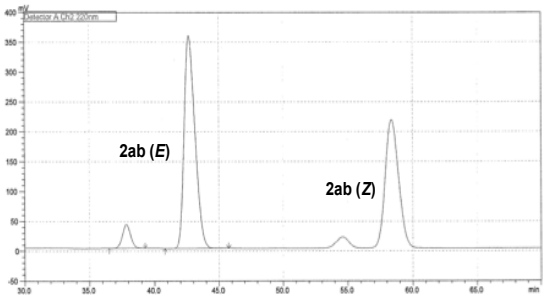

Peak#	Ret. Time	Area	Height	Area%
1	37.848	1739929	39964	7.697
2	42.673	20865572	356691	92.303
Total		22605501	396655	100.000

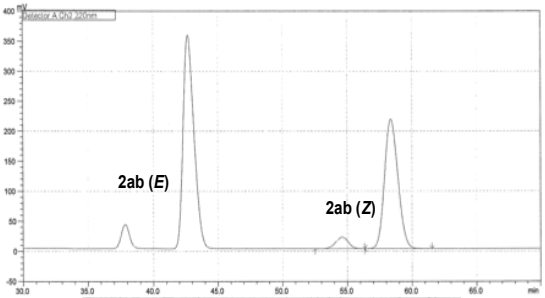

Peak#	Ret. Time	Area	Height	Area%
1	54.599	1289796	18912	7.644
2	58.361	15584373	215457	92.356
Total		16874169	234370	100.000

Peak #	Time (min)	Area (%)	Peak #	Time (min)	Area (%)
1 (*rac*)	39.389	50.239	1 (*E*)	37.848	7.697
2 (*rac*)	44.190	49.761	2 (*E*)	42.673	92.303
			1 (*Z*)	54.599	7.644
			2 (*Z*)	58.361	92.356

1.5.5 Formal Synthesis of (+)-Heliespirone A and (–)-Heliespirone C

Scheme 1.25 Application to Enantioselective Synthesis of Heliespirone A and C

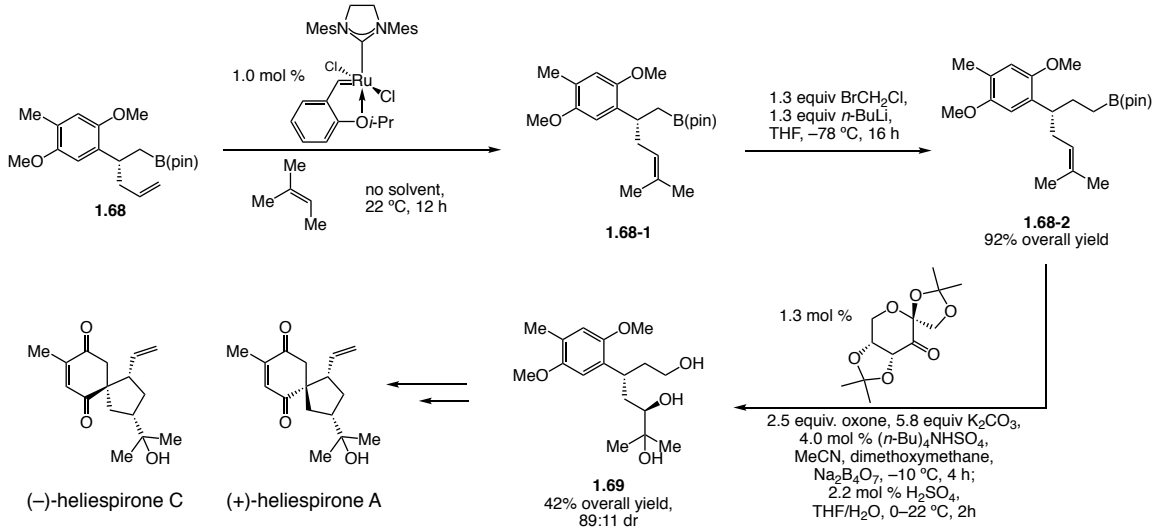

(*R*)-2-(2-(2,5-Dimethoxy-4-methylphenyl)pent-4-en-1-yl)-4,4,5,5-tetramethyl-1,3,2-dioxaborolane (1.68): In a N_2-filled glove box, a flame-dried 100 mL round-bottom flask equipped with a stir bar was charged with bisphosphine **L3b** (188 mg, 0.28 mmol), NaO*t*-Bu (742 mg, 7.7 mmol), and CuCl (26 mg, 0.26 mmol). The flask was sealed with a septum and electrical tape before removal from the glove box. Tetrahydrofuran (20 mL) was added and the resulting yellow solution was allowed to stir for 1 h under N_2 at 22 °C. A solution of $B_2(pin)_2$ (1.4 g, 5.7 mmol) in thf (15 mL) was added to the mixture at 0 °C, causing the solution to turn dark brown immediately. After 15 min, a solution of **13** (2.75 g, 15.5 mmol) in thf (5 mL) and allylphosphate (**1.11**) [0.92 mL (1.0 g), 5.15 mmol] was added by syringe. The resulting mixture was allowed to stir at 22 °C for 18 h. Then, the mixture was passed through a short plug of silica gel (4x4 cm) and eluted with Et_2O. The organic layer was concentrated under reduced pressure, affording yellow oil, which was purified by silica gel chromatography (100% hexanes→hexanes:Et_2O = 10:1) to afford **1.68** as colorless oil (1.1 g, 3.3 mmol, 64% yield) and recovered **1.67** (1.68 g, 9.4 mmol,

91%). IR (neat): 2976 (w), 2931 (w), 2830 (w), 1506 (m), 1465 (m), 1398 (m), 1369 (m), 1316 (m), 1207 (s), 1143 (s), 1046 (s), 968 (m), 846 (m), 802 (m) cm^{-1}; ^{1}H NMR (400 MHz, $CDCl_3$): δ 6.68 (1H, s), 6.64 (1H, s), 5.71 (1H, ddt, *J* = 17.2, 9.8, 7.4 Hz), 4.98–4.89 (2H, m), 3.78 (3H, s), 3.76 (3H, s), 3.36 (1H, app pent, *J* = 7.5 Hz), 2.43–2.25 (2H, m), 2.18 (3H, s), 1.22 (1H, dd, *J* = 15.6, 7.6 Hz), 1.15–1.10 (1H, m), 1.13 (6H, s), 1.10 (6H, s); ^{13}C NMR (100 MHz, $CDCl_3$): δ 151.7, 151.0, 137.8, 133.2, 124.2, 115.7, 114.4, 110.9, 82.9, 56.5, 56.2, 42.3, 34.2, 24.84, 24.81, 16.2; HRMS (DART): Calcd for $C_{20}H_{32}B_1O_4$ $[M+H]^+$: 347.2394, Found: 347.2377; Specific Rotation: $[\alpha]_D^{20}$ +36.6 (*c* 0.56, $CHCl_3$) for an enantiomerically enriched sample of 97:3 er Enantiomeric purity was determined by HPLC analysis of the alcohol product after oxidation in comparison with authentic racemic material (97:3 er shown; Chiralpak AD–H column, 99% hexanes, 1% *i*-PrOH, 0.3 mL/min, 220 nm).

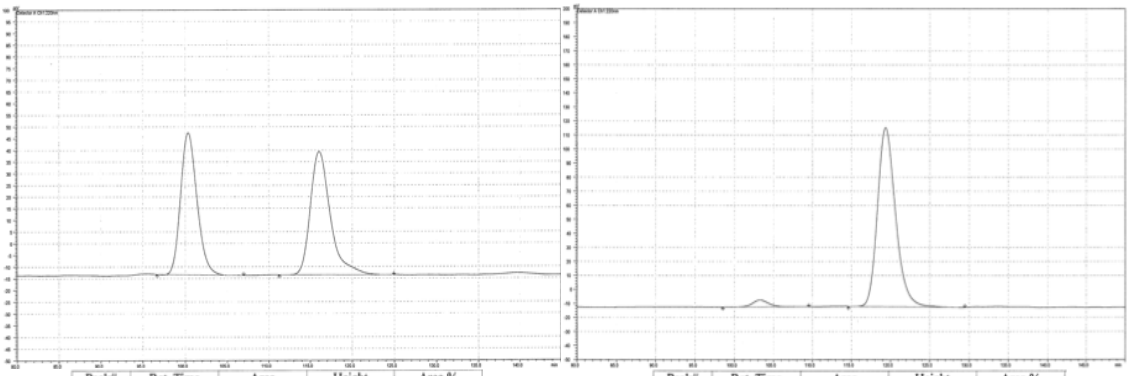

Peak#	Ret. Time	Area	Height	Area %
1	100.356	8464114	61183	49.107
2	116.048	8771942	52918	50.893
Total		17236056	114101	100.000

Peak#	Ret. Time	Area	Height	Area %
1	103.251	722520	4990	3.364
2	119.350	20758481	127762	96.636
Total		21481001	132752	100.000

Peak #	Time (min)	Area (%)	Peak #	Time (min)	Area (%)
1	100.356	49.107	1	103.251	3.364
2	116.048	50.893	2	119.350	96.636

(*R*)-2-(3-(2,5-Dimethoxy-4-methylphenyl)-6-methylhept-5-en-1-yl)-4,4,5,5-tetramethyl-1,3,2-dioxaborolane (1.68-2): Compound **1.68** was converted to **1.68-2** by

a two-step sequence olefin cross metathesis/homologation based on the reported procedures except Hoveyda-Grubbs catalyst 2nd generation was used in the cross metathesis.[40] IR (neat): 2977 (w), 2931 (w), 2854 (w), 1504 (m), 1466 (m), 1398 (m), 1372 (m), 1317 (m), 1208 (s), 1145 (m), 1049 (m), 968 (w) cm^{-1}; ^1H NMR (400 MHz, $CDCl_3$): δ 6.65 (1H, s), 6.62 (1H, s), 5.09–5.06 (1H, m), 3.77 (3H, s), 3.73 (3H, s), 3.02 (1H, app pent, *J* = 7.2 Hz), 2.35–2.19 (2H, m), 1.81 (3H, s), 1.80–1.70 (1H, m), 1.68–1.56 (4H, m), 1.54 (3H, s), 1.21 (12H, s), 0.74–0.60 (2H, m); ^{13}C NMR (100 MHz, $CDCl_3$): δ 151.9, 151.7, 132.1, 131.7, 124.2, 123.6, 114.5, 110.7, 82.9, 56.6, 56.2, 40.5, 33.8, 29.3, 25.9, 25.0, 24.9, 17.9, 16.2; HRMS (DART): Calcd for $C_{23}H_{38}B_1O_4$ $[M+H]^+$: 389.2863, Found: 389.2862; Specific Rotation: $[\alpha]_D^{20}$ +18.0 (*c* 0.50, $CHCl_3$).

(3*R*,5*R*)-3-(2,5-Dimethoxy-4-methylphenyl)-6-methylheptane-1,5,6-triol (1.69): Compound **1.68-2** was converted to **1.69** by a two step sequence enantioselective epoxidation/hydrolysis based on the reported procedures except the oxidation was performed with 2.5 equiv of oxone.[41] The spectroscopic data match those reported previously.[42] ^1H NMR (400 MHz, $CDCl_3$): δ 6.72 (1H, s), 6.66 (1H, s), 3.80 (3H, s), 3.79 (3H, s), 3.58–3.53 (2H, m), 3.46–3.35 (2H, m), 2.20 (3H, s), 2.12–2.01 (1H, m), 1.88–1.84 (1H, m), 1.74–1.59 (2H, m), 1.21 (3H, s), 1.15 (3H, s); HRMS (DART): Calcd for $C_{17}H_{28}O_5$ $[M]^+$: 312.1937, Found: 312.1939. Specific Rotation: $[\alpha]_D^{20}$ +23.4 (*c* 0.23, $CHCl_3$). Literature precedence: $[\alpha]_D^{13}$ +29.2(*c* 0.10, CH_2Cl_2).[42]

---

(40) For cross-metathesis see: Chatterjee, A. K.; Sanders, D. P.; Grubbs, R. H. *Org. Lett.* **2002,** *4,* 1939–1942. For homologation see: Kliman, L. T.; Mlynarski, S. N.; Morken, J. P. *J. Am. Chem. Soc.* **2009,** *131,* 13210–13211.

(41) Wang, Z.-X.; Tu, Y.; Frohn, M.; Zhang, J.-R.; Shi, Y. *J. Am. Chem. Soc.* **1997,** *119,* 11224–11235.

(42) Huang, C.; Liu, B. *Chem. Commun.* **2010,** *46,* 5280–5282.

1.5.6 Additional Studies Regarding the Effect of Concentration Changes on Enantioselectivity

Scheme 1.26. Additional Studies Regarding the Effect of Aryl Olefin or Allyl Electrophile Concentration on Enantioselectivity

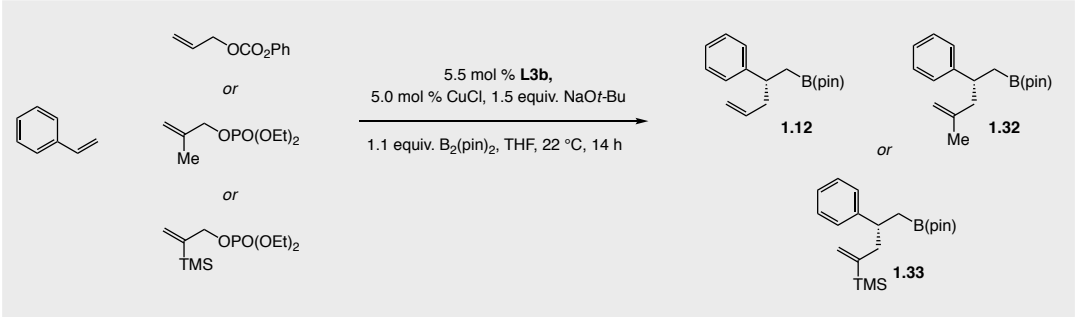

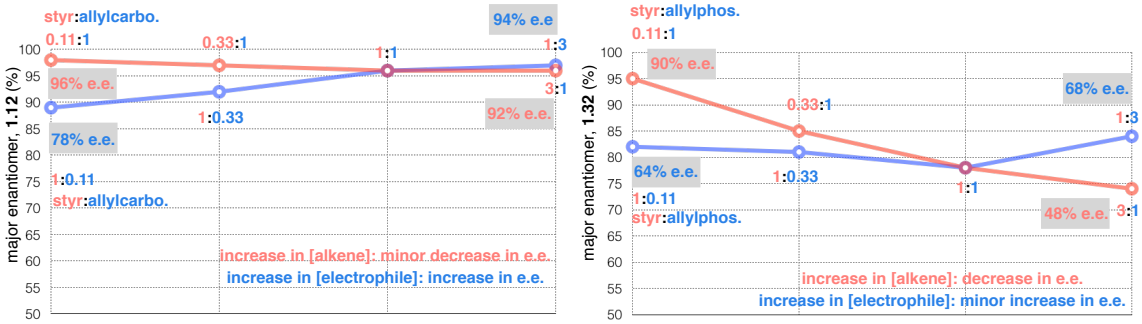

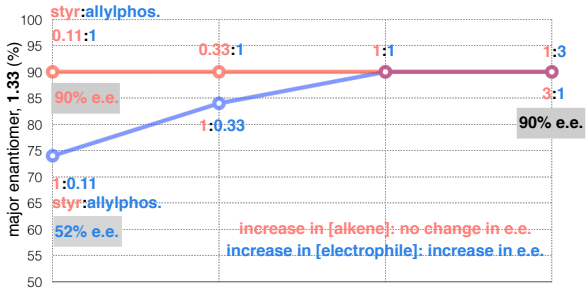

1.5.7 Study of the Possibility of Epimerization through Isotopic Labeling

Scheme 1.27. Synthesis of *E* and *Z* Deuterium-Labeled Aryl Olefins

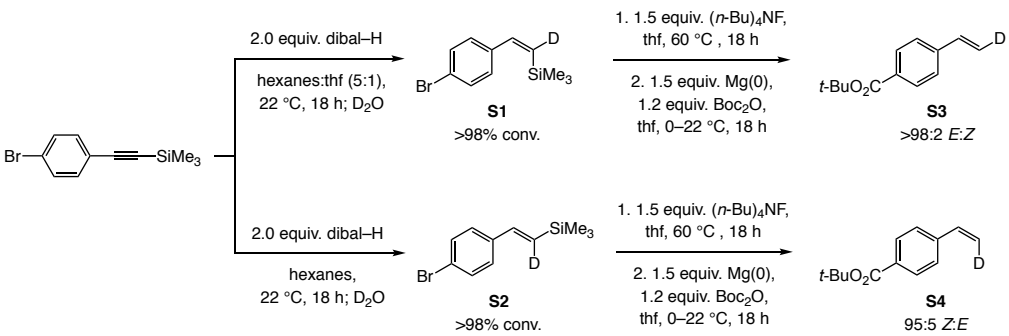

(*Z*)-(2-(4-Bromophenyl)vinyl-1-*d*)trimethylsilane (S1): To a flame-dried round bottom flask equipped with a stir bar was added hexanes (20 mL) under N_2, after which dibal–H (8.6 mL, 48 mmol, USE WITH CAUTION, PYROPHORIC) was added by a gas-tight syringe. The resulting mixture was allowed to cool to 0 °C, and a solution of trimethyl(4-bromophenylethynyl)silane (6.1 g, 24 mmol) in thf (4 mL) was added drop-wise by syringe. The mixture was allowed to stir for an additional 5 min at 0 °C and then warmed to 22 °C and allowed to stir for 23 h. The reaction was then quenched upon drop-wise addition of D_2O (1.2 mL, 72 mmol) at 0 °C and allowed to stir for 1 h at 22 °C. The mixture was transferred to a separatory funnel and Rochelle's salt (50 mL) and a saturated solution of aqueous ammonium chloride (40 mL) were added. The layers were separated, and the aqueous layer was washed with Et_2O (3 x 20 mL). The combined organic layers were dried over Na_2SO_4 and concentrated in vacuo. The resulting yellow oil was purified by silica gel chromatography (100% pentane) and Kugelrohr distillation to afford **S1**.

(*E*)-(2-(4-Bromophenyl)vinyl-1-*d*)trimethylsilane (S2): This compound was prepared similarly to **S1**, except 100% hexanes (24 mL) was used instead of using 16.7% thf.

***tert*-Butyl-(*E*)-4-(vinyl-2-*d*)benzoate (S3):** To a solution of **S1** in thf (15 mL) was added $(n\text{Bu})_4\text{NF}$ (1.0 M in thf, 8.25 mL, 8.25 mmol) at 22 °C under N_2. The mixture was allowed to stir at 60 °C for 18 hours after which it was transferred to a separatory funnel; water (25 mL) was added and the layers separated. The aqueous layer was washed with Et_2O (3x20 mL). The combined organic layers were dried over $MgSO_4$ and concentrated under reduced pressure. The resulting yellow oil was purified by Kugelrohr distillation to afford **(*E*)-1-Bromo-4-(vinyl-2-*d*)benzene** which was converted to **S3** following the

previously reported procedure.[33] The resulting colorless oil was purified by silica gel chromatography and Kugelrohr distillation to afford **S3** as colorless liquid (200 mg, >98% D, >98% *E*). IR (neat): 2979 (w), 1709 (s), 1608 (w), 1393 (m), 1291 (s), 1162 (s), 1112 (s), 1066 (s), 1067 (m), 865 (s), 771 (s), 702 (m) cm^{-1}; ^{1}H NMR ($CDCl_3$, 400 MHz): δ 7.97–7.94 (2H, m), 7.43 (2H, d, *J* = 8.4 Hz), 6.74 (1H, d, *J* = 17.6 Hz), 5.82 (1H, d, *J* = 17.6 Hz), 1.60 (9H, s); ^{13}C NMR ($CDCl_3$, 100 MHz): δ 165.6, 141.5, 136.1, 131.3, 129.8, 127.2, 126.0, 121.4, 115.9 (t, *J* = 24.3 Hz), 81.0, 28.3; HRMS (DART): Calcd for $C_{13}H_{16}DO_2$ $[M+H]^+$: 206.1291; Found: 206.1300.

***tert*-Butyl-(*Z*)-4-(vinyl-2-*d*)benzoate (S4):** To a solution of **S2** in thf (15 mL) was added $(nBu)_4NF$ (1.0 M in thf, 8.25 mL, 8.25 mmol) at 22 °C under N_2. The mixture was allowed to stir at 60 °C for 18 h after which it was transferred to a separatory funnel, water (25 mL) was added and the layers separated. The aqueous layer was washed with Et_2O (3x20 mL). The combined organic layers were dried over $MgSO_4$ and concentrated under reduced pressure. The resulting yellow oil was purified by Kugelrohr distillation to afford **(*Z*)-1-Bromo-4-(vinyl-2-*d*)benzene** which was converted to **S4** following the previously reported procedure.[33] The product was purified by silica gel chromatography and Kugelrohr distillation to afford **S4** as colorless liquid (199.4 mg, >98%D, 95:5 *Z*:*E)*. IR (neat): 2977 (w), 1707 (s), 1607 (w), 1367 (m), 1287 (s), 1161 (s), 1104 (s), 1016 (m), 848 (s), 774 (s), 706 (s), 438 (w) cm^{-1}; ^{1}H NMR ($CDCl_3$, 400 MHz): δ 7.94 (2H, d, *J*= 8.4 Hz), 7.43 (2H, d, *J* = 8.4 Hz), 6.75–6.79 (1H, m), 5.35 (1H, *J* = 10.4 Hz), 1.60 (9H, s); ^{13}C NMR ($CDCl_3$, 100 MHz): δ 165.7, 141.5, 136.2, 131.3, 129.8, 126.1, 116.0 (t, *J* = 23.5 Hz), 81.0, 28.3 HRMS (DART): Calcd for $C_{13}H_{16}DO_2$ $[M+H]^+$: 206.1291; Found: 206.1293

tert*-Butyl-4-((1*S*,2*R*)-1-(4,4,5,5-tetramethyl-1,3,2-dioxaborolan-2-yl)pent-4-en-2-yl-1-*d*)benzoate (1.26-*d from S3*):** Following the representative procedure except **L3b** and 1:3 alkene:phosphate (**1.11**) used, **1.26-*d was obtained as colorless oil (60:40 dr, determined from ^{1}H NMR of the product after oxidation). IR (neat): 2977 (w), 2929 (w), 1711 (s), 1609 (w), 1391 (m), 1364 (s), 1312 (s), 1288 (s), 1255 (m), 1164 (s), 1143 (s), 1112 (s), 850 (m) cm^{-1}; ^{1}H NMR ($CDCl_3$, 400 MHz): δ 7.88 (2H, d, *J* = 8.0 Hz), 7.24 (2H, d, *J* = 8.0 Hz), 5.63 (1H, ddt, *J* = 17.2, 10.4, 6.8 Hz), 4.96–4.90 (2H, m), 2.99 (1H, app q, *J* = 7.2 Hz), 2.35 (2H, t, *J* = 7.0 Hz), 1.58 (9H, s), 1.22 (1H, br s), 1.12 (6H, s), 1.11 (2.46H, s, minor), 1.10 (3.54H, s, major); ^{13}C NMR ($CDCl_3$, 150 MHz): δ 166.1, 151.95 (minor), 151.93 (major), 136.8, 129.8, 129.5, 127.4, 116.5, 83.2, 80.8, 43.51 (major), 43.48 (minor), 41.4, 28.4, 24.9, 24.80 (minor), 24.79 (major); HRMS (DART): Calcd for $C_{22}H_{33}D_1B_1O_4$ $[M+H]^+$: 374.2613; Found: 374.2620.

tert*-Butyl-4-((1*R*,2*R*)-1-(4,4,5,5-tetramethyl-1,3,2-dioxaborolan-2-yl)pent-4-en-2-yl-1-*d*)benzoate (1.26-*d from S4*):** Following the representative procedure except **L3b** and 1:3 alkene:phosphate (**1.11**) used, **1.26-*d was obtained as colorless oil (35:65 dr, determined from ^{1}H NMR of the product after oxidation). IR (neat): 2977 (w), 2929 (w), 1711 (s), 1609 (w), 1391 (m), 1364 (s), 1312 (s), 1288 (s), 1255 (m), 1164 (s), 1143 (s), 1112 (s), 850 (s) cm^{-1}; ^{1}H NMR ($CDCl_3$, 400 MHz): δ 7.88 (2H, d, *J* = 8.0 Hz), 7.24 (2H, d, *J* = 8.0 Hz), 5.63 (1H, ddt, *J* = 17.2, 10.4, 6.8 Hz), 4.96–4.90 (2H, m), 2.99 (1H, app q, *J* = 7.5 Hz), 2.35 (2H, t, *J* = 7.0 Hz), 1.58 (9H, s), 1.22 (1H, br s), 1.12 (6H, s), 1.11 (3.76H, s, major), 1.10 (2.24H, s, minor); ^{13}C NMR ($CDCl_3$, 150 MHz): δ 166.1, 151.95 (major), 151.93 (minor), 136.8, 129.8, 129.5, 127.4, 116.5, 83.2, 80.8, 43.51 (minor), 43.48 (major), 41.4, 28.4, 24.9, 24.80 (major), 24.79 (minor); HRMS (DART): Calcd for

$C_{22}H_{33}D_1B_1O_4$ $[M+H]^+$: 374.2613; Found: 374.2620.

***tert*-Butyl-(*E*)-3-(vinyl-2-*d*)benzoate (substrate for synthesis of *anti*-1.24-*d*):** Following the procedure for preparation of **S3** except trimethyl(3-bromophenylethynyl)silane was used. The product was obtained as >98:2 *E*:*Z*. IR (neat): 2977 (w), 1710 (s), 1367 (m), 1297 (s), 1254 (m), 1157 (s), 1079 (m), 1036 (m), 999 (m), 883 (m), 785 (w), 753 (s), 408 (w) cm^{-1}; ^1H NMR (400 MHz, $CDCl_3$): δ 8.02 (1H, s), 7.87 (1H, dt, *J* = 7.6, 1.2 Hz), 7.56–7.55 (1H, m), 7.35 (1H, t, *J* = 7.2 Hz), 6.75 (1H, d, *J* = 17.6 Hz), 5.80 (1H, d, *J* = 17.6 Hz), 1.60 (9H, s); ^{13}C NMR (100 MHz, $CDCl_3$): δ 165.7, 137.7, 136.1, 132.4, 130.1, 128.8, 128.5, 127.3, 114.7 (t, *J* = 24.3 Hz), 81.1, 28.3; HRMS (DART): Calcd for $C_{13}H_{16}D_1O_2$ $[M+H]^+$: 206.1291, Found: 206.1297.

***tert*-Butyl-(*Z*)-3-(vinyl-2-*d*)benzoate (substrate for synthesis of *syn*-1.24-*d*):** Following the procedure for preparation of **S4** except trimethyl(3-bromophenylethynyl)silane was used. The product was obtained as 90:10 *Z*:*E*. IR (neat): 2977 (w), 1711 (s), 1367 (m), 1291 (s), 1277 (s), 1156 (s), 1109 (m), 1082 (m), 848 (m), 818 (m), 755 (m), 697 (m), 406 (w) cm^{-1}; ^1H NMR (400 MHz, $CDCl_3$): δ 8.03 (1H, t, *J* = 2 Hz), 7.88 (1H, dt, *J* = 7.6, 1.6 Hz), 7.57–7.55 (1H, m), 7.37 (1H, t, *J* = 7.6 Hz), 6.74 (1H, dt, *J* = 10.8, 2.4 Hz), 5.29 (1H, d, *J* = 10.8 Hz), 1.61 (9H, s); ^{13}C NMR (100 MHz, $CDCl_3$): δ 165.7, 137.7, 136.1, 132.4, 130.1, 128.7, 128.5, 127.3, 114.6 (t, *J* = 23.5 Hz), 81.1, 28.2; HRMS (DART): Calcd for $C_{13}H_{16}D_1O_2$ $[M+H]^+$: 206.1291, Found: 206.1302.

***tert*-Butyl-3-((1*S*,2*R*)-1-(4,4,5,5-tetramethyl-1,3,2-dioxaborolan-2-yl)pent-4-en-2-yl-1-*d*)benzoate (*anti*-1.24-*d*):** IR (neat): 2977 (m), 2927 (w), 1713 (s), 1479 (w), 1366 (s), 1316 (s), 1295 (s), 1161 (s), 1145 (s), 1111 (m), 755 (m), 697 (w) cm^{-1}; ^1H NMR (400 MHz, $CDCl_3$): δ 7.83 (1H, t, *J* = 1.8 Hz), 7.78 (1H, dt, *J* = 8.0, 1.2 Hz), 7.37 (1H, dt, *J* =

7.6, 1.2 Hz), 7.30 (1H, t, *J* = 7.6 Hz), 5.66 (1H, ddt, *J* = 17.0, 10.0, 7.2 Hz), 4.99–4.90 (2H, m), 2.99 (1H, q, *J* = 7.2 Hz), 2.44–2.32 (2H, m), 1.59 (9H, s), 1.22 (1H, d, *J* = 7.6 Hz), 1.11 (6H, s), 1.10 (6H, s); ^{13}C NMR (100 MHz, $CDCl_3$): δ 166.2, 147.1, 137.0, 131.9, 131.6, 128.8, 128.1, 127.2, 116.4, 83.2, 80.9, 43.4, 41.3, 28.4, 24.9, 24.8; HRMS (DART): Calcd for $C_{22}H_{33}D_1B_1O_4$ $[M+H]^+$: 374.2613, Found: 374.2614. Enantiomeric purity was determined by HPLC analysis in comparison with authentic racemic material (87:13 er shown; Chiralcel OZ–H column, 100% hexanes, 0.3 mL/min, 220 nm).

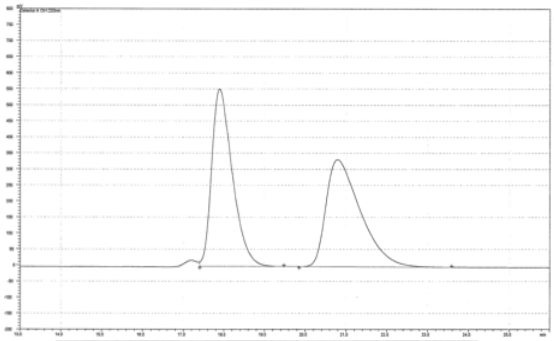

Peak#	Ret. Time	Area	Height	Area %
1	17.885	19631455	553324	50.079
2	20.783	19569298	334519	49.921
Total		39200753	887842	100.000

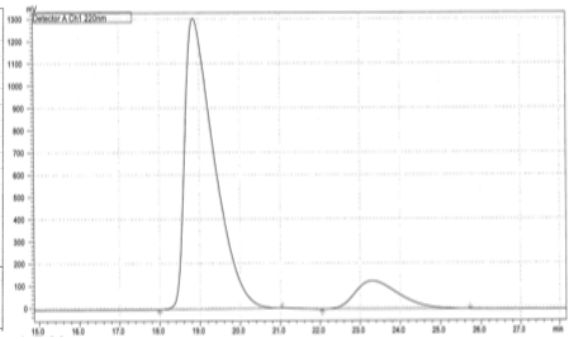

Peak#	Ret. Time	Area	Height	Conc.	Area%
1	18.855	66108118	1308800	87.254	87.254
2	23.306	9656871	126997	12.746	12.746
Total		75764989	1435797		100.000

Peak #	Time (min)	Area (%)	Peak #	Time (min)	Area (%)
1	17.885	50.079	1	18.855	87.254
2	20.783	49.921	2	23.306	12.746

***tert*-Butyl-3-((1*R*,2*R*)-1-(4,4,5,5-tetramethyl-1,3,2-dioxaborolan-2-yl)pent-4-en-2-yl-1-*d*)benzoate (*syn*-1.24-*d*):** IR (neat): 2977 (m), 2927 (w), 1713 (s), 1479 (w), 1366 (s), 1316 (s), 1295 (s), 1161 (s), 1145 (s), 1111 (m), 755 (m), 697 (w) cm^{-1}; ^{1}H NMR (400 MHz, $CDCl_3$): δ 7.83 (1H, t, *J* = 1.6 Hz), 7.78 (1H, dt, *J* = 7.6, 1.2 Hz), 7.37 (1H, dt, *J* = 8, 1.6 Hz), 7.30 (1H, t, *J* = 7.6 Hz), 5.66 (1H, ddt, *J* = 17.0, 10.0, 7.2 Hz), 4.99–4.91 (2H, m), 2.99 (1H, q, *J* = 7.2 Hz), 2.44–2.32 (2H, m), 1.59 (9H, s), 1.11 (6H, s), 1.10 (6H, s), 1.07 (1H, d, *J* = 9.2 Hz); ^{13}C NMR (100 MHz, $CDCl_3$): δ 166.2, 147.1, 137.0, 131.9,

131.6, 128.8, 128.1, 127.2, 116.5, 83.2, 80.9, 43.4, 41.3, 28.4, 24.9, 24.8; HRMS (DART): Calcd for $C_{22}H_{33}D_1B_1O_4$ $[M+H]^+$: 374.2613, Found: 374.2614. Enantiomeric purity was determined by HPLC analysis in comparison with authentic racemic material (87:13 er shown; Chiralcel OZ–H column, 100% hexanes, 0.3 mL/min, 220 nm).

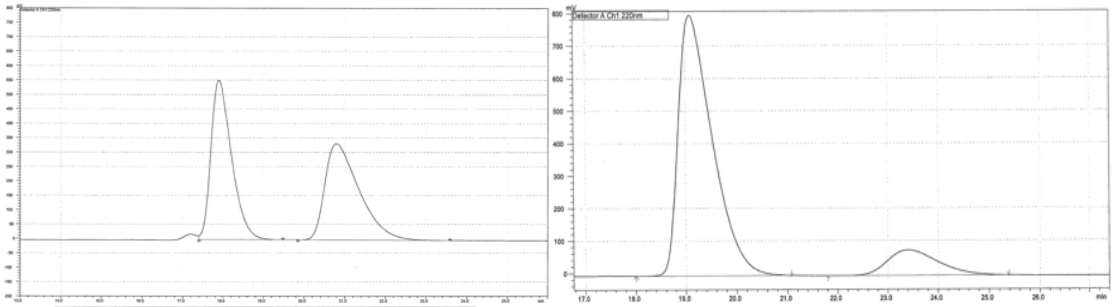

Peak#	Ret. Time	Area	Height	Area %
1	17.885	19631455	553324	50.079
2	20.783	19569298	334519	49.921
Total		39200753	887842	100.000

Peak#	Ret. Time	Area	Height	Conc.	Area%
1	19.082	37431307	801554	87.184	87.184
2	23.406	5502265	78389	12.816	12.816
Total		42933572	879943		100.000

Peak #	Time (min)	Area (%)	Peak #	Time (min)	Area (%)
1	17.885	50.079	1	19.082	87.184
2	20.783	49.921	2	23.406	12.816

Scheme 1.28. Synthesis of *E* and *Z* Deuterium-Labeled Aryl Olefins

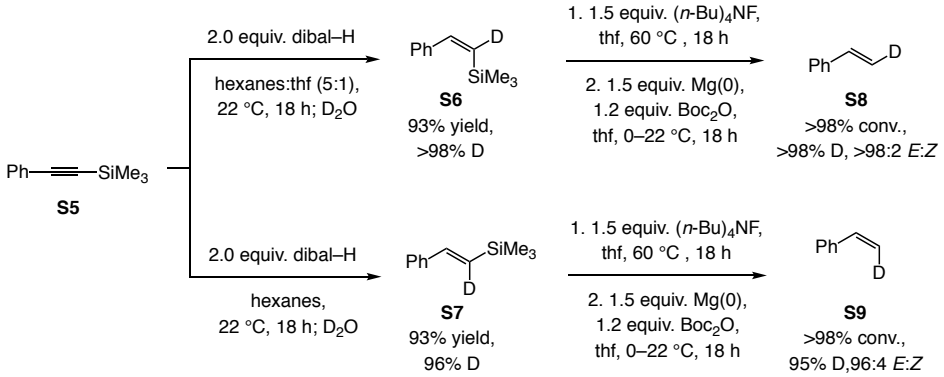

(*Z*)-Trimethyl(2-phenylvinyl-1-*d*)silane (S6): To a flame-dried round bottom flask equipped with a stir bar was added hexanes (20 mL) and thf (4 mL) under N_2 after which dibal–H (8.6 mL, 48 mmol, USE CAUTION, PYROPHORIC) was added through a gas tight syringe. The mixture was allowed to cool to 0 °C (ice/water bath) and

trimethyl(phenylethynyl)silane (4.8 mL, 24 mmol) was added by syringe drop-wise. The mixture was allowed to stir for an additional 5 min at 0 °C and then warm to 55 °C and stir for 23 h. The reaction was quenched upon drop-wise addition of D_2O (0.8 mL, 48 mmol) at 0 °C and stir for additional 1 h at 22 °C. The mixture was transferred to a separatory funnel after which Rochelle's salt (30 ml) and a saturated solution of aqueous ammonium chloride (30 ml) were added to separate the layers. The aqueous layer was washed with Et_2O (3 x 20 mL). The combined organic layers were dried over Na_2SO_4 and concentrated. The resulting yellow oil was purified by silica gel chromatography (100% pentane) and Kugelrohr distillation to afford **S6** as colorless liquid (4.0 g, 93%, >98% D). IR (neat): 2954 (w), 2897 (w), 1590 (w), 1569 (w), 1491 (w), 1247 (m), 1073 (w), 833 (s), 755 (s), 695 (s), 619 (m), 486 (m), 458 (w) cm^{-1}; ^1H NMR ($CDCl_3$, 400 MHz): 7.40–7.21 (6H, m), 0.06 (9H, s); ^{13}C NMR ($CDCl_3$, 100 MHz): δ 146.6, 128.4, 128.3, 128.0, 127.9, 127.5, 0.3; HRMS (DART): Calcd for $C_{11}H_{15}DSi$ $[M+H]^+$: 177.1084; Found: 177.1097.

(*E*)-Trimethyl(2-phenylvinyl-1-*d*)silane (S7): Prepared similarly to **S6**, 100% hexanes was used instead of using 16.7% thf to afford **S7** (4.0 g, 93%, 96% D) as a colorless liquid. IR (neat): 3025 (w), 2954 (w), 1594 (w), 1570 (w), 1494 (w), 1297 (s), 1082 (m), 922 (w), 834 (s), 754 (s), 692 (s), 485 (w) cm^{-1}; ^1H NMR ($CDCl_3$, 400 MHz): 7.47–7.41 (2H, m), 7.36–7.13 (3H, m), 6.89–6.85 (1H, m), 0.16 (9H, s); ^{13}C NMR ($CDCl_3$, 100 MHz): δ 143.7, 128.7, 128.4, 128.1, 127.9, 126.5, 125.6, –1.1, –1.6; HRMS (DART): Calcd for $C_{11}H_{15}DSi$ $[M+H]^+$: 177.1084; Found: 177.1092.

***trans*-Styrene-(β)-*d* (S8):** To a solution of (*Z*)-trimethyl(2-phenylvinyl-1-*d*)silane (2.5 g, 14 mmol) in thf (15 mL) was added $(n\text{-Bu})_4NF$ (21 mL of 1M in thf) at 22 °C under N_2. The mixture was allowed to stir at 60 °C for 18 h, after which it was transferred to a

separatory funnel. Water (25 mL) was added and the layers separated. The aqueous layer was washed with Et_2O (3 x 20 mL). The combined organic layers were dried over $MgSO_4$ and concentrated under house vacuum. The resulting yellow oil was purified by Kugelrohr distillation to afford the product (>98% *E*, >98% D) as colorless liquid. The spectroscopic data match those reported previously.[43] ^{1}H NMR ($CDCl_3$, 400 MHz): δ 7.45–7.23 (5H, m), 6.73 (1H, dt, *J* = 17.6, 1.6 Hz) 5.74 (1H, d, *J* = 17.6 Hz)

***cis*-Styrene-(β)-*d* (S9):** This compound was prepared similarly to *trans*-Styrene-(β)-d, starting from (*E*)-trimethyl(2-phenylvinyl-1-*d*)silane (2.5 g, 14 mmol) and TBAF (56 mL of 1 M in thf) for 18 hours. The product was obtained as colorless liquid (96% *Z*, 95% D). The spectroscopic data match those reported previously.[43] ^{1}H NMR ($CDCl_3$, 400 MHz): δ 7.45–7.22 (5H, m), 6.72 (1H, dt, *J* = 10.9, 2.6 Hz), 5.23 (1H, d, *J* = 10.9 Hz)

2-((1*R*,2*R*)-2,4-Diphenylpent-4-en-1-yl-1-*d*)-4,4,5,5-tetramethyl-1,3,2-dioxaborolane (*anti*-1.31-*d*): Following the representative procedure except **L3b** and 6:1 alkene:phosphate (**1.11**)used. IR (neat): 2923 (m), 2854 (w), 1453 (w), 1351 (m), 1314 (m), 1214 (w), 1143 (s), 969 (m), 896 (w), 777 (m), 734 (m), 698 (s), 547 (w) cm^{-1}; ^{1}H NMR ($CDCl_3$, 600 MHz): δ 7.40–7.36 (2H, m), 7.33–7.29 (2H, m), 7.28–7.19 (3H, m), 7.15–7.09 (3H, m), 5.15 (1H, d, *J* = 1.8 Hz), 4.83 (1H, *J* = 1.2 Hz), 2.95 (1H, q, *J* = 6.6 Hz), 2.87 (1H, dd, *J* = 13.2, 6 Hz), 2.73 (1H, dd, *J* = 12.6 7.8 Hz), 1.23 (1H, d, *J* = 6), 1.07 (6H, s), 1.05 (6H, s); ^{13}C NMR ($CDCl_3$, 150 MHz): δ 146.9, 146.8, 141.2, 128.4, 128.1, 127.6, 127.4, 126.6, 125.9, 114.5, 83.0, 45.7, 39.9, 24.9, 24.7; HRMS (DART): Calcd for $C_{22}H_{27}DBO_2$ $[M+H]^+$: 336.2245; Found: 336.2241. Enantiomeric purity was determined by HPLC analysis of the alcohol product after oxidation in comparison with

(43) Kapeller, D.; Barth, R.; Mereiter, K.; Hammerschmidt, F. 2007, *J. Am. Chem. Soc.* **2007,** *129,* 914–923.

authentic racemic material (89:11 er shown; Chiralcel OZ–H column, 99% hexanes, 1% *i*-PrOH, 0.3 mL/min, 220 nm).

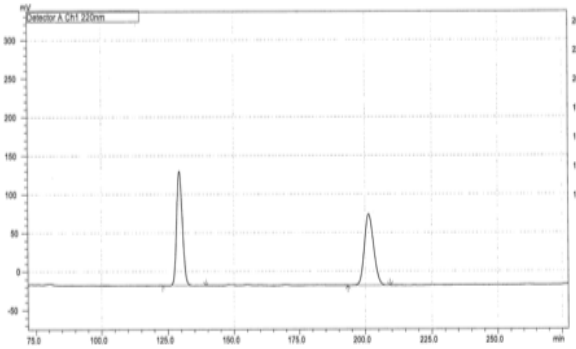

Peak#	Ret. Time	Area	Height	Conc.	Area%
1	129.355	22288828	147877	49.803	49.803
2	201.412	22465067	92552	50.197	50.197
Total		44753895	240429		100.000

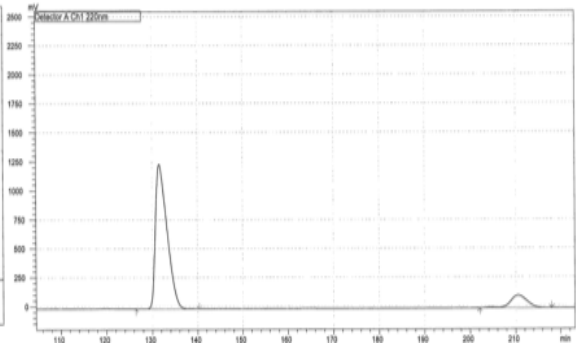

Peak#	Ret. Time	Area	Height	Conc.
1	131.578	221968013	1247086	88.668
2	210.567	28367150	110170	11.332
Total		250335164	1357256	

Peak #	Time (min)	Area (%)	Peak #	Time (min)	Area (%)
1	129.355	49.803	1	131.578	88.668
2	201.412	50.197	2	210.567	11.332

2-((1*S*,2*R*)-2,4-Diphenylpent-4-en-1-yl-1-*d*)-4,4,5,5-tetramethyl-1,3,2-dioxaborolane (*syn*-1.31-*d*): Following the representative procedure except **L3b** and 6:1 alkene:phosphate (**1.11**) used. IR (neat): 2977 (w), 2924 (m), 2854 (w), 1194 (w), 1389 (s), 1316 (s), 1142 (s), 1110 (w), 970 (m), 895 (m), 859 (m), 777 (m), 697 (s), 521 (w) cm^{-1}; ^{1}H NMR ($CDCl_3$, 600 MHz): δ 7.42–7.35 (2H, m), 7.34–7.29 (2H, m), 7.28–7.19 (3H, m), 7.14–7.09 (3H, m), 5.15 (1H, d, *J* =1.2 Hz), 4.83 (1H, s), 2.96 (1H, q, *J* = 8.4 Hz), 2.87 (1H, dd, J = 13.8, 6 Hz), 2.73 (1H, dd, *J* = 13.2, 7.8 Hz), 1.11 (1H, d, *J* = 9 Hz), 1.08 (6H, s), 1.05 (6H, s); ^{13}C NMR ($CDCl_3$, 150 MHz): δ 146.9, 146.8, 141.2, 128.4, 128.1, 127.6, 127.4, 126.7, 125.9, 114.5, 83.1, 45.6, 39.9, 24.9, 24.7; HRMS (DART): Calcd for $C_{22}H_{27}BO_2$ $[M+H]^+$: 336.2245; Found: 336.2245. Enantiomeric purity was determined by HPLC analysis of the alcohol product after oxidation in comparison with

authentic racemic material (96:4 er shown; Chiralcel OZ–H column, 99% hexanes, 1% *i*-PrOH, 0.3 mL/min, 220 nm).

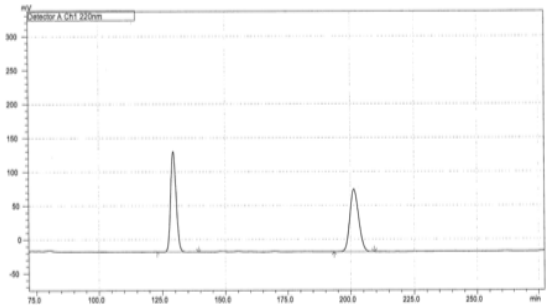

Peak#	Ret. Time	Area	Height	Conc.	Area%
1	129.355	22288828	147877	49.803	49.803
2	201.412	22465067	92552	50.197	50.197
Total		44753895	240429		100.000

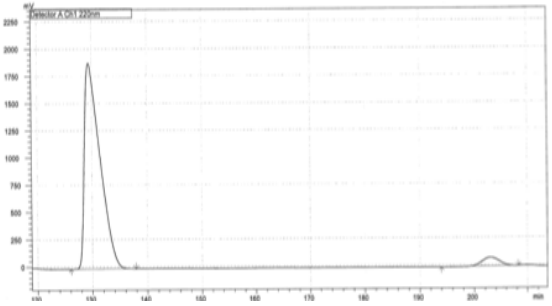

Peak#	Ret. Time	Area	Height	Conc.	Area%
1	129.403	370626114	1885975	95.564	95.564
2	202.960	17203506	78726	4.436	4.436
Total		387829619	1964701		100.000

Peak #	Time (min)	Area (%)	Peak #	Time (min)	Area (%)
1	129.355	49.803	1	129.403	95.564
2	201.412	50.197	2	202.960	4.436

(*E*)-1-(Trifluoromethyl)-4-(vinyl-2-*d*)benzene (substrate for synthesis of *anti*-1.27-*d*): Following the procedure for preparation of **S8** except 1-[(Trimethylsilyl)ethynyl]-4-(trifluoromethyl)benzene was used. The product was obtained in 91:9 *E*:*Z* selectivity. The spectroscopic data match those reported previously.[44] ^{1}H NMR (400 MHz, $CDCl_3$): δ 7.58 (2H, d, *J* = 8.4 Hz), 7.50 (2H, d, *J* = 8.4 Hz), 6.75 (1H, d, *J* = 17.6 Hz), 5.83 (1H, d, *J* = 17.6 Hz).

(*Z*)-1-(Trifluoromethyl)-4-(vinyl-2-*d*)benzene (substrate for synthesis of *syn*-1.27-*d*): Following the procedure for preparation of **S9** except 1-[(Trimethylsilyl)ethynyl]-4-(trifluoromethyl)benzene was use. The product was obtained as a 90:10 ratio of *Z*:*E* isomers. IR (neat): 2954 (m), 2925 (m), 2854 (m), 1325 (s), 1168 (m), 1129 (m), 1068 (m) cm^{-1}; ^{1}H NMR (400 MHz, $CDCl_3$): δ 7.57 (2H, d, *J* = 8.4 Hz), 7.48 (2H, d, *J* = 8.4 Hz),

(44) Gao, F.; Hoveyda, A. H. *J. Am. Chem. Soc.* **2010,** *132,* 10961–10963.

6.72 (1H, dt, J = 11.2, 2.6 Hz), 5.36 (1H, d, J = 11.2 Hz); ^{13}C NMR (100 MHz, $CDCl_3$): δ 141.1, 135.7, 129.8 (q, J = 32.4 Hz), 126.5, 125.6, 124.3 (q, J = 270.2 Hz), 116.3 (t, J = 23.6 Hz); HRMS (EI): Calcd for $C_9H_7D_1F_3$ $[M]^+$: 173.0563, Found: 173.0560.

4,4,5,5-Tetramethyl-2-((1S,2R)-2-(4-(trifluoromethyl)phenyl)pent-4-en-1-yl-1-*d*)-1,3,2-dioxaborolane (*anti*-1.27-*d*): Following the representative procedure except **L3b** used. IR (neat): 2979 (w), 2926 (w), 1359 (m), 1322 (s), 1162 (m), 1143 (m), 1120 (s), 1069 (m), 836 (m) cm^{-1}; ^{1}H NMR (400 MHz, $CDCl_3$): δ 7.51 (2H, d, J = 8.0 Hz), 7.31 (2H, d, J = 8.4 Hz), 5.64 (1H, ddt, J = 17.0, 10.2, 7.0 Hz), 4.98–4.92 (2H, m), 3.00 (1H, q, J = 7.1 Hz), 2.36 (2H, t, J = 7.2 Hz), 1.22 (1H, d, J = 1.2 Hz), 1.10 (6H, s), 1.08 (6H, s); ^{13}C NMR (100 MHz, $CDCl_3$): δ 151.1, 136.5, 128.3 (q, J = 32.1 Hz), 127.9, 125.1 (q, J = 3.8 Hz), 124.5 (q, J = 270.4 Hz), 116.7, 83.3, 43.5, 41.4, 24.8, 24.7; HRMS (DART): Calcd for $C_{18}H_{24}D_1B_1F_3O_2$ $[M+H]^+$: 342.1963, Found: 342.1961. Enantiomeric purity was determined by HPLC analysis in comparison with authentic racemic material (60:40 er shown; Chiralcel OZ–H column, 100% hexanes, 0.3 mL/min, 220 nm).

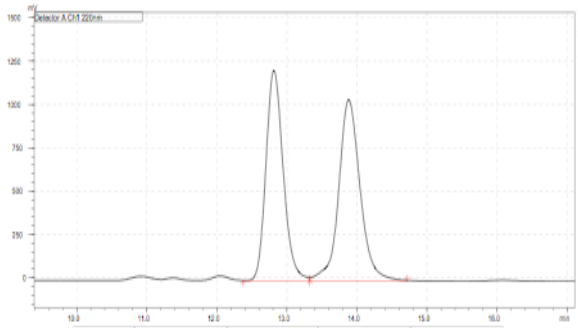

Peak#	Ret. Time	Area	Height	Area%
1	12.811	20708890	1213112	48.458
2	13.878	22027279	1042603	51.542
Total		42736169	2255714	100.000

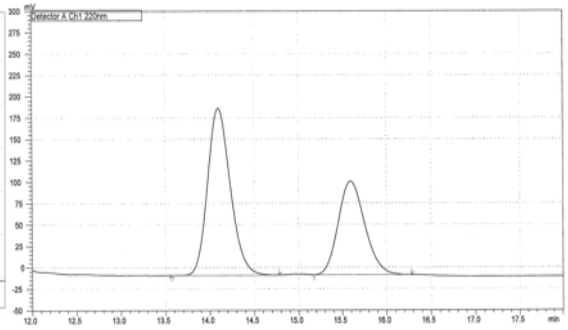

Peak#	Ret. Time	Area	Height	Area%
1	14.097	3477565	195530	60.178
2	15.594	2301245	109481	39.822
Total		5778809	305011	100.000

Peak #	Time (min)	Area (%)	Peak #	Time (min)	Area (%)
1	12.811	48.458	1	14.097	60.178
2	13.878	51.542	2	15.594	39.822

4,4,5,5-Tetramethyl-2-((1R,2R)-2-(4-(trifluoromethyl)phenyl)pent-4-en-1-yl-1-d)-1,3,2-dioxaborolane (*syn*-1.27-*d*): Following the representative procedure except **L3b** used. IR (neat): 2979 (w), 2926 (w), 1359 (m), 1322 (s), 1162 (m), 1143 (m), 1120 (s), 1069 (m), 836 (m) cm^{-1}; ^{1}H NMR (400 MHz, $CDCl_3$): δ 7.51 (2H, d, *J* = 8.4 Hz), 7.31 (2H, d, *J* = 8.4 Hz), 5.64 (1H, ddt, *J* = 17.2, 10.4, 6.8 Hz), 4.98–4.91 (2H, m), 3.00 (1H, q, *J* = 7.9 Hz), 2.36 (2H, t, *J* = 7.2 Hz), 1.10 (6H, s), 1.09 (6H, s), 1.10–1.09 (1H, m); ^{13}C NMR (100 MHz, $CDCl_3$): δ 151.1, 136.5, 128.3 (q, *J* = 32.1 Hz), 127.9, 125.1 (q, *J* = 3.8 Hz), 124.5 (q, *J* = 270.2 Hz), 116.7, 83.3, 43.5, 41.4, 24.8, 24.7; HRMS (DART): Calcd for $C_{18}H_{24}D_1B_1F_3O_2$ $[M+H]^+$: 342.1963, Found: 342.1961. Enantiomeric purity was determined by HPLC analysis in comparison with authentic racemic material (74:26 er shown; Chiralcel OZ–H column, 100% hexanes, 0.3 mL/min, 220 nm).

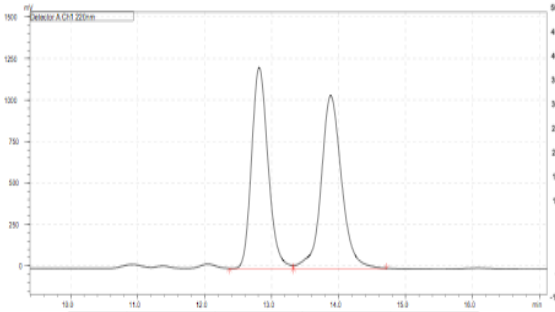

Peak#	Ret. Time	Area	Height	Area%
1	12.811	20708890	1213112	48.458
2	13.878	22027279	1042603	51.542
Total		42736169	2255714	100.000

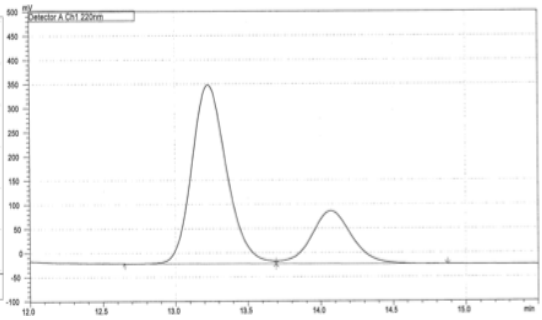

Peak#	Ret. Time	Area	Height	Area%
1	13.228	6193512	370607	74.379
2	14.070	2133423	109619	25.621
Total		8326935	480227	100.000

Peak #	Time (min)	Area (%)	Peak #	Time (min)	Area (%)
1	12.811	48.458	1	13.228	74.379
2	13.878	51.542	2	14.070	25.621

1.5.8 Study of the Possibility of Homolytic versus Heterolytic Cu–C Bond Cleavage

Scheme 1.29. Synthesis of Cyclopropane **1.39**

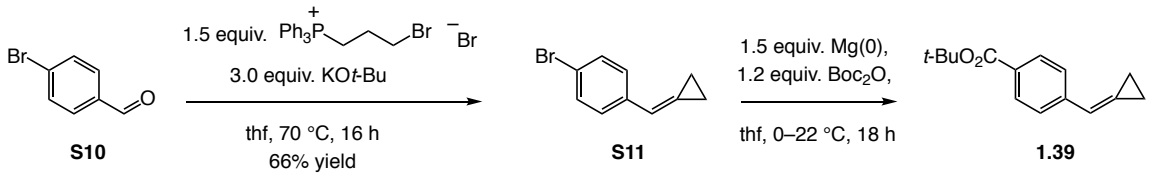

1-Bromo-4-(cyclopropylidenemethyl)benzene (S11): Prepared from aldehyde **S10** (purchased from Aldrich and used as received) by formerly reported procedure.[45] The spectroscopic data match those reported previously.[46] ^{1}H NMR (400 MHz, $CDCl_3$): δ 7.46–7.42 (2H, m), 7.40–7.38 (2H, m), 6.70–6.68 (1H, m), 1.42–1.38 (2H, m), 1.20–1.16 (2H, m).

***tert*-Butyl-4-(cyclopropylidenemethyl)benzoate (1.39):** Prepared from **S11** according to the reported procedure.[35] IR (neat): 2977 (w), 1706 (s), 1606 (m), 1367 (m), 1307 (s), 1292 (s), 1254 (m), 1161 (s), 1107 (s), 1015 (m), 863 (m), 849 (m), 757 (m) cm^{-1}; ^{1}H NMR (400 MHz, $CDCl_3$): δ 7.96 (2H, d, J = 8.4 Hz), 7.55 (2H, d, J = 8.4 Hz), 6.79–6.78 (1H, m), 1.61 (9H, s), 1.48–1.42 (2H, m), 1.22–1.18 (2H, m); ^{13}C NMR (100 MHz, $CDCl_3$): δ 165.8, 142.3, 130.1, 129.7, 127.6, 126.3, 117.9, 80.8, 28.3, 4.5, 0.8; HRMS (DART): Calcd for $C_{15}H_{19}O_2$ $[M+H]^+$: 231.1391, Found: 231.1385.

***tert*-Butyl-(*S*)-4-(1-(1-(4,4,5,5-tetramethyl-1,3,2-dioxaborolan-2-yl)cyclopropyl)but-3-en-1-yl)benzoate (1.40):** IR (neat): 2976 (w), 2932 (m), 1710 (s), 1640 (w), 1440 (m), 1409 (m), 1290 (s), 1164 (s), 1140 (s), 1113 (s), 851 (s), 708 (m), 685 (m), 420 (w) cm^{-1}; ^{1}H NMR (400 MHz, $CDCl_3$): δ 7.88 (2H, d, J = 8), 7.38 (2H, d, J =8), 5.69 (1H, ddt, J = 17.2, 9.6, 7.2), 5.00–4.95 (1H, m), 4.89–4.85 (1H, m), 2.75–2.71 (2H, m), 1.20 (1H, t, J

(45) Evans, P. A.; Inglesby, P. A.; Kilbride, K. *Org. Lett.* **2013,** *15,* 1798–1801.
(46) Katritzky, A. R.; Du, W.; Levell, J. R.; Li, J. *J. Org. Chem.* **1998,** *63*, 6710–6711.

=7.8), 1.58 (9H, s), 1.20 (12H, s), 0.74 (1H, ddd, J = 9.2, 5.6, 3.2), 0.66 (1H, ddd, J = 8, 4.8, 2.8), 0.41 (1H, ddd, J =8.4, 5.2, 3.2), 0.35 (1H, ddd, J = 8.4, 5.2, 3.2); ^{13}C NMR (100 MHz, $CDCl_3$): δ 166.1, 150.3, 138.1, 129.8, 129.2, 128.5, 115.5, 83.1, 80.7, 53.4, 38.8, 28.4, 25.0, 24.5, 14.1, 10.2; HRMS (DART): Calcd for $C_{24}H_{36}BO_4$ $[M+H]^+$: 399.2707, Found: 399.2723. Enantiomeric purity was determined by HPLC analysis of the alcohol product after oxidation in comparison with authentic racemic material (54:46 er shown; Chiralcel OZ–H column, 99% hexanes, 1% *i*-PrOH, 0.3 mL/min, 220 nm).

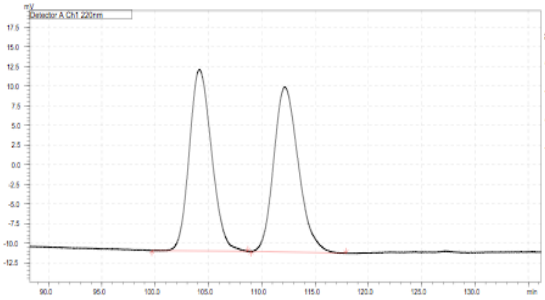

Peak#	Ret. Time	Area	Height	Area%
1	104.145	3349312	23097	49.894
2	112.153	3363590	21013	50.106
Total		6712902	44110	100.000

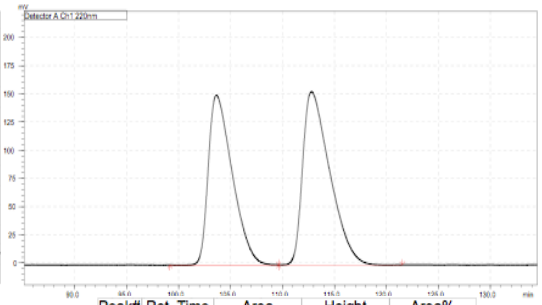

Peak#	Ret. Time	Area	Height	Area%
1	103.637	24149247	150345	46.394
2	112.787	27903537	153742	53.606
Total		52052783	304087	100.000

Peak #	Time (min)	Area (%)	Peak #	Time (min)	Area (%)
1	104.145	49.894	1	103.637	46.394
2	112.153	50.106	2	112.787	53.606

Additional support for cleavage/re-formation of the Cu–C bond is likely to be heterolytic in nature is that with diene **S15** as the substrate, cyclopentenyl product **1.45** was not detected (Scheme 1.12).

Scheme 1.30. Synthesis of Diene **1.42**

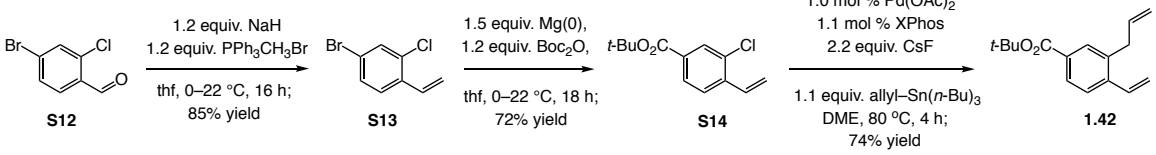

4-Bromo-2-chloro-1-vinylbenzene (S13): Prepared from aldehyde **S12** (purchased from Combi-Blocks and used as received) following the previously reported procedure.[31] IR (neat): 3089 (w), 3060 (w), 1579 (m), 1467 (s), 1371 (m), 1085 (m), 1049 (m), 985 (m), 917 (s), 867 (m), 812 (s) cm^{-1}; ^{1}H NMR (400 MHz, $CDCl_3$): δ 7.53 (1H, s), 7.42 (1H, d, *J* = 8.4 Hz), 7.36 (1H, dd, *J* = 8.4, 1.6 Hz), 7.02 (1H, dd, *J* = 17.4, 11.0 Hz), 5.74 (1H, d, *J* = 17.2 Hz), 5.41 (1H, d, *J* = 10.8 Hz); ^{13}C NMR (100 MHz, $CDCl_3$): δ 134.9, 133.9, 132.4, 132.3, 130.2, 127.7, 121.7, 117.3; HRMS (DART): Calcd for $C_8H_7Br_1Cl_1$ $[M+H]^+$: 216.9420, Found: 216.9427.

***tert*-Butyl-3-chloro-4-vinylbenzoate (S14):** Prepared from **S13** according to the reported procedure.[35] IR (neat): 2978 (w), 2933 (w), 1716 (s), 1392 (m), 1368 (m), 1298 (s), 1258 (m), 1168 (s), 1118 (s), 773 (m), 849 cm^{-1}; ^{1}H NMR (400 MHz, $CDCl_3$): δ 7.95 (1H, d, *J* = 1.6 Hz), 7.83 (1H, dd, *J* = 8.5, 2.1 Hz), 7.59 (1H, d, *J* = 8.0 Hz), 7.11 (1H, dd, *J* = 17.6, 10.8 Hz), 5.82 (1H, dd, *J* = 17.4, 0.6 Hz), 5.48 (1H, dd, *J* = 11.0, 1.0 Hz), 1.59 (9H, s); ^{13}C NMR (100 MHz, $CDCl_3$): δ 164.5, 139.5, 133.1, 132.7, 132.5, 130.8, 127.8, 126.3, 118.6, 81.7, 28.3; HRMS (DART): Calcd for $C_{13}H_{16}Cl_1O_2$ $[M+H]^+$: 239.0839,

***tert*-Butyl-3-allyl-4-vinylbenzoate (1.42):** Prepared from **S14** according to the reported procedure.[47] IR (neat): 2977 (w), 2931 (w), 1709 (s), 1367 (m), 1293 (s), 1253 (s), 1163 (s), 1118 (s), 989 (m), 914 (s), 849 (s) cm^{-1}; ^{1}H NMR (400 MHz, $CDCl_3$): δ 7.82 (1H, dd, *J* = 7.8, 1.4 Hz), 7.78 (1H, d, *J* = 1.6 Hz), 7.53 (1H, d, *J* = 8.4 Hz), 6.97 (1H, dd, *J* = 17.2, 11.2 Hz), 6.01–5.91 (1H, m), 5.73 (1H, dd, *J* = 17.4, 1.4 Hz), 5.39 (1H, dd, *J* = 11.2, 1.2 Hz), 5.10–5.06 (1H, m), 5.00–4.94 (1H, m), 3.48 (2H, dt, J = 6.4, 1.6 Hz), 1.59 (9H, s); ^{13}C NMR (100 MHz, $CDCl_3$): δ 165.8, 140.9, 137.1, 136.4, 134.1, 131.4, 131.0, 127.8,

(47) Naber, J. R.; Buchwald, S. L. *Adv. Synth. Catal.* **2008,** *350,* 957–961.

125.7, 117.5, 116.4, 81.0, 37.5, 28.3; HRMS (DART): Calcd for $C_{16}H_{21}O_2$ $[M+H]^+$: 244.1463, Found: 244.1471.

***tert*-Butyl-(*R*)-3-allyl-4-(1-(4,4,5,5-tetramethyl-1,3,2-dioxaborolan-2-yl)pent-4-en-2-yl)benzoate (1.43):** IR (neat): 2977 (w), 2930 (w), 1711 (s), 1367 (s), 1298 (s), 1253 (m), 1166 (s), 1143 (s), 1121 (m), 912 (m), 849 (m) cm^{-1}; ^1H NMR (400 MHz, $CDCl_3$): δ 7.78 (1H, dd, J = 8.0, 2.0 Hz), 7.75 (1H, d, J = 2.0 Hz), 7.27 (1H, d, J = 7.6 Hz), 6.00 (1H, ddt, J = 17.0, 10.2, 6.2 Hz), 5.70–5.60 (1H, m), 5.09–5.02 (2H, m),), 4.99–4.91 (2H, m), 3.59–3.45 (2H, m), 3.32–3.24 (1H, m), 2.36–2.23 (2H, m), 1.58 (9H, s), 1.26–1.21 (1H, m), 1.08 (6H, s), 1.05 (6H, s), 1.12–1.05 (1H, m); ^{13}C NMR (100 MHz, $CDCl_3$): δ 166.2, 150.3, 137.6, 137.3, 136.8, 130.6, 129.5, 127.6, 126.4, 116.6, 116.1, 83.2, 80.7, 43.5, 37.4, 35.6, 28.4, 24.8, 24.77; HRMS (DART): Calcd for $C_{25}H_{38}B_1O_4$ $[M+H]^+$: 413.2863, Found: 413.2858.

1.5.9 Spectroscopic Studies of Bis-Phosphine–Cu Complexes

Spectroscopic Detection of the Key Intermediates in the Catalytic Cycle

Detection of a chiral bis-phosphine–Cu complex and the corresponding aggregate structures. In an N_2-filled glove box, an oven-dried 2-dram vial was charged with CuO*t*-Bu (2.8 mg, 0.0203 mmol), bis-phosphine **L3c** (15 mg, 0.0224 mmol) and thf-d_8 (0.3 mL). The mixture was manually stirred leading to formation of a homogeneous light-green solution and was then transferred to an NMR tube after which the original vial was washed with 0.2 mL of thf-d_8. The tube was capped with a septum and sealed with paraffin before being removed from glove box.

The ^{31}P spectrum (A) was first acquired at 22 °C; there was ~30% un-coordinated bis-phosphine ligand. At –20 °C (spectrum B) peaks were generally sharper, suggesting that

there is equilibrium among various complexes. Variations in temperature and concentration of **L3c** led to only slight changes in the chemical shift of the free ligand (as judged by the coupling constant values): whereas the $J_{P\text{-}P}$ **L3c** is 21.8 Hz, it is 110-190 Hz for the derived Cu complex the same coupling constant (depending on extent of complexation).

Aggregates derived from bis-phosphine–Cu complexes and related equilibria

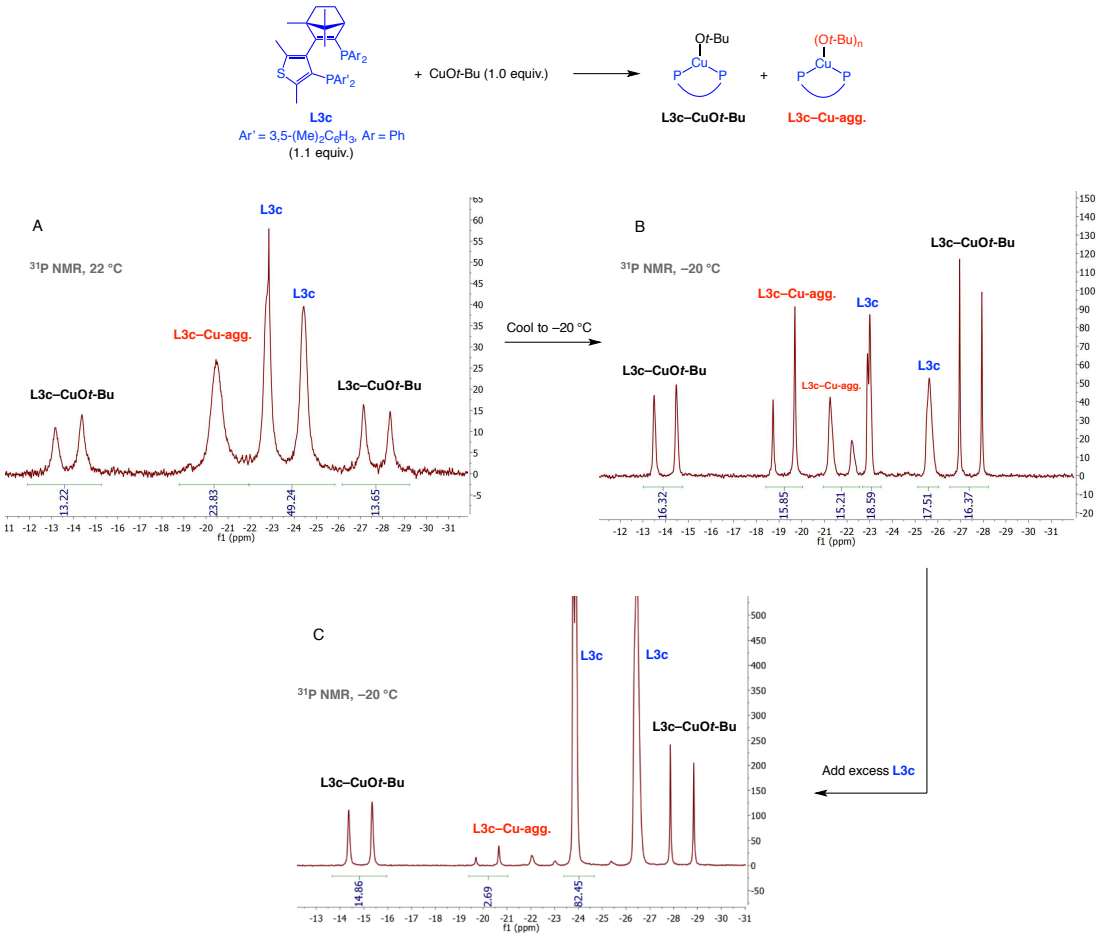

Conclusion: The increase in concentration of bis-phosphine–Cu complex (less unbound CuO*t*-Bu) due to excess **L3c** is consistent with the fact that there was considerable increase in er when excess ligand was used even with unoptimal alkene:electrophile ratio (Fig. 4c, manuscript).

Addition of styrene, *para*-trifluoromethylstyrene or pentafluorostyrene (20 equiv.) did not result in a detectable change on the concentration of any of the organocopper species.

Conclusion: An alkene does not compete with the bis-phosphine ligand for copper coordination.

When excess **L3c** were added (60 mg, 0.112 mmol; spectrum C), the amount of bis-phosphine–Cu complex increased (i.e., from ~1:1 to ~5.5 **L3c-CuO*t*-Bu:L3c-Cu-agg.**).

Conclusion: L3c-Cu-agg. contains more than one Cu atom (dimer or larger aggregate) and may be converted to monomeric species by introducing more ligand. A similar observation has been reported involving $[CuO\textit{t}\text{-}Bu(PPh_3)]_2$.[48]

Bis-phosphine–CuOt-Bu complexes undergo ligand dissociation. Metal–oxygen bonds in alkoxide complexes are largely ionic. The polarity of the metal–oxygen bond is usually attenuated through π-donation by the oxygen atom into the metal d-orbitals in early transition metal systems. With late-transition metals, the ability of alkoxide ligands to serve as a σ- and π-donor systems is negligible. In the case of Cu(I) complexes (d^{10}), alkoxide and hydroxide ligands for the most part serve as σ-donors. Thus, the oxygen atoms retain considerable Lewis basicity, which can lead to the formation of oligomeric species by alkoxo bridging[48]. The large size of bis-phosphine ligand **L3c** and the *tert*-butoxide moiety translates into accelerated oligomer formation, a process that is driven by a decrease in steric pressure (Scheme 1.31).

---

(48) Lemmen, T. H.; Goeden, G. V.; Huffman, J. C.; Geerts, R. L.; Caulton, K. G. *Inorg. Chem.* **1990,** *29,* 3680–3685.

Scheme 1.31. Alkoxide bridging leads to aggregation and reduced steric strain

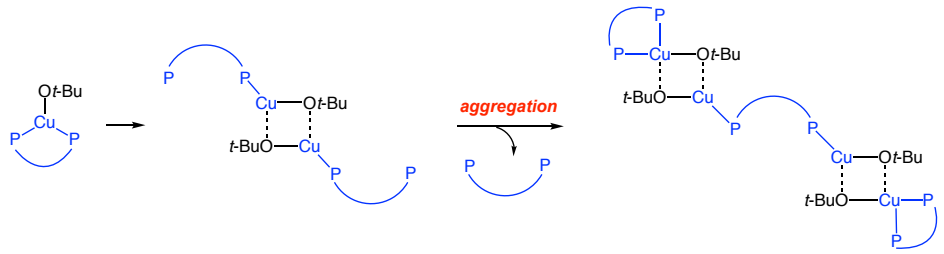

Detection of bis-phosphine–Cu–B(pin) complex at –20 °C. In a N_2-filled glove box, a solution of CuO*t*-Bu (2.8 mg, 0.0203 mmol), **L3c** (15 mg, 0.0224 mmol), and $PhCH_2Ph$ (internal standard; 4.0 μL, 0.0233 mmol) in thf-d_8 (0.3 mL) was prepared in a two-dram vial. The mixture was manually stirred upon formation of a homogeneous light-green solution and then transferred to an NMR tube, after which the vial was washed with additional 0.2 mL of thf-d_8. The tube was capped with a septum and sealed with paraffin before being removed from glove box. The tube was then placed in a dry ice/acetone bath. A solution of bis(pinacolato)diboron (11.4 mg, 0.0449 mmol) was prepared in 0.2 mL of

Excess bis-phosphine ligand decreases the amount of unbound Cu–B(pin)

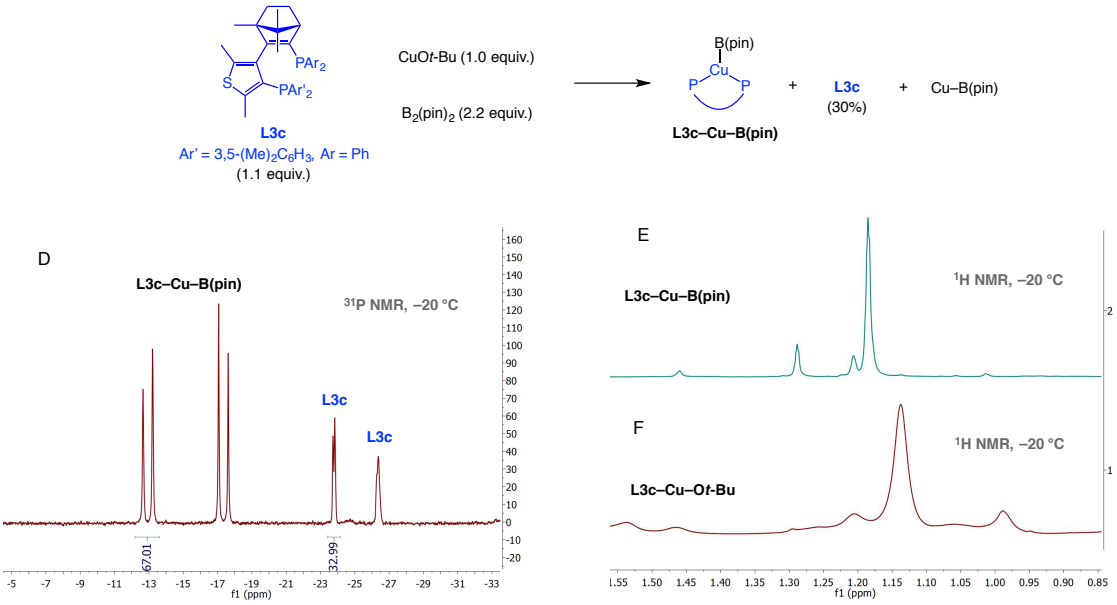

thf-d_8 in a separate vial and transferred by syringe to the solution in the NMR tube and stirred manually without removing the cooling bath to ensure minimal reaction occurring

before being placed in the spectrometer. The spectrum was acquired at –20 ºC in a precooled spectrometer.

Resonances corresponding to bis-phosphine-Cu–Bpin and free **L3c** (30%) were detected by ^{31}P NMR spectroscopy (spectrum D). Complete disappearance of the initial signals assigned to L-CuO*t*-Bu was observed by ^{1}H NMR spectroscopy (spectrum E after the addition of B_2pin_2 solution, and spectrum F before the addition of B_2pin_2 solution).

Detection of alkyl–Cu diastereomers and evidence for Cu–H elimination. In an N_2-filled glove box, a solution of CuO*t*-Bu (2.8 mg, 0.0203 mmol), bis-phosphine **L3c** (15 mg, 0.0224 mmol), *para*-trifluoromethylstyrene (5.0 μL, 0.0314 mmol) and $PhCH_2Ph$ (internal standard; 4.0 μL, 0.0233 mmol) in thf-d_8 (0.3 mL) were placed in a two-dram vial. The mixture was manually stirred upon formation of a homogeneous light-green solution and then transferred to an NMR tube, after which the vial was washed with additional 0.2 mL of thf-d_8. The tube was capped with a septum and sealed with paraffin before removal from glove box and placed into a dry ice/acetone bath. A solution of $B_2(pin)_2$ (11.4 mg, 0.0449 mmol) dissolved in 0.2 mL of thf-d_8 was at this time added and the resulting mixture was shaken/stirred manually without removing the cooling bath to minimize reaction occurring prior to positioning the tube in the spectrometer. The spectrum was then acquired at –20 °C.

As shown in spectra G and H below, the resonances corresponding to diastereomeric Cu-alkyl complexes (78% conv., 99:1 dr) were detected in the ^{1}H and ^{31}P NMR spectra; there was ~17% of uncoordinated bis-phosphine **L3c** also present. The sample was then allowed to warm to 22 °C (while in the spectrometer) and reaction progress monitored spectroscopically. There was further transformation to the Cu–alkyl complexes (93%

conv.; spectra I and J) along with diminution of dr to 72:28. Additionally, the acquired spectra indicate the generation of the corresponding *E*-β-alkenyl–B(pin) byproduct formed through Cu–H elimination with significant amounts formed after 1.5 h at 22 °C (spectra K and L). The identity of the alkenyl–B(pin) compound was confirmed by spiking the tube with an authentic sample of the same material.

Kinetic enantioselectivity of Cu–B(pin) addition and reactivity of chiral vs. achiral Cu–B(pin) complexes

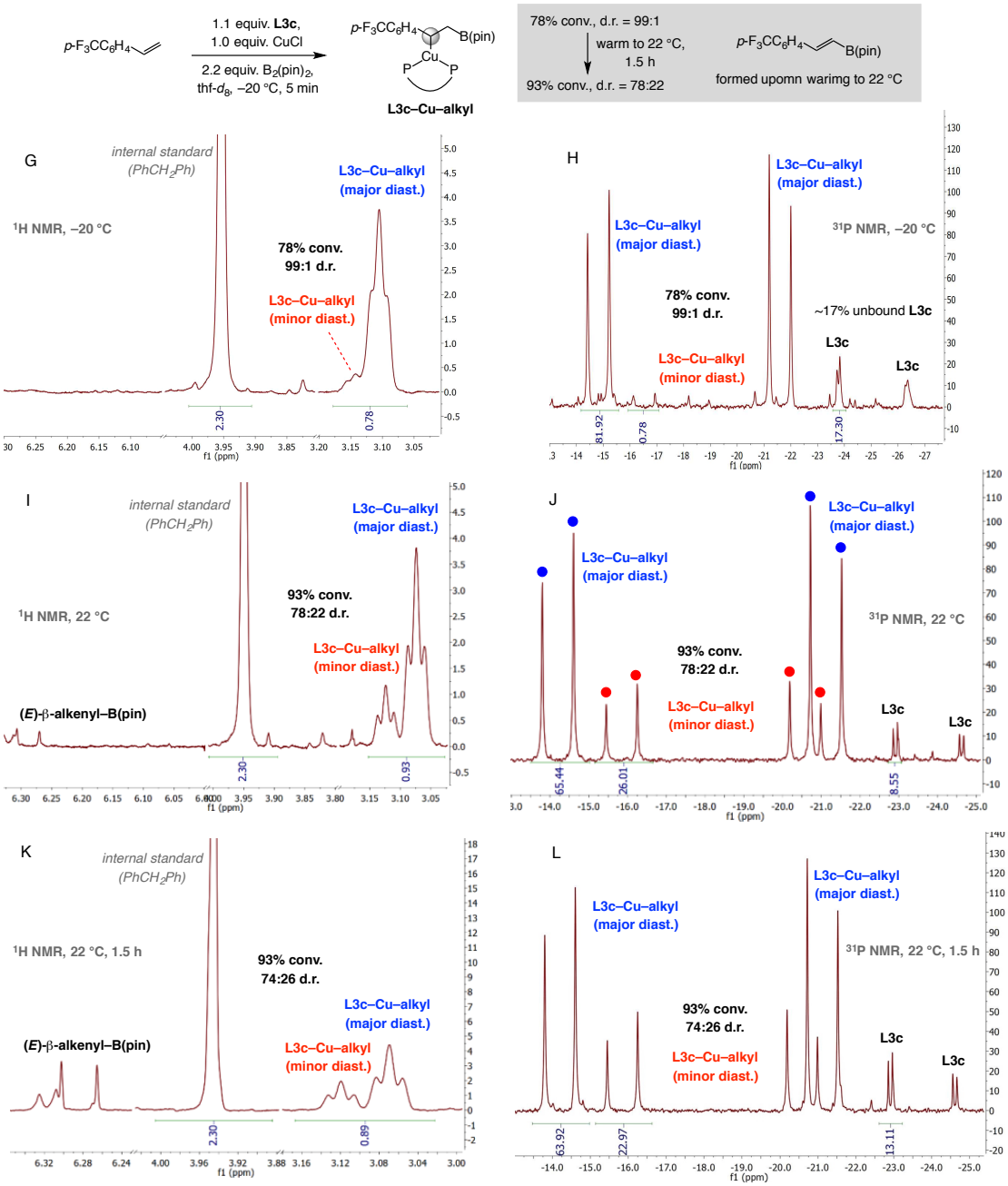

Conclusions. The above experiment show that the bis-phosphine–Cu–B(pin) complex adds to *para*-trifluoromethylstyrene readily and rapidly at –20 °C in a highly enantioselective manner. When the mixture was allowed to warm to 22 °C, the ratio between the two diastereomeric alkylcopper complexes decreased with time (from 99:1 to ~75:25) with more of the Cu–alkyl complex being formed (93% conv.). The decrease in dr may be attributed to lower reactivity of the un-coordinated Cu–B(pin) complex, which can add to the alkene substrate only at a higher temperature, supporting the notion that such a species can engender diminution in enantioselectivity in cases where the olefin is more electrophilic/reactive. Once the aryl olefin is fully converted to the corresponding alkylcopper intermediate, there can be complete bis-phosphine–Cu coordination, leaving only the excess bis-phosphine unbound. It is also possible that some of the lowering in er arises from preferential Cu–H elimination by the Cu–alkyl major diastereomer, accounting for the formation of the alkenyl–B(pin) byproduct at 22 °C.

Cu–H Addition to a β-Alkenyl–B(pin) Byproduct

Examination of bis-phosphine–Cu–H addition to an (E)-β-alkenyl–B(pin) compound. In an N_2-filled glove box, a solution of CuO*t*-Bu (2.8 mg, 0.0203 mmol), **L3c** (15 mg, 0.0224 mmol) and $PhCH_2Ph$ as the internal standard (5.0 μL, 0.03 mmol) was prepared in thf-d_8 (0.3 mL) in a two-dram vial. The mixture was manually stirred leading to the formation of a homogeneous light-green solution and was then transferred to an NMR tube. The vial was washed with an additional 0.2 mL of thf-d_8. The tube was capped with a septum and sealed with paraffin before removal from glove box and placed into a dry ice/acetone bath. A solution of polymethylhydrosiloxane (PMHS) (10 μL, 0.17 mmol) and (*E*)-2-[4-(trifluoromethyl)phenyl]vinylboronic acid pinacol ester (13.8 mg, 0.043

mmol) prepared in 0.2 mL of thf-d_8 was added by syringe and the resulting mixture was stirred manually (cooling bath retained to avoid any premature transformation). Reaction progress was monitored at 22 °C.

Regioselectivity of Cu–H addition to a β-alkenyl–B(pin) compound

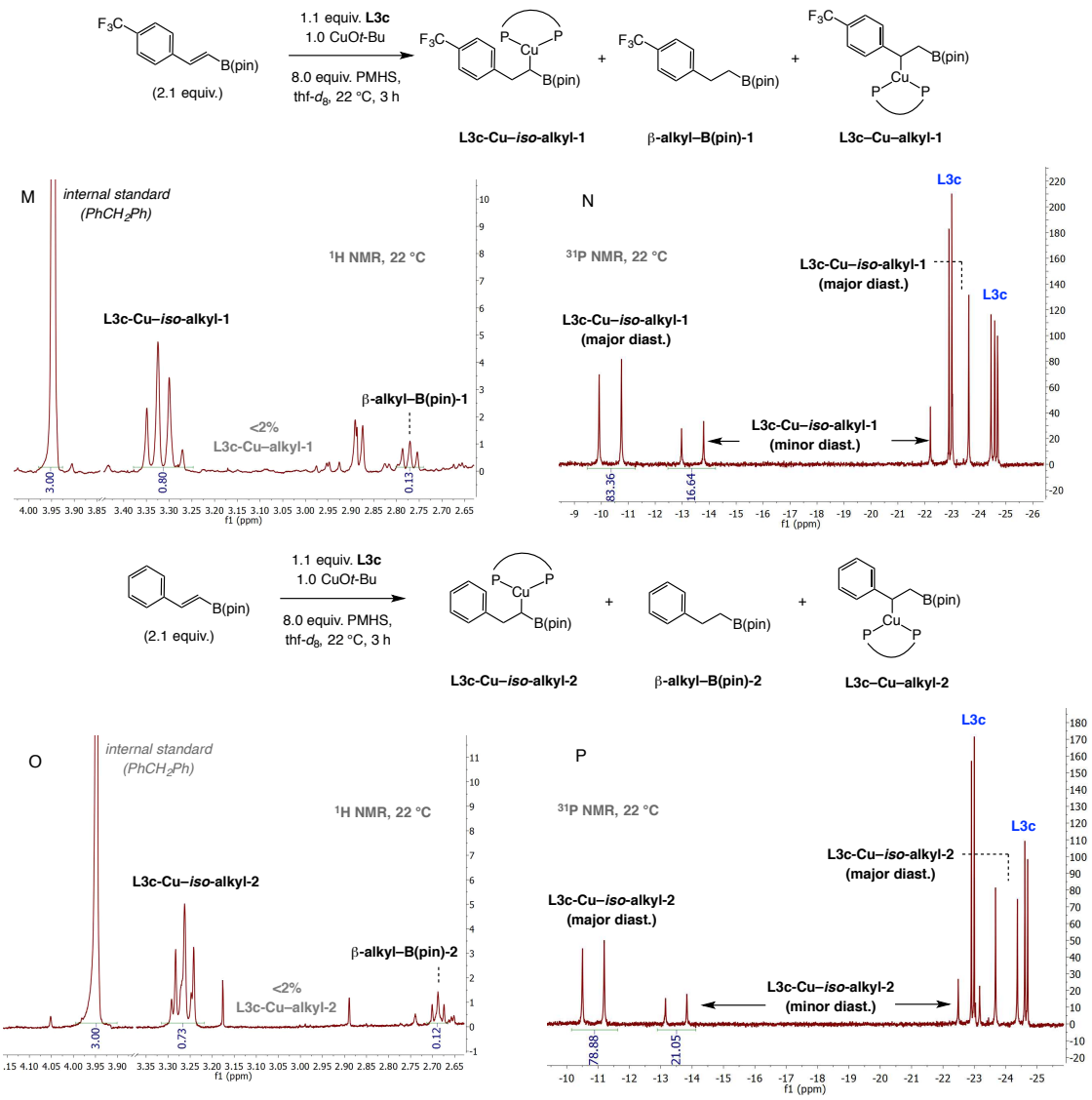

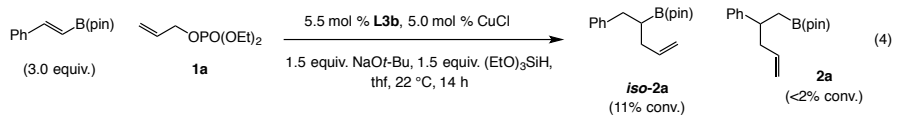

Resonances for **L3c-Cu–*iso*-alkyl-1** were detected in the ^{1}H NMR spectrum (M; ~80% conv.). The ^{31}P NMR spectrum (N) indicates 83:17 dr There were no detectable

resonances for **L3c-Cu-alkyl-1**, but ~13% of 2-(4-trifluoromethylphenyl)ethyl-1-boronic acid pinacol ester (**β-alkyl–B(pin)-1**), probably formed due to reaction of organocopper with adventitious water, was detected. The same experiment was carried out with (*E*)-2-phenyl-vinylboronic acid pinacol ester (13.8 mg, 0.043 mmol). The resonances corresponding to **L3c-Cu–*iso*-alkyl-2** were detected by ^{1}H NMR (spectrum O; 73% conv.) along with 12% **β-alkyl–B(pin)-2**. As before, dr was determined by analysis of the ^{31}P NMR spectrum (P; 78:22).

Through the experiment shown in Eq. 4 we examined the issue of Cu–H addition to (*E*)-2-phenyl-vinylboronic acid pinacol ester followed by C–C bond formation. Only ***iso*-2a** was detected (11% conv.; <2% **2a**).

Conclusions. Due to reversal in alkene polarization due to the presence of the electron-withdrawing B(pin) group, Cu–H addition to (*E*)-*β*-alkenyl–B(pin) derivatives occurs with opposite site selectivity compared to Cu–B(pin) additions (i.e., homobenzylic Cu–C bond). Preferential formation of ***iso*-2a** is consistent with a study reported by Sadighi[49]. It is unlikely that Cu–H re-addition is responsible for the loss in enantioselectivity. We could not detect **L3c-Cu-alkyl-1** or **L3c-Cu-alkyl-2**.

Probing the feasibility of Cu–H elimination/re-addition leading to loss of enantiomeric purity of a Cu–alkyl species; a cross-over experiment. In an N_2-filled glove box, a solution of CuO*t*-Bu (2.8 mg, 0.0203 mmol), **L3c** (15 mg, 0.0224 mmol), styrene (2.4 μL, 0.0203 mmol) and $PhCH_2Ph$ (internal standard; 4.0 μL, 0.0233 mmol) in thf-d_8 (0.3 mL) was prepared in a two-dram vial. The mixture was manually stirred leading to the formation of a homogeneous light-green solution and then transferred to an NMR tube,

(49) Laita, D. S.; Tsui, E. Y.; Sadighi, J. P. *Organometallics* **2006,** *25,* 2405–2408.

after which the vial was washed with additional 0.2 mL of thf-d_8. The tube was sealed with a septum and paraffin before removal from the glove box and introduced into a dry ice/acetone bath. A solution of bis(pinacolato)diboron (11.4 mg, 0.0449 mmol) in 0.2 mL thf-d_8 was then added by syringe and the mixture stirred manually without removing the cooling bath (to avoid premature transformation prior to the tube being placed in the spectrometer).

Resonances for diastereomers **L3c-Cu–alkyl-2** were detected by ^{1}H NMR (spectrum Q; 96% conv., 15 min, 22 °C); the corresponding alkenyl–B(pin) was detected in trace amounts (<5%). The ^{31}P NMR (spectrum R) indicates 81:19 dr for the formation of **L3c-Cu-alkyl-2**.

A solution of (*E*)-2-[4-(trifluoromethyl)phenyl]vinylboronic acid pinacol ester (13.8 mg, 0.043 mmol, 2.1 equiv.) in 0.2 mL thf-d_8 was added to the mixture transferred by syringe. After 2 h at 22 °C, spectroscopic analysis (spectra S and T) indicated depletion of **L3c-Cu-alkyl-2** concomitant with the appearance of resonances for **L3c-Cu-*iso*-alkyl-1** (17% conv.; 75:25 dr based on ^{31}P NMR spectrum T). Also shown for comparison are ^{31}P NMR spectra T, U and V, indicating the absence of any product from Cu–H addition to less electrophilic/reactive **β-alkenyl–B(pin)-2**.

Conclusions. A bis-phosphine–Cu–H complex can be generated from reaction of a Cu–alkyl complex generated from Cu–B(pin) addition to an alkene, and may subsequently be transferred by a Cu–H elimination/re-addition sequence to a different alkenyl–B(pin)

Evidence for Cu–H elimination; a cross-over experiment

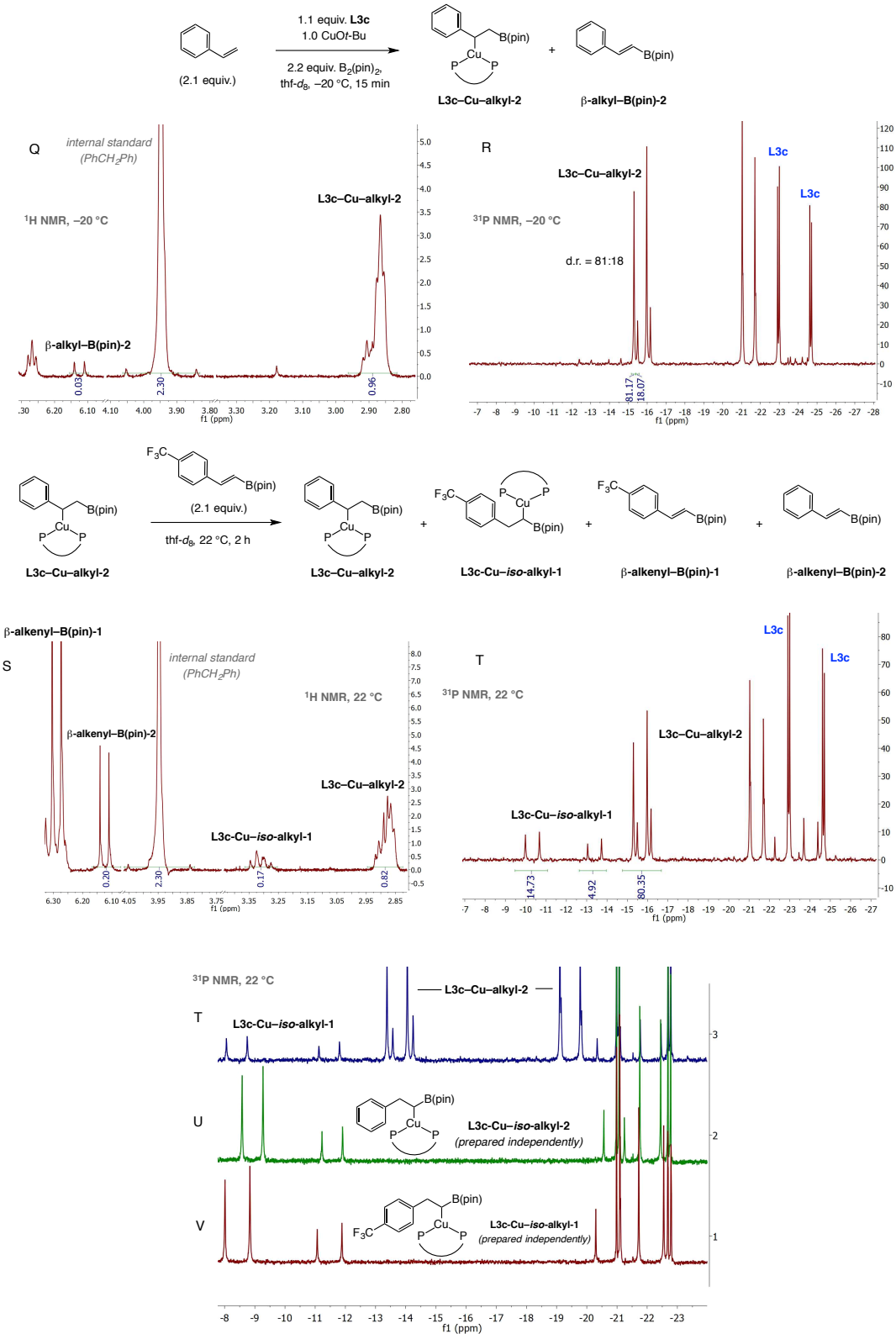

compound but with the opposite regiochemistry (from benzylic to homobenzylic Cu–C

bond); this is further illustrated in Scheme 1.32. It is therefore unlikely that Cu–H re-

Scheme 1.32. Regiochemistry of Cu–H elimination/re-addition

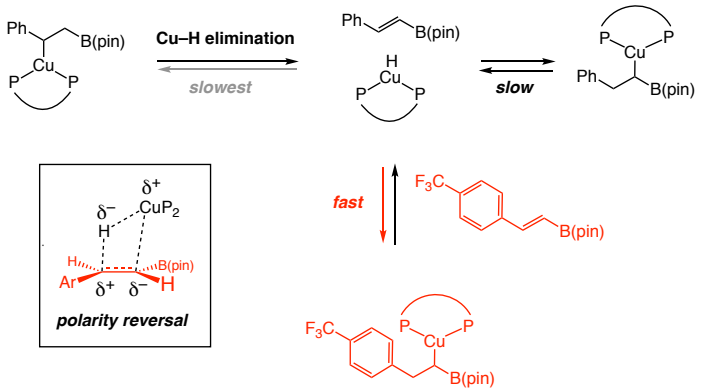

addition from the opposite face of the same alkene can occur without dissociation from the original alkenyl–B(pin) by product. Furthermore, the observation that Cu–H can dissociate and then add to a different alkenyl–B(pin) compound points to a weak bis-phosphine–Cu–H⋯alkenyl–B(pin) coordination. The possibility of Cu–H re-addition to the same alkenyl–B(pin) is rendered especially unlikely considering the presence of substantially larger amounts of terminal alkene substrate under the catalytic condition (vs. any released alkenyl–B(pin)).

1.5.10 Relevance to Catalytic Processes that Involve Cu–H Additions

(*S*)-*N*,*N*-Dibutyl-1,2,3,4-tetrahydronaphthalen-1-amine (1.70): Following the previously reported procedure except 1:3 alkene:hydroxylamine was used. The spectroscopic data are consistent with those reported formerly.[8b] ^{1}H NMR (400 MHz, $CDCl_3$): δ 8.07 (1H, dt, *J* = 7.8, 1.2 Hz), 7.53 (4H, d, *J* = 7.3 Hz), 7.38 (4H, dd, *J* = 8.2, 6.9 Hz), 7.32–7.22 (3H, m), 7.17 (1H, tt, *J* = 7.3, 1.1 Hz), 7.09 (1H, d, *J* = 7.9 Hz), 4.00 (1H, dd, *J* = 10.2, 5.7 Hz), 3.87 (2H, d, *J* = 13.6 Hz), 3.54 (2H, d, *J* = 13.6 Hz), 2.91–2.66 (2H, m), 2.32–2.14 (1H, m), 2.06 (1H, dtt, *J* = 13.7, 5.6, 3.1 Hz), 1.85 (1H, tdd, *J* = 12.5, 10.1, 2.8 Hz), 1.76–1.58 (1H, m); Specific Rotation: $[\alpha]_D^{20}$ –62.0 (*c* 1.00, $CHCl_3$) for an

enantiomerically enriched sample of 97:3 e.r. Enantiomeric purity was determined by HPLC analysis in comparison with authentic racemic material (97:3 e.r. shown; Chiralcel OJ–H column, 97% hexanes, 3% *i*-PrOH, 0.8 mL/min, 220 nm).

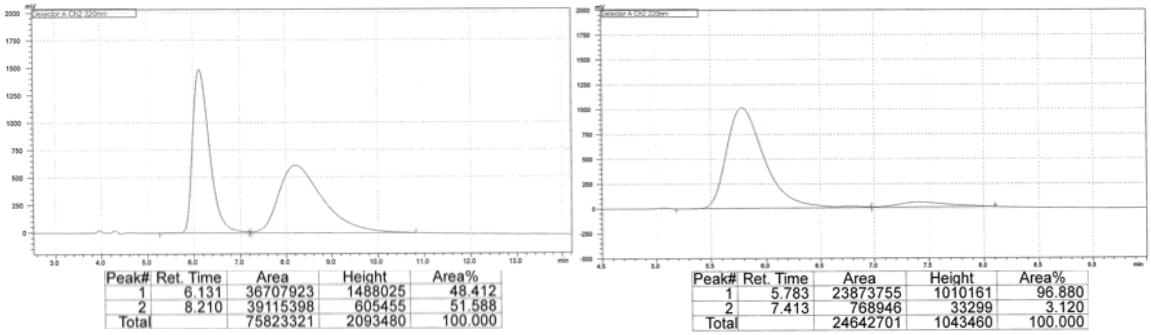

Peak #	Time (min)	Area (%)	Peak #	Time (min)	Area (%)
1	6.131	48.412	1	5.783	96.880
2	8.210	51.588	2	7.413	3.120

***(R)*-2-(1-(3,4-Dihydroisoquinolin-2(1H)-yl)octyl)-2,3-dihydro-1H-naphtho[1,8-de][1,3,2]diazaborinine (1.71):** Following the previously reported procedure except 40 mol % of **L2** was used. The spectroscopic data match those reported previously.[10] ^{1}H NMR (400 MHz, $CDCl_3$): δ 7.10–7.01 (7H, m), 6.88 (1H, d, *J* = 6.8 Hz), 6.00 (2H, dd, 6.8, 1.6 Hz), 5.66 (2H, bs), 3.81 (1H, d, *J* = 14.8 Hz), 3.55 (1H, d, *J* = 14.8 Hz), 2.86–2.79 (1H, m), 2.73–2.55 (3H, m), 1.78 (1H, dd, *J* = 9.2, 4.4 Hz), 1.71–1.64 (1H, m), 1.59–1.50 (1H, m), 1.46–1.37 (1H, m), 1.33–1.24 (9H, m), 0.89 (3H, t, *J* = 6.8 Hz); Enantiomeric purity was determined by HPLC analysis in comparison with authentic racemic material (97:3 e.r. shown; Chiralcel OD–H column, 95% hexanes, 5% *i*-PrOH, 0.5 mL/min, 330 nm).

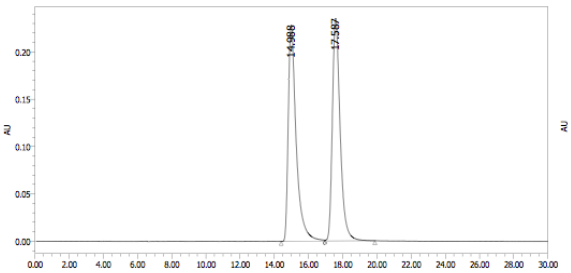

	保持時間 (分)	面積 (μV秒)	%面積	高さ (μV)
1	14.988	7375266	49.72	228425
2	17.587	7458781	50.28	235465

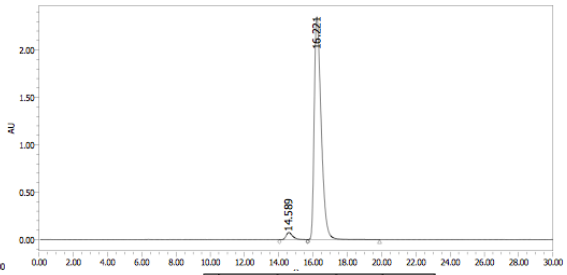

	保持時間 (分)	面積 (μV秒)	%面積	高さ (μV)
1	14.589	2038125	2.99	75250
2	16.221	66191474	97.01	2351533

Peak #	Time (min)	Area (%)	Peak #	Time (min)	Area (%)
1	14.988	49.72	1	14.589	2.99
2	17.587	50.28	2	16.221	97.01

1.5.11 Determination of Absolute Stereochemistry

Other than comparison of specific rotation of **1.69** to the reported values suggesting a (*R*) configuration of the products, we synthesized (***R*)-1.76** and obtained the X-ray crystal structure to ascertain the absolute stereochemical identity of the products.

Scheme 1.33. Synthesis of Lactone **1.76**

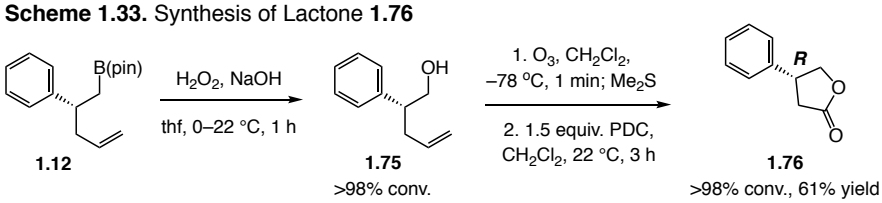

Compound (***R*)-1.75** was synthesized from enantiomerically enriched **1.12** (95:5 e.r.), as illustrated in Scheme 1.33. **(*R*)-4-Phenyldihydrofuran-2(3*H*)-one [(*R*)-1.76]**: The spectroscopic data match those reported previously.[50] ^{1}H NMR (400 MHz, $CDCl_3$): δ 7.40–7.22 (5H, m), 4.67 (1H, dd, *J* = 8.8, 8.0 Hz), 4.28 (1H, dd, *J* = 9.0, 8.2 Hz), 3.79

(50) Malkov, A. V.; Friscourt, F.; Bell, M.; Swarbrick, M. E.; Kočovský, P. *J. Org. Chem.* **2008,** *73,* 3996–4003.

(1H, app pent, J = 8.5 Hz), 2.93 (1H, dd, J = 17.6 and 8.8 Hz), 2.68 (1H, dd, J = 17.6, 8.8 Hz); Specific Rotation: $[\alpha]_D^{20}$ –40.8 (c 0.50, $CHCl_3$). The absolute configuration of **(*R*)-1.76** was established by X-ray analysis, which was assigned to be (*R*). Compound **1.12** is thus assigned to possess the (*R*) configuration. The absolute stereochemistry for other enantiomerically enriched products has been assigned by inference.

1.5.12 Data for X-ray Crystallography of (*R*)-1.76

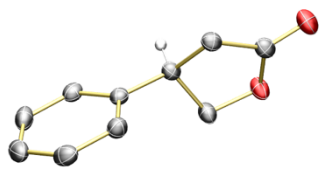

Table 1.2 Crystal data and structure refinement for $C_{10}H_{10}O_2$

Identification code	C10H10O2
Empirical formula	C10 H10 O2
Formula weight	162.18
Temperature	100(2) K
Wavelength	1.54178 Å
Crystal system	Monoclinic
Space group	$P2_1$
Unit cell dimensions	a = 6.1692(7) Å
	b = 7.7518(8) Å
	c = 8.6969(9) Å
Volume	415.33(8) $Å^3$
Z	2

Density (calculated)	1.297 Mg/m^3
Absorption coefficient	0.729 mm^{-1}
F(000)	172
Crystal size	0.600 x 0.070 x 0.050 mm^3
Theta range for data collection	5.092 to 66.613°.
Index ranges	-7<=h<=7, -8<=k<=9, -10<=l<=10
Reflections collected	4434
Independent reflections	1435 [R(int) = 0.0455]
Completeness to theta = 67.679°	98.2 %
Absorption correction	Semi-empirical from equivalents
Max. and min. transmission	0.7528 and 0.5867
Refinement method	Full-matrix least-squares on F^2
Data / restraints / parameters	1435 / 1 / 109
Goodness-of-fit on F^2	1.091
Final R indices [I>2sigma(I)]	R1 = 0.0341, wR2 = 0.0848
R indices (all data)	R1 = 0.0346, wR2 = 0.0858
Absolute structure parameter	-0.05(11)
Extinction coefficient	na
Largest diff. peak and hole	0.145 and -0.213 e. $Å^{-3}$

Table 1.3. Atomic coordinates ($x10^4$) and equivalent isotropic displacement parameters ($Å^2$ x 10^3) for $C_{10}H_{10}O_2$. U(eq) is defined as one third of the trace of the

orthogonalized U^{ij} tensor

	x	y	z	U(eq)
O(1)	4872(2)	3283(2)	344(2)	29(1)
O(2)	8163(2)	4179(2)	-234(2)	34(1)
C(1)	6684(3)	4254(3)	609(2)	25(1)
C(2)	6464(3)	5329(3)	2029(2)	23(1)
C(3)	4017(3)	5331(3)	2238(2)	22(1)
C(4)	3365(3)	3581(3)	1546(2)	26(1)
C(5)	3258(3)	5568(2)	3851(2)	21(1)
C(6)	4294(3)	4761(3)	5124(2)	26(1)
C(7)	3475(4)	4930(3)	6572(2)	31(1)
C(8)	1594(4)	5872(3)	6774(2)	32(1)
C(9)	571(3)	6695(3)	5510(3)	31(1)
C(10)	1411(3)	6549(3)	4071(2)	24(1)

Table 1.4. Bond lengths [Å] and angles [°] for $C_{10}H_{10}O_2$

O(1)-C(1)	1.357(3)
O(1)-C(4)	1.453(2)

O(2)-C(1)	1.202(3)
C(1)-C(2)	1.502(3)
C(2)-C(3)	1.530(3)
C(2)-H(2A)	0.9900
C(2)-H(2B)	0.9900
C(3)-C(5)	1.513(3)
C(3)-C(4)	1.530(3)
C(3)-H(3)	1.0000
C(4)-H(4A)	0.9900
C(4)-H(4B)	0.9900
C(5)-C(10)	1.392(3)
C(5)-C(6)	1.396(3)
C(6)-C(7)	1.388(3)
C(6)-H(6)	0.9500
C(7)-C(8)	1.390(3)
C(7)-H(7)	0.9500
C(8)-C(9)	1.393(3)
C(8)-H(8)	0.9500
C(9)-C(10)	1.384(3)
C(9)-H(9)	0.9500
C(10)-H(10)	0.9500

C(1)-O(1)-C(4)	110.01(15)
O(2)-C(1)-O(1)	120.97(19)
O(2)-C(1)-C(2)	129.3(2)
O(1)-C(1)-C(2)	109.77(17)
C(1)-C(2)-C(3)	103.33(16)
C(1)-C(2)-H(2A)	111.1
C(3)-C(2)-H(2A)	111.1
C(1)-C(2)-H(2B)	111.1
C(3)-C(2)-H(2B)	111.1
H(2A)-C(2)-H(2B)	109.1
C(5)-C(3)-C(4)	112.65(16)
C(5)-C(3)-C(2)	117.74(15)
C(4)-C(3)-C(2)	101.13(16)
C(5)-C(3)-H(3)	108.3
C(4)-C(3)-H(3)	108.3
C(2)-C(3)-H(3)	108.3
O(1)-C(4)-C(3)	105.02(16)
O(1)-C(4)-H(4A)	110.7
C(3)-C(4)-H(4A)	110.7
O(1)-C(4)-H(4B)	110.7
C(3)-C(4)-H(4B)	110.7

H(4A)-C(4)-H(4B)	108.8
C(10)-C(5)-C(6)	118.66(18)
C(10)-C(5)-C(3)	119.28(17)
C(6)-C(5)-C(3)	121.98(18)
C(7)-C(6)-C(5)	120.31(19)
C(7)-C(6)-H(6)	119.8
C(5)-C(6)-H(6)	119.8
C(6)-C(7)-C(8)	120.6(2)
C(6)-C(7)-H(7)	119.7
C(8)-C(7)-H(7)	119.7
C(7)-C(8)-C(9)	119.20(18)
C(7)-C(8)-H(8)	120.4
C(9)-C(8)-H(8)	120.4
C(10)-C(9)-C(8)	120.0(2)
C(10)-C(9)-H(9)	120.0
C(8)-C(9)-H(9)	120.0
C(9)-C(10)-C(5)	121.13(19)
C(9)-C(10)-H(10)	119.4
C(5)-C(10)-H(10)	119.4

Symmetry transformations used to generate equivalent atoms:

Table 1.5. Anisotropic displacement parameters ($Å^2x10^3$) for $C_{10}H_{10}O_2$. The anisotropic displacement factor exponent takes the form: $-2\pi^2[h^2 a^{*2}U^{11} + ... + 2 h k a^* b^* U^{12}]$

	U^{11}	U^{22}	U^{33}	U^{23}	U^{13}	U^{12}
O(1)	25(1)	38(1)	24(1)	-7(1)	4(1)	-6(1)
O(2)	28(1)	46(1)	30(1)	-1(1)	8(1)	0(1)
C(1)	24(1)	28(1)	23(1)	3(1)	0(1)	1(1)
C(2)	20(1)	24(1)	25(1)	2(1)	0(1)	-1(1)
C(3)	21(1)	24(1)	22(1)	3(1)	0(1)	1(1)
C(4)	23(1)	34(1)	23(1)	-4(1)	3(1)	-3(1)
C(5)	21(1)	18(1)	24(1)	-2(1)	1(1)	-3(1)
C(6)	29(1)	23(1)	26(1)	1(1)	2(1)	2(1)
C(7)	42(1)	24(1)	25(1)	0(1)	-2(1)	-5(1)
C(8)	40(1)	31(1)	27(1)	-9(1)	9(1)	-10(1)
C(9)	25(1)	31(1)	37(1)	-11(1)	6(1)	0(1)
C(10)	21(1)	21(1)	30(1)	-2(1)	-2(1)	-2(1)

Table 1.6. Hydrogen coordinates ($x10^4$) and isotropic displacement parameters ($Å^2$ $x10^3$) for $C_{10}H_{10}O_2$

	x	y	z	U(eq)

H(2A)	7011	6515	1879	28
H(2B)	7263	4805	2930	28
H(3)	3343	6256	1569	27
H(4A)	3494	2663	2336	31
H(4B)	1850	3610	1109	31
H(6)	5564	4094	4998	31
H(7)	4208	4395	7435	37
H(8)	1014	5954	7761	39
H(9)	-704	7357	5636	37
H(10)	715	7129	3218	29

Table 1.7. Torsion angles [°] for $C_{10}H_{10}O_2$

C(4)-O(1)-C(1)-O(2)	178.59(19)
C(4)-O(1)-C(1)-C(2)	-1.5(2)
O(2)-C(1)-C(2)-C(3)	161.0(2)
O(1)-C(1)-C(2)-C(3)	-18.9(2)
C(1)-C(2)-C(3)-C(5)	153.11(17)
C(1)-C(2)-C(3)-C(4)	29.95(18)
C(1)-O(1)-C(4)-C(3)	21.5(2)

C(5)-C(3)-C(4)-O(1)	-158.08(16)
C(2)-C(3)-C(4)-O(1)	-31.48(18)
C(4)-C(3)-C(5)-C(10)	-100.7(2)
C(2)-C(3)-C(5)-C(10)	142.14(19)
C(4)-C(3)-C(5)-C(6)	76.0(2)
C(2)-C(3)-C(5)-C(6)	-41.1(3)
C(10)-C(5)-C(6)-C(7)	0.5(3)
C(3)-C(5)-C(6)-C(7)	-176.25(19)
C(5)-C(6)-C(7)-C(8)	1.3(3)
C(6)-C(7)-C(8)-C(9)	-2.0(3)
C(7)-C(8)-C(9)-C(10)	0.9(3)
C(8)-C(9)-C(10)-C(5)	0.9(3)
C(6)-C(5)-C(10)-C(9)	-1.6(3)
C(3)-C(5)-C(10)-C(9)	175.24(19)

Symmetry transformations used to generate equivalent atoms:

1.5.13 Representative Products of Bis-Phosphine–Cu-Catalyzed Reactions

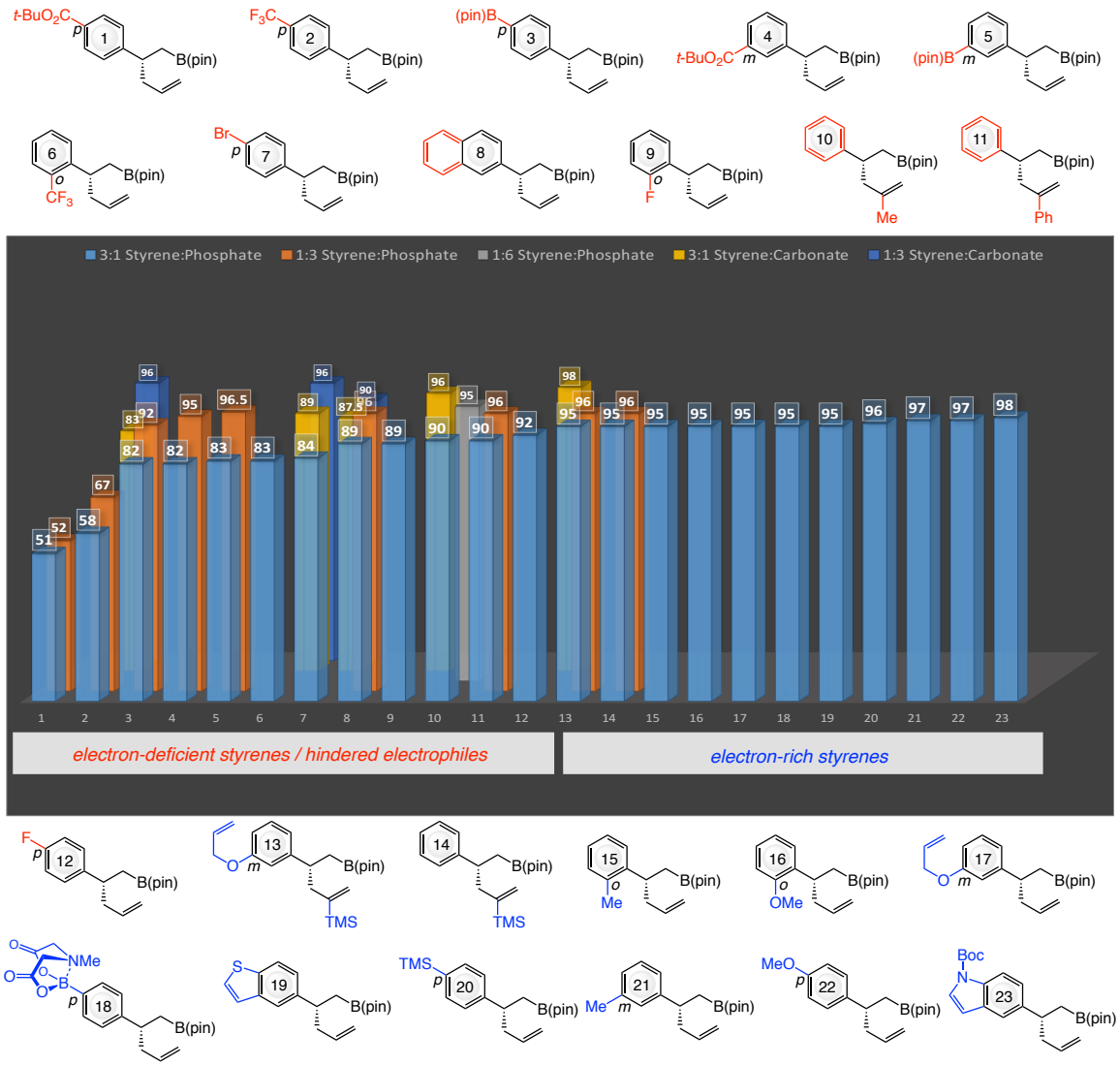

1.5.14 Density Functional Theory (DFT) Calculations

(**Please Note:** In the following section, the term Cu–rev is synonymous with the term Cu–*iso* used above.)

DFT computations[51] were performed with the Gaussian 09 suite of programs[52]. Geometries were optimized with density functional ωB97XD[53] and the Def2SVP basis set[54]. The effect of a polar reaction medium (tetrahydrofuran, THF) was approximated by means of the SMD solvation model[55]. Stationary points were probed through vibrational analysis and Gibbs free energy corrections were performed under standard conditions (298.15 K, 1.0 atm). Intrinsic reaction coordinate (IRC) calculations have been performed starting from selected transition states (**ts**) employing the L(ocal) Q(uadratic) A(approximation) method, followed by subsequent optimization to obtain structures and energies for educt (**ed**) and product (**prod**) on either side of the transition state[56]. We furthermore probed the performance of various density functionals through single point

---

(51) For reviews on application of DFT calculations to the chemistry of transition metal complexes see: (a) Cramer, C. J.; Truhlar, D. G. *Phys. Chem. Chem. Phys.* **2009,** *11,* 10757–10816. (b) Grimme, S.; Ehrlich, S.; Goerigk, L. *J. Comp. Chem*. **2001,** *32,* 1456–1465. (c) Peverati, R.; Truhlar, D. G. *Phil. Trans. R. Soc. A* **2014,** *372*:20120476.

(52) Frisch, M. J.; Trucks, G. W.; Schlegel, H. B.; Scuseria, G. E.; Robb, M. A.; Cheeseman, J. R.; Scalmani, G.; Barone, V.; Mennucci, B.; Petersson, G. A.; Nakatsuji, H.; Caricato, M.; Li, X.; Hratchian, H. P.; Izmaylov, A. F.; Bloino, J.; Zheng, G.; Sonnenberg, J. L.; Hada, M.; Ehara, M.; Toyota, K.; Fukuda, R.; Hasegawa, J.; Ishida, M.; Nakajima, T.; Honda, Y.; Kitao, O.; Nakai, H.; Vreven, T.; Montgomery, Jr., J. A.; Peralta, J. E.; Ogliaro, F.; Bearpark, M.; Heyd, J. J.; Brothers, E.; Kudin, K. N.; Staroverov, V. N.; Kobayashi, R.; Normand, J.; Raghavachari, K.; Rendell, A.; Burant, J. C.; Iyengar, S. S.; Tomasi, J.; Cossi, M.; Rega, N.; Millam, J. M.; Klene, M.; Knox, J. E.; Cross, J. B.; Bakken, V.; Adamo, C.; Jaramillo, J.; Gomperts, R.; Stratmann, R. E.; Yazyev, O.; Austin, A. J.; Cammi, R.; Pomelli, C.; Ochterski, J. W.; Martin, R. L.; Morokuma, K.; Zakrzewski, V. G.; Voth, G. A.; Salvador, P.; Dannenberg, J. J.; Dapprich, S.; Daniels, A. D.; Farkas, Ö.; Foresman, J. B.; Ortiz, J. V.; Cioslowski, J.; Fox, D. J. *Gaussian 09, Revision **D.01**,* Gaussian, Inc., Wallingford CT **2009**.

(53) Chai, J.-D.; Head-Gordon, M. *Phys. Chem. Chem. Phys.*, **2008,** *10,* 6615–6620.

(54) Weigend, F.; Ahlrichs, R. *Phys. Chem. Chem. Phys.* **2005**, *7*, 3297–3305.

(55) Marenich, A. V.; Cramer, C. J.; Truhlar, D. G. *J. Phys. Chem. B.* **2009,** *113,* 6378–6396.

(56) (a) Page, M.; McIver Jr., J. W. *J. Chem. Phys.* **1998,** *88,* 922–935. (b) Page, M.; Doubleday Jr., C.; McIver Jr., J. W. *J. Chem. Phys.* **1990,** *93,* 5634–5642.

energy calculations at the geometries optimized at the levels described above by means of the SMD solvation model[55] with THF as solvent and the larger Def2TZVPP[54] basis set. Since the correct density functional is not known we tested several state of the art approaches that have been developed over the past decade[51, 57]: ωB97XD[53], M06[58], MN12SX[59], MN12L[59], M06L[58], BP86-D3BJ[51b, 60] and PBE0-D3BJ[51b, 61] (Figure 1–9). Electronic and Gibbs free energies for Figure 1–10 are provided in doi:10.1038/nchem.2861 and the entries used as the basis for Figures 6–7 are highlighted in red. A file for convenient viewing of computed geometries with the program Mercury 3.3 is appended as separate "coordinates.xyz" file in doi:10.1038/nchem.2861[62].

---

(57) For selected examples highlighting the importance of including treatment of dispersion interactions in modeling olefin metathesis reactions promoted by Ru carbene complexes see: (a) Torker, S.; Merki, D.; Chen. P. *J. Am. Chem. Soc.* **2008,** *130,* 4808–4814. (b) Minenkov, Y.; Occhipinti, G.; Singstad, A.; Jensen, V. R. *Dalton Trans.* **2012,** *41,* 5526–5541. (c) Minenkov, Y.; Occhipinti, G.; Jensen, V. R. *Organometallics* **2013,** *32,* 2099–2111. (d) Torker, S.; Khan, R. K. M.; Hoveyda, A. H. *J. Am. Chem. Soc.* **2014,** *136,* 3439–3455. (e) Khan, R. K. M.; Torker, S.; Hoveyda, A. H. *J. Am. Chem. Soc.* **2014,** *136,* 14337–14340. (f) Torker, S.; Koh, M. J.; Khan, R. K. M.; Hoveyda, A. H. *Organometallics* **2016,** *35,* 543–562. (g) Mikus, M. S.; Torker, S.; Hoveyda, A. H. *Angew. Chem. Int. Ed.* **2016,** *55,* 4997–5002. For modeling allyl addition to CF_3-ketones see: (h) Lee, K.; Silverio, D. L.; Torker, S.; Robbins, D. W.; Haeffner, F.; Hoveyda, A. H. *Nat. Chem.* **2016,** *8,* 768–777.

(58) Zhao, Y.; Truhlar, D. G. *Acc. Chem. Res.* **2008,** *41,* 157–167.

(59) Peverati, R.; Truhlar, D. G. *Phys. Chem. Chem. Phys.* **2012,** *14,* 16187–1619.

(60) (a) Becke, A. D. *Phys. Rev. A: At. Mol. Opt. Phys.* **1988***, 38,* 3098–3100. (b) Perdew, J. P.; Yue, W. *Phys. Rev. B* **1986,** *33,* 8800–8802.

(61) Adamo, C.; Barone, V. *J. Chem. Phys.* **1999,** *110,* 6158–6169.

(62) Lichtenberger, D. L.; Gladysz, J. A. *Organometallics* **2014,** *33,* 835−835. The "coordinates.xyz" file can be generated by copying all the coordinates in doi:10.1038/nchem.2861 into a text file without empty lines and changing the extension to ".xyz".

Scheme 1.34. General reaction sequence for Cu–B(pin) addition/allylic substitution including competitive side reactions (β-H or Cu–H elimination/re-addition).

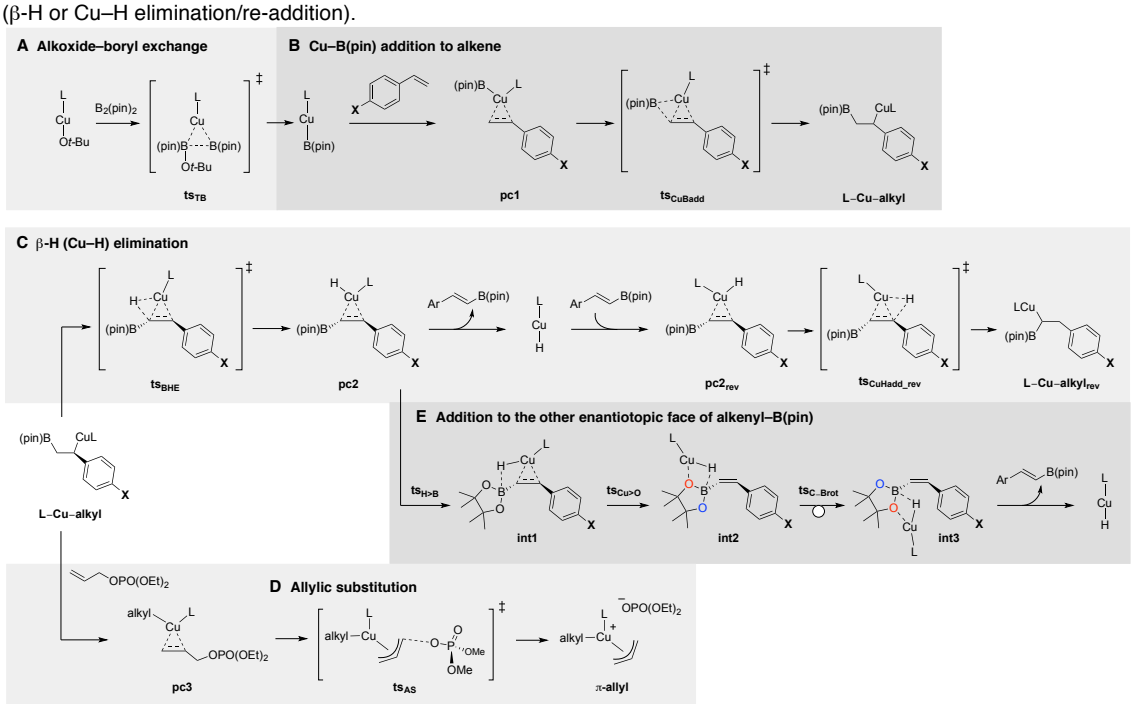

Abbreviations: **TB**, transborylation [conversion of Cu–alkoxide to Cu–B(pin)]; **BHE**, β-hydride (or Cu–H) elimination; **pc**, π-complex; $\mathbf{ts_{H>B}}$, transition state for hydride migration to boron; $\mathbf{ts_{Cu>O}}$, transition state for Cu migration to oxygen on Bpin; $\mathbf{ts_{C\text{-}Brot}}$, transition state for C–B bond rotation; $\mathbf{ts_{CuHadd\_rev}}$, transition state Cu–H addition leading to Cu–alkyl$_{rev}$ species with opposite regiochemistry; **int**, intermediate; **Cu–H**, linear Cu-hydride species.

Background

Linear CuO*t*-Bu species that contain neutral ligands are labeled as **L–Cu–O*t*-Bu** [L = bis-phosphine **L3a**, a model NHC (**NHCMe$_2$**) and phosphine (**PMe$_3$**), tetrahydrofuran (thf) or an aryl olefin with *para* substituent X]. Formation of linear **L–Cu–B(pin)** complex is expected to occur by reaction with $B_2(pin)_2$ via transition state $\mathbf{ts_{TB}}$. In Figures 1–10, **ed** and **prod** denote the minima on either side of $\mathbf{ts_{TB}}$, which was obtained by IRC calculations and subsequent optimization. Complex **L–Cu–B(pin)** undergoes Cu–B(pin) addition through the following sequence: **pc1** → $\mathbf{ts_{CuBadd}}$ → **L–Cu–alkyl**. Complex **L–Cu–alkyl** can either participate in an allylic substitution reaction (**pc3** → $\mathbf{ts_{AS}}$ → **π-allyl**) or Cu–H elimination via transition state $\mathbf{ts_{BHE}}$ to generate π-complex **pc2**. Upon dissociation of the alkenyl–B(pin) species linear **L–Cu–H** is formed, which might then

re-add with the opposite site selectivity [Cu at the carbon bearing the B(pin) unit] to form alkylcopper species **L–Cu–alkyl$_{rev}$** (**pc2$_{rev}$** → **ts$_{CuHadd_rev}$**).

Questions to be Addressed

Issues concerning the DFT calculations. The difficulty associated with modeling reactions that contain multiple ionic species notwithstanding, a number of DFT calculations were performed. Comparison of absolute free energies of transition states with different character (e.g., **ts$_{CuBadd}$** vs. **ts$_{AS}$**) is challenging and probably subject to somewhat large relative errors. This is particularly an issue with transtition state structures that may be envisioned for the allylic substitution (AS) step, such as those where the phosphate moiety is cleaved without the assistance of Na chelation and those where Na coordination is involved (but not necessarily intramolecular, see below).

ts$_{AS}$ without Na alkoxide **ts$_{AS}$** with Na alkoxide

Specific questions investigated. The major goal of these studies was to address the following questions:

(1) What is the most plausible stereochemical model for L–Cu–B(pin) addition to an aryl olefin with L being bis-phosphine ligand **L3a**?

(2) What are the most likely steps where the presence of an electron-deficient aryl olefin can lead to a lowering of enantioselectivity? Is it possible that electron-deficient alkene might be capable of activating Cu–O*t*-Bu clusters, breaking them into smaller,

more reactive species, due to their ability to provide stronger back-bonding (lower energy π*)?

(3) Alternatively, does an electron-deficient aryl olefin allow for a more competitive Cu–B(pin) addition with an achiral complex?

(4) Why does the allylic substitution step seem to be more difficult with bis-phosphine **L3a**, particularly with bulkier allyl elecrophiles? Does this allow for alternative reaction pathways to compete, leading to lower e.r. (enantiomeric ratio)?

(5) Is β–H (Cu–H) elimination within the alkylcopper intermediates critical to enantioselectivity fluctuations and, if so, is it followed by subsequent Cu–H re-addition from the opposite enantiotopic face?

(6) What is the basis for reactions, regardless of whether they contain an NHC or a phosphine ligand, being highly S_N2'-selective?

(7) Does displacement of the bis-phosphine ligand by an aryl olefin or a Lewis basic solvent molecule (i.e., thf) take place to a degree that influences the observed e.r. fluctuations? This might have several advantages: Although phosphines are better donors (compared to olefins) and should therefore bind more strongly to the metal center, the smaller size and π-accepting properties of styrenes could exert a positive influence on the rate of C–B bond formation. However, a competitive and non-selective Cu–B addition pathway starting form **L3a –Cu–B(pin)** would likely be second-order in the alkene (i.e., one styrene needed for displacement of **L3a** and another one is involved in Cu–B addition; Scheme 1.35). See the discussion associated with Figures 6–7 below.

Scheme 1.35. Enantioselective Cu–B(pin) addition and competitive bimolecular reaction.

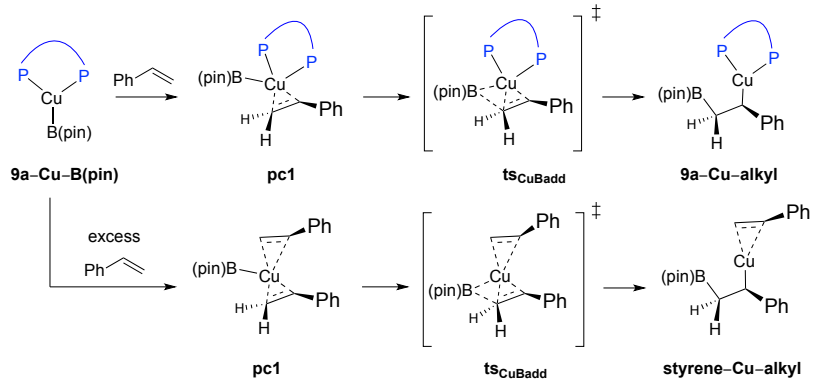

Stereochemical Model for Addition of L3a–Cu–B(pin) to an Aryl Olefin (Figure 1.1–1.2)

The free energy surface for Cu–B(pin) addition with ligand **L3a** at the M06/Def2TZVPP$_{THF(SMD)}$//ωB97XD/ Def2SVP$_{THF(SMD)}$ level are shown in Figure 1.1. Reaction of **L3a–Cu–O*t*-Bu** generates **L3a–Cu–B(pin)** irreversibly (G_{rel} = 0.0 kcal/mol) via transition state **ts$_{TB}$** (G_{rel} = 36.3 kcal/mol). Two modes of addition were considered that might afford the major diastereomer of **L3a-Cu–alkyl** complex [**major01** with the phenyl group on styrene pointing to the front (G_{rel} = 16.9 kcal/mol) and **major02** with the phenyl ring facing to the rear (G_{rel} = 23.4 kcal/mol); Figure 1.1]. The same applies to the pathways leading to the minor diastereomer of **L3a–Cu–alkyl** [**minor01** (G_{rel} = 18.9 kcal/mol) and **minor02** (G_{rel} = 21.8 kcal/mol)]. The computed energies are in agreement with the experimental observations. Investigation with other density functionals (ωB97XD, MN12SX, MN12L, M06L, BP86-D3BJ and PBE0-D3BJ) revealed qualitatively similar trends albeit with some differences in the absolute energies (e.g., with BP86 including Grimme's D3 dispersion the reaction barriers relative to **L3a–Cu–B(pin)** are underestimated, likely due to overestimation of dispersion; 4.1 kcal/mol for **ts$_{CuBadd_major01}$**; Figure 1.2).

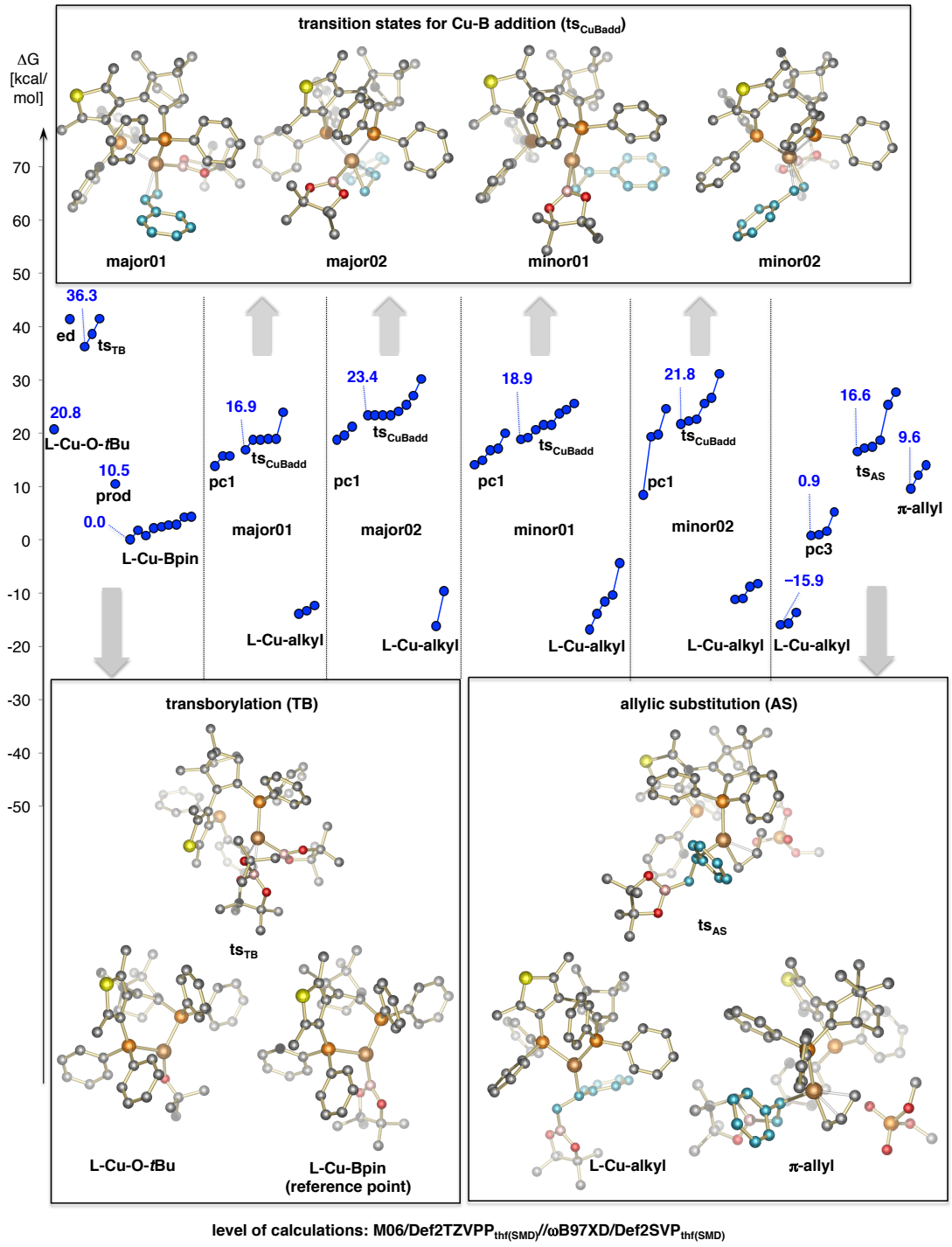

Figure 1.1. Free energy surfaces for the enantioselective Cu–B(pin) addition (CuBadd)/allylic substitution (AS) sequence with bis-phosphine **L3a** at the M06/DefTZVPP$_{thf(SMD)}$//ωB97XD/Def2SVP$_{thf(SMD)}$ level. Several conformers are shown for the two modes of addition leading to the major (**major01** and **major02**) and the minor enantiomer (**minor01** and **minor02**). The free energies have been referenced to the most stable **L3a–Cu–B(pin)** conformer. Only the AS transition states leading to the major enantiomer are shown. The computed structures of the lowest conformer for a given species are displayed. Abbreviations: **TB**, transborylation [conversion of Cu–alkoxide to Cu–B(pin)]; **pc**, π-complex.

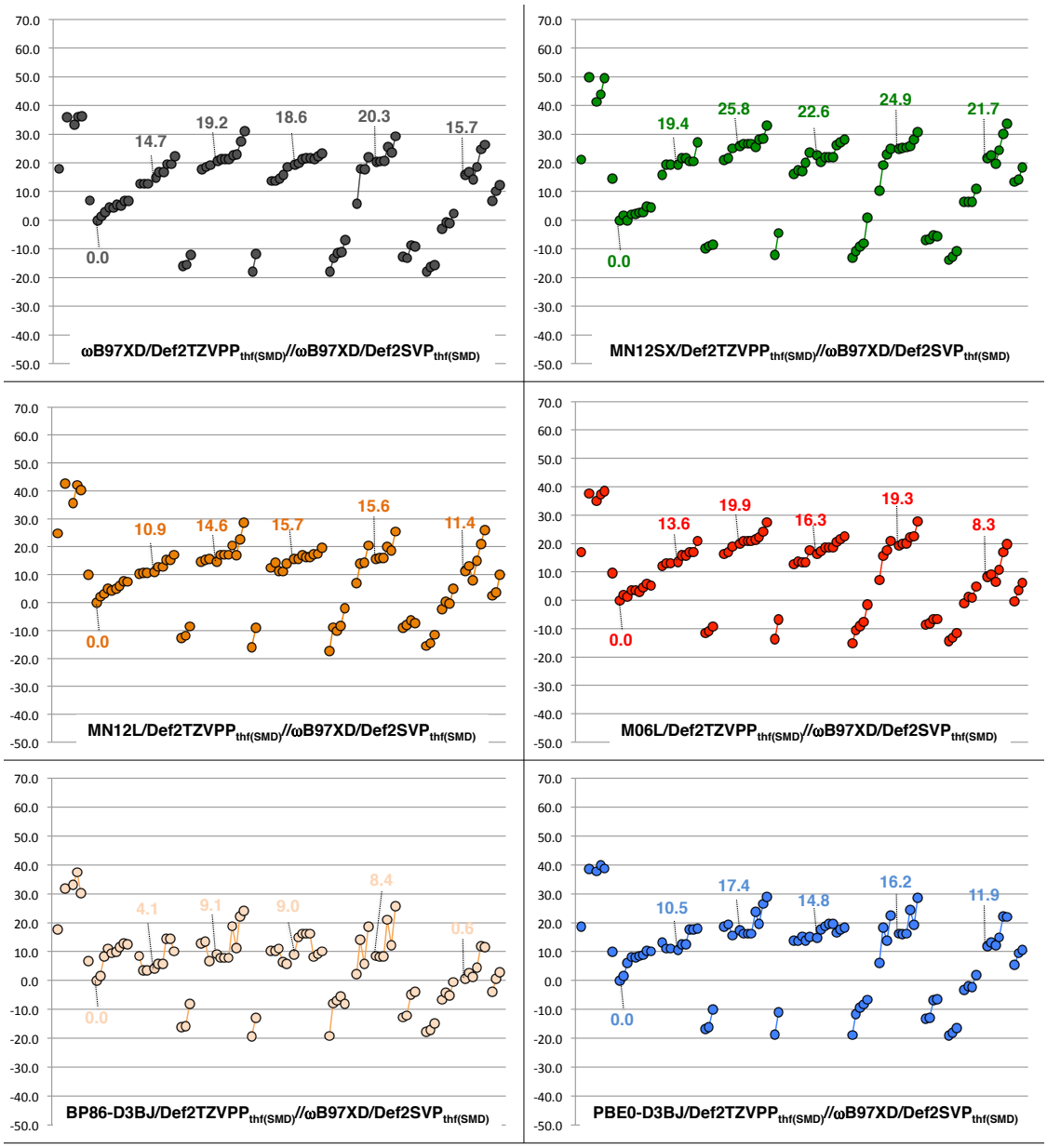

Figure 1.2. Free energy surfaces for the enantioselective Cu–B(pin) addition (CuBadd)/allylic substitution (AS) sequence with ligand **L3a** at the M06/DefTZVPP$_{thf(SMD)}$//ωB97XD/Def2SVP$_{thf(SMD)}$ level. Several conformers are shown for the two modes of addition that lead to the major (**major01** and **major02**) as well as the minor enantiomer (**minor01** and **minor02**). The free energies have been referenced to the most stable **L3a–Cu–B(pin)** conformer; only AS transition states leading to the major enantiomer are shown; the computed structures of the lowest conformer for a given species are displayed. Abbreviations: **TB** [conversion of Cu–alkoxide to Cu–B(pin)], transborylation; **pc**, π-complex.

Following Cu–B(pin) addition, the major alkylcopper diastereomer may undergo allylic substitution via $\mathbf{ts_{AS}}$ (G_{rel} = 16.6 kcal/mol for the most accessible conformer)[63,64,65,66]. Due to higher conformational complexity of $\mathbf{ts_{AS}}$ compared to $\mathbf{ts_{CuBadd}}$ we did not perform calculations for allylic substitution with the minor alkylcopper diastereomer; we judged that the energy difference relative to the major pathway would be masked by significant uncertainty.

Several structural features are worth highlighting, which explain why the major enantiomer is generated preferentially and shed light on coordination chemistry of the bis-phosphine ligands (Scheme 1.36). In the pathway leading to the major alkylcopper enantiomer there is, in addition to several edge-to-face aromatic interactions[67], a weak H-bonding association between one of the oxygen atoms of the B(pin) moiety and an *ortho*-hydrogen atom of an arylphosphine ring (Scheme 1.36a). Rather than consider this H-bonding interaction as purely attractive, this geometry may be viewed as the least

---

(63) For mechanistic considerations regarding nucleophilic reaction promoted by Cu(I) species see: Yoshikai, N.; Nakamura, E. *Chem. Rev.* **2012,** *112,* 2339–2372. For a computational report regarding the nucleophilicity of d-orbitals in Cu-alkyl species see: Mori, S.; Hirai, A.; Nakamura, M.; Nakamura, E. *Tetrahedron* **2000,** *56,* 2805–2809.

(64) For an early computational report regarding site selectivity in allylic substitution (AS) reactions involving anionic hetereocuprates see: (a) Yoshikai, N.; Zhang, S.-L.; Nakamura, E. *J. Am. Chem. Soc.* **2008,** *130,* 12862–12863.. For a report discussing regioselectivity during reductive elimination from Cu(III) π-allyl species see: (b) Yamanaka, M.; Kato, S.; Nakamura, E. *J. Am. Chem. Soc.* **2004,** *126,* 6287–6293.

(65) For a dissusion of enantioselective allylic substitution promoted by Cu–R entities bearing NHC ligands with a pendant sulfonate group see: (a) Shi, Y.; Jung, B.; Torker, S.; Hoveyda, A. H. *J. Am. Chem. Soc.* **2015,** *137,* 8948–8964. (b) Lee, J.; Torker, S.; Hoveyda, A. H. *Angew. Chem. Int. Ed.* **2017,** *56,* 821–826.

(66) For additional stereochemical models regarding 1,4- or 1,6-additions to enoates or dienoates that also suggest the involvement of an intramolecular coordination of the substrate to a metal counterion see: (a) Meng, F.; Li, X.; Torker, S.; Shi, Y.; Shen, X.; Hoveyda, A. H. *Nature* **2016,** *537,* 387–393. (b) Li, X.; Meng, F.; Torker, S.; Shi, Y.; Hoveyda, A. H. *Angew. Chem. Int. Ed.* **2016,** *55,* 9997–10002.

(67) (a) Quan, R. W.; Li Z.; Jacobsen, E. N. *J. Am. Chem. Soc.* **1996,** *118,* 8156–8157. For a review on aromatic interactions see: (b) Hunter, C. A.; Lawson, K. R.; Perkins, J.; Urch, C. J. *J. Chem. Soc., Perkin Trans.* **2001,** *2* 651–669.

repulsive; in other words, there is probably minimal electron density on that particular ortho proton on the phenyl ring, which favors propinquity with the B(pin) moiety.

The presence of the four *meta*-methyl groups of the diarylphosphine moieties in bis-phosphine **L3c** causes enantioselectivity reversal (20:80 e.r.); we propose this is because the aforementioned weak H-bonding interaction is sterically and electronically disrupted. It is also likely that the phosphine ligand adopts a more flexible coordination mode.

Scheme 1.36. Key structural features in the transition states for Cu–B(pin) addition and allylic substitution with ligand **L3a**.

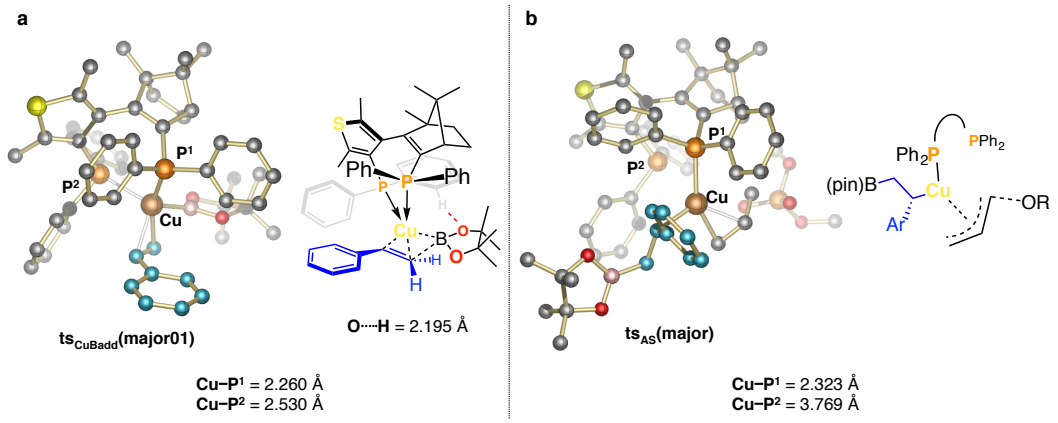

While bis-phosphine **L3a** probably coordinates to Cu in a bidentate manner during Cu–B(pin) addition (with a dissymmetric coordination of the two phosphine atoms; Cu–P^1 = 2.260 Å vs. Cu–P^2 = 2.530 Å; Scheme 1.36a), its coordination mode is monodentate during the allylic substitution process; this adjustment is required for accommodating the square planar geometry involving a π-allyl group (Scheme 1.36b). One of the phosphine atoms may therefore be displaced from Cu as reflected in a comparatively long Cu–P^2 distance (3.769 Å; Scheme 1.36b). The additional and undesired enthalpic penalty associated with cleavage of the Cu–P^2 bond implies that

allylic substitution reactions, particularly those with sterically hindered electrophiles, are challenging and can allow side reactions to become more competitive.

Influence of Electronic Attributes of Aryl Olefins on the Barriers for Cu–B(pin) Addition, β-Hydride (Cu–H) Elimination and Allylic Substitution (Figures 2–3)

To gain insight vis-à-vis the impact of electronic alterations of aryl olefins, we probed the free energy surface for Cu–B(pin) addition with model NHC or phosphine ligands at the M06/Def2TZVPP$_{thf(SMD)}$//ωB97XD/ Def2SVP$_{thf(SMD)}$ level (Figure 2.1–2.2 for L = **NHCMe$_2$** and Figure 3.1–3.2 for L = **PMe$_3$**). We considered examining a model system to be more effective approach because the key electronic effects could be masked by large conformational complexity. We have referenced the energies relative to **L3a–Cu–B(pin)** and, as a result, the free energies in Figure 2.1 include that needed for displacement of the neutral bis-phosphine ligand [i.e., **L3a–Cu–B(pin)** + **Me$_2$NHC** → **Me$_2$NHC–Cu–B(pin)** + **L3a**].

Complex **Me$_2$NHC–Cu–O*t*-Bu** is likely monomeric (13.6 kcal/mol relative to **L3a–Cu–B(pin)** compared to 16.7 kcal/mol for the derived dimer; blue curve in Figure 2.1); it reacts with $B_2(pin)_2$ via transition state **ts$_{TB}$** (22.5 kcal/mol) to generate **Me$_2$NHC–Cu–B(pin)**, which is 2.8 kcal/mol more stable relative to **L3a–Cu–B(pin)**, suggesting that **NHCMe$_2$** coordinates more strongly to Cu than bis-phosphine **L3a**. **Me$_2$NHC–Cu–B(pin)** reacts irreversibly with styrene (11.6 kcal/mol for **ts$_{CuBadd}$**) to generate **Me$_2$NHC–Cu–alkyl** species (–19.9 kcal/mol for the conformer obtained by IRC calculation/optimization). Complex **Me$_2$NHC–Cu–alkyl** can either undergo Cu–H

elimination via $\mathbf{ts_{BHE}}$ (5.1 kcal/mol) or allylic substitution (1.7 kcal/mol for $\mathbf{ts_{AS}}$). Although these data suggest that reaction with the allyl phosphate ($\mathbf{ts_{AS}}$) is more favorable than formation of the alkenyl–B(pin) ($\mathbf{ts_{BHE}}$), a more rigorous estimate of the relationship between $\mathbf{ts_{BHE}}$ and $\mathbf{ts_{AS}}$ would be difficult to establish. Firstly, unimolecular as opposed to bimolecular processes will show different dependencies on concentration. Secondly, as already mentioned, the precise idendity of $\mathbf{ts_{AS}}$ is probably unknown, although a structure resembling a π-allyl species should likely be entertained[63,64].

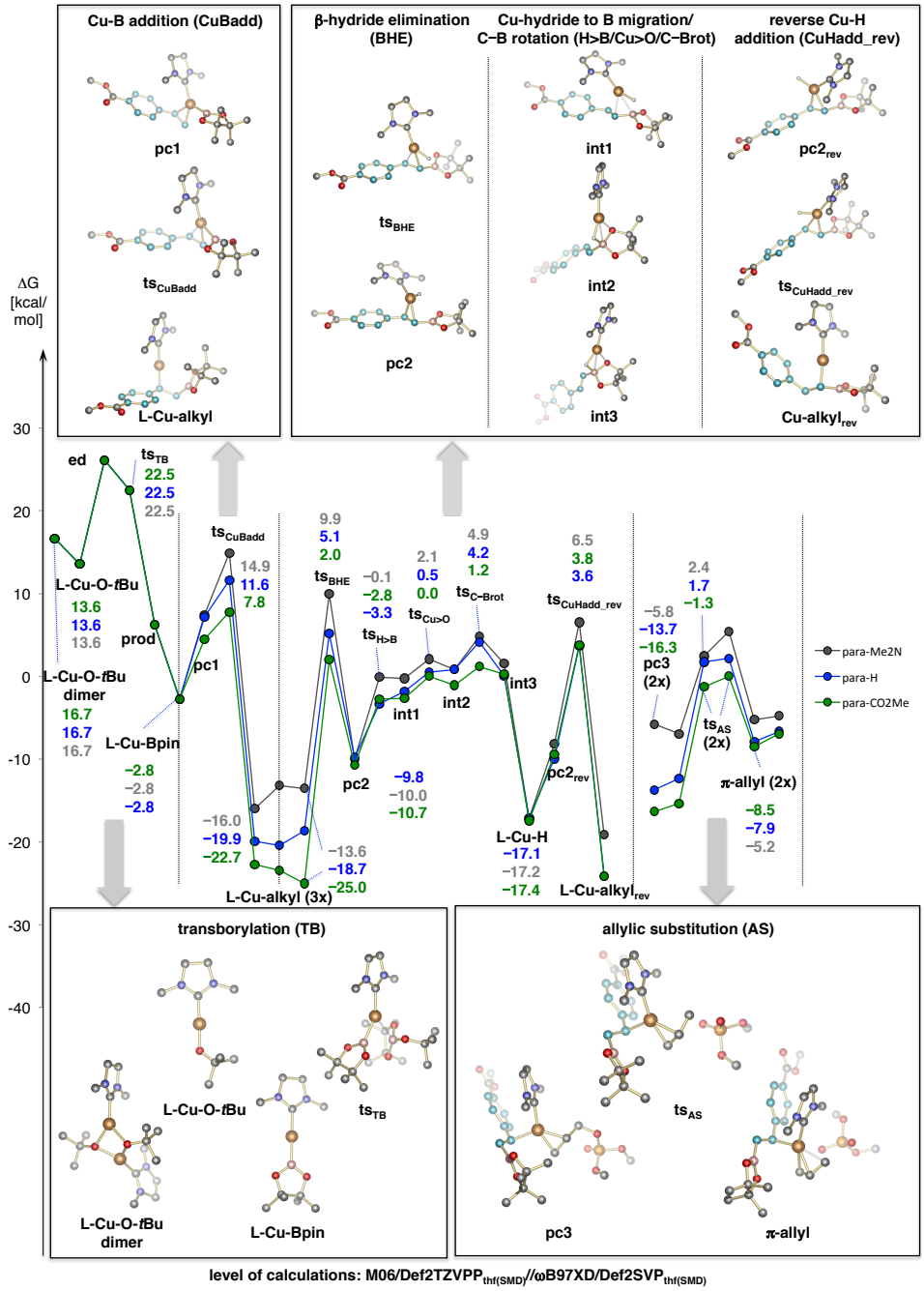

Figure 2.1. Free energy surfaces for the enantioselective Cu–B(pin) addition (CuBadd)/allylic substitution (AS) sequence with a model NHC ligand (**NHCMe$_2$**) for reaction with various aryl olefins (***p*-Me$_2$N**, grey; ***p*-H**, blue; ***p*-CO$_2$Me**, green) at the M06/DefTZVPP$_{thf(SMD)}$//ωB97XD/Def2SVP$_{thf(SMD)}$ level. Several conformers are shown for **ts$_{AS}$** and **L–Cu–alkyl**. The free energies have been referenced to the most stable **L3a–Cu–B(pin)** conformer, which takes into account the free energy for ligand displacement (cf. Figure 6.1); the computed structures for L = ***p*-CO$_2$Me-styrene** are displayed. Abbreviations: **TB**, transborylation [conversion of Cu–alkoxide to Cu–B(pin)]; **BHE**, β-hydride (or Cu–H) elimination; **pc**, π-complex; **ts$_{H>B}$**, transition state for hydride migration to boron; **ts$_{Cu>O}$**, transition state for Cu migration to oxygen on Bpin; **ts$_{C\text{-}Brot}$**, transition state for C–B bond rotation; **ts$_{CuHadd_rev}$**, transition state Cu–H addition leading to Cu–alkyl$_{rev}$ species with opposite regiochemistry; **int**, intermediate; **Cu–H**, linear Cu-hydride species.

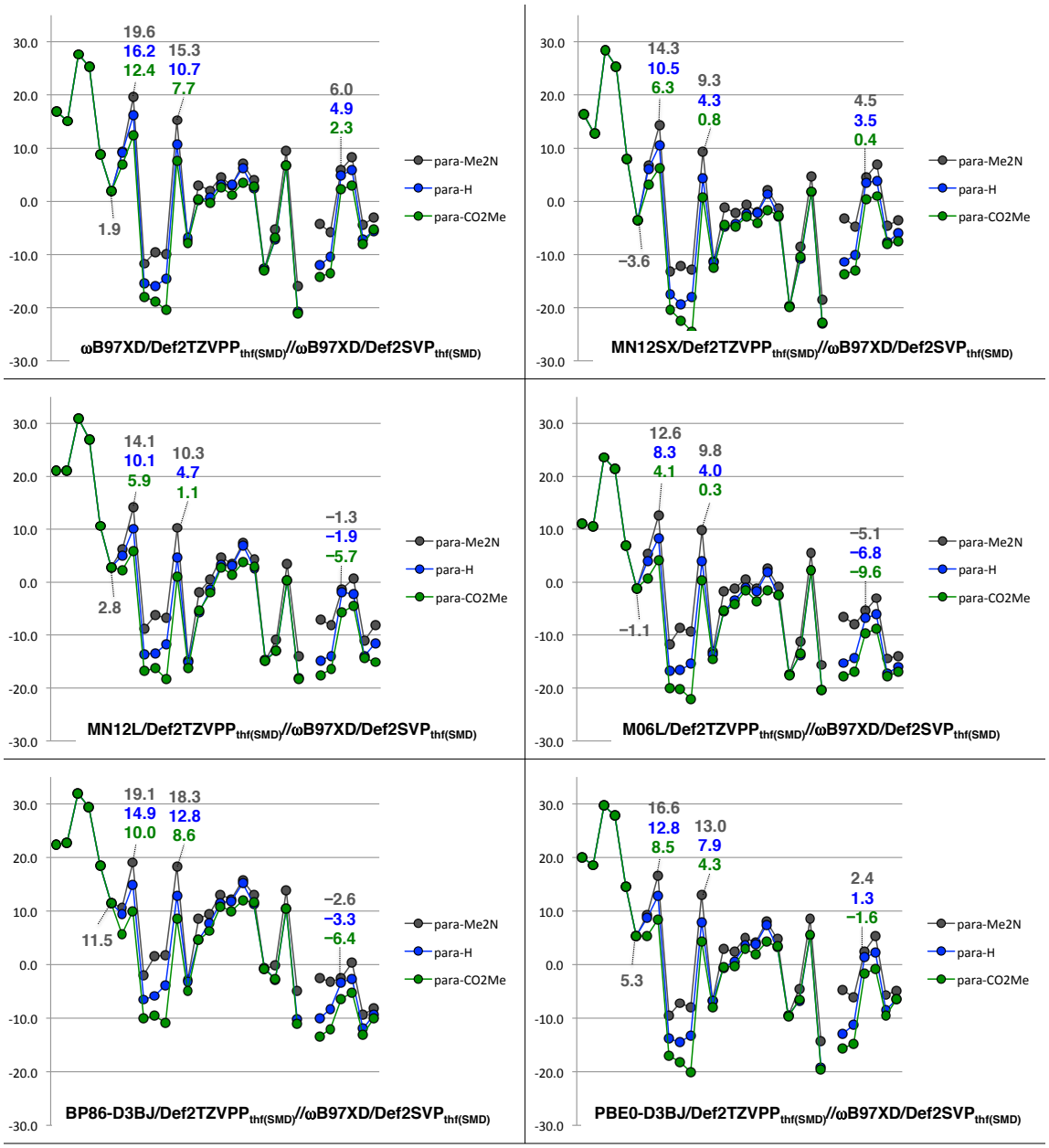

Figure 2.2. Free energy surfaces for the enantioselective Cu–B(pin) addition (CuBadd)/allylic substitution (AS) sequence with a model NHC ligand (**NHCMe$_2$**) for reaction with various styrene derivatives (***p*-Me$_2$N**, grey; ***p*-H (styrene)**, blue; ***p*-CO$_2$Me**, green) with various density functionals after optimization with ωB97XD/Def2SVP$_{thf(SMD)}$. For details, see Figure 2.1.

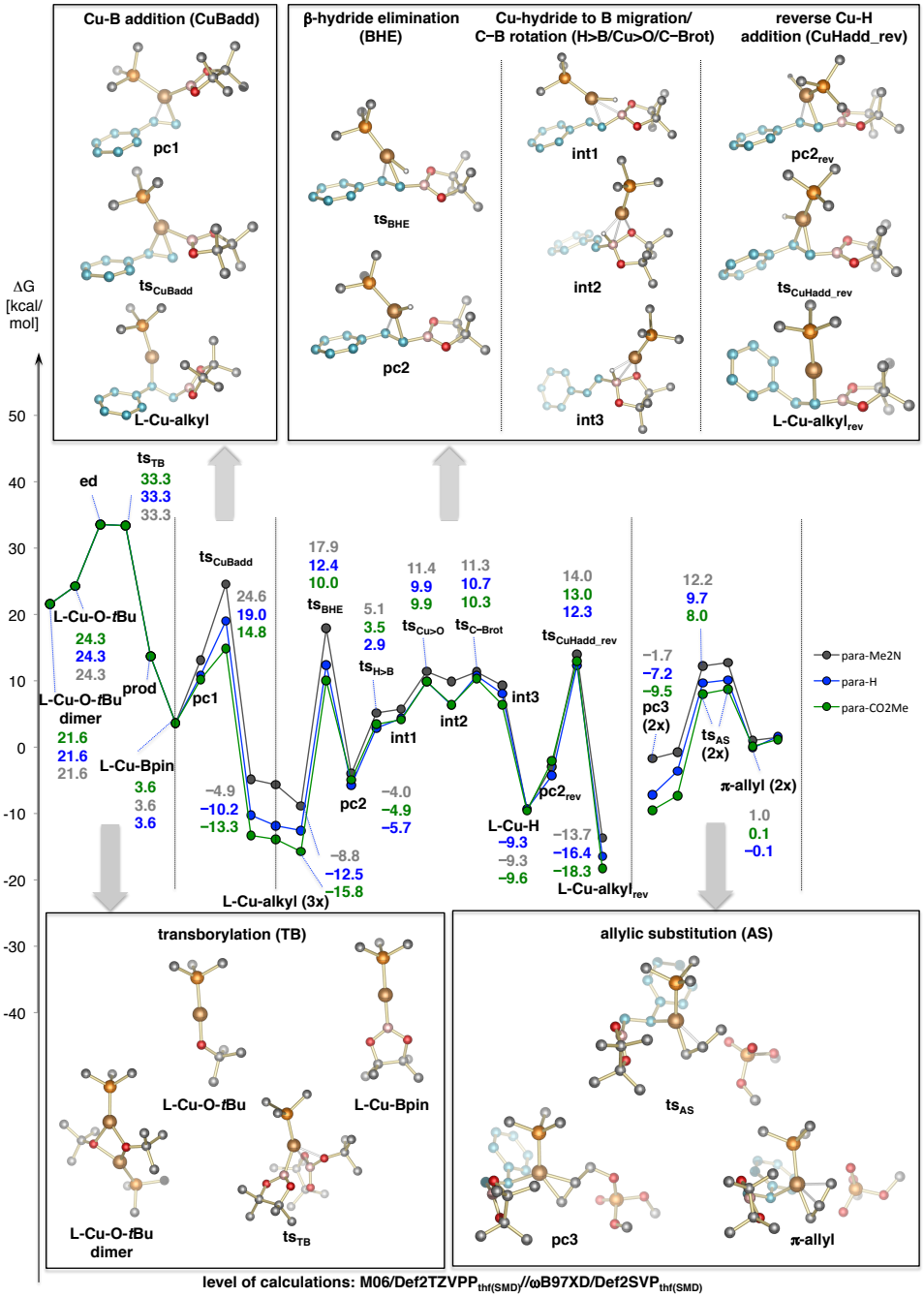

Figure 3.1. Free energy surfaces for the enantioselective Cu–B(pin) addition (CuBadd)/allylic substitution (AS) sequence with a model phosphine ligand (**PMe$_3$**) for reaction with various aryl olefins (***p*-Me$_2$N**, grey; ***p*-H (styrene)**, blue; ***p*-CO$_2$Me**, green) at the M06/DefTZVPP$_{thf(SMD)}$//ωB97XD/Def2SVP$_{thf(SMD)}$ level. Several conformers are shown for **ts$_{AS}$** and **L–Cu–alkyl**. The free energies have been referenced to the most stable **L3a**-Cu-Bpin conformer, which takes into account the free energy for ligand displacement (see Figure 6.1); the computed structures for L = ***p*-CO$_2$Me-styrene** are displayed. Abbreviations: **TB**, transborylation [conversion of Cu–alkoxide to Cu–B(pin)]; **BHE**, β-hydride (or Cu–H) elimination; **pc**, π-complex; **ts$_{H>B}$**, transition state for hydride migration to boron; **ts$_{Cu>O}$**, transition state for Cu migration to oxygen on Bpin; **ts$_{C-Brot}$**, transition state for C–B bond rotation; **ts$_{CuHadd_rev}$**, transition state Cu–H addition leading to Cu–alkyl$_{rev}$ species with reversal of regiochemistry; **int**, intermediate; **Cu–H**, linear Cu-hydride species.

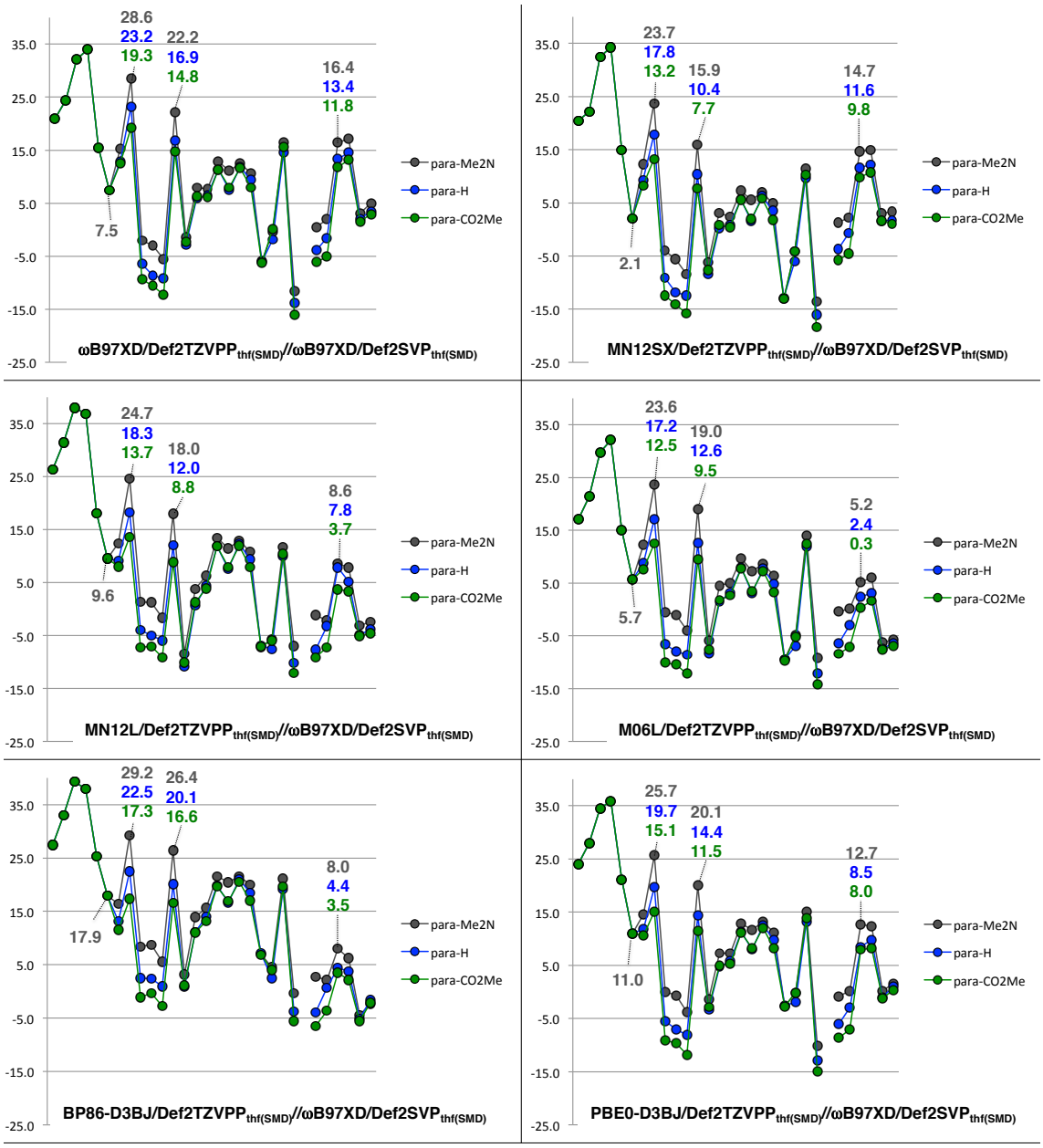

Figure 3.2. Free energy surfaces for the enantioselective Cu–B(pin) addition (CuBadd)/allylic substitution (AS) sequence with a model phosphine ligand (**PMe$_3$**) for reaction with various aryl olefins (***p*-Me$_2$N**, grey; ***p*-H (styrene)**, blue; ***p*-CO$_2$Me**, green) with various density functionals after optimization with ωB97XD/Def2SVP$_{thf(SMD)}$. For details, see Figure 3.1.

Feasibility of Cu–H re-addition as a possible reason for lowering of e.r. In search of a rationale regarding the diminution in enantioselectivity when allyl phosphate concentration is decreased, we first considered a Cu–H elimination/re-addition sequence. Nonetheless, Cu–H addition to the opposite enantiotopic face of the *same* alkenyl–B(pin) molecule seems unlikely, especially considering the substantial amounts of unreacted aryl olefin present.

Nevertheless, one feasible mechanism for Cu–H re-addition to the opposite face of the alkenyl–B(pin) without dissociation from that olefin might be as follows: migration of **L–Cu–H** from the double bond in **pc2** toward boron to generate borate[68] species **int2** (Figure 2.1), which would allow for rotation around the C–B bond (**ts**$_{\textbf{Cu-Brot}}$, 3.6 kcal/mol) and addition to the opposite face of the olefin. Computational studies reveal that such a pathway would be energetically much less favored compared to formation of the separated entities [i.e., **L–Cu–H** + alkenyl–B(pin), −17.1 kcal/mol]. The absence of a stable adduct with the linear **L–Cu–H** species suggests that olefin exchange followed by Cu–H addition to a different olefin is preferred. What is more, we have been unable to locate a stable adduct between **L–Cu–H** and the aromatic ring moiety of the model alkenyl–B(pin) complex. Unlike bent β-diketiminate-Cu species (shown below), reported to form isolable adducts with toluene[68c], binding of a linear **L–Cu–H** species is unfavorable due to the energy required to distort the linear geometry (see Figure 10.1 for the **L–Cu–Me** species).

---

(68) Copper–borohydride complexes are isolable compounds: (a) Lippard, S. J.; Melmed, K. M. *J. Am. Chem. Soc.* **1967,** *89,* 3929–3930. (b) Lippard, S. J.; Ucko, D. A. *Inorg. Chem.* **1968,** *7,* 1051–1056. (c) Nako, A. E.; White, A. J. P.; Crimmin, M. R. *Dalton Trans.* **2015,** *44,* 12530–12534. For a review on three-center/two-electron bonds in inorganic compounds see: (d) Green, J. C.; Green, M. L. H.; Parkin, G. *Chem. Commun.* **2012,** *48,* 11481–11503.

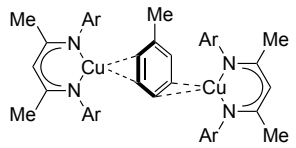

Site Selectivity of Cu–H addition to an aryl-substituted alkenyl–B(pin) compound. Cu–H addition to an alkenyl–B(pin) compound probably occurs with the opposite site selectivity compared to a monosubstituted aryl olefin (3.6 kcal/mol for $\mathbf{ts_{CuHadd\_rev}}$ vs. 5.1 kcal/mol for $\mathbf{ts_{BHE}}$), leading to linear $\mathbf{NHCMe_2{-}Cu{-}alkyl_{rev}}$ species with the Cu atom bound to homobenzylic carbon bearing the Bpin group (Figure 2.1). The latter scenario has been verified through spectroscopic investigations (see NMR experiments, 1.5.9) with ligand **L3c** (i.e., **L3c–Cu–H** generation from PHMS and **L3c–Cu–O*t*-Bu**, followed by addition to alkenyl–B(pin) substrates, synthesized independently, leads to generation of $\mathbf{L3c{-}Cu{-}alkyl_{rev}}$). The proposed site selectivity of Cu–H addition to an alkenyl–B(pin) is supported by the pioneering report of Sadighi[69].

Next, we investigated the significance of the electronic properties of aryl olefin substrates. Cu–B(pin) addition is significantly more favored with *p*-methylesterstyrene (7.8 kcal/mol for $\mathbf{ts_{CuBadd}}$) compared to *p*-dimethylaminostyrene (14.9 kcal/mol), which is also reflected in the greater reaction exothermicity (–25.0 kcal/mol for the lowest **L–Cu–alkyl** conformer; green curve in Figure 2.1). The positive effect of an electron-withdrawing aryl substituent on reaction rate suggests that background reactivity starting from phosphine-free CuO*t*-Bu species might be significantly higher than association of bis-

(69) Laitar, D. S.; Tsui, E. Y.; Sadighi, J. P. *Organometallics* **2006,** *25,* 2405–2408.

phosphine **L3a** with the phosphine-free Cu–Bpin intermediate (see Figure 4a in the manuscript).

The effect of an electron-withdrawing substituent on rate (transition state effect) appears to be considerably larger than the ability of an electron-withdrawing styrene to stabilize various $(CuO\textit{t}\text{-}Bu)_n$ species (ground state effect), ruling out styrene assisted deaggregation of oligomeric/polymeric $(CuO\textit{t}\text{-}Bu)_n$ species as reason for e.r. fluctuations (see also the discussion associated with Figures 8–9 below). Furthermore, the decreased nucleophilicity of the **Me_2NHC–Cu–alkyl** species derived from *p*-methylesterstyrene reduces the rate of allylic substitution (–1.3 kcal/mol for $\mathbf{ts_{AS}}$, which corresponds to a barrier of 26.3 kcal/mol relative to the most stable **Me_2NHC–Cu–alkyl** species; green curve, Figure 2.1). In the case of the substrate bearing a *p*-dimethylaminoaryl moiety the energy of $\mathbf{ts_{AS}}$ is 2.4 kcal/mol, corresponding to a barrier of only 18.4 kcal/mol (relative to the most stable **Me_2NHC–Cu–alkyl** species; grey curve, Figure 2.1). The lower reactivity of the **Me_2NHC–Cu–alkyl** species derived from *p*-methylesterstyrene towards allylic substitution (AS) renders the alternative Cu–H elimination pathway more competitive (2.0 kcal/mol for $\mathbf{ts_{BHE}}$, which is only 3.3 kcal/mol above $\mathbf{ts_{AS}}$). With *p*-dimethylaminoaryl system the energy difference between $\mathbf{ts_{BHE}}$ and $\mathbf{ts_{AS}}$ is larger (7.5 kcal/mol).

Similar trends are obtained when the calculations are performed in presence of a neutral **PMe_3** model ligand (Figure 3 compared to L = **$NHCMe_2$**, Figure 2). Notable distinctions are the greater propensity of the **Me_3P–Cu–O*t*-Bu** species to dimerize (21.6 kcal/mol for dimer vs. 24.3 kcal/mol for monomer; Figure 3.1), likely reflecting the lower

nucleophilicity of the d orbitals on Cu in **Me_3P–Cu–O*t*-Bu**[63]. Further, **Me_3P–Cu–B(pin)** is 3.6 kcal/mol above **L3a–Cu–B(pin)**, whereas **Me_2NHC–Cu–B(pin)** is more stable than the reference point with ligand **L3a** (–2.8 kcal/mol; Figure 2.1). The lower binding affinity of phosphine as opposed to NHC ligands likely renders reactions promoted by phosphines more prone to undesired reactivity resulting from ligand loss.

Differences Between Density Functionals in Figures 2 & 3

Despite the similarity in trends between various density functionals there are notable distinctions. For example, **Me_2NHC–Cu–B(pin)** is more stable than **L3a–Cu–B(pin)** only with functionals M06, MN12SX and M06L (–2.8, –3.6 and –1.1 kcal/mol, respectively; Figure 2.2). PBE0-D3BJ and particularly BP86-D3BJ, which tend to overestimate dispersion when the large bis-phosphine **L3a** is involved, predict **Me_2NHC–Cu–B(pin)** to be 5.3 and 11.5 kcal/mol, respectively, less stable than **L3a–Cu–B(pin)** (Figure 2.2). Presumably, the energy for binding of the bis-phosphine ligand to Cu is overestimated. (Because spectroscopic experiments, as detailed in 1.5.9, indicate facile loss of the chiral ligand, the results with BP86-D3BJ are unlikely to be correct). Another instance where appropriate modeling of dispersion forces is central relates to the comparison of unimolecular (e.g., hydride Cu–H elimination) as opposed to bimolecular pathways (e.g., allylic substitution). For example, while there is a small energy gap between $\mathbf{ts_{BHE}}$ and $\mathbf{ts_{AS}}$ with functional M06 (5.1 vs. 1.7 kcal/mol; blue curve in Figure 2.1), with functional BP86-D3BJ $\mathbf{ts_{AS}}$ is favored significantly over $\mathbf{ts_{BHE}}$ (–3.3 vs. 12.8 kcal/mol; blue curve in Figure 2.2). Functional BP86-D3BJ probably provides an unsatisfactory representation of the mechanism, since the experimental results suggest competitiveness between Cu–H elimination and allylic substitution. The smallest energy

gap between $\mathbf{ts_{BHE}}$ and $\mathbf{ts_{AS}}$ is predicted with functional MN12SX (4.3 vs. 3.5 kcal/mol; blue curve in Figure 2.2). Nearly identical trends to those described for L = $\mathbf{NHCMe_2}$ are observed with L = $\mathbf{PMe_3}$ as the model phosphine (Figure 3.2).

Regarding Displacement of a Bis-phosphine from a Cu Complex by an Aryl Olefin or a Solvent Molecule (Figures 4–7)

Comparison of free energy surfaces for Cu–B(pin) addition with various supporting ligands (L) at the M06/Def2TZVPP$_{thf(SMD)}$//ωB97XD/Def2SVP$_{thf(SMD)}$ level are shown in Figure 6.1. (For the individual free energy surfaces with L = styrene or thf, see Figures 4 and 5, respectively.) The graphs in Figure 6.1 offer insight regarding the ability of a select number of neutral ligands to stabilize intermediates and transition states along the catalytic cycle. For example, replacement of **L3a** from **L3a–Cu–B(pin)** (0.0 kcal/mol; grey curve in Figure 6.1) by $\mathbf{NHCMe_2}$ leads to an energy gain of 2.8 kcal/mol (red curve). Likewise, substitution of $\mathbf{PMe_3}$ affords a slightly less stable structure (3.6 kcal mol; brown curve).

Styrene and thf are relatively inferior Cu ligands (13.6 and 16.0 kcal/mol; blue and light blue curves). The high energies for transitions states $\mathbf{ts_{CuBadd}}$ and $\mathbf{ts_{BHE}}$ for L = thf (39.2 and 33.8 kcal/mol) rule out the feasibility of solvent-stabilized species as reactive intermediates. The situation is less straightforward with styrene. Changing the reference point from a common **L3a–Cu–B(pin)** intermediate to each individual **L–Cu–B(pin)** species (Figure 7) sheds some light on the impact of the electronic nature of L and the facility of each step. It appears that while π-donor ligands (thf) destabilize square planar transitions states $\mathbf{ts_{CuBadd}}$ and $\mathbf{ts_{BHE}}$ (23.2 and 17.8 kcal/mol; light blue curve in Figure 7),

π-acceptor ligands exert a more positive impact in this regard (e.g., styrene; 9.3 and 4.8 kcal/mol; blue curve in Figure 7). Competitive π-back-donation from Cu to the styrene molecules may facilitate movement of the B(pin) nucleophile across the lobes of the transition metal's d_{xy} orbital. In other words, Cu–styrene coordination through σ-donation becomes more important, rendering the π*-orbital on styrene more electrophilic [more facile Cu–B(pin) addition]. These considerations suggest that, at sufficiently high styrene concentration, a Cu–B(pin) addition pathway that is bimolecular in styrene (cf. Scheme 1.35) might become competitive (23.0 and 16.9 kcal/mol for $\mathbf{ts_{CuBadd}}$ with L = styrene and L = **L3a**, respectively; Figures 6.1). Based on similar principles, β–H (or Cu–H) elimination might be favored with a π-accepting (electron-deficient) aryl olefin (4.8 and 17.8 kcal/mol for $\mathbf{ts_{BHE}}$ with L = styrene and L = thf; blue and light blue curves, Figure 7). It is therefore plausible that an aryl olefin might negatively impact enantioselectivity because competition between styrene and an allyl electrophile for **L3a–Cu–alkyl** could result in loss of the bis-phosphine ligand, followed by styrene-promoted Cu–H elimination via $\mathbf{ts_{BHE}}$ (L = styrene, 18.4 kcal/mol; blue curve, Figures 6.1); such a process is capable of being competitive with allylic substitution involving bis-phosphine–Cu–alkyl complex ($\mathbf{ts_{AS}}$ with L = **L3a** is 16.6 kcal/mol; grey curve, Figures 6.1). The findings illustrated in Figure 7 further illustrate that allylic substitution processes involving **L3a–Cu–alkyl** might be particularly challenging due to steric hindrance. Whereas $\mathbf{ts_{CuBadd}}$ (15.4 kcal/mol) is significantly higher in energy compared to $\mathbf{ts_{AS}}$ (6.1 kcal/mol) with the smaller PMe_3 ligand, the two transition states have nearly identical energies with ligand **L3a** (16.9 and 16.6 kcal/mol, respectively; Figure 7).

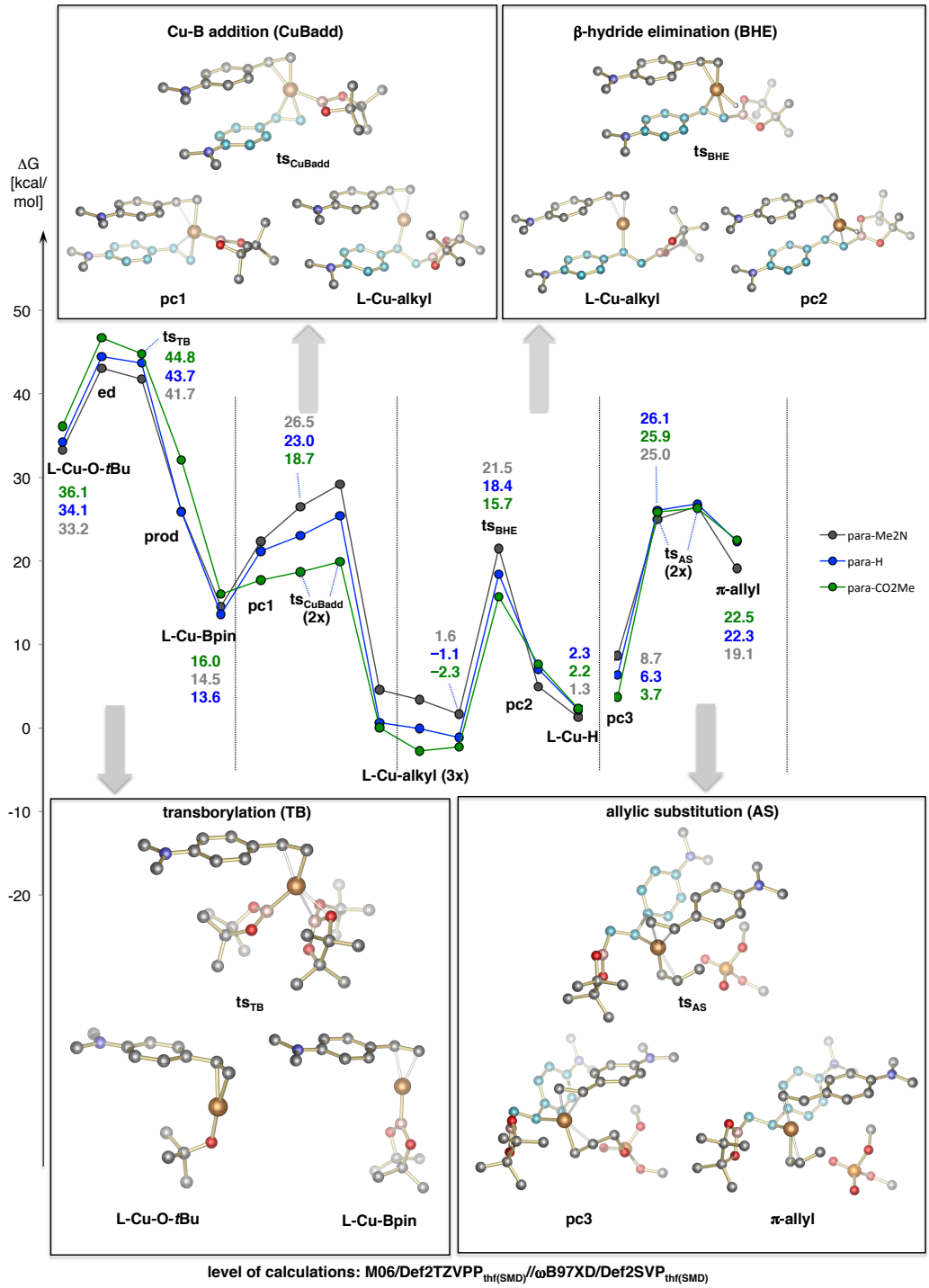

Figure 4.1. Free energy surfaces for the enantioselective Cu–B(pin) addition (CuBadd)/allylic substitution (AS) sequence with styrene derivatives as the supporting ligand (***p*-Me$_2$N**, grey; ***p*-H (styrene)**, blue; ***p*-CO$_2$Me**, green) at the M06/DefTZVPP$_{thf(SMD)}$//ωB97XD/Def2SVP$_{thf(SMD)}$ level. Several conformers are shown for **ts$_{CuBadd}$**, **ts$_{AS}$** and **L–Cu–alkyl**. The free energies have been referenced to the most stable **L3a–Cu–B(pin)** conformer, which takes into account the free energy for ligand displacement (see Figure 6.1); the computed structures for L = ***p*-Me$_2$N-styrene** are displayed. Abbreviations: **TB**, transborylation [conversion of Cu–alkoxide to Cu–B(pin)]; **BHE**, β-hydride (Cu–H) elimination; **pc**, π-complex.

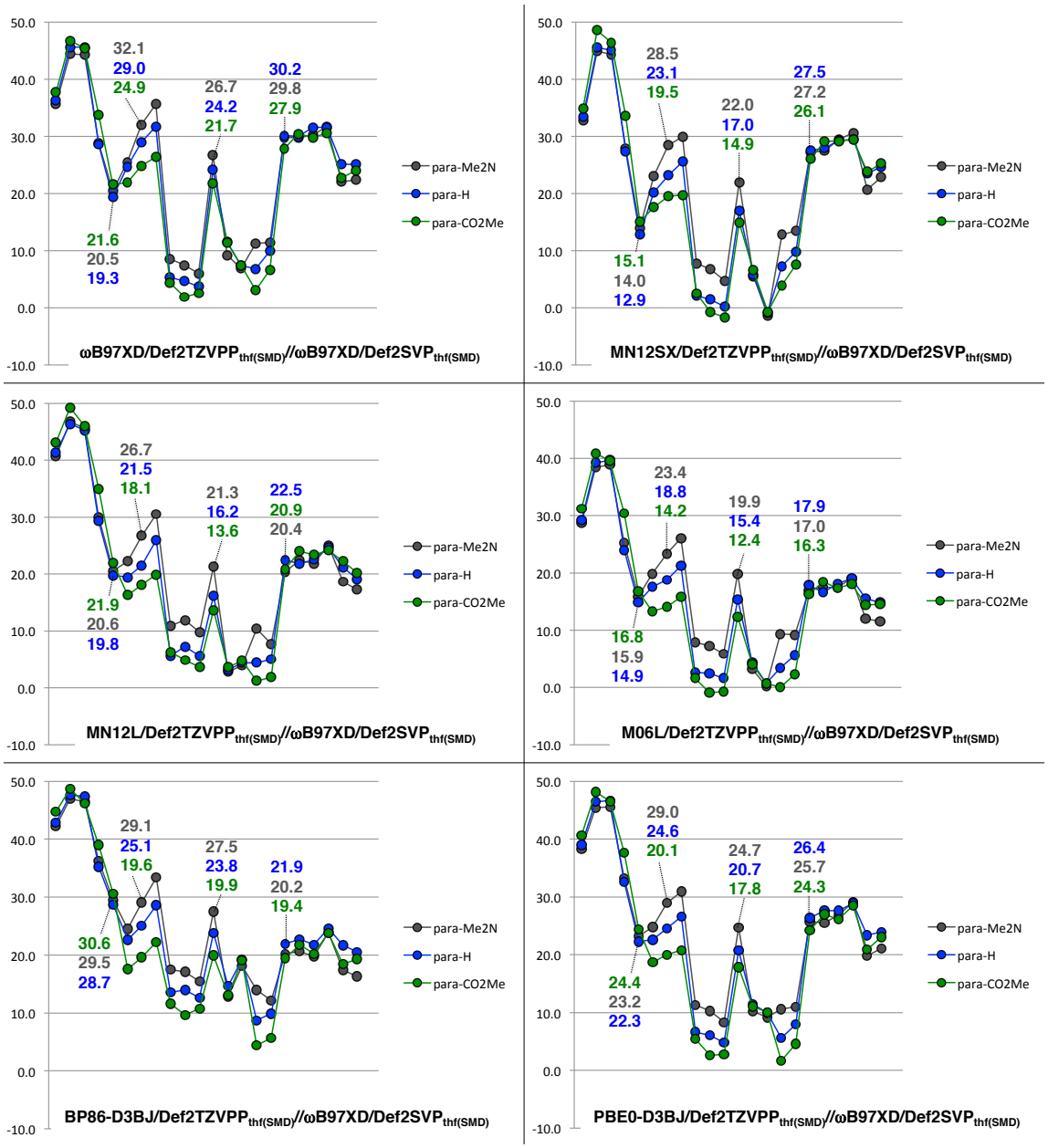

Figure 4.2. Free energy surfaces for the enantioselective Cu–B(pin) addition (CuBadd)/allylic substitution (AS) sequence with styrene derivatives as the supporting ligand (***p*-Me$_2$N**, grey; ***p*-H (styrene)**, blue; ***p*-CO$_2$Me**, green) with various density functionals after optimization with ωB97XD/Def2SVP$_{THF(SMD)}$. For more details, see Figure 4.1.

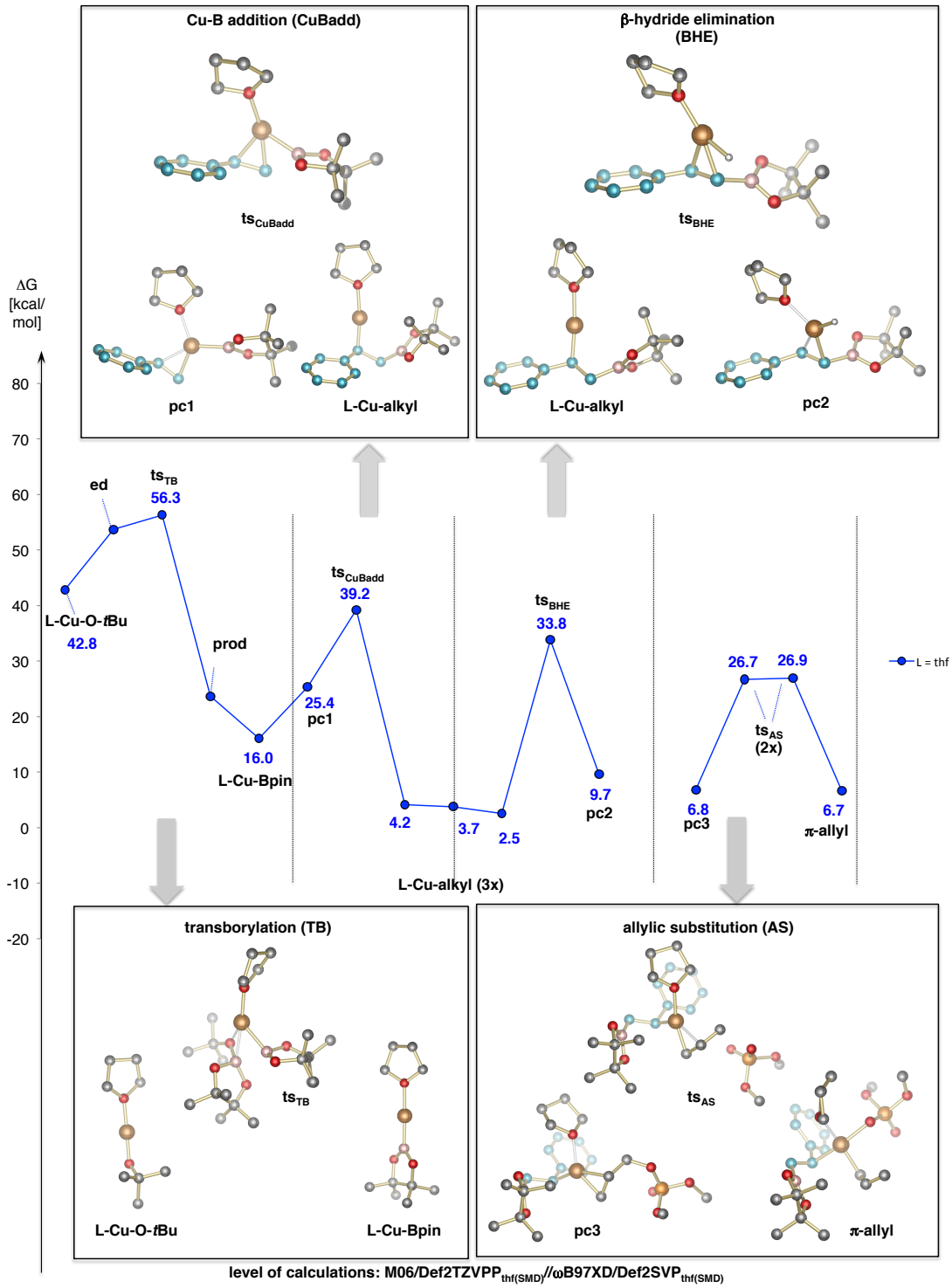

Figure 5.1. Free energy surfaces for the enantioselective Cu–B(pin) addition (CuBadd)/allylic substitution (AS) sequence with a thf molecule as the supporting ligand at the M06/DefTZVPP$_{thf(SMD)}$//ωB97XD/Def2SVP$_{thf(SMD)}$ level. Several conformers are shown for **ts$_{AS}$** and **L–Cu–alkyl**. The free energies have been referenced to the most stable **L3a–Cu–Bpin** conformer, which takes into account the free energy for ligand displacement (cf. Figure 6.1). Abbreviations: **TB**, transborylation [conversion of Cu–alkoxide to Cu–B(pin)]; **BHE**, β-hydride (Cu–H) elimination; **pc**, π-complex.

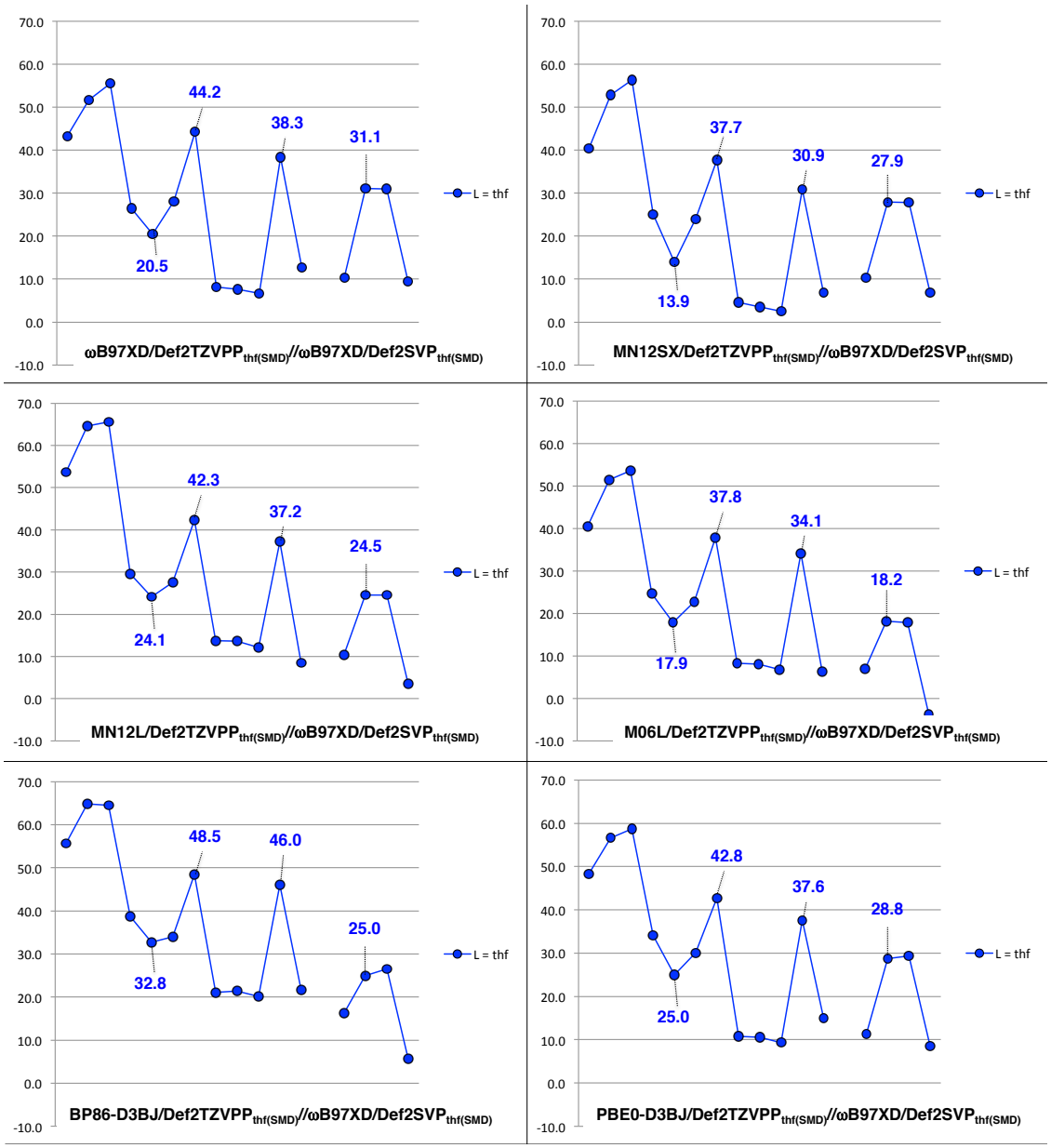

Figure 5.2. Free energy surfaces for the enantioselective Cu–B(pin) addition (CuBadd)/allylic substitution (AS) sequence with a thf molecule as the supporting ligand with different density functionals after optimization with ωB97XD/Def2SVP$_{THF(SMD)}$. For details, see Figure 5.1.

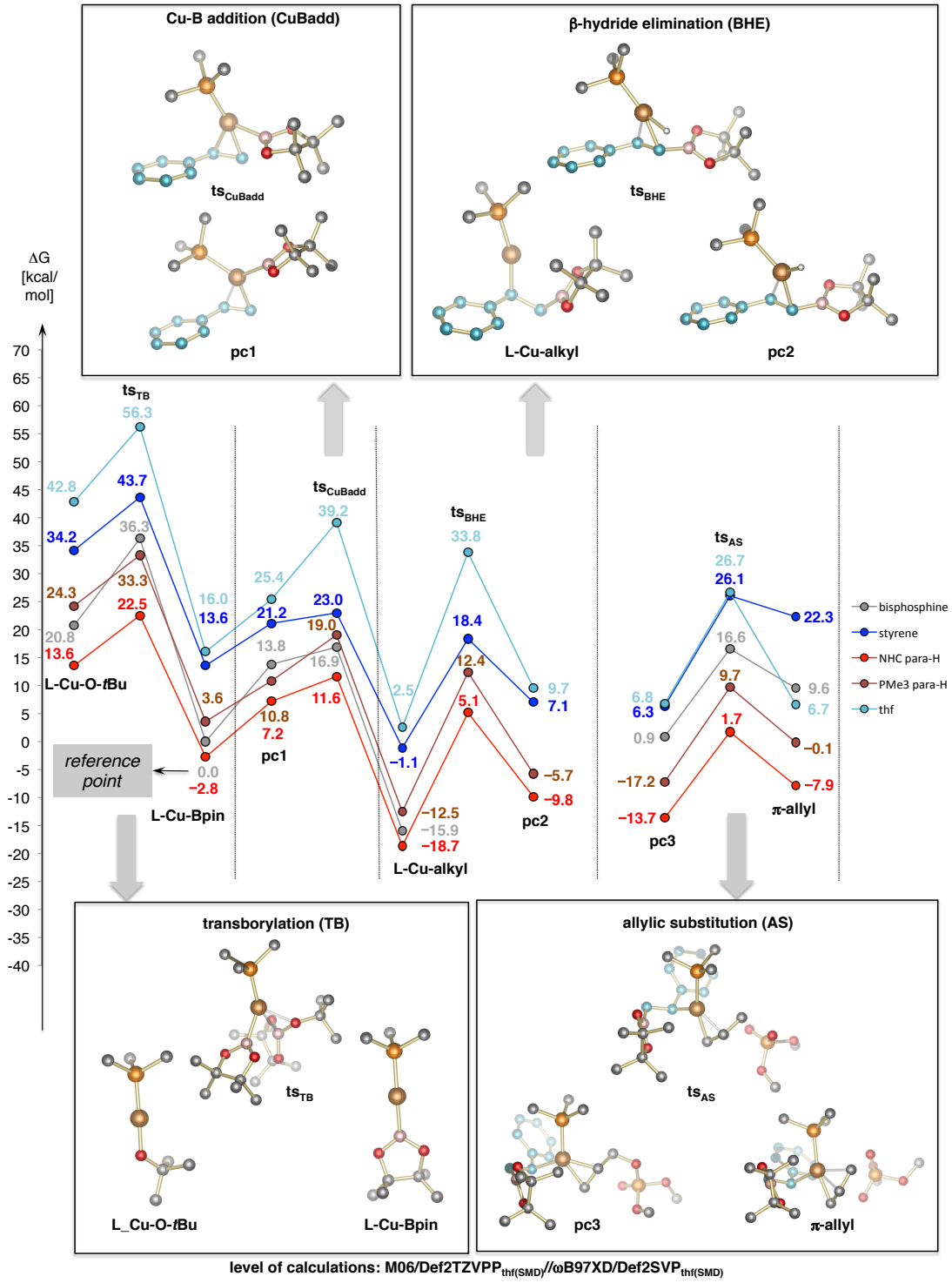

Figure 6.1. Free energy surfaces for the enantioselective Cu–B(pin) addition (CuBadd)/allylic substitution (AS) sequence in presence of various ligands L (**L3a**, grey; **styrene**, blue; model NHC ligand **NHCMe$_2$**, red; model phosphine ligand **PMe$_3$**, brown; **thf**, light blue) at the M06/DefTZVPP$_{thf(SMD)}$//ωB97XD/Def2SVP$_{thf(SMD)}$ level. All free energies have been referenced to the **L3a–Cu–B(pin)** species, which takes into account the free energy of ligand exchange; only computed structures for L = **PMe$_3$** are shown. Abbreviations: **TB**, transborylation [conversion of Cu–alkoxide to Cu–B(pin)]; **BHE**, β-hydride (Cu–H) elimination; **pc**, π-complex.

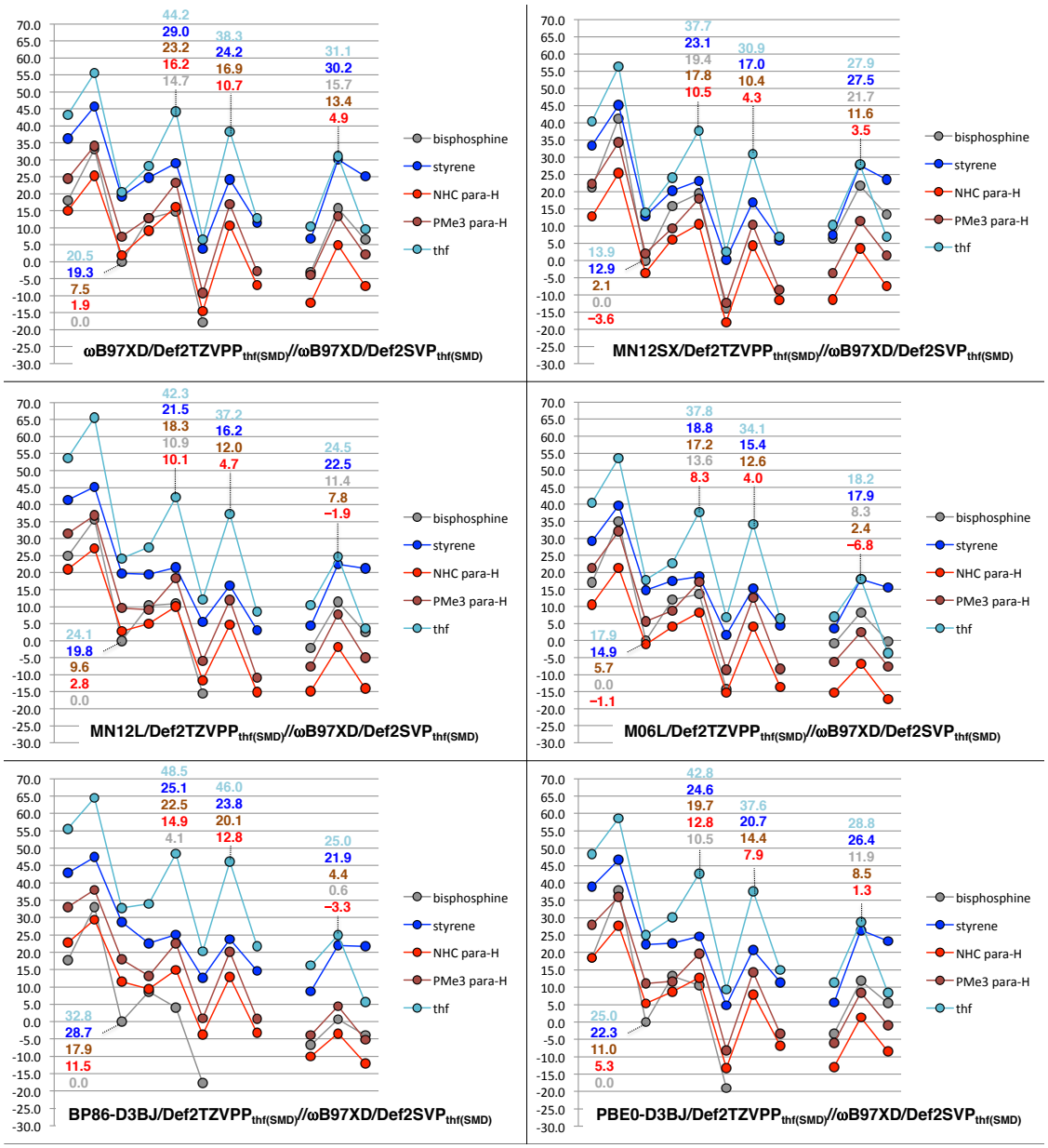

Figure 6.2. Free energy surfaces for the enantioselective Cu–B(pin) addition (CuBadd)/allylic substitution (AS) sequence in presence of various ligands L (**L3a**, grey; **styrene**, blue; model NHC ligand **NHCMe$_2$**, red; model phosphine ligand **PMe$_3$**, brown; **thf**, light blue) with various density functionals after optimization with ωB97XD/Def2SVP$_{thf(SMD)}$. For more details, see Figure 6.1.

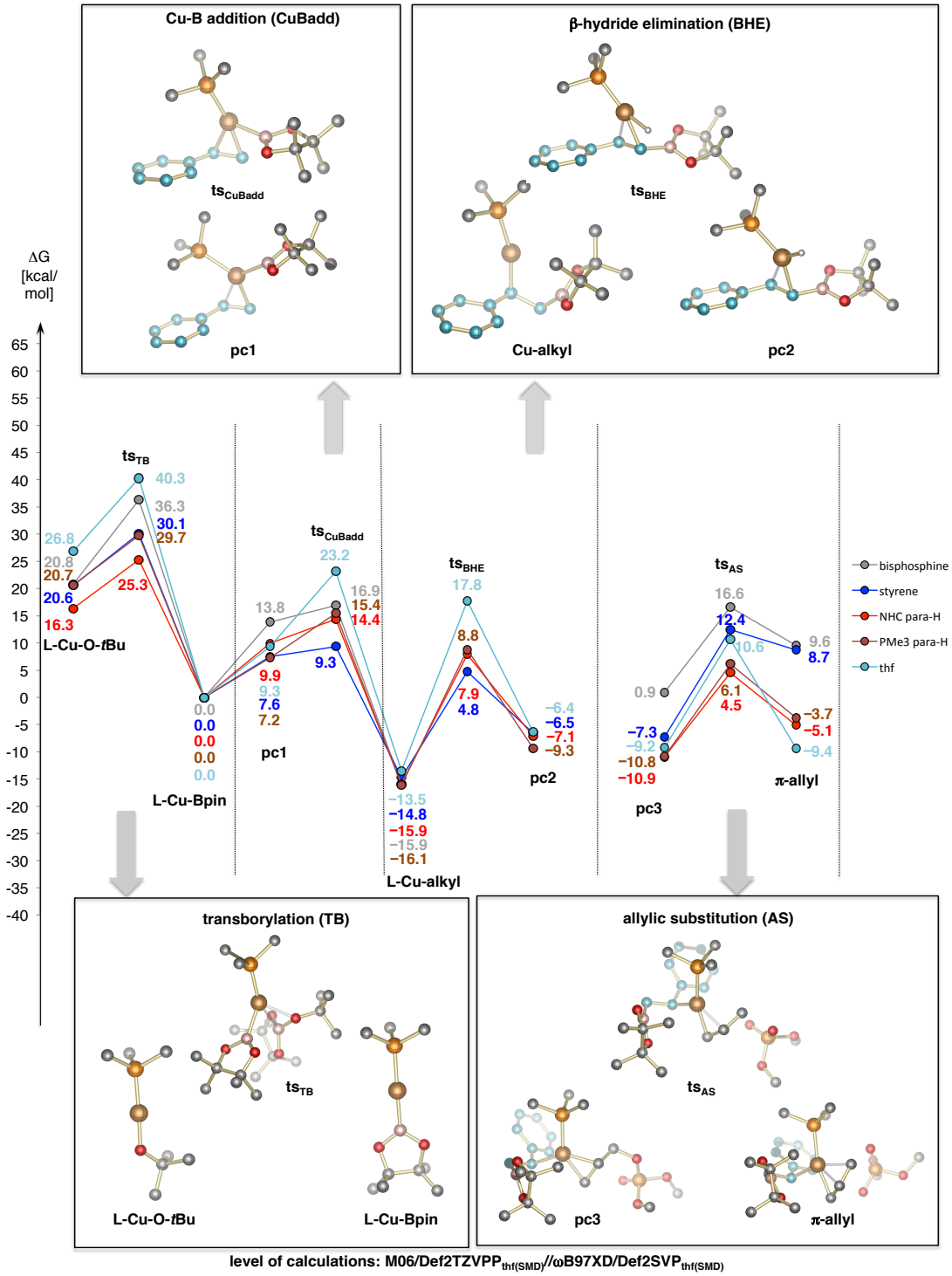

Figure 7. Free energy surfaces for the enantioselective Cu–Bpin addition (CuBadd)/allylic substitution (AS) sequence in presence of various ligands L (**L3a**, grey; **styrene**, blue; model NHC ligand **NHCMe$_2$**, red; model phosphine ligand **PMe$_3$**, brown; **thf**, light blue) at the M06/DefTZVPP$_{thf(SMD)}$//ωB97XD/Def2SVP$_{thf(SMD)}$ level. The free energies for a given ligand L have been referenced to the L–Cu–B(pin) species, which does not take into account the free energy of ligand exchange; only computed structures for L = **PMe$_3$** are shown. Abbreviations: **TB**, transborylation [conversion of Cu–alkoxide to Cu–B(pin)]; **BHE**, β-hydride (Cu–H) elimination; **pc**, π-complex.

Differences Between Density Functionals and the Negative Impact that an Aryl Olefins Might Have on Enantioselectivity (Figure 6.2)

There are noteworthy differences between various density functionals regarding the probability of competitive pathways, which would entail loss of bis-phosphine **L3a** and a pathway that is second-order in aryl olefin (see Scheme 1.35). For instance $\mathbf{ts_{CuBadd}}$ with L = **L3a** is less than 7 kcal/mol more stable than $\mathbf{ts_{CuBadd}}$ with L = styrene with M06 (6.1 kcal/mol; Figure 6.1), MN12SX (3.7 kcal/mol; Figure 6.2) and M06L (5.2 kcal/mol; Figure 6.2). (It should be noted that there is significant excess of styrene compared to bis-phosphine **L3a**.) With other density functionals a non-selective Cu–B(pin) addition mechanism that is second-order in styrene seems less likely. Similarly, styrene-induced β-hydride (Cu–H) elimination through the sequence entailing replacement of bis-phosphine **L3a**, followed by $\mathbf{ts_{BHE}}$ with L = styrene, could be responsible for lowering of enantioselectivty if predictions made with functionals M06 and particularly MN12SX were correct. That is, with MN12SX allylic substitution involving **L3a–Cu–alkyl** (21.7 kcal/mol; grey curve, Figure 6.2) is energetically more demanding than $\mathbf{ts_{BHE}}$ with L = styrene (17.0 kcal/mol; blue curve, Figure 6.2). In contrast, if the results with BP86-D3BJ, a functional, which tends to overestimate dispersion forces involving the bulky bisphosphine ligand, were correct (which is unlikely), a mechanism entailing styrene-promoted loss of ligand **L3a** could be entirely ruled out (i.e., the grey curve for L = **L3a** is significantly below the blue curve for L = styrene, Figure 6.2).

Coordinating Affinity of Aryl Olefins to CuO*t*-Bu, CuO*t*-Bu dimer, Cu(O*t*-Bu)$_2^-$ and Cu(O*t*-Bu)$_2^-$Na$^+$ (cf. Figures 8–9)

To examine the relationship between the electronic attributes of an aryl olefin and its ability to coordinate with various (CuO*t*-Bu)$_n$ entities, we carried out the calculations illustrated in Figures 8–9 (M06/Def2TZVPP$_{thf(SMD)}$// ωB97XD/Def2SVP$_{thf(SMD)}$). These data show that replacement of bis-phosphine **L3a** from CuO*t*-Bu by styrene is significantly endergonic (13.4 kcal/mol, Figures 8.1) and that electron-rich aryl olefins stabilize linear alkene···Cu–O*t*-Bu structures more effectively (12.4 vs. 15.3 kcal/mol for *p*-dimethylaminostyrene vs. *p*-methylesterstyrene, respectively; Figure 8.1). The trend is reversed for the dimeric systems, where it appears that π-backbonding to the olefin becomes more of a factor (9.8, 9.6 and 8.8 kcal/mol for *p*-dimethylaminostyrene, styrene and *p*-methylesterstyrene, respectively; Figure 8.1). However, such ground states effects are unlikely to have a major impact on e.r. fluctuations because of the relatively small energy difference resulting from electronic attributes of an aryl olefin together with the relatively low binding affinity of olefins to CuO*t*-Bu species[70] comapred to a bis-phosphine.

Similar trends regarding the electronic nature of aryl olefins are observed vis-à-vis binding Cu–(O*t*-Bu)$_2^-$ and Cu–(O*t*-Bu)$_2^-$Na$^+$ (Figure 9.1). Association of *p*-methylesterstyrene is favored by 3.8 kcal/mol relative to *p*-NMe$_2$-styrene, although binding is overall highly endergonic (16.7 kcal/mol for *p*-CO$_2$Me-styrene; Figure 9.1);

---

(70) For a review on the chemistry of olefin–Cu(I) complexes, see: (a) Wang, X.-S.; Zhao, H.; Li, Y.-H.; Xiong, R.-G.; You, X.-Z. *Topics in Catalysis* **2005,** *35,* 43–61. For the intramolecular chelation of olefins to Cu-O*t*Bu clusters see: (b) Hakansson, M.; Lopes, C.; Jagner, S. *Organometallics* **1998,** *17,* 210–215. (c) Bellot, B. J.; Girolami, G. S. *Organometallics* **2009,** *28,* 2046–2052. π-Backbonding is typically more pronounced in complexes with more nucleophilic anionic dinitrogen-containing ligands: (d) Oguadinma, P. O.; Schaper, F. *Organometallics* **2009,** *28,* 6721–6731.

this might be attributed to the increase in repulsion between the alkoxide oxygen non-bonding electrons when they reside in a cis relationship[71]. In contrast, binding to the $Cu(O\textit{t}\text{-}Bu)_2^{-}Na^{+}$ species is only slightly exergonic, with a slight preference for electron-deficient aryl olefins (0.5 and 1.1 kcal/mol relative stabilization for *p*-methylesterstyrene compared to *p*-NMe_2-styrene on the ΔG and ΔE surfaces, respectively; Figure 9.1). Here, repulsion caused by the alkoxide oxygen non-bonding electrons is countered by a Na ion[71], which can favor alkene–Cu association (G_{rel} = –0.7 kcal/mol for *p*-methylesterstyrene; Figure 9.1).

Factors that Impact S_N2' Selectivity (Figure 10)

The free energy transition states for the allylic substitution (AS) step was carried out with a system that contains a model phosphine (**PMe_3**) and NHC (**$NHCMe_2$**) ligand at the M06/Def2TZVPP$_{thf(SMD)}$//ωB97XD/Def2SVP$_{thf(SMD)}$ level (Figure 10.1). With L = **PMe_3** reaction of the linear nucleophilic L–Cu–Me species[63b] with allylphosphate in a S_N2'-type fashion (24.7 kcal/mol) is predicted to be 1.4 kcal/mol lower in free energy (compared to the S_N2-type transition state, 26.1 kcal/mol). A similar trend is observed with L = **$NHCMe_2$** (24.7 vs. 27.2 kcal/mol). Furthermore, it appears that the presence of an NHC ligand does not mean faster allylic substitution (compared to a phosphine); this can be attributed to the relatively high energy required to distort the L–Cu–Me species from its linear geometry into a bent form (18.0 kcal/mol required to reach a 115 º angle vs. 14.5 kcal/mol for the corresponding PMe_3 species; Figure 10.1). It is likely that a

(71) A similar phenomenon has been described during polytopal rearrangements and olefin metathesis reactions of Ru carbene complexes. See: (a) Torker, S.; Khan, R. K. M.; Hoveyda, A. H. *J. Am. Chem. Soc.* **2014,** *136,* 3439–3455. (b) Khan, R. K. M.; Torker, S.; Hoveyda, A. H. *J. Am. Chem. Soc.* ***2013,*** *135,* 10258–10261.

potential positive influence of an NHC ligand may be attributed to diminished tendency for aggregate formation (as discussed above). As shown by Nakamura in connection to anionic cuprate complexes[63,64a], such "hetero-cuprate" Cu(I)–alkyl species in their bent form (Scheme 1.37a; stronger Me compared to weaker NHC/phosphine donor) display an increased orbital coefficient on the d_{xy} orbital lobe that is *cis* to the more nucleophilic alkyl group (HOMO at an angle of 115º; Scheme 1.37b); this favors addition of the allyl electrophile so that the larger coefficient on C3 is *trans* to less nucleophilc/neutral NHC/phoshpine ligand (Scheme 1.37c). In addition to these electronic effects, the involvement of a chelate interaction between a phosphate/carboxylate leaving group with either a cyanide ligand (as proposed by Nakamura) [64a] or a pendant sulfonate group[65] is probably not a necessary prerequisite for obtaining high S_N2'-selectivity, but it can assist in difficult cases such as those where a bulky allyl electrophile is involved. In other words, reactions promoted by alkyl–Cu–PR_3 species and a small/unsubstituted allyl electrophile are highly S_N2' selective (cf. Figure 4d in the manuscript). Our studies further show that allylic substitution transition state **$ts_{AS}(S_N2')$** is relatively early in character (i.e., it resembles the square-planar olefin π-complex generated from complexation to the C2=C3 double bond) with a relatively short Cu–C3 bond length of 1.978 Å and a comparatively extended Cu–C1 bond (2.468 Å). On the other hand, **$ts_{AS}(S_N2)$** is more "product-like" (that is, it more resembles the high-energy, square-planar π-allyl species), as indicated by the smaller difference between the Cu–C1 and Cu–C3 bond lengths (2.330 and 2.063 Å, respectively), which is in agreement with an earlier report[64a].

Scheme 1.37. S_N2' selectivity in allylic substitution (AS) promoted by "heterocuprate-like" **Me_2NHC–Cu–Me**; (a) HOMO of linear ground state; (b) HOMO of bent ground state (Me–Cu–C^{NHC} = 115 º); (c) transition state for S_N2'-type mode of addition; (d) transition state for S_N2-type mode of addition.

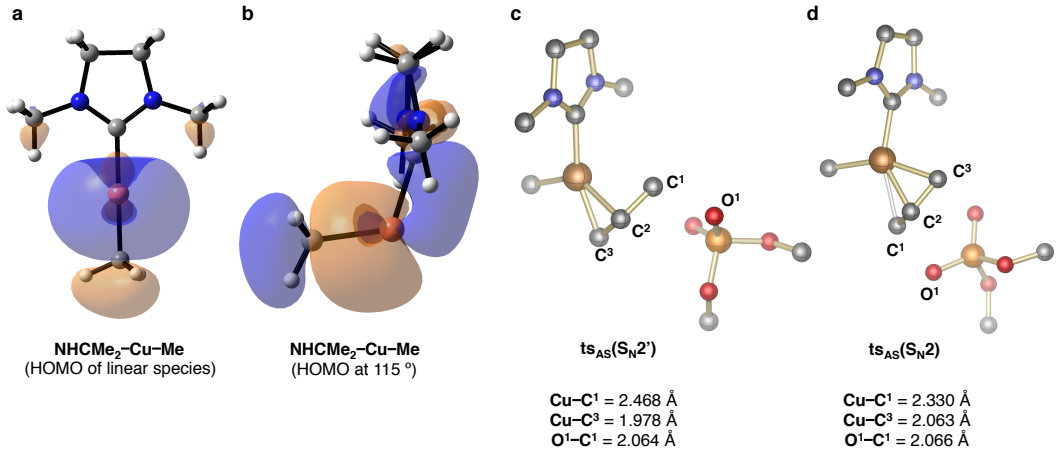

A similar trend, as described for Cu species bearing neutral NHC or phosphine ligands, is observed for the reaction catalyzed by **L–Cu–Me** (L = Na-O*t*Bu). The energies for **$ts_{AS}(S_N2')$** and **$ts_{AS}(S_N2)$** are 24.6 and 26.4 kcal/mol, respectively (left graph, Figure 10.1). (It should be noted that there is no intermolecular coordination between the phosphate leaving group and the Na counterion). In the alternative cases with intramolecular coordination of the phosphate leaving group to the Na cation bound to the alkoxide there is significant stabilization of both types of transition states (18.4 and 14.8 kcal/mol, respectively for **$ts_{AS}(S_N2')_{chelate}$** and **$ts_{AS}(S_N2)_{chelate}$**; cf. Figure 10.1), although this lowering in energy is likely overestimated and subject to significant uncertainties due to the presumably more complex coordination environment in solution (i.e., larger chelate structures with additional molecules of base, etc). Nonetheless, trends in energies and structural features might provide a hint for why background reactions [i.e., those catalyzed by **L–Cu–Me** (L = NaO*t*-Bu)] are less regioselective (Scheme 1.38). In case of the S_N2'-type transition state with a chelating interaction, the Na–O^1 and Na–O^2 bond lengths are 2.194 and 2.196 Å, respectively. This is significantly longer than when the Cu

center displaces the phosphate with its d_{z^2} orbital through an S_N2-type mechanism (2.161 and 2.147 Å for Na–O^1 and Na–O^2, respectively; Scheme 1.38). These findings imply that **$ts_{AS}(S_N2')_{chelate}$** might be more strained, which is reflected in the larger entropy corrections to the free energy (ΔG_{corr} = 15.0 vs. 10.8 kcal/mol for **$ts_{AS}(S_N2')_{chelate}$** vs. **$ts_{AS}(S_N2)_{chelate}$**, respectively; doi:10.1038/nchem.2861).

Scheme 1.38. Geometries of transition states for allylic substitution (AS) for background reaction with a chelate bridge between *tert*-butoxide and phosphate through a Na counterion.

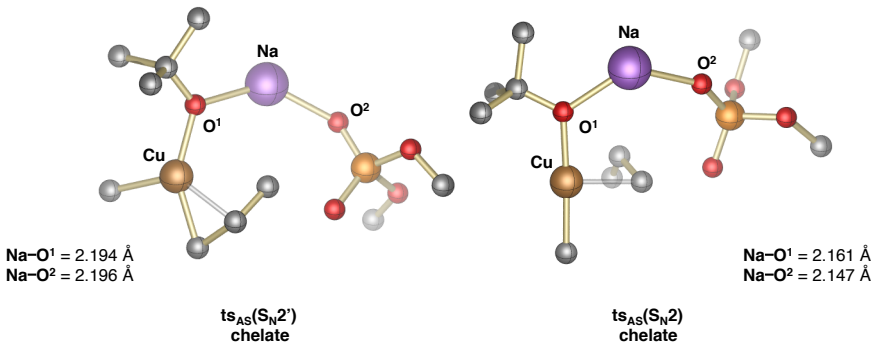

Intramolecular coordination of the phosphate leaving group to the Na cation bound to the alkoxide leads to significant stabilization of both types of transition states (18.4 and 14.8 kcal/mol, respectively for **$ts_{AS}(S_N2')_{chelate}$** and **$ts_{AS}(S_N2)_{chelate}$**; cf. Figure 10.1), although this lowering in energy is likely overestimated and subject to significant uncertainties due to the presumably more complex coordination environment in solution (i.e., larger chelate structures with additional molecules of base, etc). Nonetheless, trends in energies and structural features might provide a hint for why background reactions are less regioselective (Scheme 1.38). In case of the S_N2'-type transition state with a chelating interaction, the Na–O^1 and Na–O^2 bond lengths are 2.194 and 2.196 Å, respectively. This is significantly longer than when the Cu center displaces the phosphate with its d_{z^2} orbital through an S_N2-type mechanism (2.161 and 2.147 Å for Na–O^1 and Na–O^2, respectively; Scheme 1.38). These findings imply that **$ts_{AS}(S_N2')_{chelate}$** might be more strained, which is

reflected in the larger entropy corrections to the free energy (ΔG_{corr} = 15.0 vs. 10.8 kcal/mol for $\mathbf{ts_{AS}(S_N2')_{chelate}}$ vs. $\mathbf{ts_{AS}(S_N2)_{chelate}}$, respectively; doi:10.1038/nchem.2861).

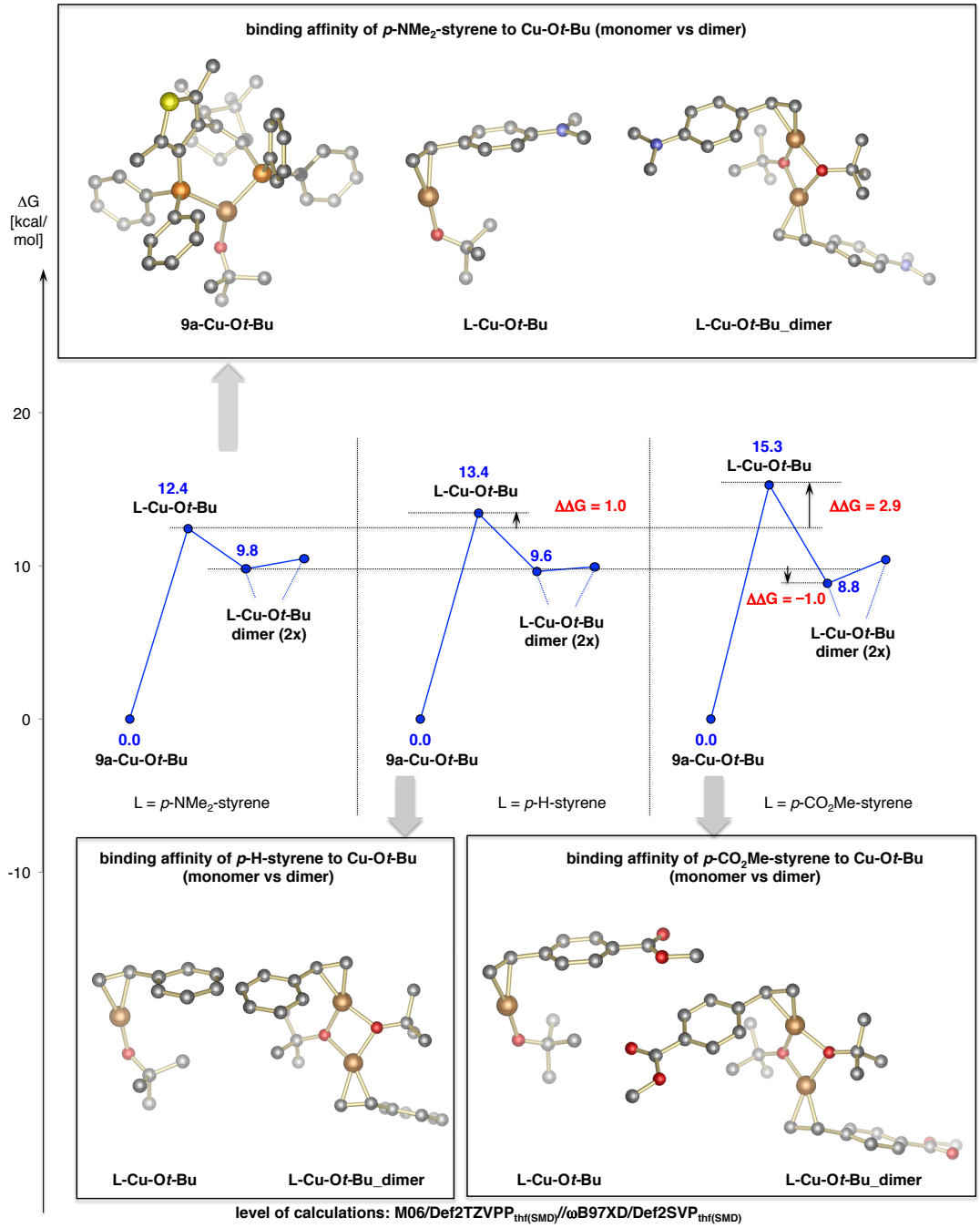

Figure 8.1. Free energy surfaces for binding affinity of various styrene derivatives (***p*-Me$_2$N**, left; ***p*-H (styrene)**, center; ***p*-CO$_2$Me**, right) to the **CuO*t*-Bu** monomer or dimer (**CuO*t*-Bu-dimer**) at the M06/DefTZVPP$_{thf(SMD)}$// ωB97XD/Def2SVP$_{thf(SMD)}$ level. Several conformers are shown for **L–CuO*t*-Bu-dimer**; the free energies have been referenced to **3La–Cu—O*t*-Bu**, which takes into account the free energy for ligand displacement (cf. Figure 6.1).

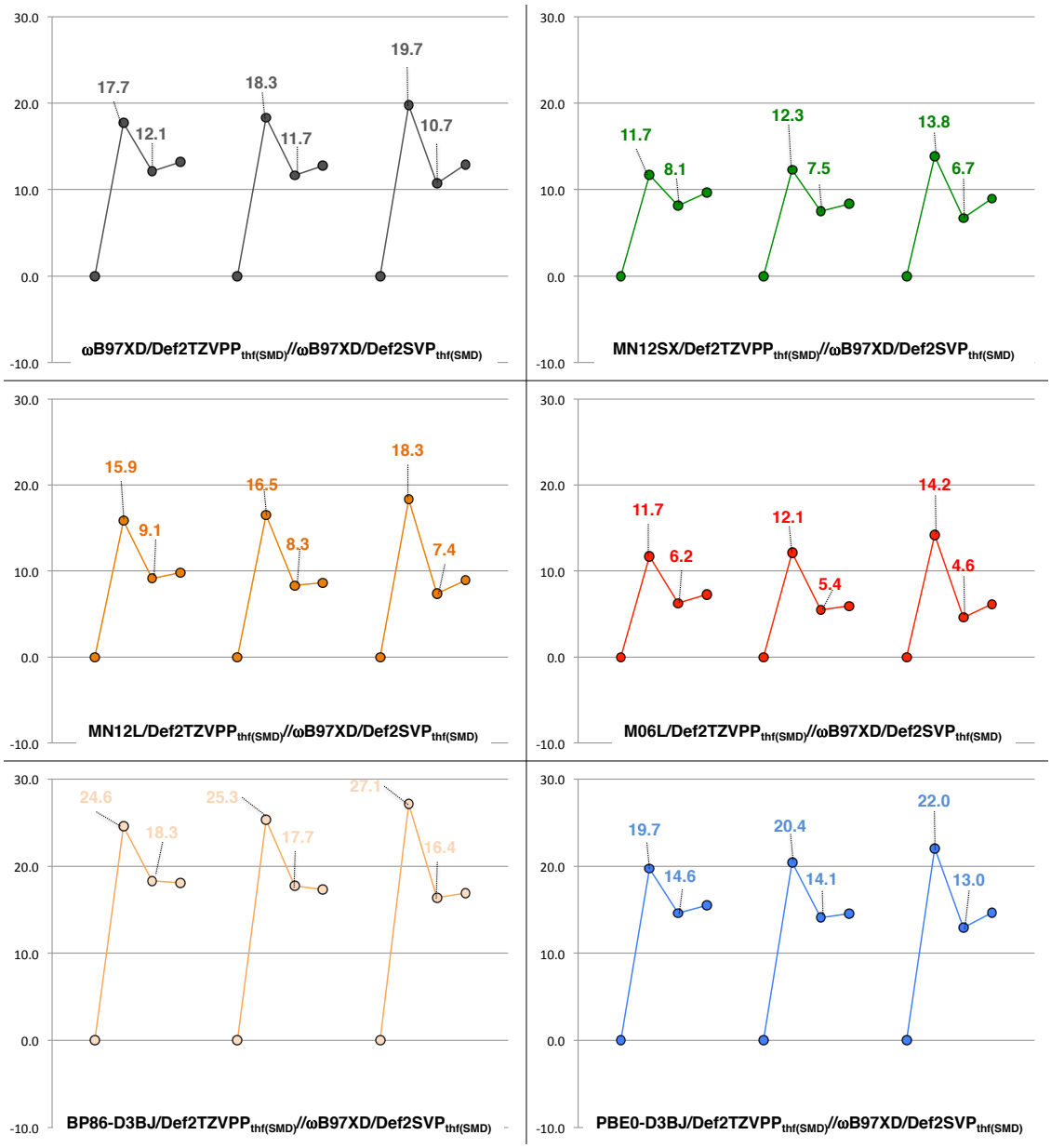

Figure 8.2. Free energy surfaces for binding affinity of various styrene derivatives (***p*-Me$_2$N**, left; ***p*-H (styrene)**, center; ***p*-CO$_2$Me**, right) to the **CuO*t*-Bu** monomer or dimer (**CuO*t*-Bu-dimer**) with various density functionals after optimization with ωB97XD/Def2SVP$_{thf(SMD)}$. For details, see Figure 8.1.

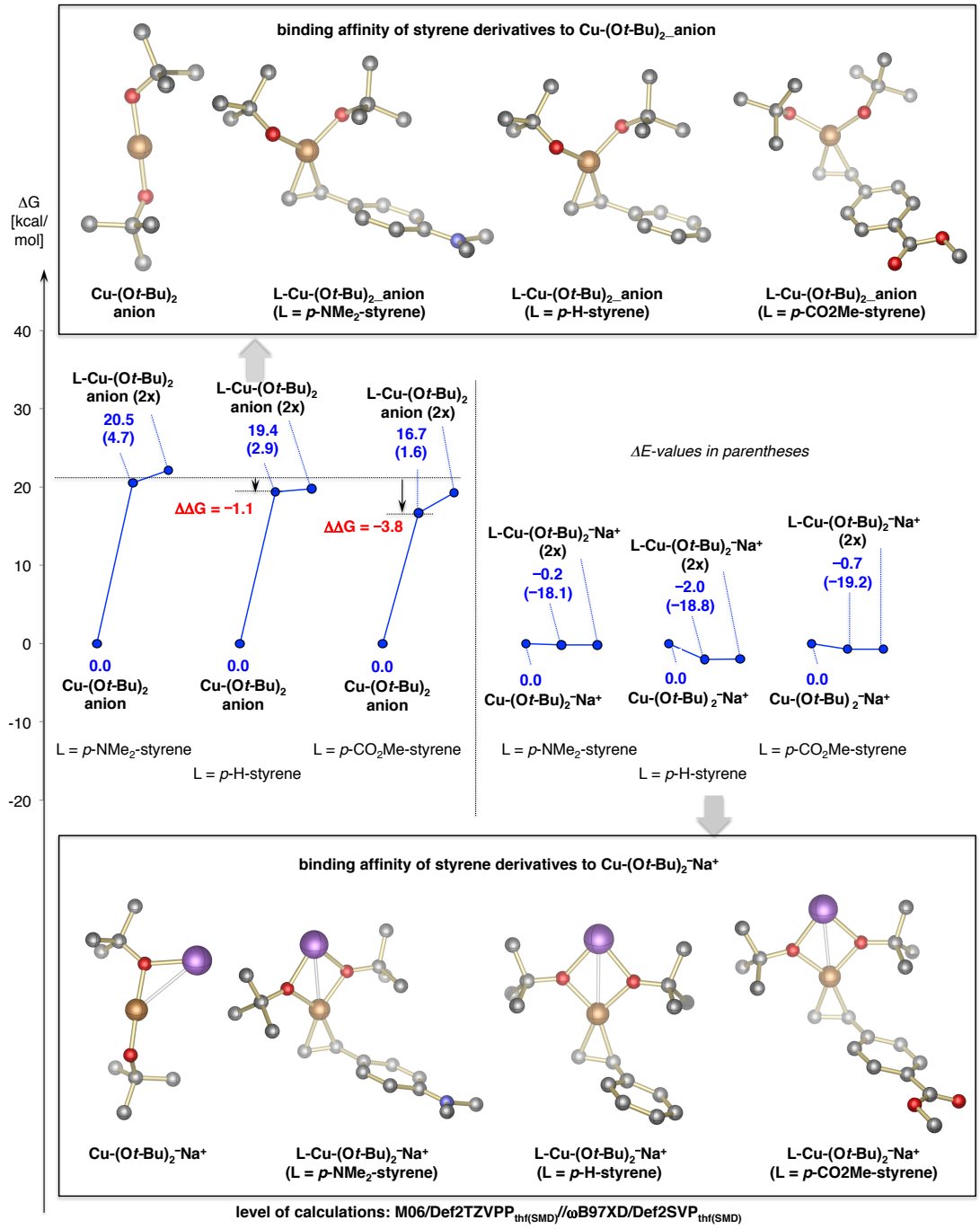

Figure 9.1. Free energy surfaces for binding affinity of various styrene derivatives (***p*-Me$_2$N**, ***p*-H** (styrene)and ***p*-CO$_2$Me**) to the **Cu–O*t*-Bu)$_2^-$** (left) and the species bound to Na (**Cu–O*t*-Bu)$_2^-$Na$^+$** (left) at the M06/DefTZVPP$_{thf(SMD)}$// ωB97XD/Def2SVP$_{thf(SMD)}$ level. Several conformers are shown. The free energies have been referenced to the linear structures for **Cu–O*t*-Bu)$_2^-$** and **Cu–O*t*-Bu)$_2^-$Na$^+$.**

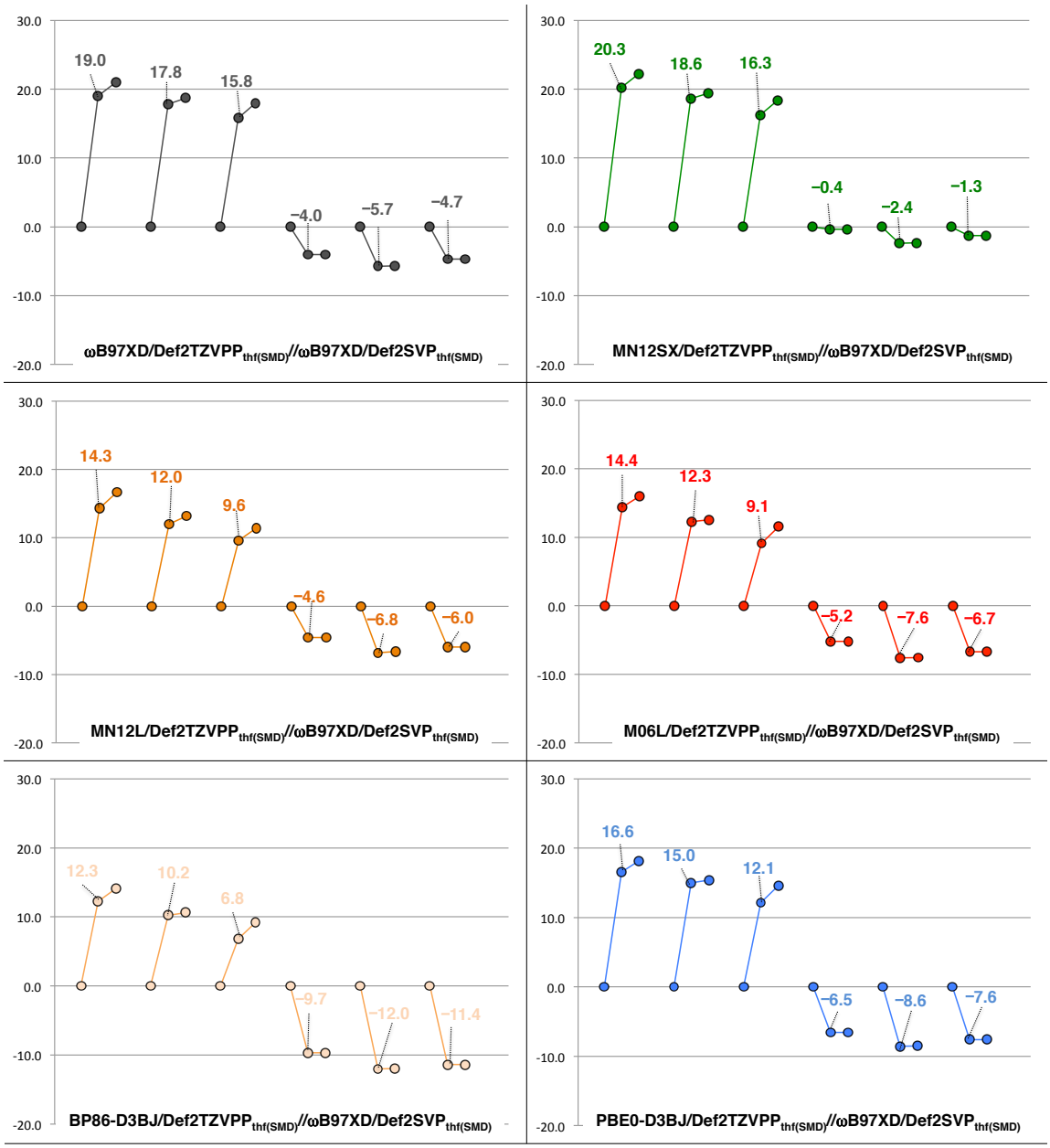

Figure 9.2. Free energy surfaces for binding affinity of various styrene derivatives (***p*-Me$_2$N**, ***p*-H** and ***p*-CO$_2$Me**) to the **Cu–O*t*-Bu)$_2^-$** (left) and the species bound to Na (**Cu–O*t*-Bu)$_2^-$Na$^+$** (left) with various density functionals after optimization with ωB97XD/Def2SVP$_{thf(SMD)}$. For details, see Figure 9.1.

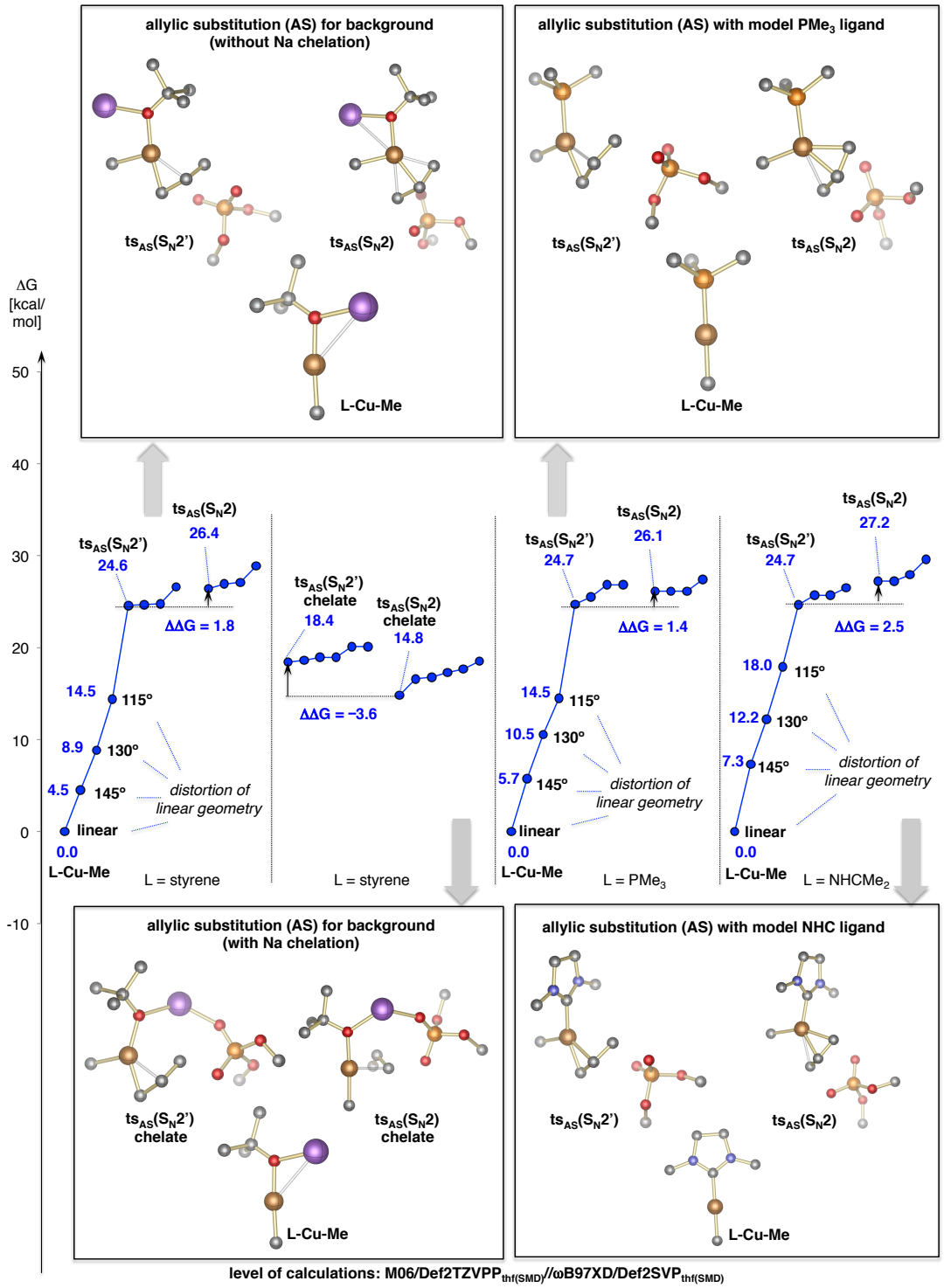

Figure 10.1. Free energy surfaces for S_N2'- and S_N2-type allylic substitution (AS) transition states with either a NaO*t*-Bu molecule, model phoshpine ligand (**PMe$_3$**) or model NHC ligand (**NHCMe$_2$**) as the supporting ligand at the M06/DefTZVPP$_{thf(SMD)}$//ωB97XD/Def2SVP$_{thf(SMD)}$ level. Several conformers are shown for **ts$_{AS}$(S$_N$2')** and **ts$_{AS}$(S$_N$2)**. The free energies have been referenced to linear Cu-alkyl species (**L–Cu–Me**); the alkyl group has been approximated by methyl (Me); only computed structures for the most stable conformers are displayed.

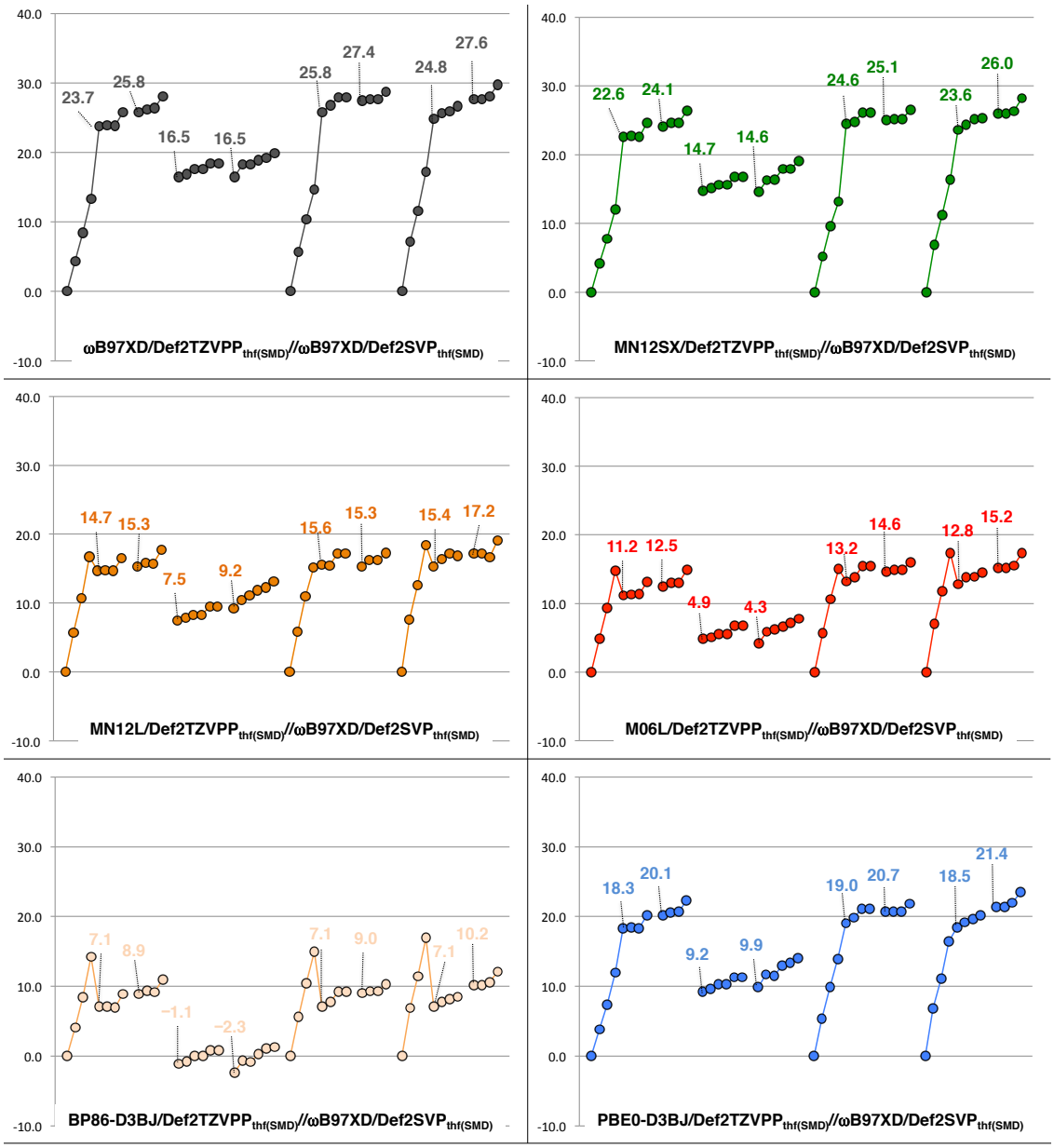

Figure 10.2. Free energy surfaces for S_N2'- and S_N2-type allylic substitution (AS) transition states with either a NaO*t*-Bu molecule, model phoshpine ligand (**PMe$_3$**) or model NHC ligand (**NHCMe$_2$**) as the supporting ligand with various density functionals after optimization with ωB97XD/Def2SVP$_{thf(SMD)}$. For details, see Figure 10.1.

1.5.15 NMR Spectra

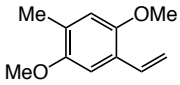

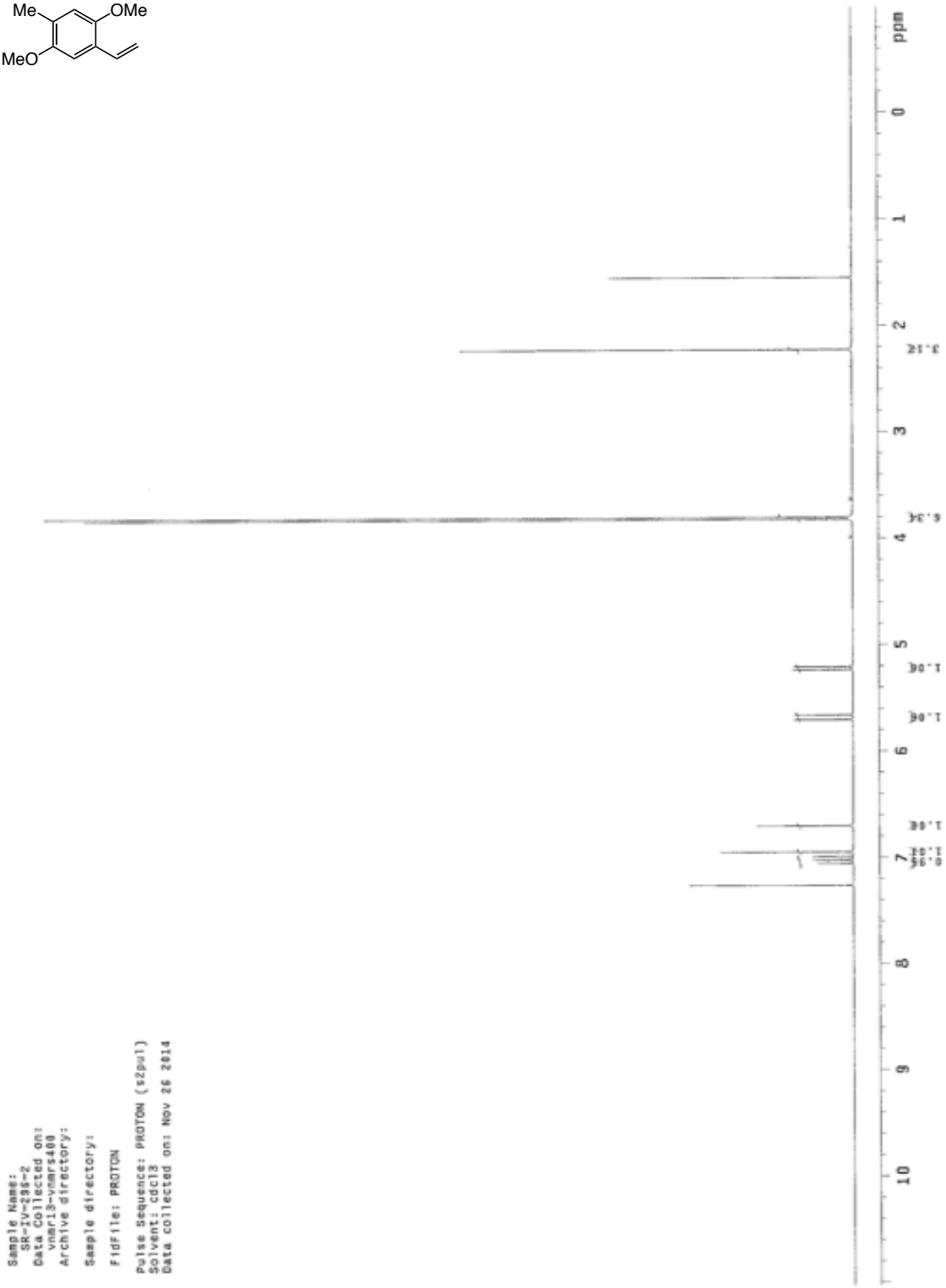

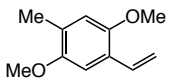
Me
OMe
MeO

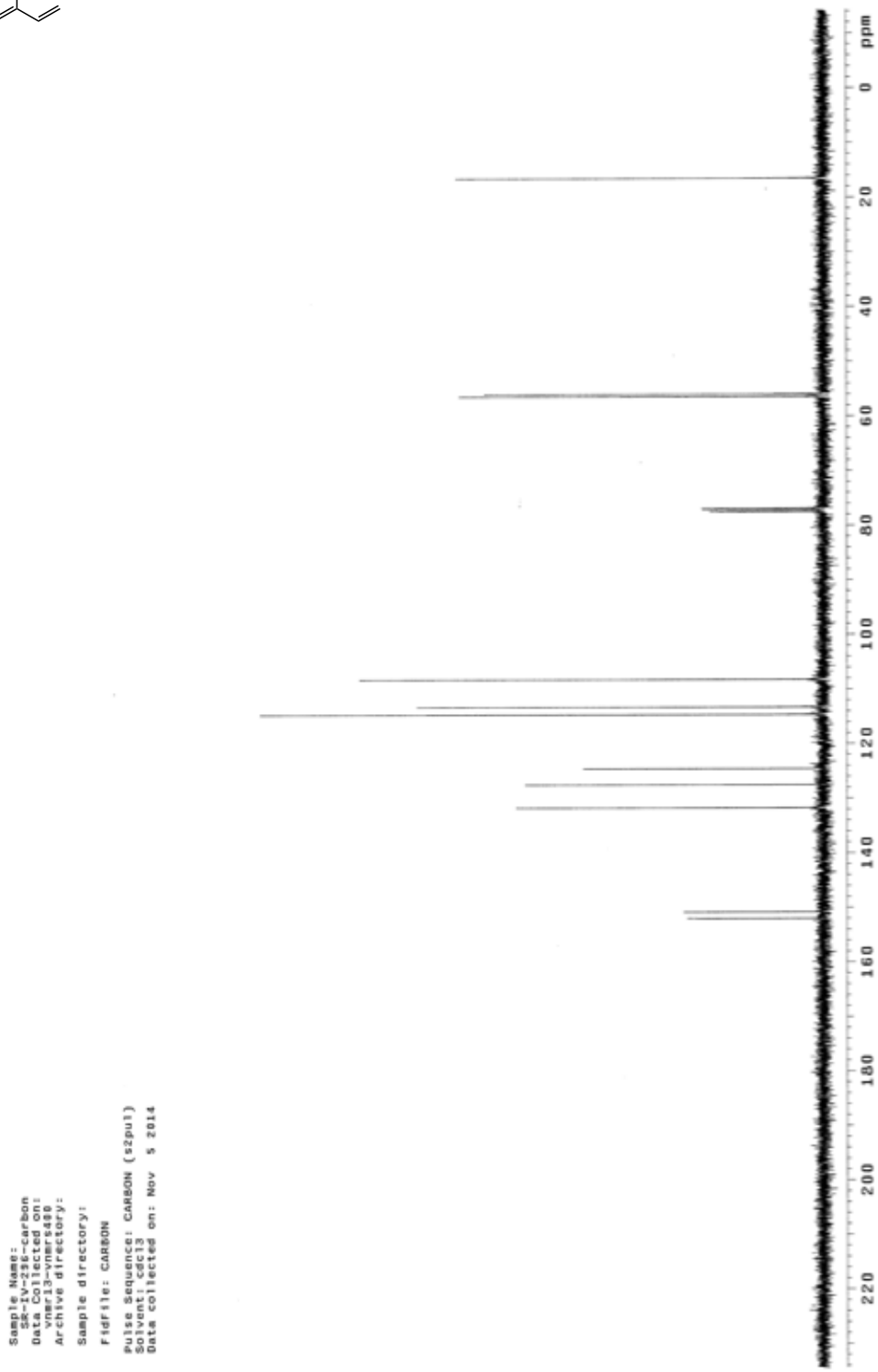
Sample Name:
SR-IV-256-carbon
Data Collected on:
vnmrj3-mercury
Archive directory:
Sample directory:
Fidfile: CARBON
Pulse Sequence: CARBON (s2pul)
Solvent: cdcl3
Data collected on: Nov 5 2014
ppm
0
20
40
60
80
100
120
140
160
180
200
220

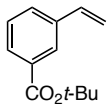
CO2t-Bu

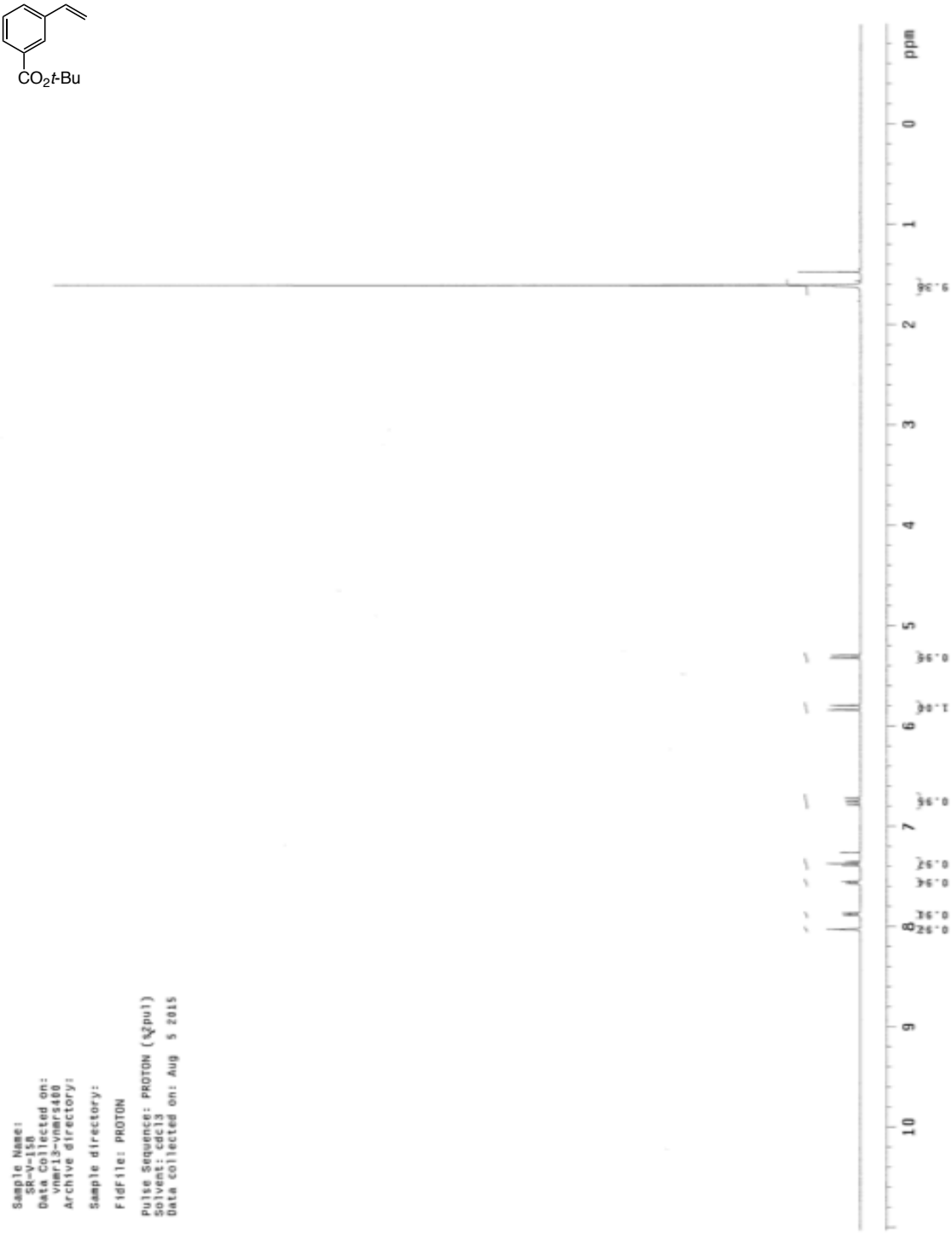
Sample Name:
SR-V-158
Data Collected on:
vnmr13-vnmrs400
Archive directory:
Sample directory:
FidFile: PROTON
Pulse Sequence: PROTON (%pu1)
Solvent: cdcl3
Data collected on: Aug 5 2015
ppm
0
1
2
3
4
5
6
7
8
9
10
9.36
1.00
0.96
0.96
0.94
0.94
0.92

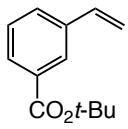
CO2t-Bu

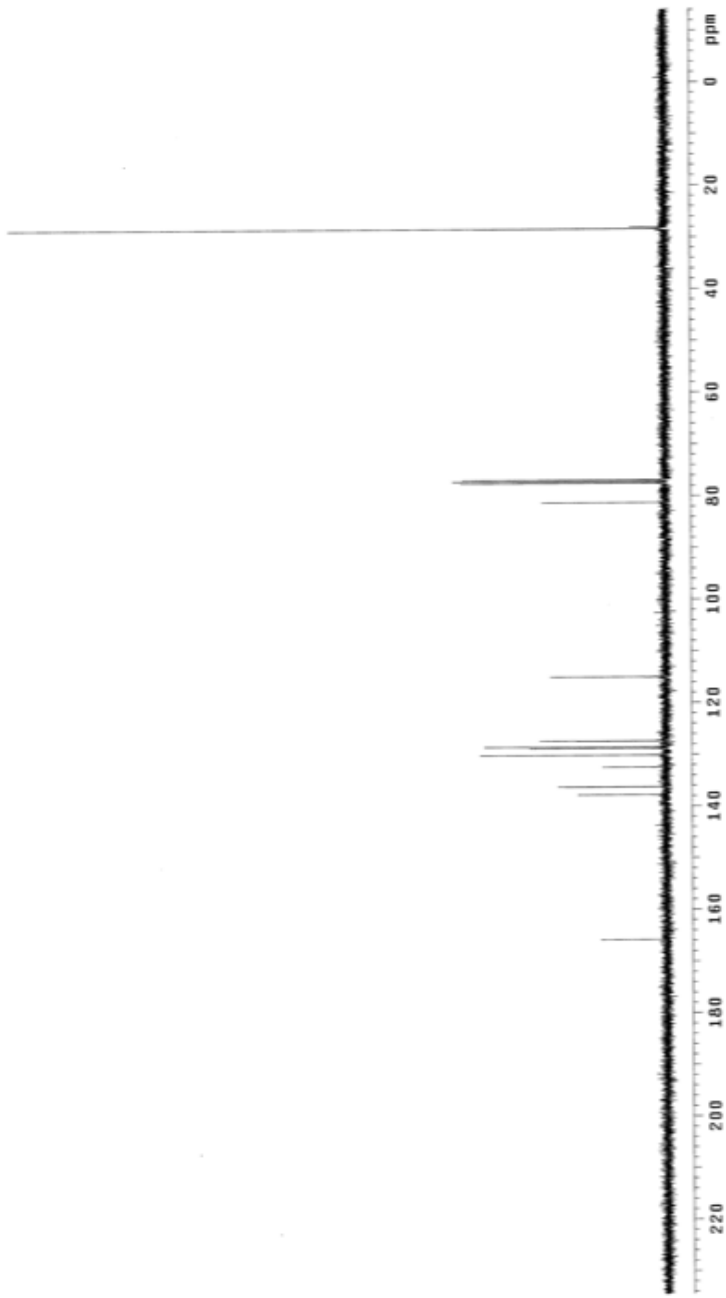
Sample Name:
SR-V-158-carbon
Data Collected on:
vnmr13-vnmrs400
Archive directory:
Sample directory:
FidFile: CARBON
Pulse Sequence: CARBON (s2pul)
Solvent: cdcl3
Data collected on: Aug 5 2015
ppm
0
20
40
60
80
100
120
140
160
180
200
220

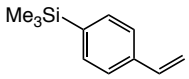
Me3Si

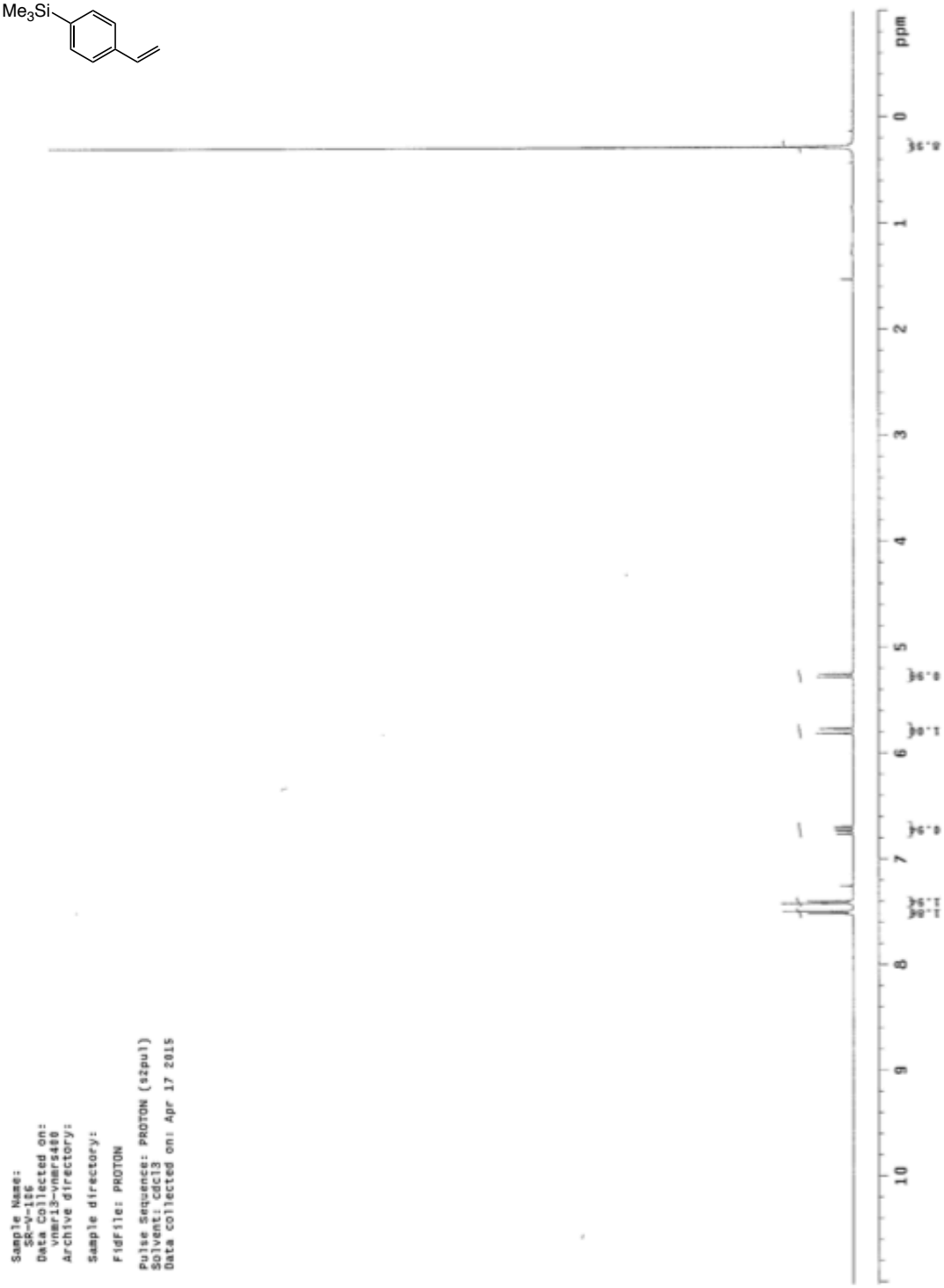
Sample Name:
SR-V-156
Data Collected on:
vnmr13-vnmrs400
Archive directory:
Sample directory:
Fidfile: PROTON
Pulse Sequence: PROTON (s2pul)
Solvent: cdcl3
Data collected on: Apr 17 2015
ppm
10
9
8
7
6
5
4
3
2
1
0

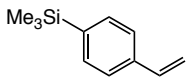
Me3Si

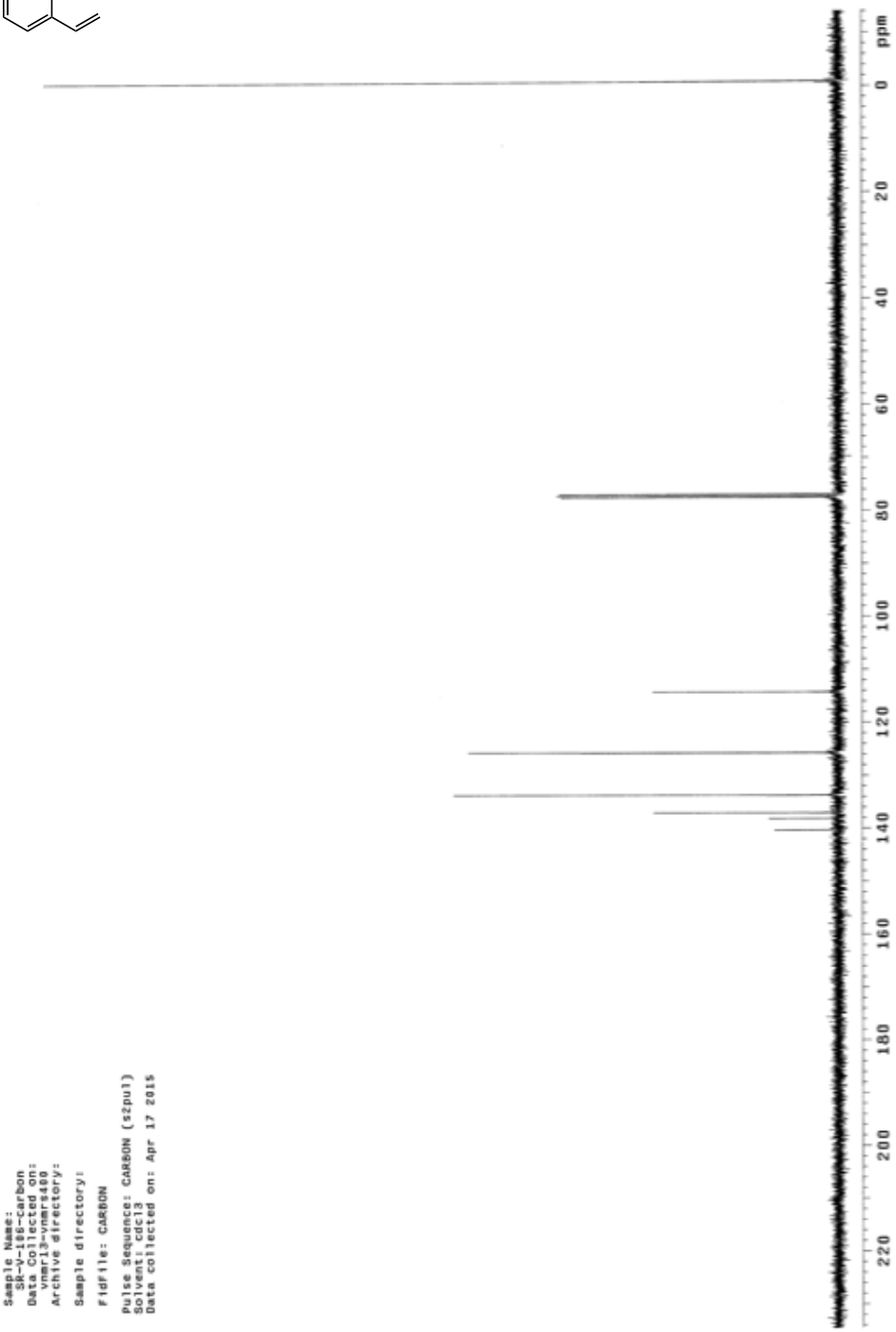
Sample Name:
SR-V-186-carbon
Data Collected on:
vnmr13-vnmrs400
Archive directory:
Sample directory:
Fidfile: CARBON
Pulse Sequence: CARBON (s2pul)
Solvent: cdcl3
Data collected on: Apr 17 2015
ppm
0
20
40
60
80
100
120
140
160
180
200
220

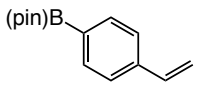
(pin)B

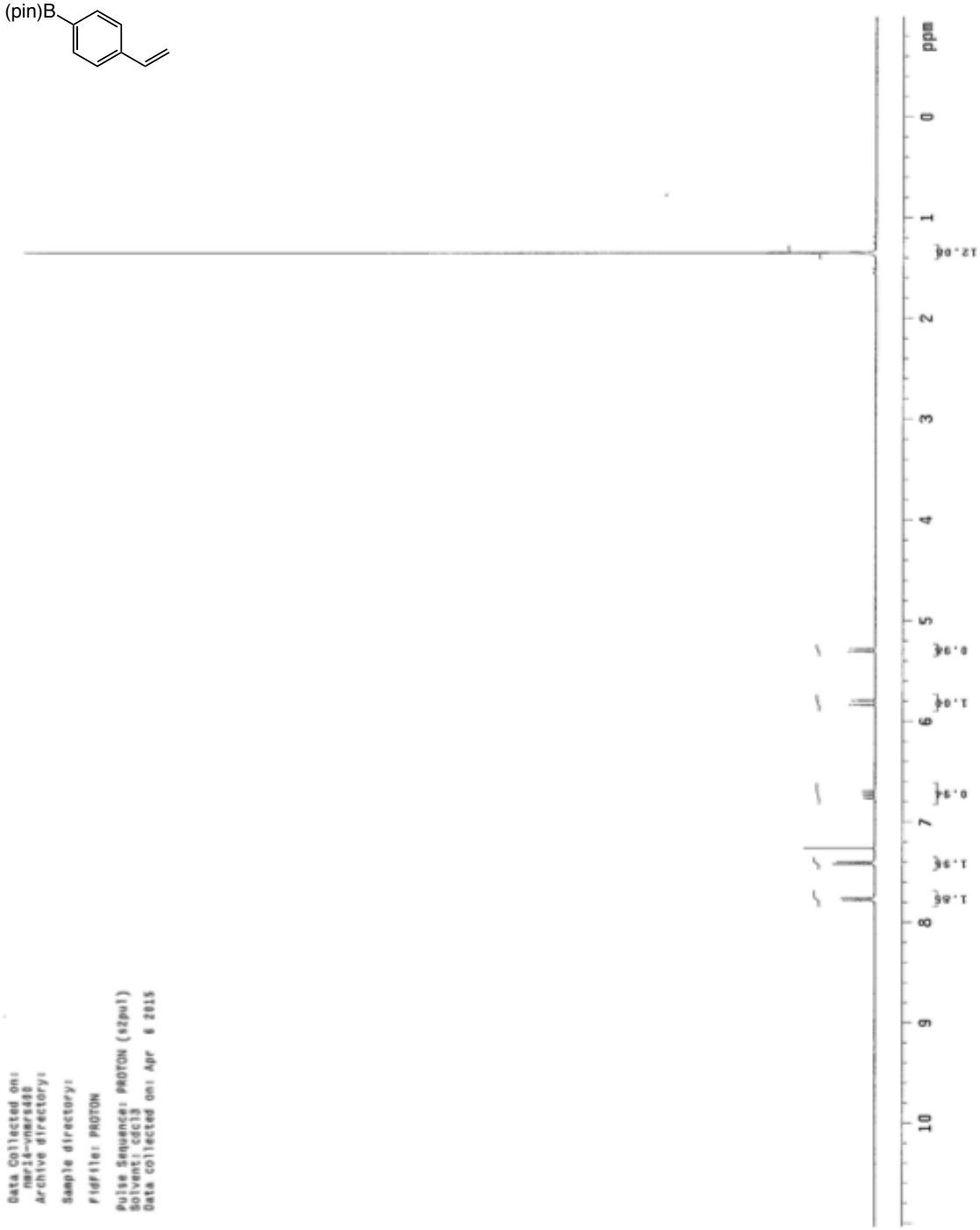
Data Collected on:
nmr14-vnmr4dd
Archive directory:
Sample directory:
FidFile: PROTON
Pulse Sequence: PROTON (s2pul)
Solvent: cdcl3
Data collected on: Apr 6 2015
ppm
12.06
0.94
1.04
0.94
1.94
1.06

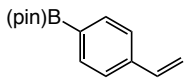
(pin)B

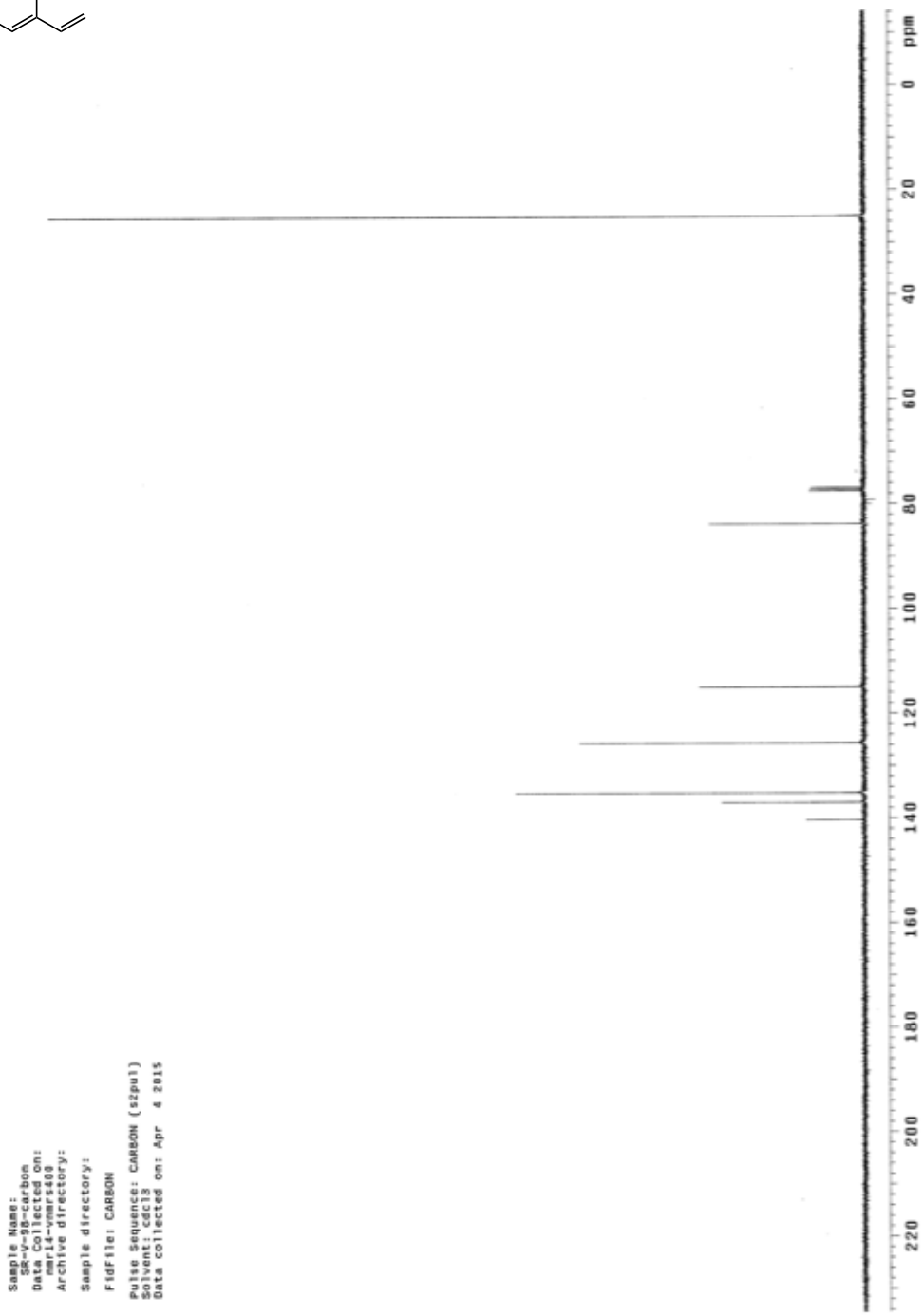
Sample Name:
SR-V-88-carbon
Data Collected on:
mmr14-vmmrs400
Archive directory:
Sample directory:
FidFile: CARBON
Pulse Sequence: CARBON (s2pul)
Solvent: cdcl3
Data collected on: Apr 4 2015
ppm
0
20
40
60
80
100
120
140
160
180
200
220

(pin)B

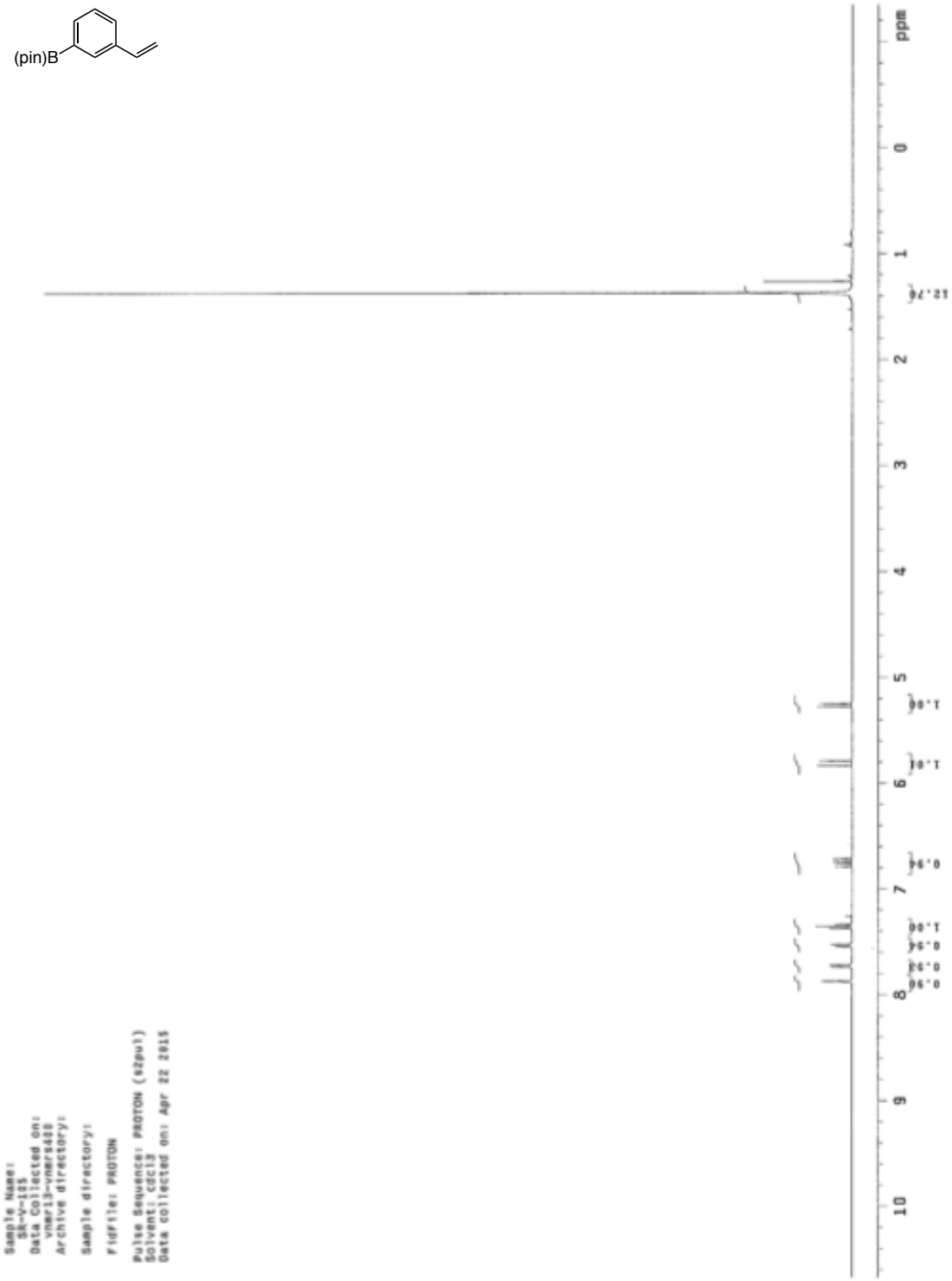
Sample Name:
SR-V-115
Data Collected on:
vnmr13-vnmrs400
Archive directory:
Sample directory:
Fidfile: PROTON
Pulse Sequence: PROTON (s2pul)
Solvent: CDCl3
Data collected on: Apr 22 2015
ppm
12.76
1.00
1.00
0.96
1.00
0.96
0.96
0.96

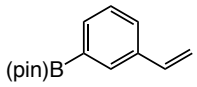
(pin)B

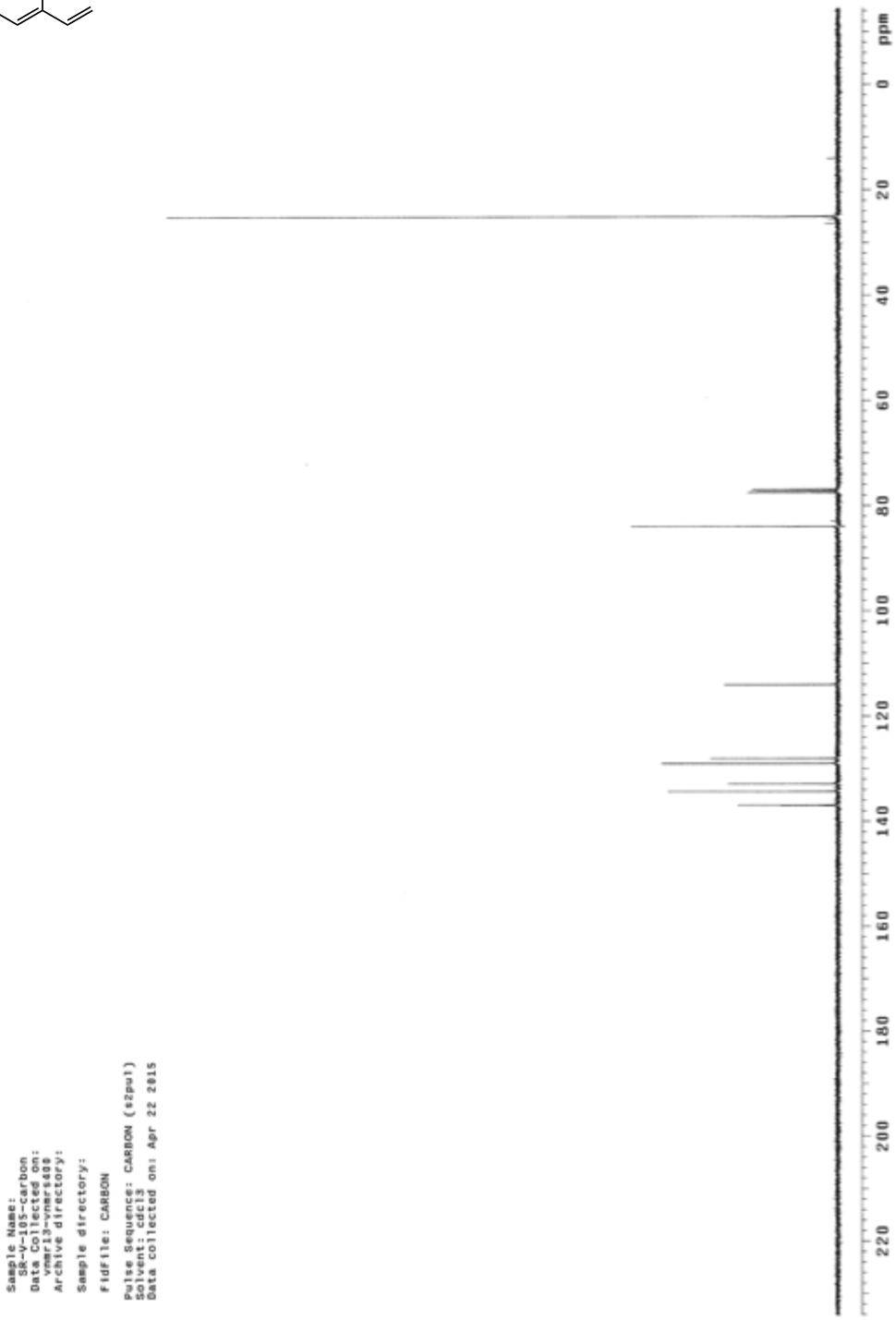
Sample Name:
SR-V-105-carbon
Data Collected on:
vnmr13-vnmrsa@
Archive directory:
Sample directory:
Fidfile: CARBON
Pulse Sequence: CARBON (s2pul)
Solvent: cdcl3
Data collected on: Apr 22 2015
ppm
220
200
180
160
140
120
100
80
60
40
20
0

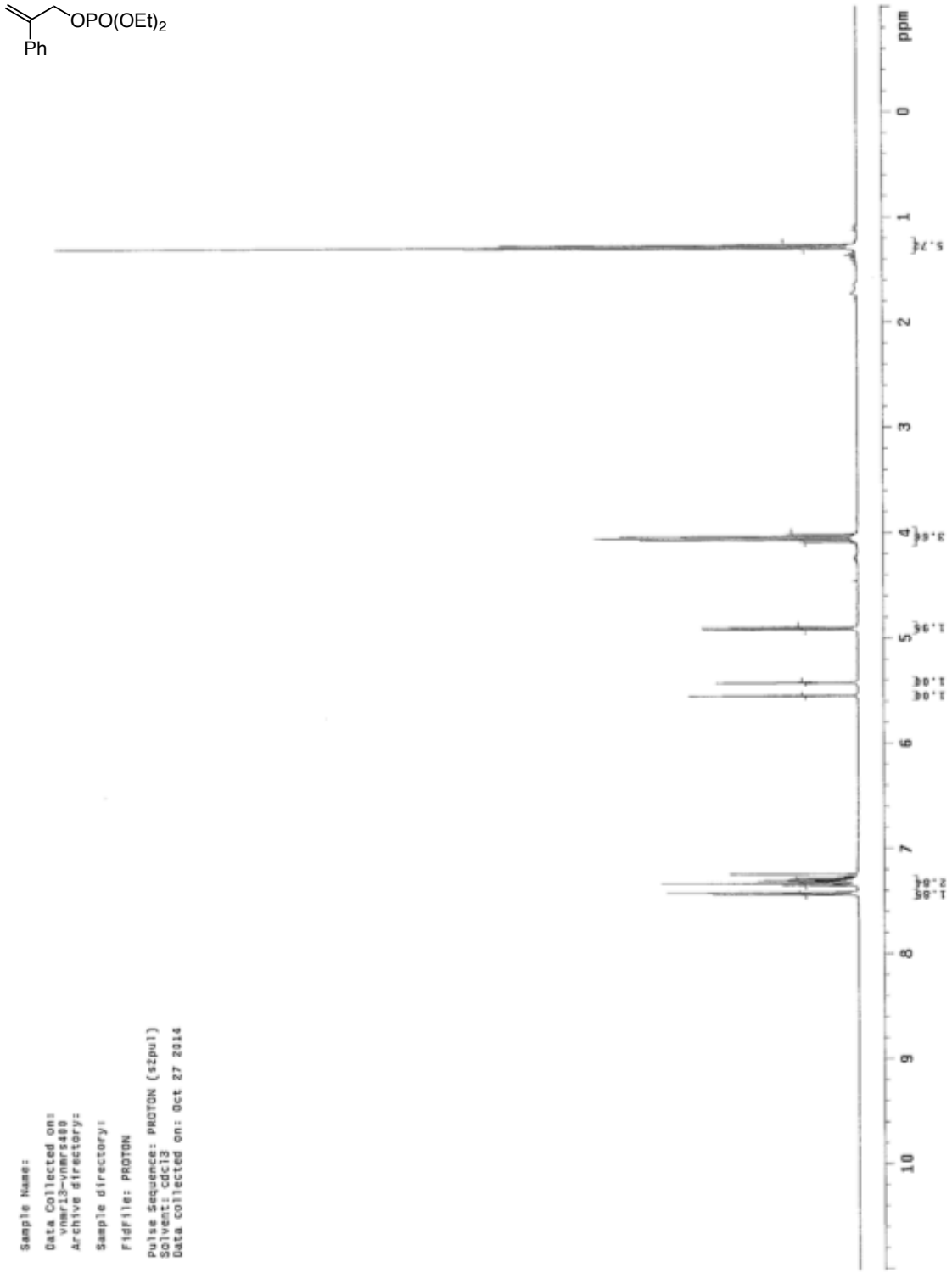
OPO(OEt)2
Ph
Sample Name:
Data Collected on:
vnmr13-vnmrs400
Archive directory:
Sample directory:
Fidfile: PROTON
Pulse Sequence: PROTON (s2pul)
Solvent: cdcl3
Data collected on: Oct 27 2014
ppm
0
1
2
3
4
5
6
7
8
9
10
5.74
3.66
1.95
1.04
1.04
2.04
1.05

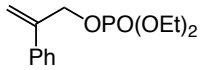
OPO(OEt)2
Ph

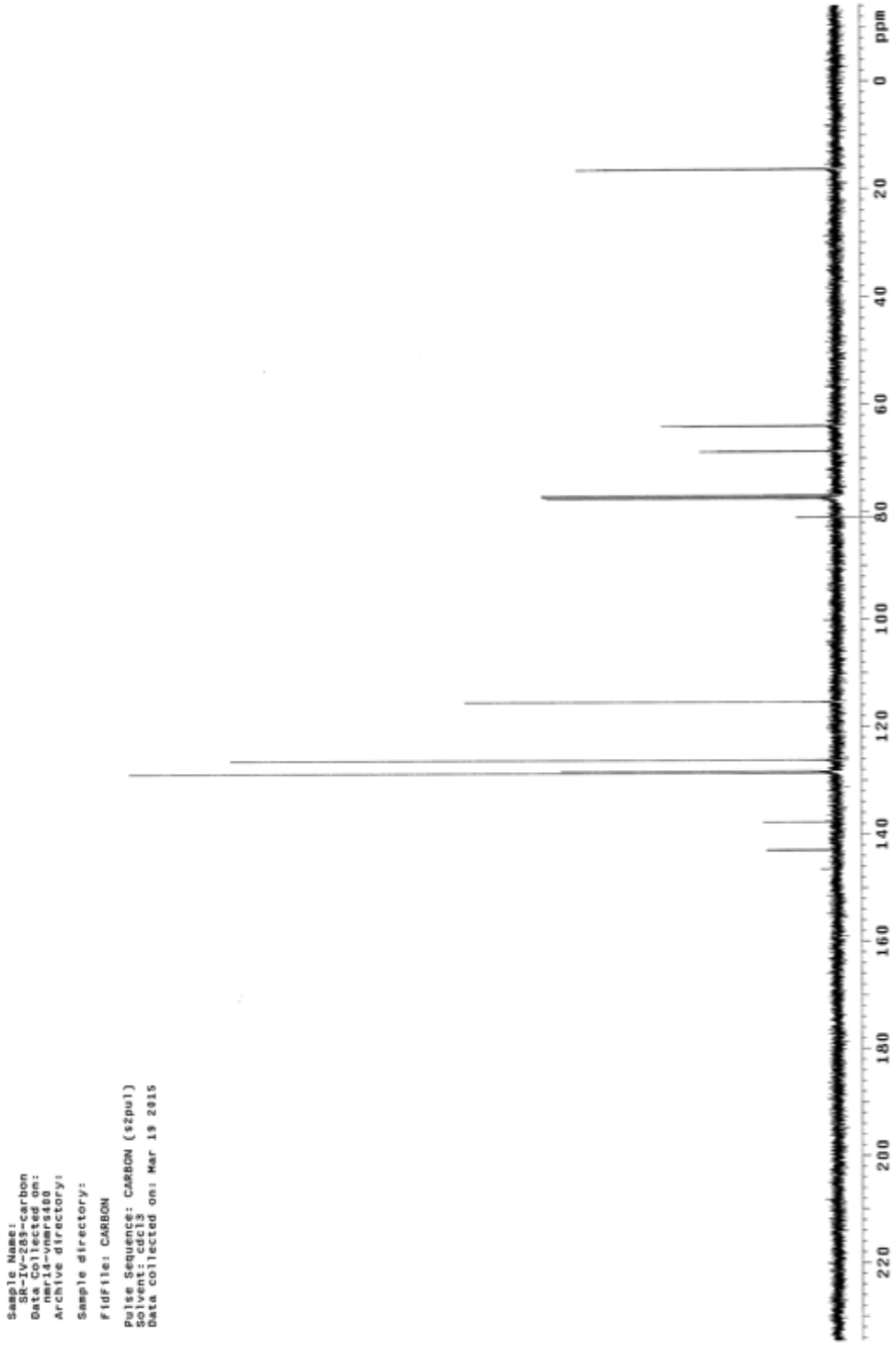
Sample Name:
SR-IV-285-carbon
Data Collected on:
nmr14-vnmrs400
Archive directory:
Sample directory:
Fidfile: CARBON
Pulse Sequence: CARBON (s2pul)
Solvent: cdcl3
Data collected on: Mar 19 2015
ppm
0
20
40
60
80
100
120
140
160
180
200
220

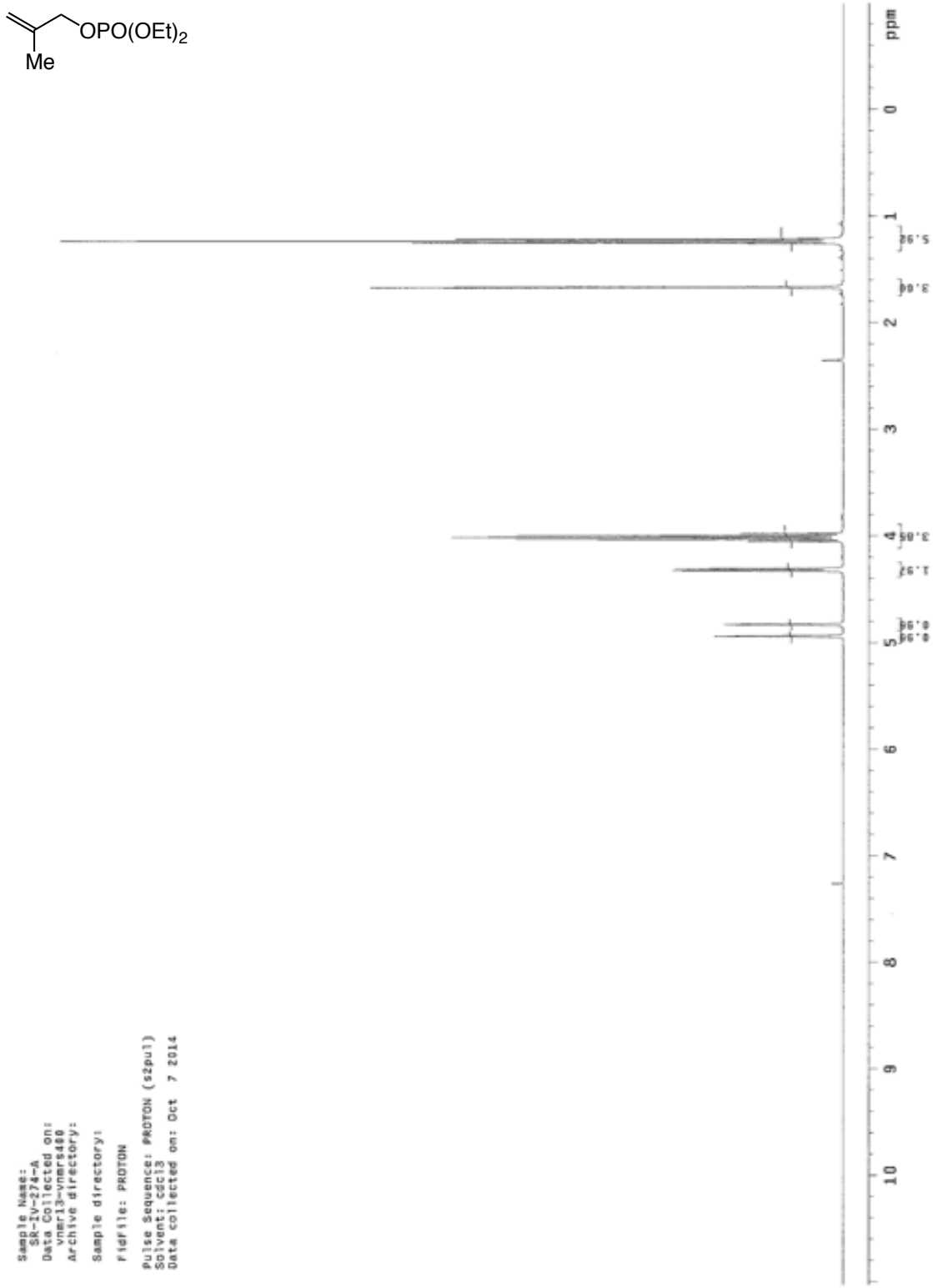
OPO(OEt)2
Me
Sample Name:
SR-IV-274-A
Data Collected on:
vnmr13-vnmrs400
Archive directory:
Sample directory:
FidFile: PROTON
Pulse Sequence: PROTON (s2pul)
Solvent: cdcl3
Data collected on: Oct 7 2014
ppm
0
1
2
3
4
5
6
7
8
9
10
5.92
3.04
3.05
1.97
0.96
0.96

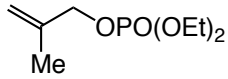
OPO(OEt)2
Me

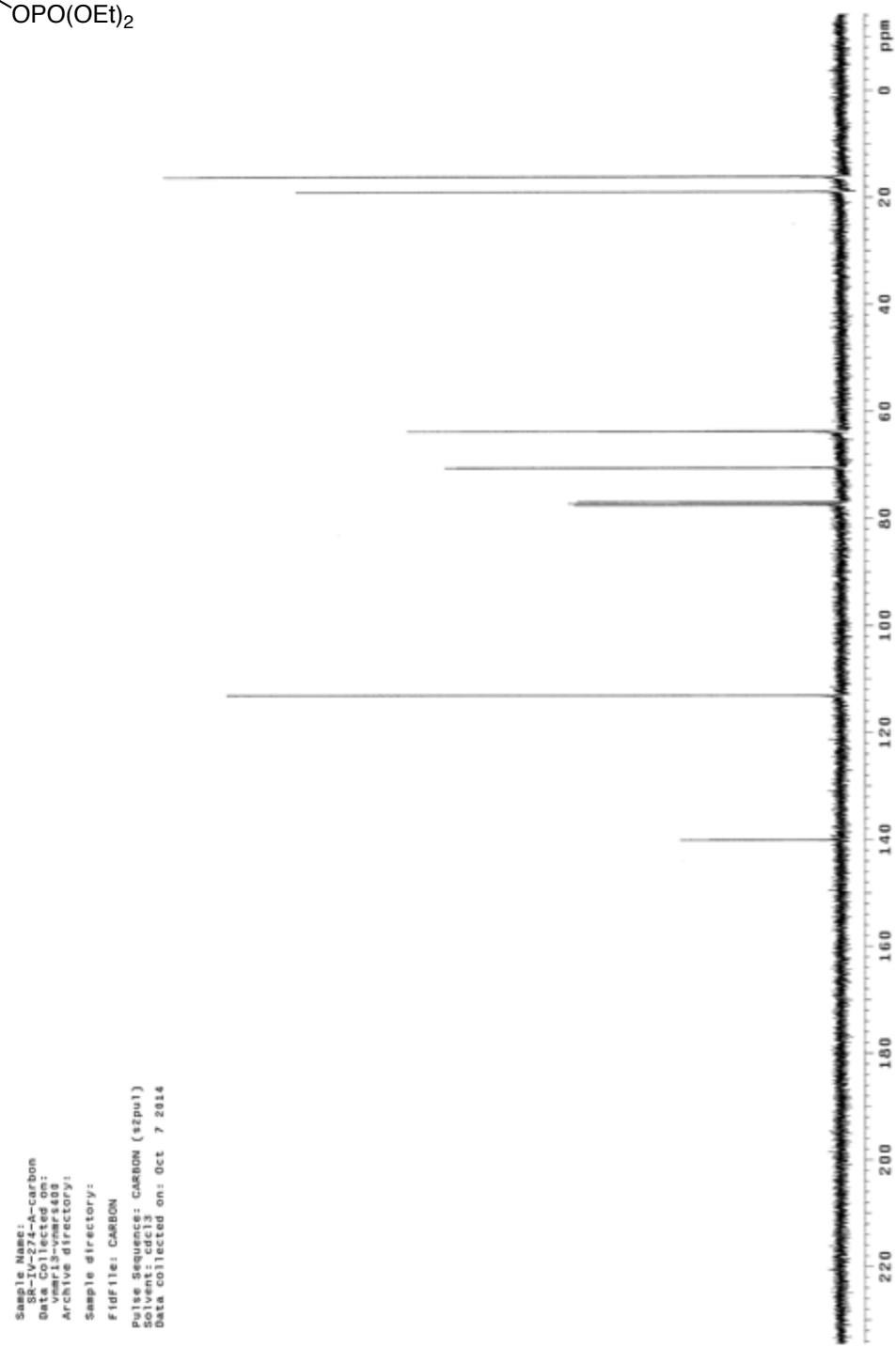
Sample Name:
SR-IV-274-A-carbon
Data Collected on:
vmar13-vmar400
Archive directory:
Sample directory:
FidFile: CARBON
Pulse Sequence: CARBON (s2pul)
Solvent: cdcl3
Data collected on: Oct 7 2014
ppm
220
200
180
160
140
120
100
80
60
40
20
0

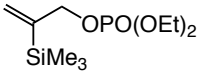
OPO(OEt)2
SiMe3

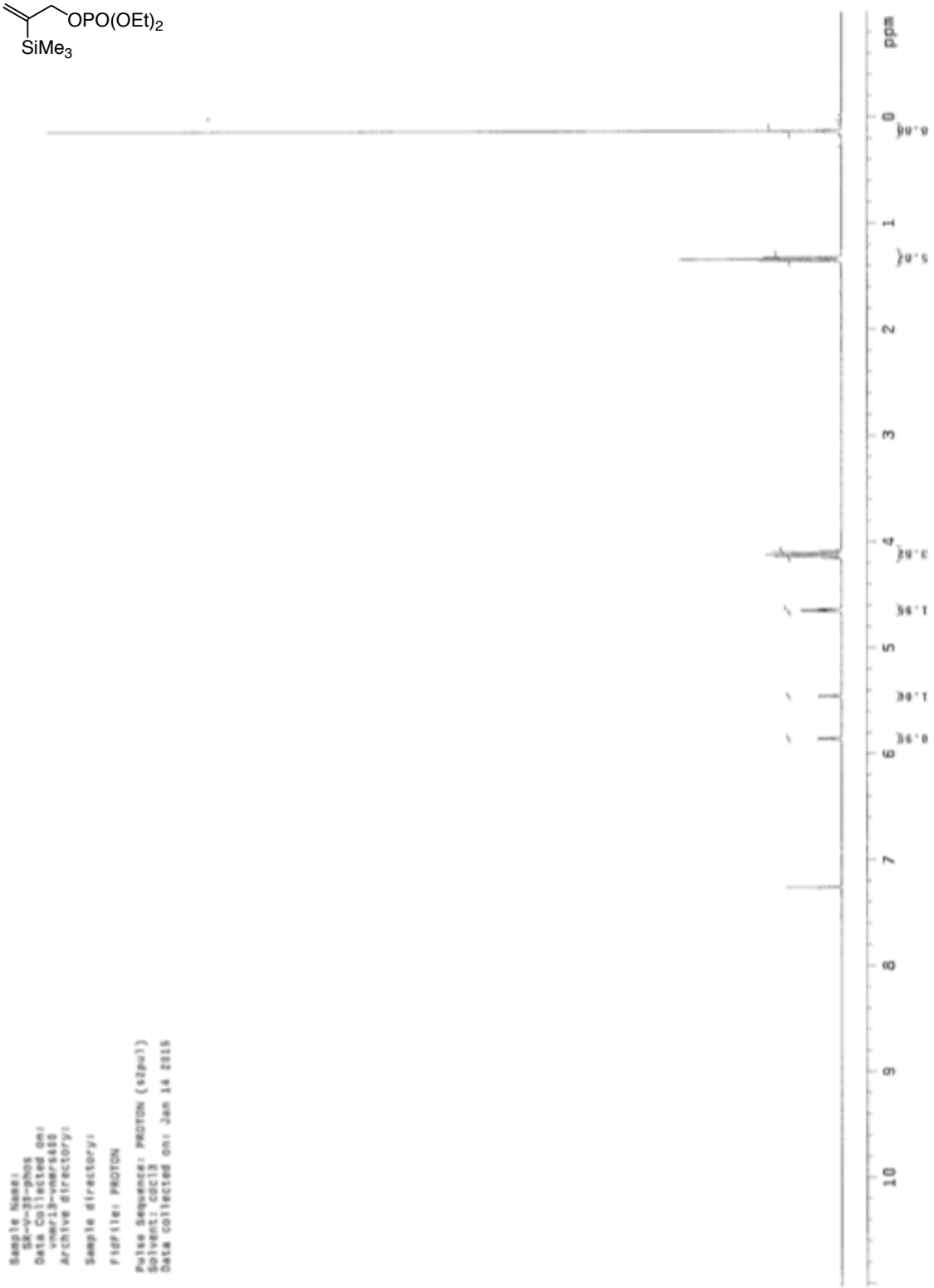
Sample Name:
SR-V-39-phos
Data Collected on:
vmar18-vmar5488
Archive directory:
Sample directory:
Fidfile: PROTON
Pulse Sequence: PROTON (s2pul)
Solvent: cdcl3
Data collected on: Jan 14 2015
ppm
0.00
0.95
3.02
1.96
1.00
0.98
0
1
2
3
4
5
6
7
8
9
10

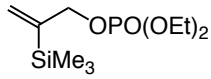
OPO(OEt)2
SiMe3

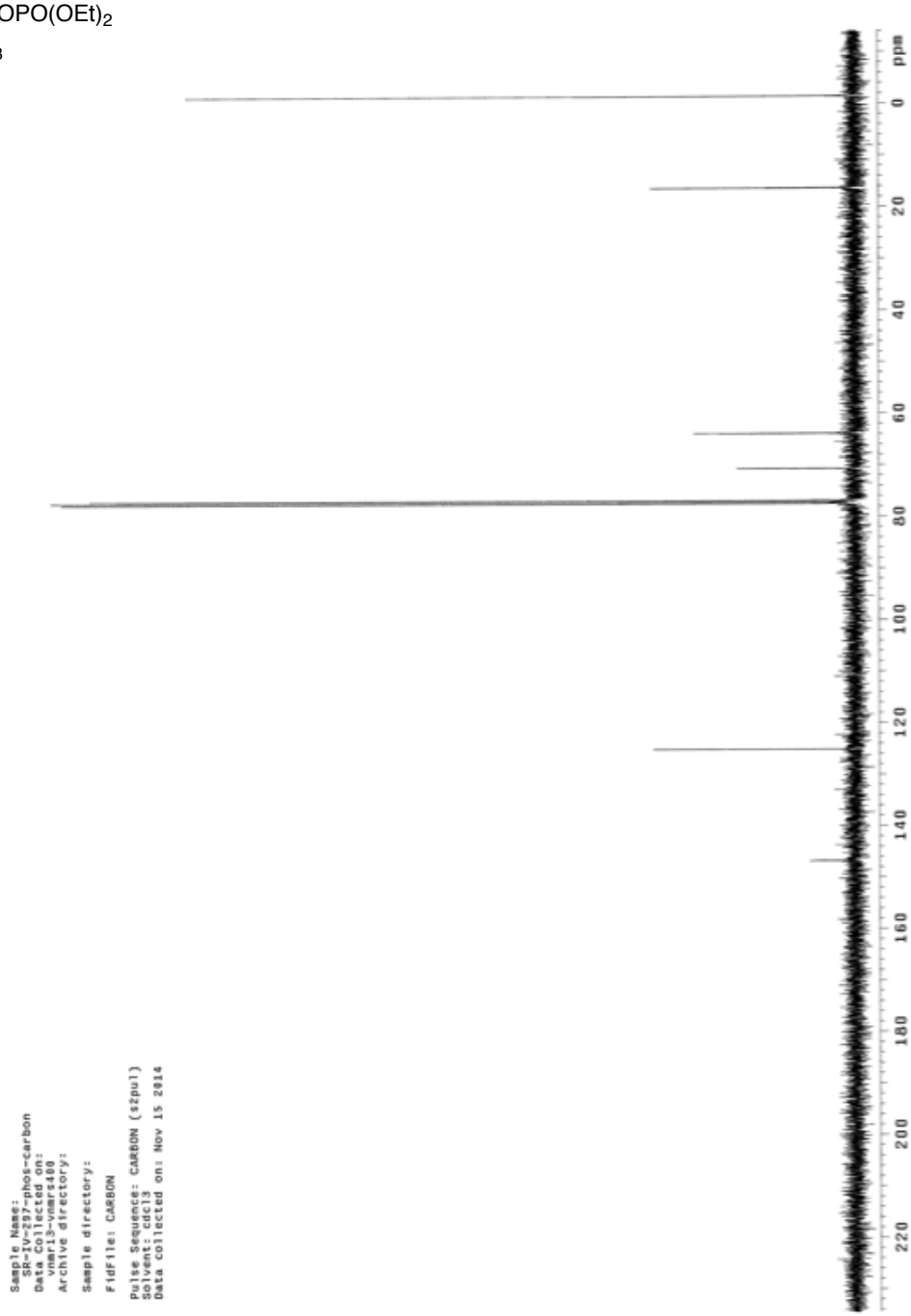
Sample Name:
SR-IV-287-phos-carbon
Data Collected on:
vnmr13-vnmrs400
Archive directory:
Sample directory:
Fidfile: CARBON
Pulse Sequence: CARBON (s2pul)
Solvent: cdcl3
Data collected on: Nov 15 2014
ppm
0
20
40
60
80
100
120
140
160
180
200
220

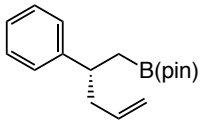
B(pin)

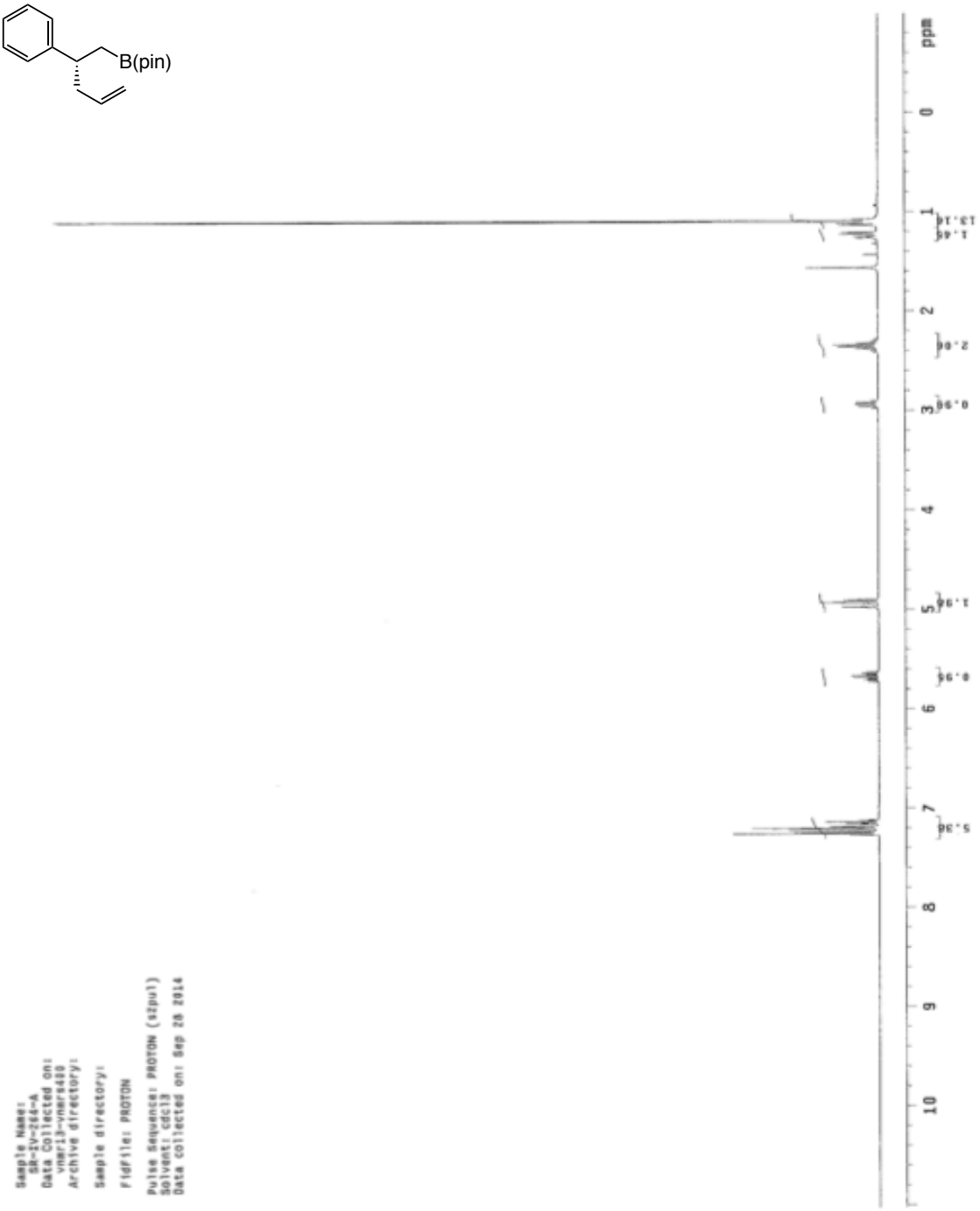
Sample Name:
SB-IV-264-A
Data Collected on:
vnmr13-vnmrs480
Archive directory:
Sample directory:
Fidfile: PROTON
Pulse Sequence: PROTON (s2pul)
Solvent: cdcl3
Data collected on: Sep 28 2014
ppm
0
1
2
3
4
5
6
7
8
9
10
13.14
1.65
2.04
0.96
1.94
0.94
5.34

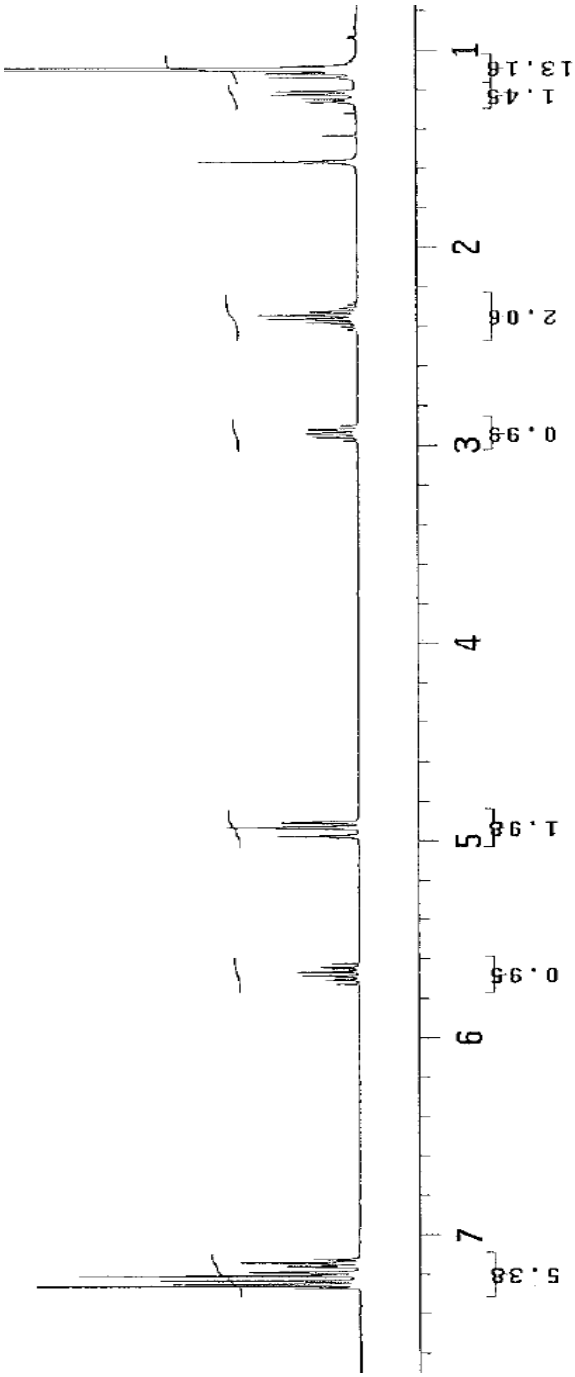
1
2
3
4
5
6
7
13.16
1.45
2.06
0.98
1.98
0.95
5.38

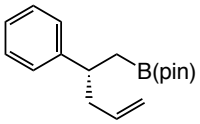
B(pin)

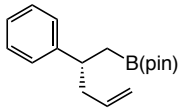
B(pin)

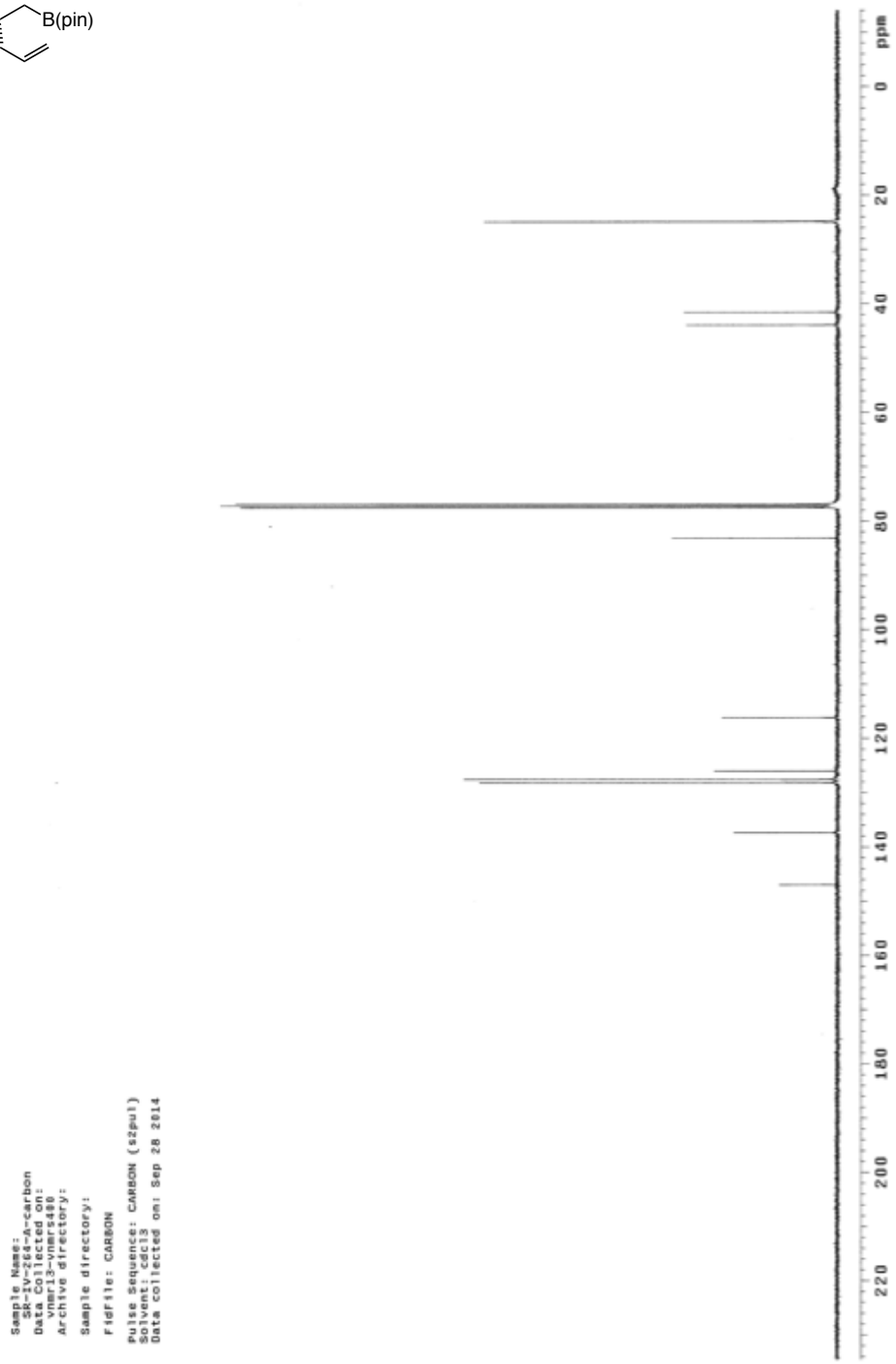
Sample Name:
SP-IV-264-A-carbon
Data Collected on:
vnmr13-vnmrs400
Archive directory:
Sample directory:
Fidfile: CARBON
Pulse Sequence: CARBON (s2pul)
Solvent: cdcl3
Data collected on: Sep 28 2014
ppm
220
200
180
160
140
120
100
80
60
40
20
0

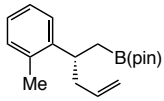
B(pin)
Me

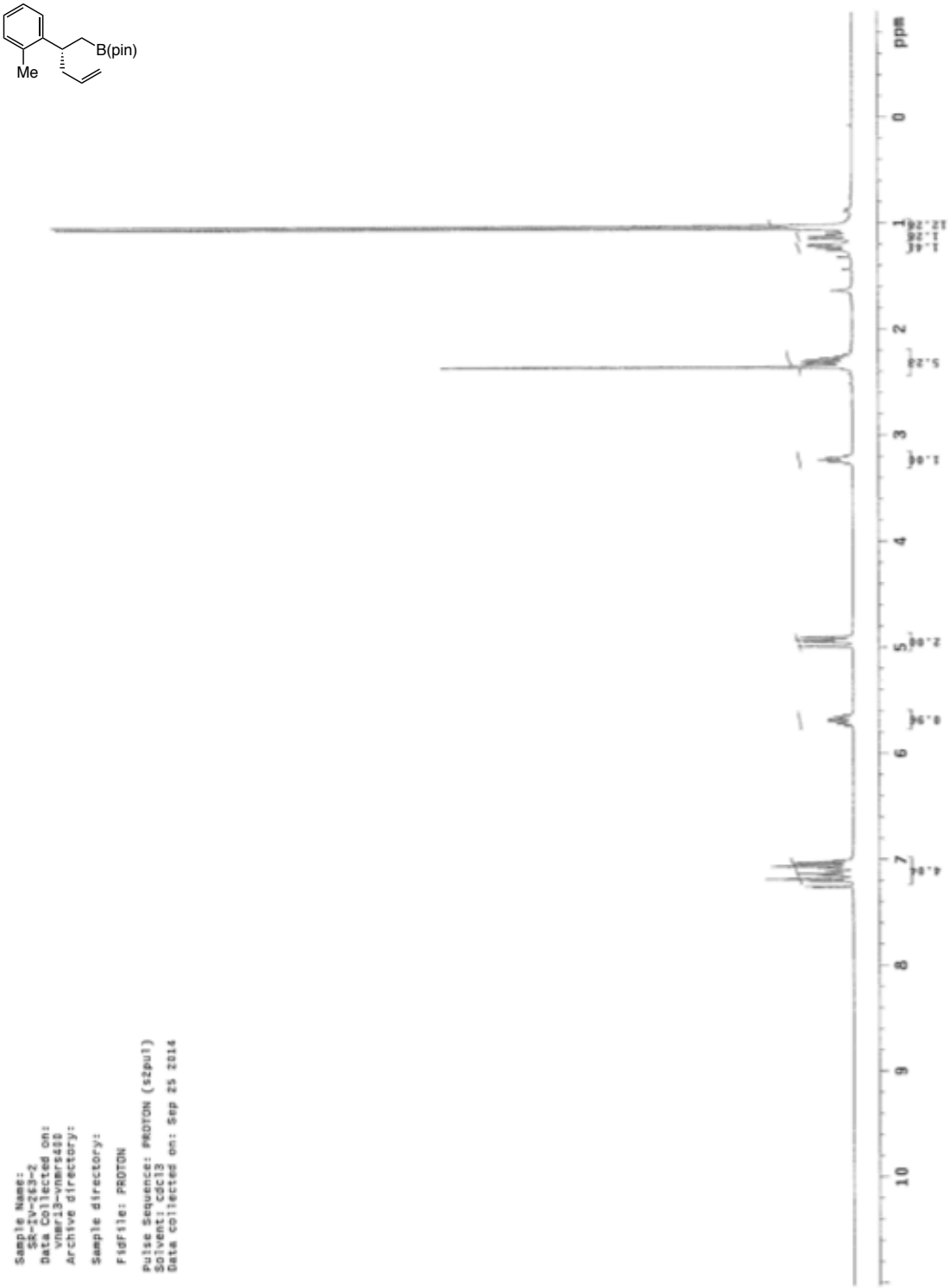
Sample Name:
SR-IV-163-2
Data Collected on:
vnmr13-vnmrs410
Archive directory:
Sample directory:
FidFile: PROTON
Pulse Sequence: PROTON (s2pul)
Solvent: CdCl3
Data collected on: Sep 25 2014
ppm
0
1
2
3
4
5
6
7
8
9
10

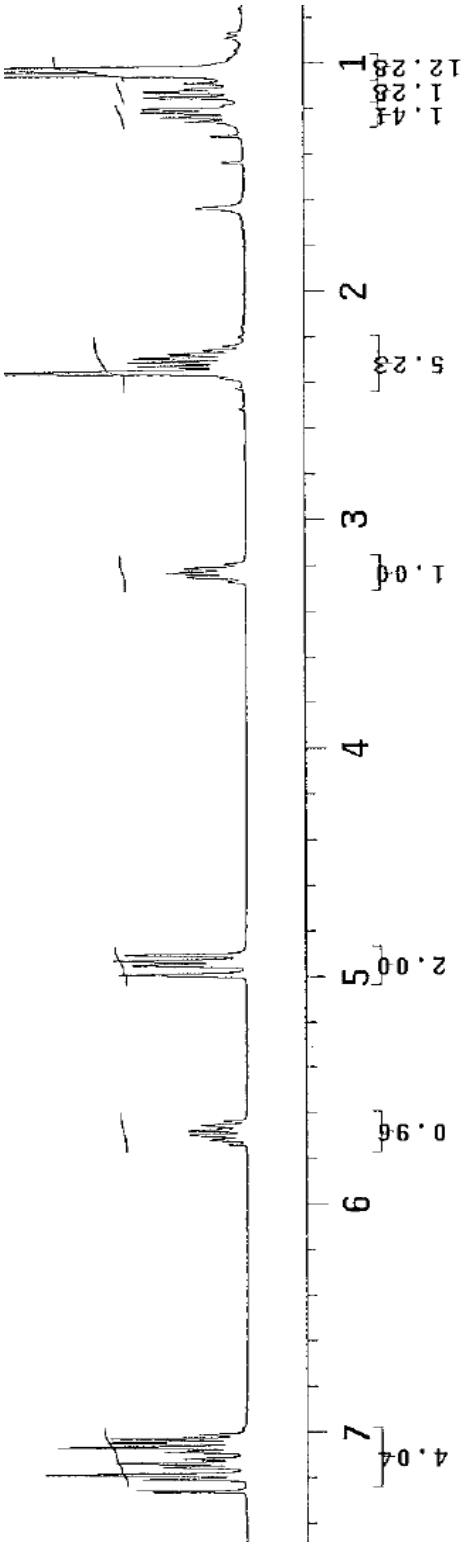
12.28
1.28
1.41
5.23
1.00
2.00
0.96
4.04
1
2
3
4
5
6
7

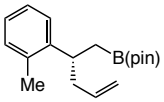
B(pin)
Me

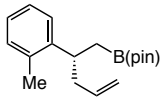
B(pin)
Me

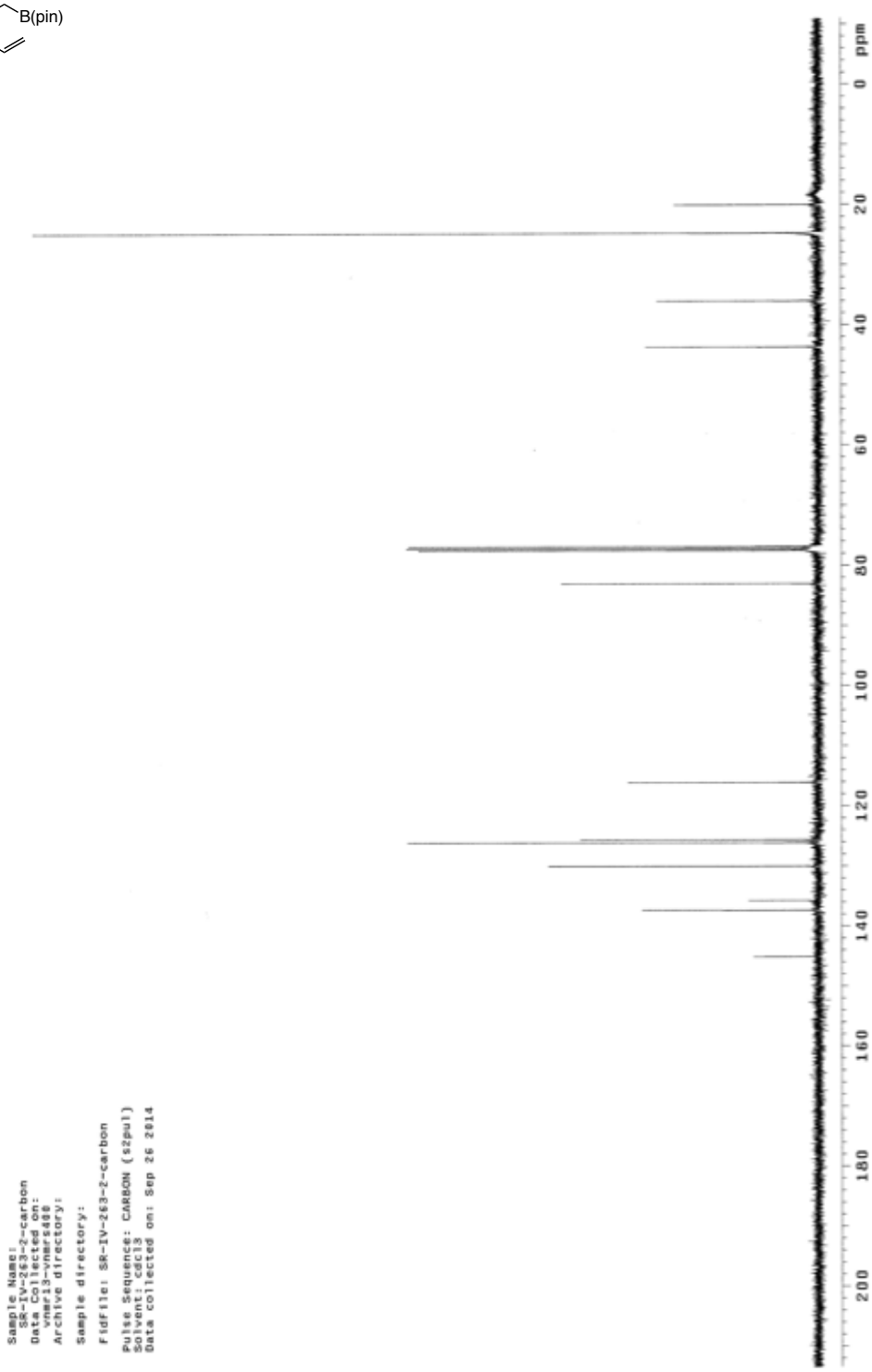
Sample Name:
SR-IV-263-2-carbon
Data Collected on:
vnmrs13-vnmrs400
Archive directory:
Sample directory:
Fidfile: SR-IV-263-2-carbon
Pulse Sequence: CARBON (s2pul)
Solvent: cdcl3
Data collected on: Sep 26 2014
ppm
0
20
40
60
80
100
120
140
160
180
200

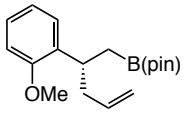
B(pin)
OMe

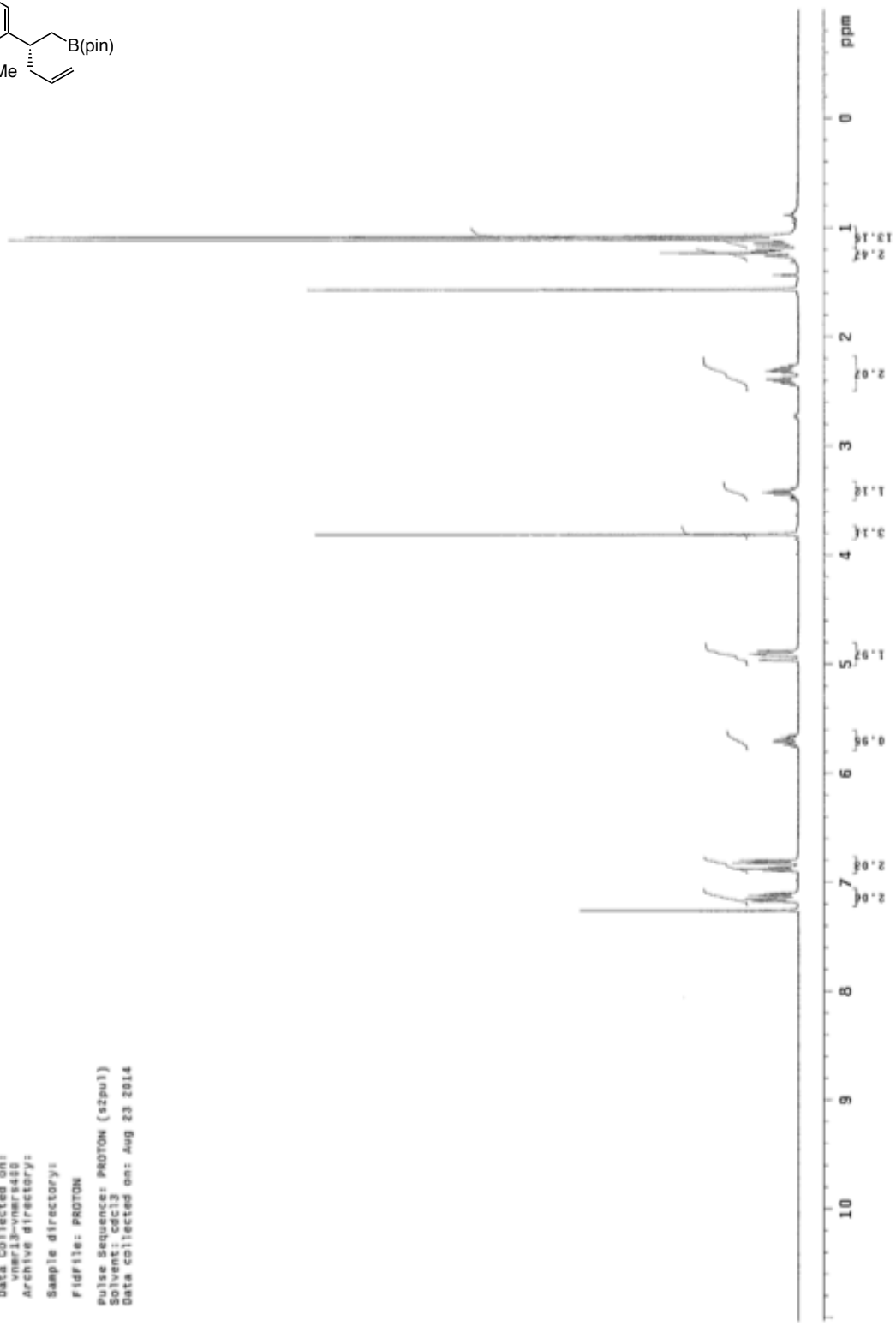
ppm
0
1
2
3
4
5
6
7
8
9
10
13.16
2.42
2.02
1.16
3.14
1.92
0.96
2.04
2.04
Sample Name:
SK-IV-251-B
Data Collected on:
vnmr13-vnmrs440
Archive directory:
Sample directory:
FidFile: PROTON
Pulse Sequence: PROTON (s2pul)
Solvent: CdCl3
Data collected on: Aug 23 2014

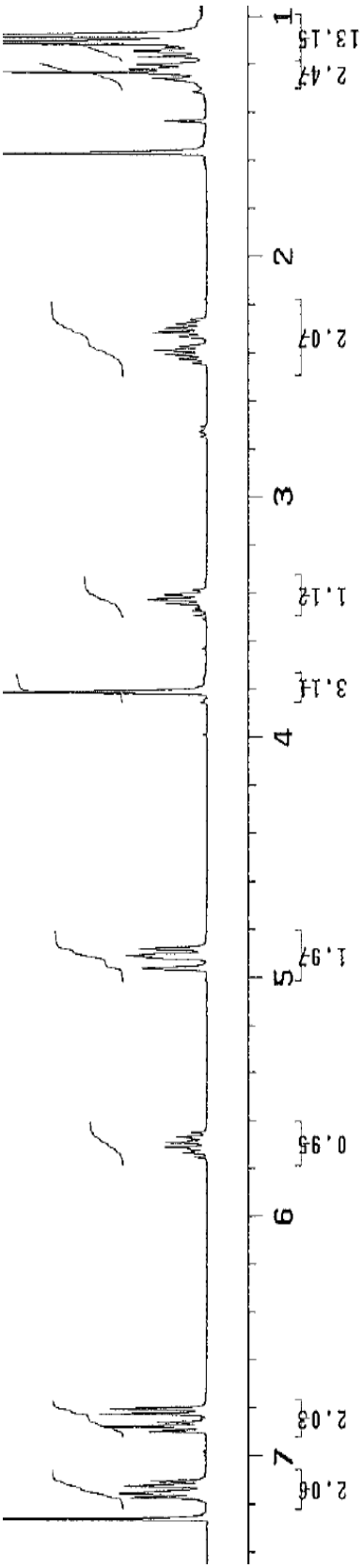
13.15
2.47
2.07
1.12
3.14
1.97
0.95
2.03
2.06
1
2
3
4
5
6
7

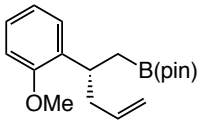
B(pin)
OMe

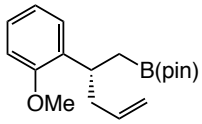
B(pin)
OMe

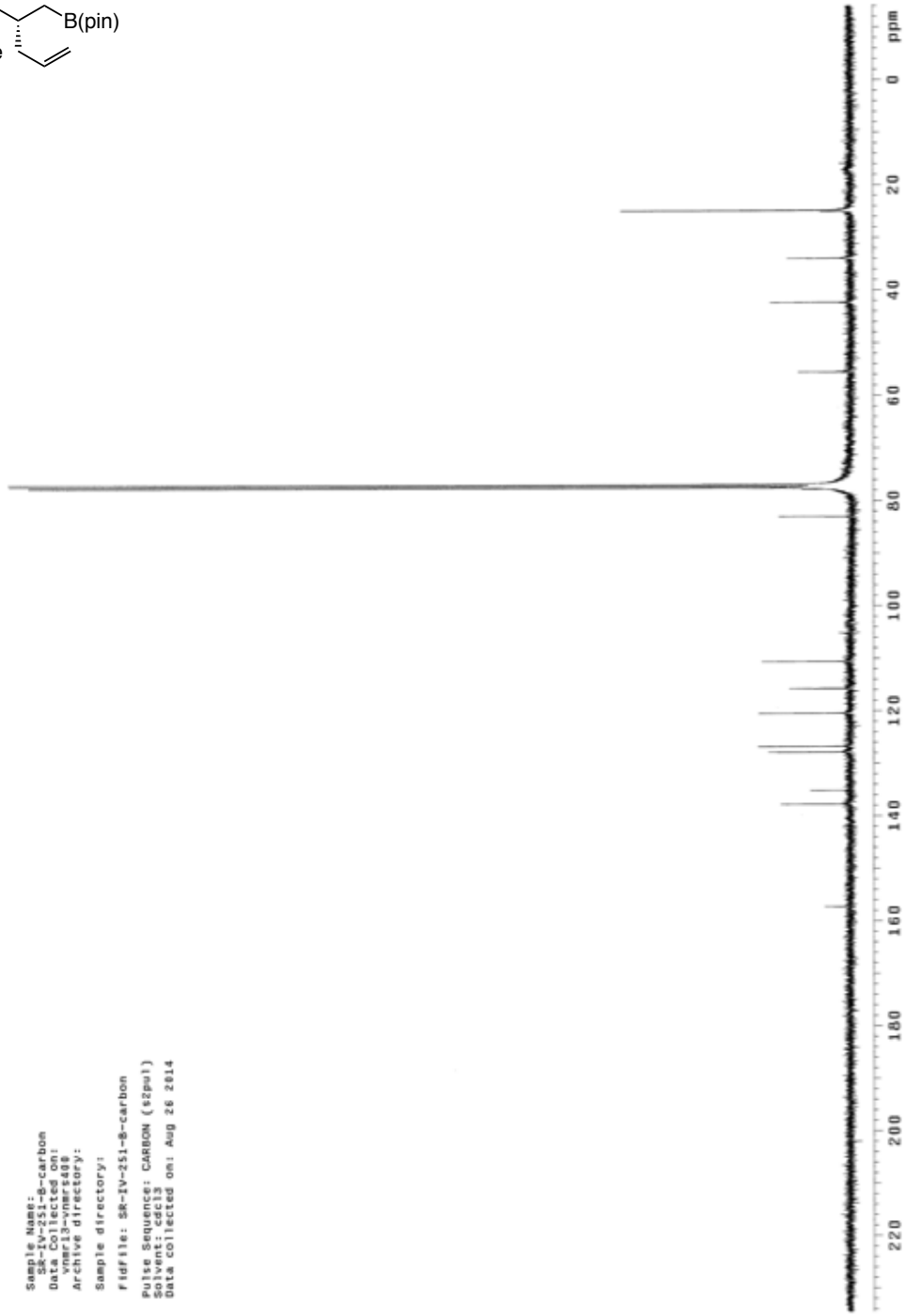
Sample Name:
SR-IV-251-B-carbon
Data Collected on:
vnmr13-vnmrs400
Archive directory:
Sample directory:
Fidfile: SR-IV-251-B-carbon
Pulse Sequence: CARBON (s2pul)
Solvent: cdcl3
Data collected on: Aug 26 2014
ppm
220
200
180
160
140
120
100
80
60
40
20
0

B(pin)
CF3

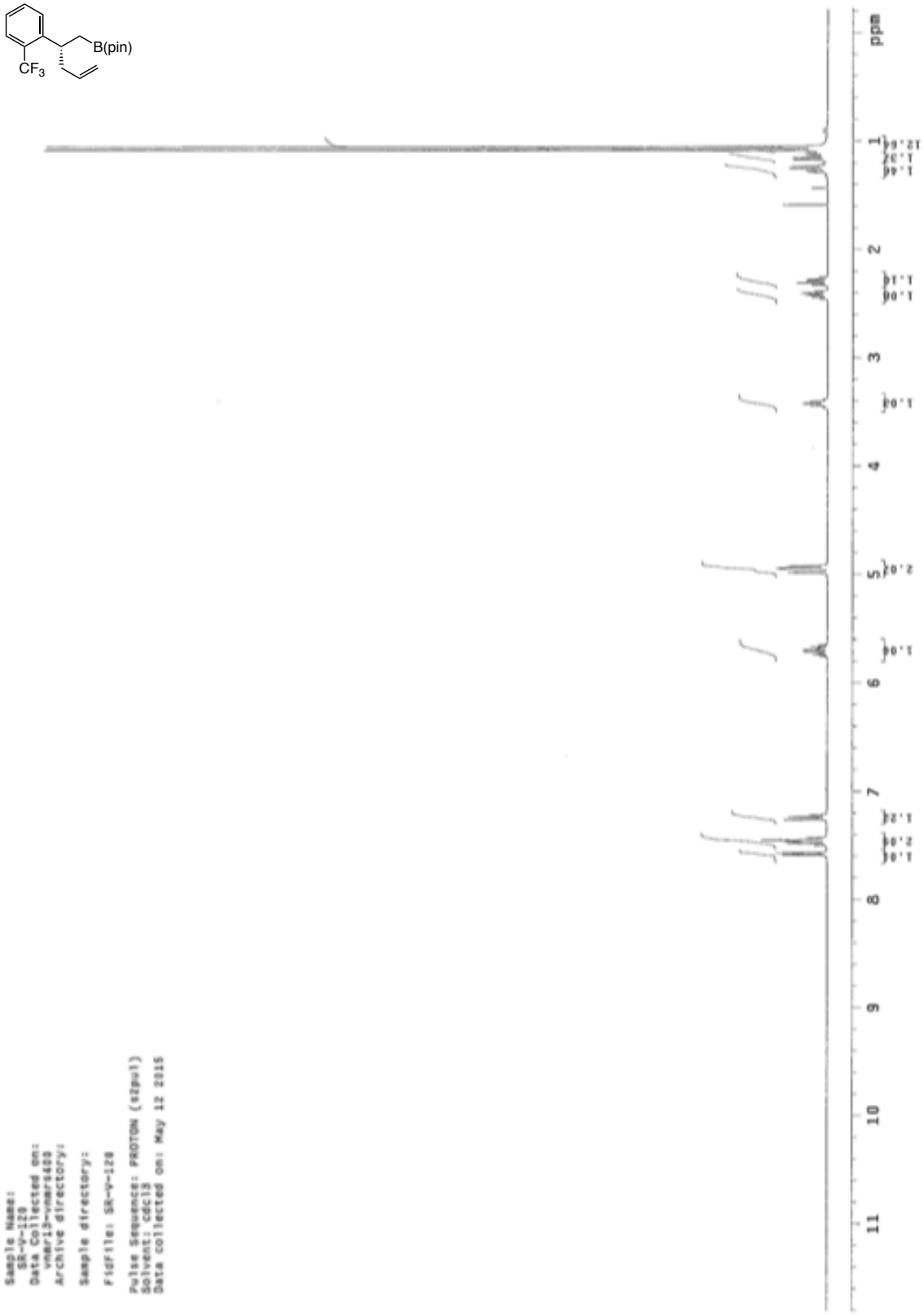
Sample Name:
SR-V-128
Data Collected on:
vmar15-vmars489
Archive directory:
Sample directory:
Fidfile: SR-V-128
Pulse Sequence: PROTON (t2pul)
Solvent: CdCl3
Data collected on: May 12 2015
ppm
12.64
1.34
1.46
1.14
1.06
1.04
2.02
1.04
1.24
2.04
1.04

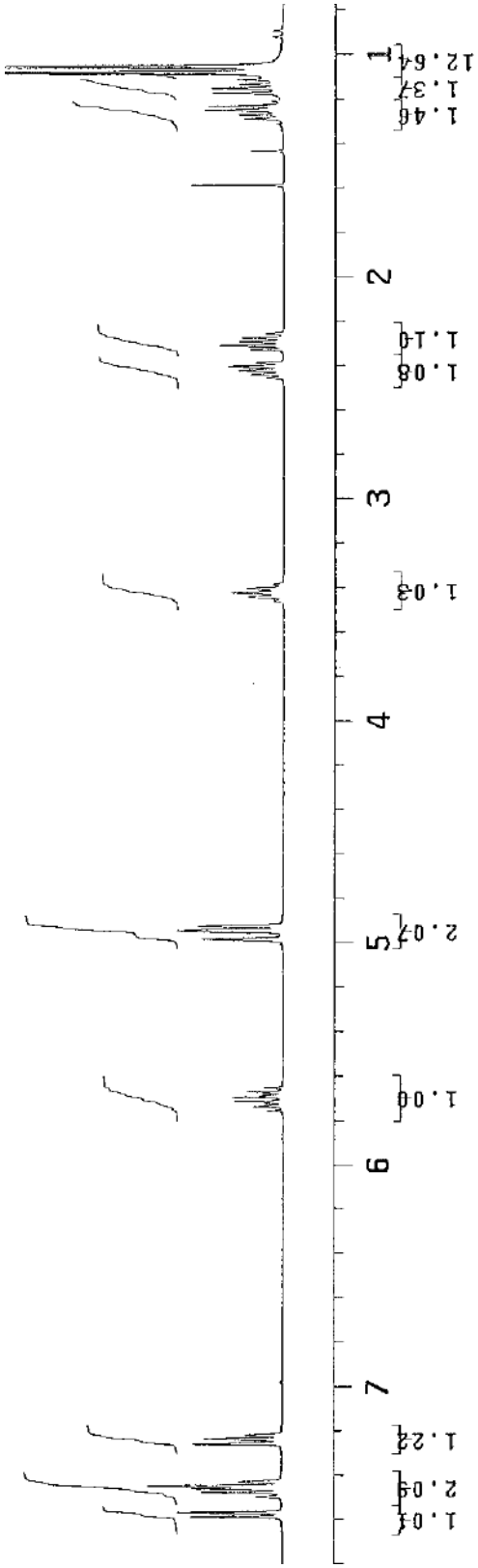
12.64
1.37
1.46
1.10
1.08
1.03
2.07
1.00
1.22
2.09
1.01
1
2
3
4
5
6
7

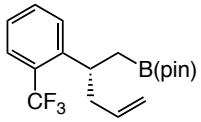
B(pin)
CF3

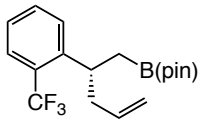
B(pin)
CF3

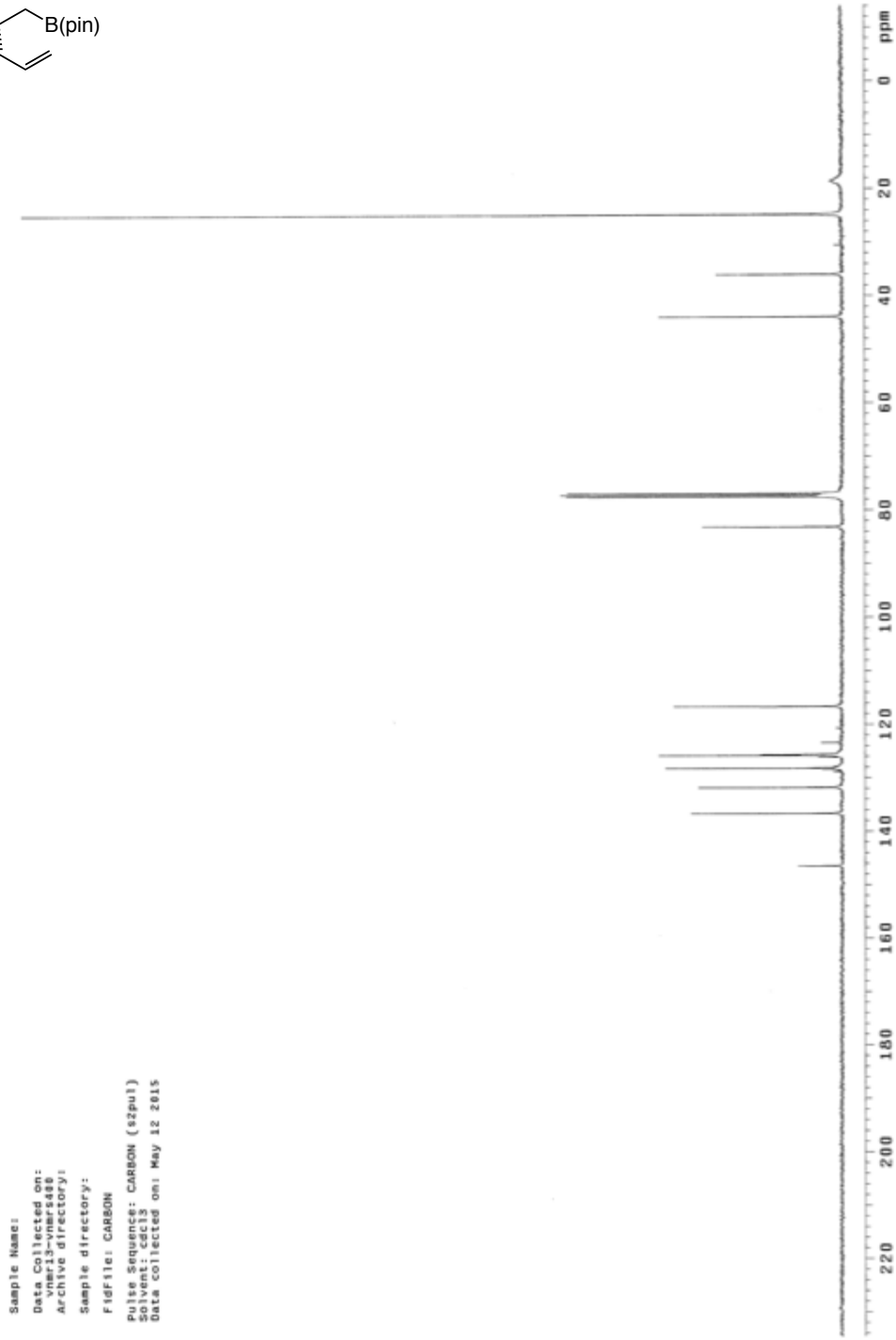
Sample Name:
Data Collected on:
vnmr13-vnmrs400
Archive directory:
Sample directory:
FidFile: CARBON
Pulse Sequence: CARBON (s2pul)
Solvent: cdcl3
Data collected on: May 12 2015
ppm
0
20
40
60
80
100
120
140
160
180
200
220

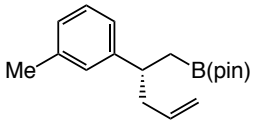
Me
B(pin)

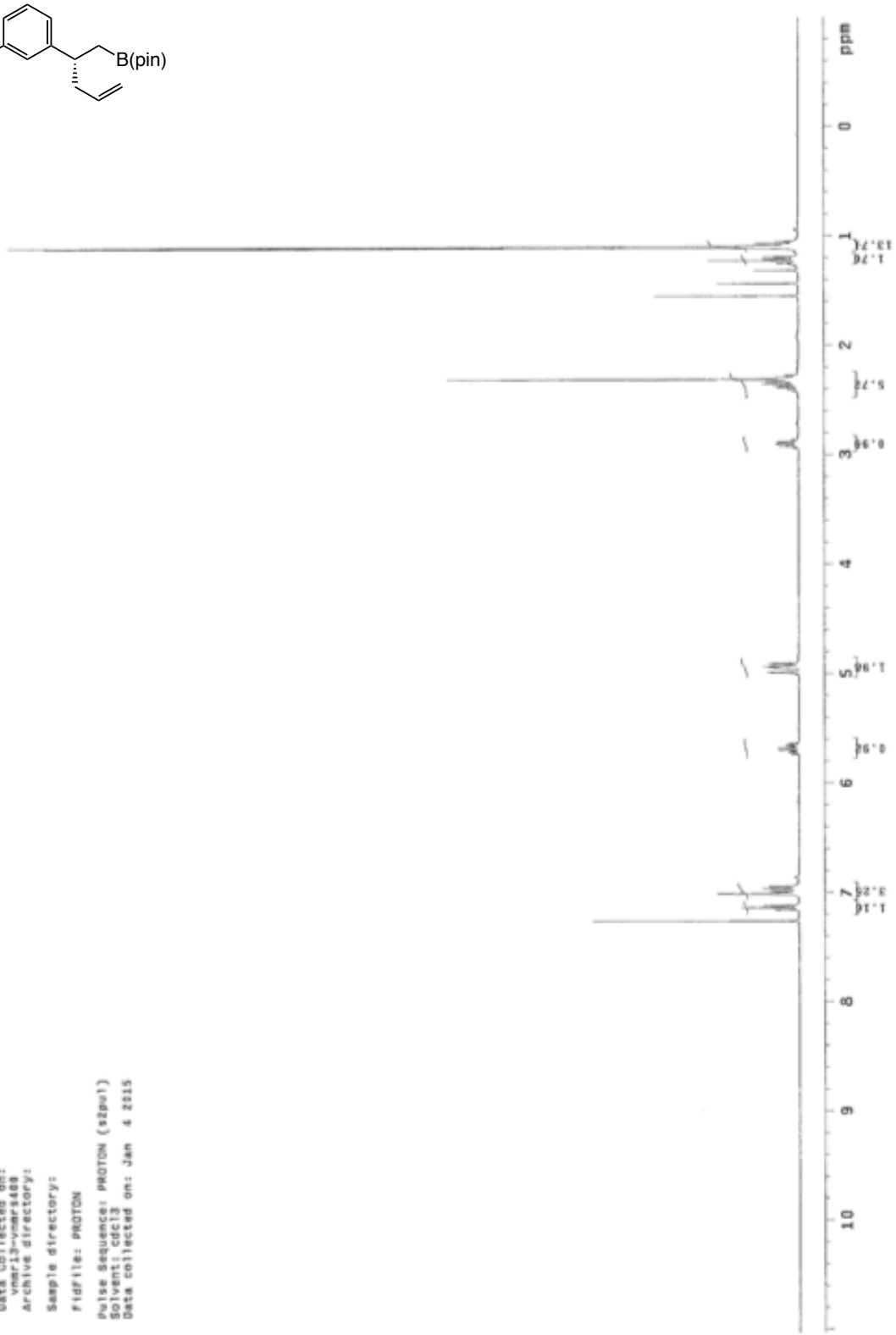
Sample Name:
SR-V-33
Data Collected on:
vnmrj3-vnmrs400
Archive directory:
Sample directory:
Fidfile: PROTON
Pulse Sequence: PROTON (s2pul)
Solvent: cdcl3
Data collected on: Jan 4 2015
ppm
13.74
1.74
5.74
0.94
1.94
0.94
3.26
1.14

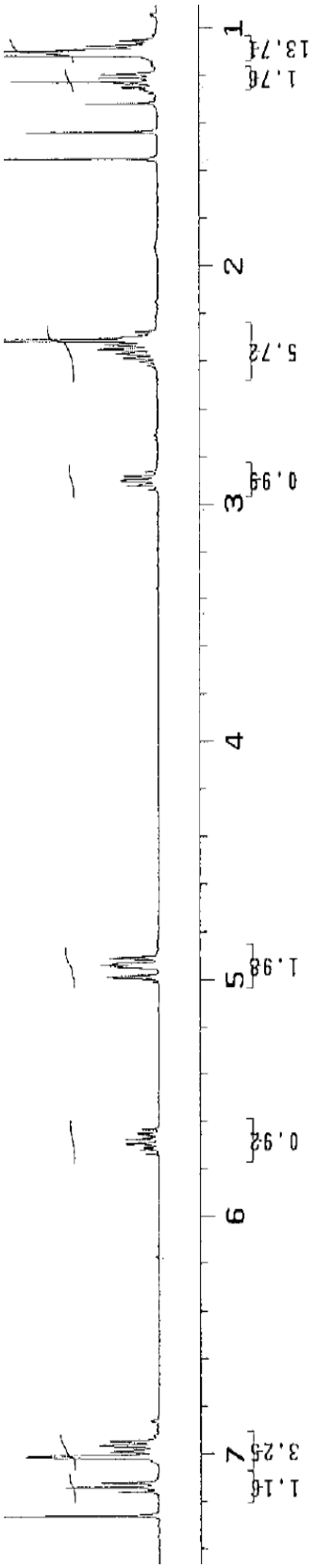
13.74
1.76
5.72
0.99
1.98
0.92
3.25
1.16
1
2
3
4
5
6
7

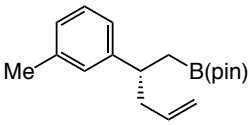
Me
B(pin)

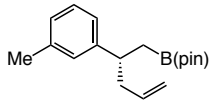

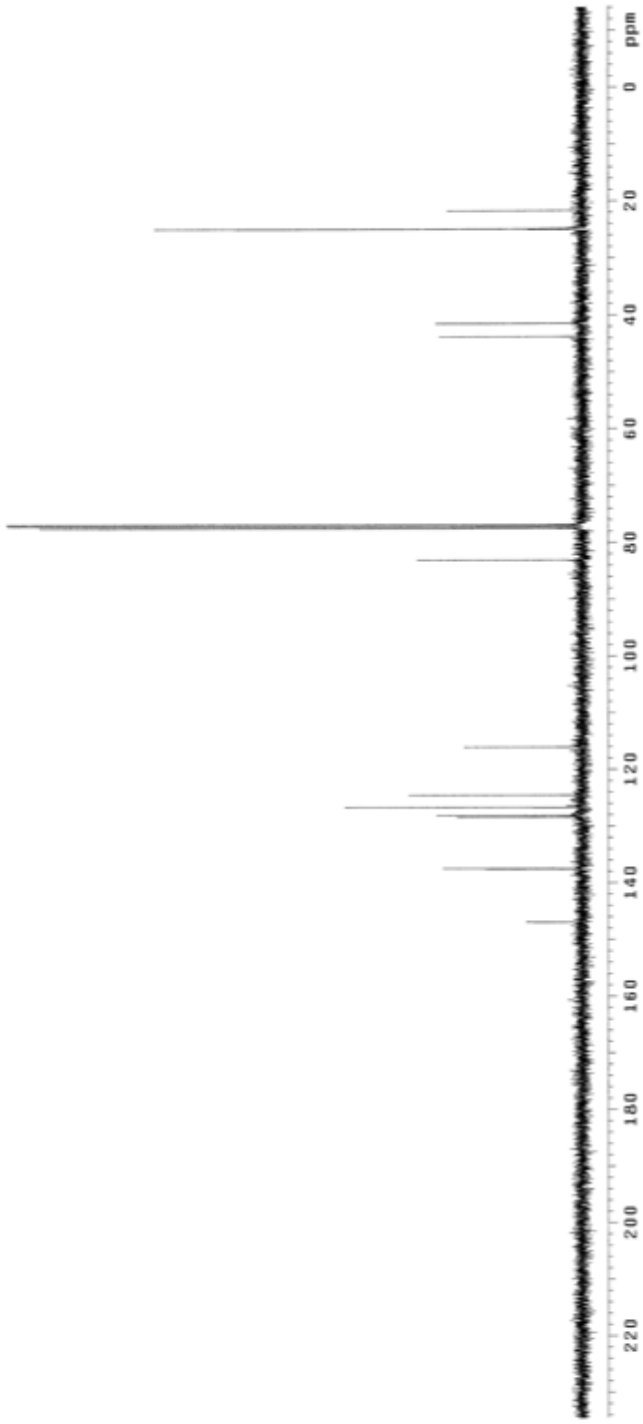

Sample Name:
SR-V-33-carbon
Data Collected on:
vmar13-vmar1400
Archive directory:

Sample directory:

Fidfile: CARBON

Pulse Sequence: CARBON (s2pul)
Solvent: cdcl3
Data collected on: Dec 23 2014

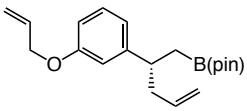
O
B(pin)

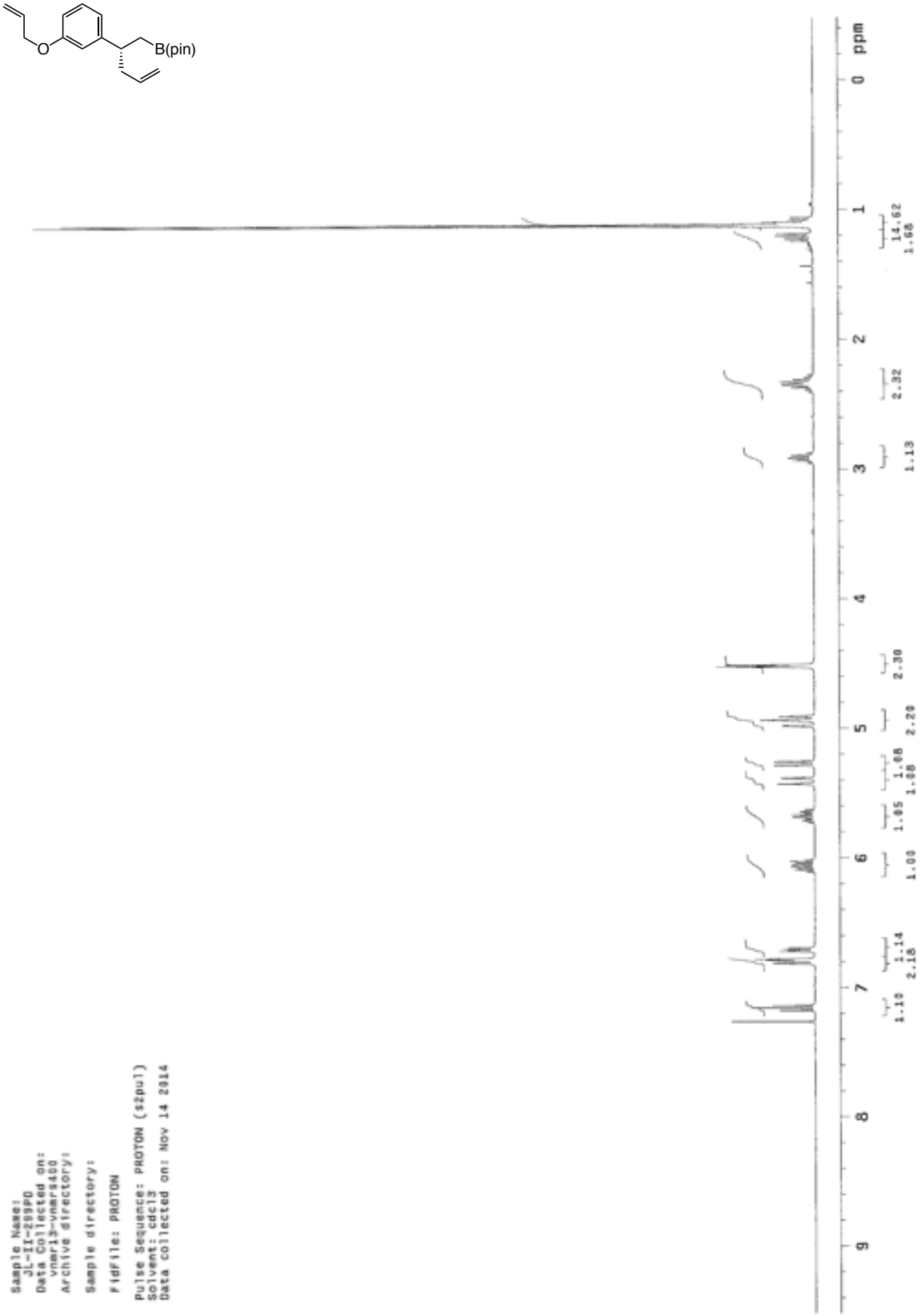
Sample Name:
JL-II-299PD
Data Collected on:
vnmr13-vnmrs400
Archive directory:
Sample directory:
FidFile: PROTON
Pulse Sequence: PROTON (s2pul)
Solvent: cdcl3
Data collected on: Nov 14 2014
ppm
9
8
7
6
5
4
3
2
1
0
1.10
1.14
2.18
1.00
1.05
1.08
1.08
2.20
2.30
1.13
2.32
14.62
1.68

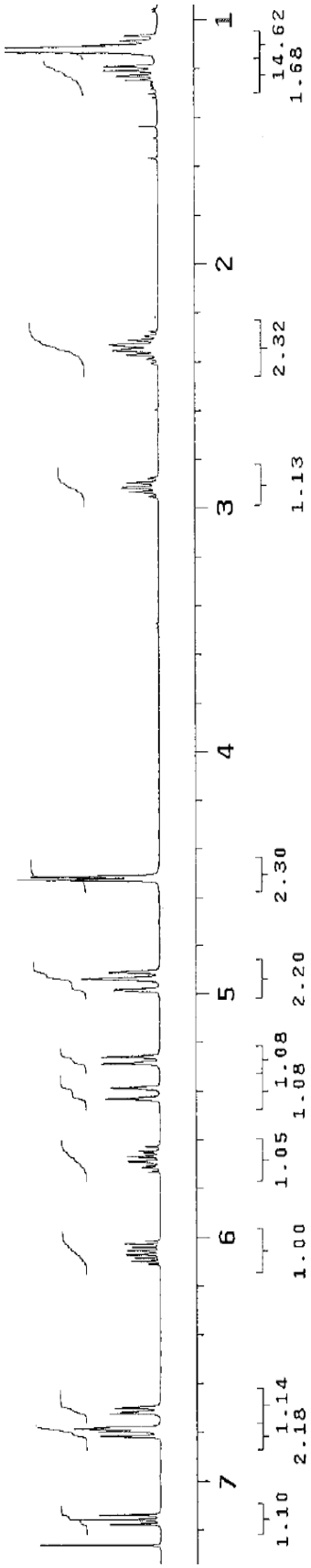
1.10
1.14
2.18
1.00
1.05
1.08
1.08
2.20
2.30
1.13
2.32
14.62
1.68
7
6
5
4
3
2
1

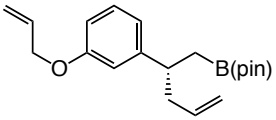
O
B(pin)

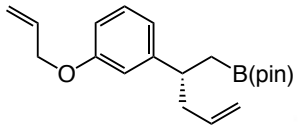
O
B(pin)

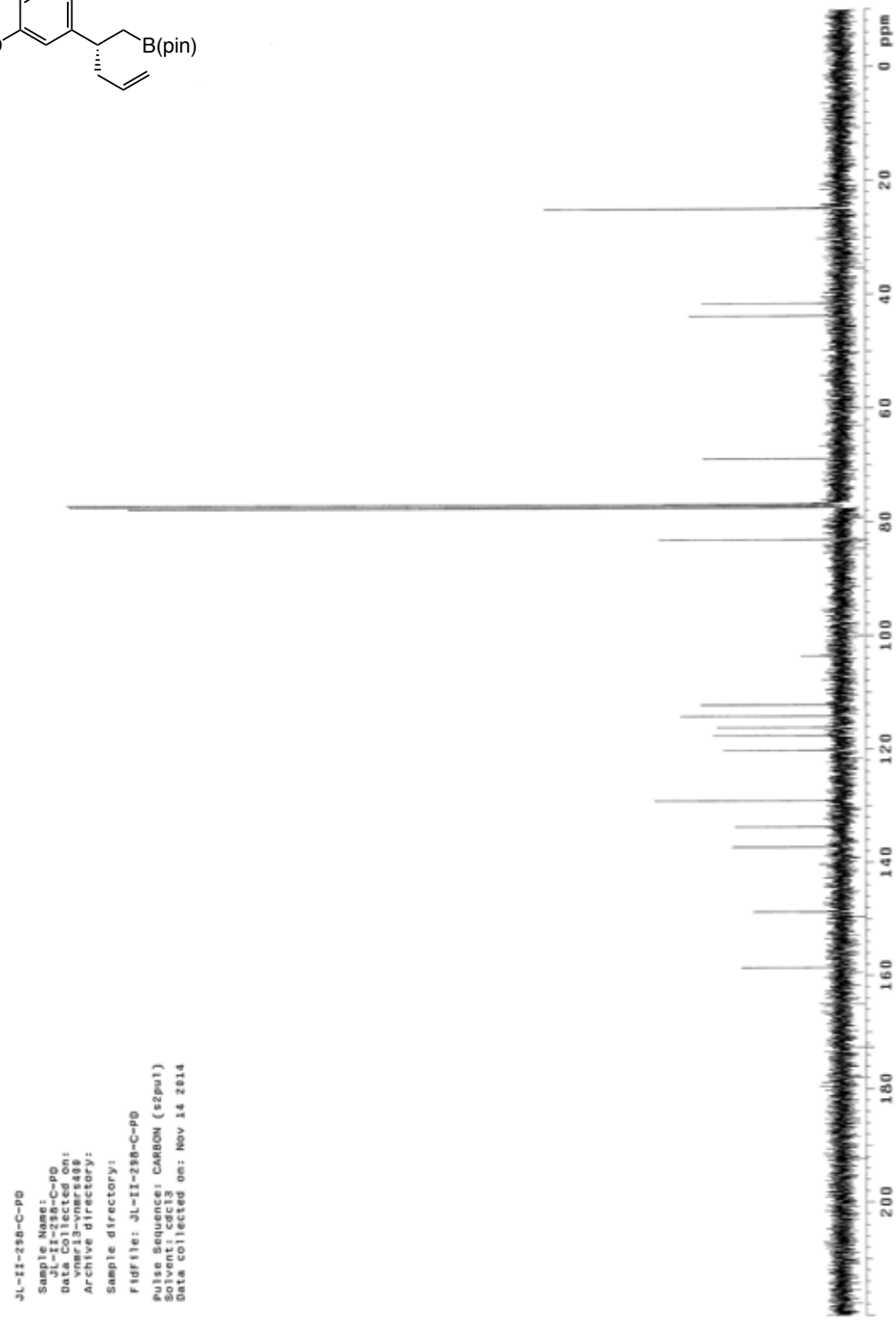
JL-II-298-C-PD
Sample Name:
JL-II-298-C-PD
Data Collected on:
vnmrs13-vnmrs400
Archive directory:
Sample directory:
Fidfile: JL-II-298-C-PD
Pulse Sequence: CARBON (s2pul)
Solvent: cdcl3
Data collected on: Nov 14 2014
0 ppm
20
40
60
80
100
120
140
160
180
200

t-BuO2C
B(pin)

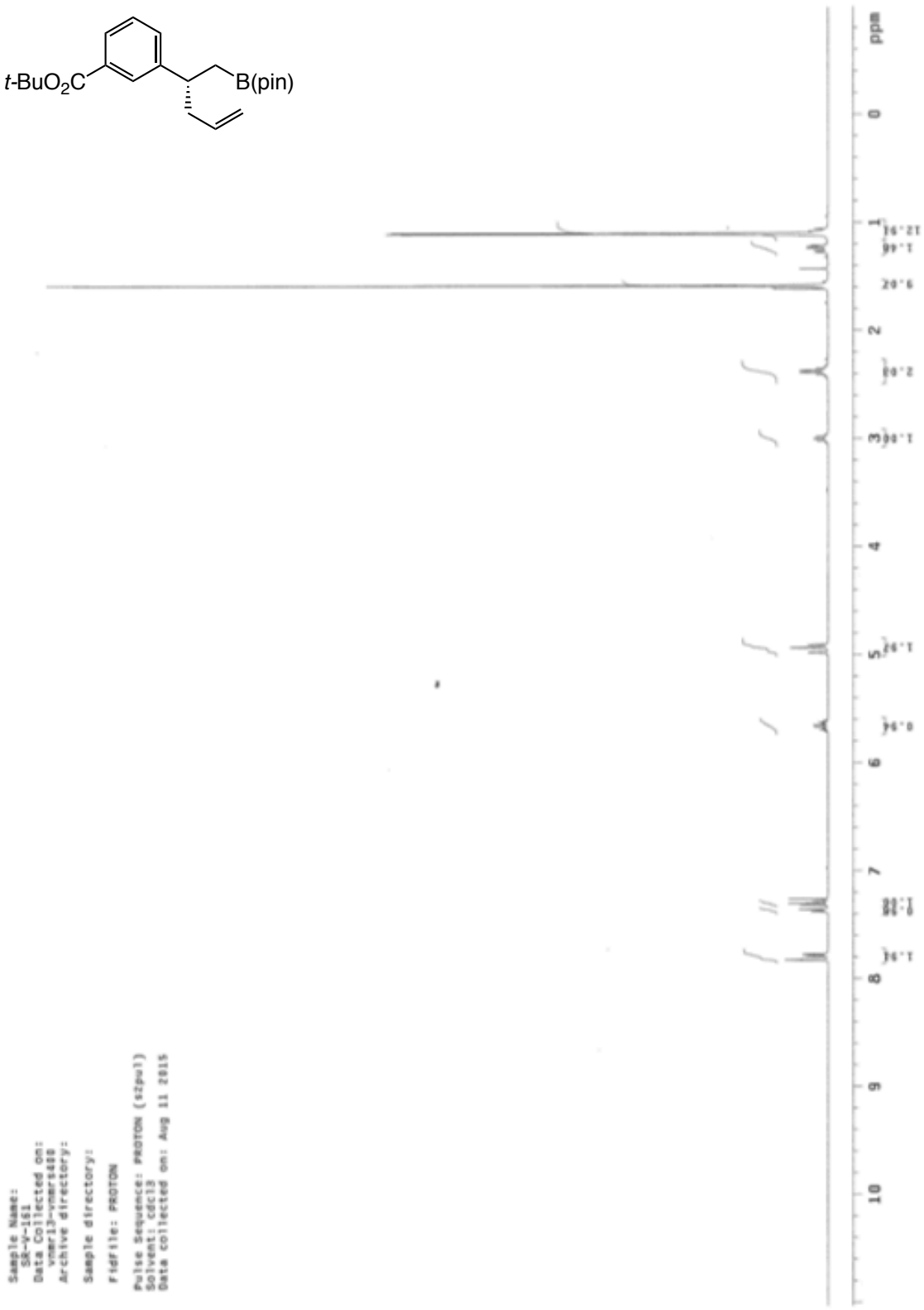
Sample Name:
SR-V-161
Data Collected on:
vnmr13-vnmrs400
Archive directory:
Sample directory:
FidFile: PROTON
Pulse Sequence: PROTON (s2pul)
Solvent: cdcl3
Data collected on: Aug 11 2015
ppm

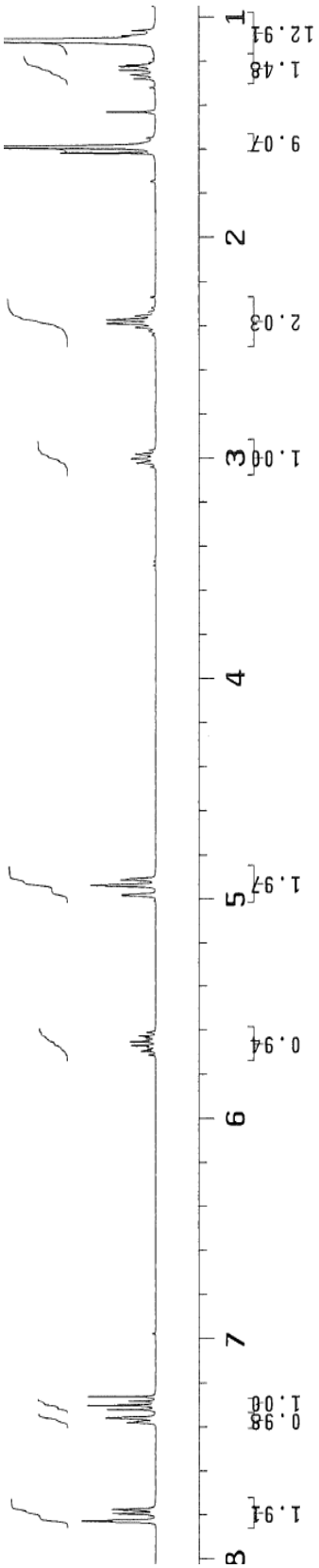
12.91
1.48
9.07
2.03
1.00
1.97
0.94
1.00
0.98
1.91
1
2
3
4
5
6
7
8

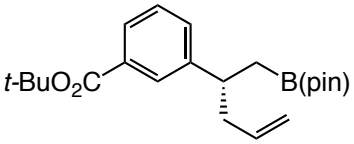
t-BuO2C
B(pin)

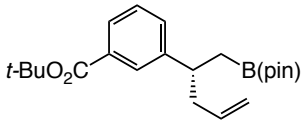
t-BuO2C
B(pin)

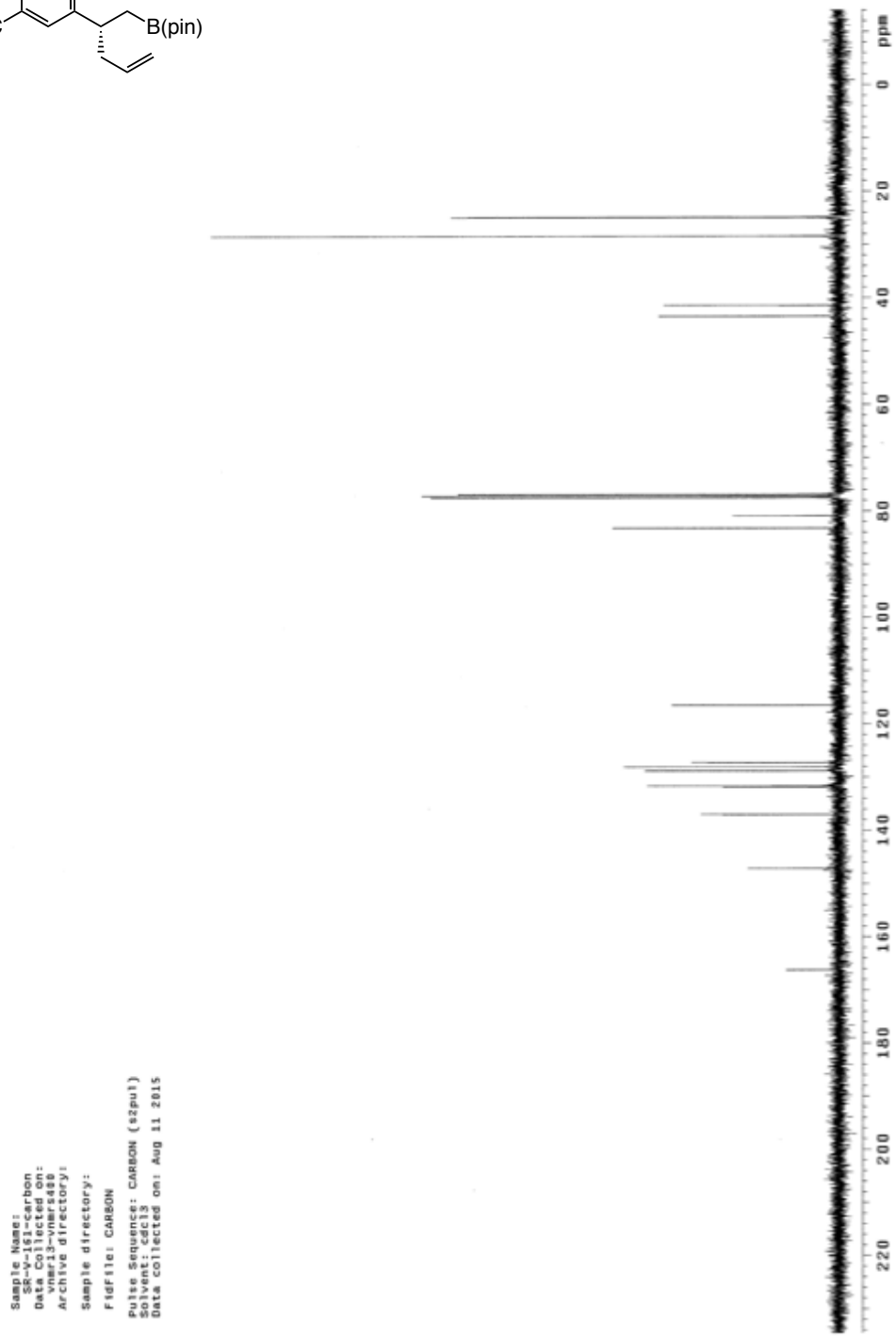
Sample Name:
SR-V-151-carbon
Data Collected on:
Pulse Sequence: CARBON (s2pul)
Solvent: cdcl3
Data collected on: Aug 11 2015
ppm
0
20
40
60
80
100
120
140
160
180
200
220

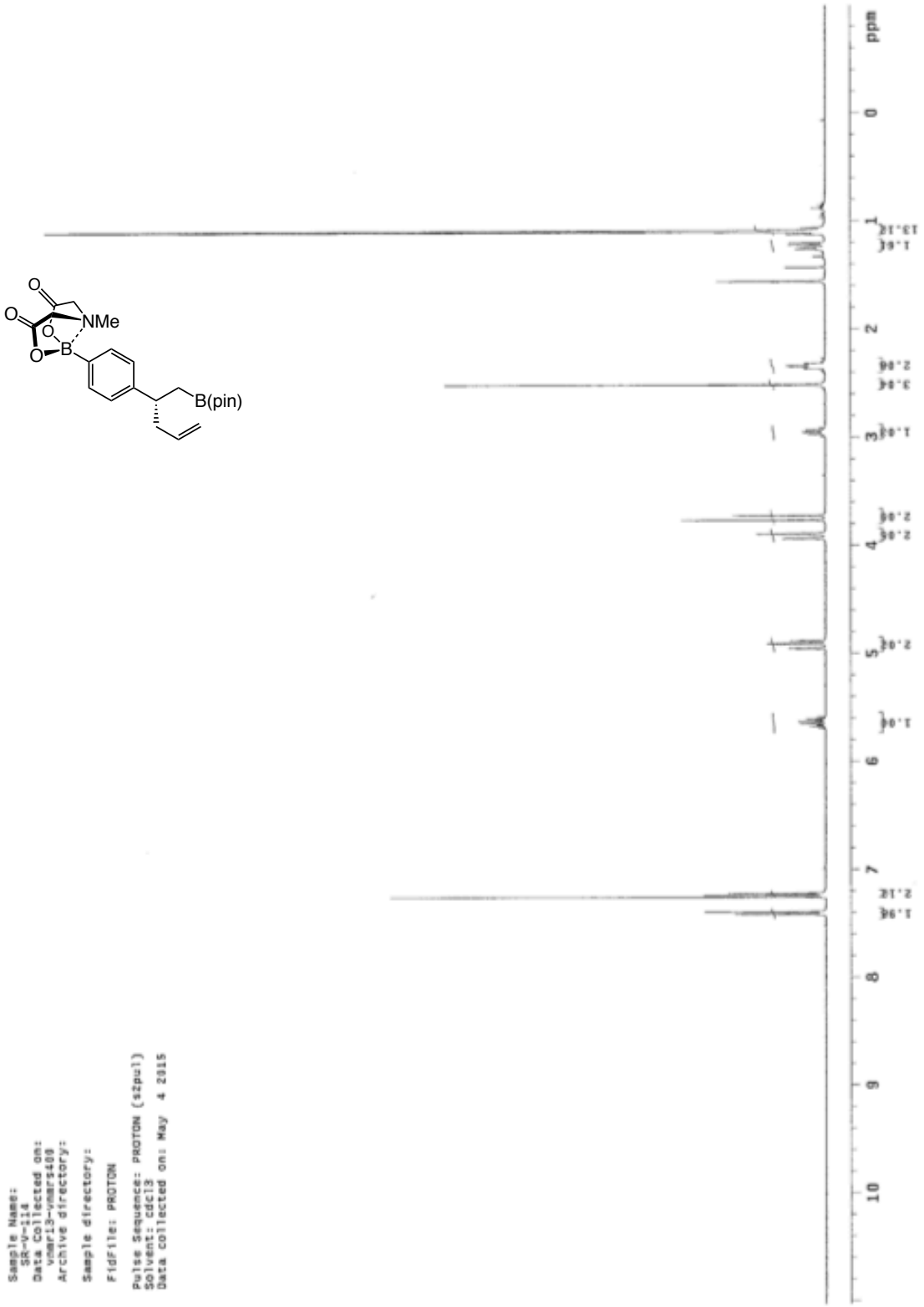
O
O
NMe
O
B
O
B(pin)
Sample Name:
SR-V-114
Data Collected on:
vmqr13-vmqrs400
Archive directory:
Sample directory:
FidFile: PROTON
Pulse Sequence: PROTON (s2pul)
Solvent: cdcl3
Data collected on: May 4 2015
ppm
0
1
2
3
4
5
6
7
8
9
10
13.12
1.64
2.06
3.84
1.00
2.06
2.06
2.06
1.00
2.12
1.94

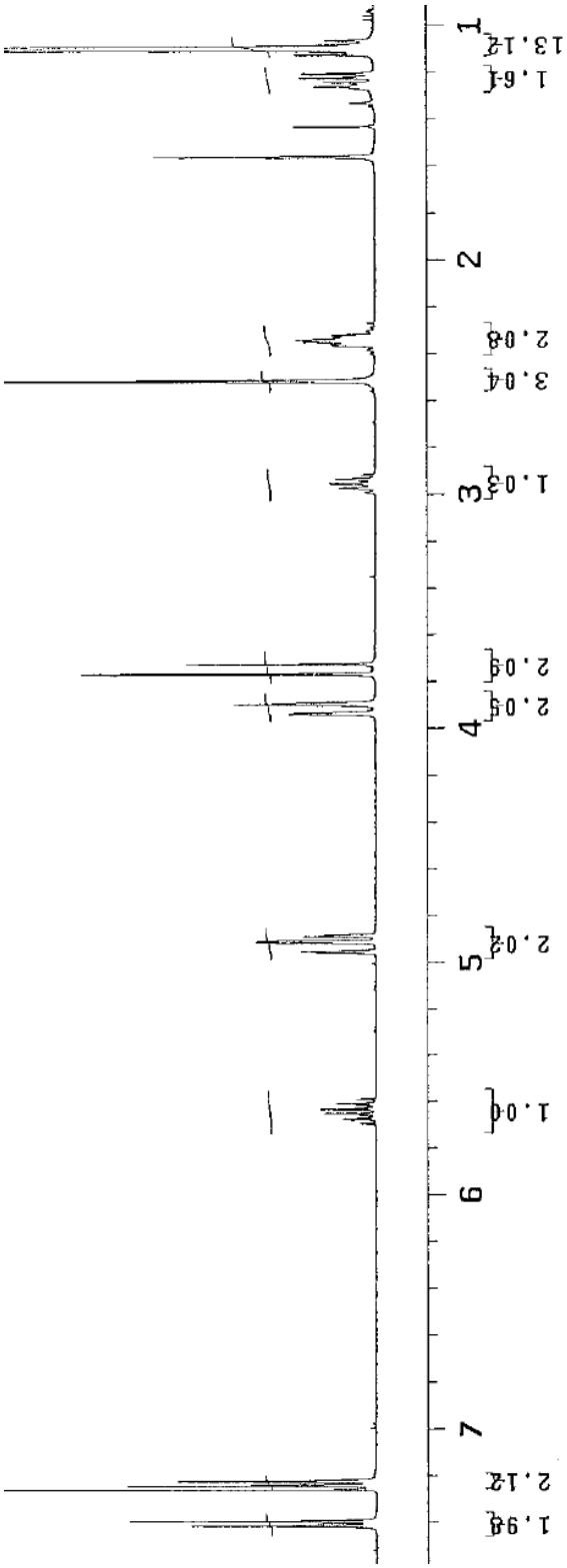
1.94
2.12
1.00
2.02
2.05
2.05
1.03
3.04
2.08
1.61
13.12
7
6
5
4
3
2
1

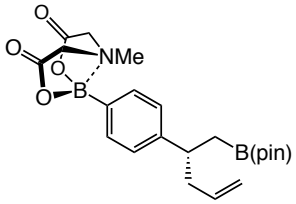
O
O
NMe
O
O
B
B(pin)

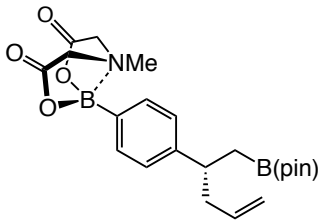
O
O
NMe
O
B
O
B(pin)

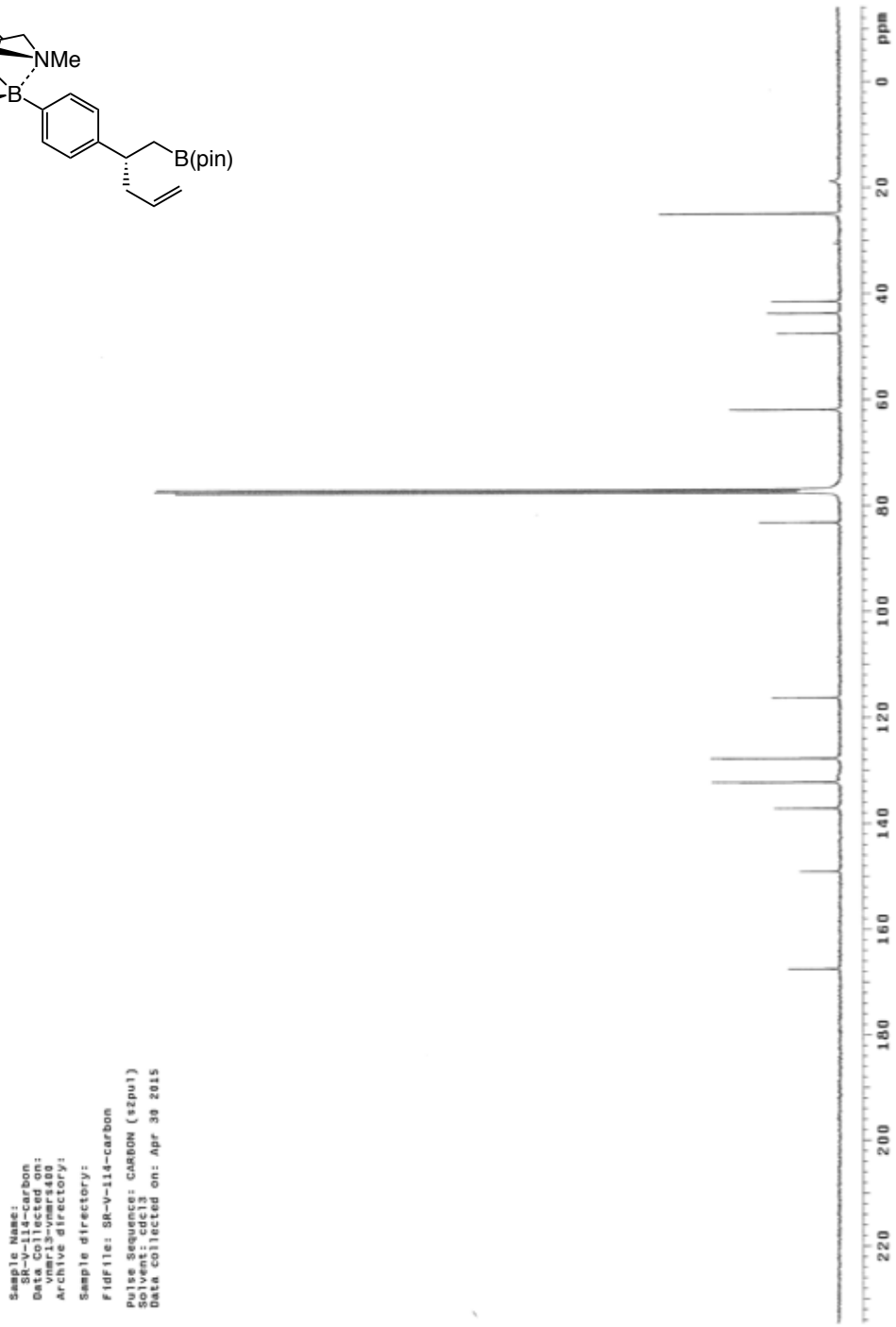
Sample Name:
SR-V-114-carbon
Data Collected on:
Varian 3Superb400
Archive directory:
Sample directory:
Fidfile: SR-V-114-carbon
Pulse Sequence: CARBON (s2pul)
Solvent: cdcl3
Data collected on: Apr 30 2015
ppm
0
20
40
60
80
100
120
140
160
180
200
220

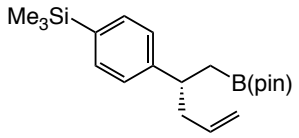
Me3Si
B(pin)

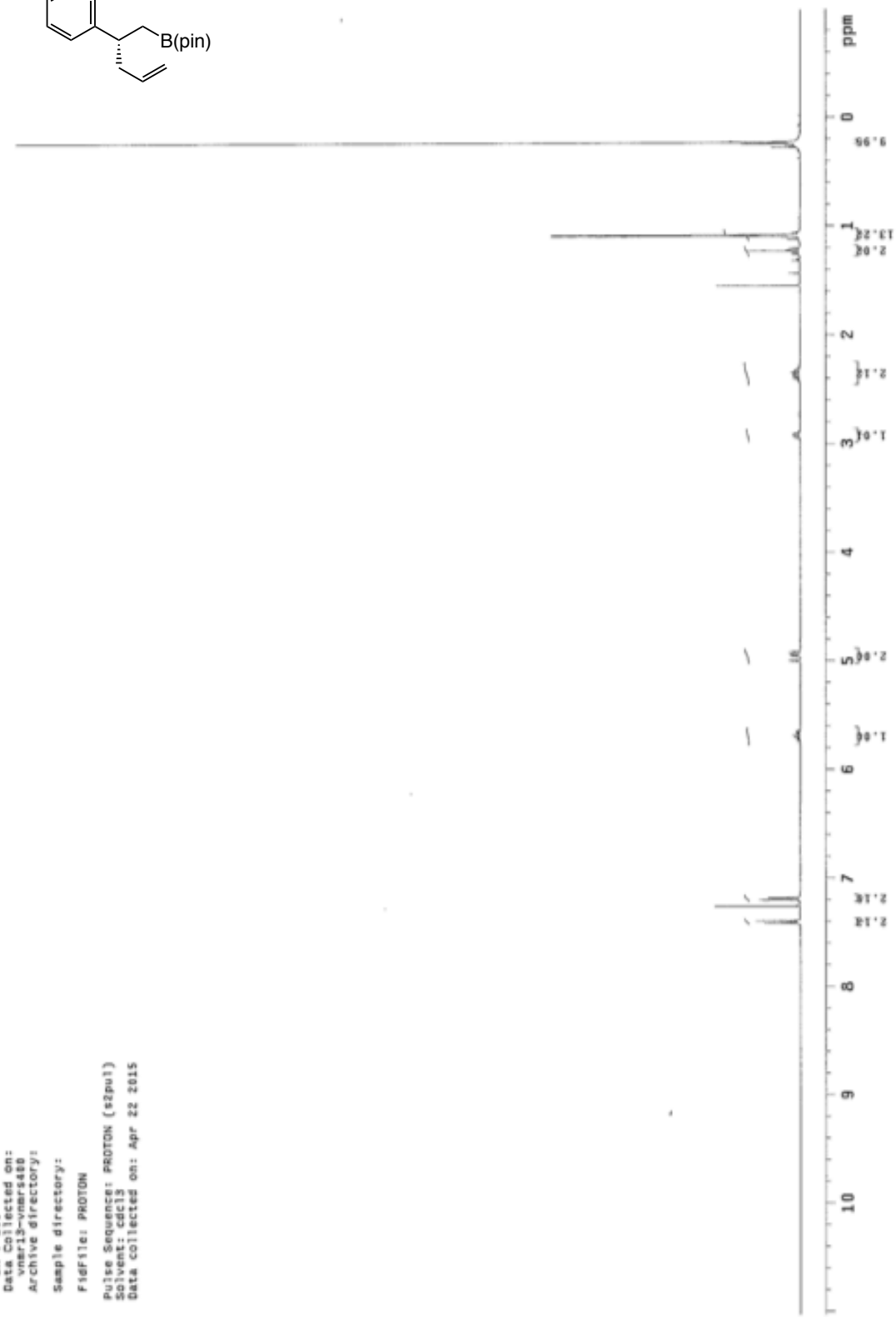
Sample Name:
SR-V-189
Data Collected on:
vnmr13-vnmrs400
Archive directory:
Sample directory:
FidFile: PROTON
Pulse Sequence: PROTON (s2pul)
Solvent: cdcl3
Data collected on: Apr 22 2015
ppm
0
1
2
3
4
5
6
7
8
9
10
9.95
13.26
2.06
2.12
1.06
2.06
1.06
2.16
2.12

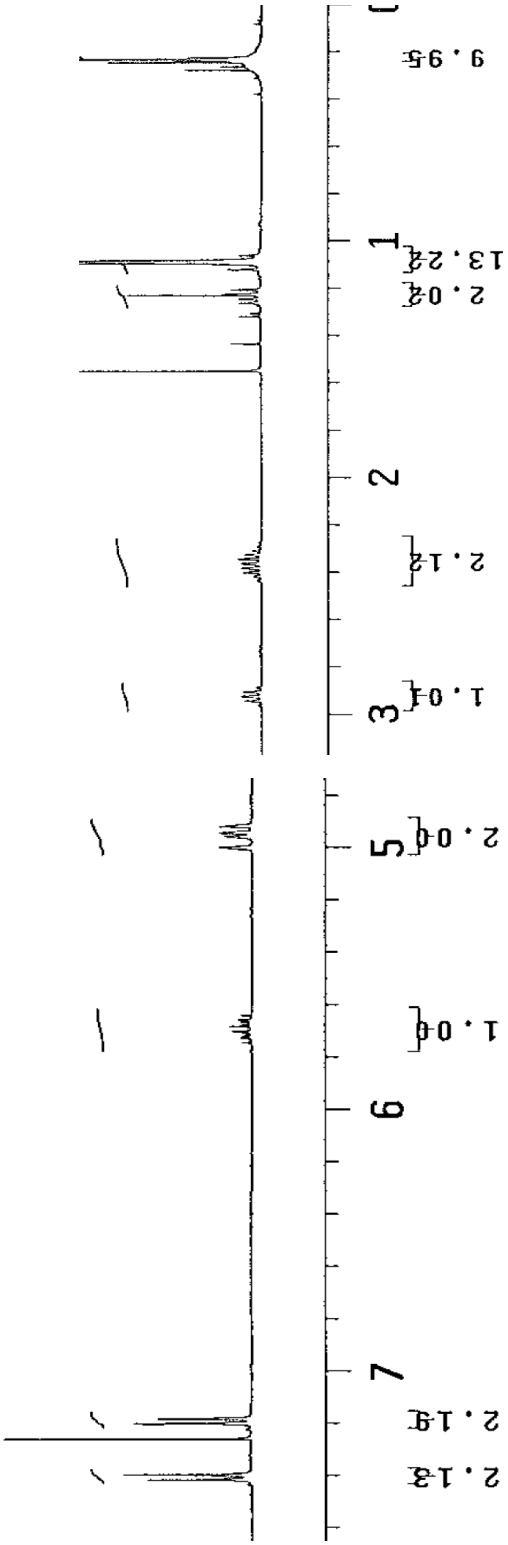
9.95
13.24
2.04
2.12
1.01
2.00
1.00
2.13
2.18
7
6
5
3
2
1

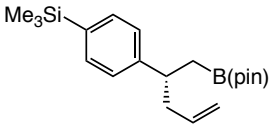
Me3Si
B(pin)

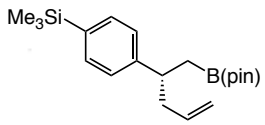
Me3Si
B(pin)

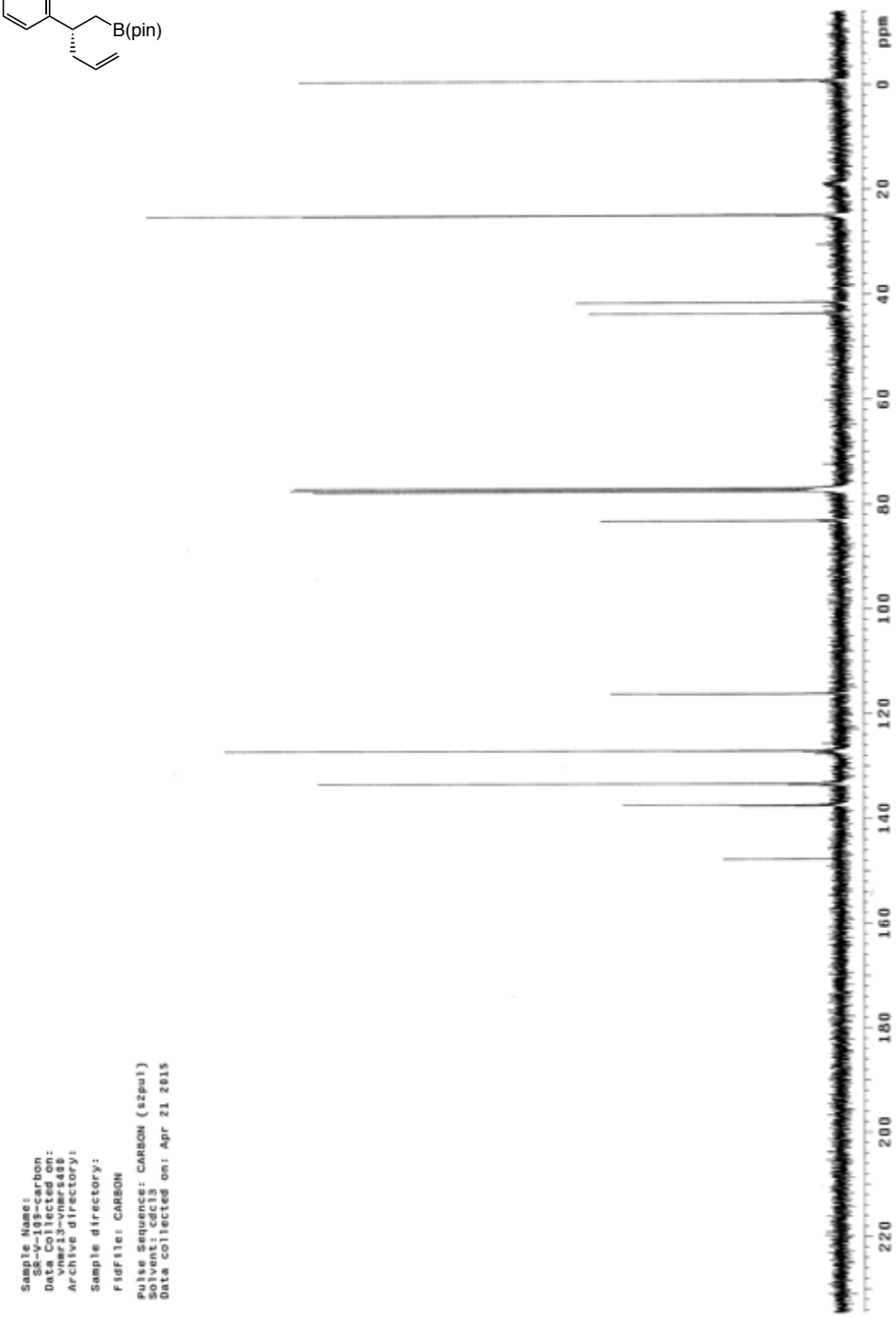
Sample Name:
SA-V-189-carbon
Data Collected on:
vnmr13-vnmrs400
Archive directory:
Sample directory:
FidFile: CARBON
Pulse Sequence: CARBON (s2pul)
Solvent: cdcl3
Data collected on: Apr 21 2015
ppm
0
20
40
60
80
100
120
140
160
180
200
220

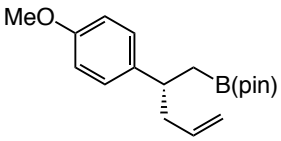
MeO
B(pin)

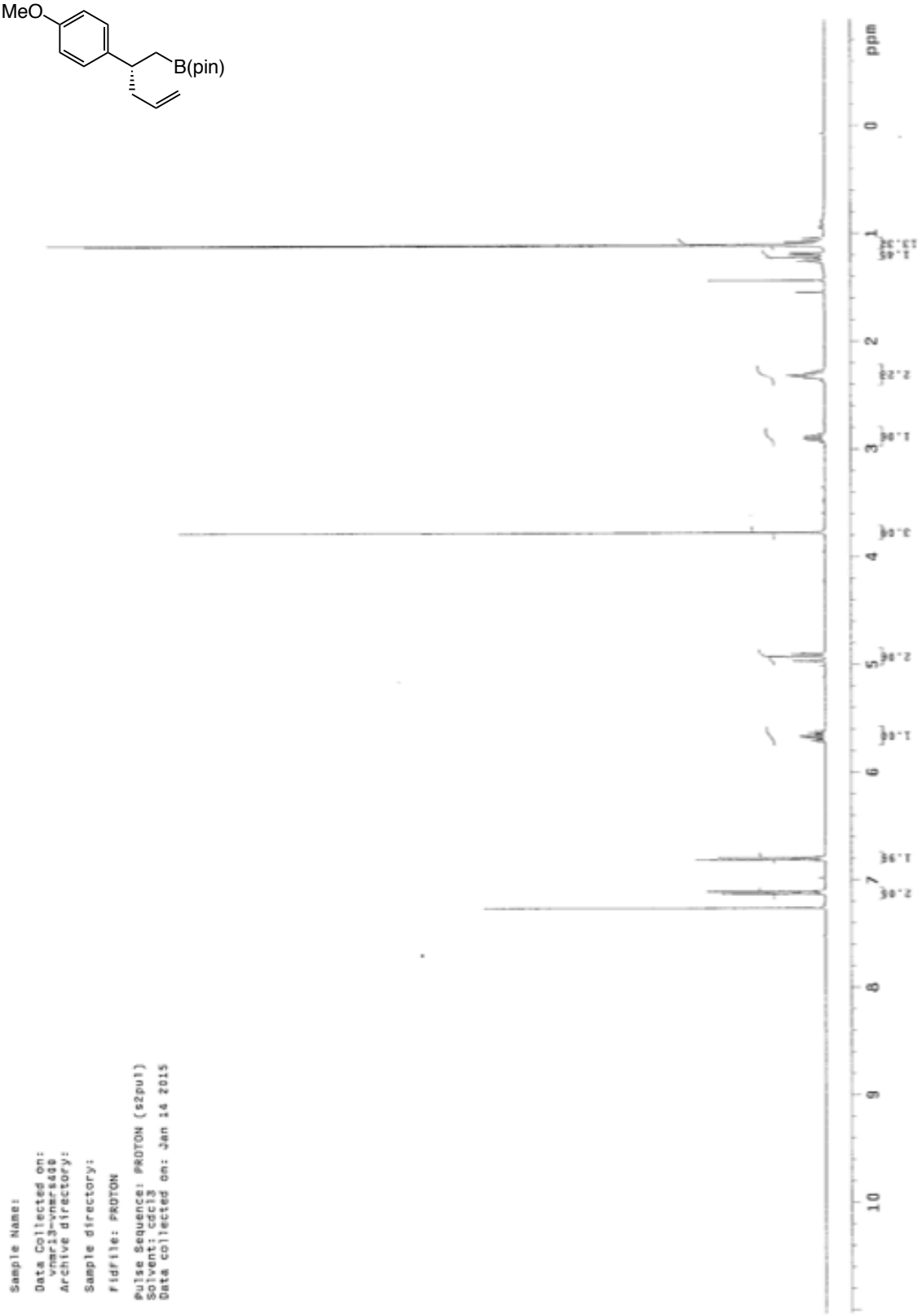
Sample Name:
Data Collected on:
vnmrs13-vnmrs400
Archive directory:
Sample directory:
Fidfile: PROTON
Pulse Sequence: PROTON (s2pul)
Solvent: cdcl3
Data collected on: Jan 14 2015
ppm
0
1
2
3
4
5
6
7
8
9
10

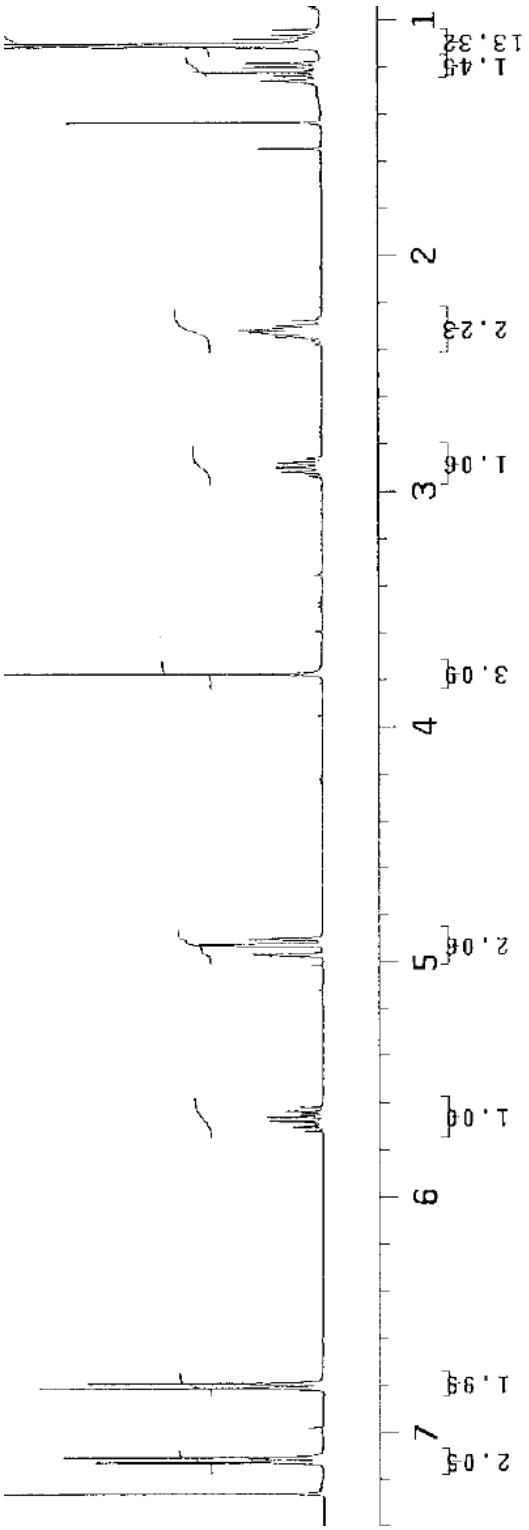
1.45
13.32
2.23
1.06
3.09
2.06
1.06
1.99
2.05
1
2
3
4
5
6
7

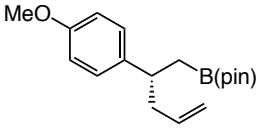
MeO
B(pin)

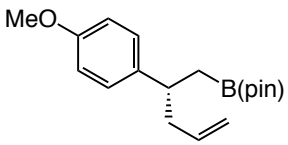
MeO
B(pin)

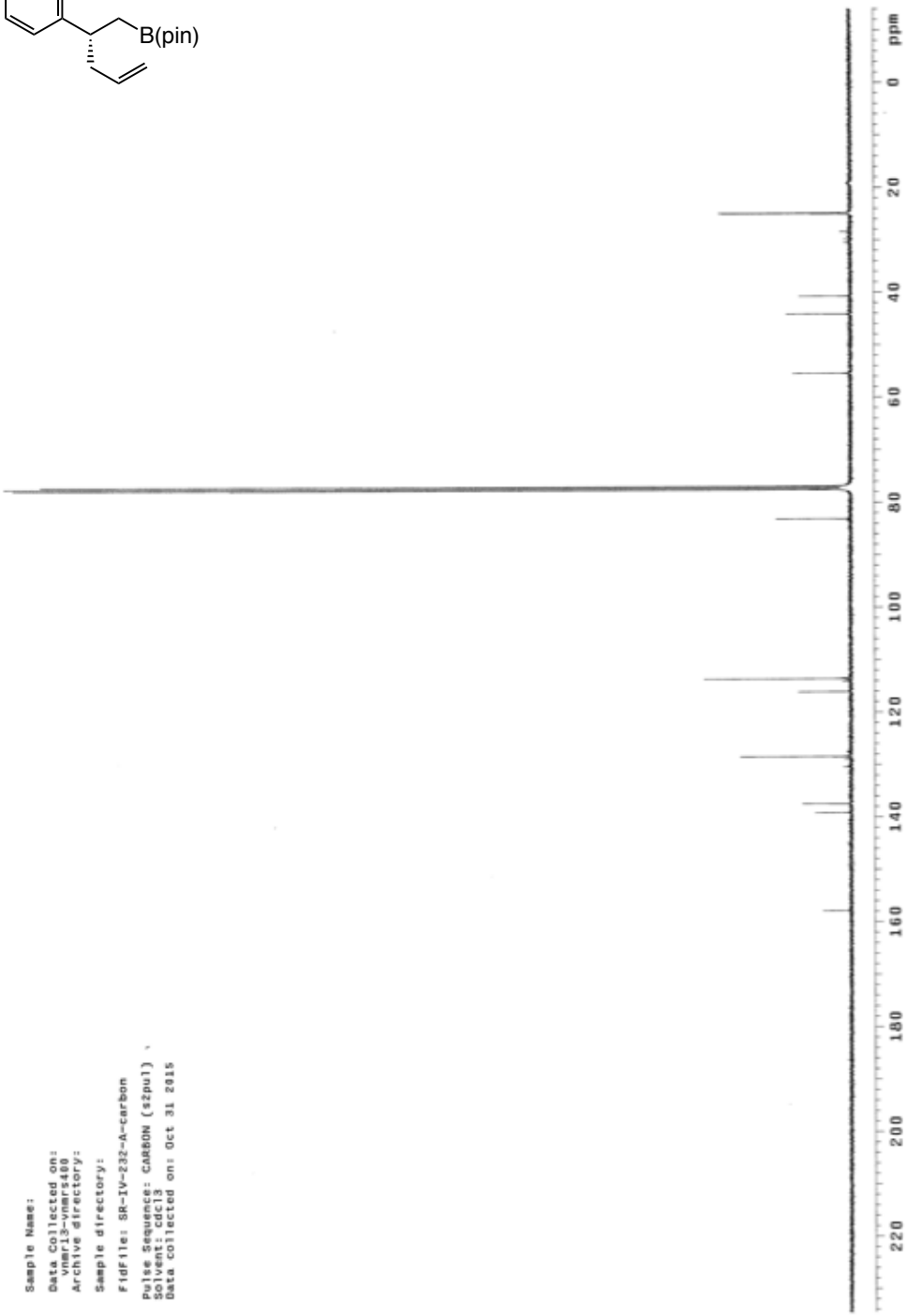
Sample Name:
Data Collected on:
vnmr13-vnmrs400
Archive directory:
Sample directory:
FidFile: SR-IV-232-A-carbon
Pulse Sequence: CARBON (s2pul)
Solvent: cdcl3
Data collected on: Oct 31 2015
ppm
220
200
180
160
140
120
100
80
60
40
20
0

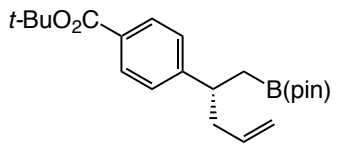
t-BuO2C
B(pin)

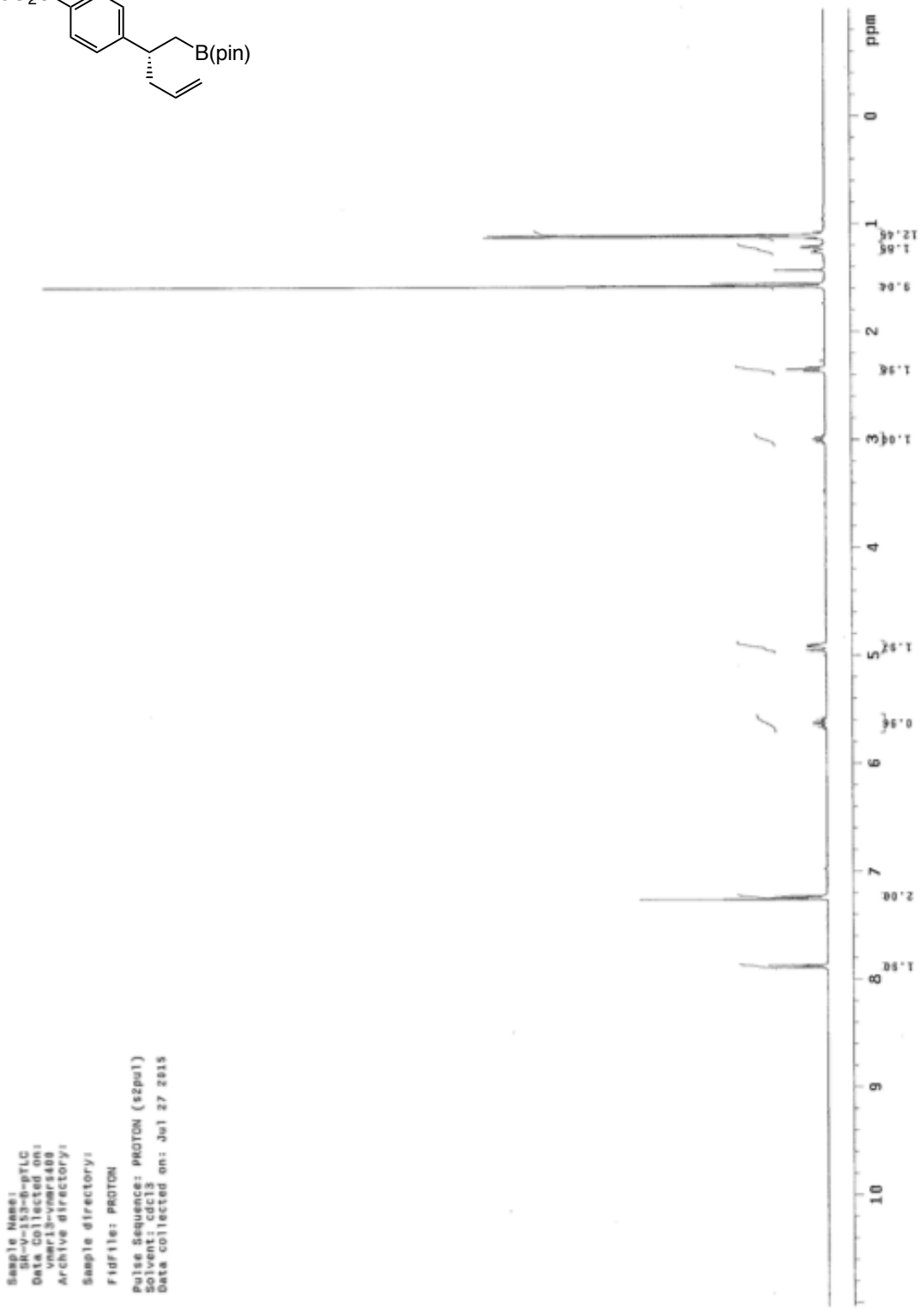
Sample Name:
SA-V-153-B-pTLC
Data collected on:
vmar13-vmars400
Archive directory:
Sample directory:
Fidfile: PROTON
Pulse Sequence: PROTON (s2pul)
Solvent: cdcl3
Data collected on: Jul 27 2015
ppm
12.65
1.85
9.04
1.96
1.00
1.92
0.96
2.08
1.98

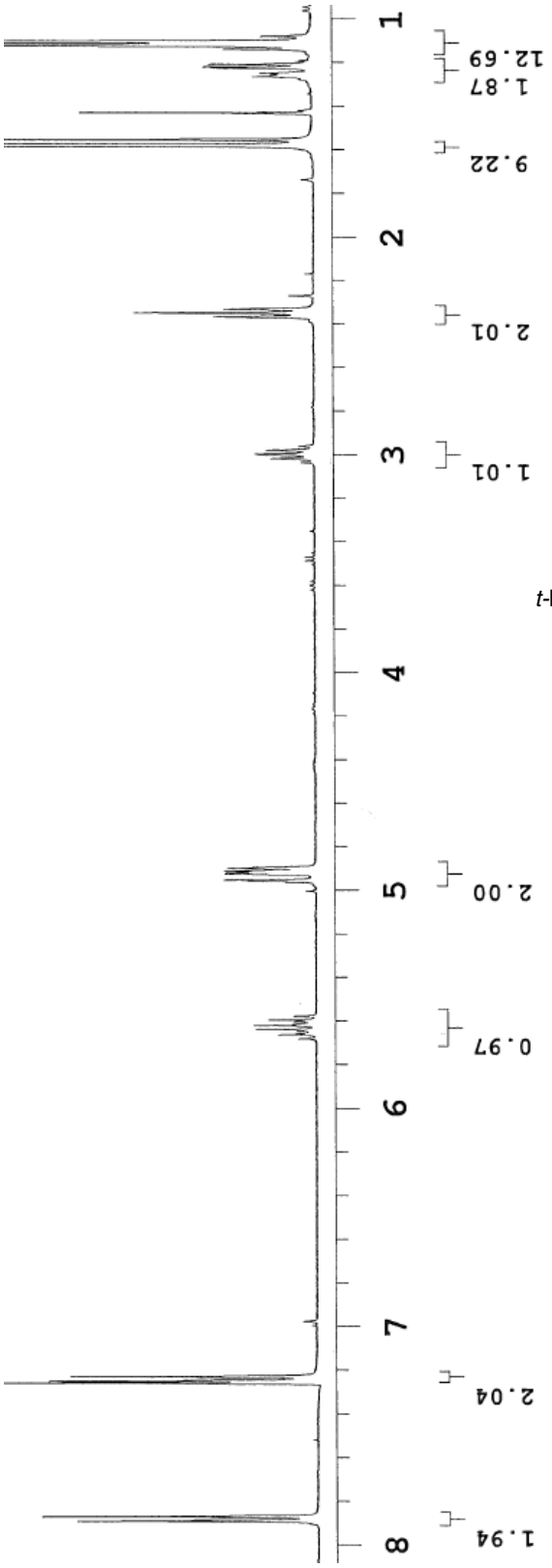
8
7
6
5
4
3
2
1
1.94
2.04
0.97
2.00
1.01
2.01
9.22
1.87
12.69

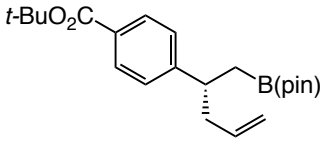
t-BuO2C
B(pin)

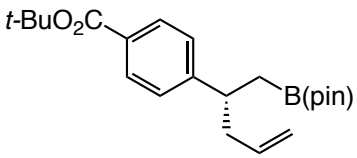
t-BuO2C
B(pin)

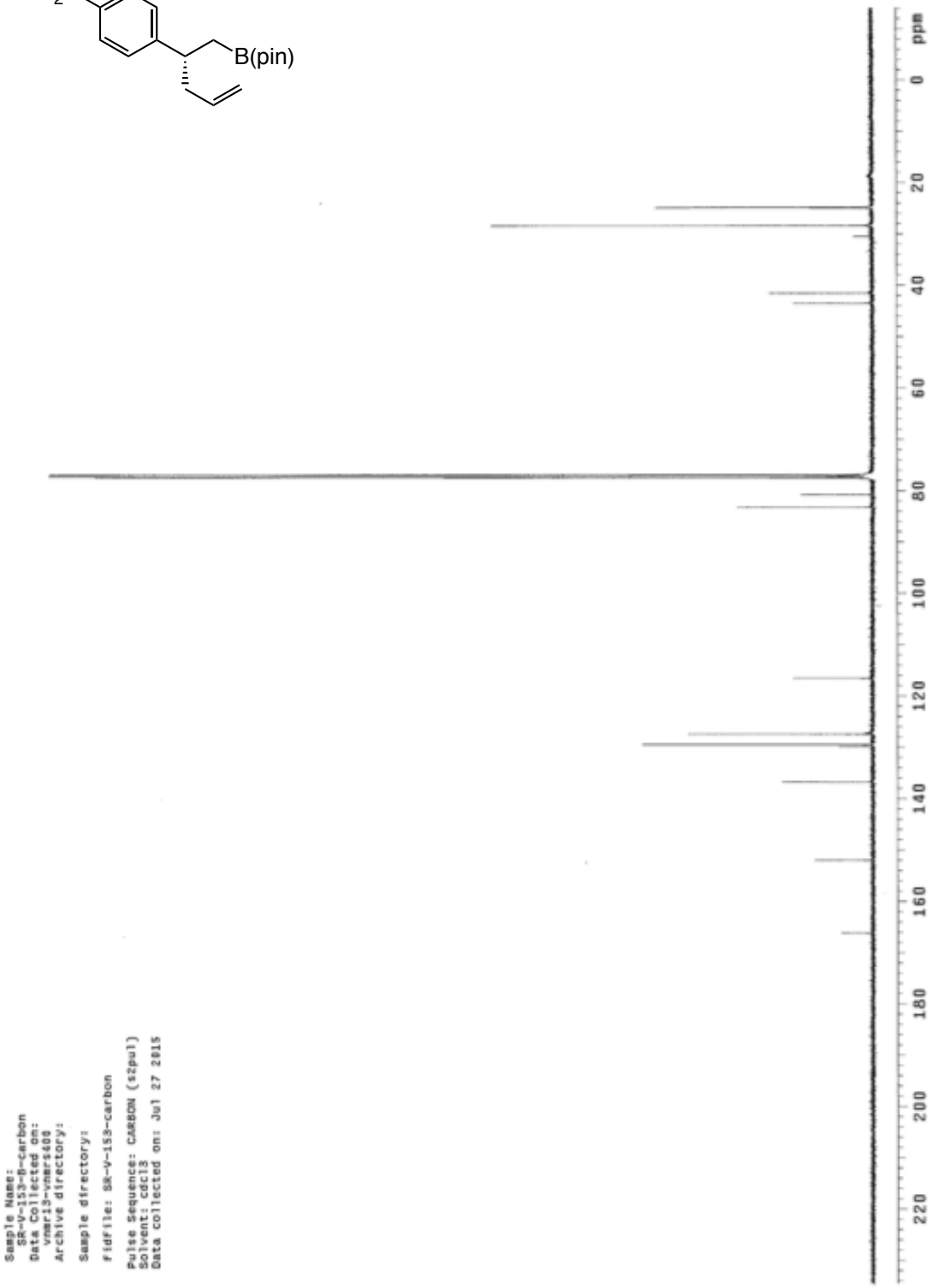
Sample Name:
SR-V-153-B-carbon
Data Collected on:
vnmr13-vnmrs600
Archive directory:
Sample directory:
fidfile: SR-V-153-carbon
Pulse Sequence: CARBON (s2pul)
Solvent: cdcl3
Data collected on: Jul 27 2015
ppm
0
20
40
60
80
100
120
140
160
180
200
220

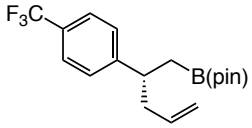
F3C
B(pin)

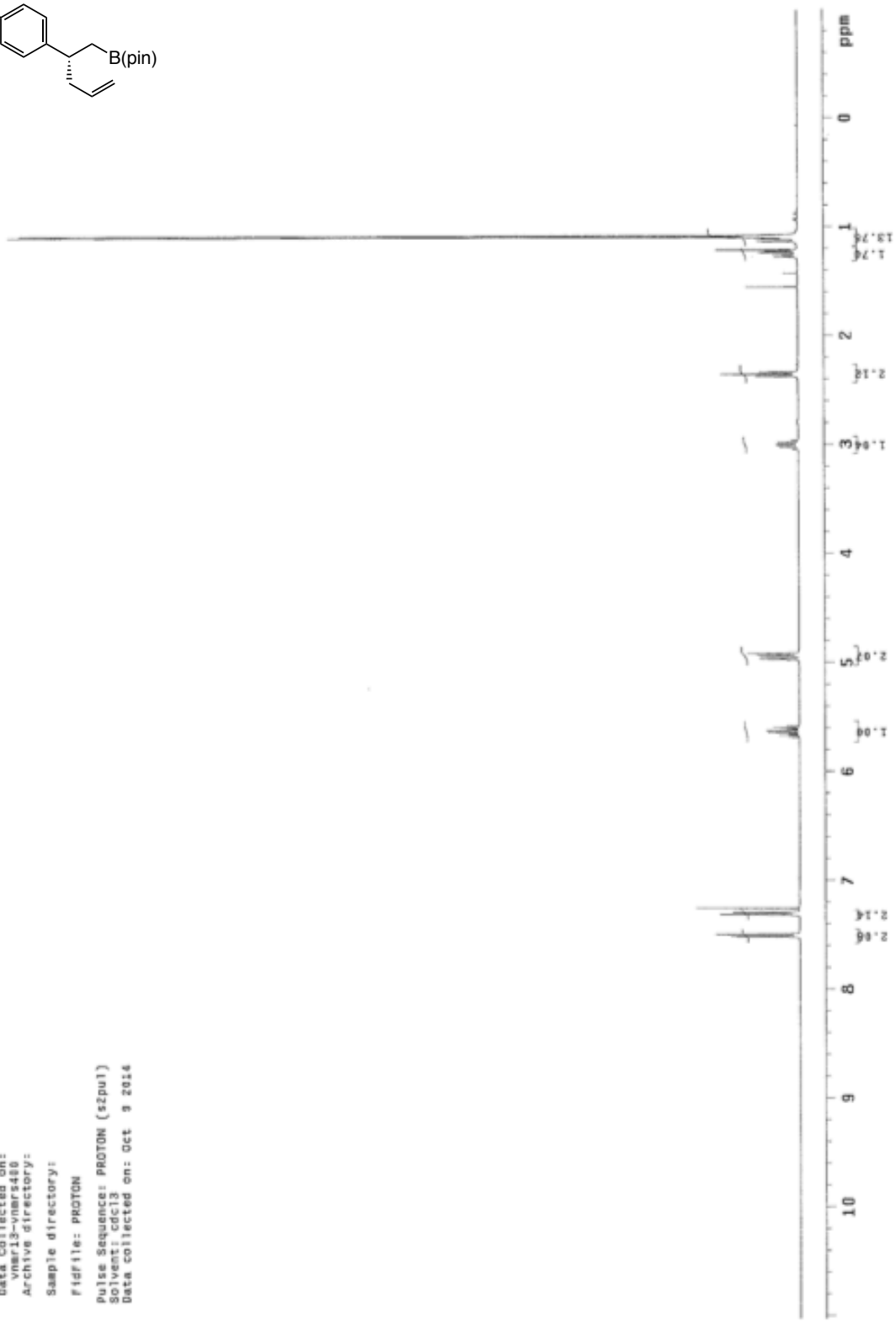
Sample Name:
SR-IV-278-D-rac
Data Collected on:
vnmr13-vnmrs400
Archive directory:
Sample directory:
Fidfile: PROTON
Pulse Sequence: PROTON (s2pul)
Solvent: cdcl3
Data collected on: Oct 3 2014
ppm
0
1
2
3
4
5
6
7
8
9
10
13.74
1.74
2.14
1.84
2.04
1.04
2.14
2.04

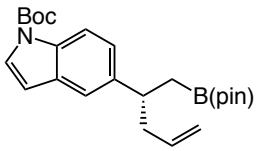
Boc
N
B(pin)

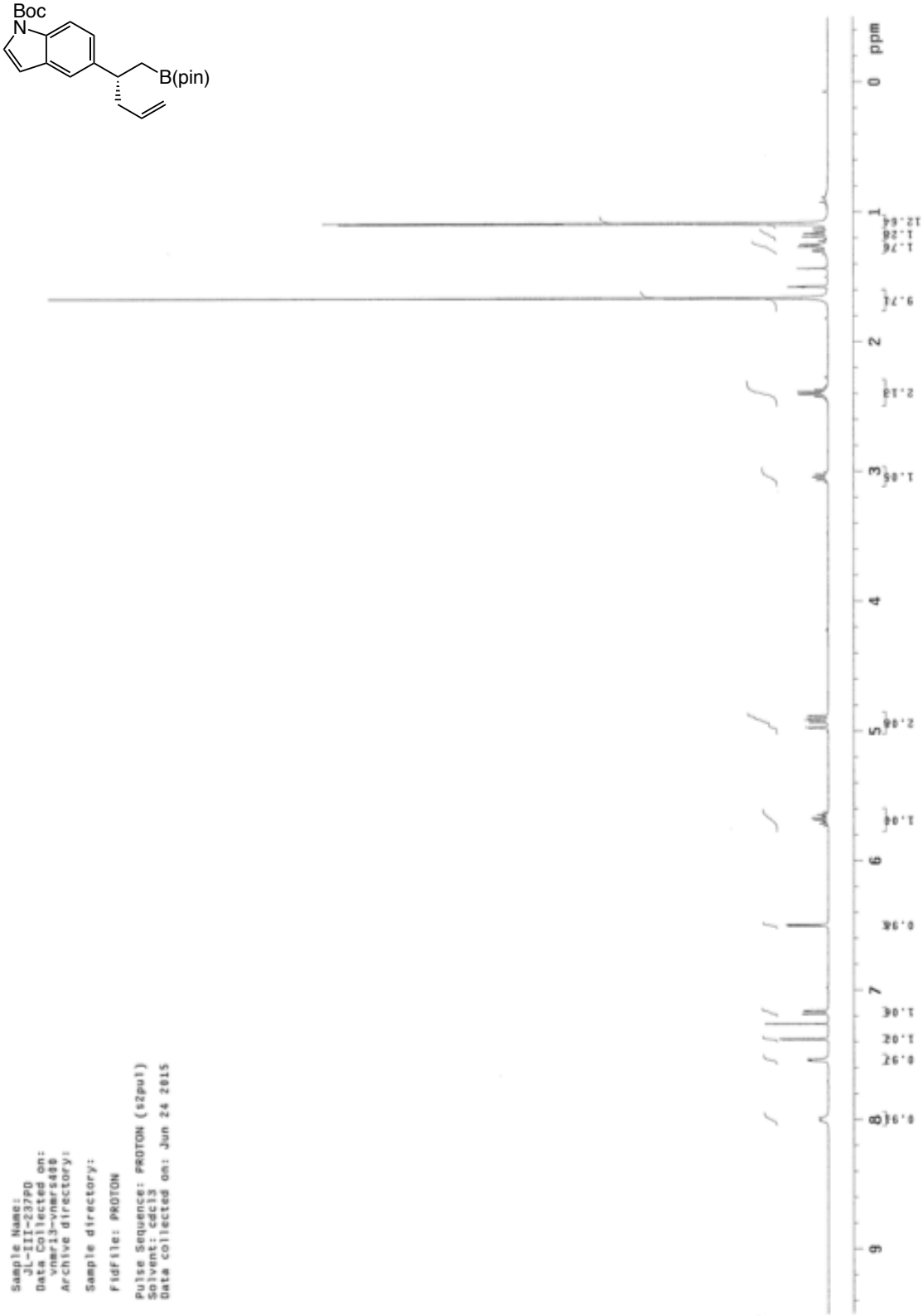
Sample Name:
JL-III-237PD
Data Collected on:
vnmr13-vnmrs400
Archive directory:
Sample directory:
FidFile: PROTON
Pulse Sequence: PROTON (s2pul)
Solvent: cdcl3
Data collected on: Jun 24 2015
ppm
12.64
1.76
1.74
1.26
9.74
2.12
1.05
2.04
1.04
0.96
1.06
1.02
0.97
0.96

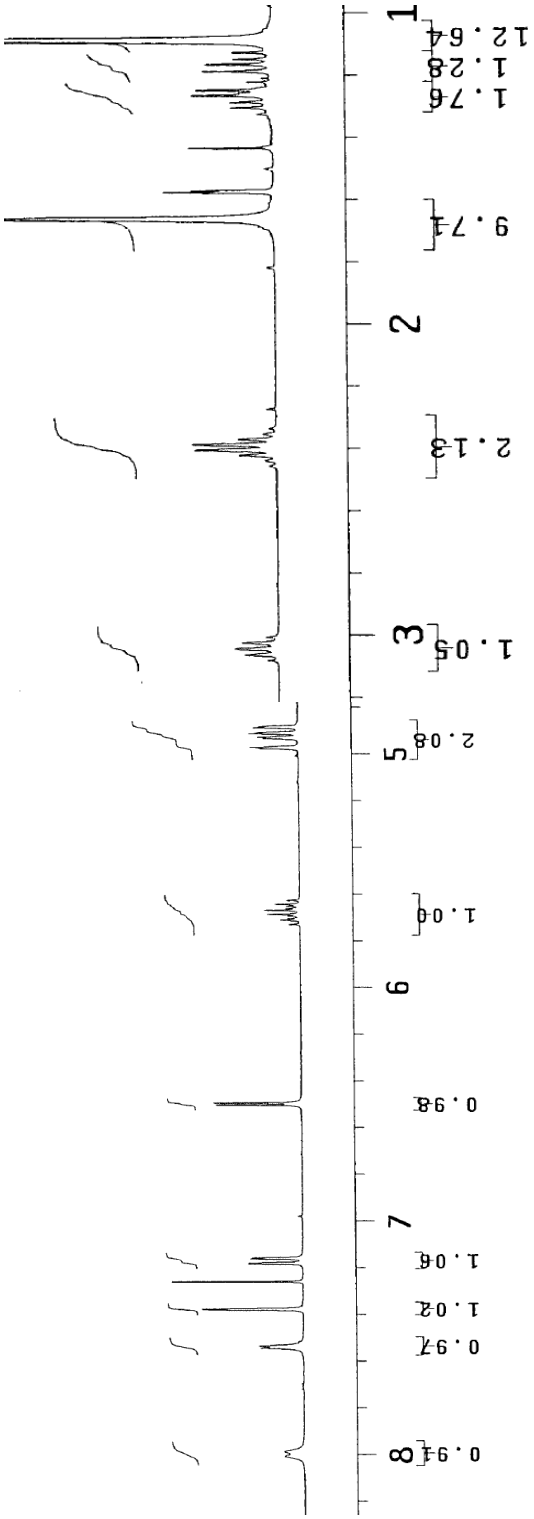
12.64
1.28
1.76
9.74
2.13
1.05
2.08
1.00
0.98
1.06
1.02
0.97
0.94
1
2
3
5
6
7
8

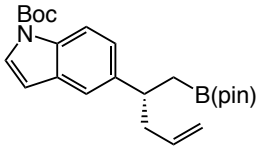
Boc
N
B(pin)

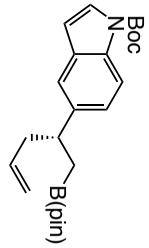
Boc
N
B(pin)

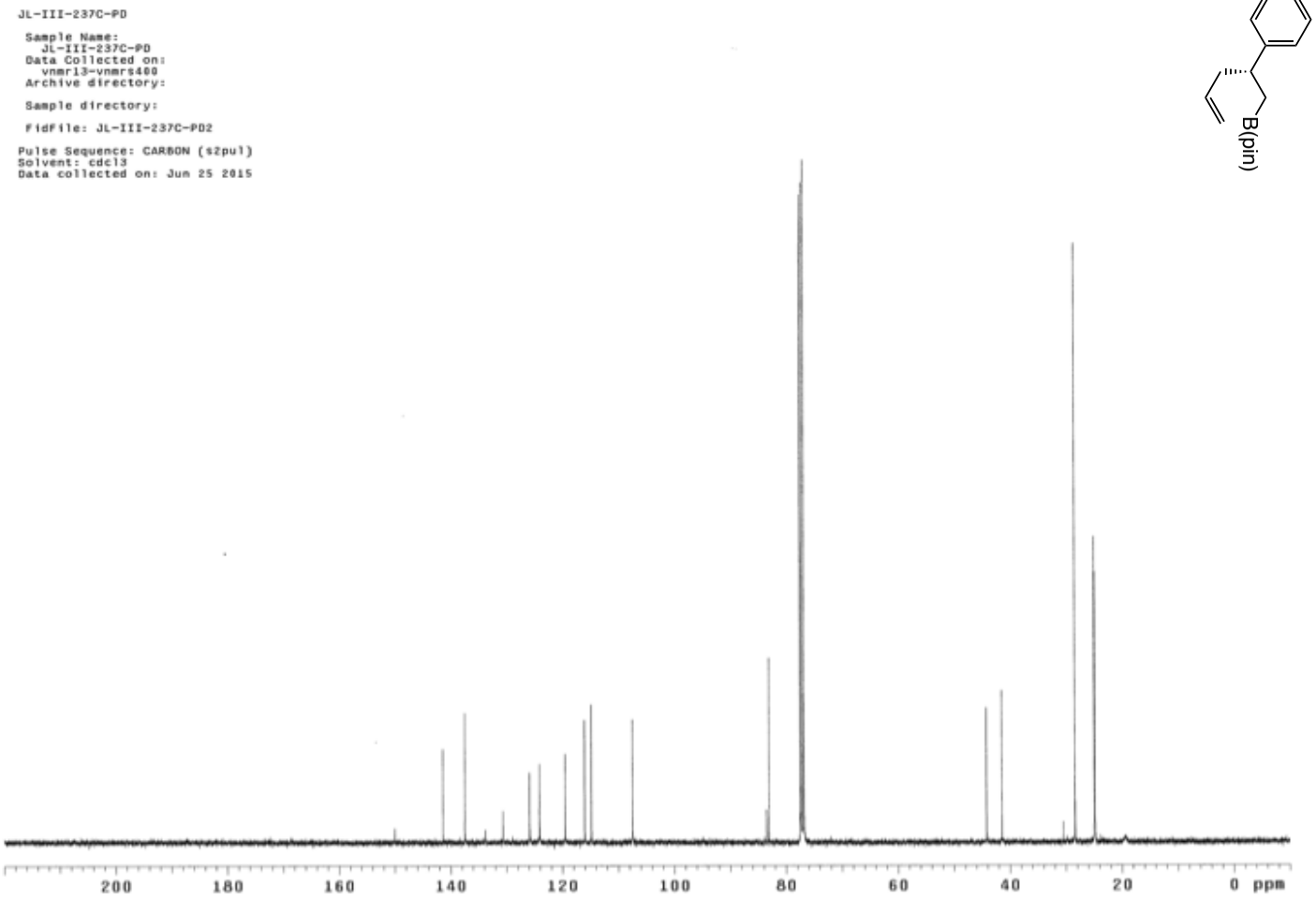
JL-III-237C-PD
Sample Name:
JL-III-237C-PD
Data Collected on:
vnmr13-vnmrs400
Archive directory:
Sample directory:
FidFile: JL-III-237C-PD2
Pulse Sequence: CARBON (s2pul)
Solvent: cdcl3
Data collected on: Jun 25 2015
200
180
160
140
120
100
80
60
40
20
0 ppm

S
B(pin)

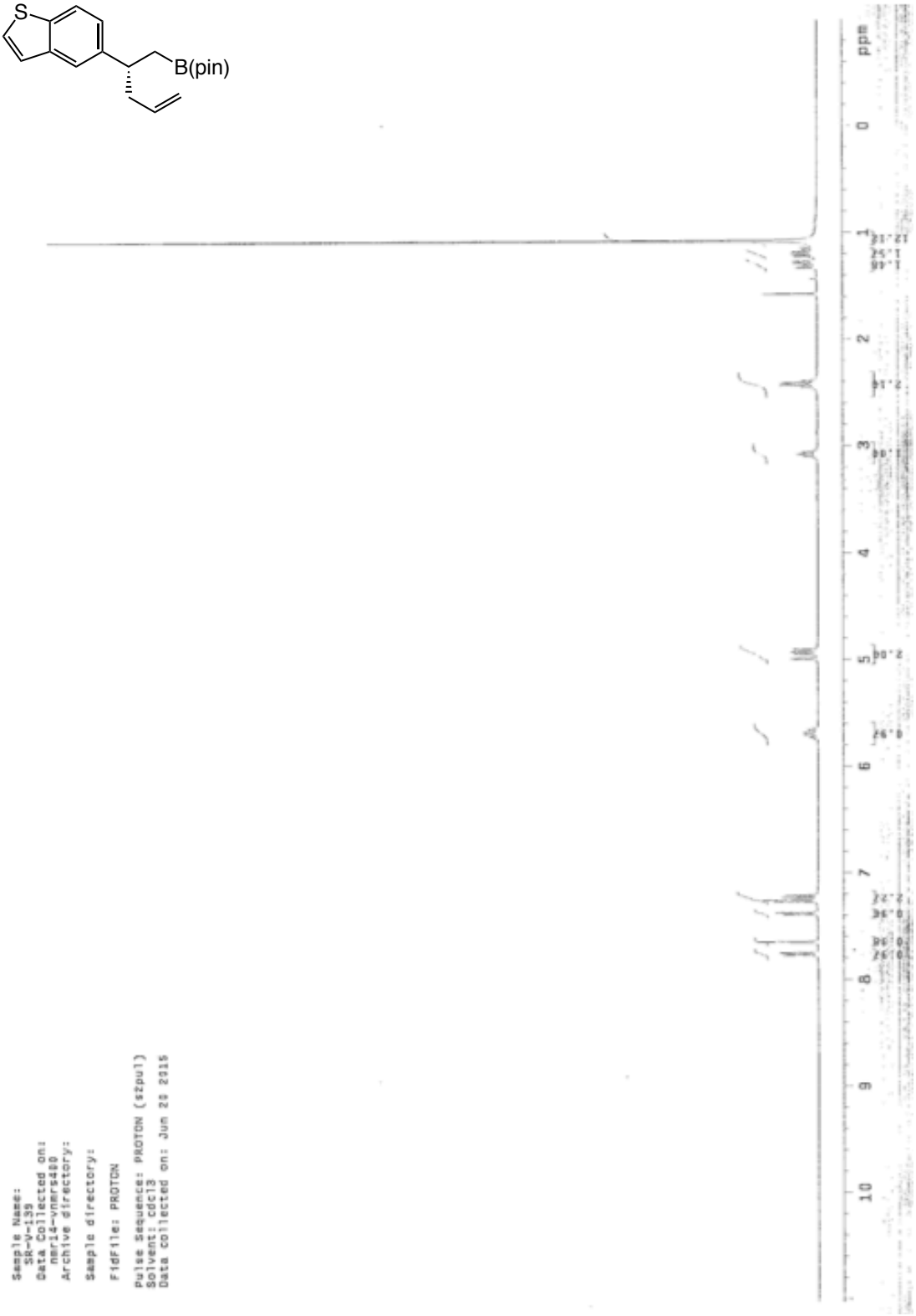
Sample Name:
SR-V-139
Data Collected on:
nmr14-vnmrs400
Archive directory:
Sample directory:
FidFile: PROTON
Pulse Sequence: PROTON (szpul)
Solvent: cdcl3
Data collected on: Jun 20 2015
ppm
10
9
8
7
6
5
4
3
2
1
0

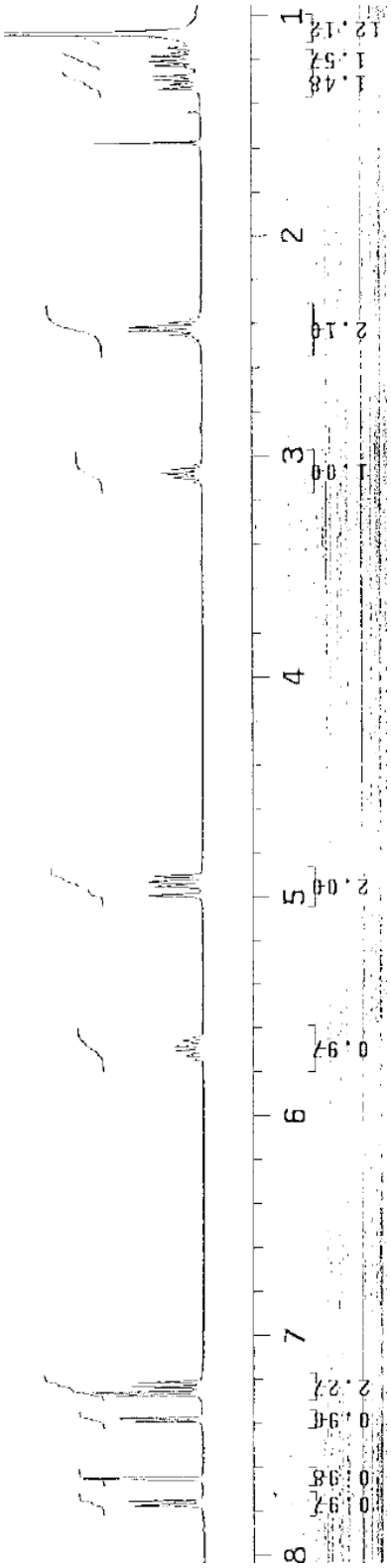
12.18
1.57
1.48
2.16
1.00
2.00
0.97
2.27
0.96
0.97
0.98
1
2
3
4
5
6
7
8

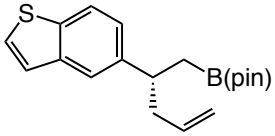
S
B(pin)

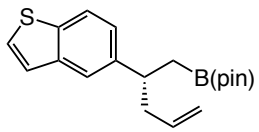
S
B(pin)

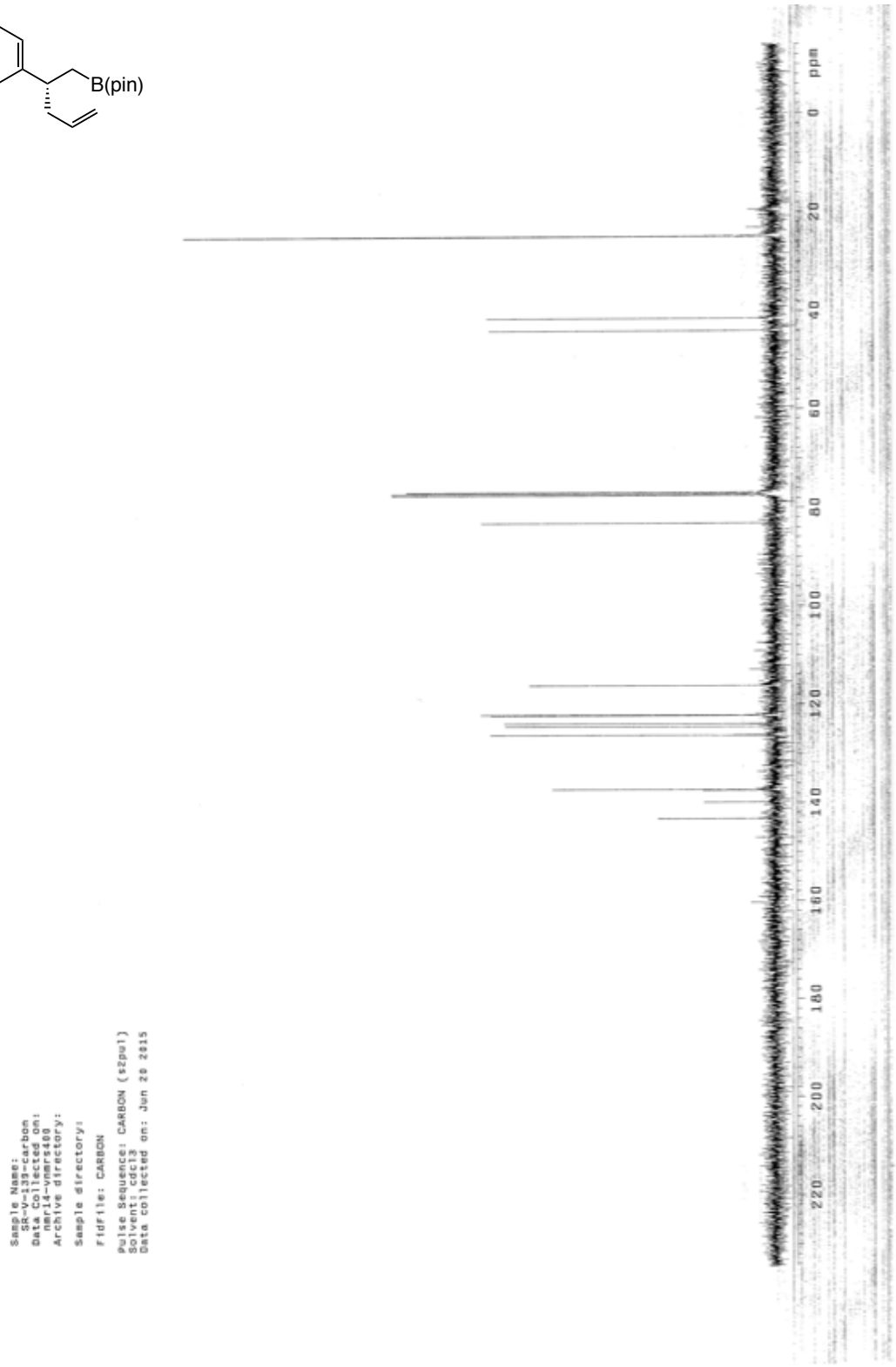
Sample Name:
SR-V-133-carbon
Data Collected on:
nmr14-vnmrs400
Archive directory:
Sample directory:
Fidfile: CARBON
Pulse Sequence: CARBON (s2pul)
Solvent: cdcl3
Data collected on: Jun 28 2015
220
200
180
160
140
120
100
80
60
40
20
0
ppm

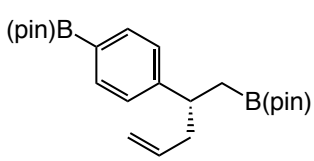
(pin)B
B(pin)

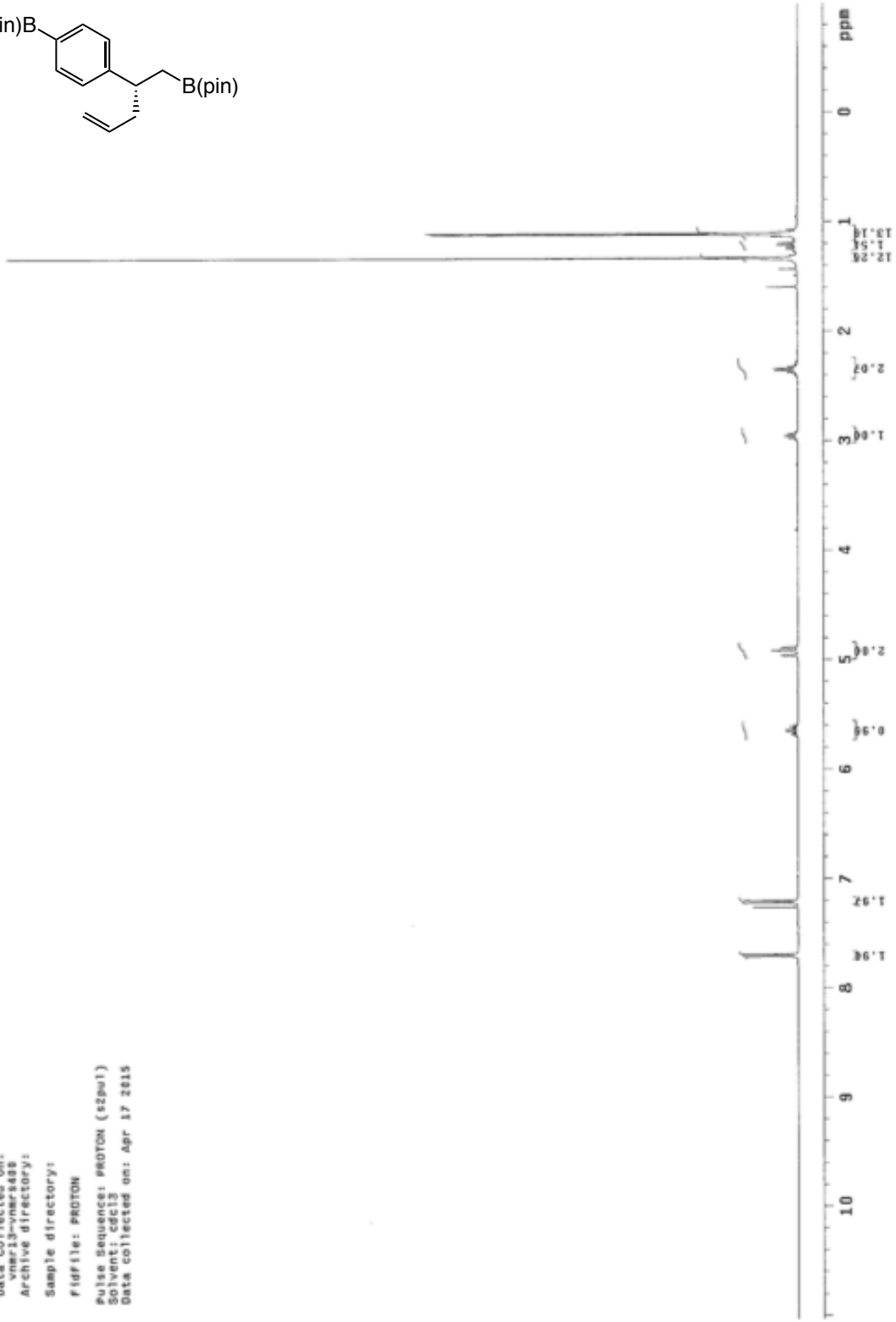
Sample Name:
SR-V-184
Data Collected on:
vnmr13-vnmrs4dd
Archive directory:
Sample directory:
Fidfile: PROTON
Pulse Sequence: PROTON (s2pul)
Solvent: cdcl3
Data collected on: Apr 17 2015
ppm
0
1
2
3
4
5
6
7
8
9
10
13.16
1.55
12.28
2.07
1.00
2.00
0.98
1.92
1.96

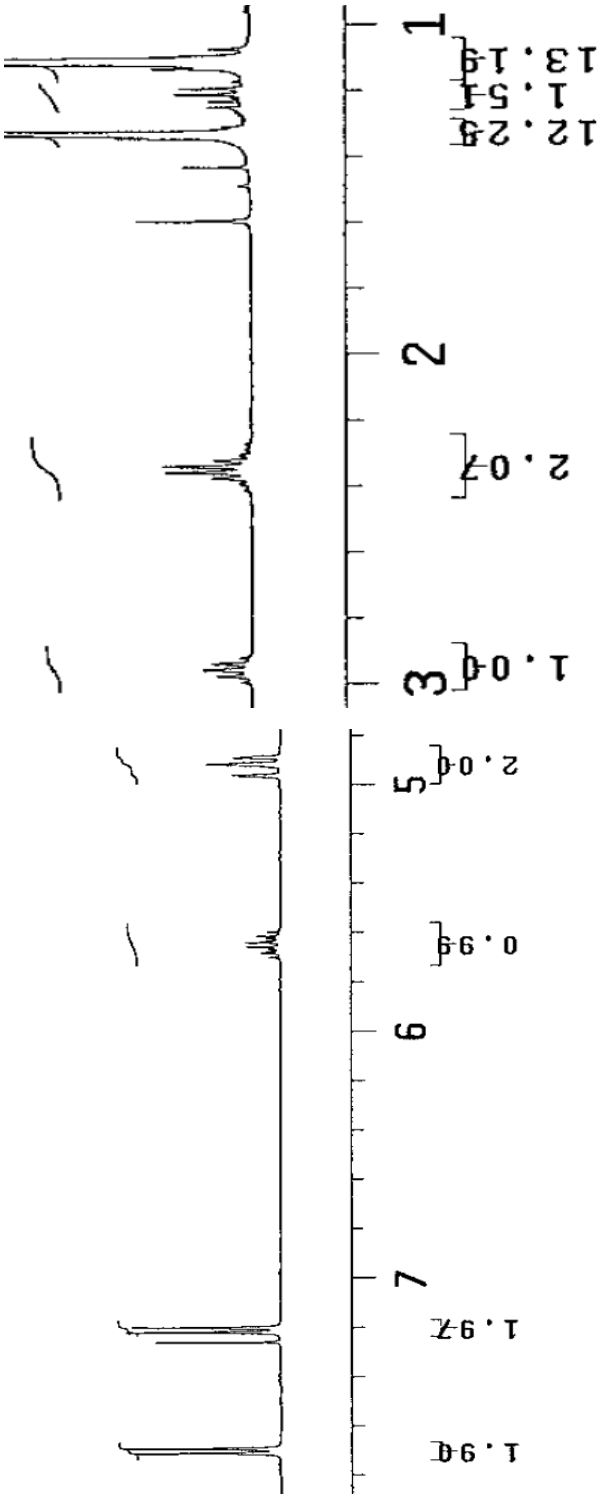
1.00
2.07
12.24
1.51
13.19
2.00
0.99
1.97
1.90
1
2
3
5
6
7

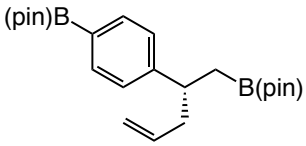
(pin)B
B(pin)

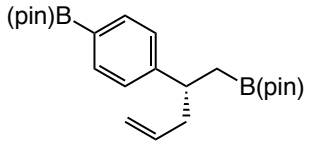
(pin)B
B(pin)

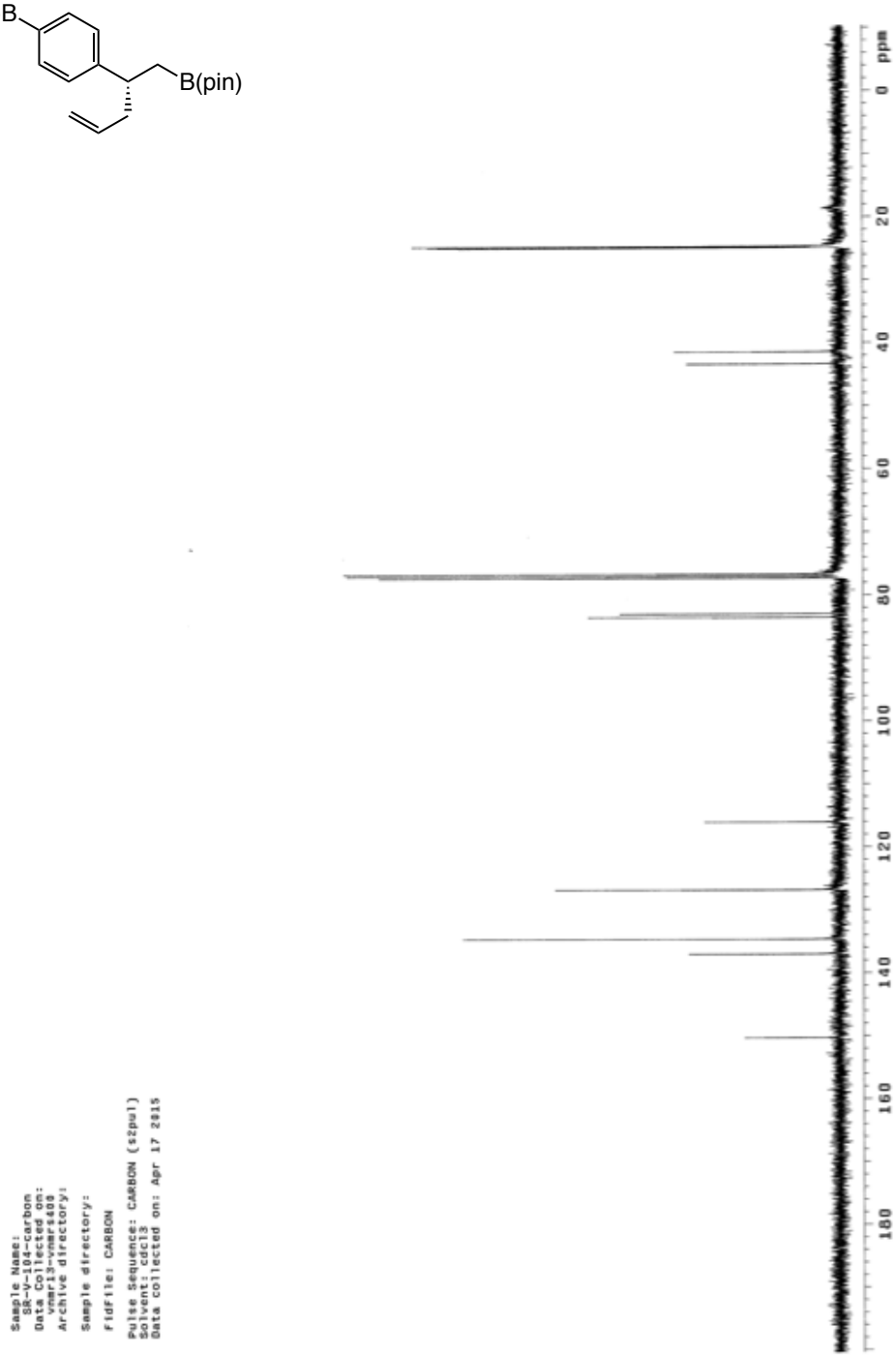
Sample Name:
SR-V-104-carbon
Data Collected on:
vnmrs3-nmrfarm
Archive directory:
Sample directory:
FidFile: CARBON
Pulse Sequence: CARBON (s2pul)
Solvent: cdcl3
Data collected on: Apr 17 2015
ppm
0
20
40
60
80
100
120
140
160
180

(pin)B
B(pin)

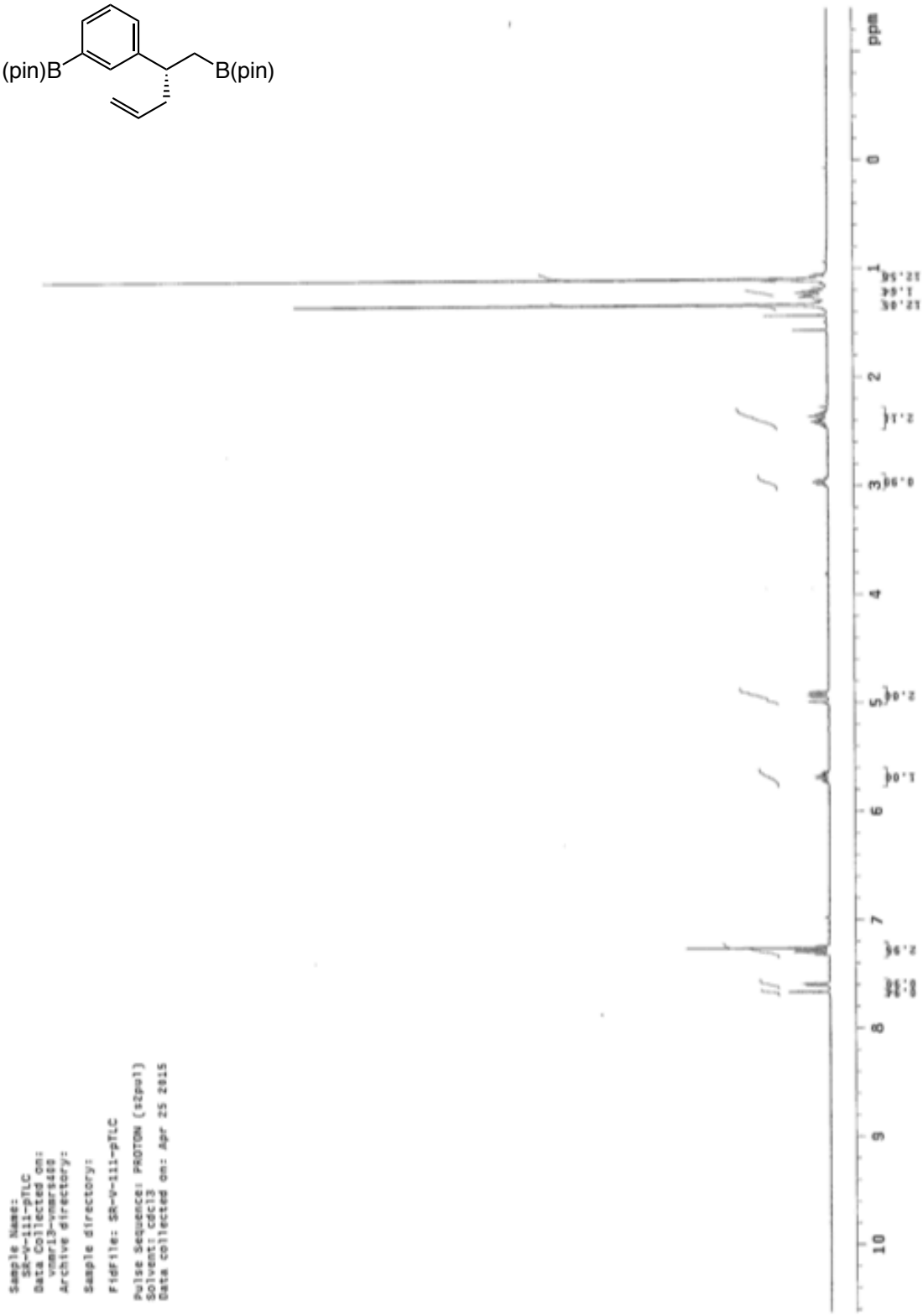
Sample Name:
SR-V-111-pTLC
Data Collected on:
vnmr13-vnmrs400
Archive directory:
Sample directory:
Fidfile: SR-V-111-pTLC
Pulse Sequence: PROTON (s2pul)
Solvent: CdCl3
Data collected on: Apr 25 2015
ppm
0
1
2
3
4
5
6
7
8
9
10

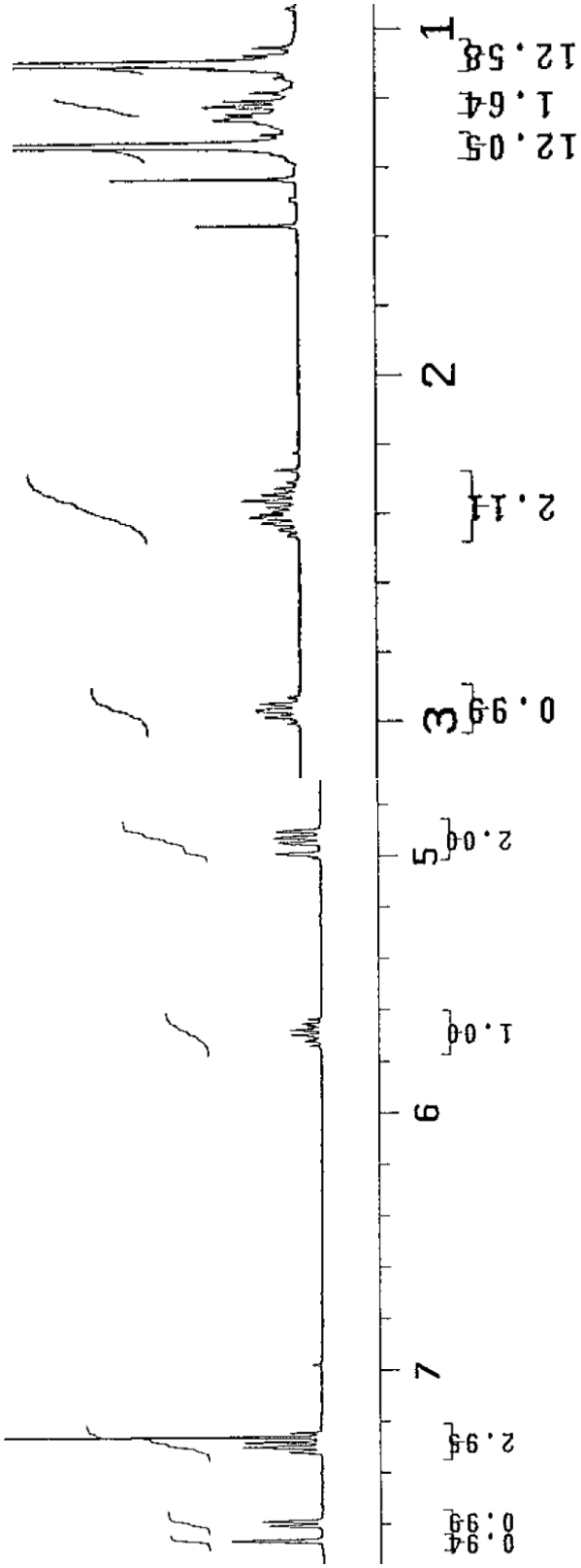
0.94
0.99
2.95
7
1.00
6
2.00
5
0.99
3
2.11
2
12.05
1.64
12.58
1

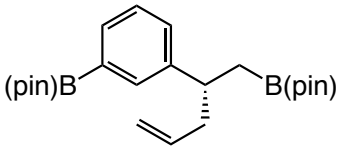
(pin)B
B(pin)

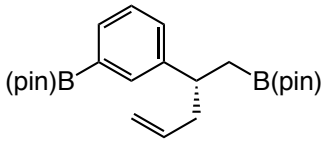
(pin)B
B(pin)

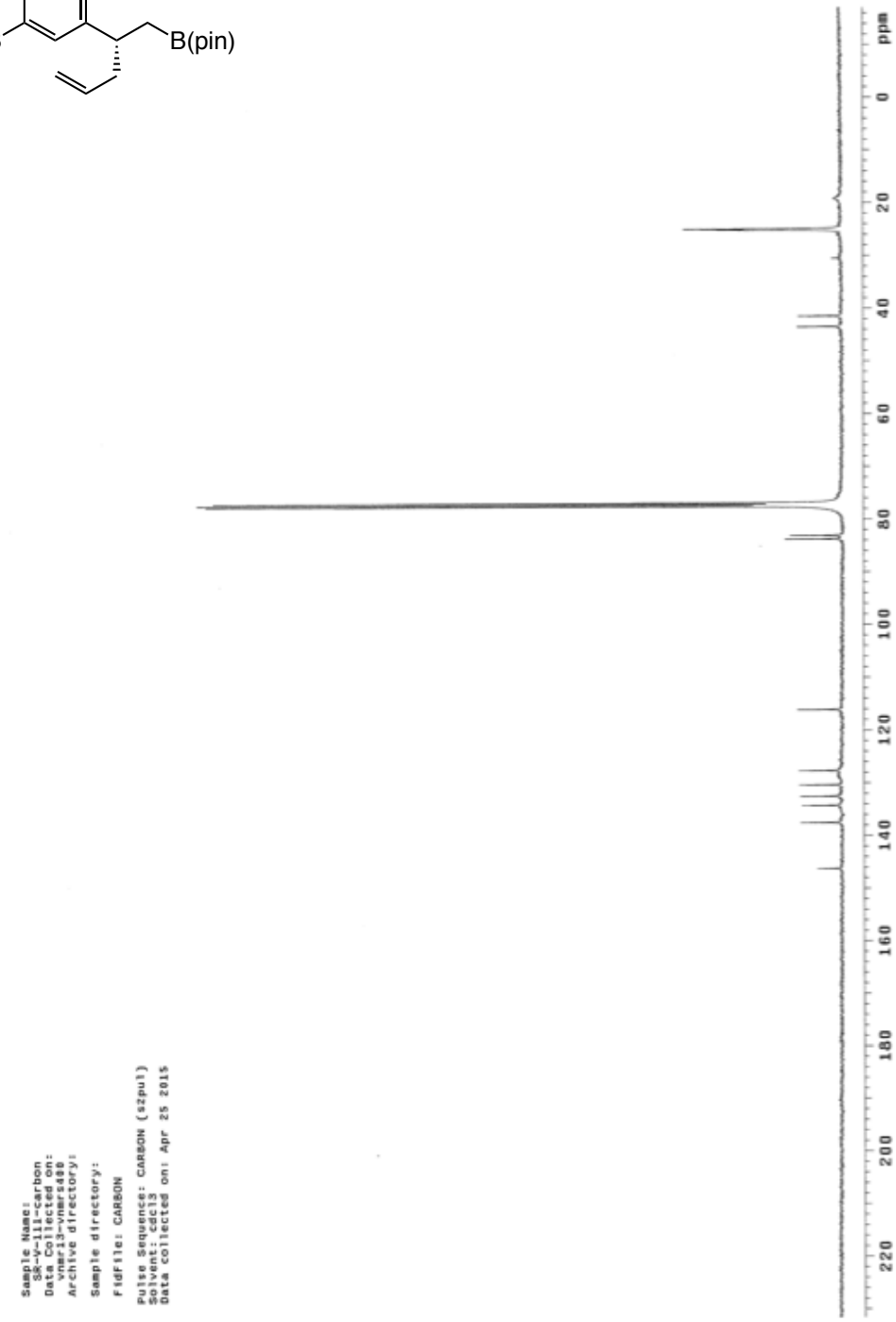
Sample Name:
SR-V-111-carbon
Date Collected on:
varian3-vnmrs480
Archive directory:
Sample directory:
FidFile: CARBON
Pulse Sequence: CARBON (s2pul)
Solvent: cdcl3
Data collected on: Apr 25 2015
ppm
220
200
180
160
140
120
100
80
60
40
20
0

B(pin)

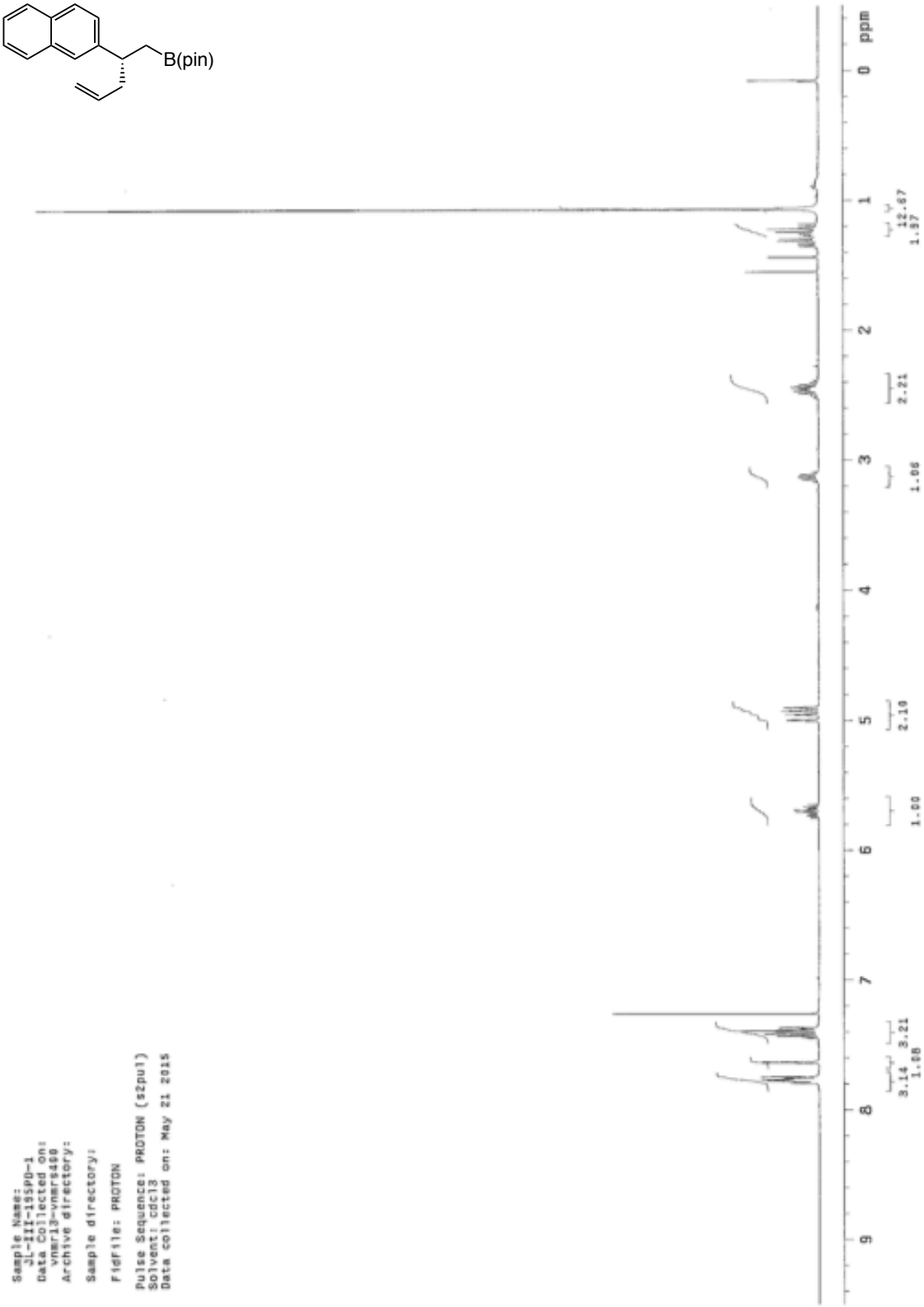
Sample Name:
JL-III-195PD-1
Data Collected on:
vnmr13-vnmrs400
Archive directory:
Sample directory:
FidFile: PROTON
Pulse Sequence: PROTON (s2pul)
Solvent: cdcl3
Data collected on: May 21 2015
ppm
0
1
2
3
4
5
6
7
8
9
12.67
1.97
2.21
1.06
2.10
1.00
3.14
3.21
1.08

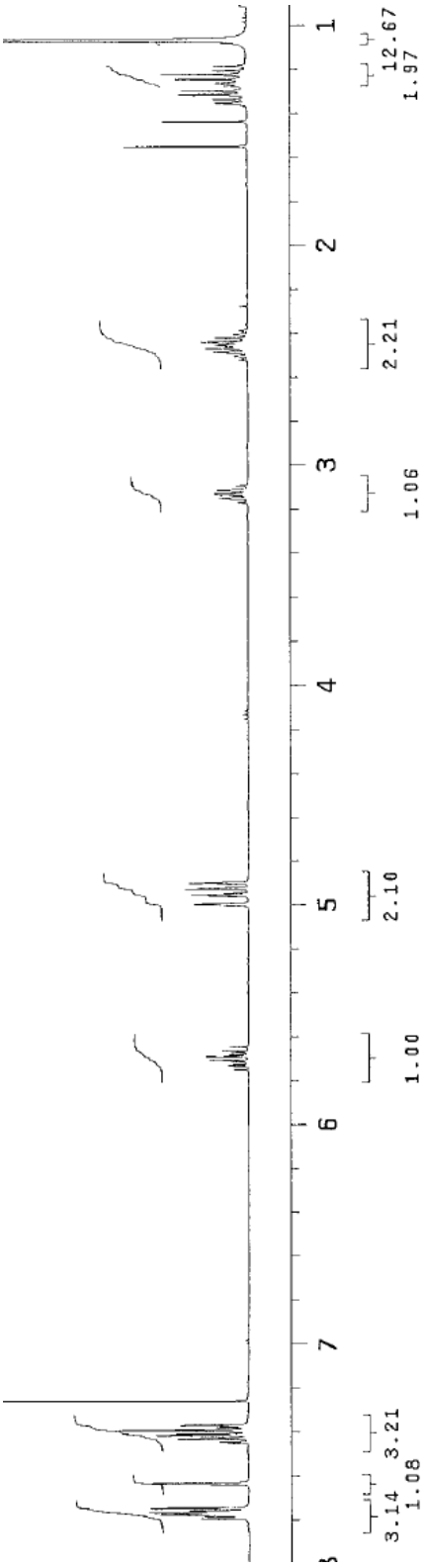
1
2
3
4
5
6
7
8
12.67
1.97
2.21
1.06
2.10
1.00
3.21
3.14
1.08

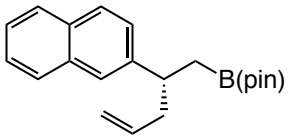
B(pin)

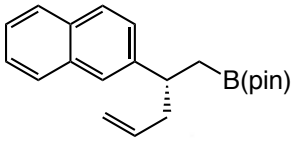
B(pin)

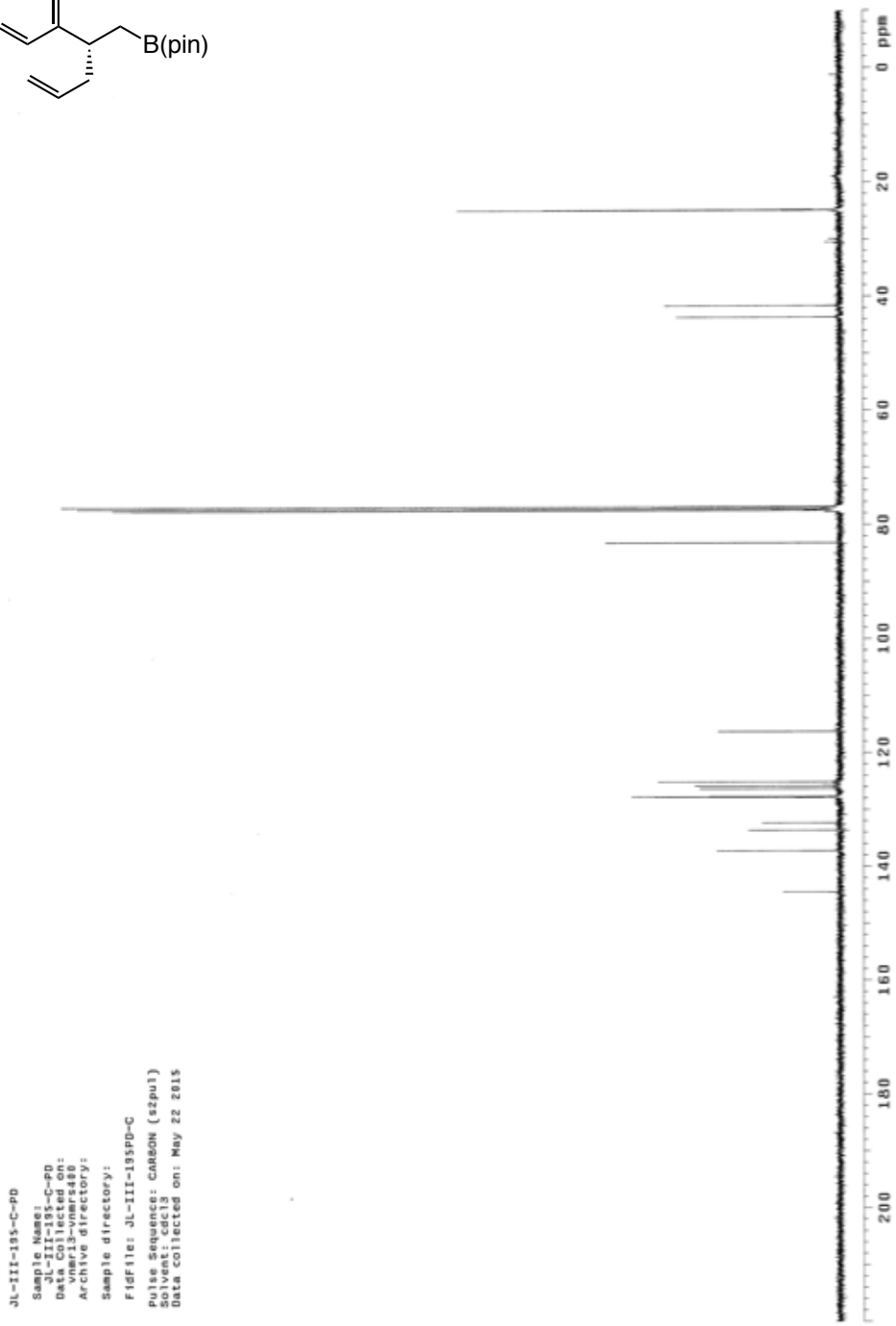
JL-III-195-C-PD
Sample Name:
JL-III-195-C-PD
Date Collected on:
vnmrs13-vnmrs480
Archive directory:
Sample directory:
FidFile: JL-III-195PD-C
Pulse Sequence: CARBON (s2pul)
Solvent: cdcl3
Data collected on: May 22 2015
200
180
160
140
120
100
80
60
40
20
0 ppm

B(pin)
Ph

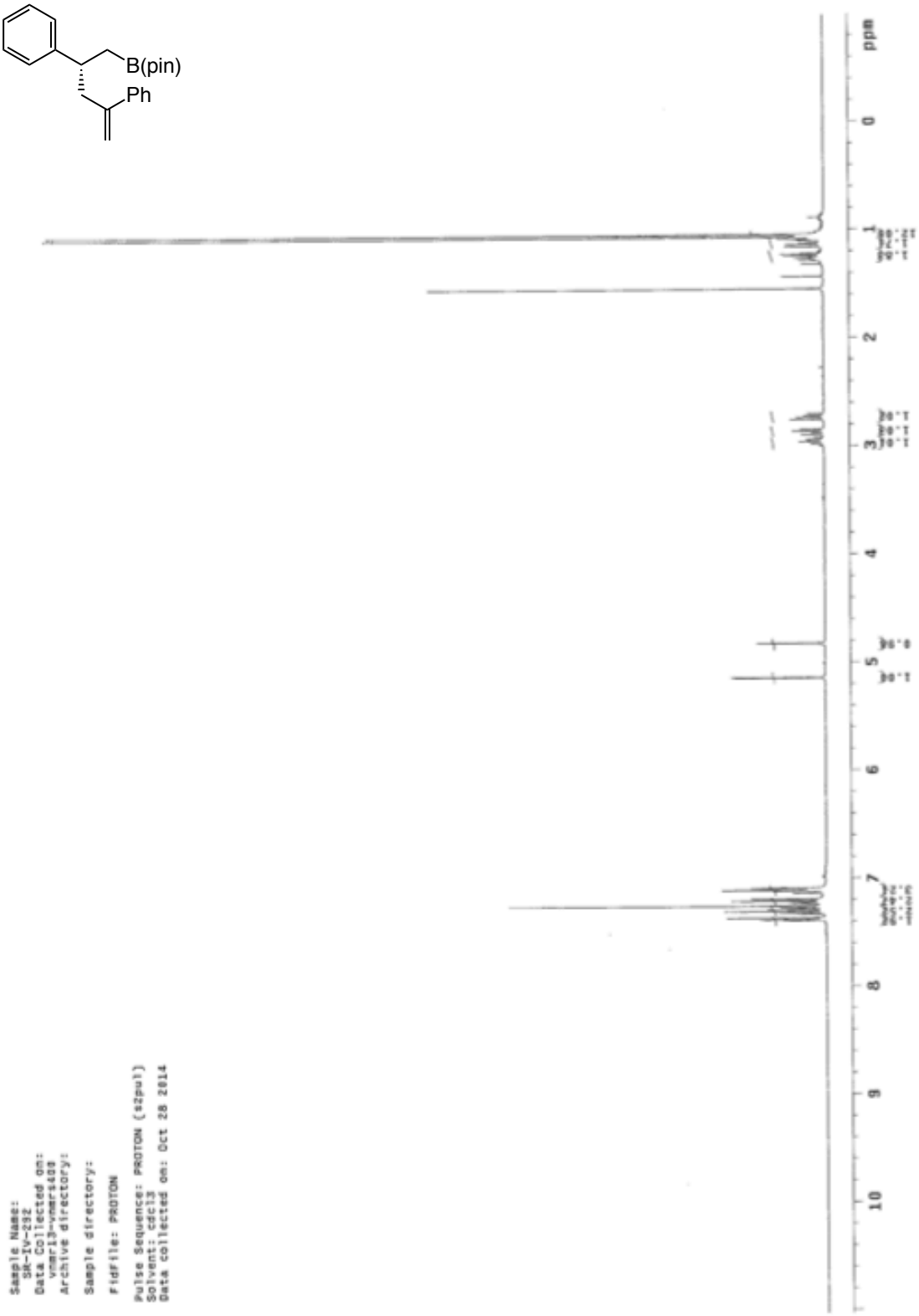
Sample Name:
SR-IV-292
Data Collected on:
vmarl3-vmars400
Archive directory:
Sample directory:
Fidfile: PROTON
Pulse Sequence: PROTON (s2pul)
Solvent: cdcl3
Data collected on: Oct 28 2014
ppm
0
1
2
3
4
5
6
7
8
9
10

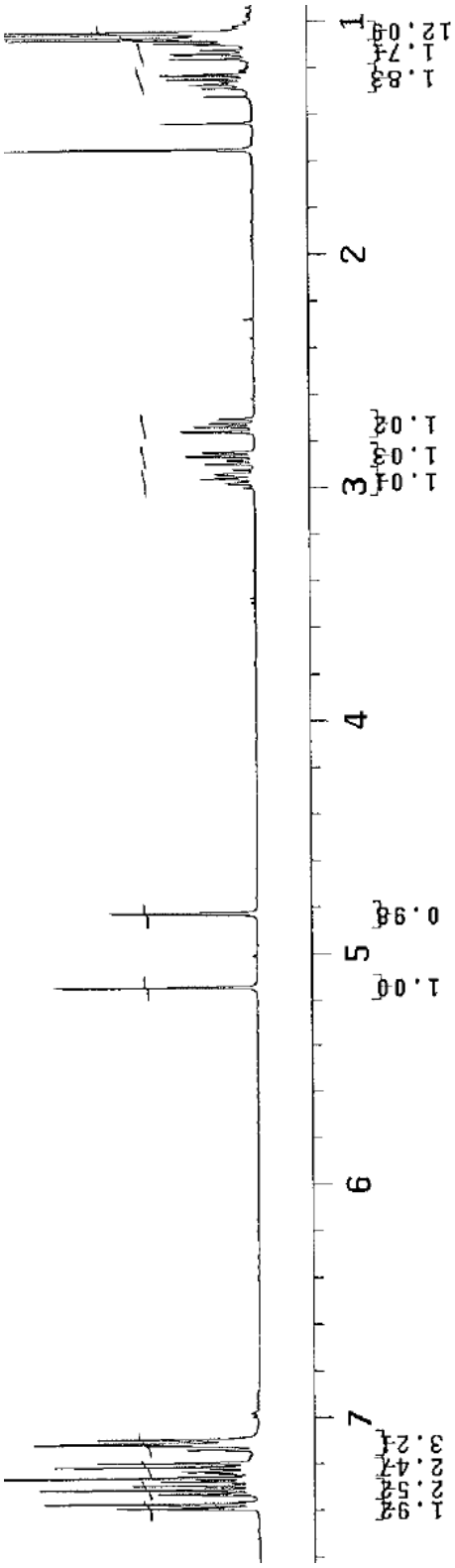
12.04
1.74
1.83
1.02
1.03
1.01
0.98
1.00
3.21
2.47
2.54
1.92
1
2
3
4
5
6
7

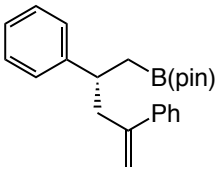
B(pin)
Ph

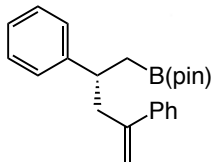
B(pin)
Ph

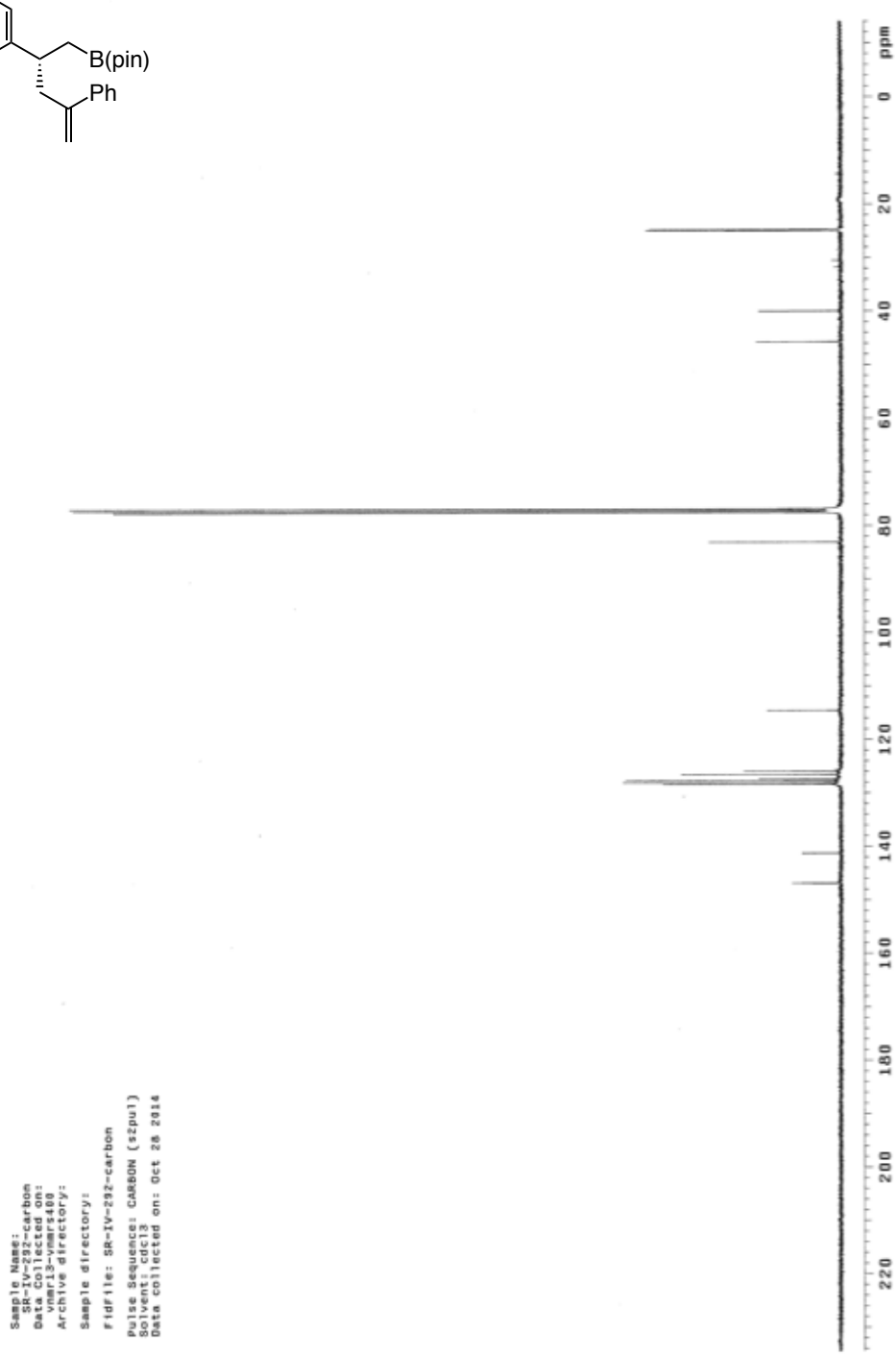
Sample Name:
SR-IV-292-carbon
Data Collected on:
Vnmr3 Vnmr400
Archive directory:
Sample directory:
Fidfile: SR-IV-292-carbon
Pulse Sequence: CARBON (s2pul)
Solvent: cdcl3
Data collected on: Oct 28 2014
ppm
0
20
40
60
80
100
120
140
160
180
200
220

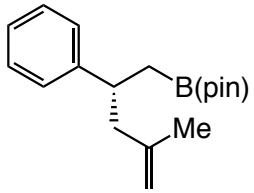

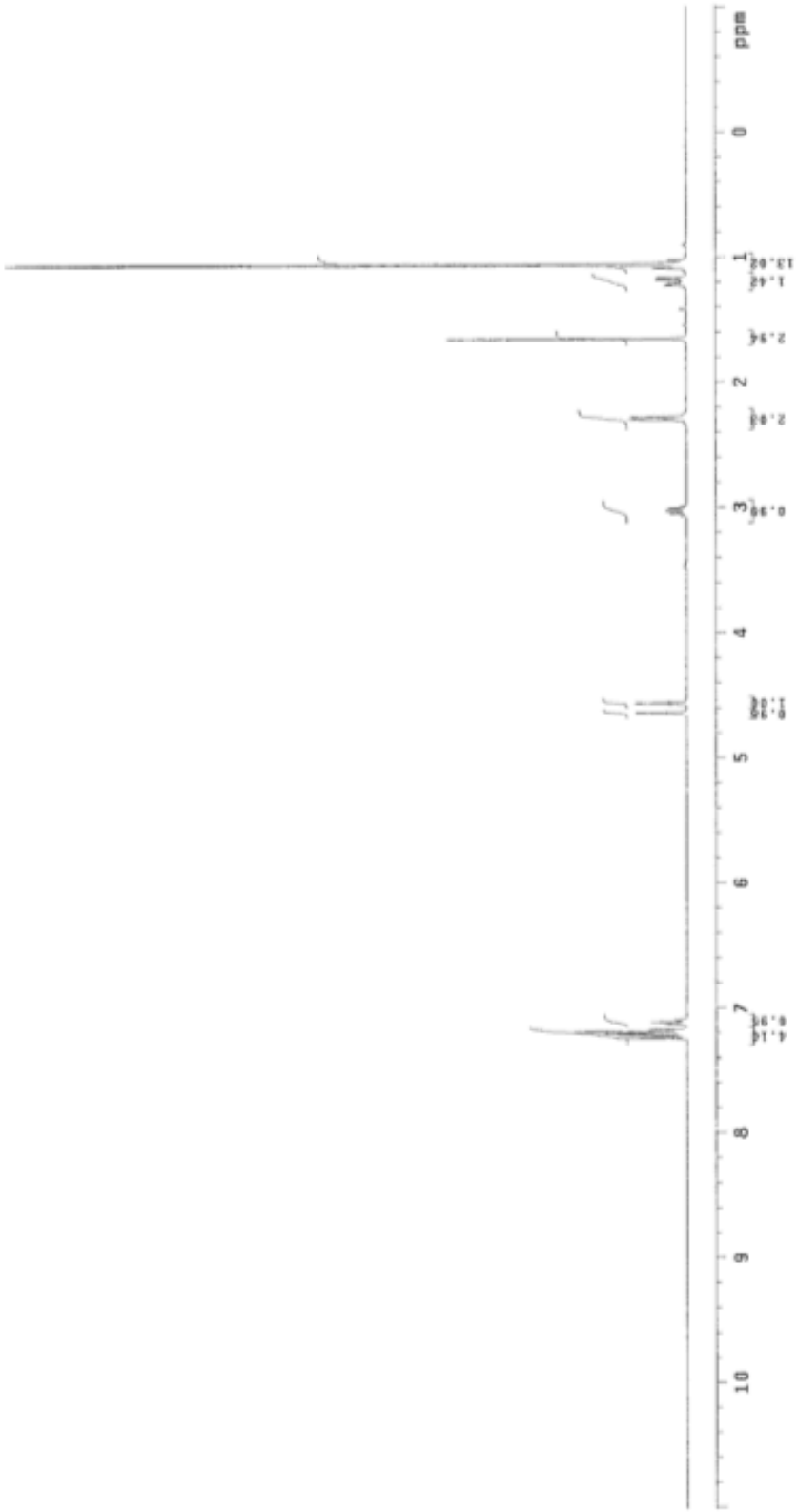

Sample Name:

Data Collected on:
vnmr13-vnmrs400
Archive directory:

Sample directory:

Fidfile: Pb-Me-product

Pulse Sequence: PROTON (s2pul)
Solvent: cdcl3
Data collected on: Jan 13 2015

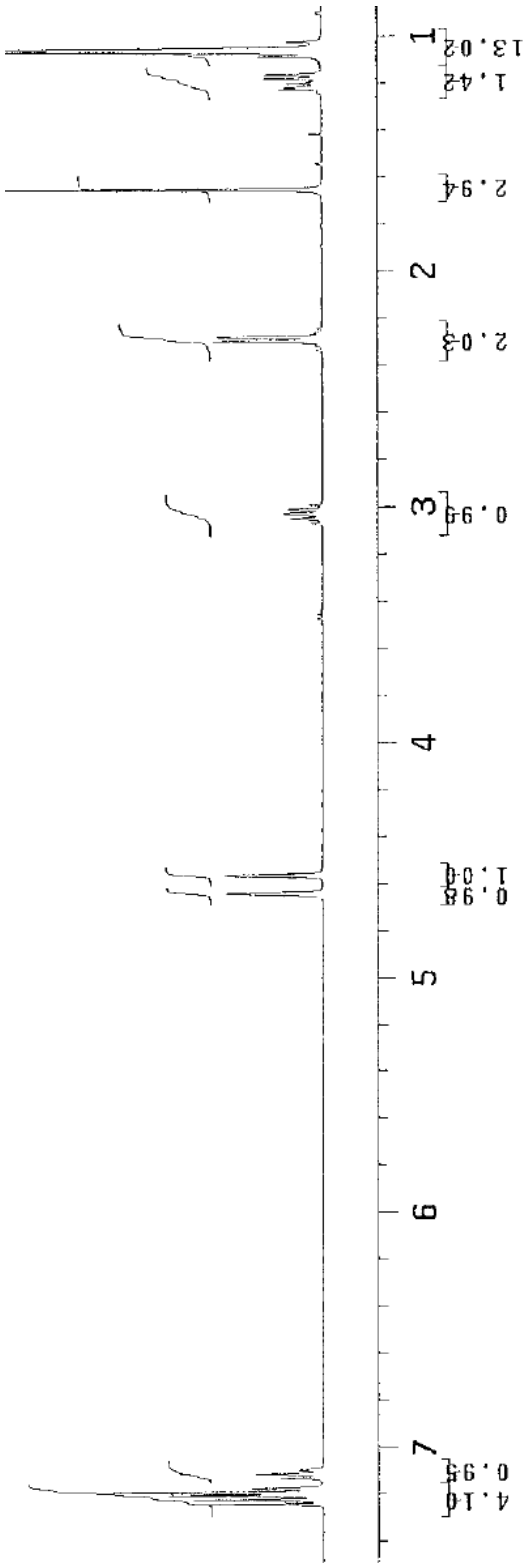
13.02
1.42
2.94
2.03
0.99
1.04
0.98
0.95
4.10
1
2
3
4
5
6
7

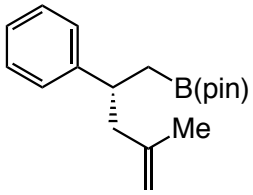
B(pin)
Me

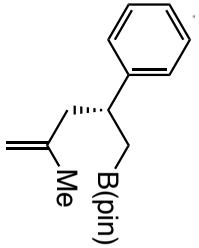

Sample Name:

Data Collected on:
vnmr13-vnmrs400
Archive directory:

Sample directory:

FidFile: CARBON

Pulse Sequence: CARBON (s2pul)
Solvent: cdcl3
Data collected on: Jan 13 2015

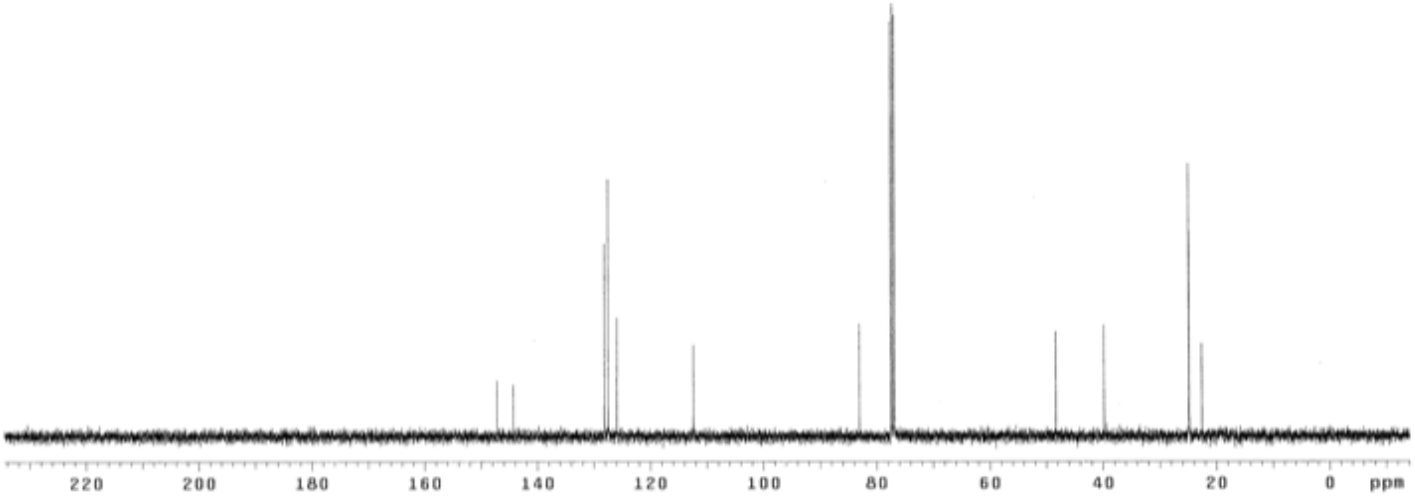

B(pin)
SiMe3

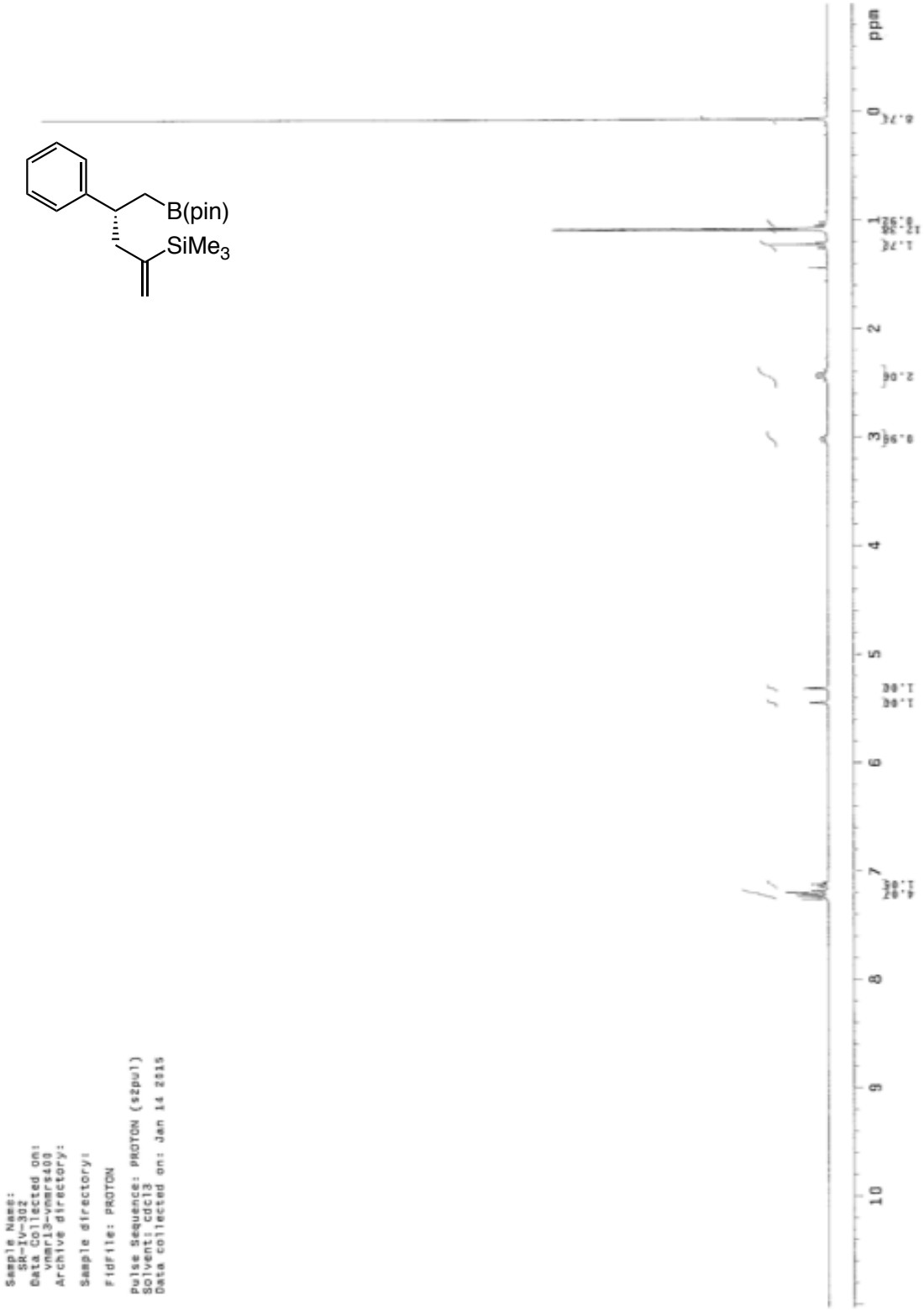
Sample Name:
SR-IV-302
Data Collected on:
vnmrj3-vnmrs400
Archive directory:
Sample directory:
Fidfile: PROTON
Pulse Sequence: PROTON (s2pul)
Solvent: cdcl3
Data collected on: Jan 14 2015
ppm
0
1
2
3
4
5
6
7
8
9
10

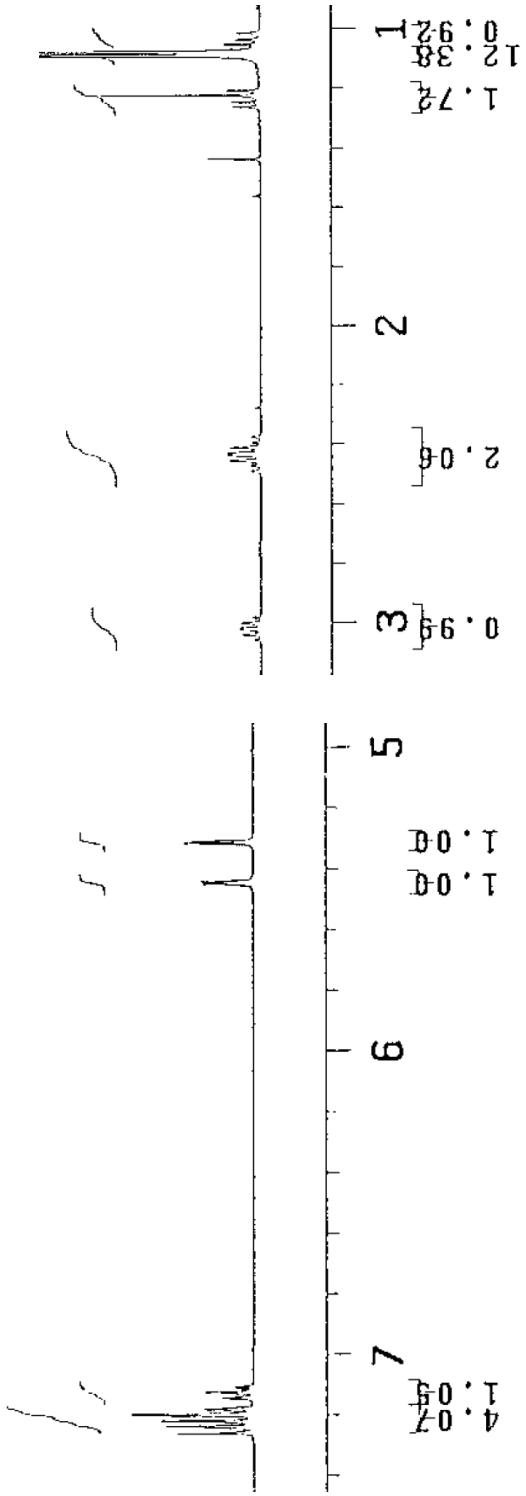
1.00
1.00
1.05
4.07
1.74
12.38
0.92
0.99
2.06
7
6
5
3
2
1

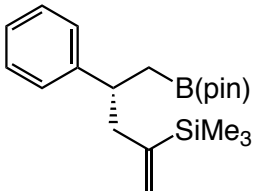
B(pin)
SiMe3

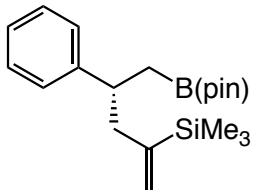
B(pin)
SiMe3

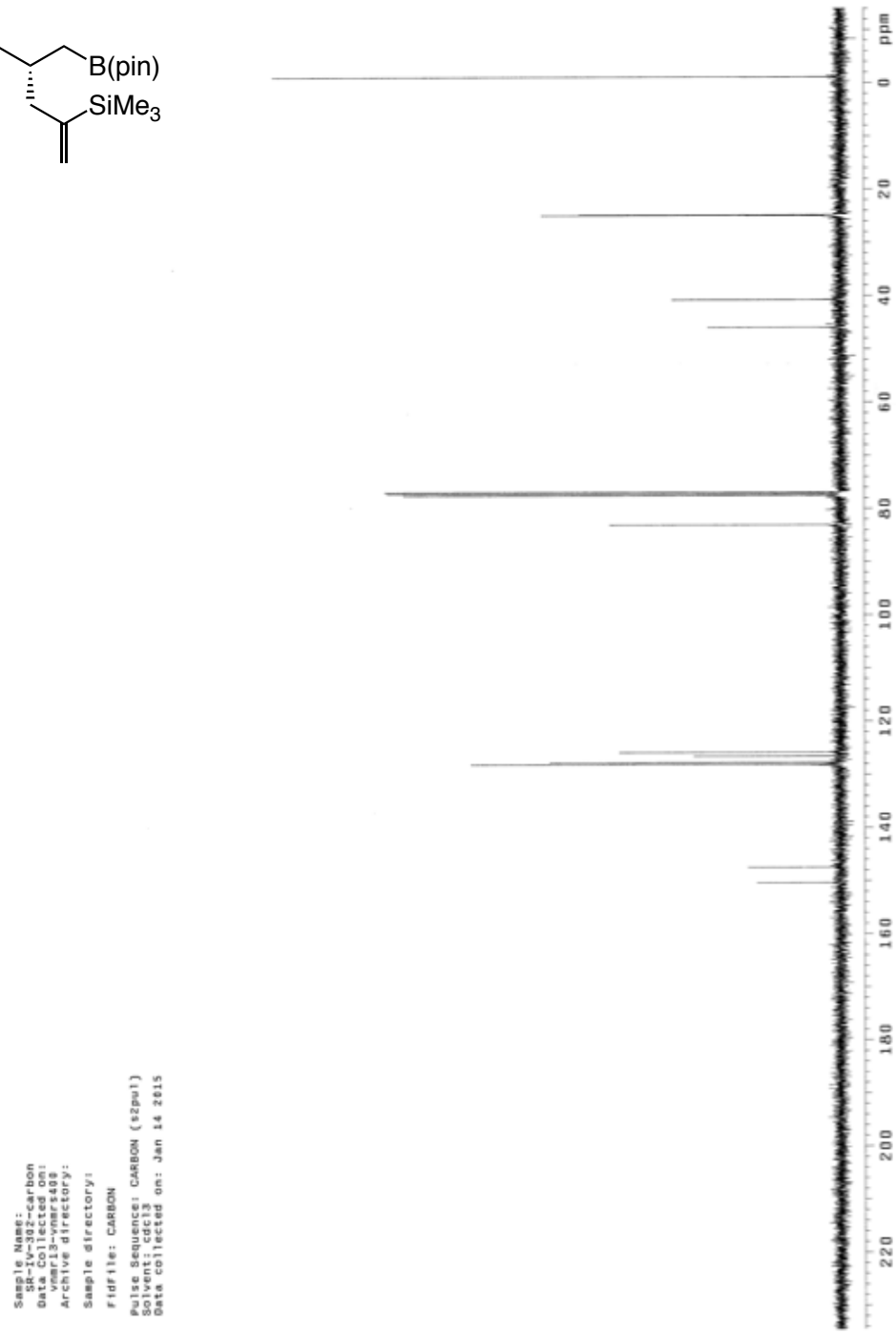
Sample Name:
SR-Iy-302-carbon
Data Collected on:
vnmrs-ser408
Archive directory:
Sample directory:
Fidfile: CARBON
Pulse Sequence: CARBON (s2pul)
Solvent: cdcl3
Data collected on: Jan 14 2015
ppm
0
20
40
60
80
100
120
140
160
180
200
220

O
B(pin)
SiMe3

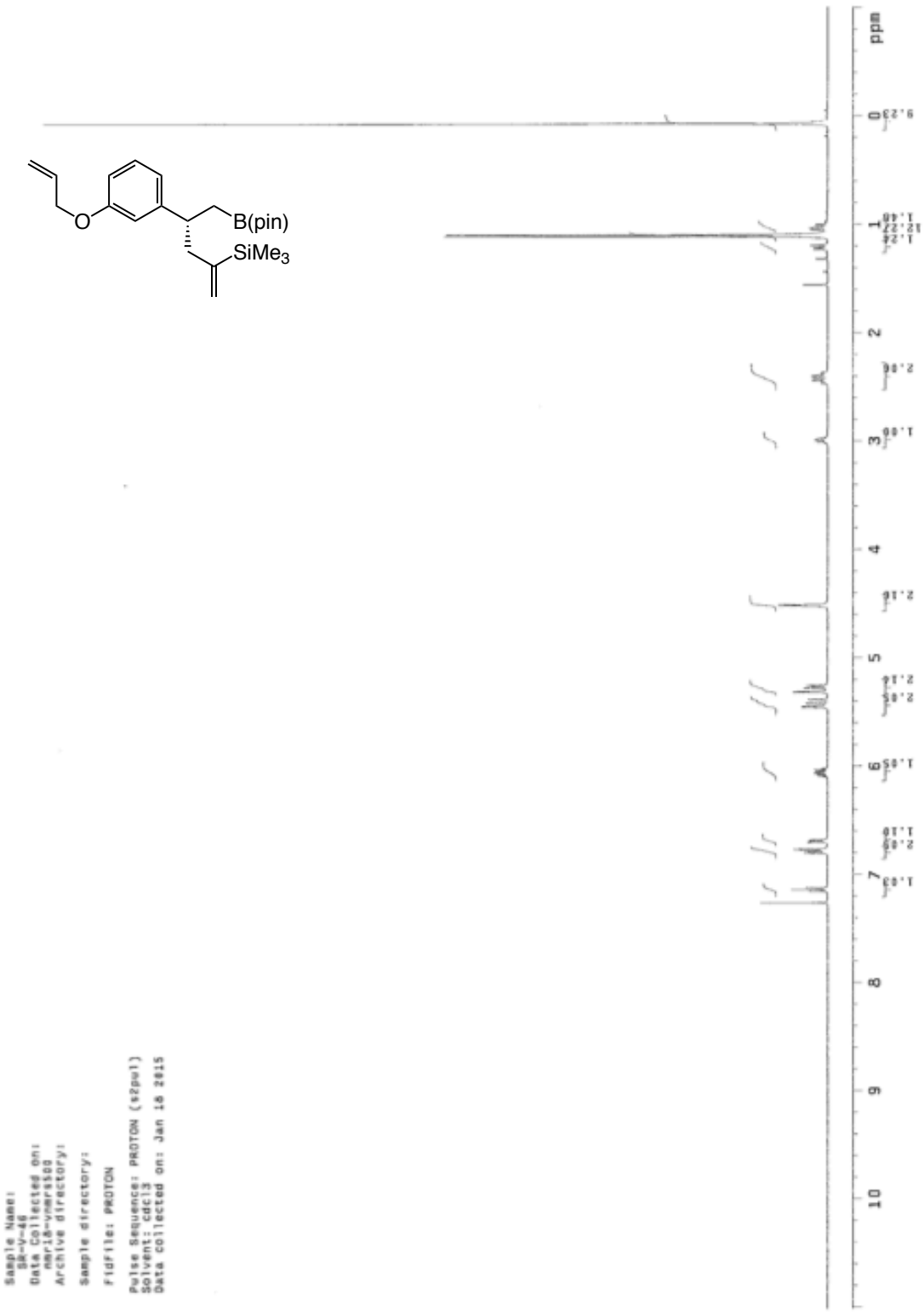
Sample Name:
SA-V-46
Data Collected on:
nmr16-vmrs500
Archive directory:
Sample directory:
Fidfile: PROTON
Pulse Sequence: PROTON (s2pul)
Solvent: cdcl3
Data collected on: Jan 18 2015
ppm

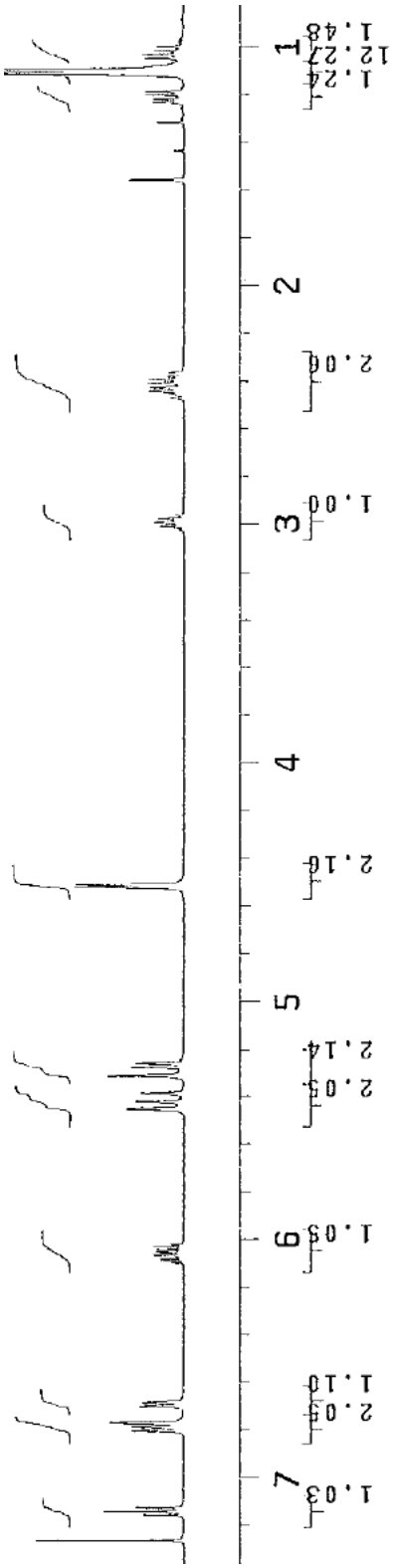
1.48
12.27
1.24
2.06
1.00
2.10
2.14
2.03
1.03
1.10
2.03
1.03
1
2
3
4
5
6
7

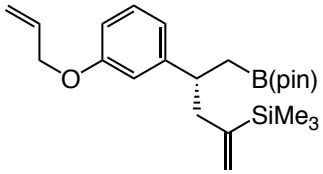
O
B(pin)
SiMe3

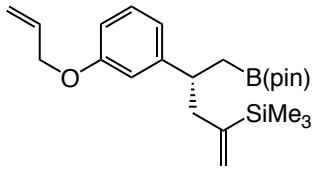
O
B(pin)
SiMe3

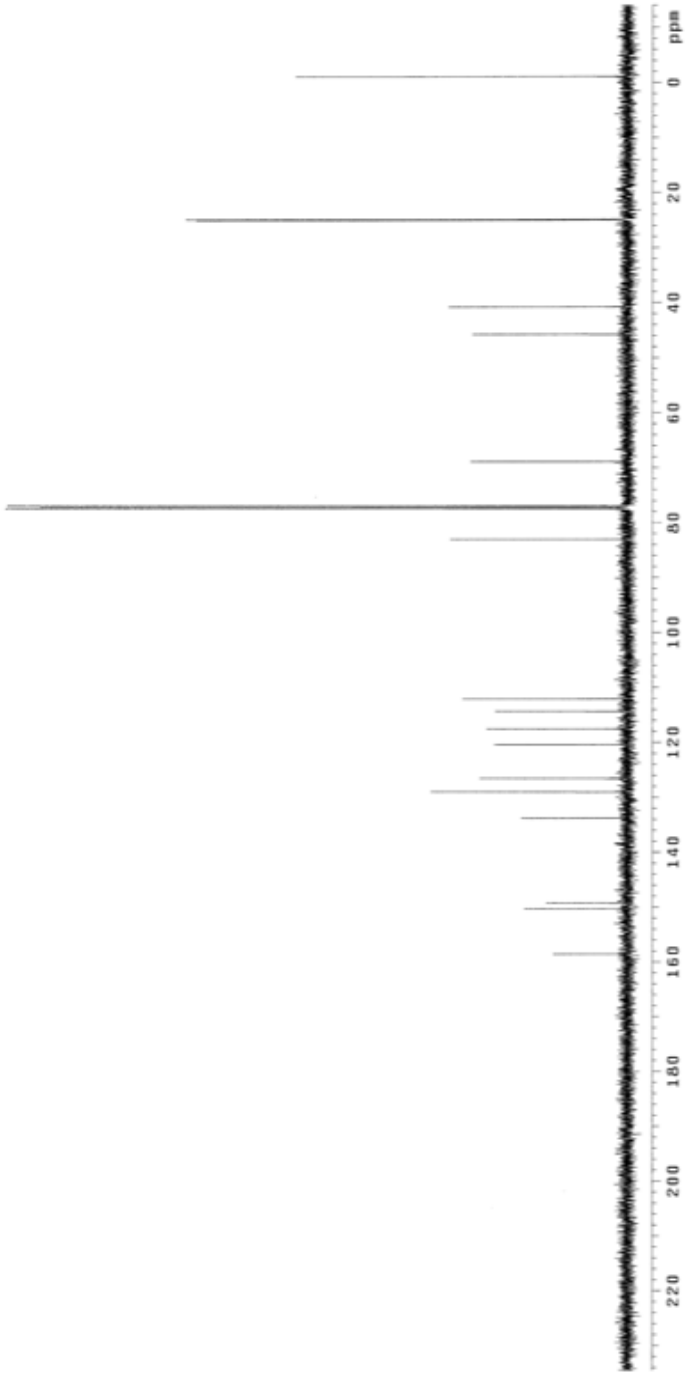
Sample Name:
SS4-13C-carbon
Date Collected on:
mar18-vnmrs59
Archive directory:
Sample directory:
FidFile: CARBON
Pulse Sequence: CARBON (s2pul)
Solvent: cdcl3
Data collected on: Jan 18 2015
ppm
0
20
40
60
80
100
120
140
160
180
200
220

F
B(pin)

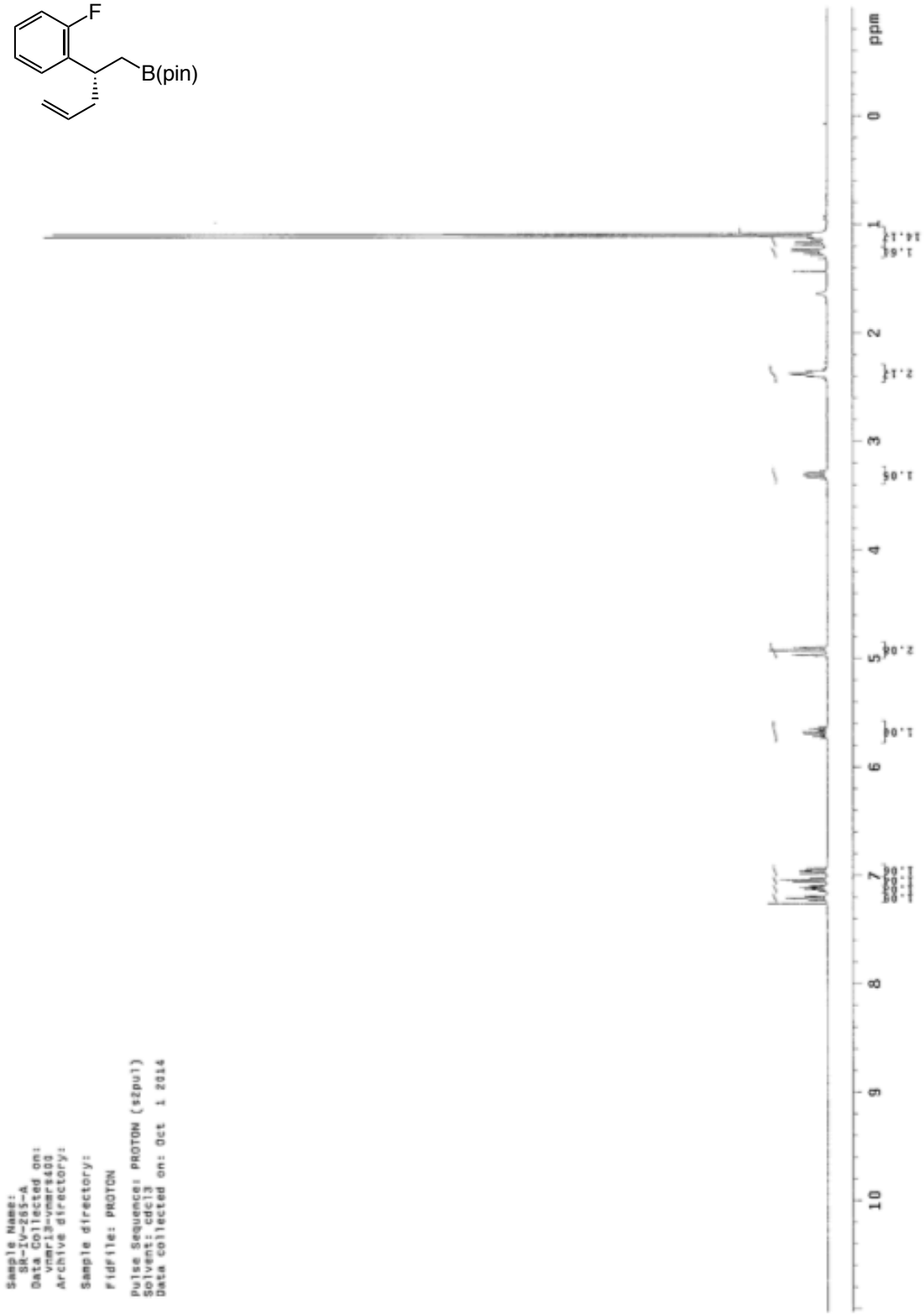
Sample Name:
SR-IV-265-A
Data Collected on:
vnmrj3-vmars400
Archive directory:
Sample directory:
Fidfile: PROTON
Pulse Sequence: PROTON (s2pul)
Solvent: cdcl3
Data collected on: Oct 1 2014
ppm
0
1
2
3
4
5
6
7
8
9
10
14.12
1.65
2.12
1.05
2.04
1.04

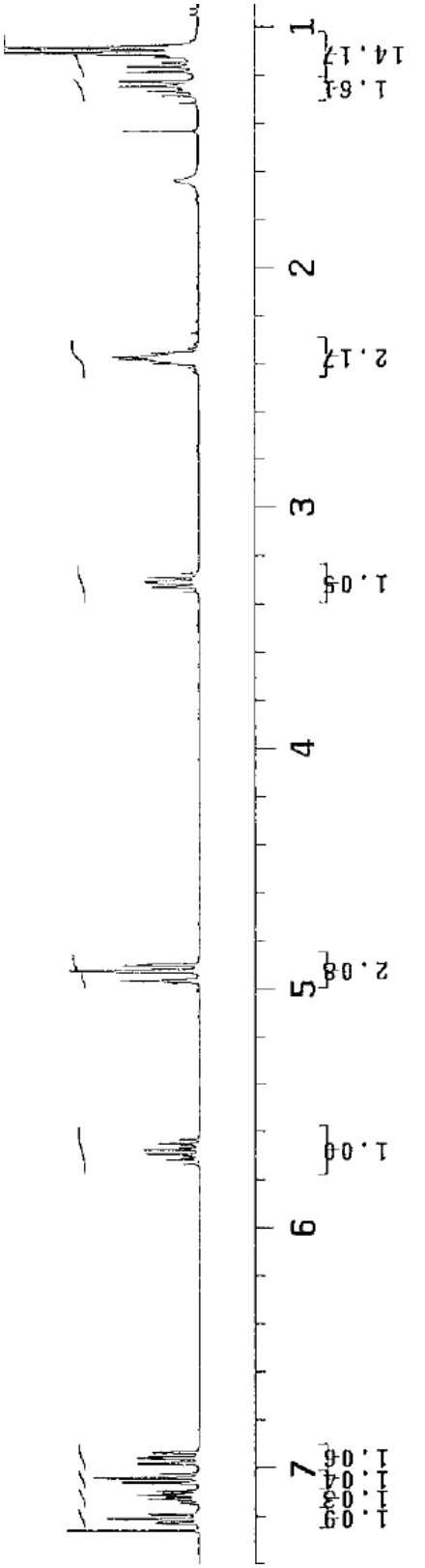
1
2
3
4
5
6
7
14.17
1.61
2.17
1.05
2.08
1.00
1.06
1.04
1.03
1.09

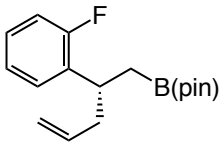
F
B(pin)

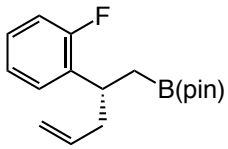
F
B(pin)


Sample Name:
SR-IV-265-A-carbon
Data Collected on:
vnmrj3-vnmrs40
Archive directory:
Sample directory:
Fidfile: CARBON
Pulse Sequence: CARBON (s2pul)
Solvent: cdcl3
Data collected on: Oct 1 2014

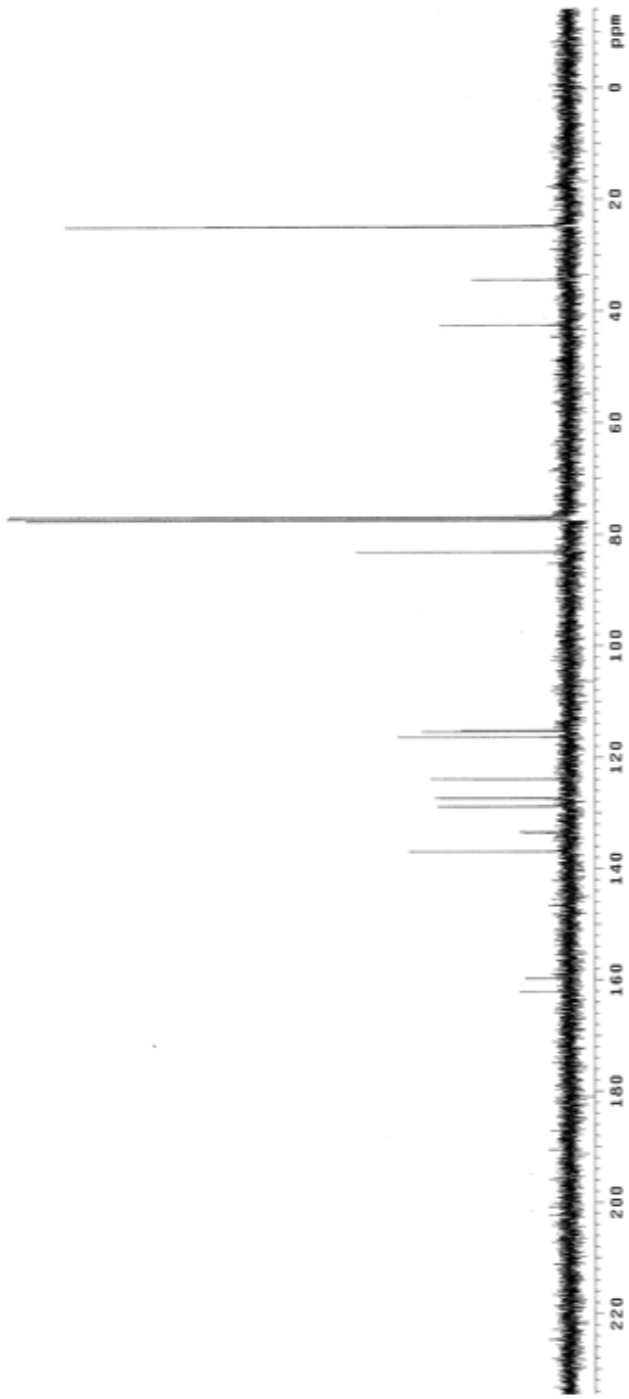
ppm
0
20
40
60
80
100
120
140
160
180
200
220

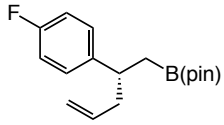
F
B(pin)

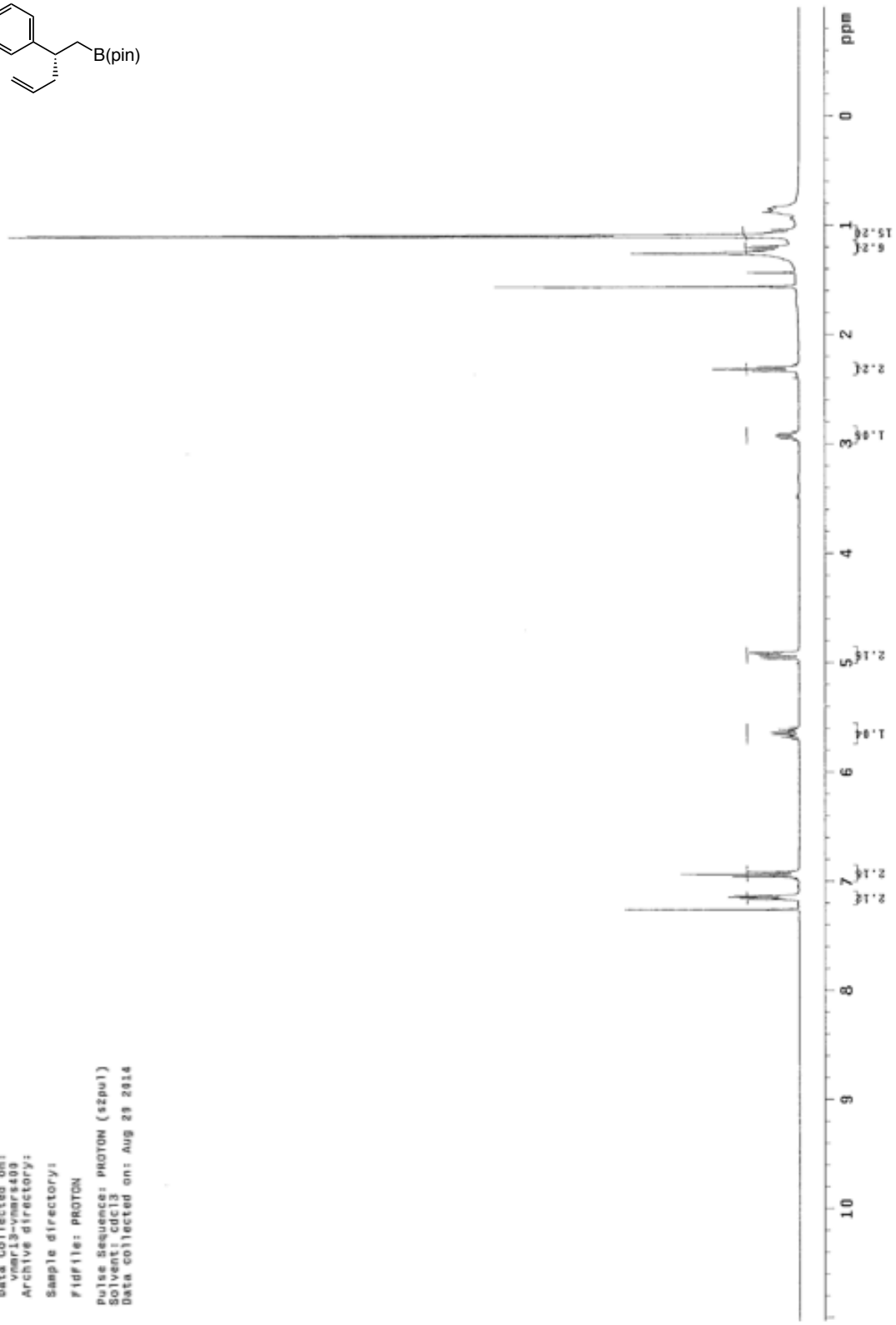
Sample Name:
SR-IV-252-A
Data Collected on:
vmar13-vmar400
Archive directory:
Sample directory:
Fidfile: PROTON
Pulse Sequence: PROTON (szpul)
Solvent: cdcl3
Data collected on: Aug 29 2014
ppm
0
1
2
3
4
5
6
7
8
9
10
15.26
6.26
2.2
1.06
2.16
1.06
2.16
2.16

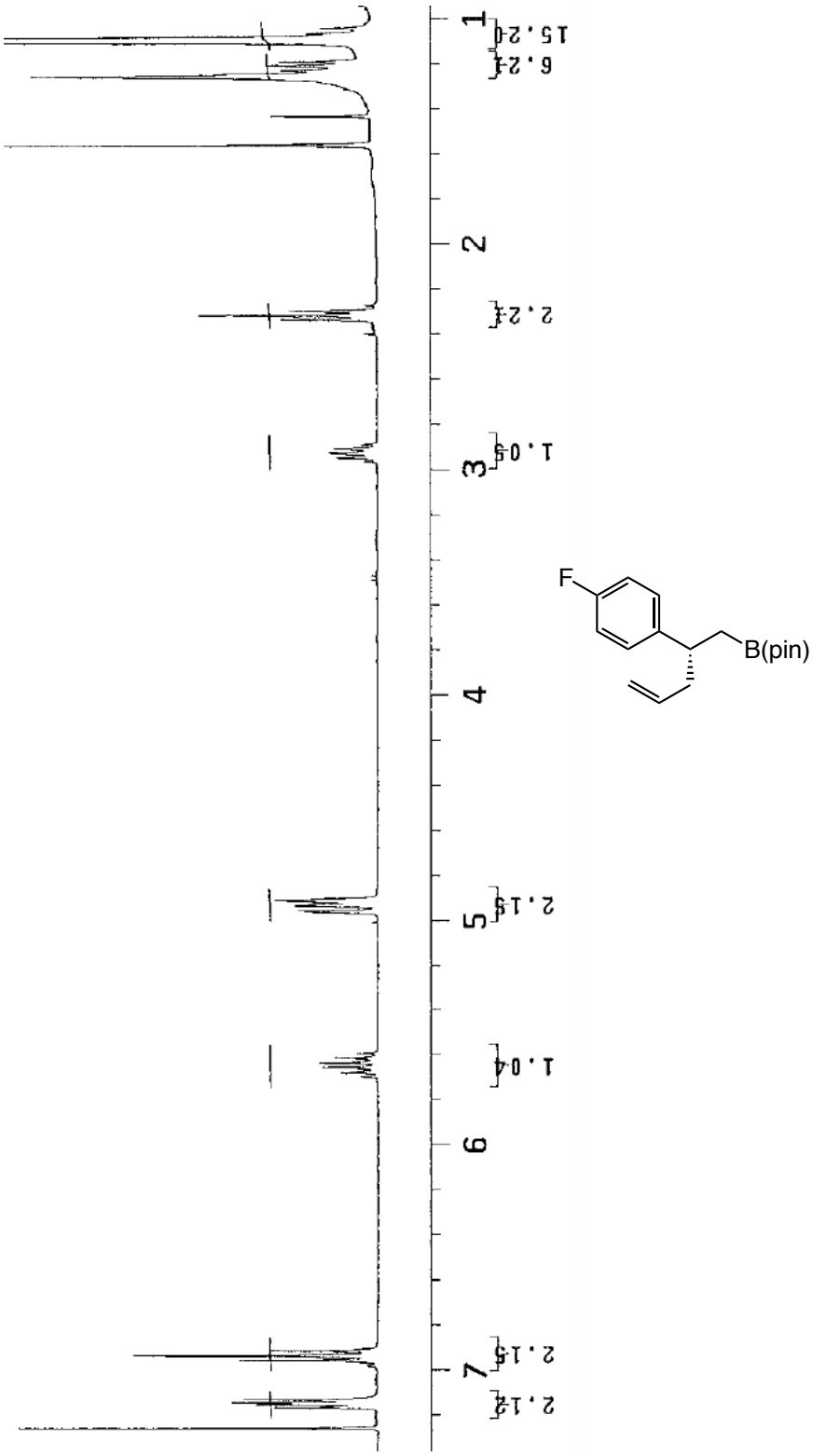
F
B(pin)
15.24
6.24
2.24
1.05
2.15
1.04
2.15
2.14
1
2
3
4
5
6
7

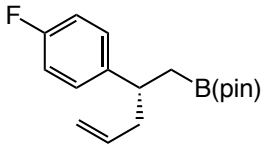
F
B(pin)

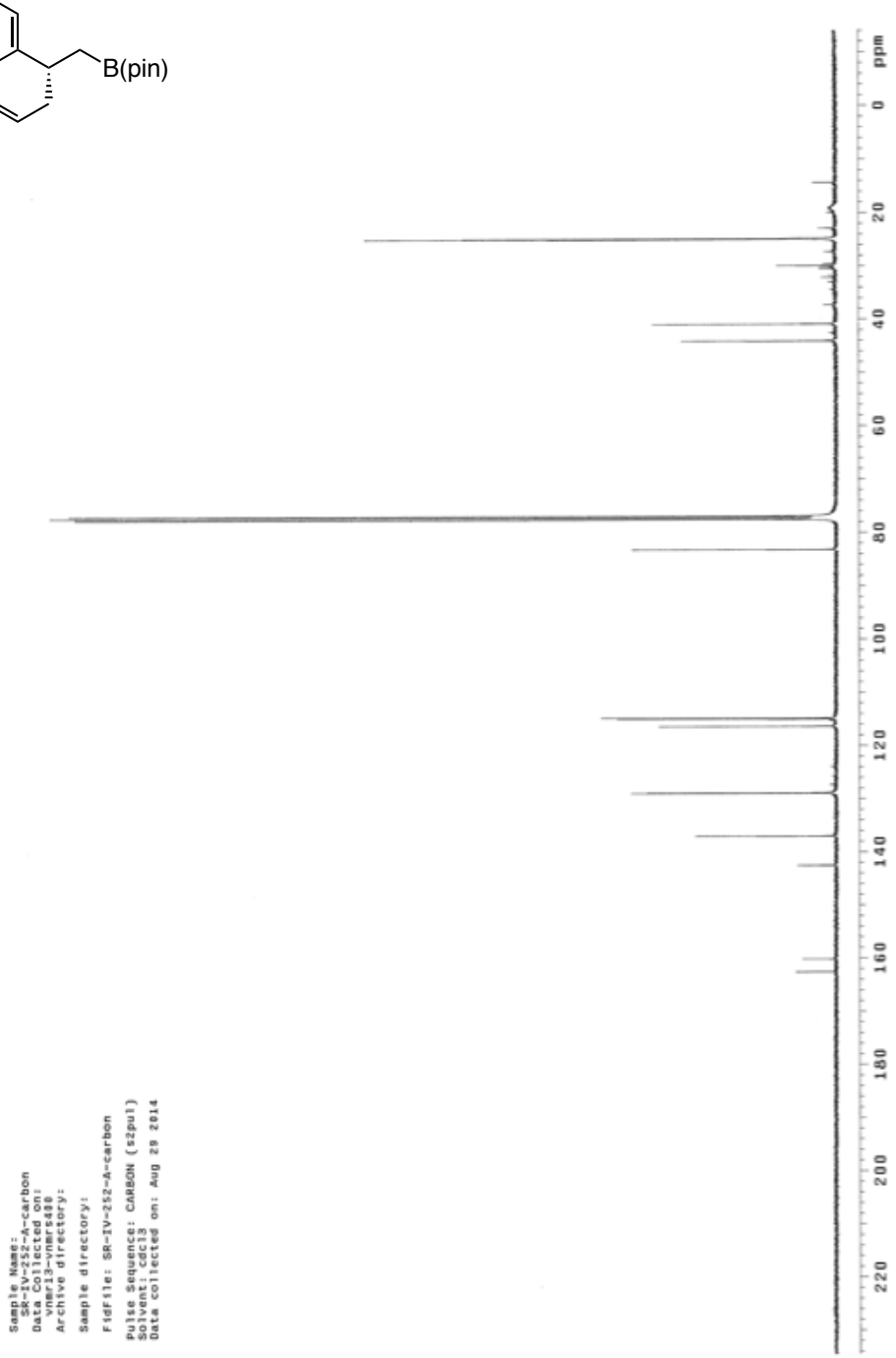
Sample Name:
SR-IV-252-A-carbon
Data Collected on:
nuvera300-400
Archive directory:
Sample directory:
FidFile: SR-IV-252-A-carbon
Pulse Sequence: CARBON (s2pul)
Solvent: CdCl3
Data collected on: Aug 29 2014
ppm
0
20
40
60
80
100
120
140
160
180
200
220

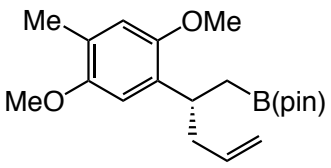
Me
OMe
MeO
B(pin)

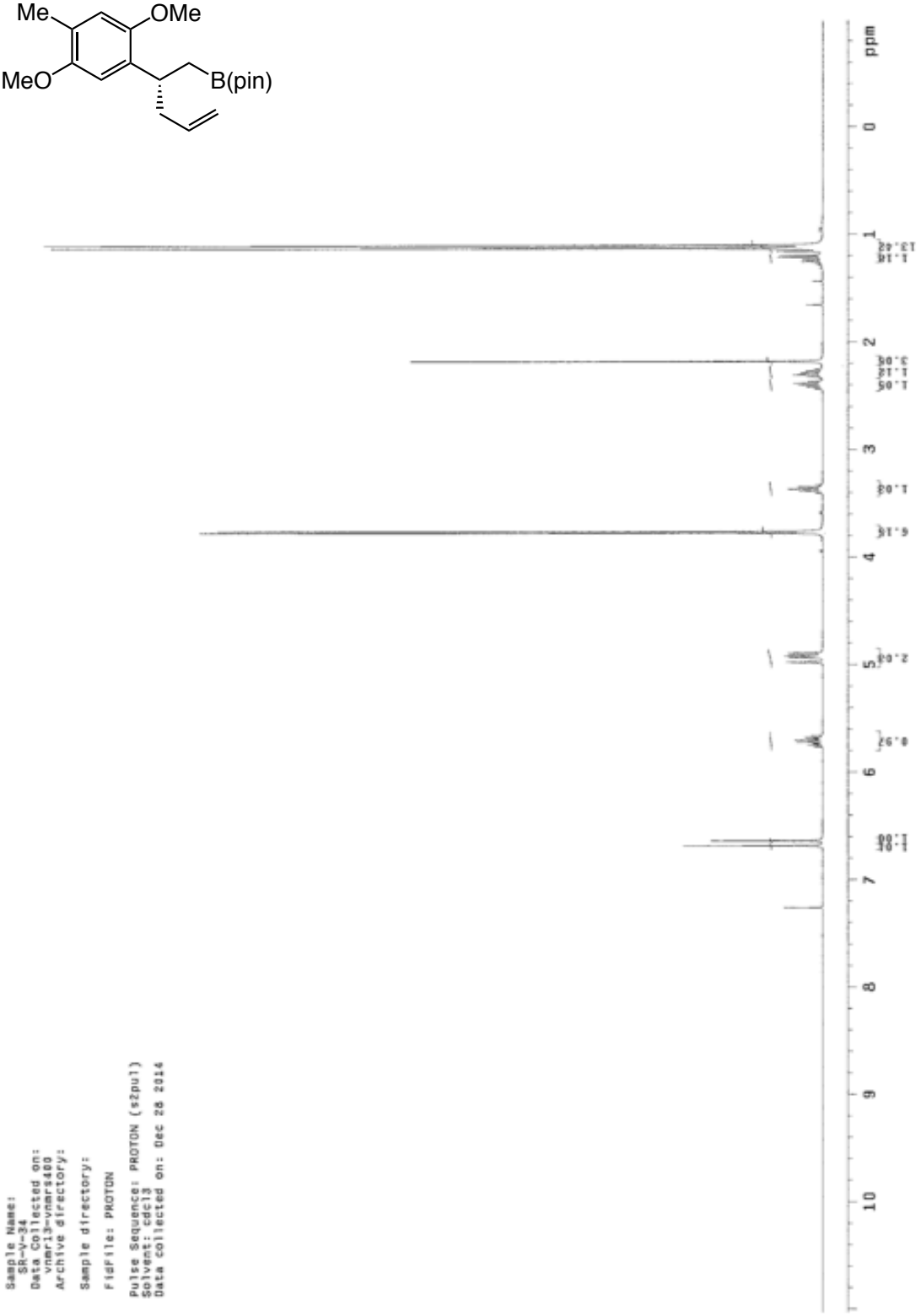
Sample Name:
SR-V-34
Data Collected on:
vnmr13-vnmr400
Archive directory:
Sample directory:
FidFile: PROTON
Pulse Sequence: PROTON (s2pul)
Solvent: cdcl3
Data collected on: Dec 28 2014
ppm
0
1
2
3
4
5
6
7
8
9
10

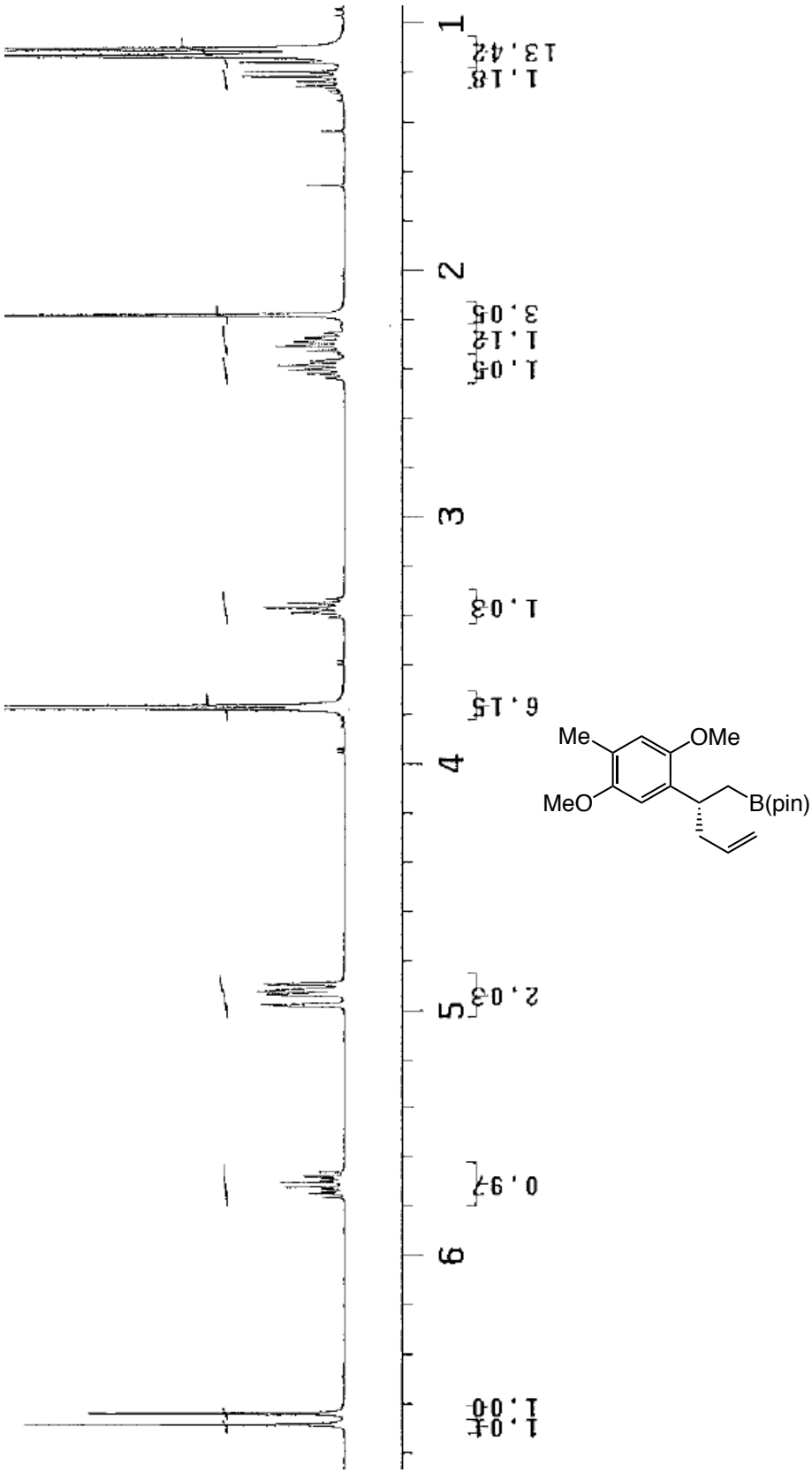
Me
OMe
MeO
B(pin)

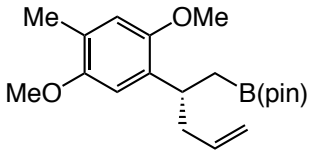
Me
OMe
MeO
B(pin)

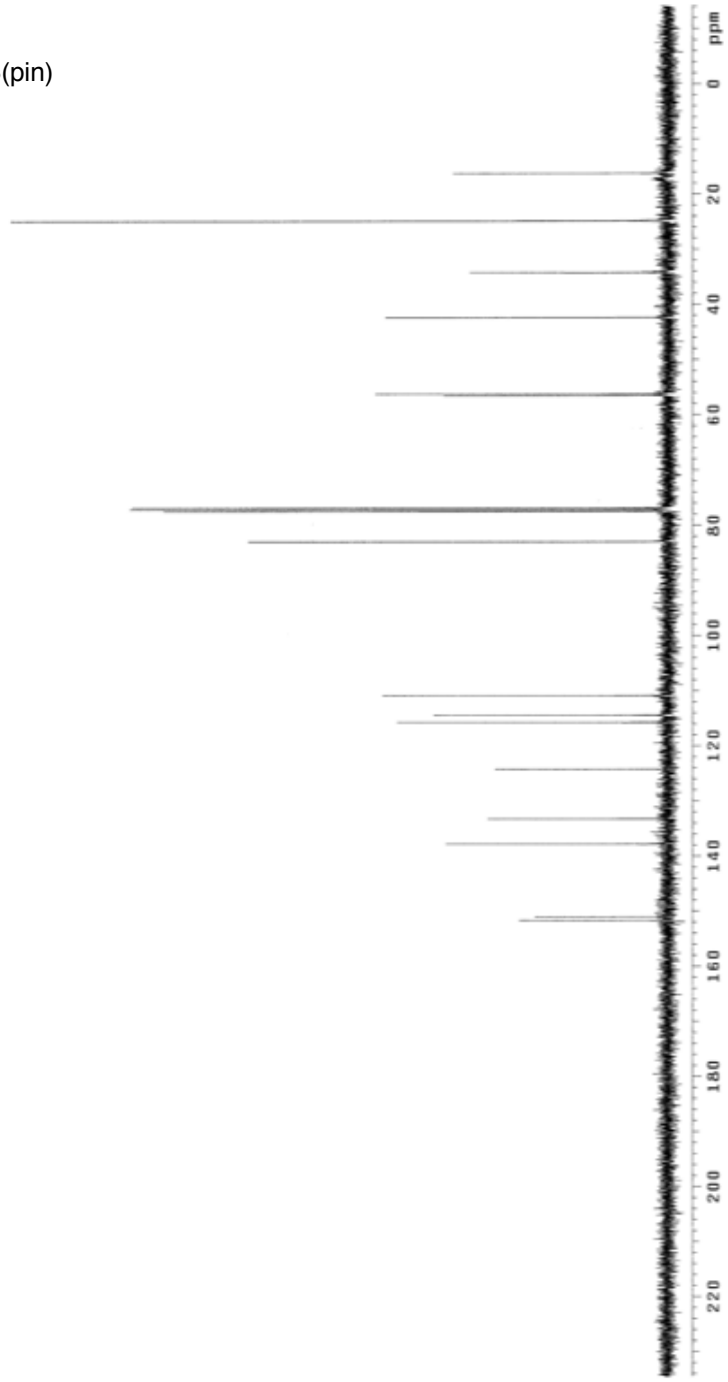
Sample Name:
Pulse Sequence: CARBON (s2pul)
Solvent: cdcl3
Data collected on: Dec 28 2014
ppm
220
200
180
160
140
120
100
80
60
40
20
0

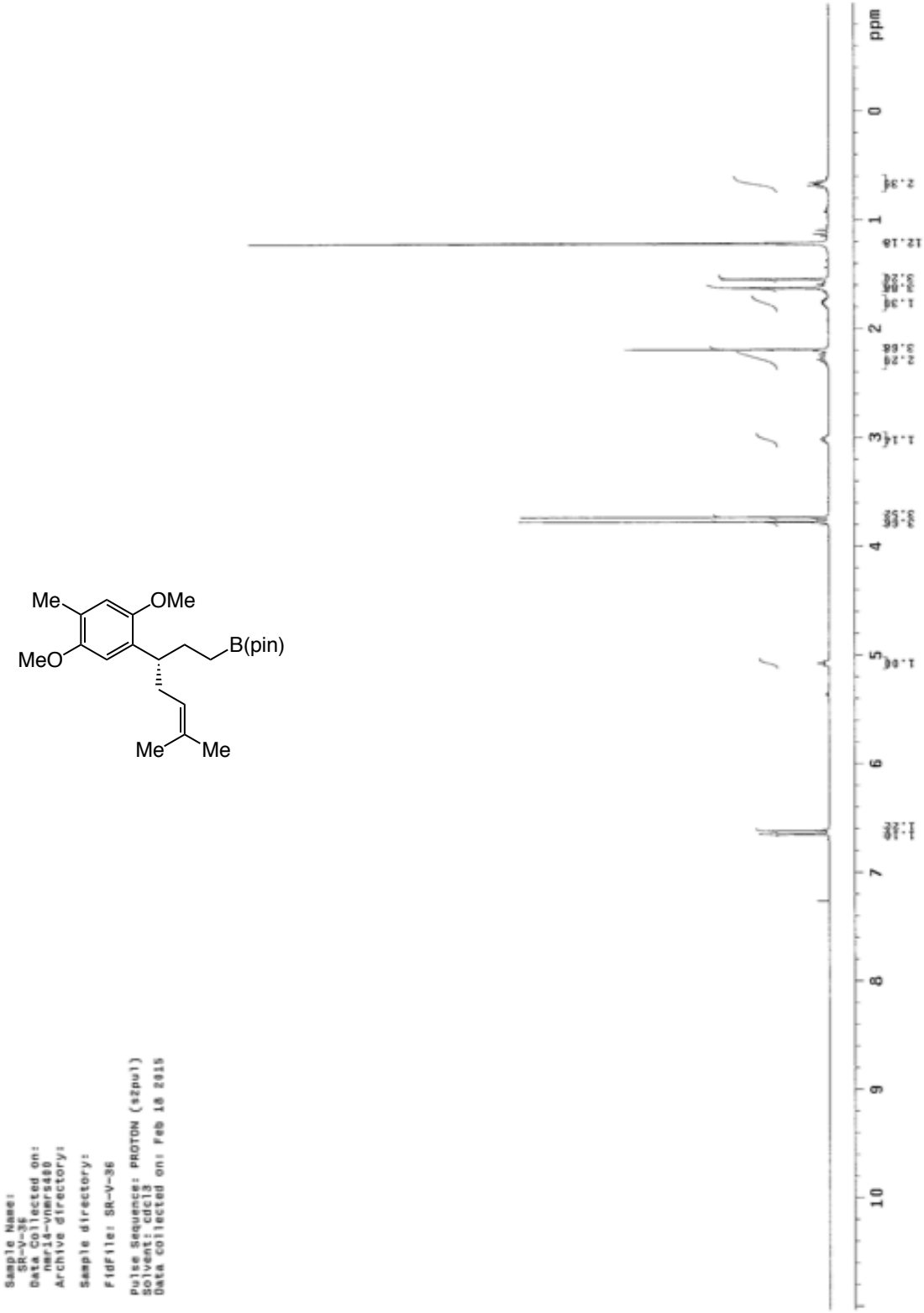
Sample Name:
SR-V-36
Data Collected on:
nmr14-vnmrs400
Archive directory:
Sample directory:
FidFile: SR-V-36
Pulse Sequence: PROTON (s2pul)
Solvent: cdcl3
Data collected on: Feb 18 2015
Me
OMe
MeO
B(pin)
Me
Me
ppm
0
1
2
3
4
5
6
7
8
9
10
2.34
12.18
1.34
2.24
1.14
1.00

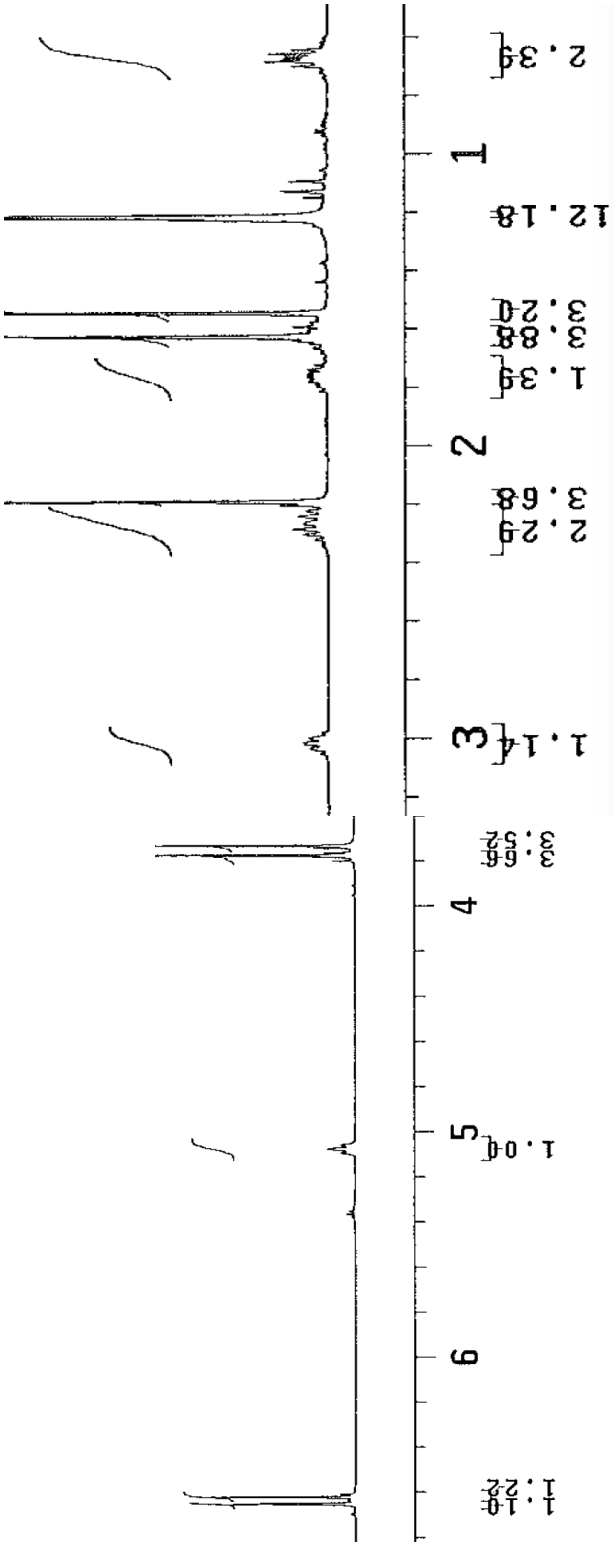
1.10
1.22
1.04
3.65
3.52
1.14
2.29
3.68
1.39
3.88
3.20
12.18
2.39
1
2
3
4
5
6

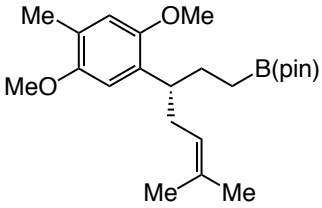
Me
OMe
MeO
B(pin)
Me
Me

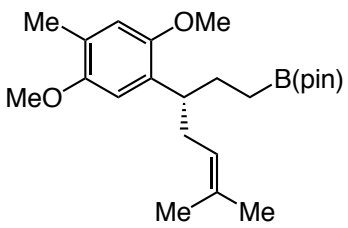
Me
OMe
MeO
B(pin)
Me
Me

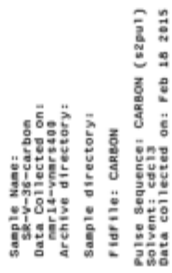
Sample Name:
SR-V-36-carbon
Data Collected on:
mar14-vnmrs400
Archive directory:
Sample directory:
Fidfile: CARBON
Pulse Sequence: CARBON (s2pul)
Solvent: cdcl3
Data collected on: Feb 18 2015

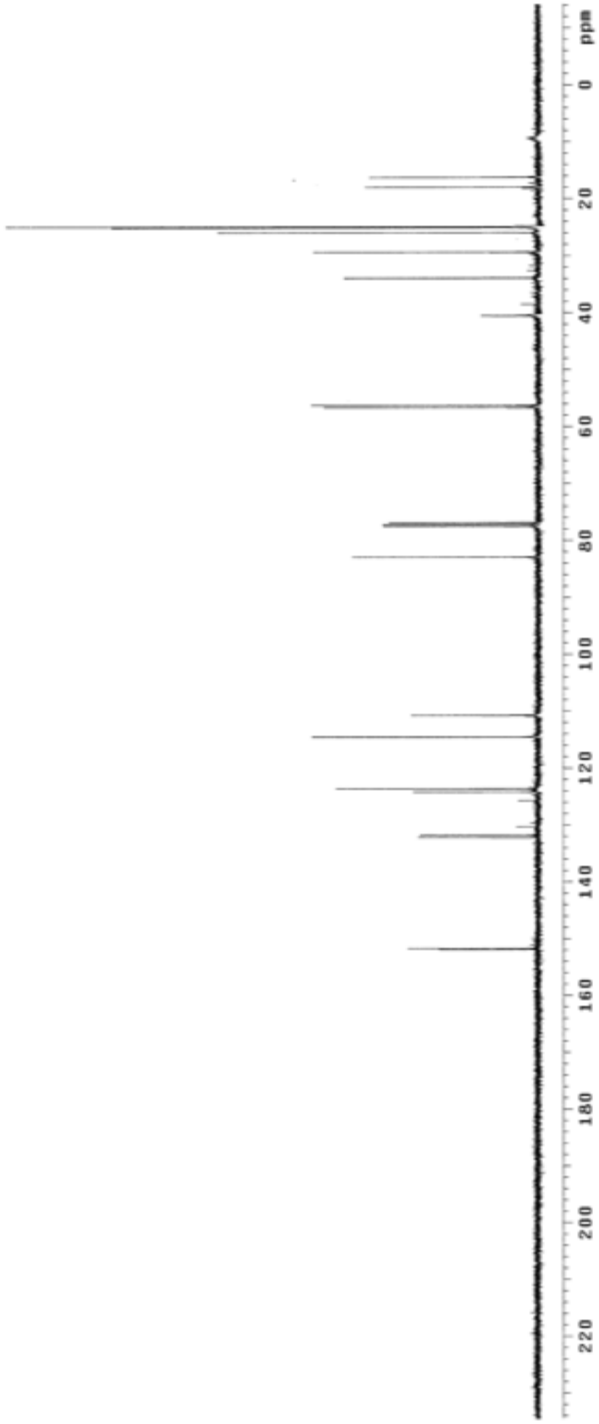
ppm
0
20
40
60
80
100
120
140
160
180
200
220

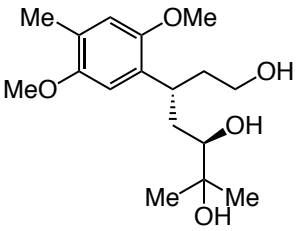
Me
OMe
MeO
OH
OH
Me
Me
OH

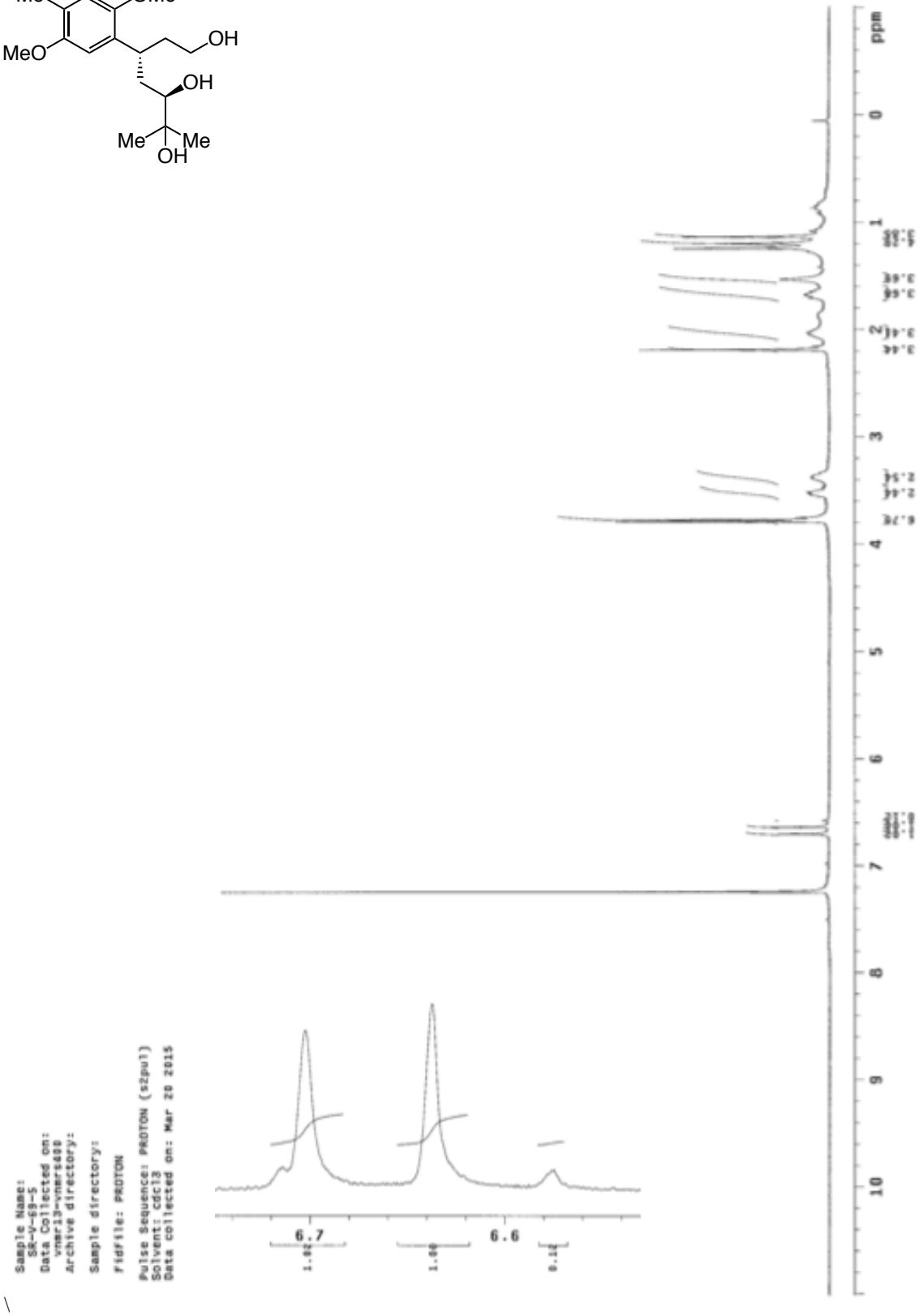
Sample Name:
SA-V-69-5
Data Collected on:
vnmr13-vnmr5400
Archive directory:
Sample directory:
Fidfile: PROTON
Pulse Sequence: PROTON (s2pul)
Solvent: cdcl3
Data collected on: Mar 20 2015
6.7
6.6
1.02
1.00
0.12
ppm
0
1
2
3
4
5
6
7
8
9
10

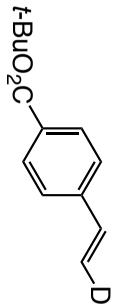

JL-IV-44PD

Sample Name:
JL-IV-44PD
Data Collected on:
vnmr13-vnmrs400
Archive directory:

Sample directory:

FidFile: JL-IV-44PD

Pulse Sequence: PROTON (s2pul)
Solvent: cdcl3
Data collected on: Oct 7 2015

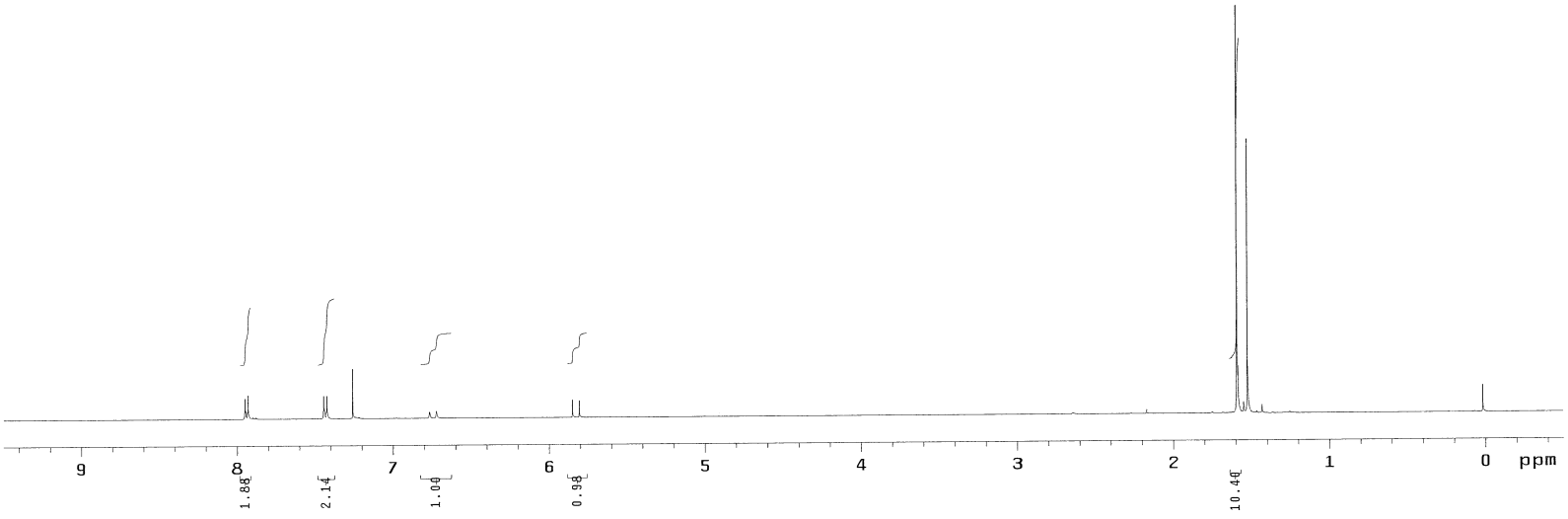

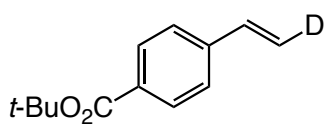

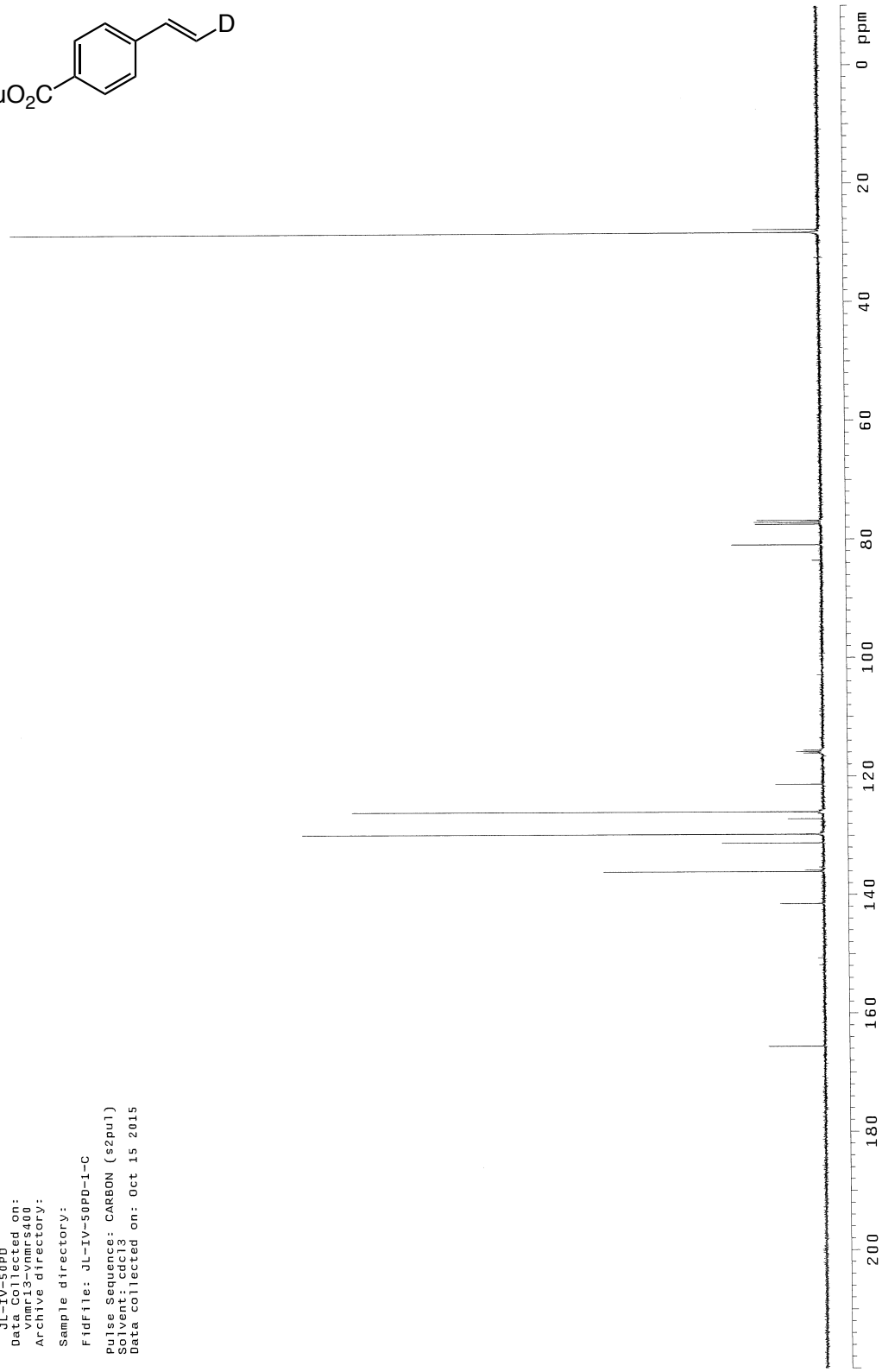

JL-IV-50PD

Sample Name:
JL-IV-50PD
Data Collected on:
vnmrs13-vnmrs400
Archive directory:

Sample directory:

FidFile: JL-IV-50PD-1-C

Pulse Sequence: CARBON (s2pul)
Solvent: cdcl3
Data collected on: Oct 15 2015

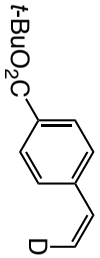

JL-IV-45PD

Sample Name:
JL-IV-45PD
Data Collected on:
vnmr13-vnmrs400
Archive directory:

Sample directory:

FidFile: JL-IV-45PD

Pulse Sequence: PROTON (s2pul)
Solvent: cdcl3
Data collected on: Oct 7 2015

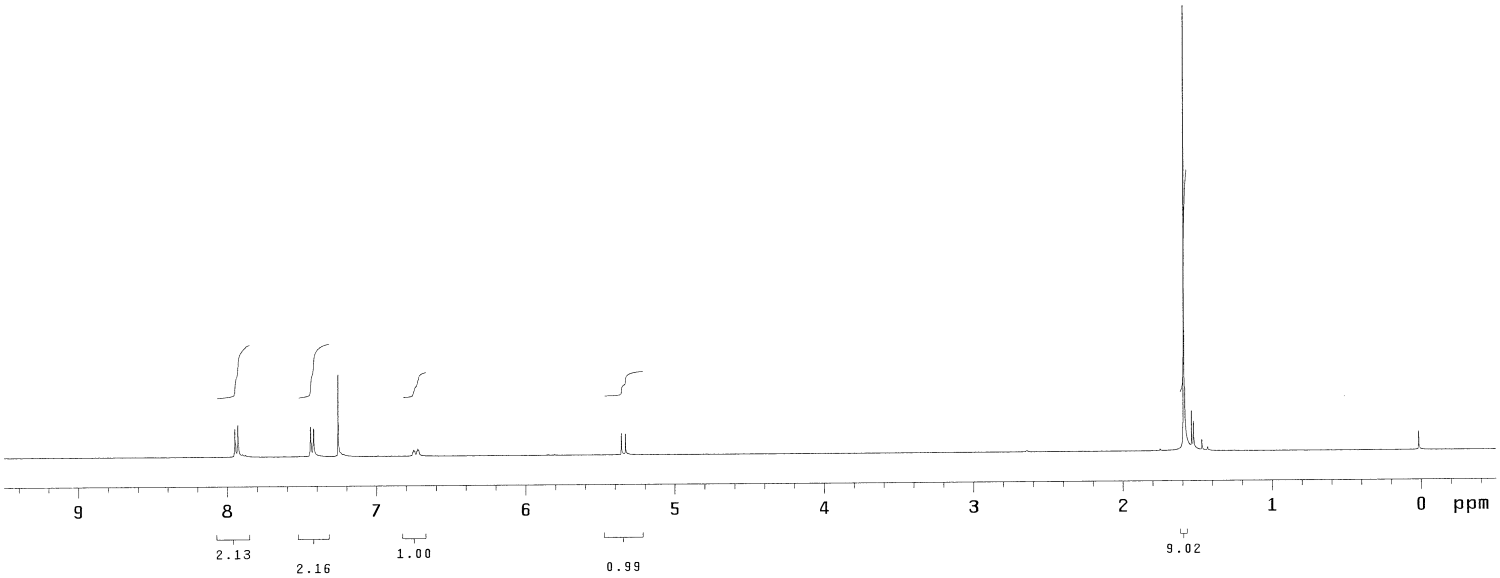

t-BuO2C
D

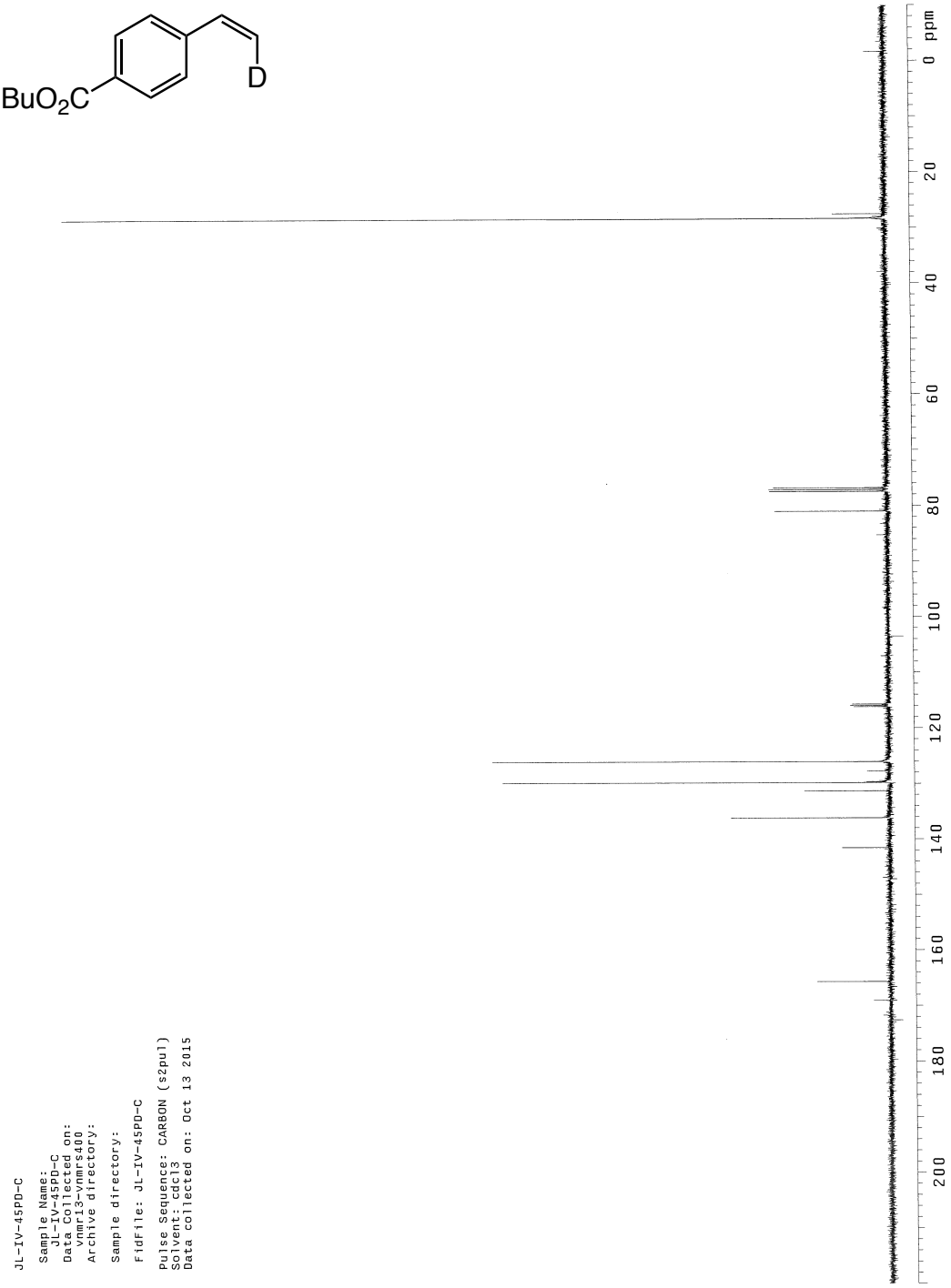
JL-IV-45PD-C
Sample Name:
JL-IV-45PD-C
Data Collected on:
vnmr13-vnmrs400
Archive directory:
Sample directory:
FidFile: JL-IV-45PD-C
Pulse Sequence: CARBON (s2pul)
Solvent: cdcl3
Data collected on: Oct 13 2015
ppm
0
20
40
60
80
100
120
140
160
180
200

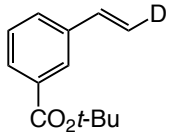

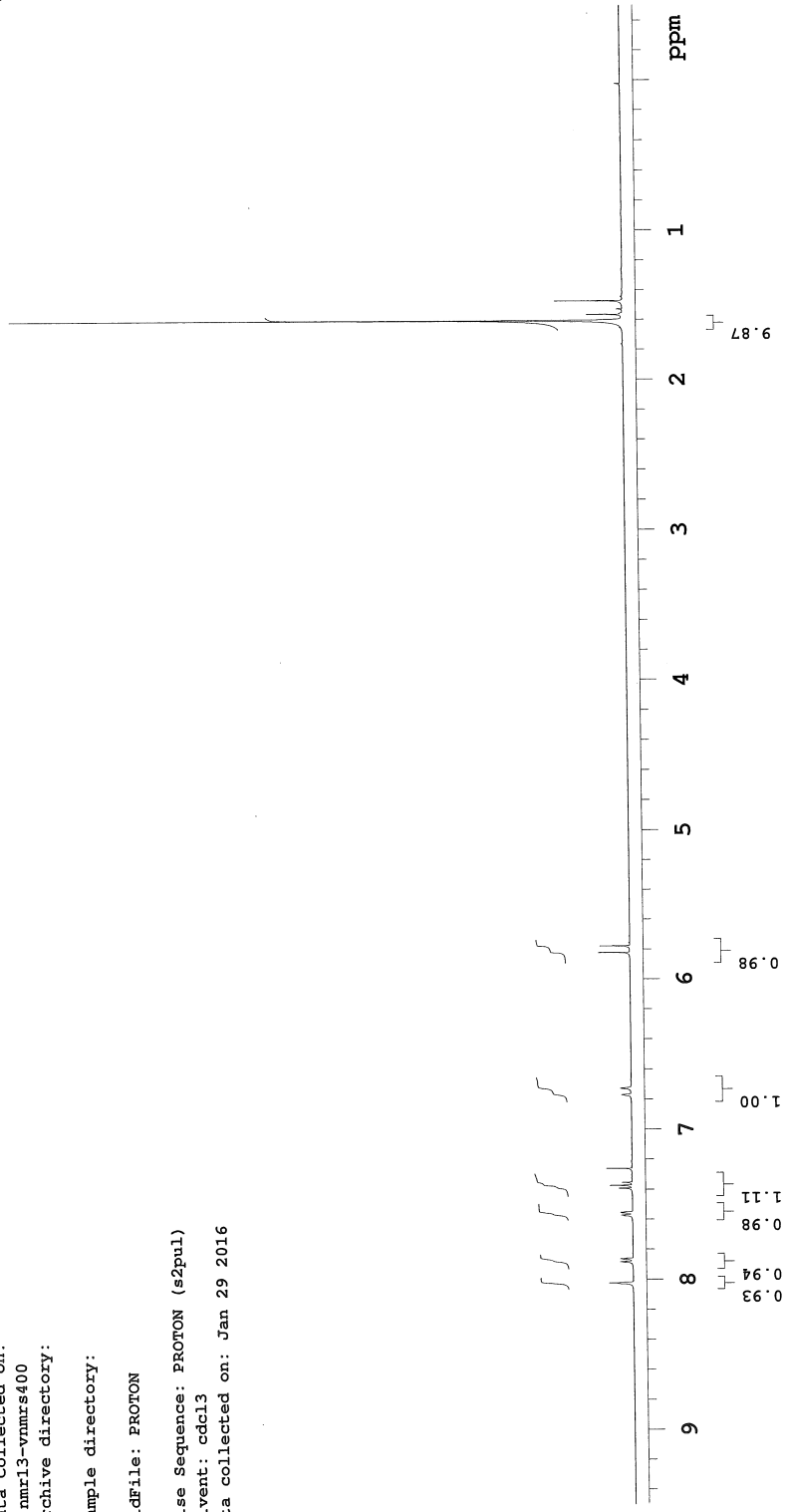

JL-IV-179PD

Sample Name:
JL-IV-179PD
Data Collected on:
nmr13-vnmrs400
Archive directory:

Sample directory:

FidFile: PROTON

Pulse Sequence: PROTON (s2pul)
Solvent: cdcl3
Data collected on: Jan 29 2016

JL-IV-179PD-C

Sample Name:
JL-IV-179PD-C
Data Collected on:
nmr13-vnmrs400
Archive directory:

Sample directory:

FidFile: CARBON

Pulse Sequence: CARBON (s2pul)
Solvent: cdcl3
Data collected on: Jan 30 2016

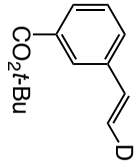

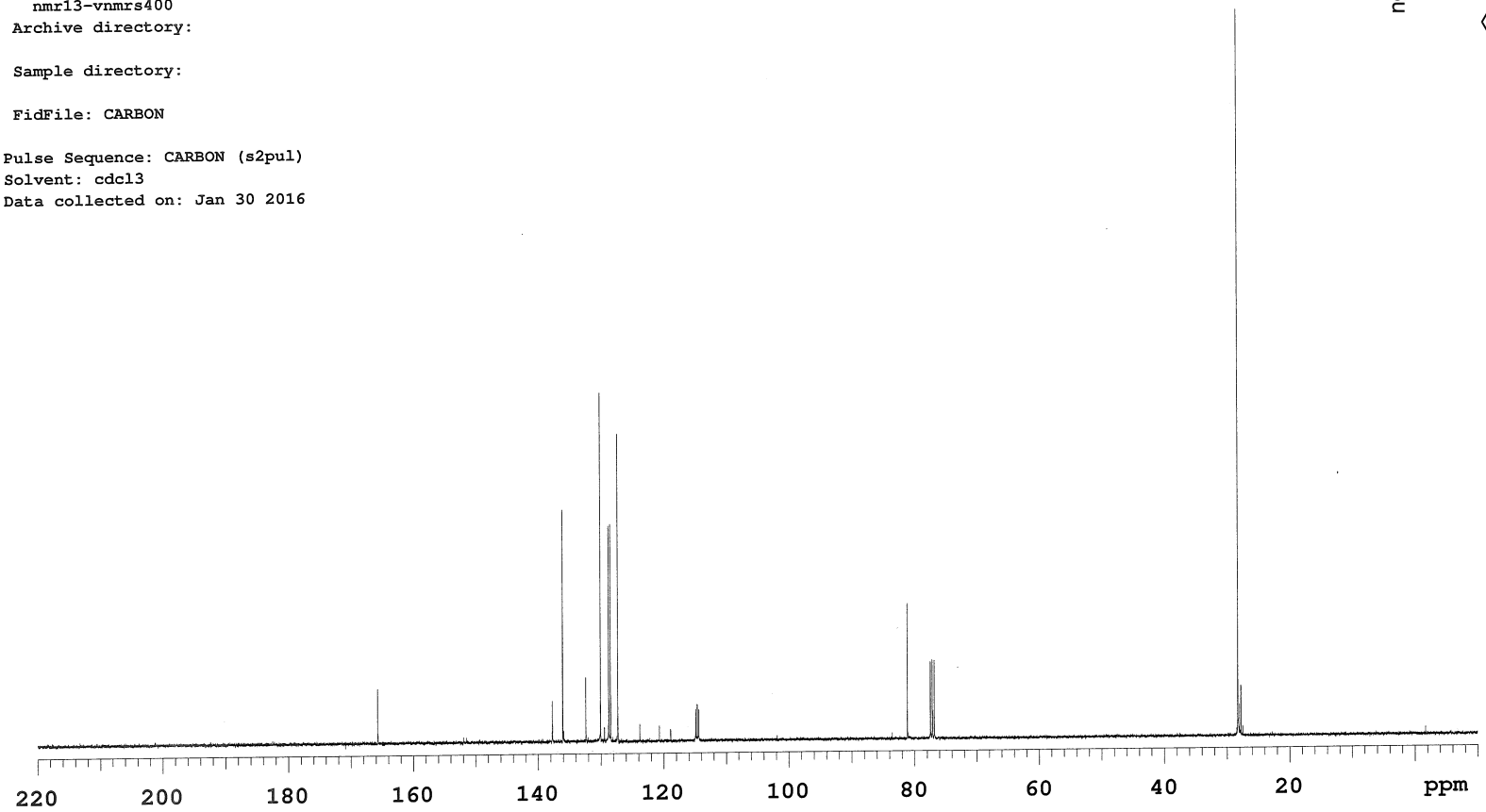

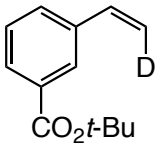

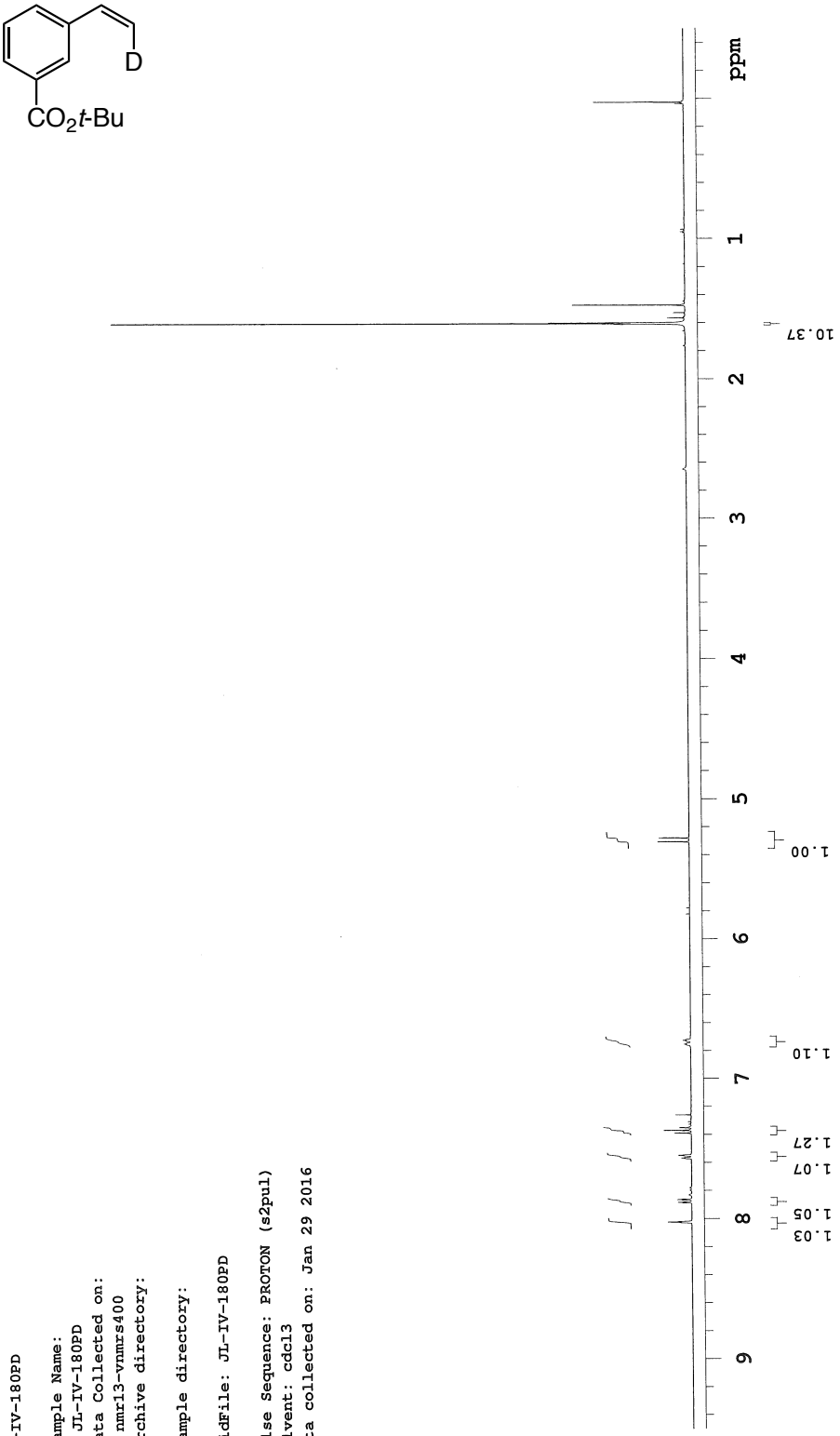

JL-IV-180PD

Sample Name:
JL-IV-180PD
Data Collected on:
nmr13-vnmrs400
Archive directory:

Sample directory:

FidFile: JL-IV-180PD

Pulse Sequence: PROTON (s2pul)
Solvent: cdcl3
Data collected on: Jan 29 2016

JL-IV-180PD-C

Sample Name:
JL-IV-180PD-C
Data Collected on:
nmr13-vnmrs400
Archive directory:

Sample directory:

FidFile: CARBON

Pulse Sequence: CARBON (s2pul)
Solvent: cdcl3
Data collected on: Jan 30 2016

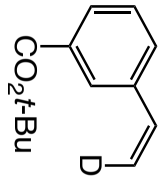

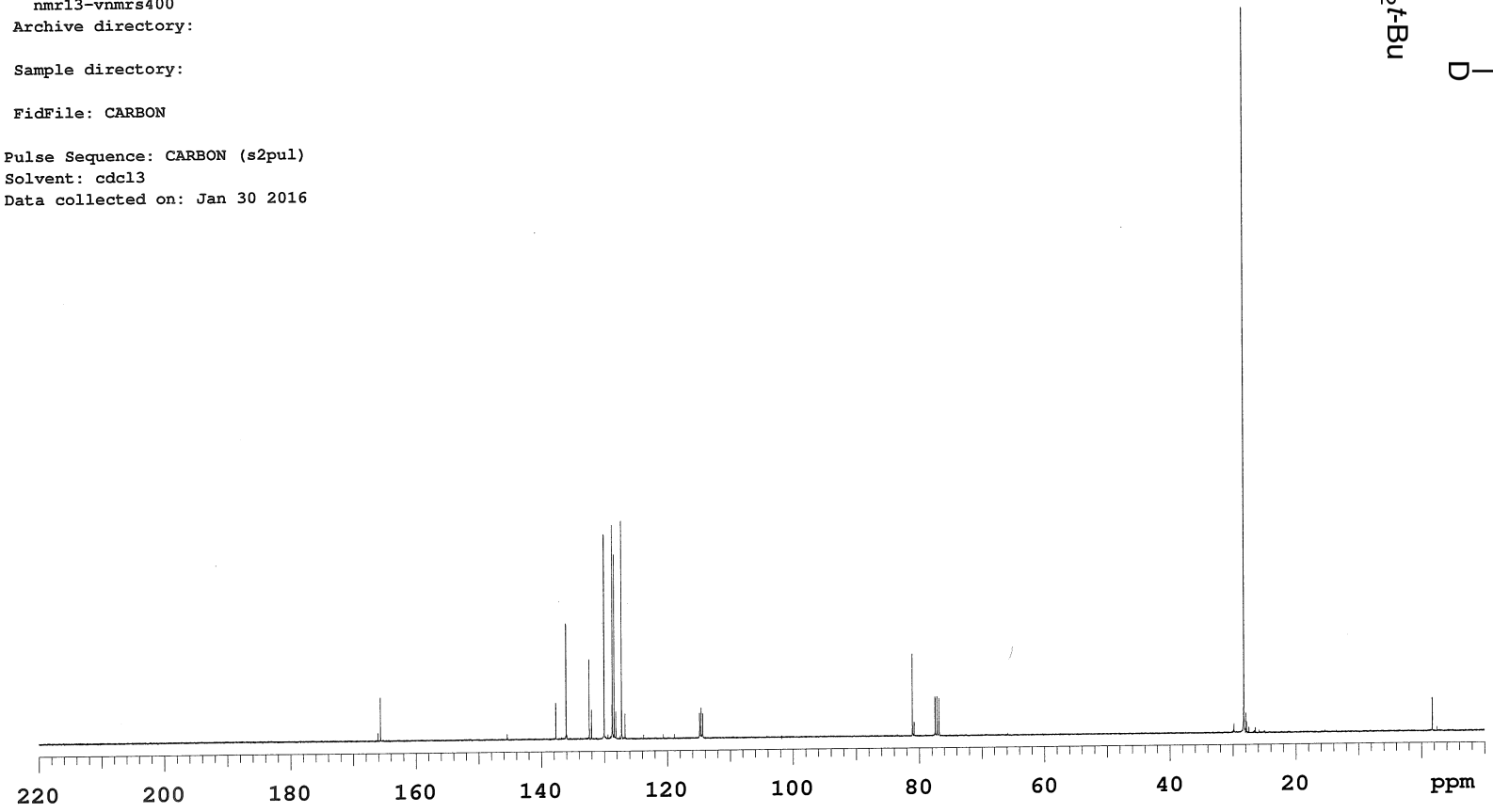

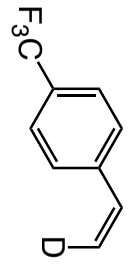

JL-IV-180PD-C

Sample Name:
JL-IV-180PD-C
Data Collected on:
nmr13-vnmrs400
Archive directory:

Sample directory:

FidFile: CARBON

Pulse Sequence: CARBON (s2pul)
Solvent: cdcl3
Data collected on: Jan 30 2016

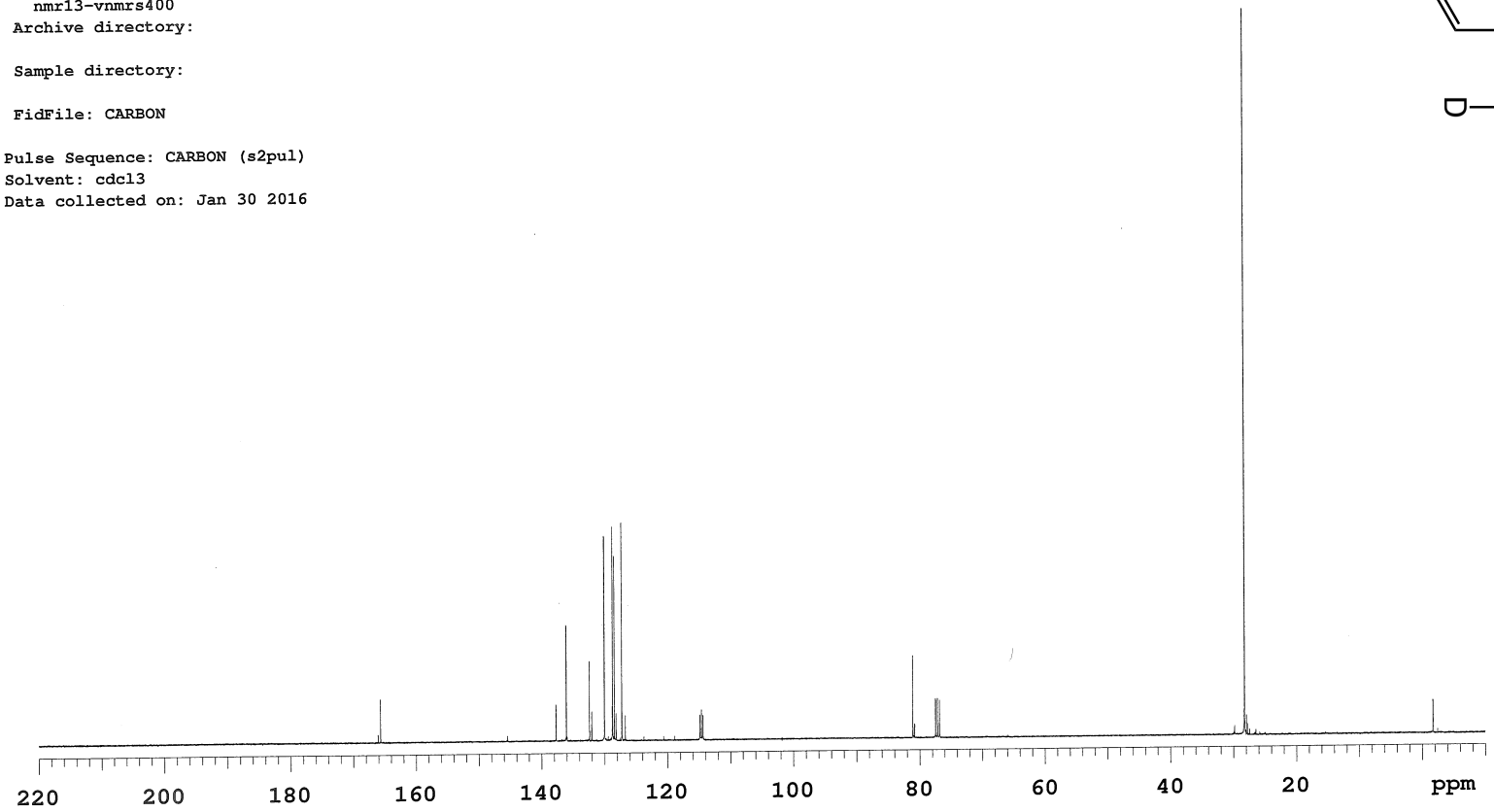

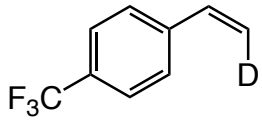
F3C
D

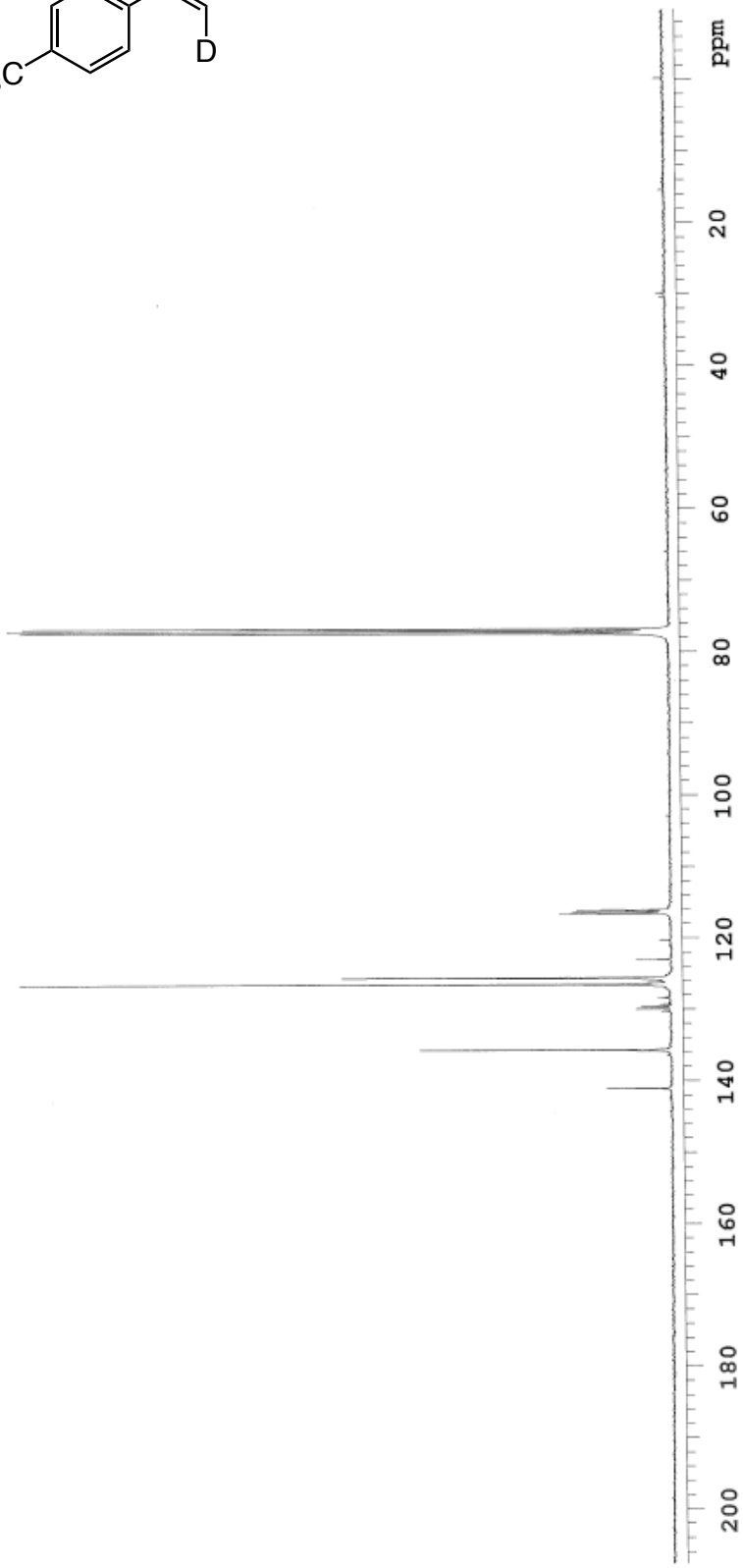
ppm
20
40
60
80
100
120
140
160
180
200

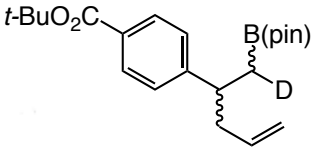

from *E* olefin

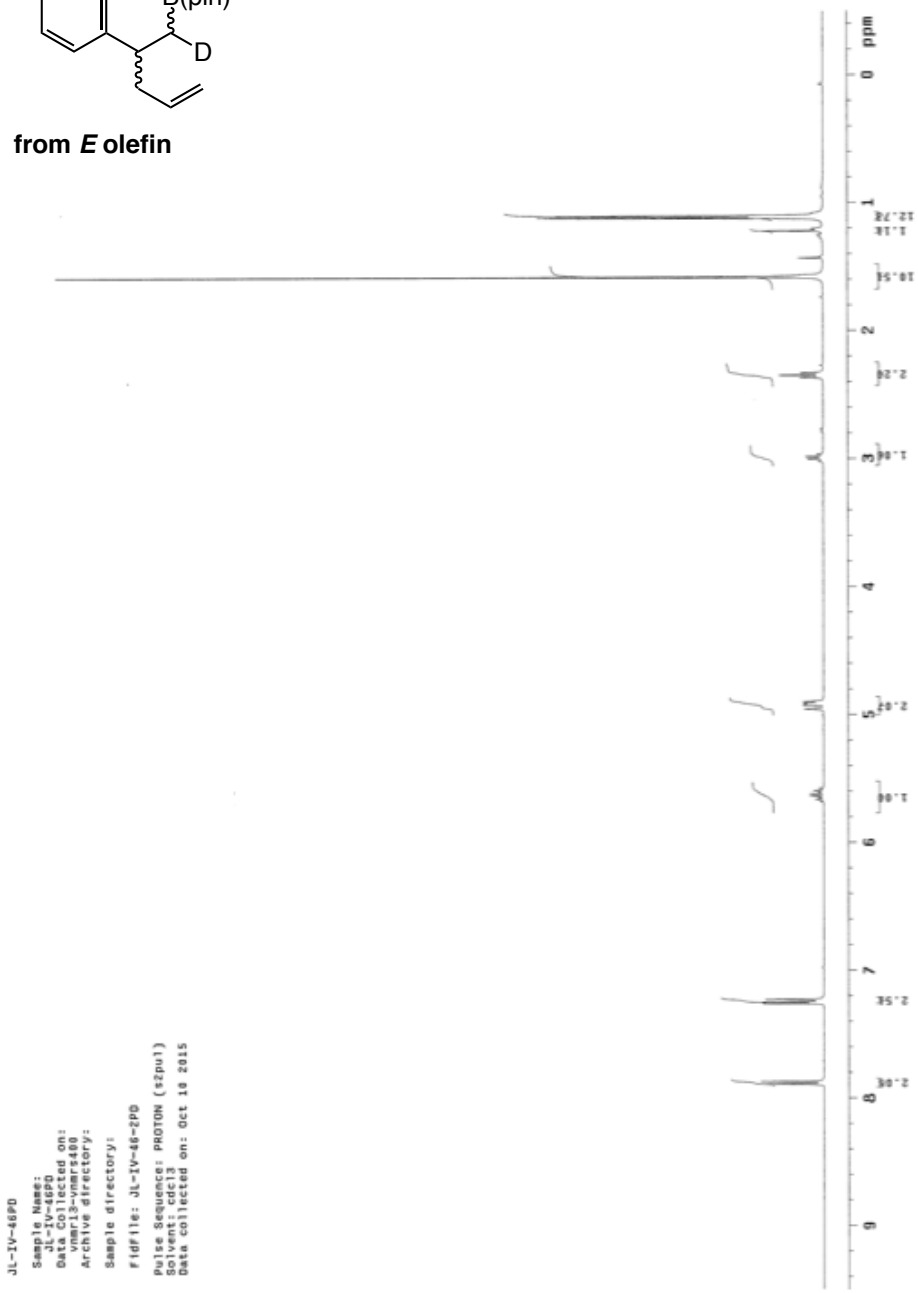

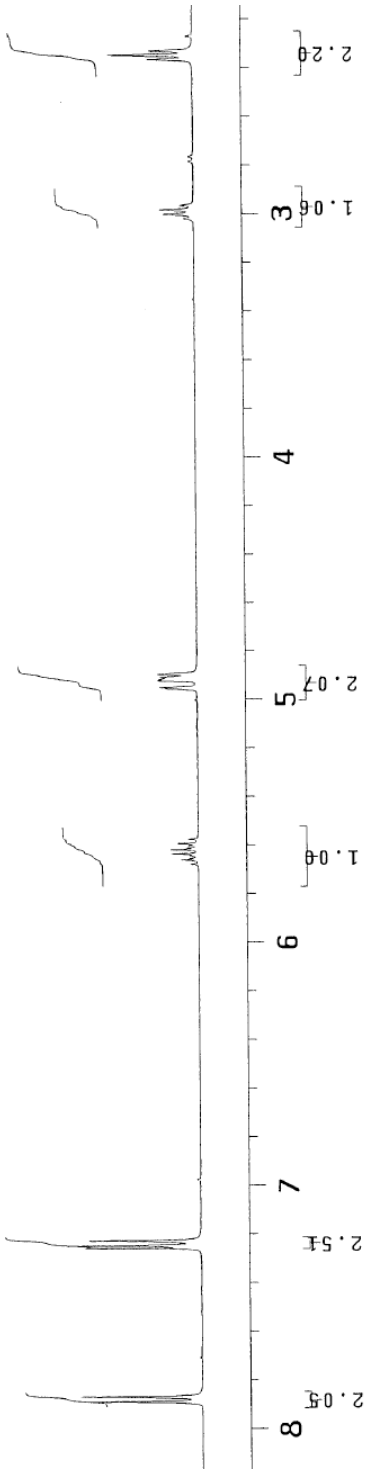

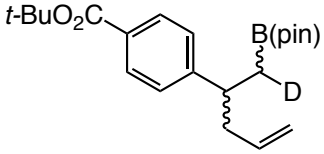

from *E* olefin

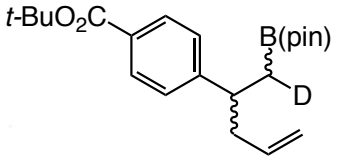

from *E* olefin

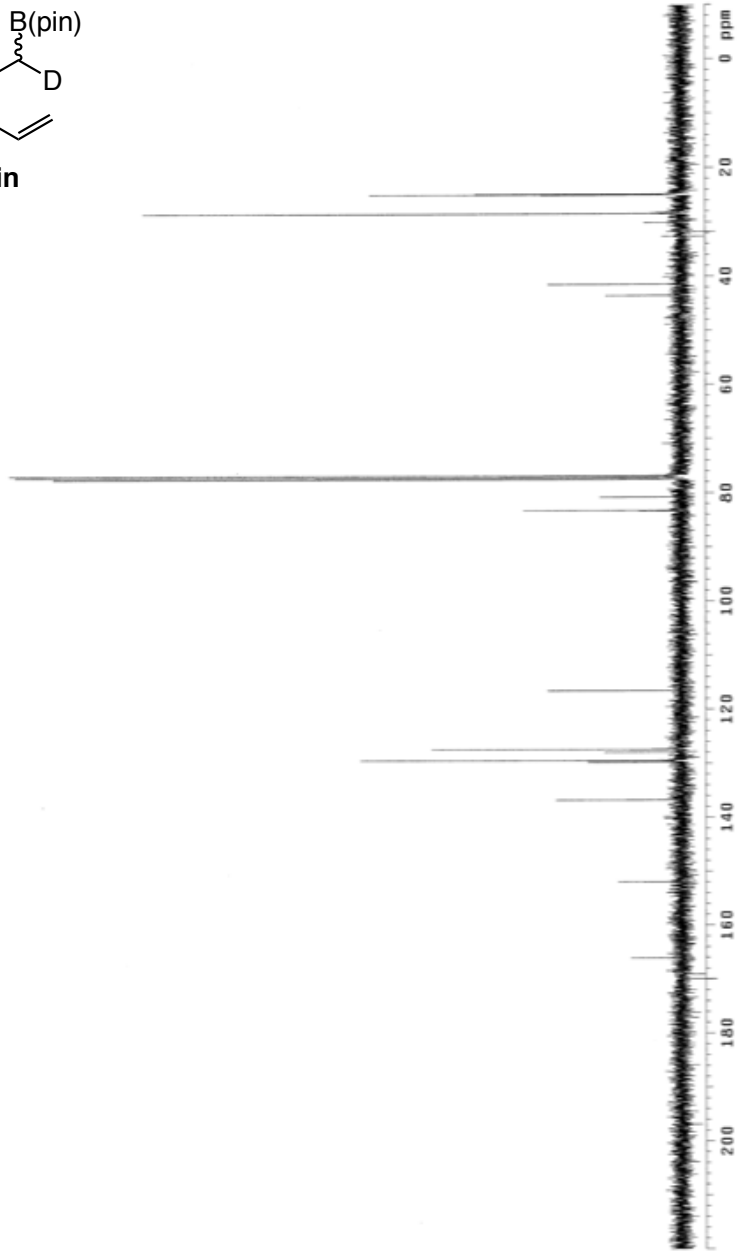

JL-IV-46PD

Sample Name:
JL-IV-46PD
Data Collected on:
Varian Unityinova480
Archive directory:

Sample directory:

Fidfile: JL-IV-46PD-C

Pulse Sequence: CARBON (s2pul)
Solvent: cdcl3
Data collected on: Oct 10 2015

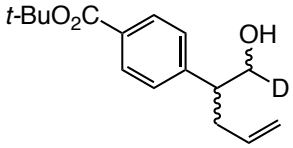

from *E* olefin
60:40 dr

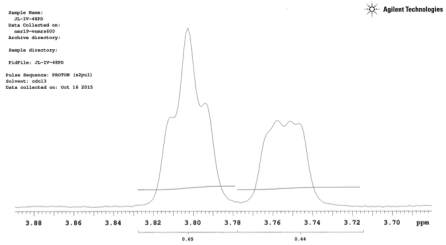

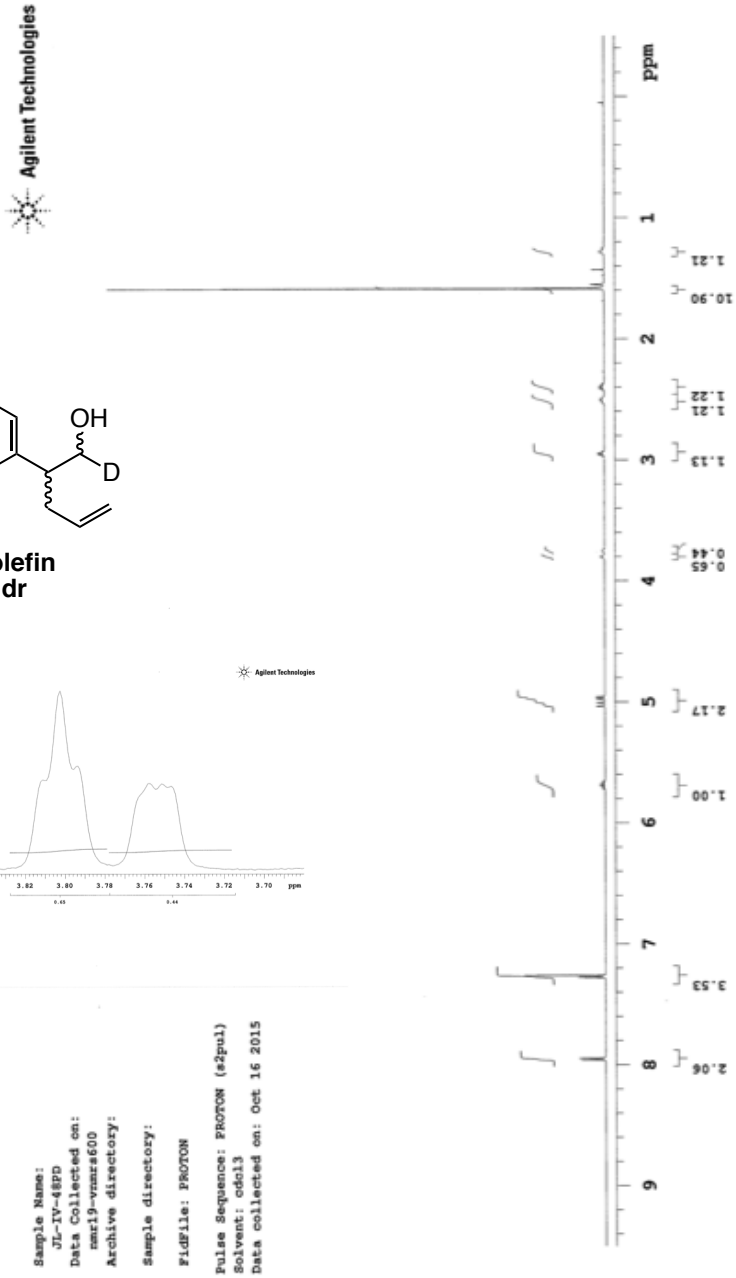

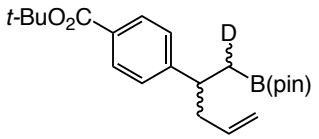

from *Z* olefin

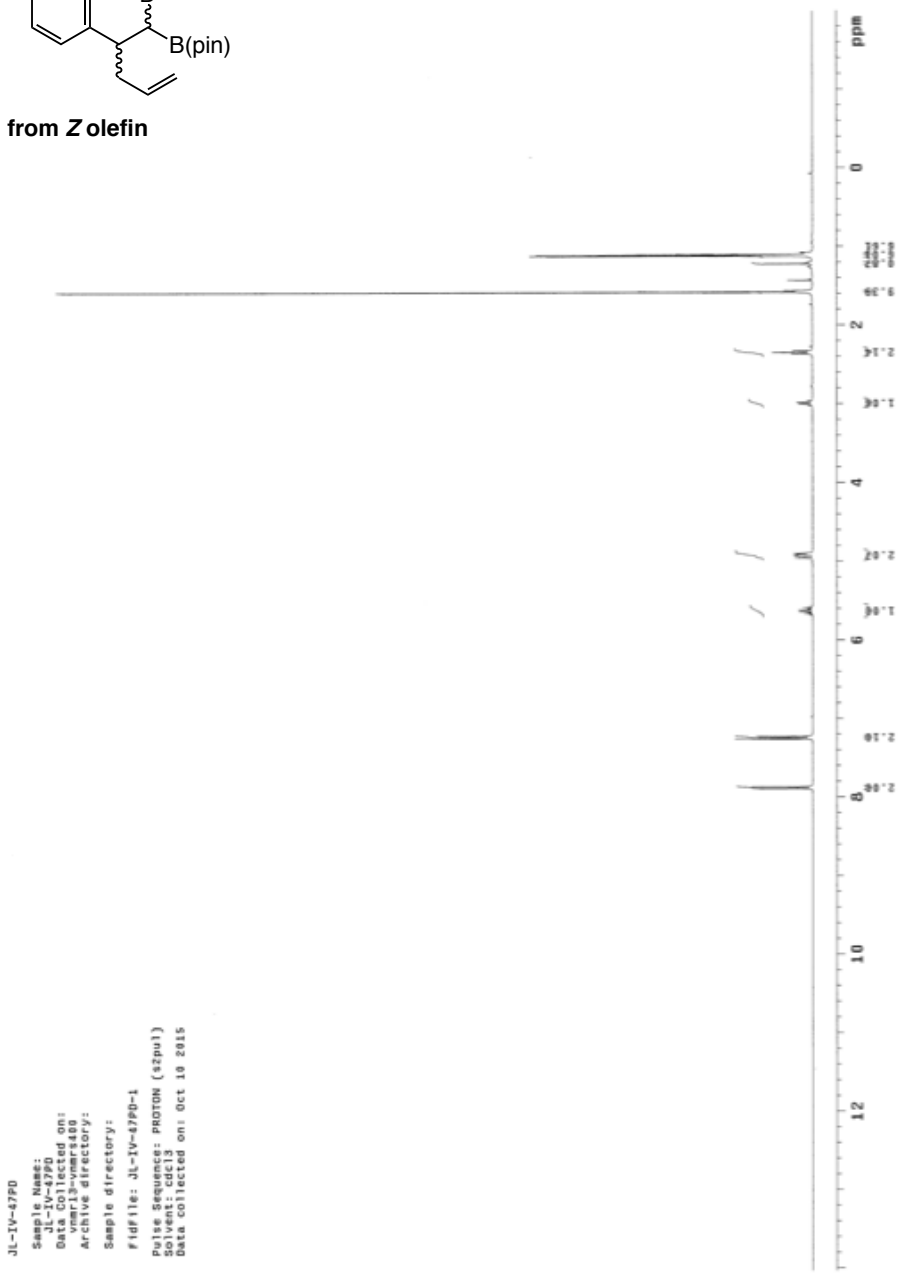

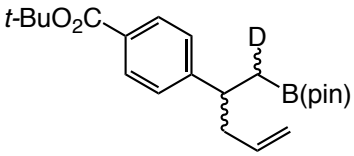

from *Z* olefin

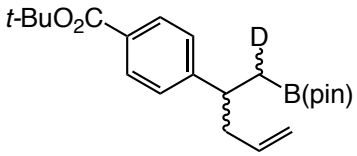

from *Z* olefin

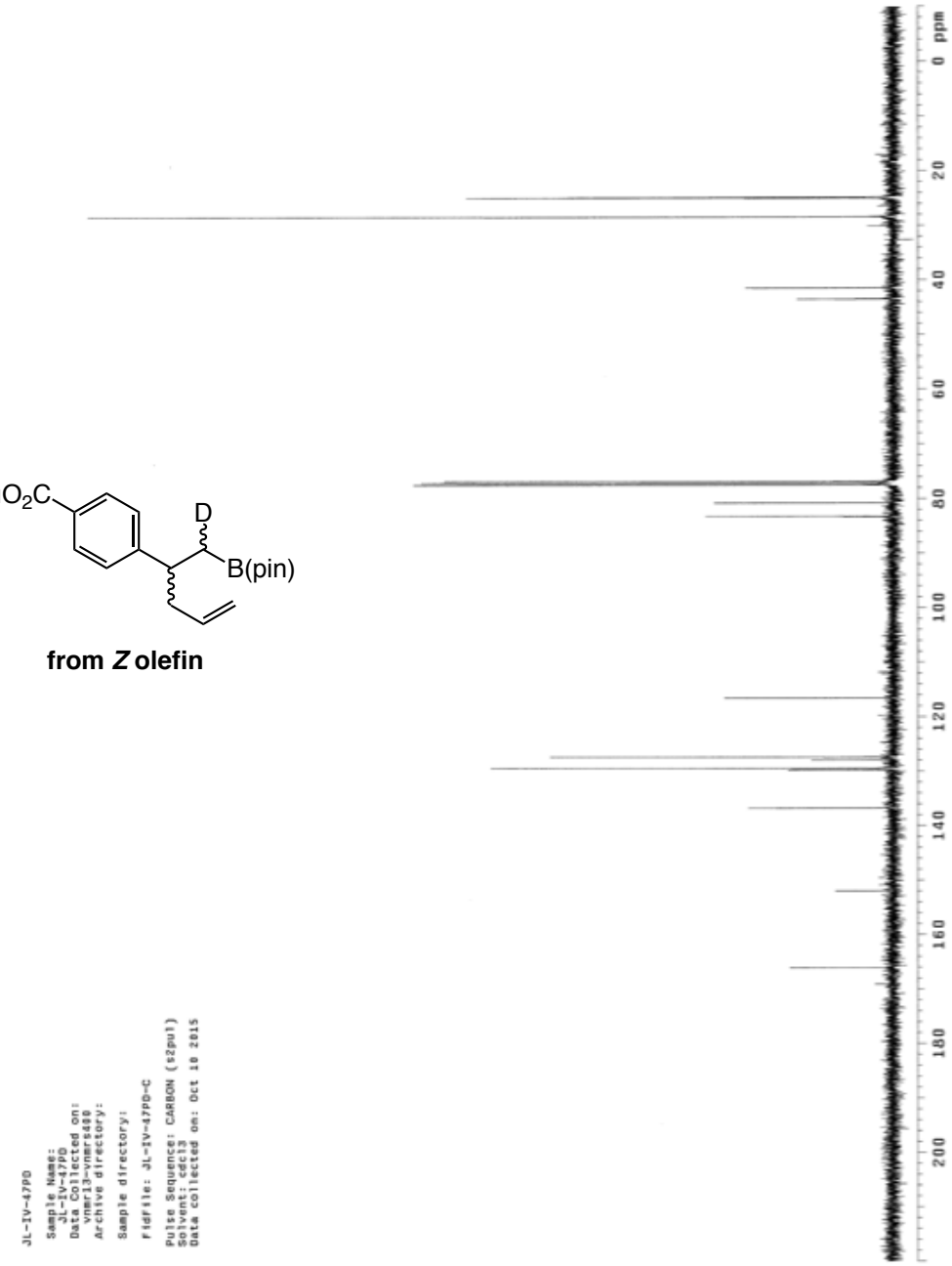

from *Z* olefin
35:65 dr

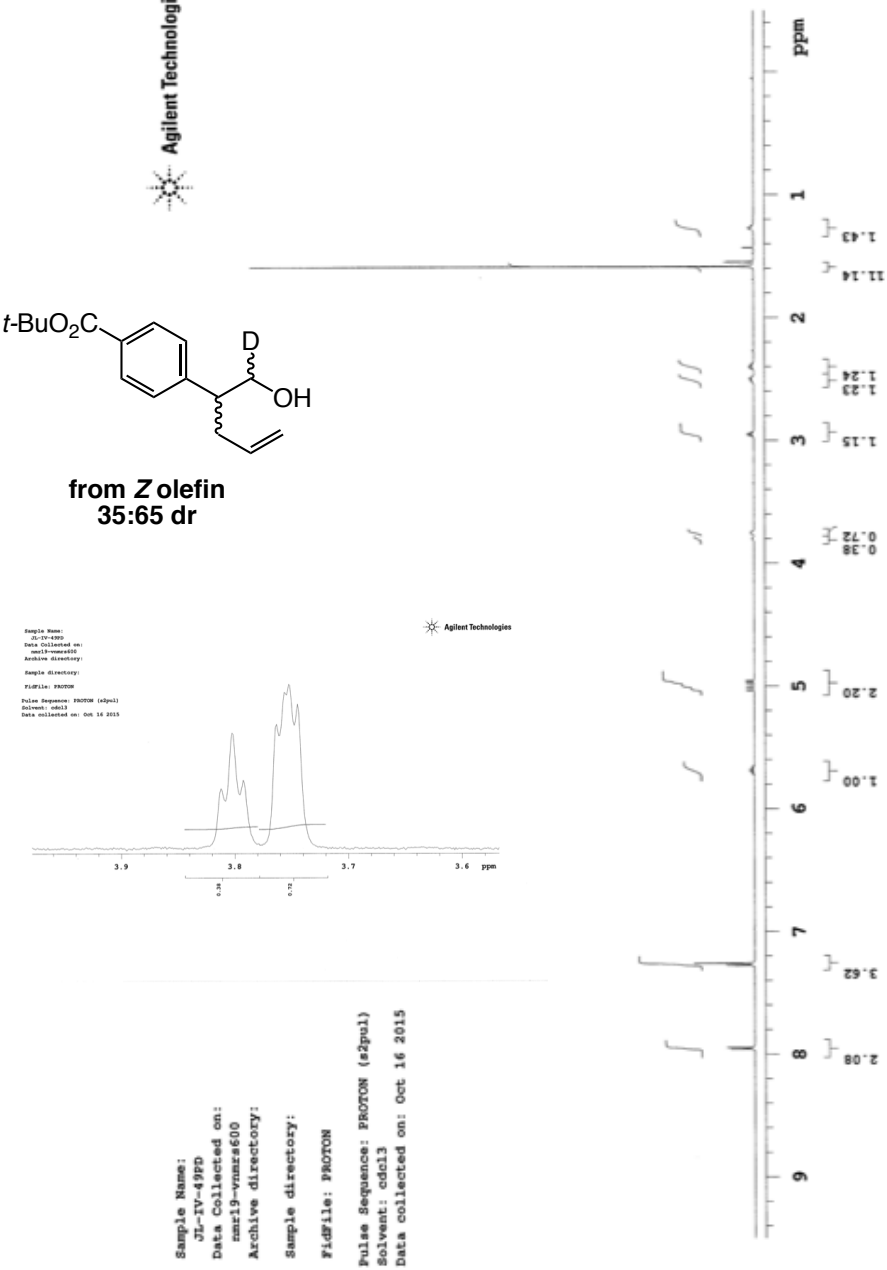

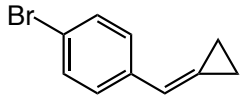

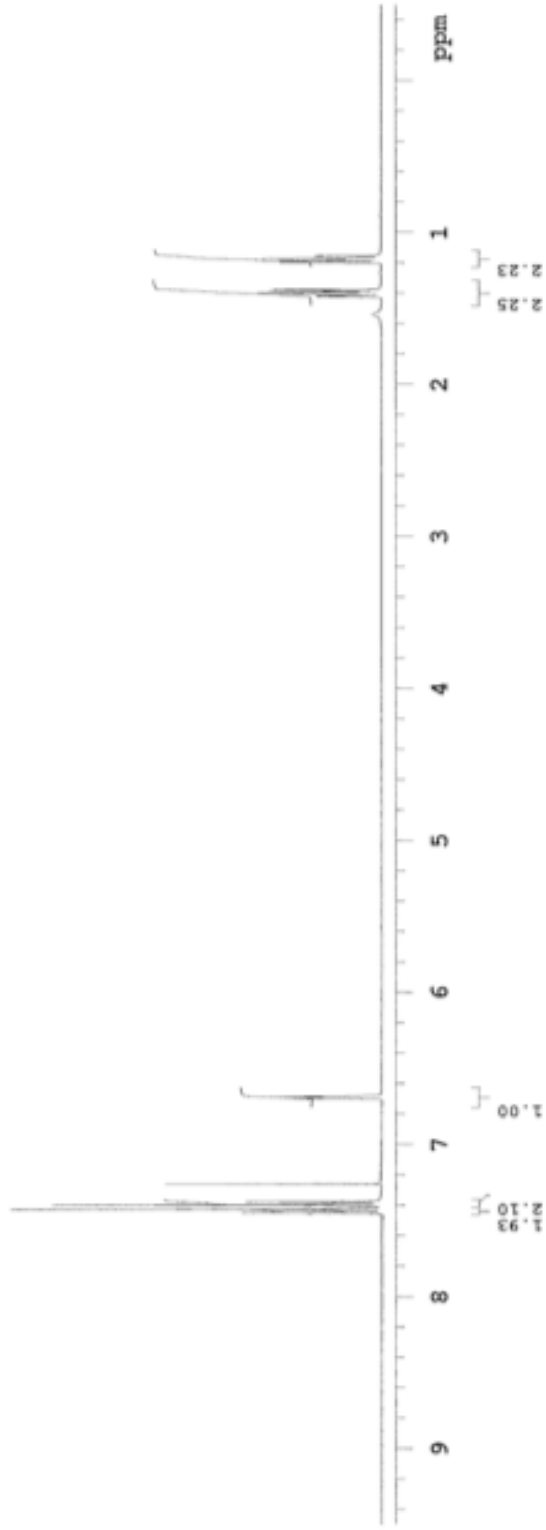

JL-IV-57PD

Sample Name:
JL-IV-57PD
Data Collected on:
vnmr13-vnmrs400
Archive directory:

Sample directory:

FidFile: JL-IV-57PD

Pulse Sequence: PROTON (s2pul)
Solvent: cdcl3
Data collected on: Oct 30 2015

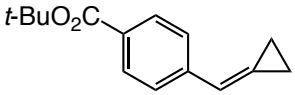

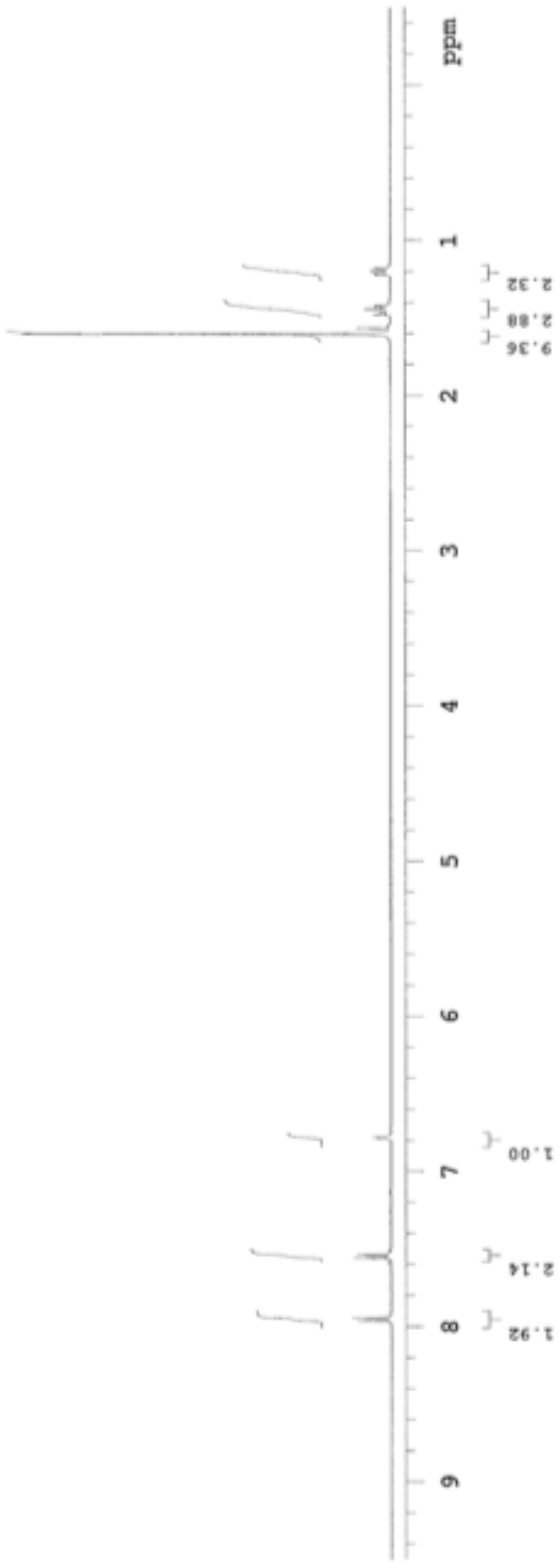

JL-IV-67CD

Sample Name:
JL-IV-67CD
Data Collected on:
vnmrj3-vnmrs400
Archive directory:

Sample directory:

FidFile: JL-IV-67ZD

Pulse Sequence: PROTON (s2pul)
Solvent: cdcl3
Data collected on: Nov 5 2015

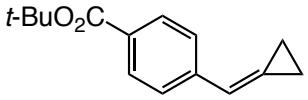
t-BuO2C

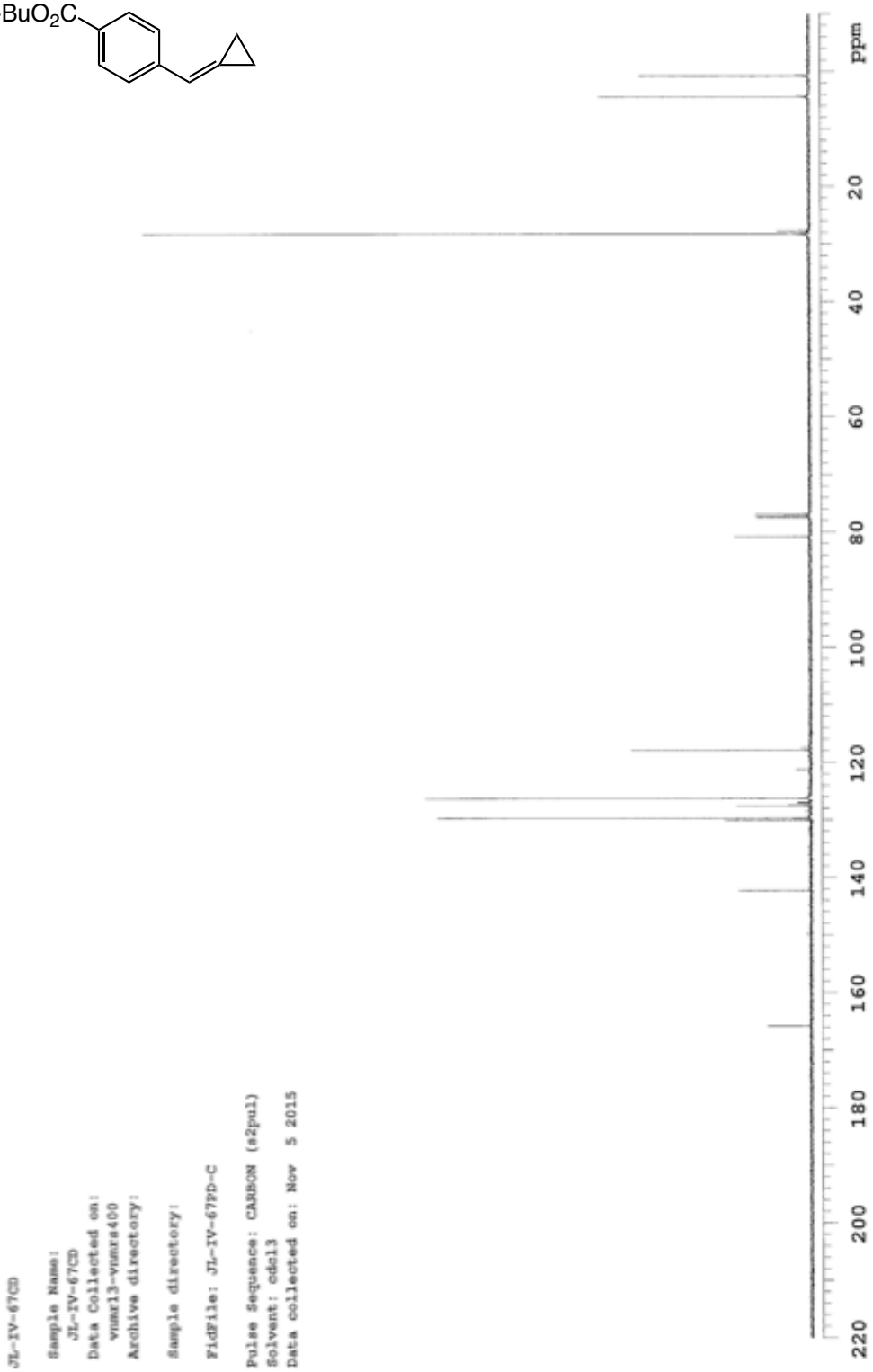
JL-IV-67CD
Sample Name:
JL-IV-67CD
Data Collected on:
vnmr13-vnmrs400
Archive directory:
Sample directory:
FidFile: JL-IV-67PD-C
Pulse Sequence: CARBON (s2pul)
Solvent: cdcl3
Data collected on: Nov 5 2015
ppm
220
200
180
160
140
120
100
80
60
40
20

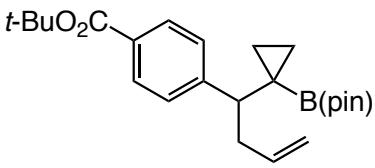
t-BuO2C
B(pin)

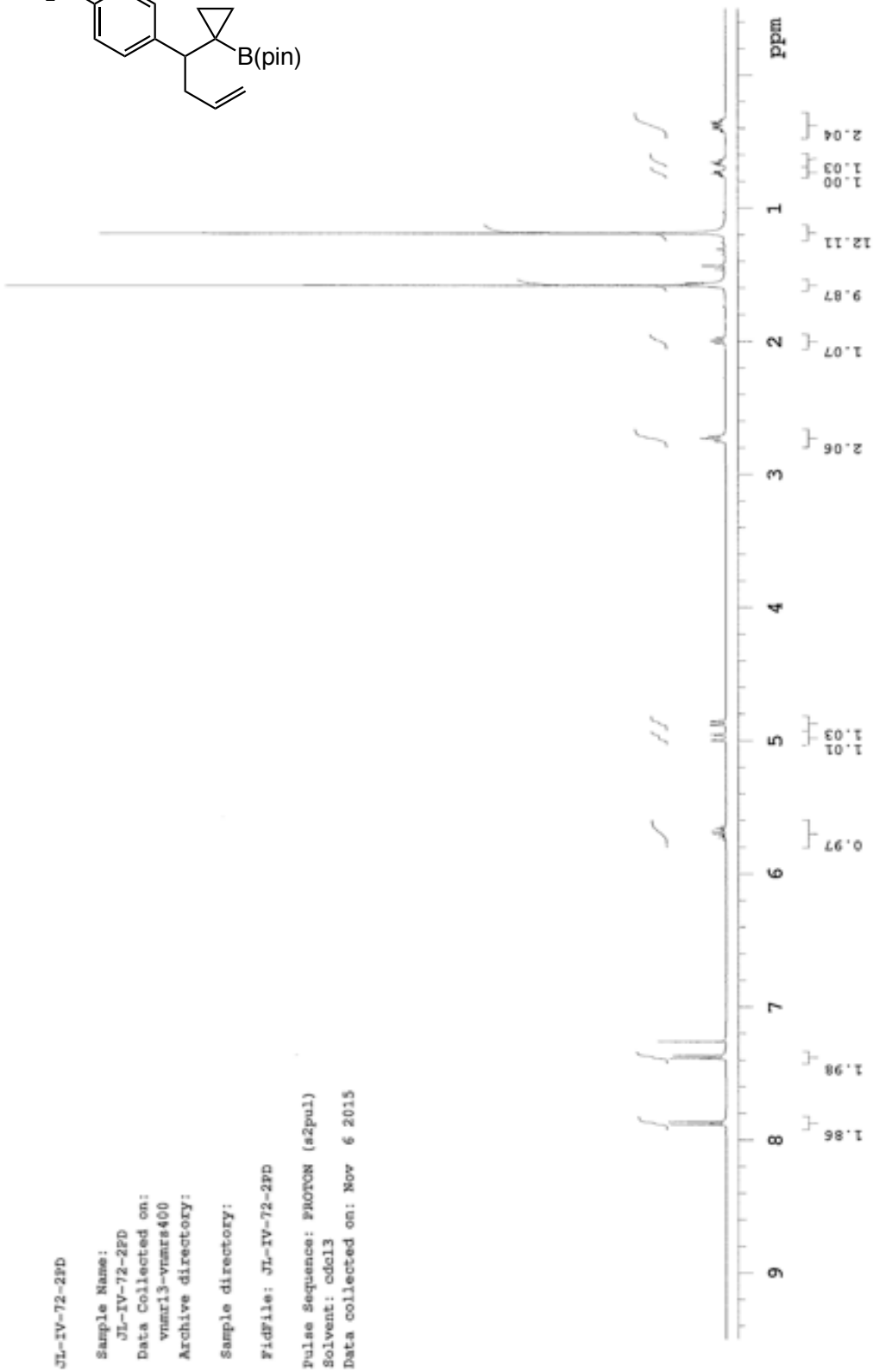
JL-IV-72-2PD
Sample Name:
JL-IV-72-2PD
Data Collected on:
vnmr13-vnmrs400
Archive directory:
Sample directory:
FidFile: JL-IV-72-2PD
Pulse Sequence: PROTON (s2pul)
Solvent: cdcl3
Data collected on: Nov 6 2015
ppm
1.86
1.98
0.97
1.03
1.01
2.06
1.07
9.87
12.11
1.00
1.03
2.04

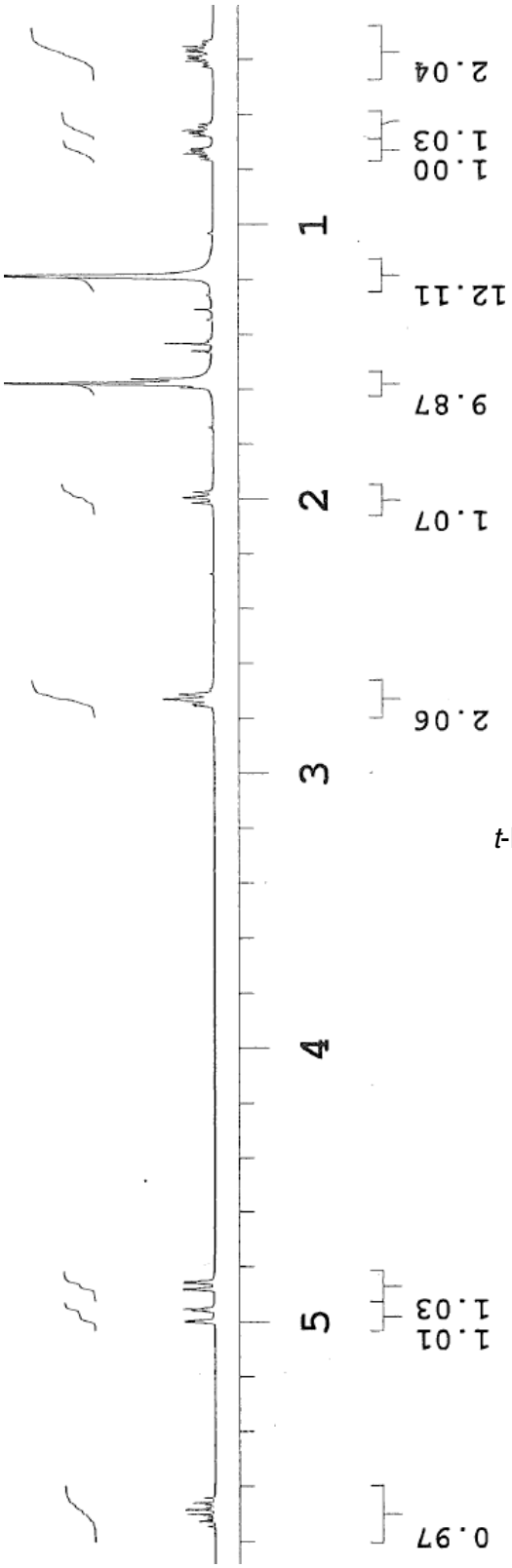
2.04
1.00
1.03
12.11
9.87
1.07
2.06
1.01
1.03
0.97
1
2
3
4
5

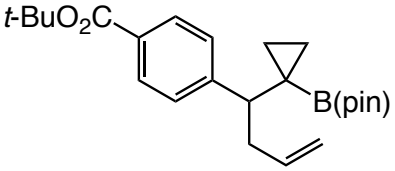
t-BuO2C
B(pin)

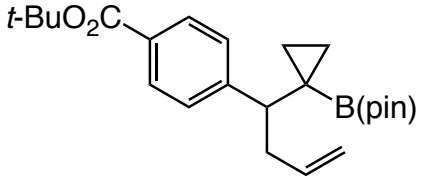
t-BuO2C
B(pin)

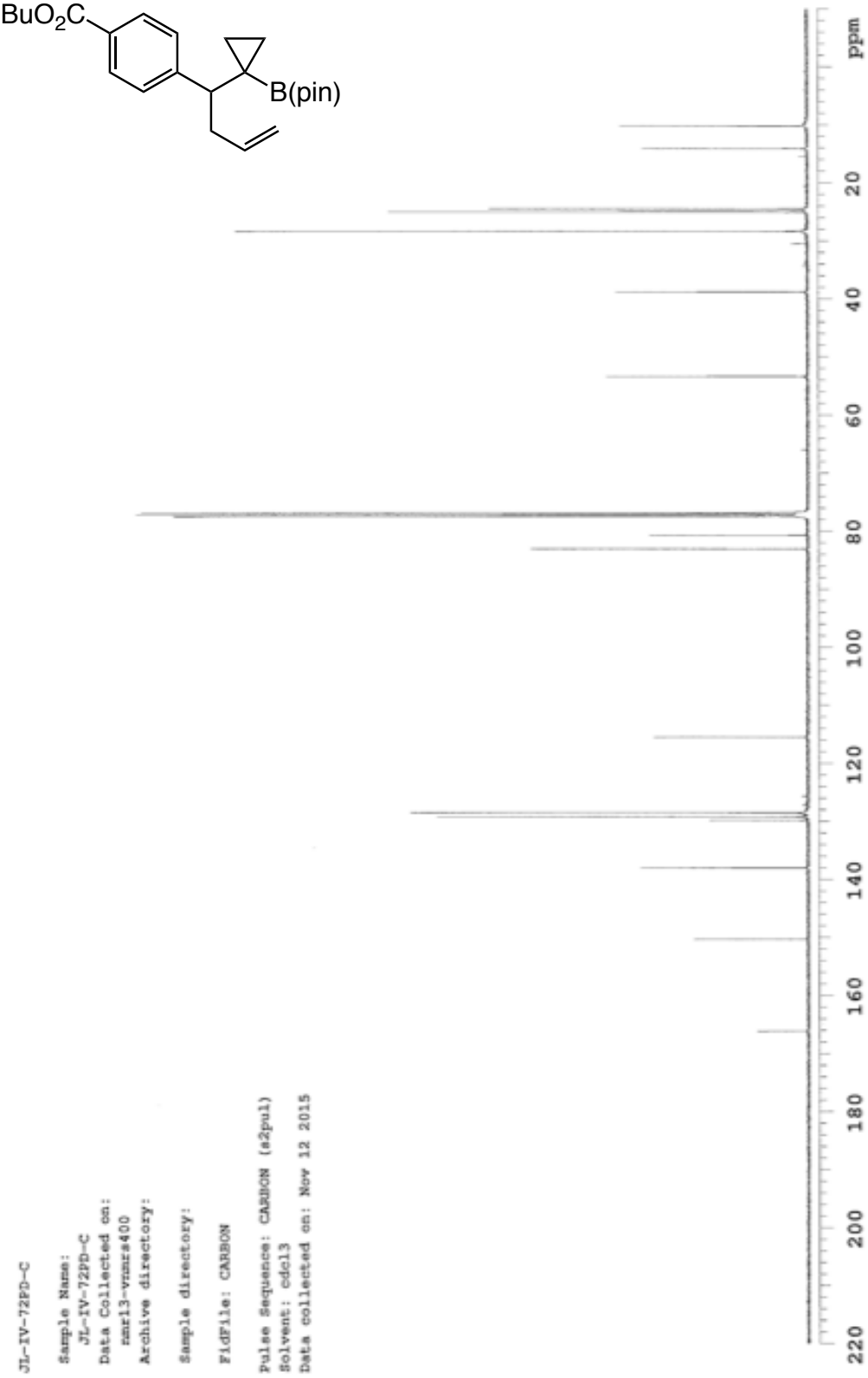
JL-IV-72PD-C
Sample Name:
JL-IV-72PD-C
Data Collected on:
nmr13-vnmrs400
Archive directory:
Sample directory:
FidFile: CARBON
Pulse Sequence: CARBON (s2pul)
Solvent: cdcl3
Data collected on: Nov 12 2015
ppm
220
200
180
160
140
120
100
80
60
40
20

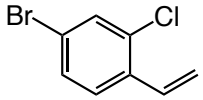
Br
Cl

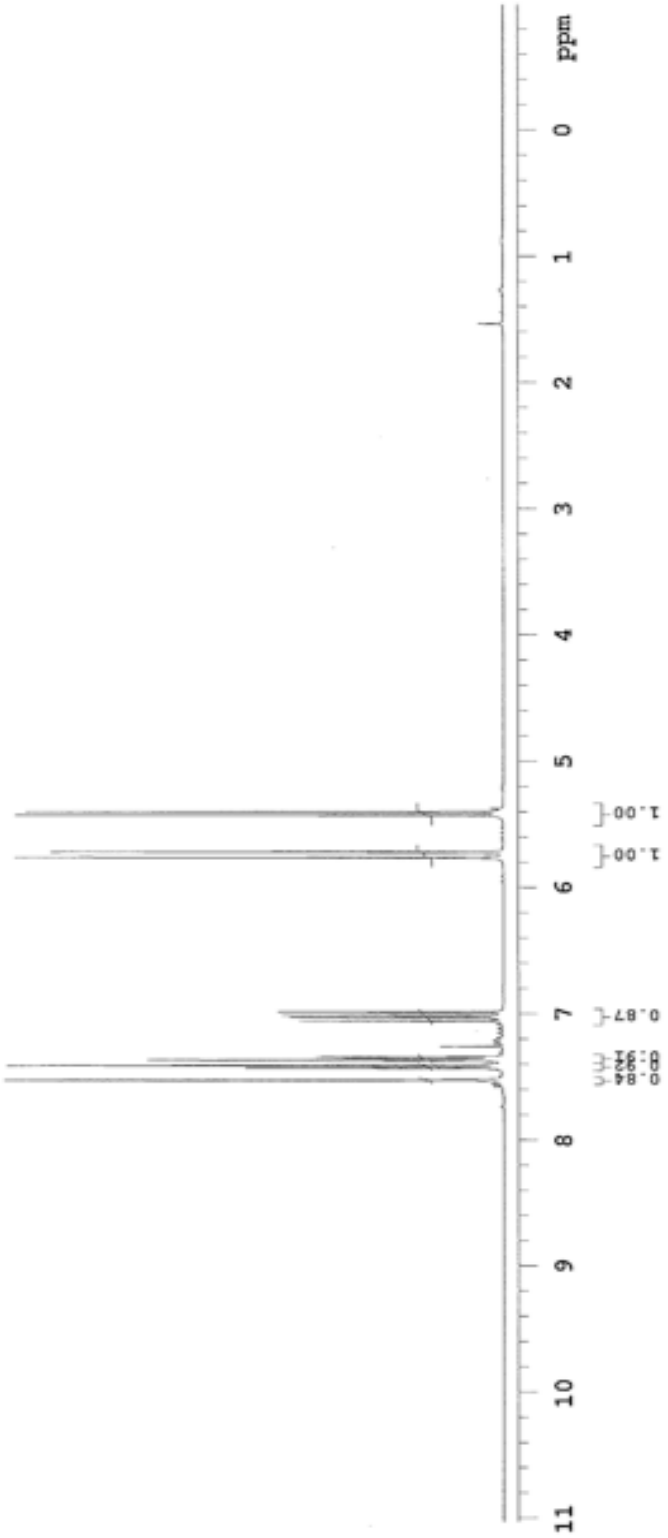
ppm
0
1
2
3
4
5
6
7
8
9
10
11
1.00
1.00
0.87
0.84
0.92
0.91

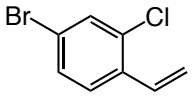
Br
Cl

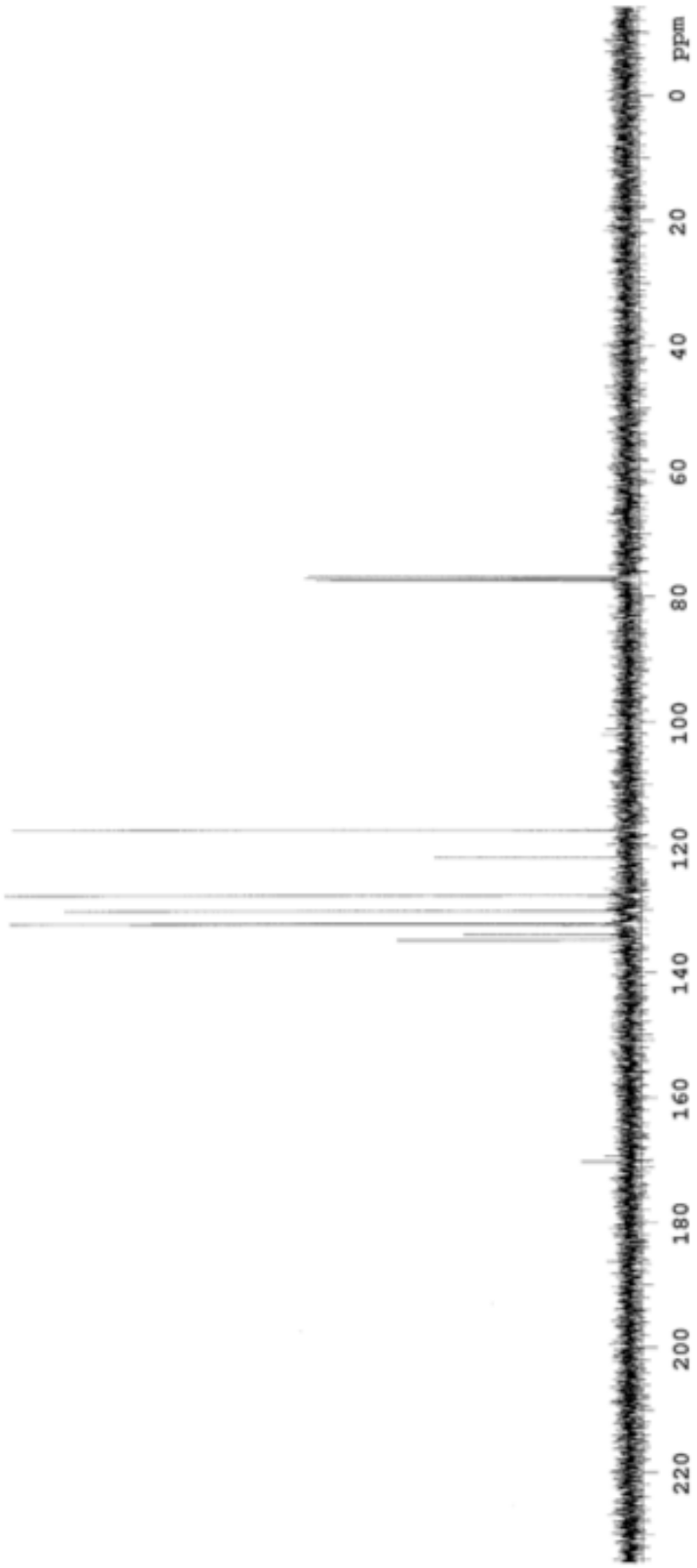
ppm
0
20
40
60
80
100
120
140
160
180
200
220

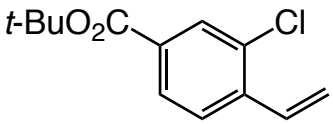
t-BuO2C
Cl

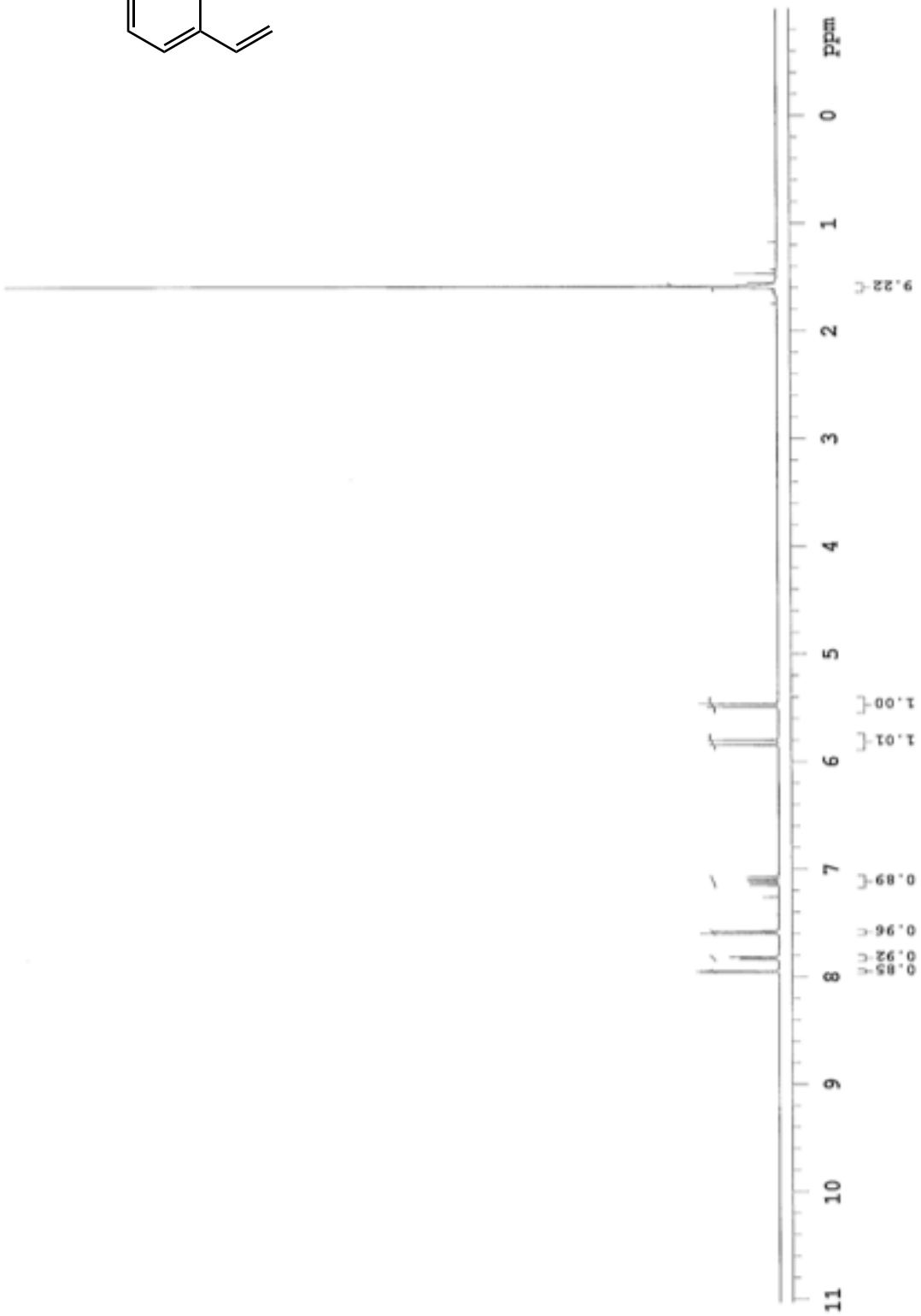
ppm
0
1
2
3
4
5
6
7
8
9
10
11
9.22
1.00
1.01
0.89
0.96
0.92
0.85

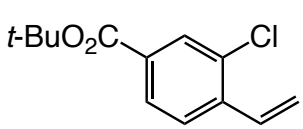
t-BuO2C
Cl

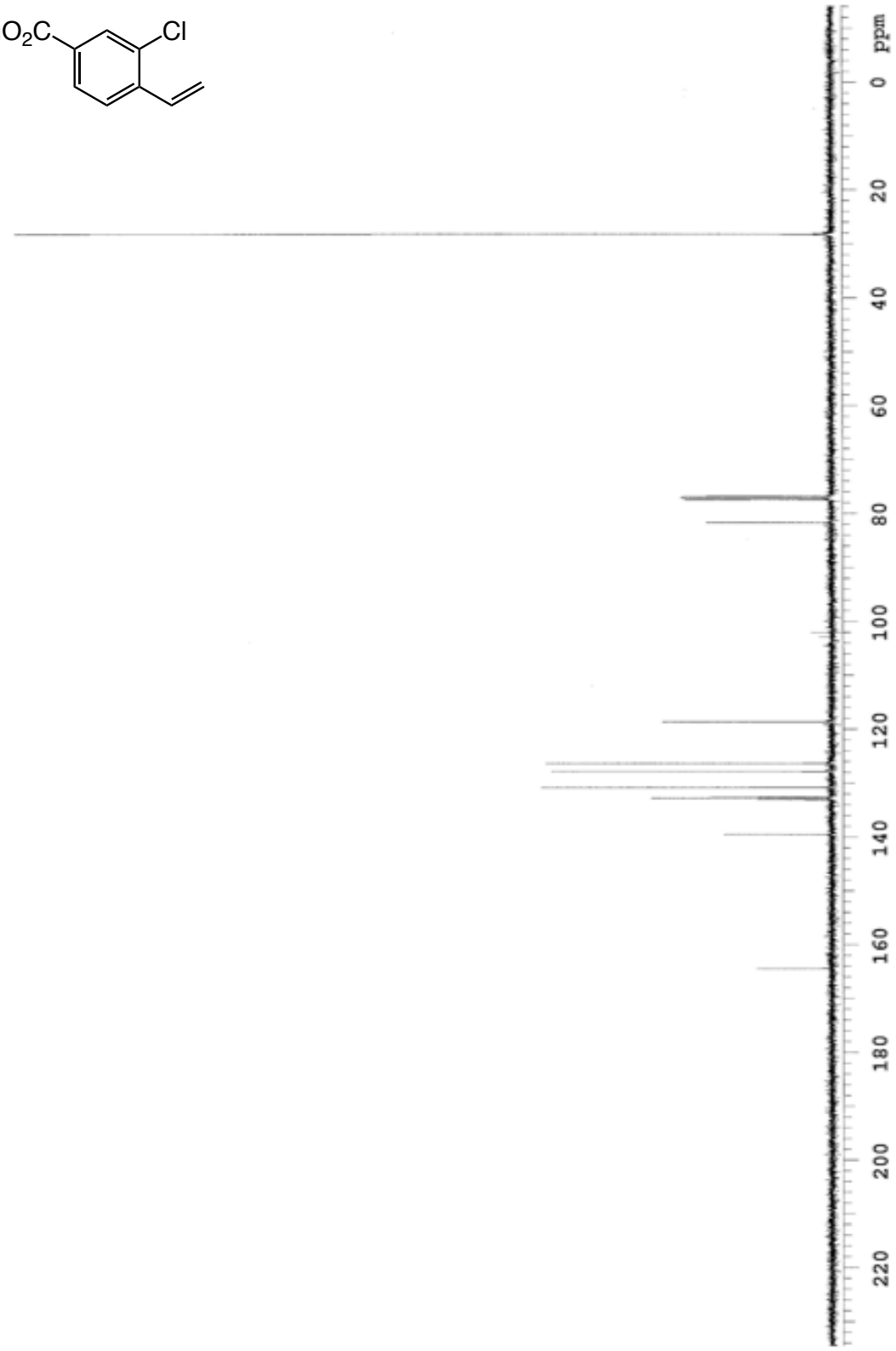
ppm
0
20
40
60
80
100
120
140
160
180
200
220

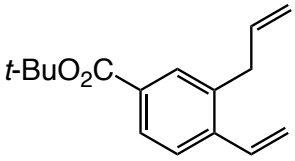
t-BuO2C

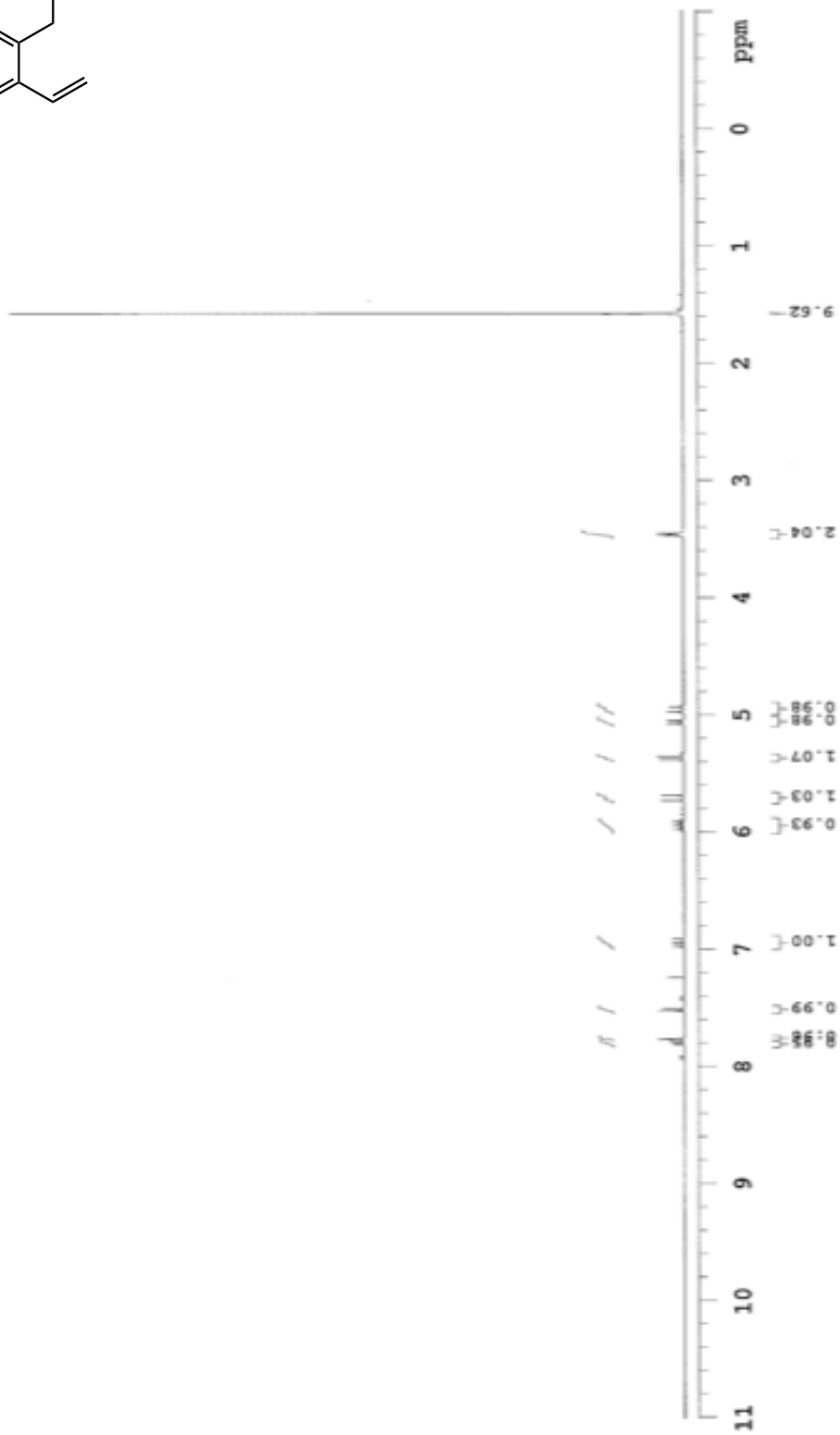
ppm
0
1
2
3
4
5
6
7
8
9
10
11
9.62
2.04
0.98
0.98
1.07
1.03
0.93
1.00
0.99
0.98
0.98

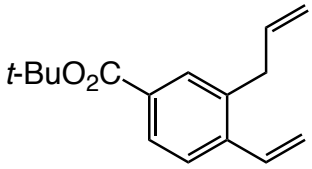
t-BuO2C

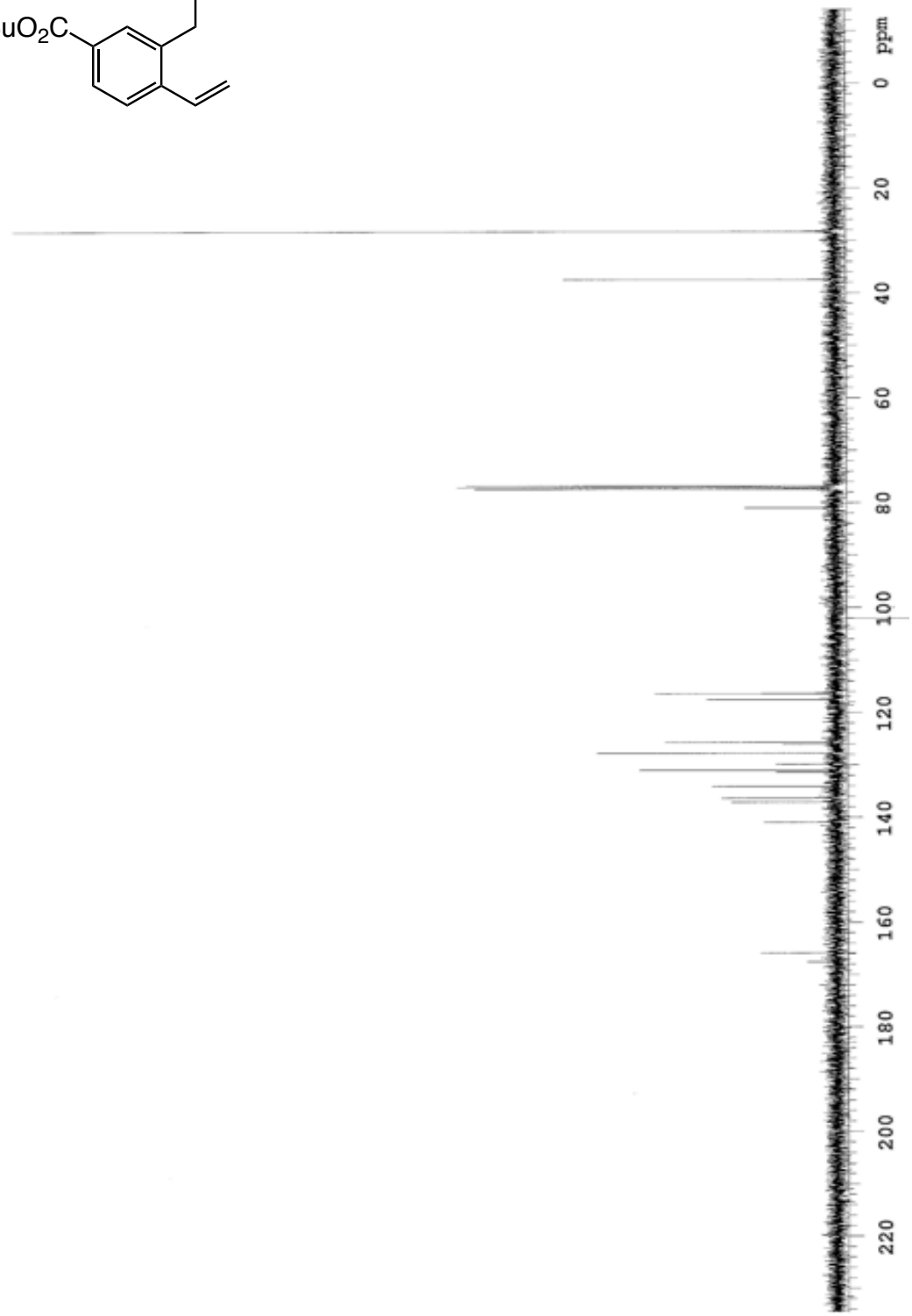
ppm
0
20
40
60
80
100
120
140
160
180
200
220

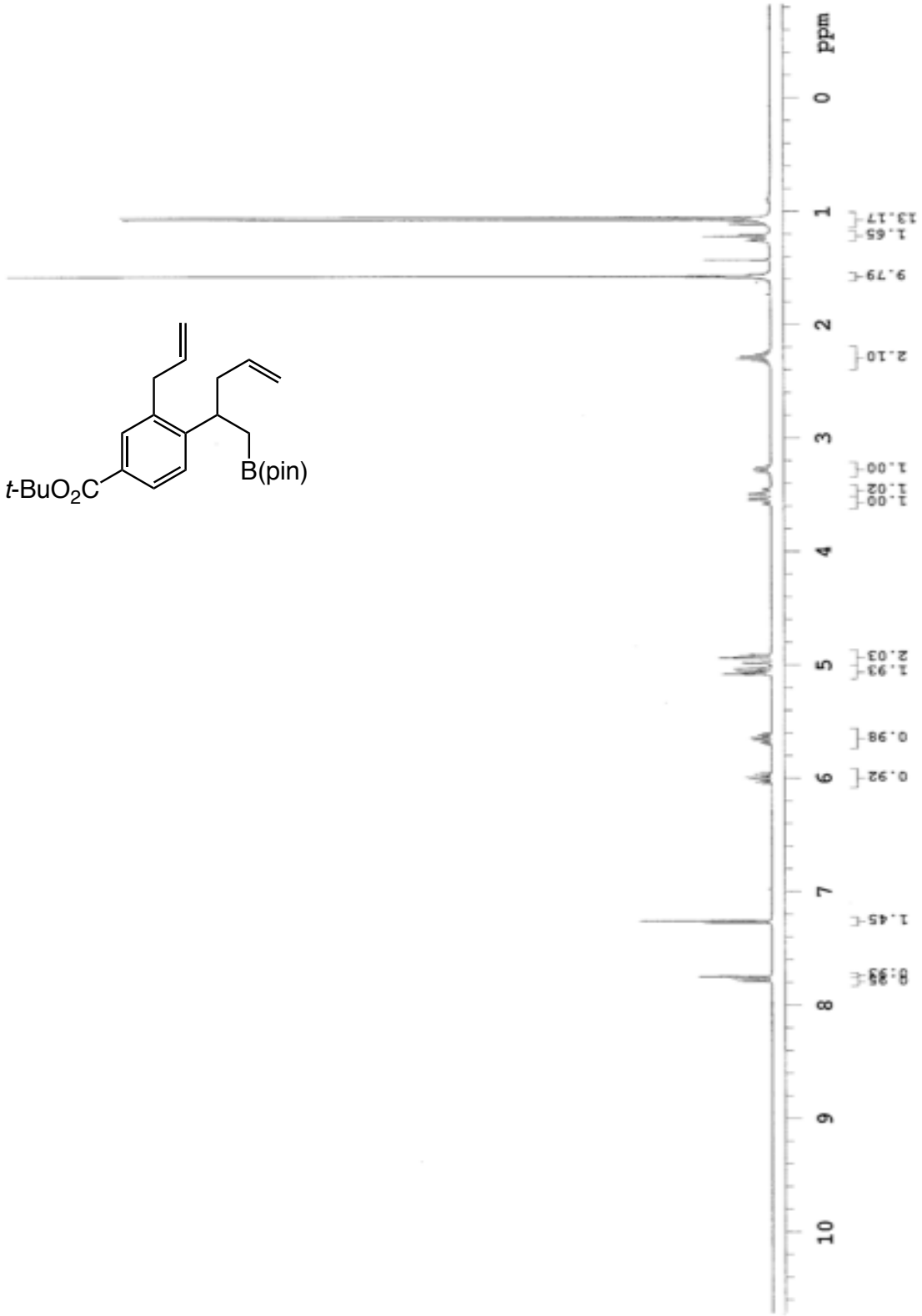
t-BuO2C
B(pin)
ppm
0
1
2
3
4
5
6
7
8
9
10
13.17
1.65
9.79
2.10
1.00
1.02
1.00
2.03
1.93
0.98
0.92
1.45
0.99
0.99

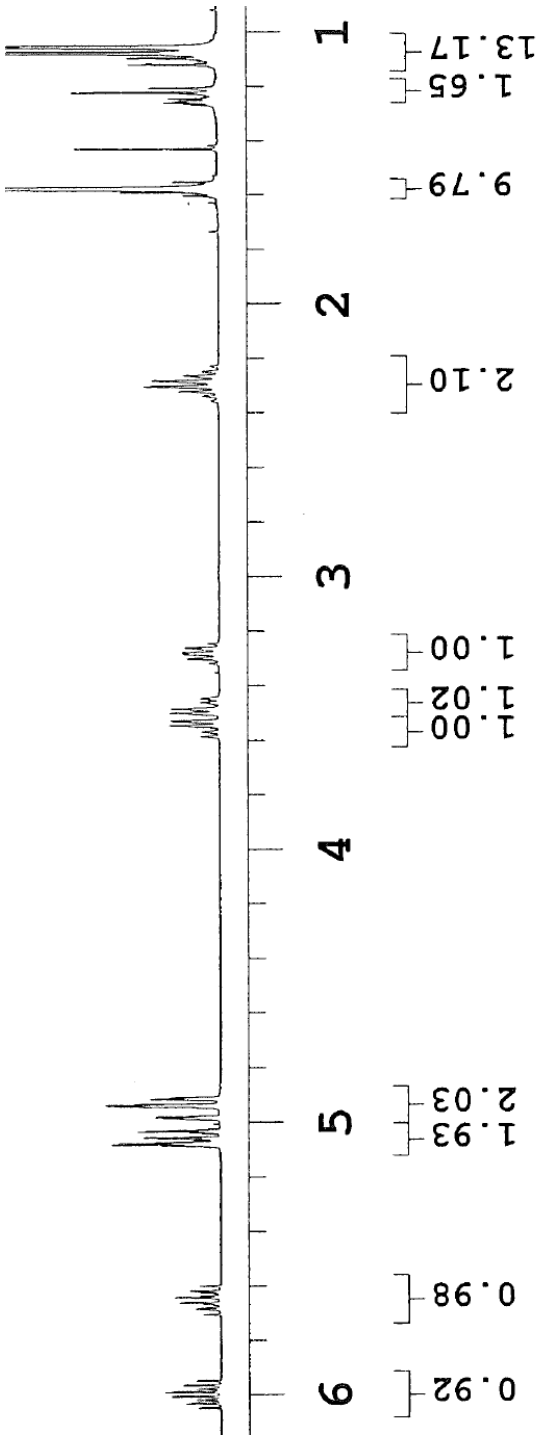
13.17
1.65
9.79
2.10
1.00
1.02
1.00
2.03
1.93
0.98
0.92
1
2
3
4
5
6

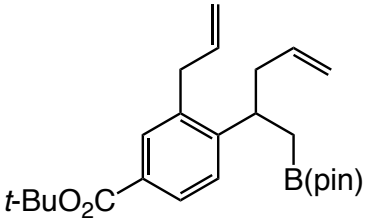
t-BuO2C
B(pin)

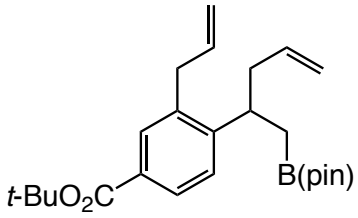
t-BuO2C
B(pin)

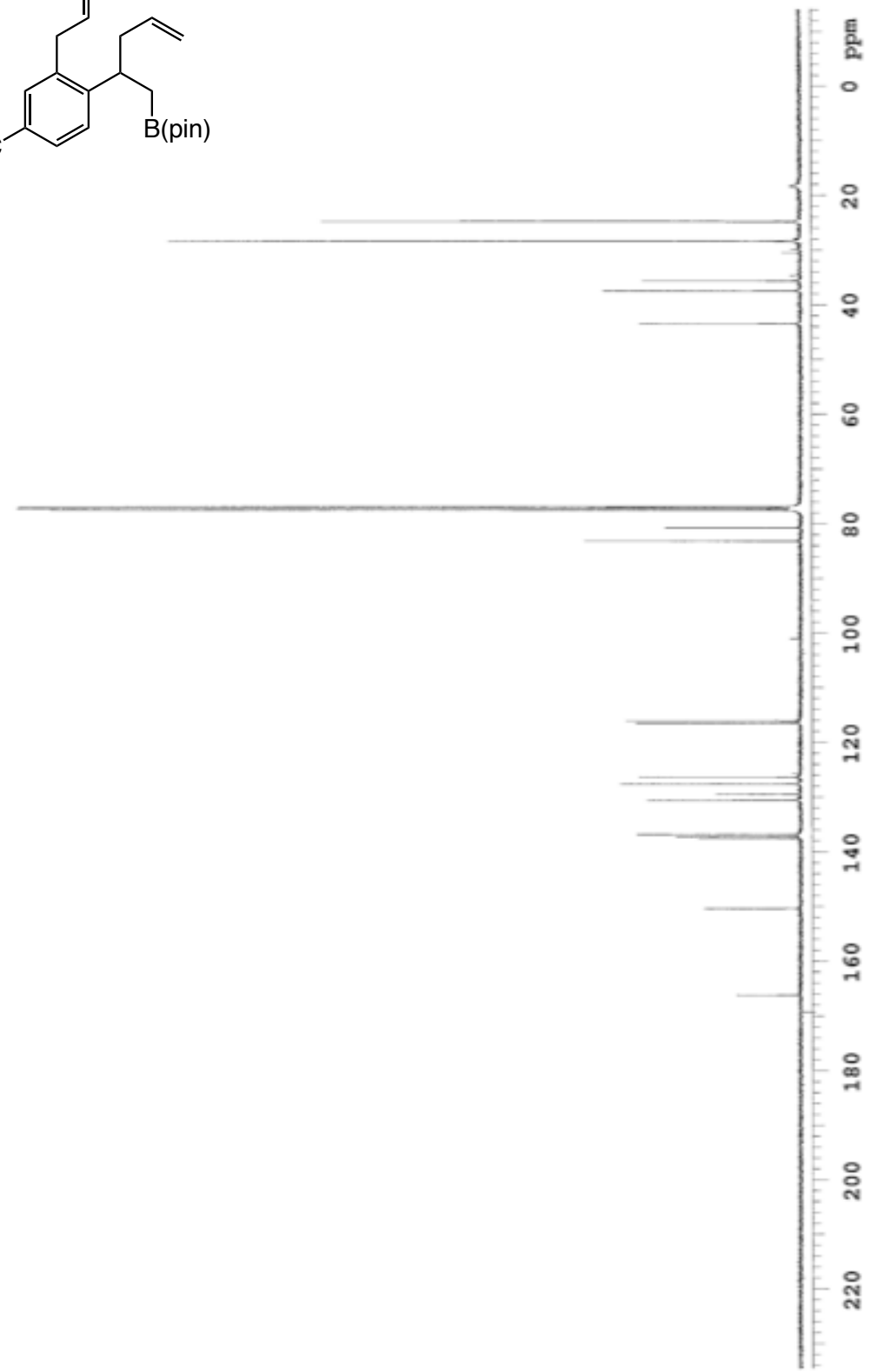
ppm
0
20
40
60
80
100
120
140
160
180
200
220

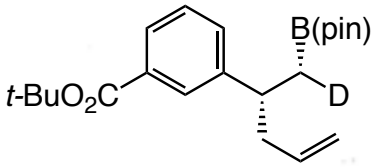
B(pin)
t-BuO2C
D

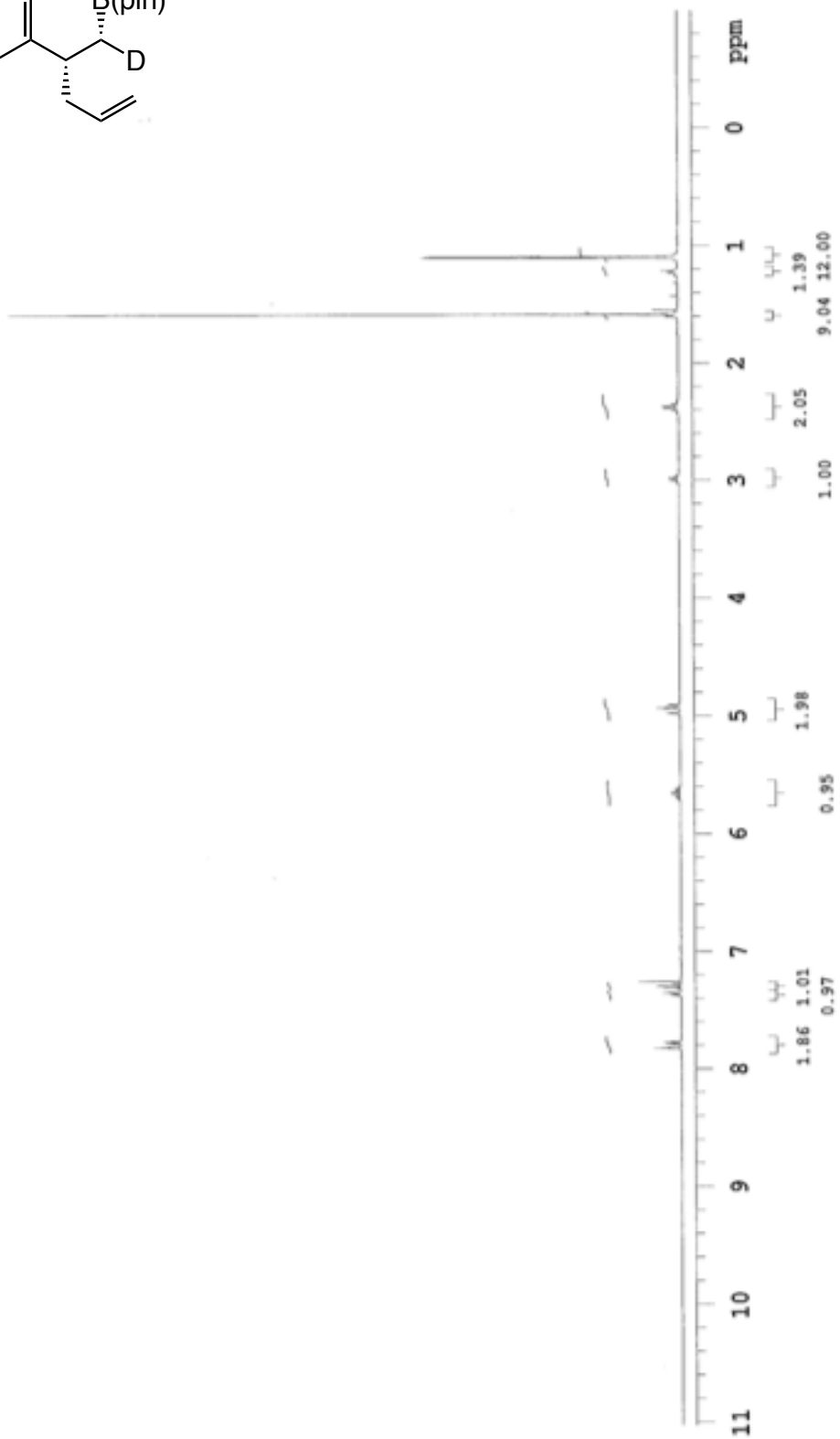
ppm
0
1
2
3
4
5
6
7
8
9
10
11
1.39
9.04
12.00
2.05
1.00
1.98
0.95
1.86
1.01
0.97

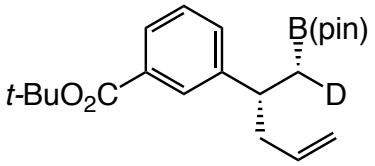
B(pin)
t-BuO2C
D

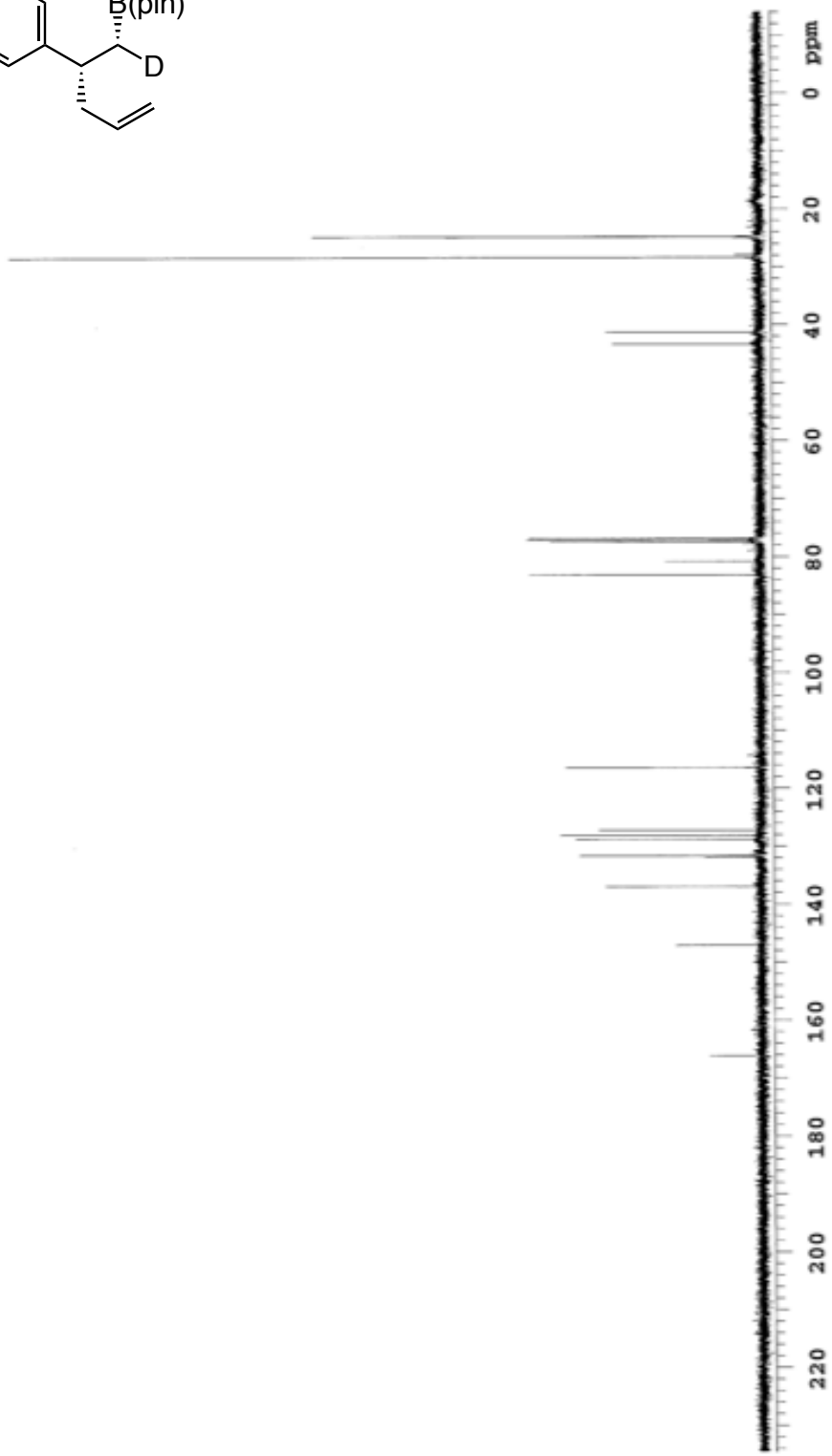
ppm
0
20
40
60
80
100
120
140
160
180
200
220

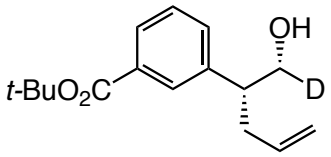
OH
D
t-BuO2C

>98:2 dr

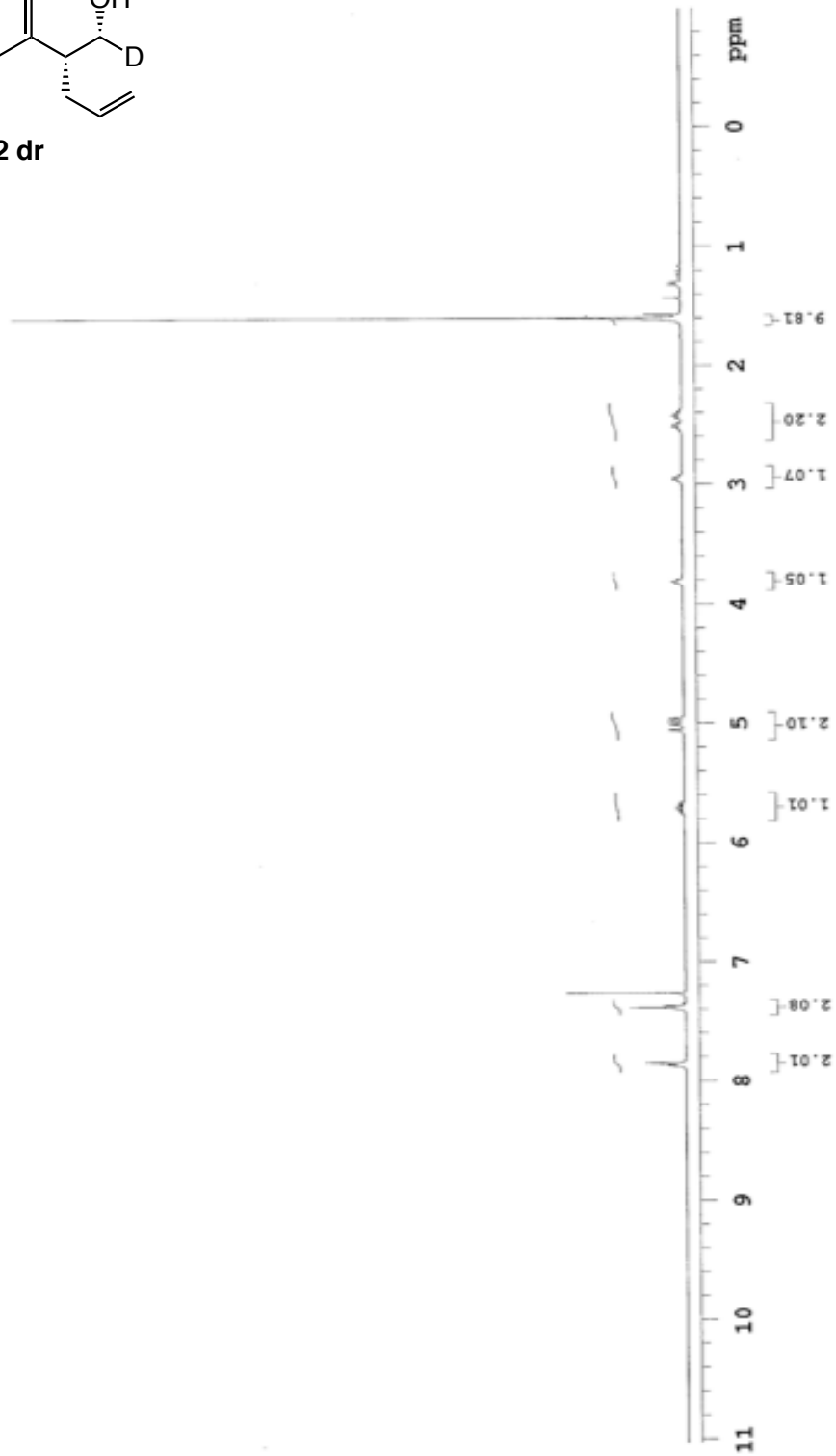
ppm
0
1
2
3
4
5
6
7
8
9
10
11
9.81
2.20
1.07
1.05
2.10
1.01
2.08
2.01

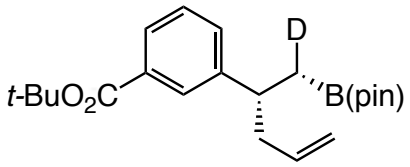
D
t-BuO2C
B(pin)

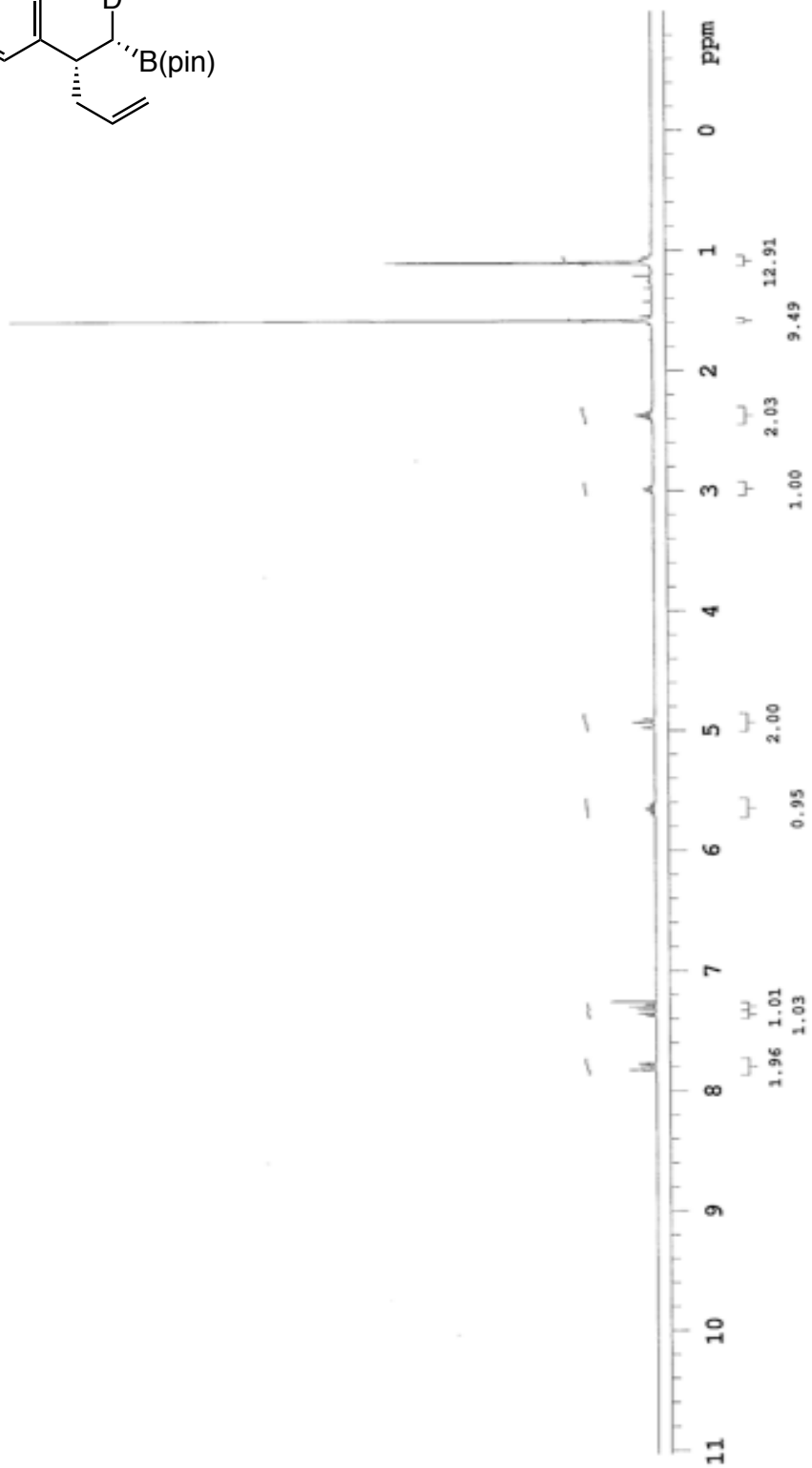
ppm
0
1
2
3
4
5
6
7
8
9
10
11
12.91
9.49
2.03
1.00
2.00
0.95
1.96
1.01
1.03

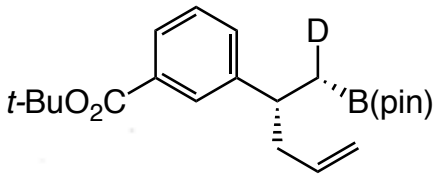
D
t-BuO2C
B(pin)

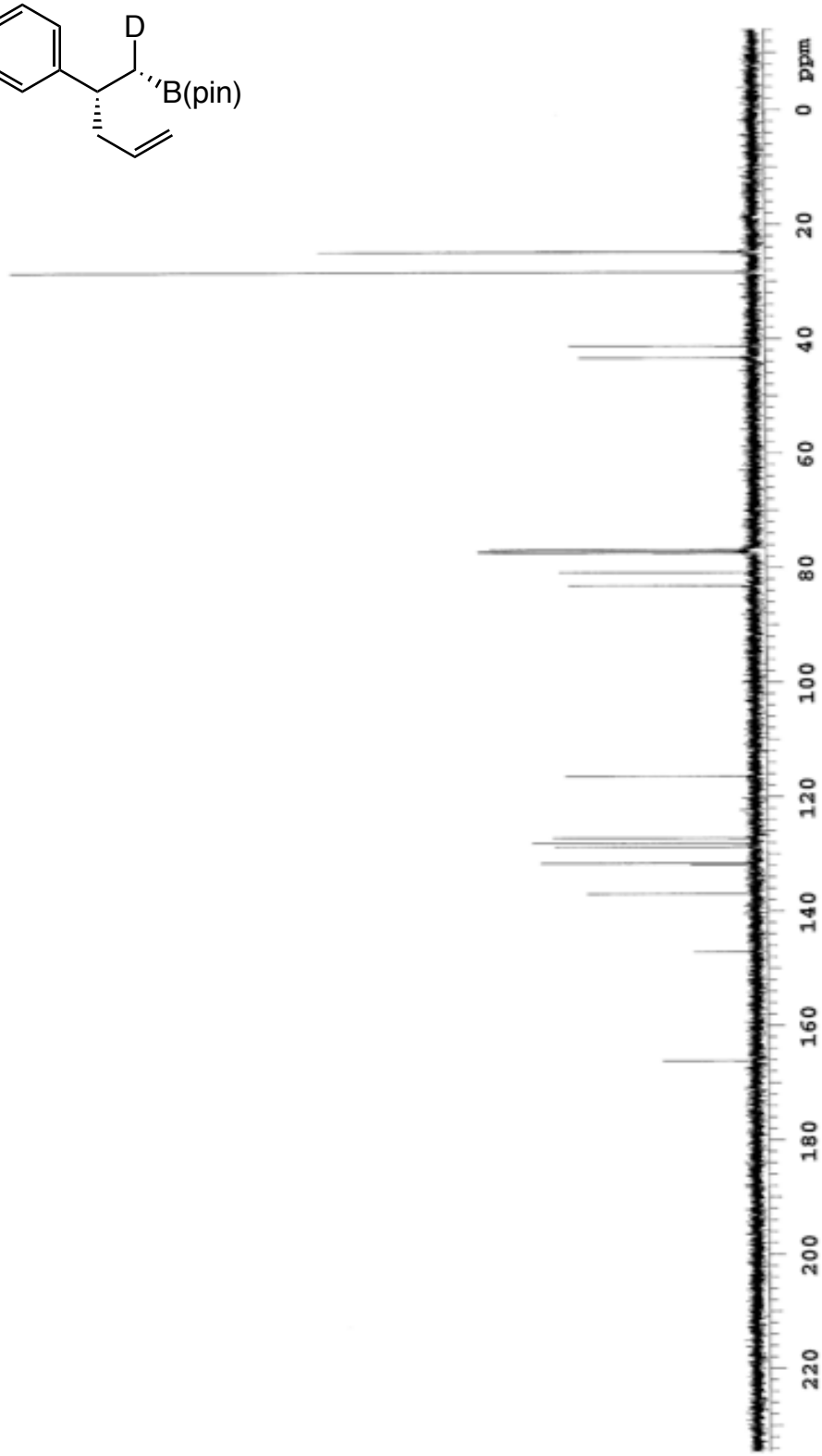
ppm
0
20
40
60
80
100
120
140
160
180
200
220

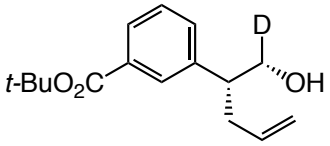

89:11 dr
(from 90:10 *Z:E*)

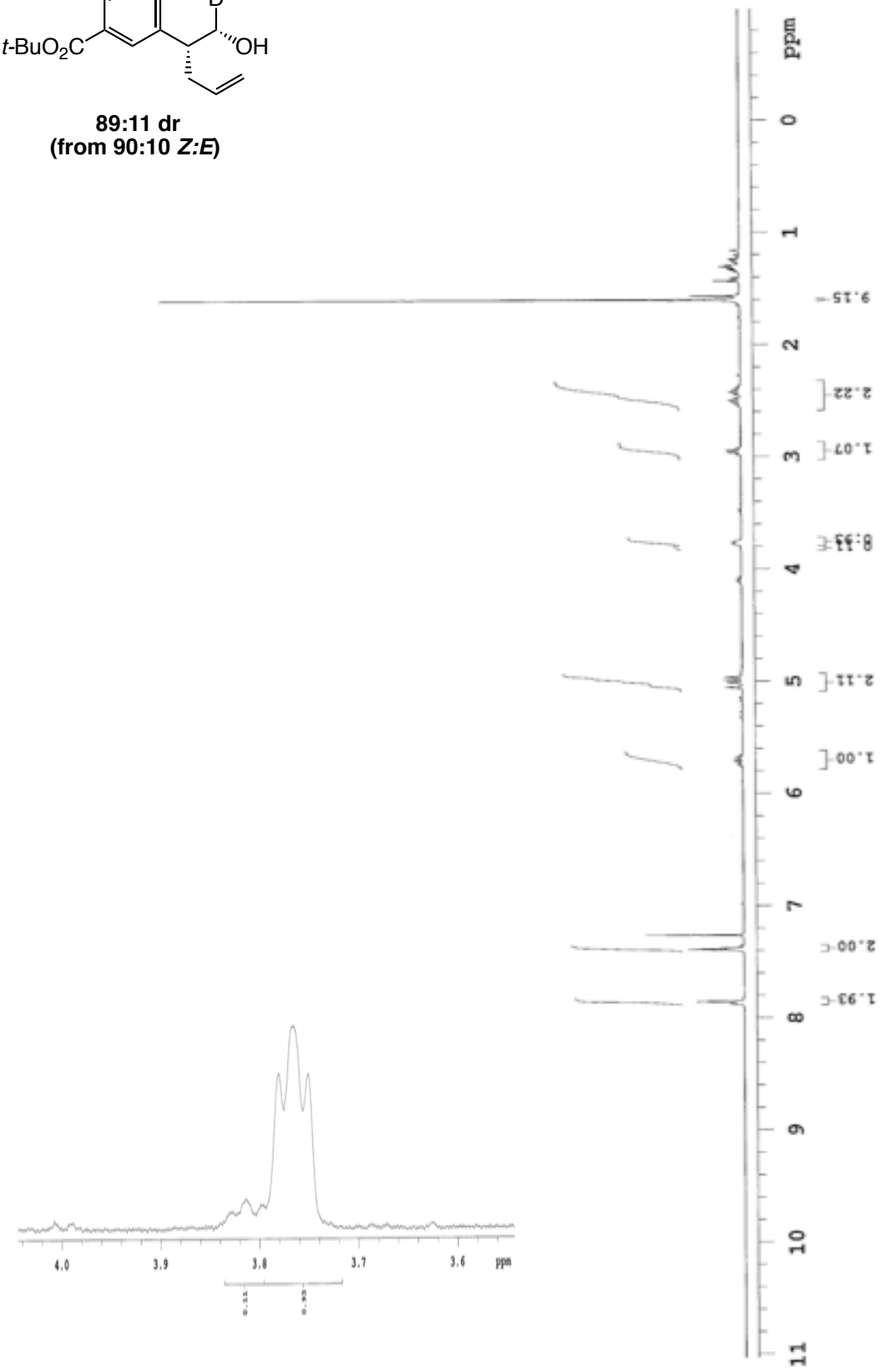

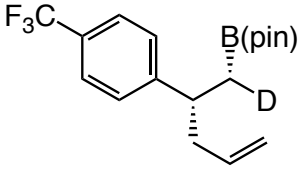
F3C
B(pin)
D

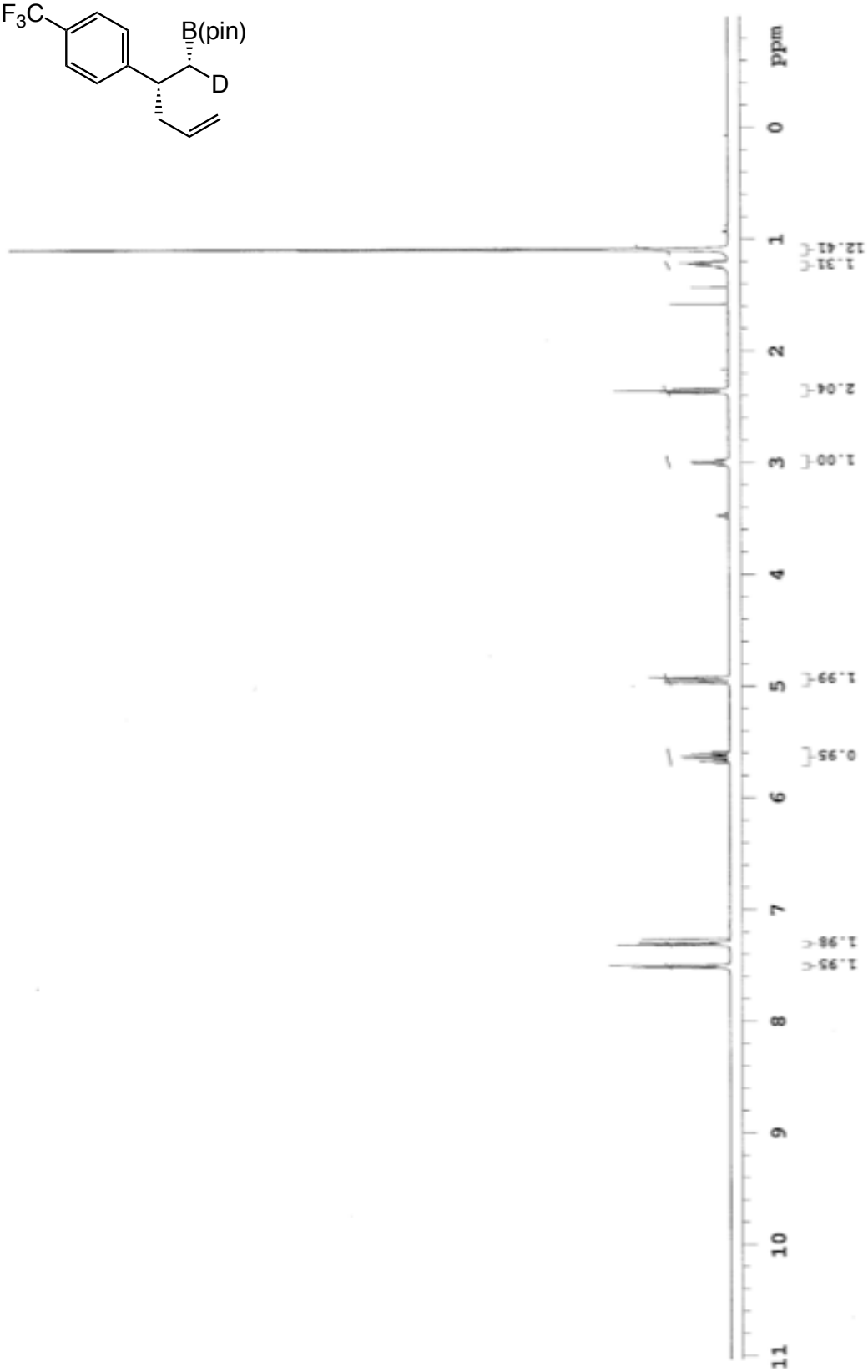
ppm
0
1
2
3
4
5
6
7
8
9
10
11
12.41
1.31
2.04
1.00
1.99
0.95
1.98
1.95

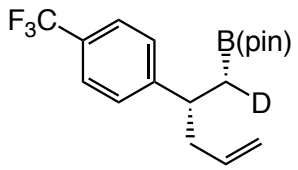
F3C
B(pin)
D

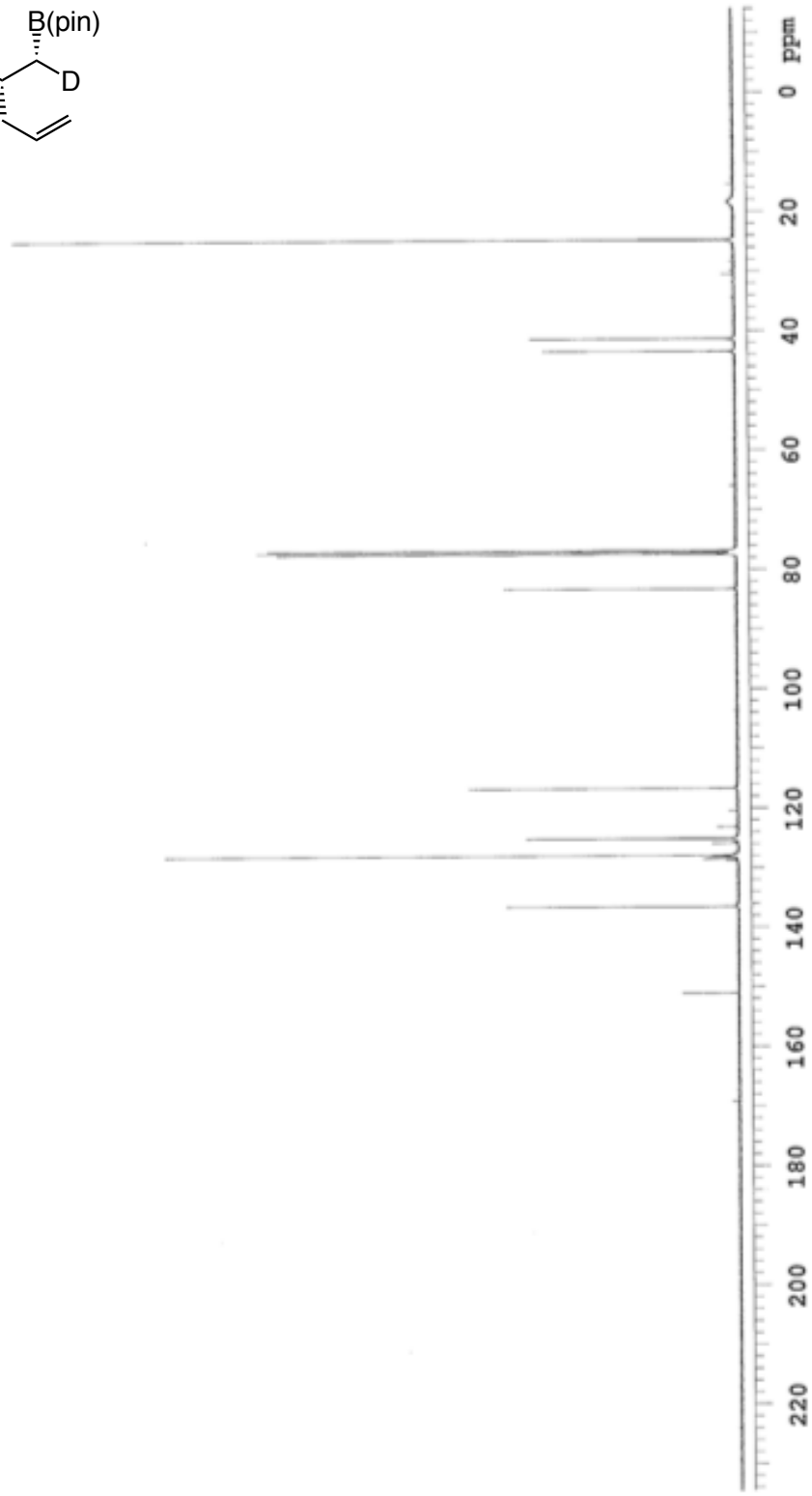
ppm
0
20
40
60
80
100
120
140
160
180
200
220

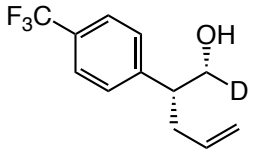

92:8 dr
(from 91:9 *E:Z alkene)*

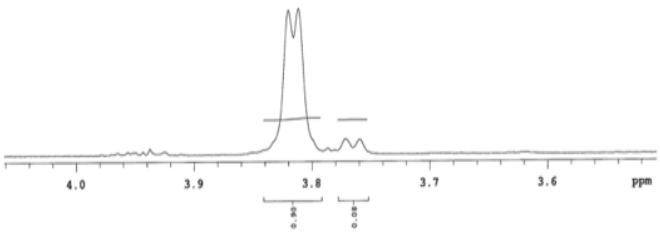

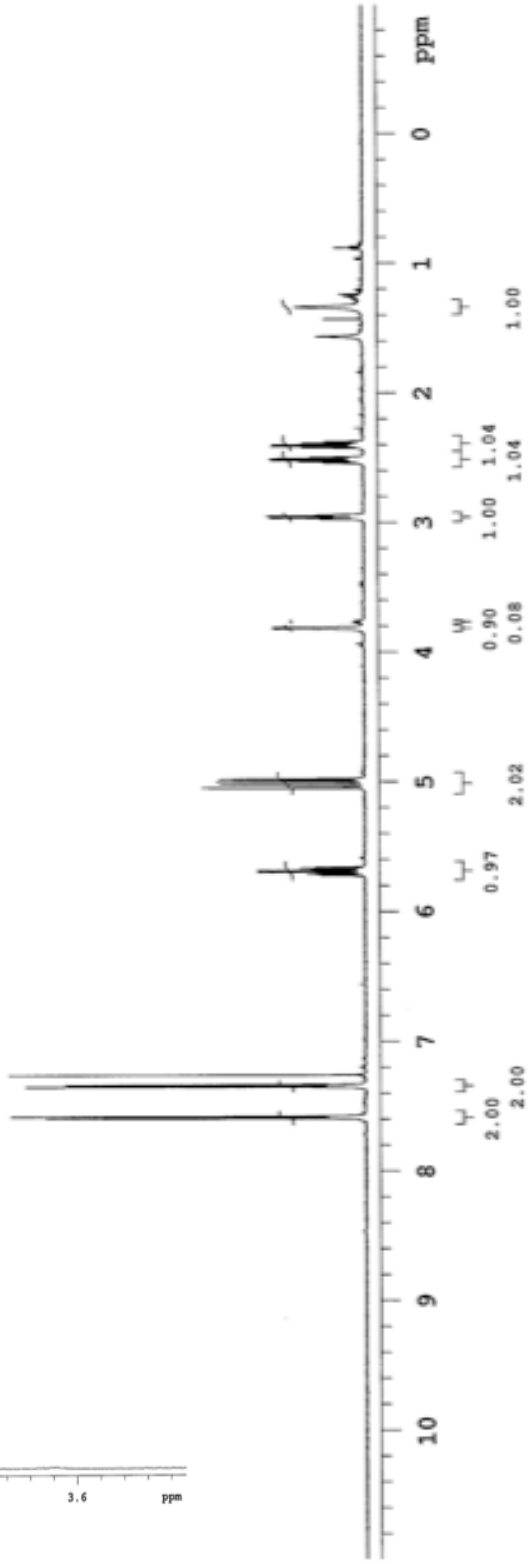

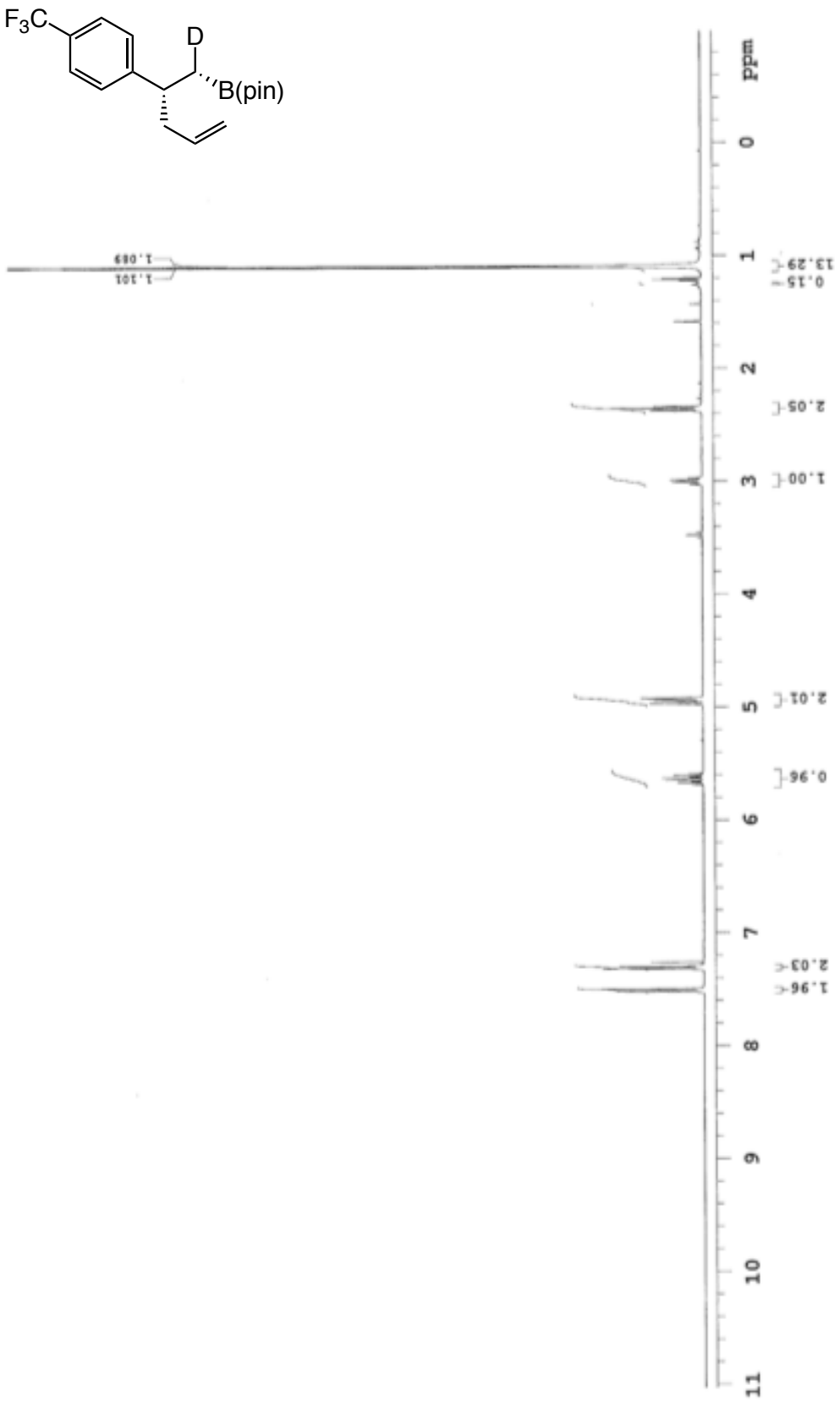
F3C
D
B(pin)
ppm
0
1
2
3
4
5
6
7
8
9
10
11
1.089
1.101
13.29
0.15
2.05
1.00
2.01
0.96
2.03
1.96

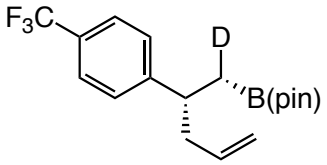
F3C
D
B(pin)

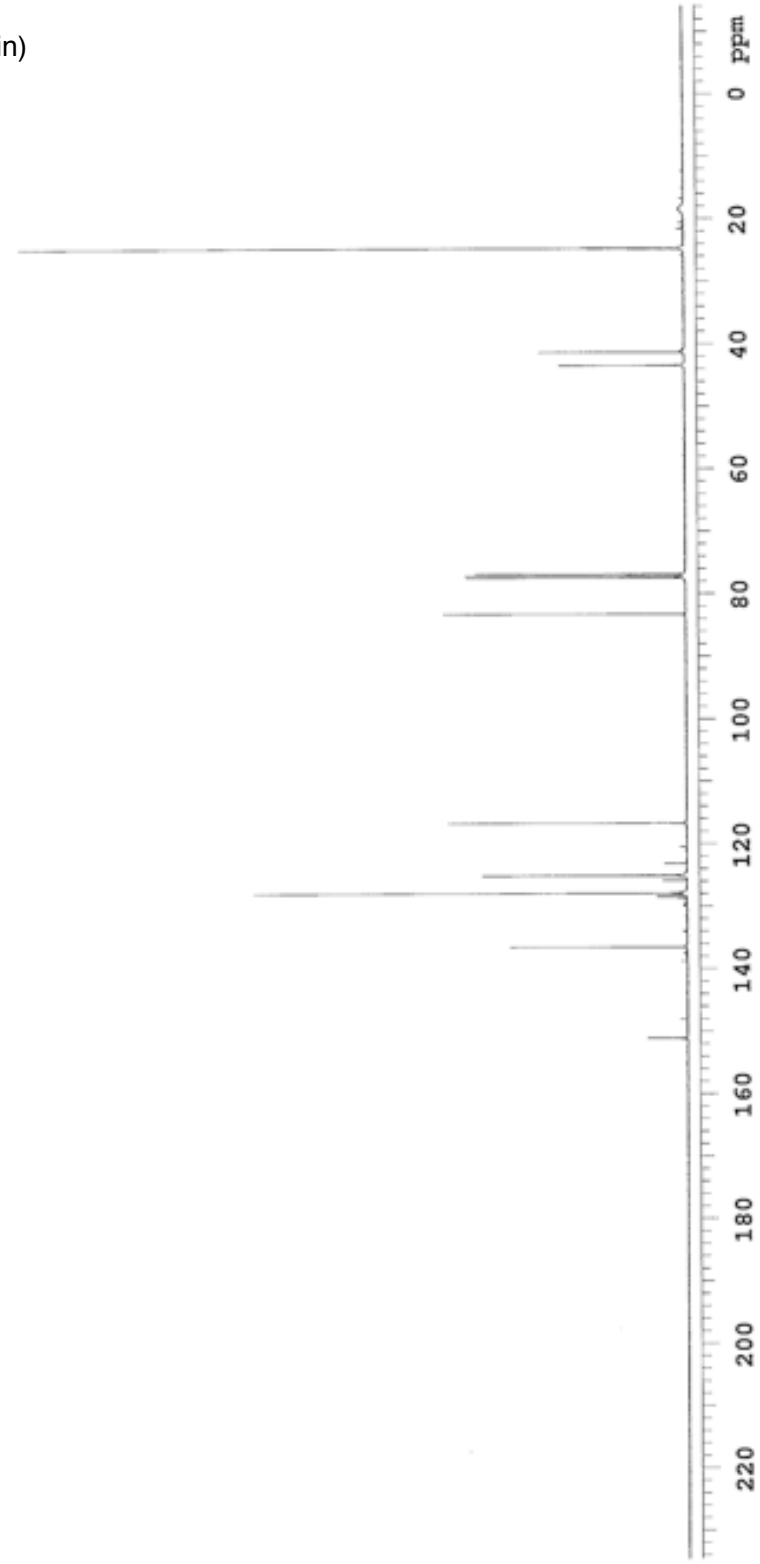
ppm
0
20
40
60
80
100
120
140
160
180
200
220

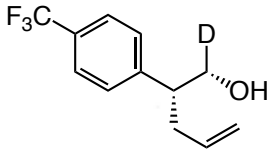

92:8 dr
(from 90:10 *Z:E alkene)*

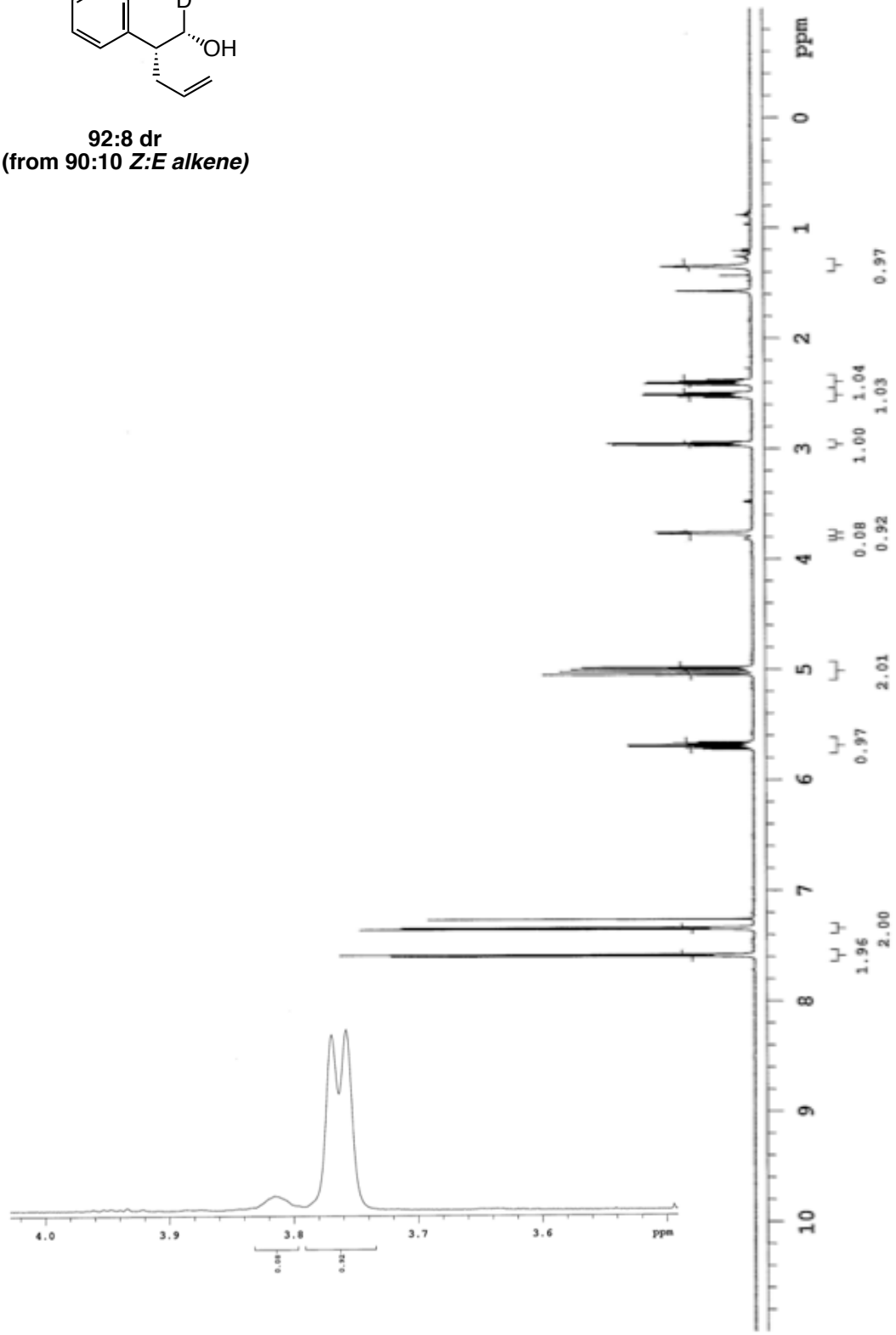

>98:2 dr
(from >98:2 *E:Z* alkene)

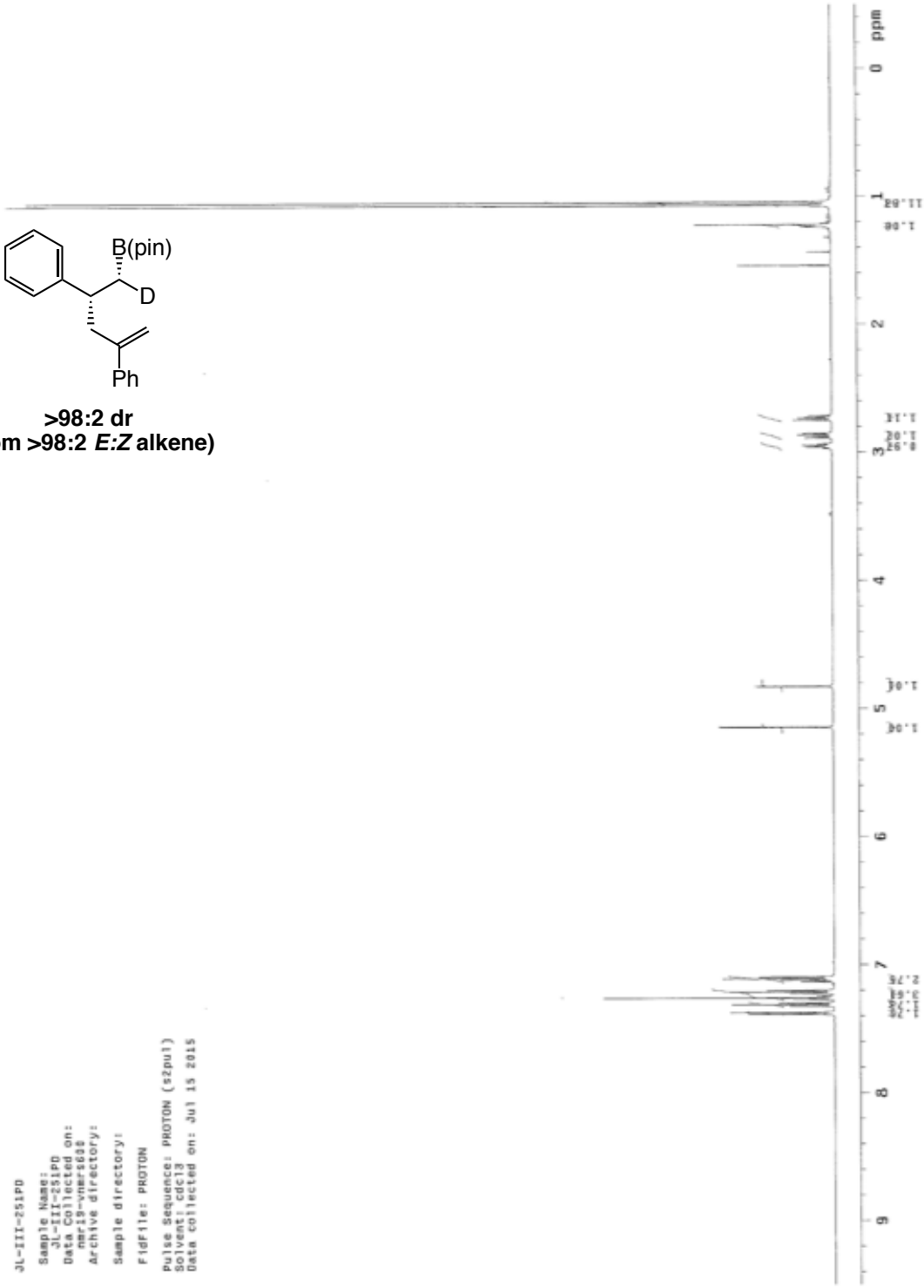

>98:2 dr
(from >98:2 *E:Z* alkene)

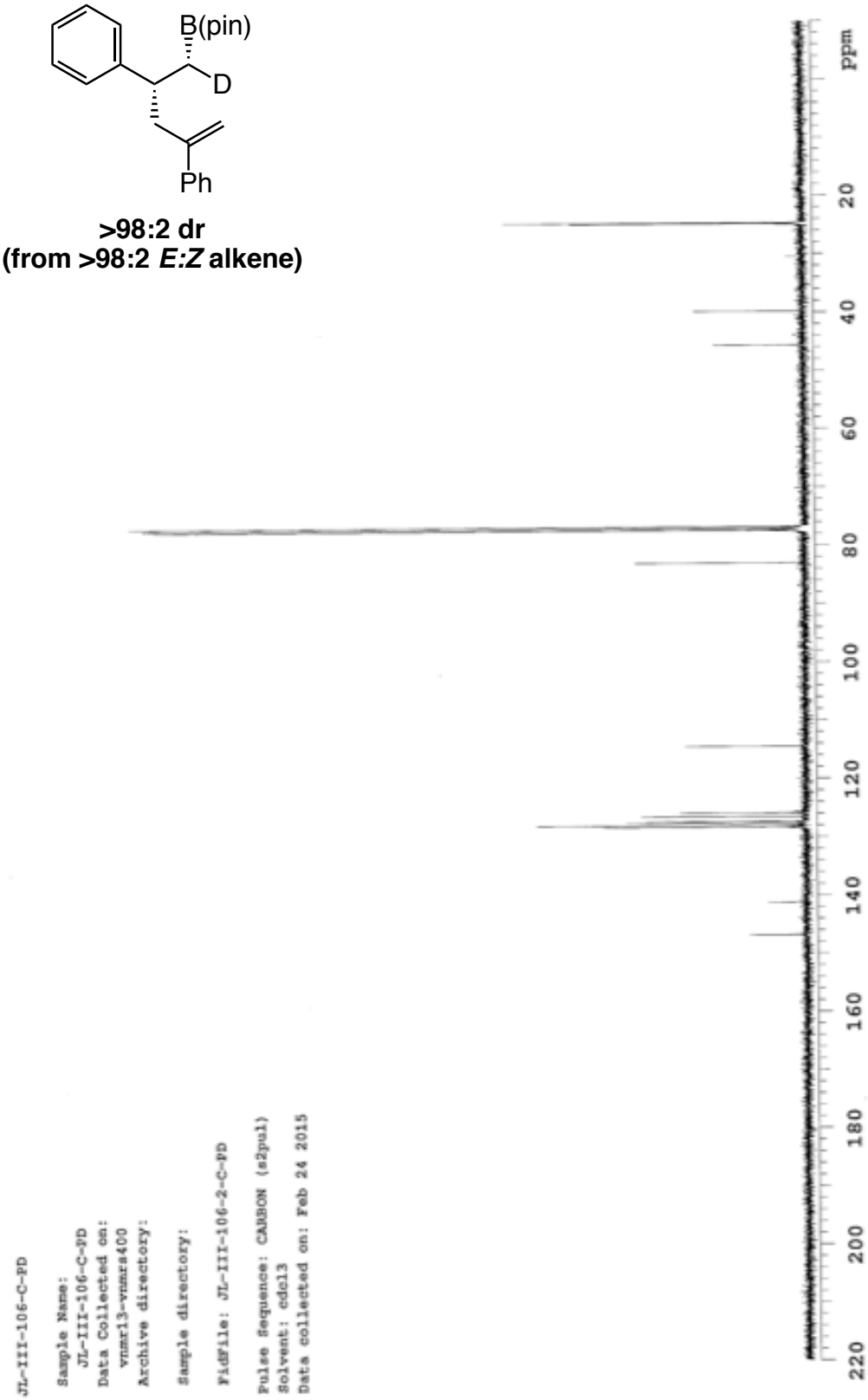

>95:5 dr
(from 96:4 *Z:E* alkene)

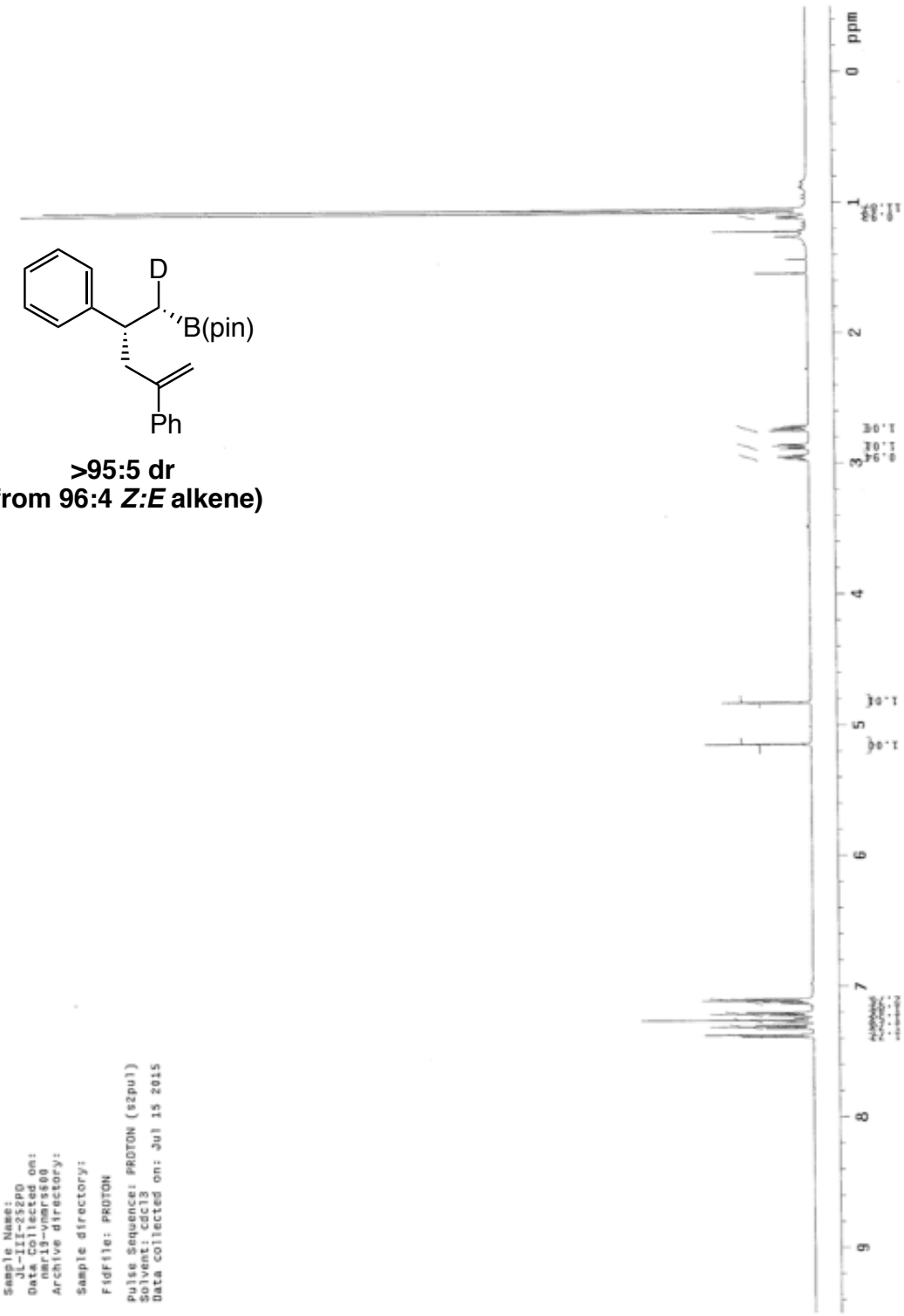

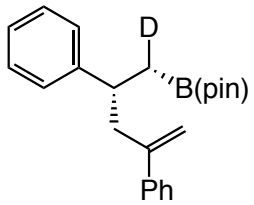

>95:5 dr
(from 96:4 *Z:E* alkene)

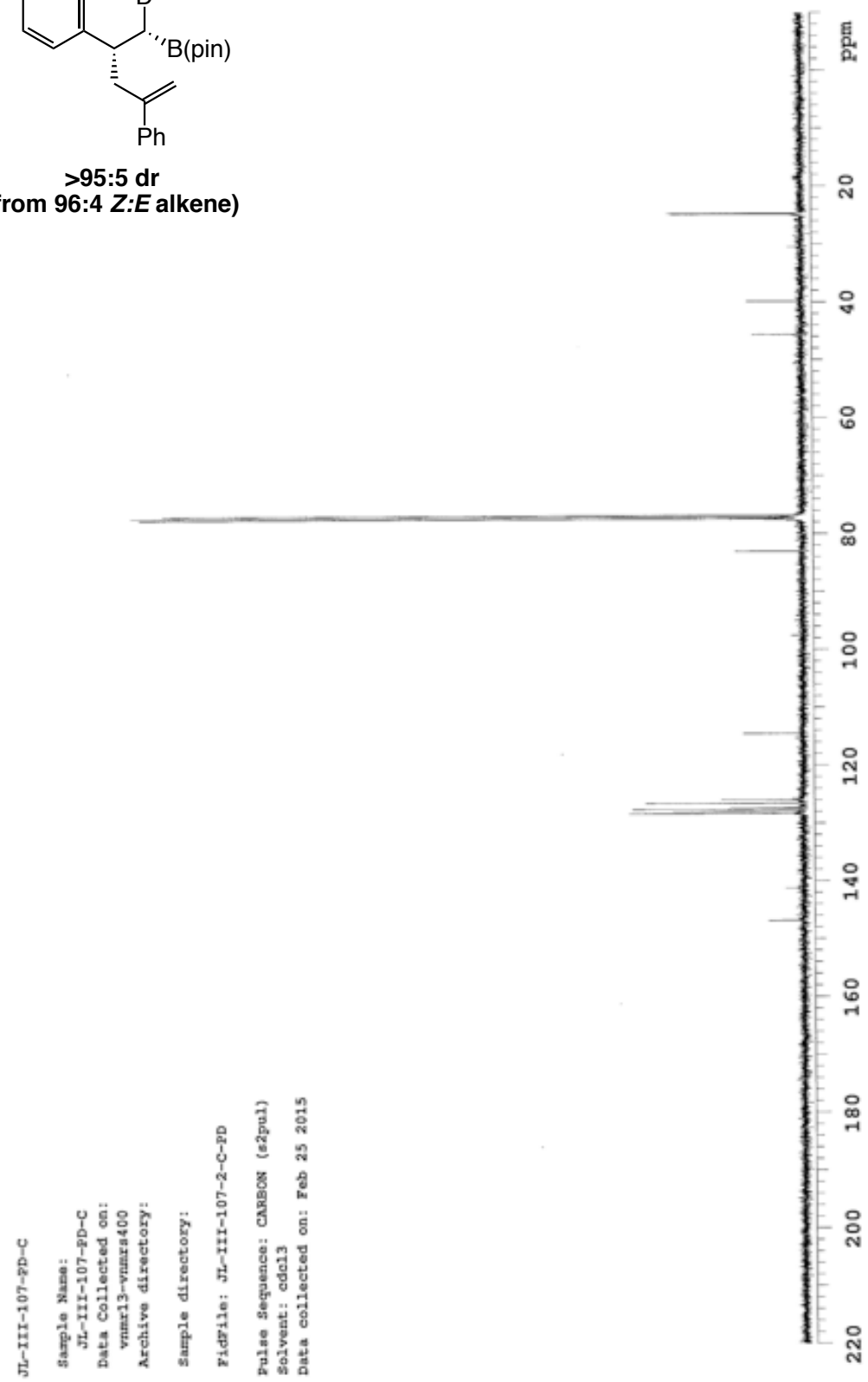

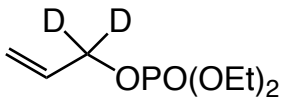
D
D
OPO(OEt)2

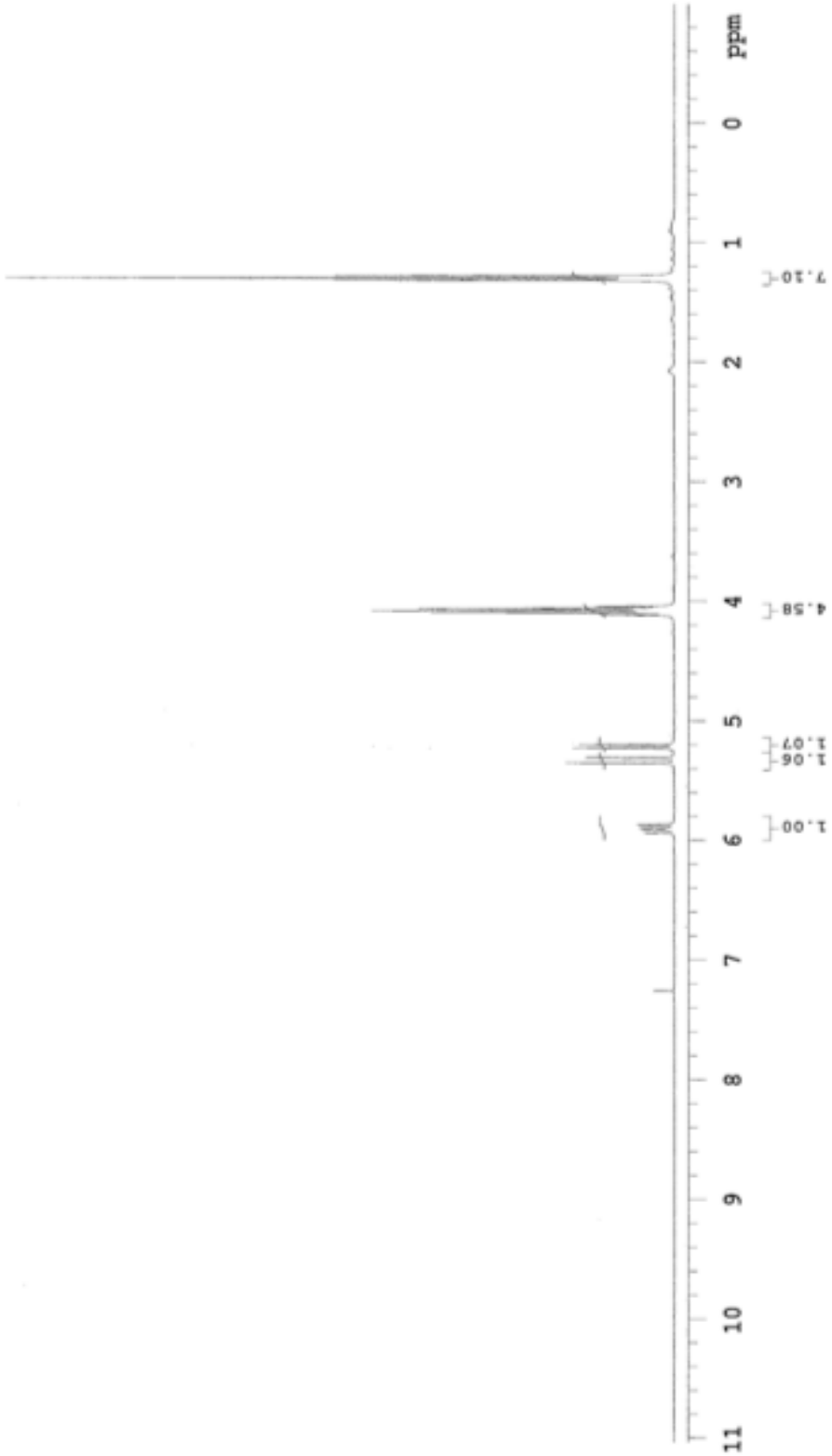
ppm
0
1
2
3
4
5
6
7
8
9
10
11
7.10
4.58
1.07
1.06
1.00

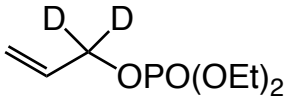
D
D
OPO(OEt)2

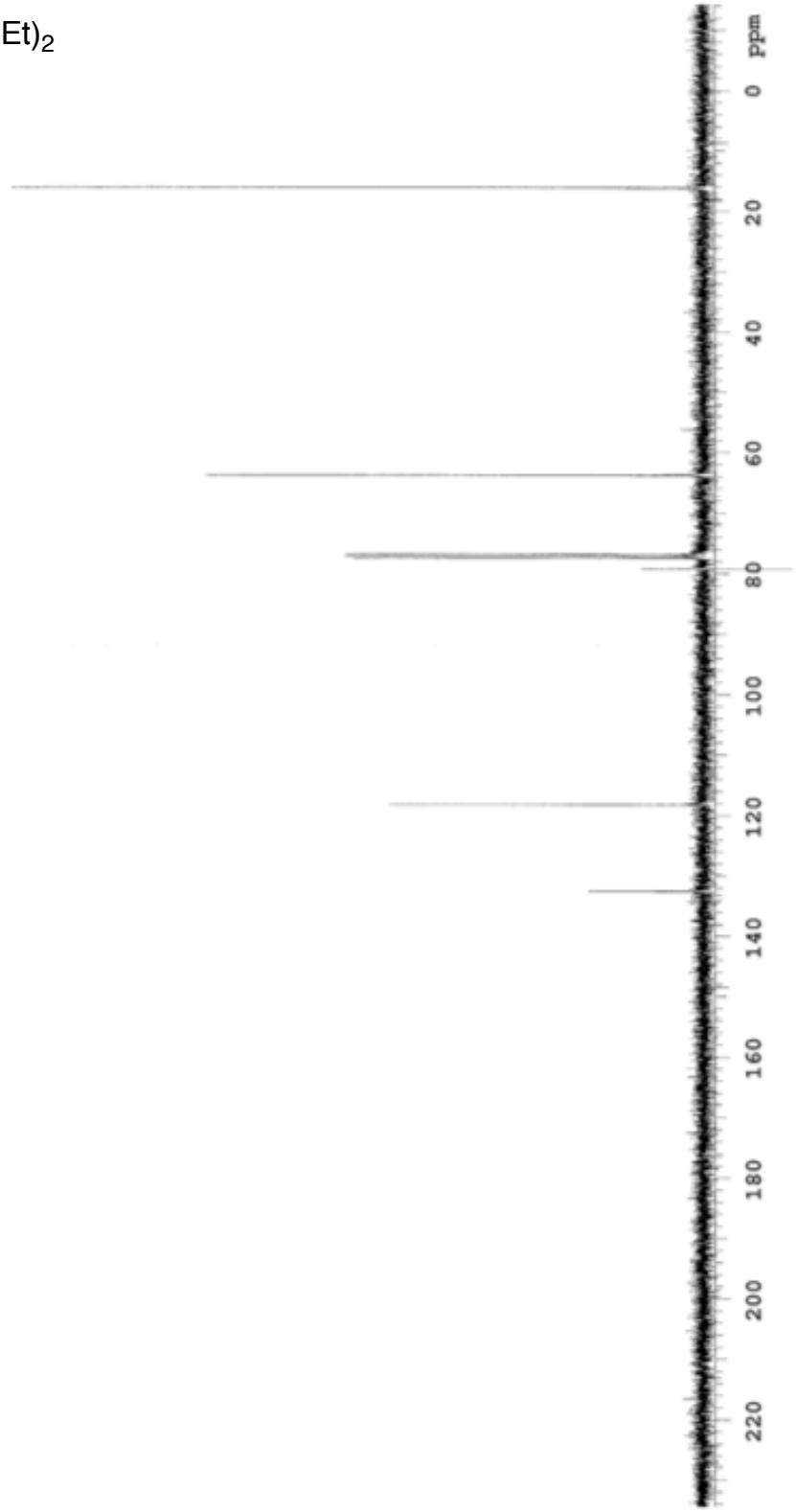
ppm
0
20
40
60
80
100
120
140
160
180
200
220

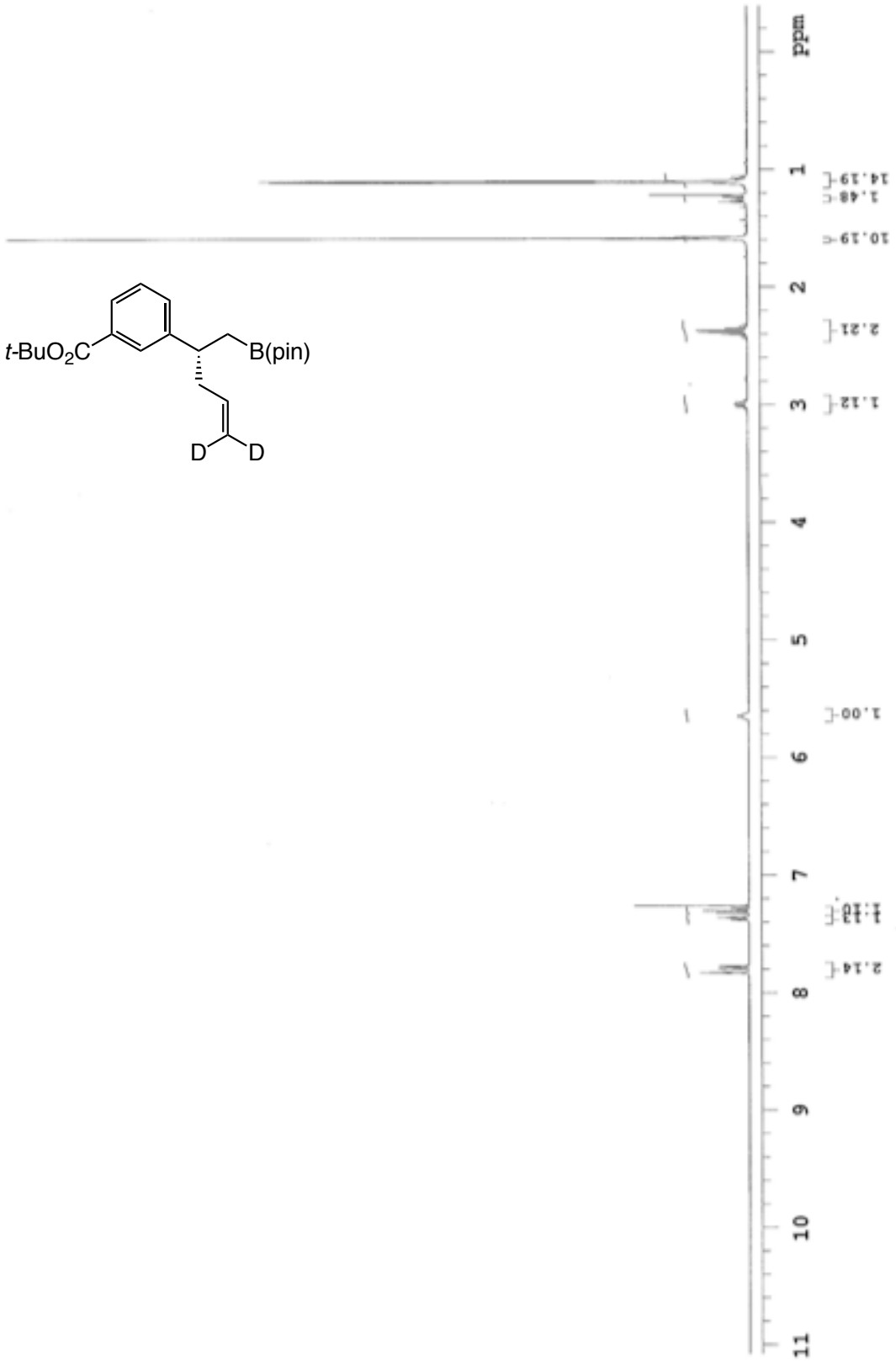
t-BuO2C
B(pin)
D
D
ppm
14.19
1.48
10.19
2.21
1.12
1.00
1.13
1.10
2.14
1
2
3
4
5
6
7
8
9
10
11

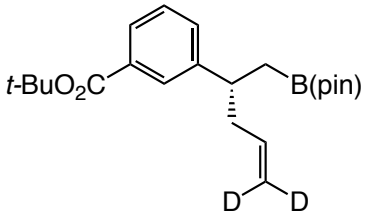
t-BuO2C
B(pin)
D
D

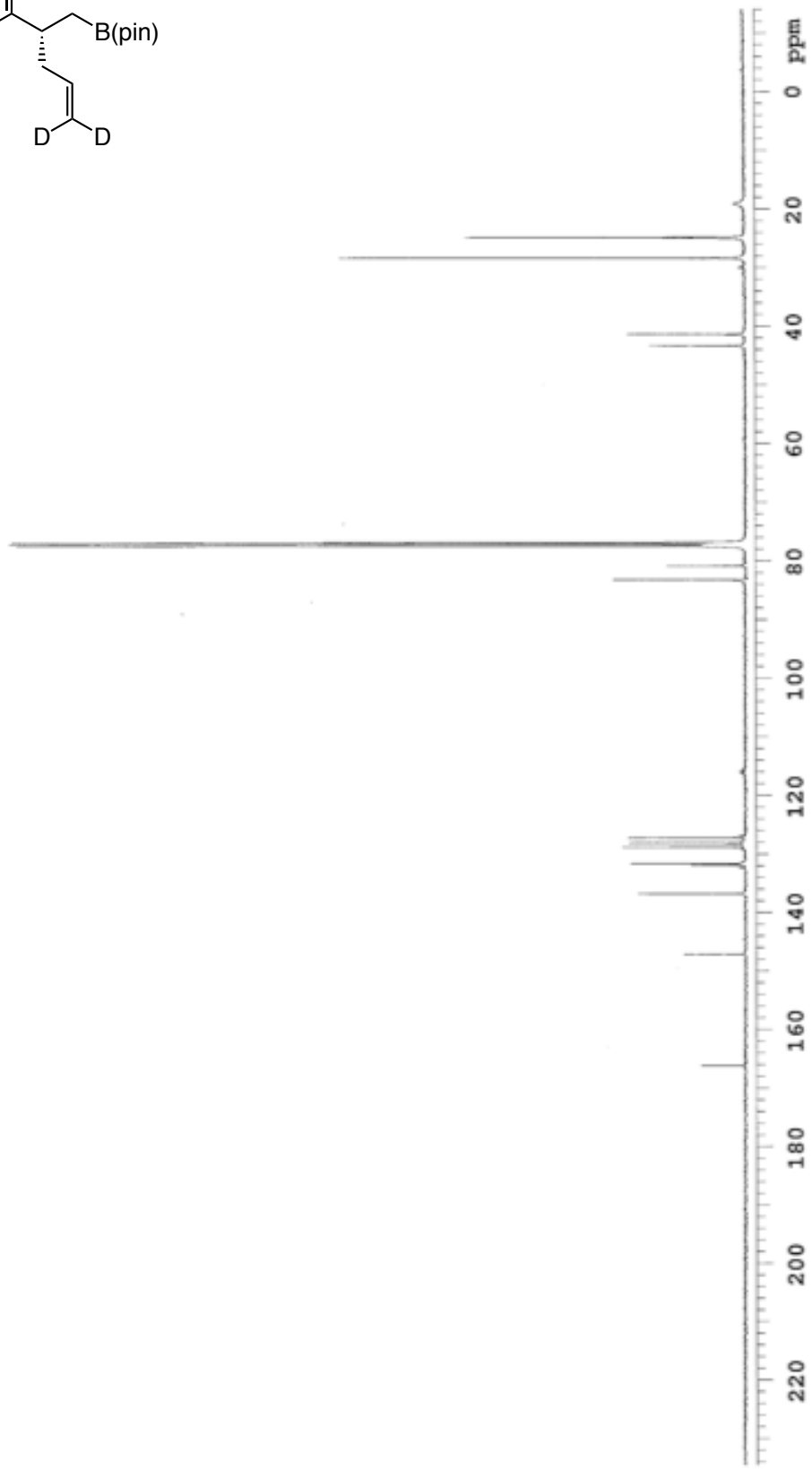
ppm
0
20
40
60
80
100
120
140
160
180
200
220

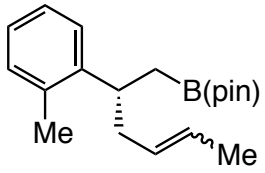
B(pin)
Me
Me

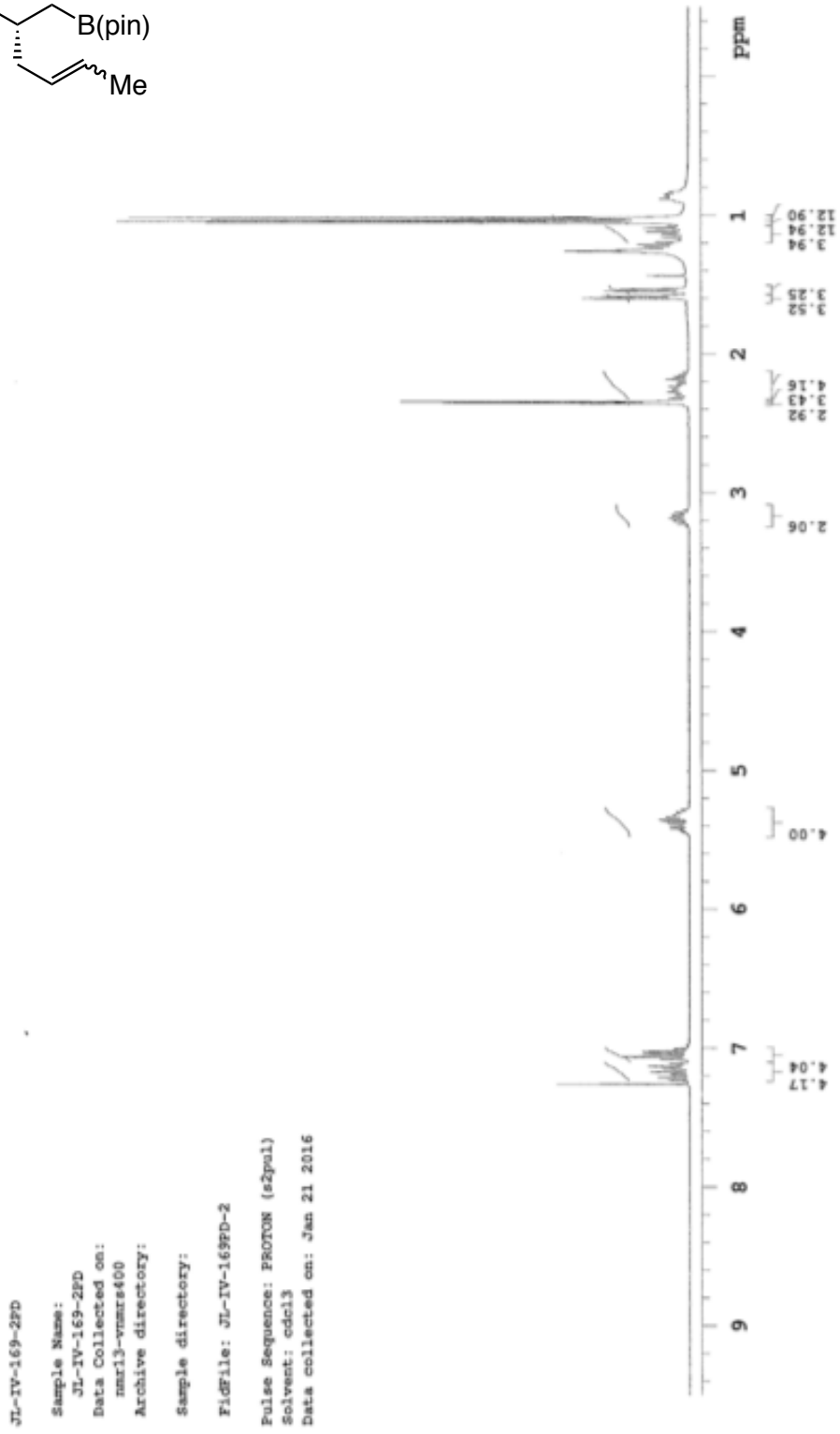
JL-IV-169-2PD
Sample Name:
JL-IV-169-2PD
Data Collected on:
nmr13-vnmrs400
Archive directory:
Sample directory:
FidFile: JL-IV-169PD-2
Pulse Sequence: PROTON (s2pul)
Solvent: cdcl3
Data collected on: Jan 21 2016
ppm
1
2
3
4
5
6
7
8
9
12.90
12.94
3.94
3.52
3.25
4.16
3.43
2.92
2.06
4.00
4.04
4.17

B(pin)

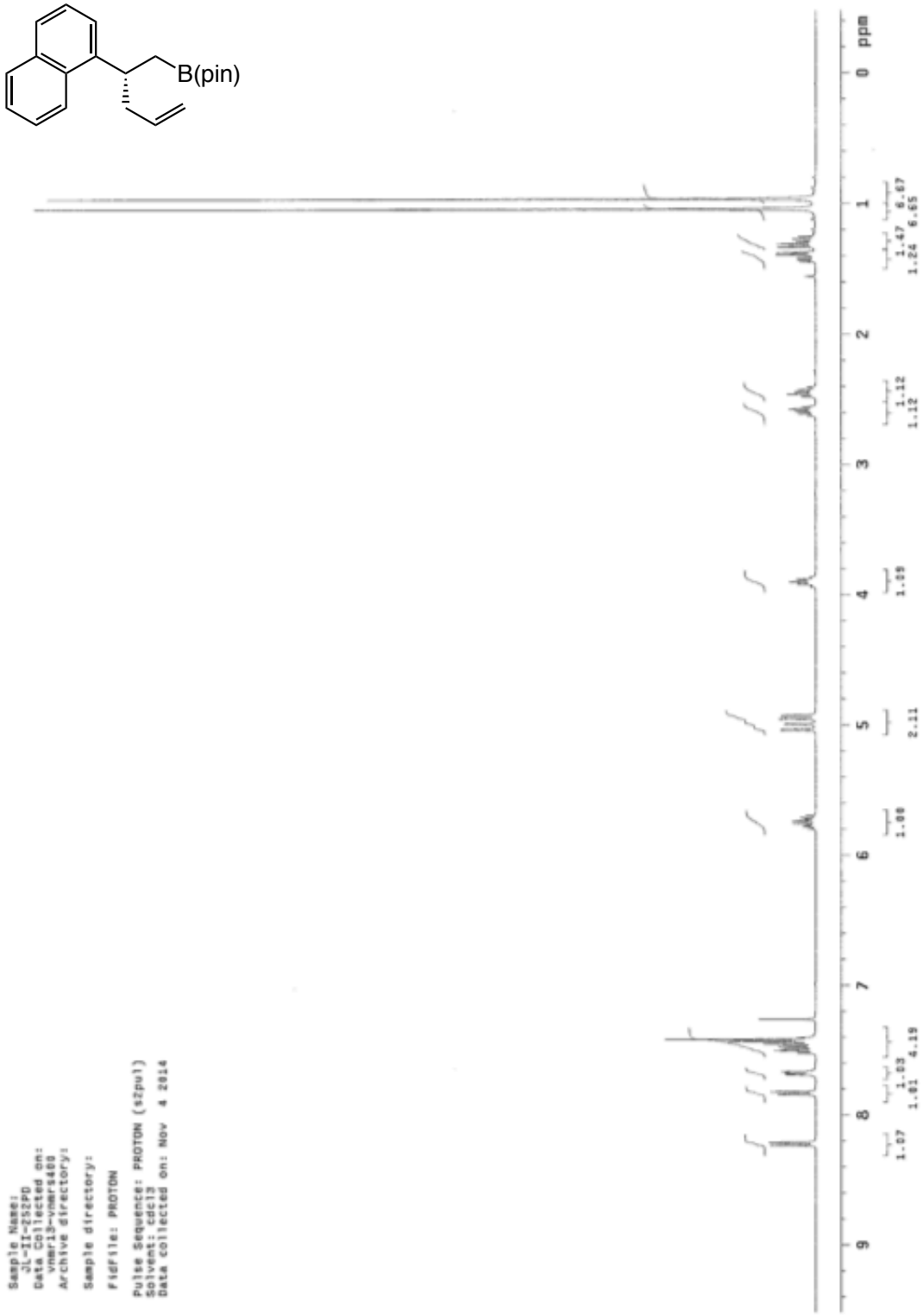
Sample Name:
2L-II-252PD
Data Collected on:
vnmr13-vnmr1469
Archive directory:
Sample directory:
Fidfile: PROTON
Pulse Sequence: PROTON (s2pul)
Solvent: cdcl3
Data collected on: Nov 4 2014
ppm
0
1
2
3
4
5
6
7
8
9
1.47 6.67
1.24 6.65
1.12
1.12
1.09
2.11
1.08
1.03
1.07 1.01 4.19

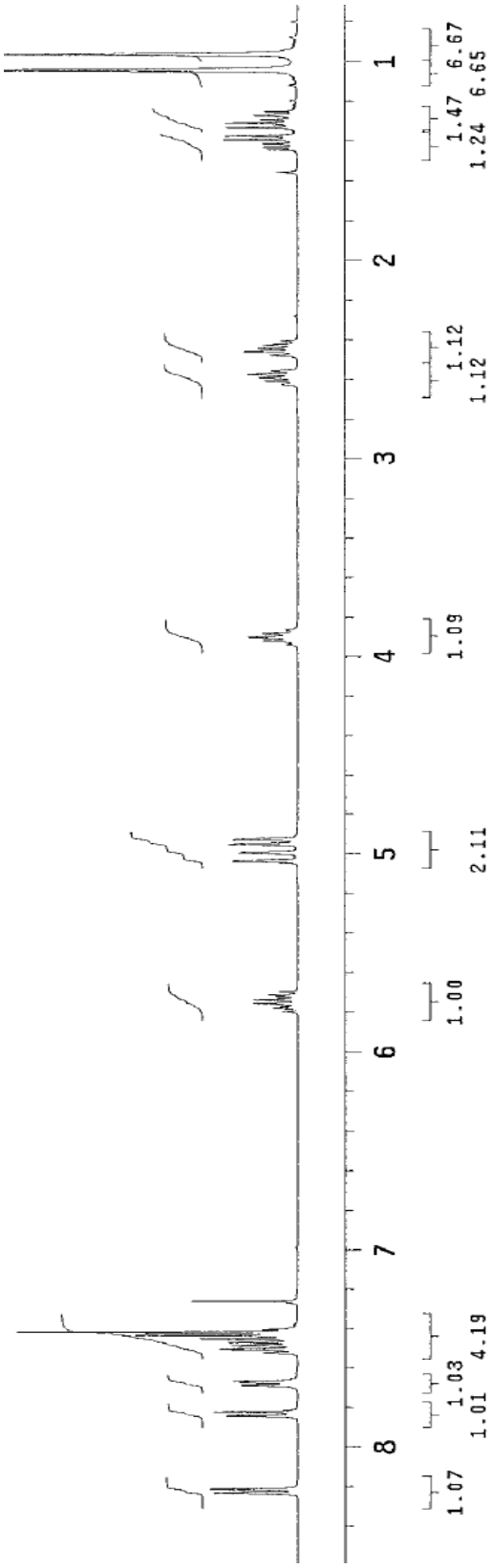
1.07
1.01
1.03
4.19
1.00
2.11
1.09
1.12
1.12
1.47
1.24
6.67
6.65
8
7
6
5
4
3
2
1

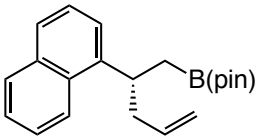
B(pin)

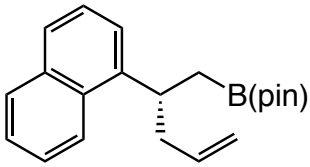
B(pin)

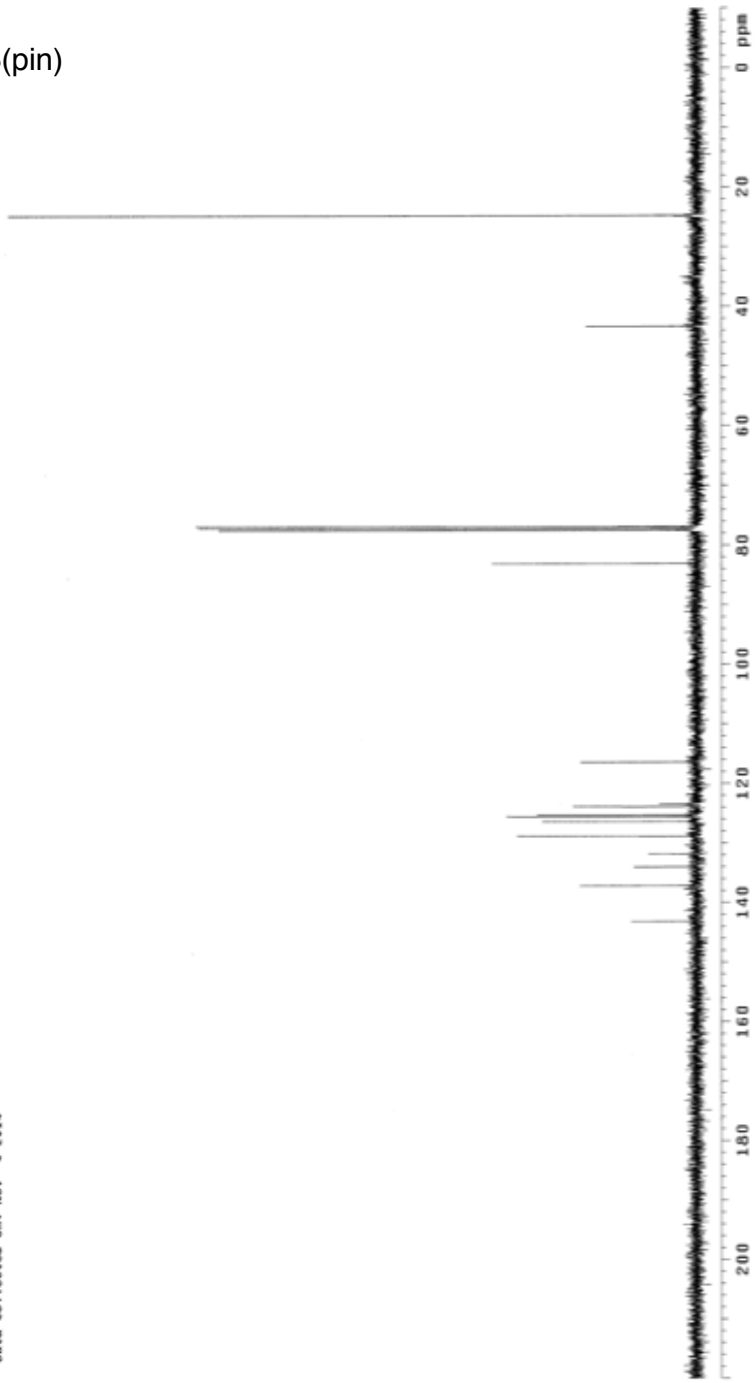
JL-II-252PD-C
Sample Name:
JL-II-252PD-C
Data Collected on:
Varian 500-MHz
Archive directory:
Sample directory:
FidFile: JL-II-252PD-C
Pulse Sequence: CARBON (s2pul)
Solvent: CDCl3
Data collected on: Nov 4 2014
200
180
160
140
120
100
80
60
40
20
0 ppm

Me
B(pin)

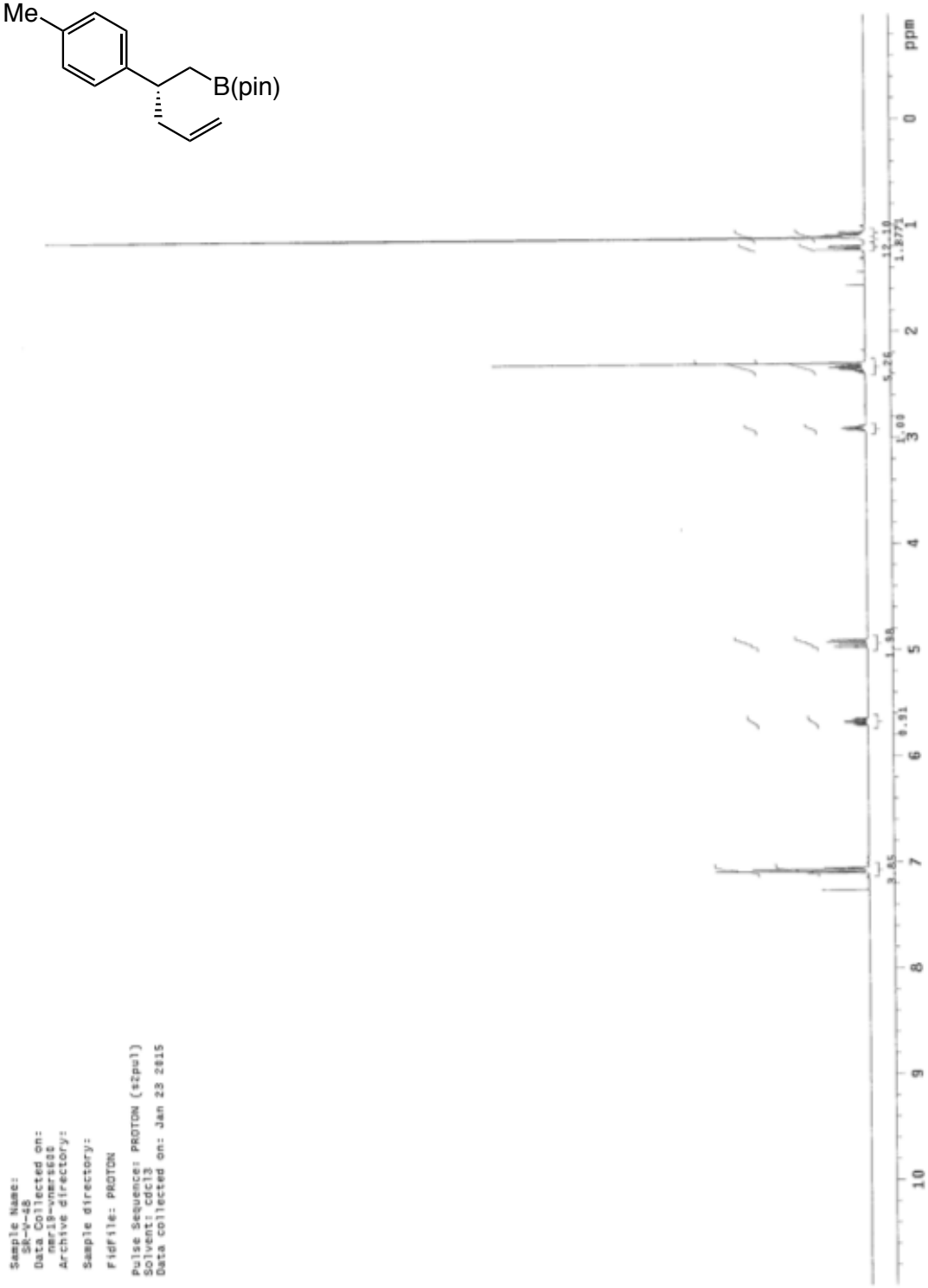
Sample Name:
SK-2-48
Data Collected on:
nmr19-nmrsis6
Archive directory:
Sample directory:
Fidfile: PROTON
Pulse Sequence: PROTON (s2pul)
Solvent: cdcl3
Data collected on: Jan 23 2015
ppm
0
1
2
3
4
5
6
7
8
9
10
12.10
1.3771
5.26
1.00
1.86
0.91
3.85

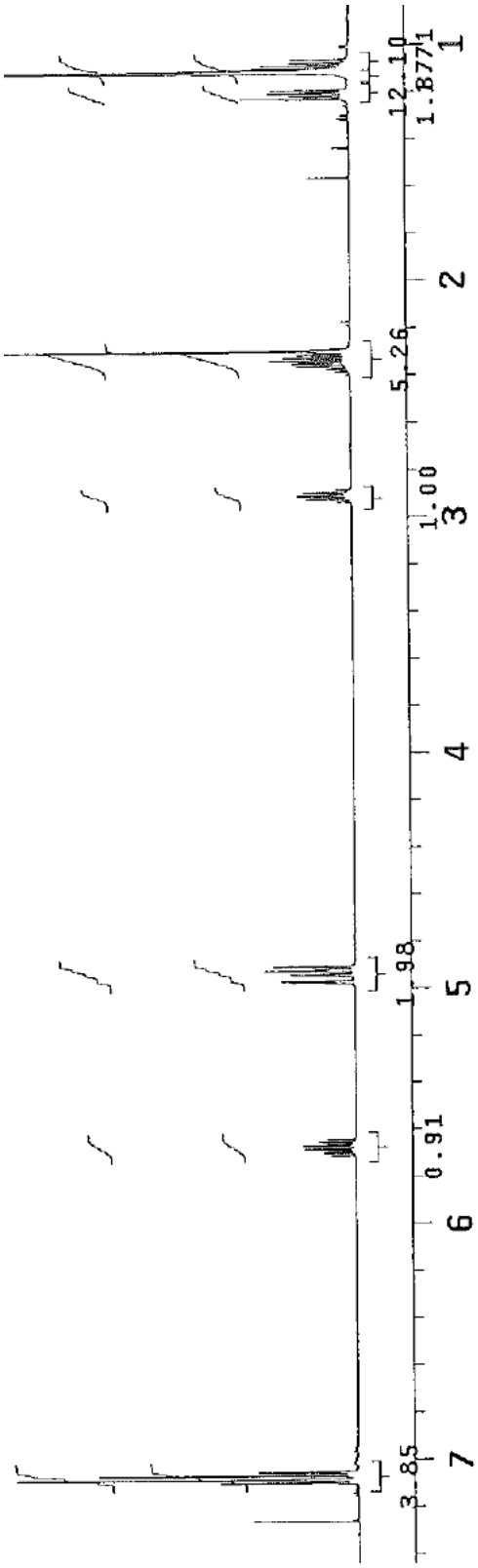
12.10
1.8771
5.26
1.00
1.98
0.91
3.85
1
2
3
4
5
6
7

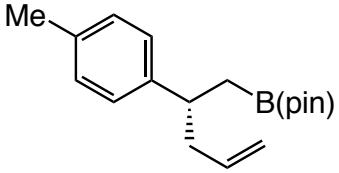
Me
B(pin)

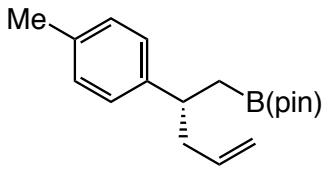
Me
B(pin)

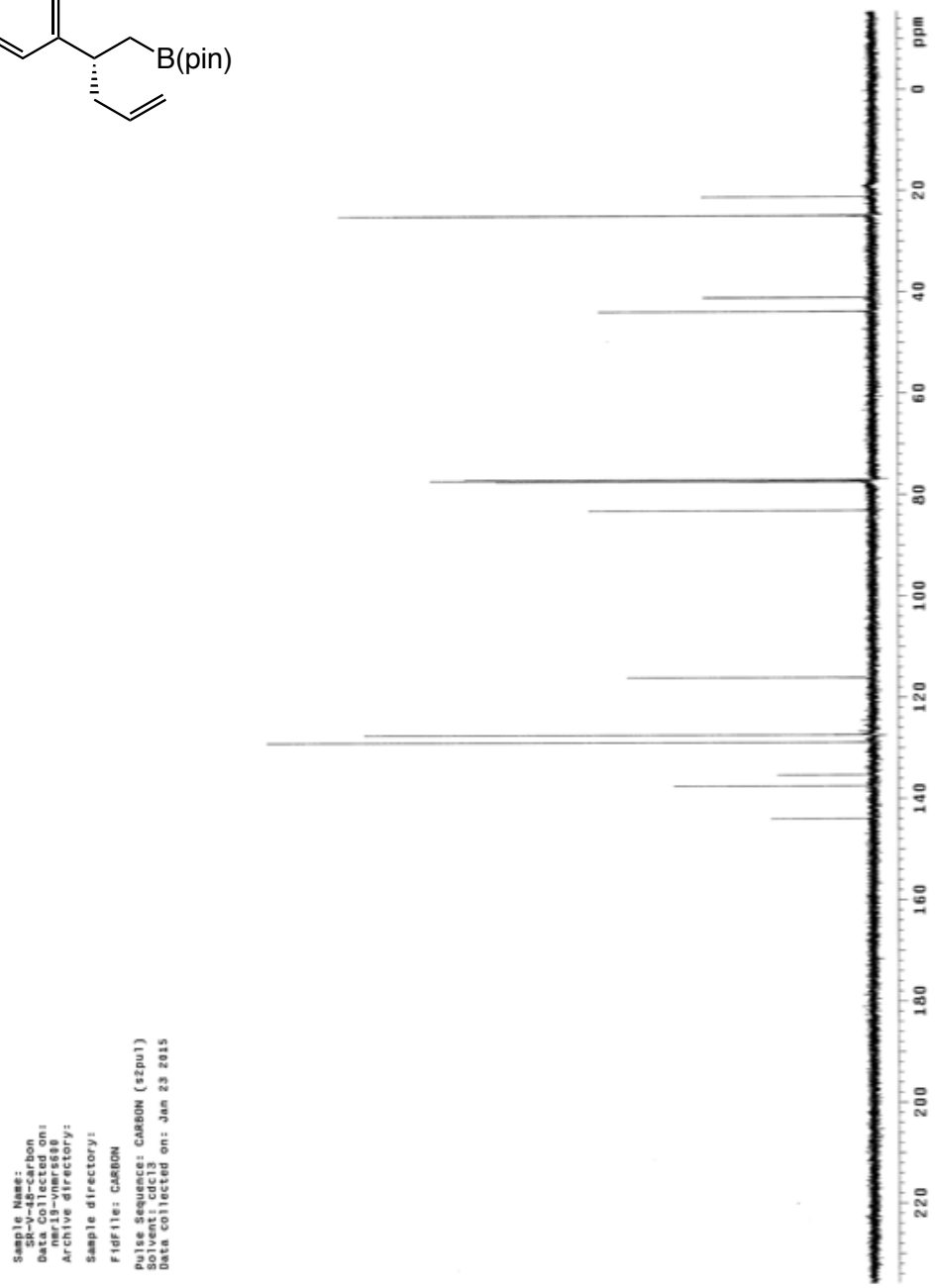
Sample Name:
SR-V-48-carbon
Data Collected on:
nmr19-vnmrs600
Archive directory:
Sample directory:
FidFile: CARBON
Pulse Sequence: CARBON (s2pul)
Solvent: cdcl3
Data collected on: Jan 23 2015
ppm
0
20
40
60
80
100
120
140
160
180
200
220

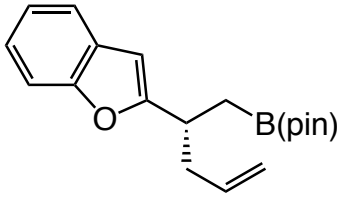
O
B(pin)

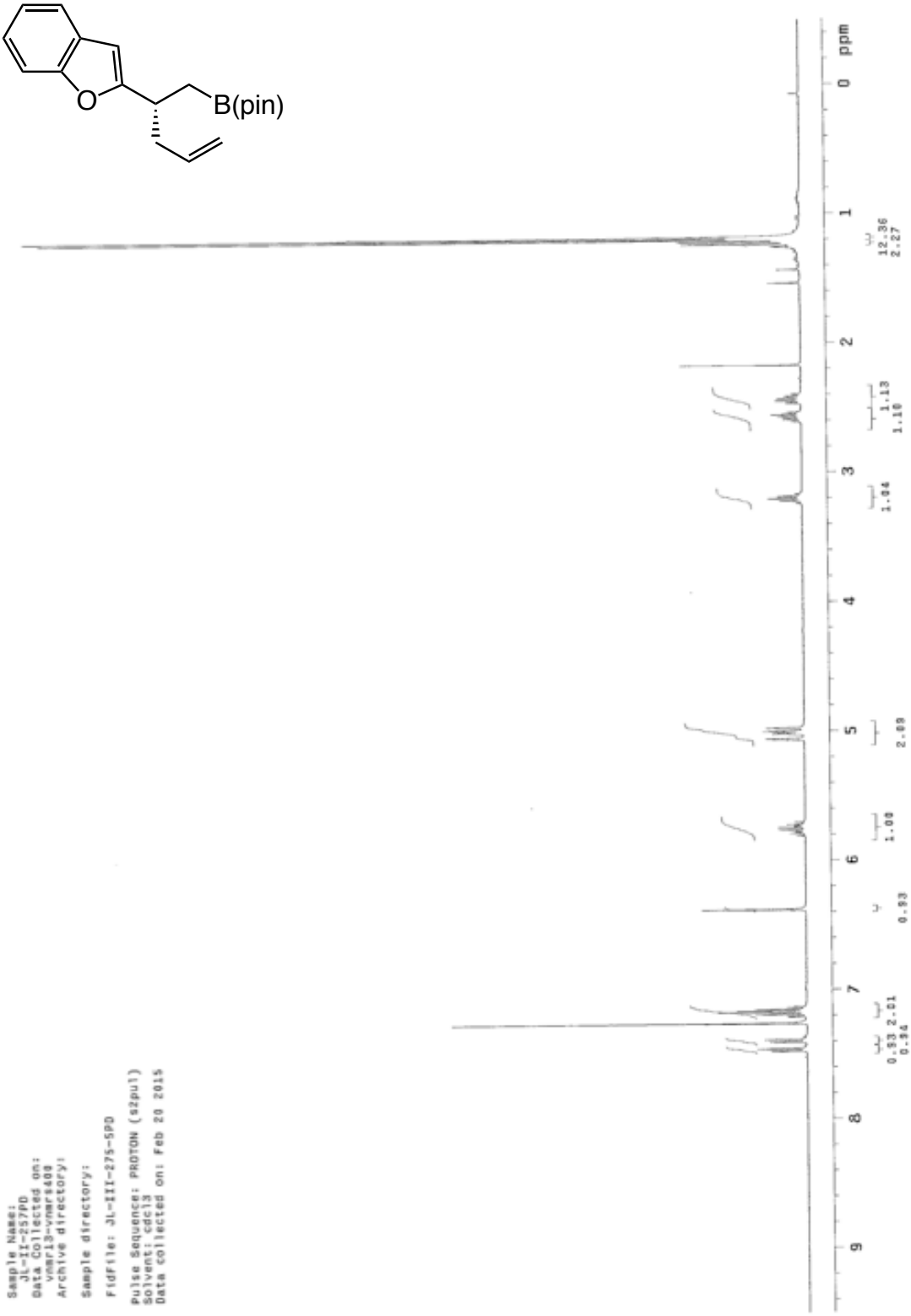
Sample Name:
JL-II-257PD
Data Collected on:
vnmr13-vnmrs400
Archive directory:
Sample directory:
FidFile: JL-III-275-SPD
Pulse Sequence: PROTON (s2pul)
Solvent: cdcl3
Data collected on: Feb 20 2015
ppm
0
1
2
3
4
5
6
7
8
9
12.36
2.27
1.13
1.10
1.04
2.08
1.08
0.93
0.93 2.01
0.94

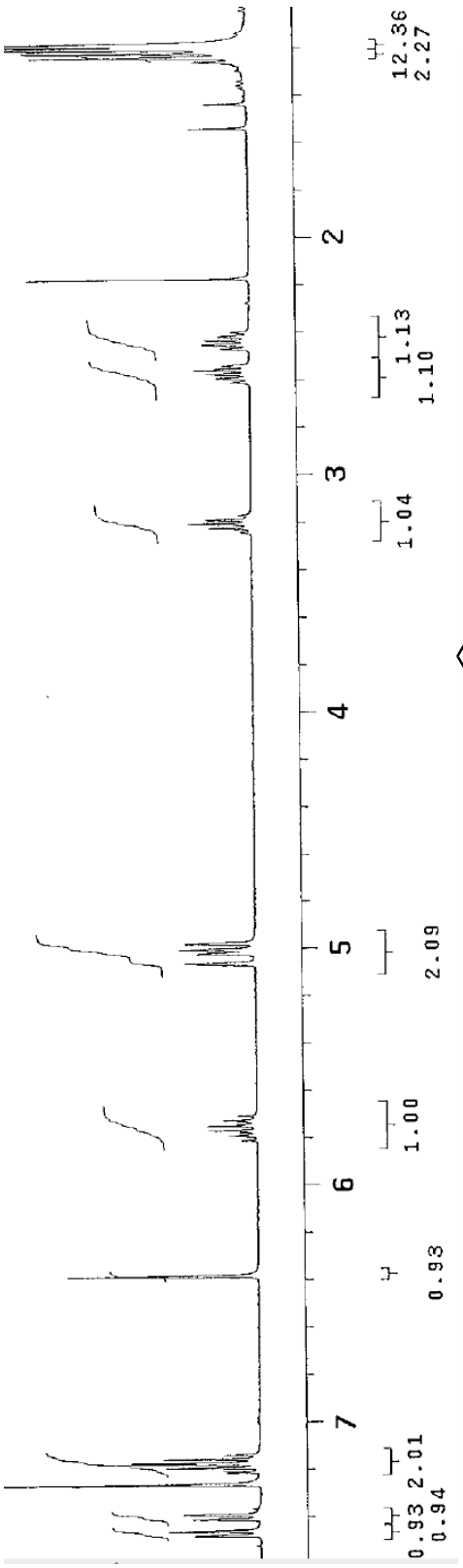
12.36
2.27
1.13
1.10
1.04
2.09
1.00
0.93
2.01
0.94
7
6
5
4
3
2

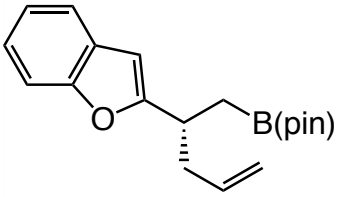
O
B(pin)

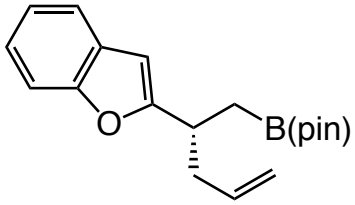
O
B(pin)

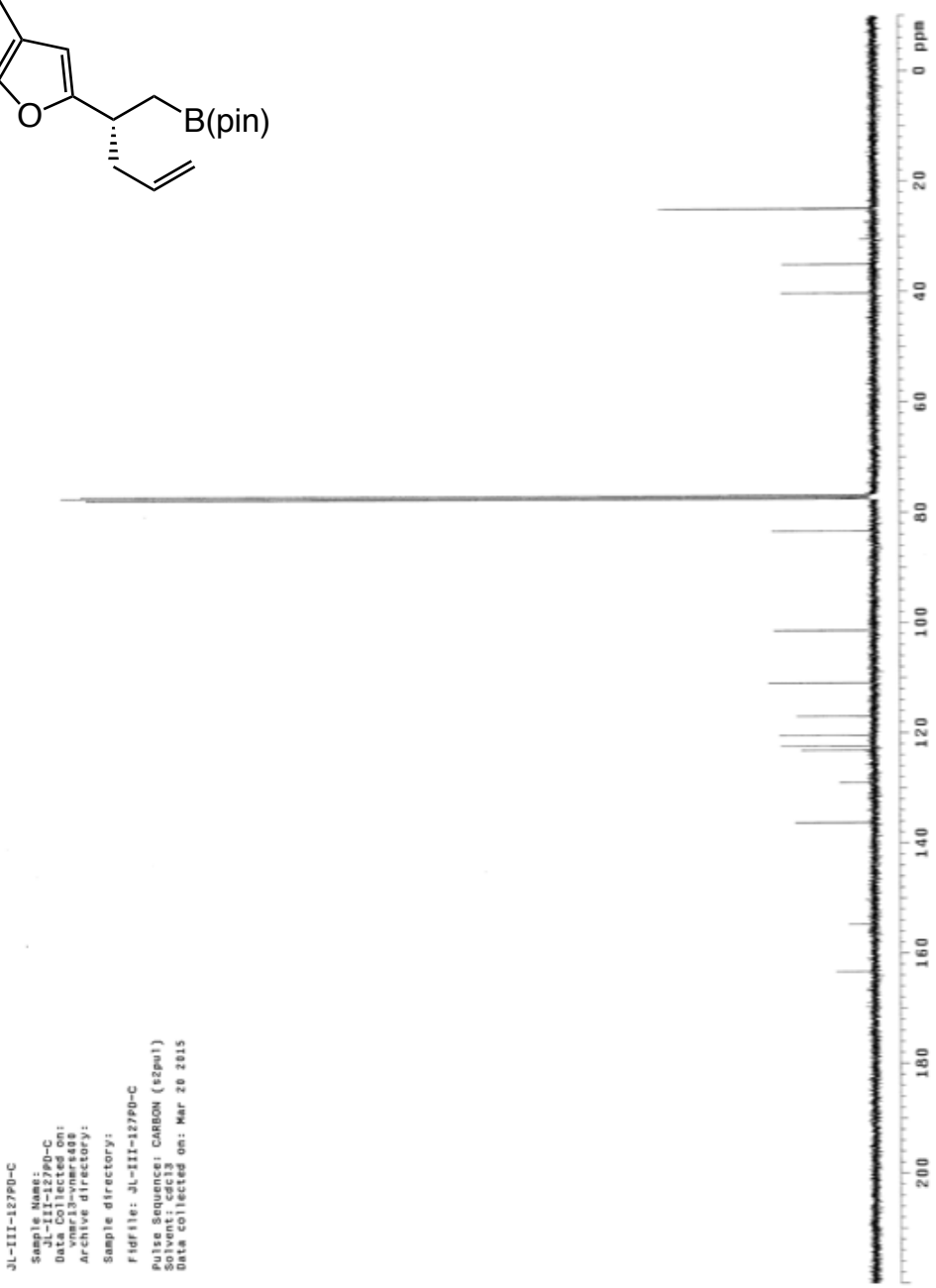
JL-III-127PD-C
Sample Name:
JL-III-127PD-C
Data Collected on:
vnmrs-3-nmrsdg
Archive directory:
Sample directory:
Fidfile: JL-III-127PD-C
Pulse Sequence: CARBON (s2pul)
Solvent: cdcl3
Data Collected on: Mar 20 2015
200
180
160
140
120
100
80
60
40
20
0 ppm

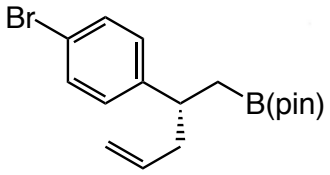
Br
B(pin)

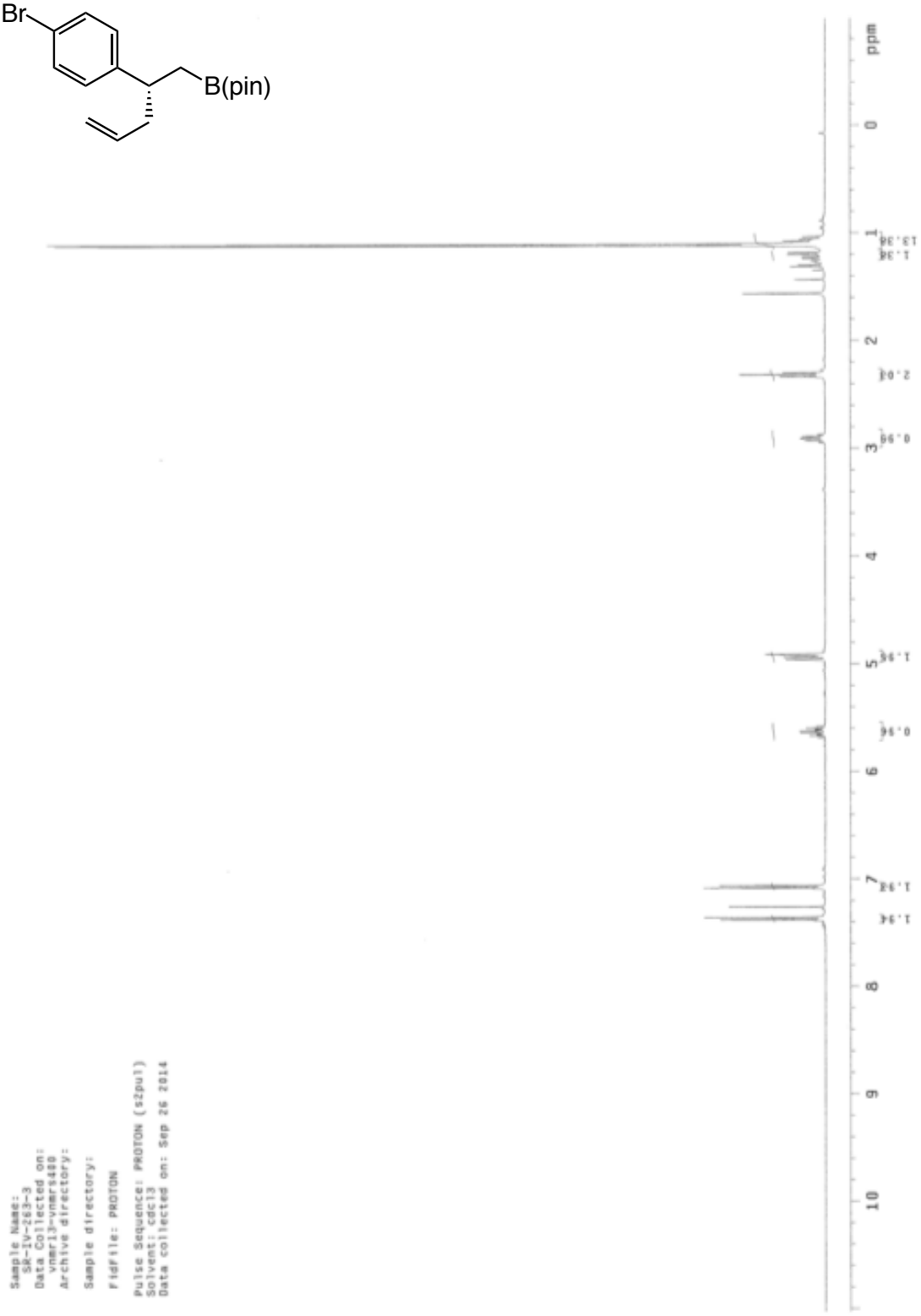
Sample Name:
SR-IV-263-3
Data Collected on:
vnmr13-vnmrs400
Archive directory:
Sample directory:
FidFile: PROTON
Pulse Sequence: PROTON (s2pul)
Solvent: cdcl3
Data collected on: Sep 26 2014
ppm
0
1
2
3
4
5
6
7
8
9
10
13.34
1.34
2.04
0.96
1.96
0.96
1.92
1.94

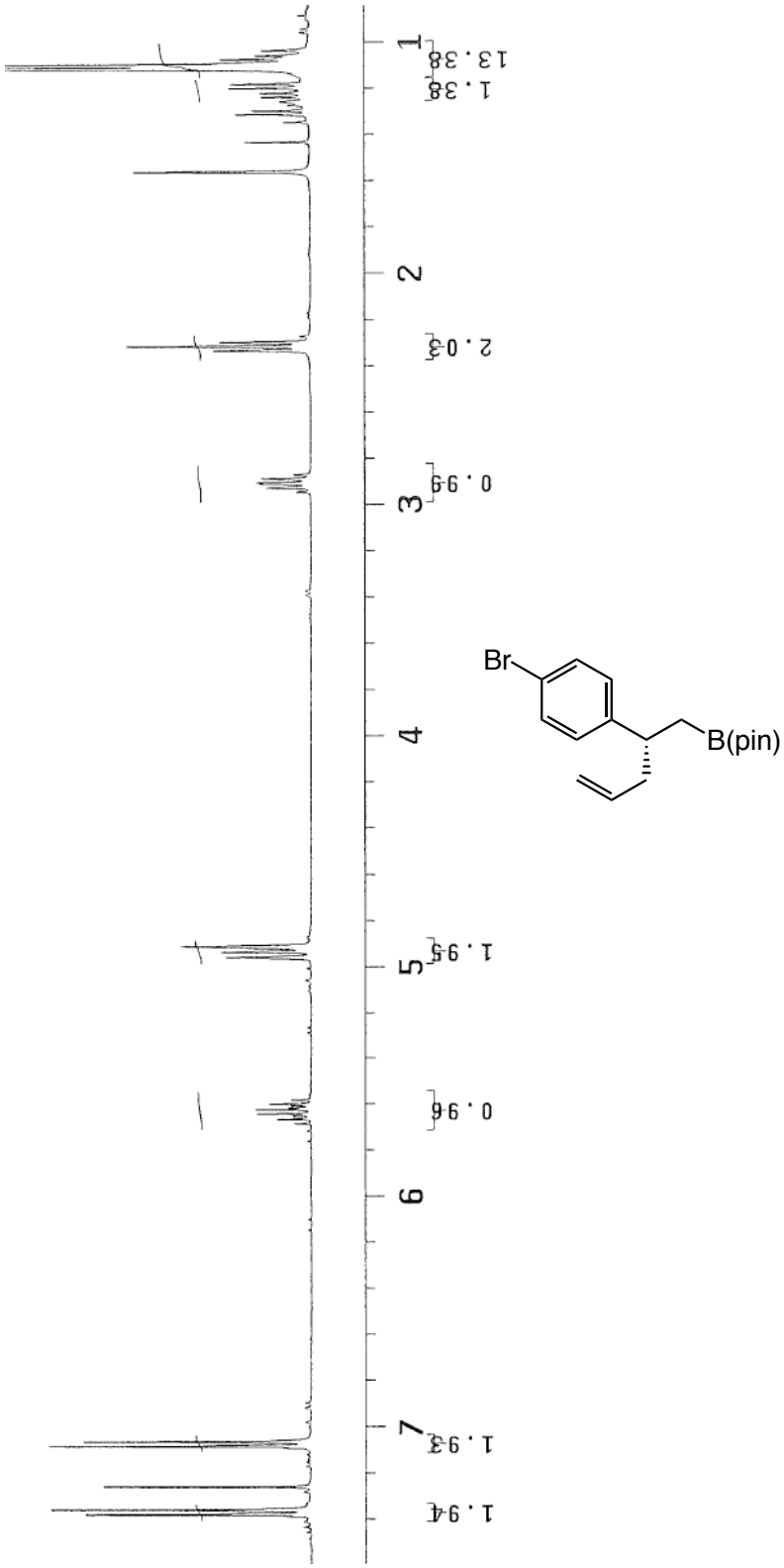
Br
B(pin)
1.94
1.93
0.96
1.95
0.99
2.03
1.38
13.38
7
6
5
4
3
2
1

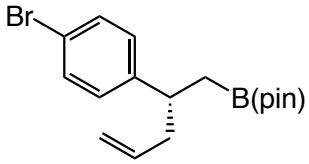
Br
B(pin)

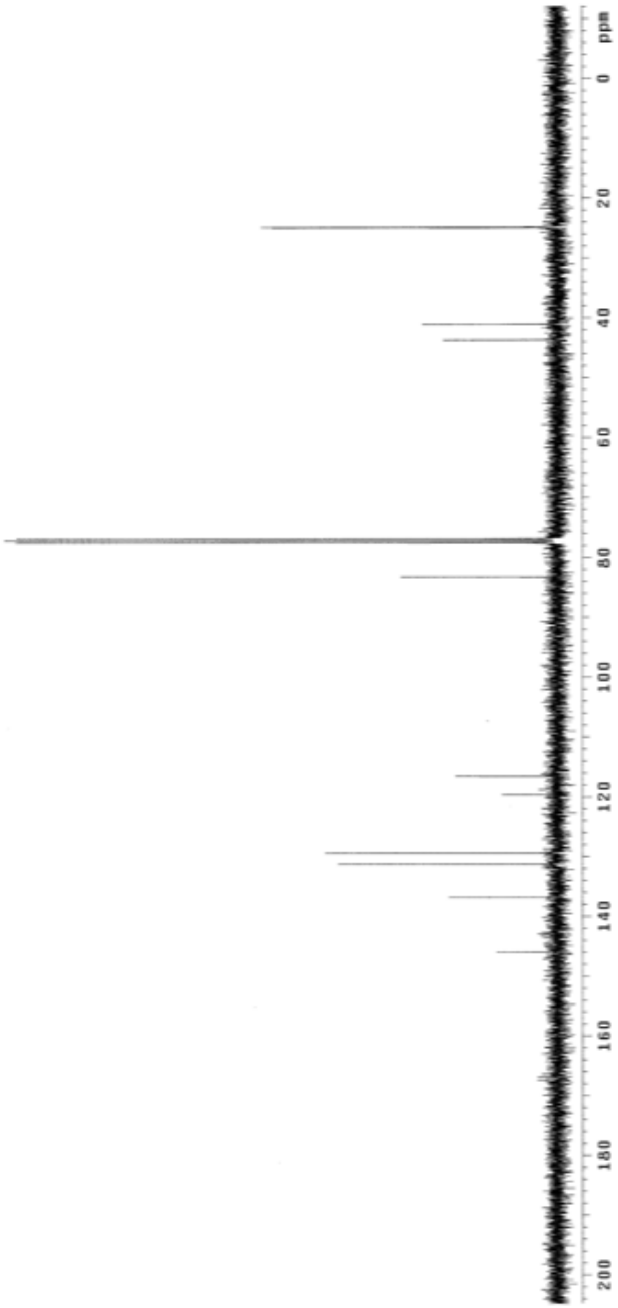
Sample Name:
SR-IV-263-3-carbon
Data Collected on:
vnmrj1-vnmrs600
Archive directory:
Sample directory:
Fidfile: SR-IV-263-3-carbon
Pulse Sequence: CARBON (s2pul)
Solvent: cdcl3
Data collected on: Sep 26 2014
ppm
0
20
40
60
80
100
120
140
160
180
200

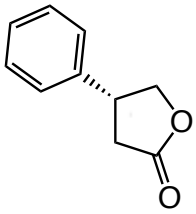

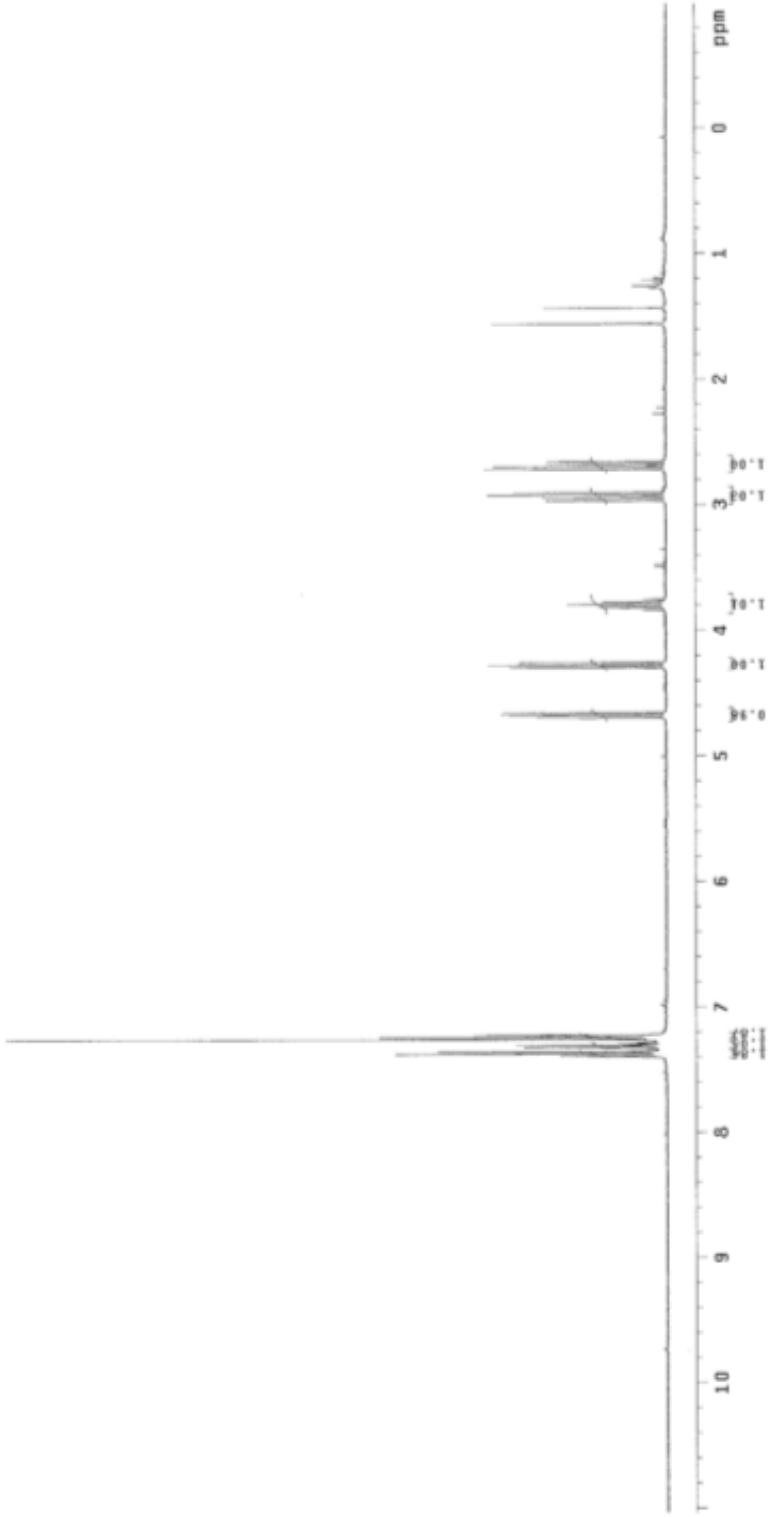
Sample Name:
SR-IV-266-oxid
Data Collected on:
nmr14-vnmrs400
Archive directory:
Sample directory:
FidFile: PROTON
Pulse Sequence: PROTON (s2pul)
Solvent: CdCl3
Data collected on: Mar 26 2015
ppm
0
1
2
3
4
5
6
7
8
9
10
1.00
1.00
1.00
1.00
0.96

CHAPTER 2

Versatile Homoallylic Boronates by Chemo-, S_N2'-, Diastereo- and Enantioselective Catalytic Sequence of Cu–H Addition to Vinyl-B(pin)/Allylic Substitution

2.1 Introduction

Catalytic methods for enantioselective preparation of boron-substituted stereogenic center are highly desired in organic chemistry.[1] To generate such entities, the Hoveyda laboratory has developed a sulfonate-containing chiral NHC–Cu catalyzed regio-, chemo-, S_N2'-, diastereo-, and enantioselective multicomponent reaction through Cu–H addition to readily available vinyl–B(pin) followed by allylic substitution to deliver homoallylic boronates. The derived homoallylic alcohols can be used as building blocks of biologically active molecules (see section 2.3.4 for applications). As discussed previously, high regio-, chemo-, and enantioselectivity are crucial to generate the desired products (see Chapter 1 for more details). In addition, development of high S_N2'- and diastereoselective allylic substitutions with 1,2-disubsituted allylic electrophiles remains a challenging problems even if the required organo-copper complex would be generated

(1) (a) Hartmann, E.; Vyas, D. J.; Oestreich, M. *Chem. Commun.* **2011,** *47,* 7917–7932. (b) Takaya, J.; Iwasawa, N. *ACS Catal.* **2012,** *2,* 1993–2006.

at the first stage.

2.2 Background

Recent enantioselective hydroboration of alkenes with precious Rh- or Ir-based complexes[2] are used to generate boron-substituted stereogenic centers. Pt-, Pd-, or carbohydrates-derived catalysts[1b,3] can also be used through the addition of diborons to various alkenes (Scheme 2.1). More complex multicomponent catalytic methods for the enantioselective preparation of valuable boron-containing organic molecules have been

Scheme 2.1. Previously Reported Catalytic Enantioselective Methods and New Strategy

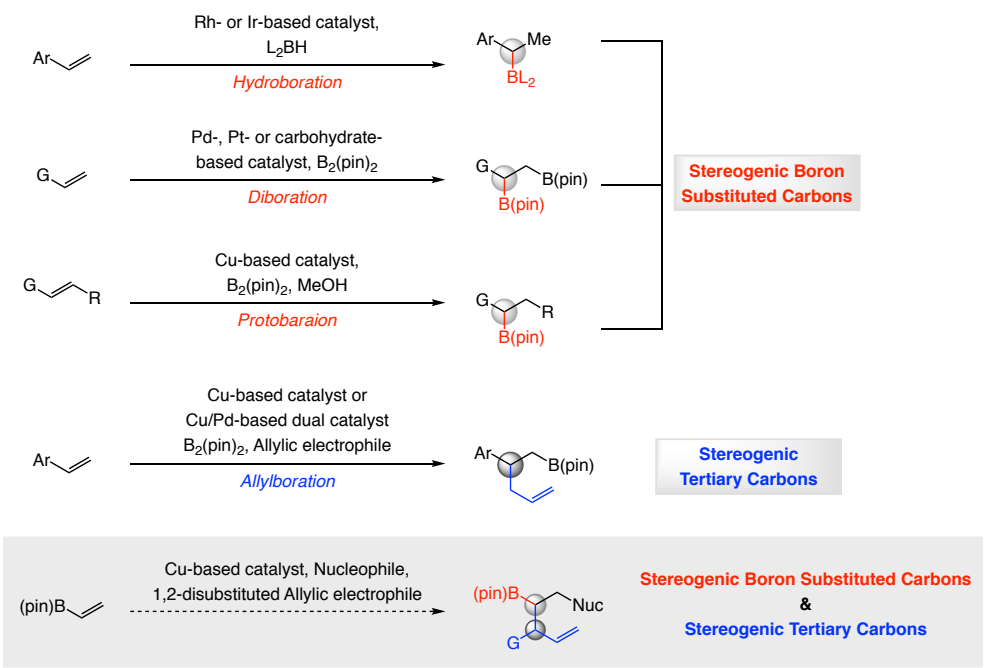

pin, pinacolato; L, ligand; G & R, various functionla groups; Nuc, nucleophile

developed through Cu–B addition to an alkene followed by in-situ protonation (proto-boryl addition, Scheme 2.1)[4] or allylic substitution (boron-allyl addition, Scheme 2.1)[5].

---

(2) Carroll, A.-M.; O'Sullivan, T. P.; Guiry, P. J. *Adv. Synth. Catal.* **2005,** *347,* 609 –631.

(3) (a) Burks, H. E.; Morken, J. P. *Chem. Commun.* **2007,** 4717–4725. (b) Coombs, J. R.; Morken, J. P. *Angew. Chem. Int. Ed.* **2016,** *55,* 2636–2649. (c) Fang, L.; Yuan, L.; Haeffner, F.; Morken, J. P. *J. Am. Chem. Soc.* **2016,** *138,* 2508–2511.

(4) (a) Lee, Y.; Hoveyda, A. H. *J. Am. Chem. Soc.* **2009,** *131,* 3160–3161. (b) Lee, Y.; Jang, H.; Hoveyda, A. H. *J. Am. Chem. Soc.* **2009,** *131,* 18234–18235. (c) Coberán, R.; Mszar, N. W.; Hoveyda, A. H. *Angew. Chem. Int. Ed.* **2011,** 50, 7079–7082. (d) Meng, F.; Jang, H.; Hoveyda, A. H. *Chem. Eur. J.* **2013,** *19,*

Although the previous systems provide useful alternative pathways to furnish boron containing complex molecules, they are limited to generate only either stereogenic boron substituted carbons or stereogenic tertiary carbons (Scheme 2.1). We envisioned that a complementary disconnection to generate both stereogenic boron and alkly substituted carbons would entail enantioselective Cu–H addition[6] to commercially available vinyl-B(pin) and an ensuing S_N2' selective allylic substitution involving a 1,2-disubsituted alkene (Scheme 2.1).

2.2.1 Importance and Challenges of the Desired Reaction

According to the reported Cu–H catalyzed non-boron-related multicomponent allylic substitution reactions, it is very difficult to produce the desired products in high

Scheme 2.2. Callenge of S_N2'- and Diastereoselective Multicomponent Reaction with 1,2-Disubstituted Electrophile

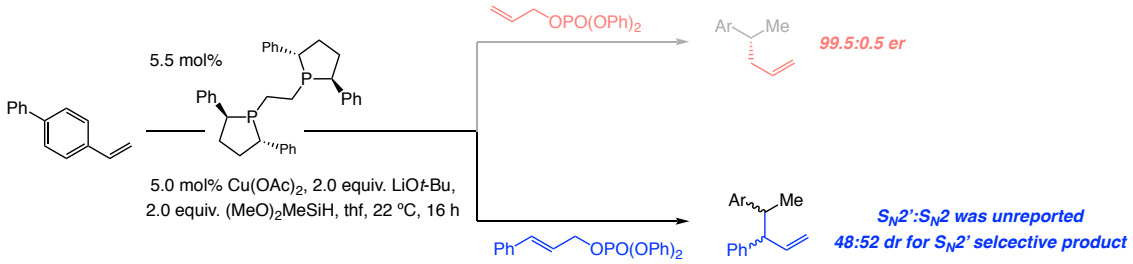

diastereoselectivity despite Cu–H addition to alkenes being highly enantioselective[6f] (Scheme 2.2). The same issue was found in the reaction involving (*E*)-1,2-disubstituted alkenyl-B(pin) substrates and allylphosphate with bis-phosphine-Cu catalysts. The

---

3204–3214.

(5) (a) Jia, T.; Cao, P.; Wang, B.; Lou, Y.; Yin, X.; Wang, M.; Liao, J. *J. Am. Chem. Soc.* **2015,** *137,* 13760–13763. (b) Lee, J.; Radomkit, S.; Torker, S.; del Pozo, J.; Hoveyda, A. H. *Nat. Chem.* **2018,** *10,* 99–108.

(6) For representative studies regarding catalytic processes that commence with an enantioselective Cu–H addition to an alkene, see: (a) Noh, D.; Chea, H.; Ju, J.; Yun, J. *Angew. Chem. Int. Ed.* **2009,** *48,* 6062–6064. (b) Miki, Y.; Hirano, K.; Satoh, T.; Miura, M. *Angew. Chem. Int. Ed.* **2013,** *52,* 10830–10834. (c) Miki, Y.; Hirano, K.; Satoh, T.; Miura, M. *Org. Lett.* **2014,** *16,* 1498–1501. (d) Nishikawa, D.; Hirano, K.; Miura, M. *J. Am. Chem. Soc.* **2015,** *137,* 15620–15623. (e) Pirnot, M. T.; Wang, Y.-M.; Buchwald, S. L. *Angew. Chem. Int. Ed.* **2016,** 55, 48 –57 (f) Wang, Y.-M.; Buchwald, S. L. *J. Am. Chem. Soc.* **2016,** *138,* 5024–5027. (g) Bandar, J. S.; Ascic, E.; Buchwald, S. L. *J. Am. Chem. Soc.* **2016,** *138,* 5821–5824. (h) Yang, Y.; Perry, I. B.; Lu, G.; Liu, P.; Buchwald, S. L. *Science* **2016,** *353,* 144–150.

method is very useful to generate products with a single stereogenic center. However, the

Scheme 2.3. Multicomponent Strategy vs Previously Reported Strategy

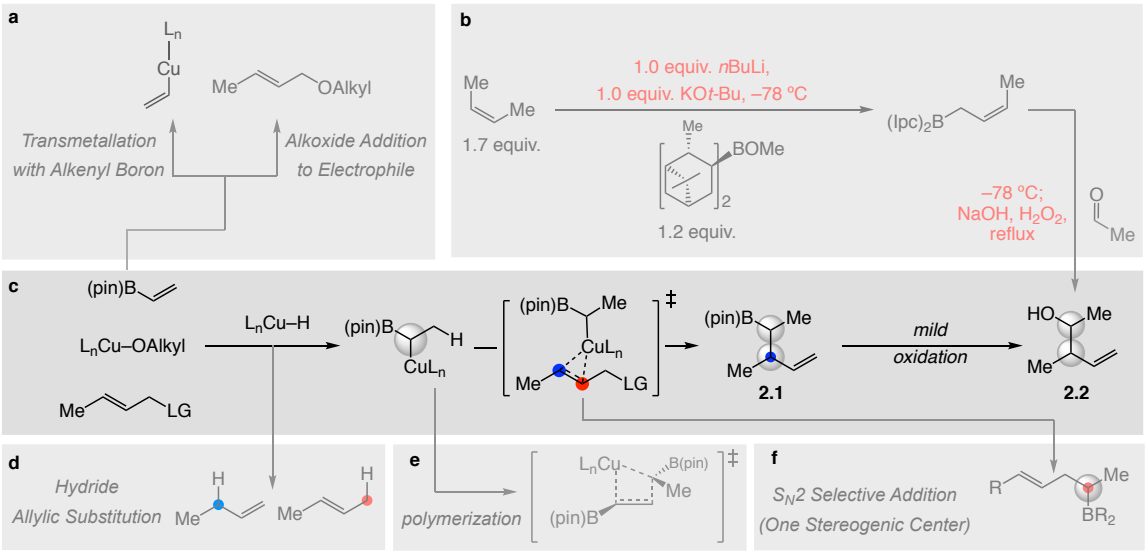

L_n, lignad; LG, leaving group; pin, pinacolato

only reported case with an (*E*)-1,2-disubstituted allylic phosphate furnished the desired product in 78:22 dr and 73:27 er.[7] The new approach from the Hoveyda laboratory to obtain a homoallylic (pin)B-substituted carbon stereogenic center under mild catalytic conditions could provide a solution to most of the difficulties associated with the S_N2'- and diastereoselective allylic substitution steps (Scheme 2.3c vs Scheme 2.3e). The desired product with (*E*)-butenyl electrophile is particularly interesting and important since the secondary alcohol product (**2.2**, Scheme 2.3) from **2.1** could also be expected from the stereoselective crotyl addition to acetaldehyde (Scheme 2.3b)[8] which generally requires superbase and cryogenic temperature to get high selectivities, and to the best of our knowledge, catalytic diastereo- and enantioselective crotylations[9] have not been

(7) Han, J. T.; Jang, W. J.; Kim, N.; Yun, J. *J. Am. Chem. Soc.* **2016,** *138,* 15146–15149.
(8) Brown, H. C.; Bhat, K. *J. Am. Chem. Soc.* **1986,** *108,* 5919–5923.
(9) For reports regarding related types of catalytic enantioselective additions to other types of aldehydes see: (a) Kim, I. S.; Han, S. B.; Krische, M. J. *J. Am. Chem. Soc.* **2009,** *131,* 2514–2520. (b) Gao, X.; Townsend, I. A.; Krische, M. J. *J. Org. Chem.* **2011,** *76,* 2350–2354. (c) McInturff, E. L.; Yamaguchi, E.; Krische, M. J. *J. Am. Chem. Soc.* **2012,** *134,* 20628–20631. (d) Zbieg, J. R.; Yamaguchi, E.; McIntruff, E. L.; Krische, M. J. *Science* **2012,** *336,* 324–327. (e) Liang, T.; Zhang, W.; Chen, T.-Y.; Nguyen, K. D.;

developed yet for transformation of **2.2**. For the successful multicomponent reaction to occur, a chiral catalyst must promote efficient, diastereo-, and enantioselective Cu–H addition followed by allylic substitution in preference to two potentially competing routes. One pathway could involve reaction of Cu-alkoxide with vinyl-B(pin) (vs. a hydride reagent) to yield a vinyl-Cu complex (Scheme 2.2a), which might then react with an allylic electrophile;[10] alternatively, the Cu–H might react directly with the allyl electrophile (Scheme 2.2d).[11] The organo-copper complex does not participate in the polymerization pathway presumably because of the high energy barrier caused by two bulky B(pin) groups approaching each other (Scheme 2.2e). Additionally, controlling stereoselectivities in alkylation step is very difficult (Scheme 2.2c and Scheme 2.2f). Despite the number of challenges, our group demonstrated that a sulfonate-containing chiral NHC–Cu complex can efficiently promote the general transformation in Scheme 2.3c with high chemo-, S_N2'-, diastereo-, and enantioselectivity.[12]

2.3 Catalytic Stereoselective Functionalization of Vinyl-B(pin)

2.3.1 Identification of an Effective Stereoselective Cu-Based Catalyst

Various commercially available chiral phosphine ligands were tested to promote the process involving vinyl-B(pin), (*E*)-1,2-disubstituted allylic phosphate **2.3** with polymethylhydrosiloxane (PMHS).[13] In most cases, the product from S_N2 mode of addition was the major and exclusive component with very poor stereoselectivity (low

---

Krische, M. J. *J. Am. Chem. Soc.* **2015,** *137,* 13066–13071.

(10) (a) Gao, F.; Carr, J. L.; Hoveyda, A. H. *Angew. Chem. Int. Ed.* **2012,** *51,* 6613–6617. (b) Gao, F.; Carr, J. L.; Hoveyda, A. H. *J. Am. Chem. Soc.* **2014,** *136,* 2149–2161.

(11) Nguyen, T. N. T.; Thiel, N. O.; Pape, F.; Teichert, J. F. *Org. Lett.* **2016,** *18,* 2455–2458.

(12) For non-diastereo- and non-enantioselective catalytic methods for synthesis of similar types of products through reaction of 1,1-diborylalkanes and allylic electrophiles, see: (a) Kim, J.; Park, S.; Park, J.; Cho, S. H. *Angew. Chem. Int. Ed.* **2016,** *55,* 1498–1501. (b) Zhang, Z.-Q.; Zhang, B.; Lu, X.; Liu, J.-H.; Liu, X.-Y.; Xiao, B.; Fu, Y. *Org. Lett.* **2016,** *18,* 952–955.

(13) Senapati, K. K. *Synlett* **2005,** 1960–1961.

dr/er, entry 1–8, Table 2.1). This was somewhat surprising since those chiral phosphines

Table 2.1. Examination of Different Types of Cu Complexes[a]

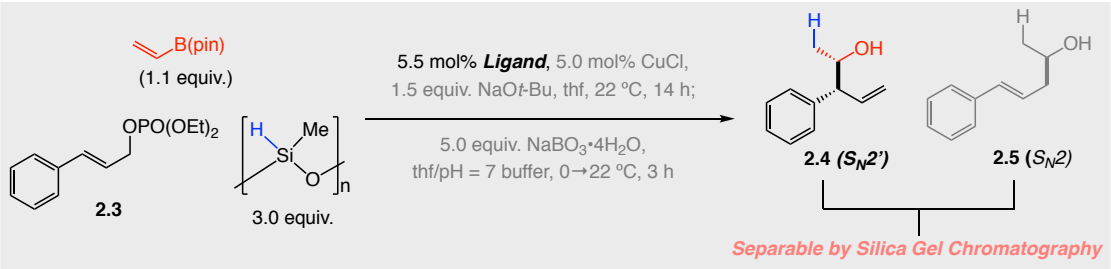

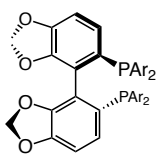

L2
Ar = 4-OMe-3,5-*t*-BuC$_6$H$_2$

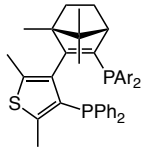

L3b
Ar = 3,5-(Me)$_2$C$_6$H$_3$

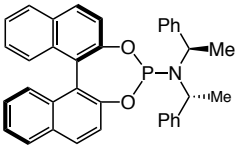

L5

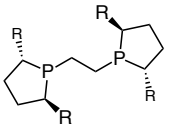

L6 R = Me, **L7** R = Ph

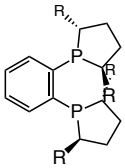

L8 R = Me, **L9** R = *i*-Pr

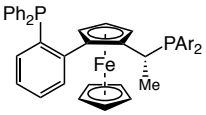

L10
Ar = 3,5-(CF$_3$)$_2$C$_6$H$_3$

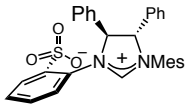

NHC-6

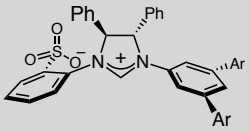

NHC-8
Ar = 2,4,6,-(*i*-Pr)$_3$C$_6$H$_2$

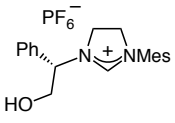

NHC-9

Entry	Ligand	Conv. (%)§	Yield (%)§§	S_N2':S_N2 (%)†	er (S_N2)††	dr (S_N2')†	er (S_N2')††
1	**L2**	>98	ND (S_N2'), 25 (S_N2)	21:79	47:53	62:38	ND
2	**L3b**	>98	ND (S_N2'), 25 (S_N2)	28:72	47:53	68:32	ND
3	**L5**	50	ND (S_N2'), 25 (S_N2)	27:73	52:48	68:32	ND
4	**L6**	>98	NA (S_N2'), 95 (S_N2)	2:>98	55:44	NA	NA
5	**L7**	>98	ND (S_N2'), 44 (S_N2)	2:98	50:50	ND	ND
6	**L8**	75	NA (S_N2'), 31 (S_N2)	2:>98	51:49	NA	NA
7	**L9**	>98	NA (S_N2'), 61 (S_N2)	2:>98	41:59	NA	NA
8	**L10**	80	30 (S_N2'), ND (S_N2)	67:33	ND	92:8	60:40 (major diast.)
9	**NHC-6**	>98	74 (S_N2'), NA (S_N2)	>98:2	NA	13:87	80:20 (major diast.)
10	**NHC-8**	83	59 (S_N2'), ND (S_N2)	94:6	ND	94:6	94:6 (major diast.)
11	**NHC-9**	85	58 (S_N2'), 8 (S_N2)	69:31	ND	31:69	47:53 (major diast.)

a Reactions were perfomed under N_2 atmosphere. § Conversion (conv.) was based on the disappearance of the limiting reagent (2.3) and determined by analysis of the ^{1}H NMR spectra of the unpurified mixtures; the variance of values is estimated to be <±2%. §§ Yield of isolated and purified product; the variance of values is estimated to be <±5%. † S_N2'- and diastereoselectivity were determined by NMR analysis; the variance of values is estimated to be <±2%. †† Enantiomeric ratios were determined by HPLC analysis; the variance of values is estimated to be <±1%. See the Experimental section for details. ND, not determined. NA, not applicable; Mes, 2,4,6-trimethylphenyl; pin, pinacolato.

have been shown to be optimal in several transformations that begin with enantioselective Cu–H addition to an alkene (**L2,**[6d,14] **L7,**[6f–h] and **L10**[7], Table 2.1). We took these findings

(14) (a) Zhu, S.; Niljianskul, N.; Buchwald, S. L. *J. Am. Chem. Soc.* **2013,** *135,* 15746–15749. (b) Zhu, S.;

as an indication that the desired sequence of reactions demands a distinct set of catalysts. Results were more encouraging with *N*-heterocyclic carbine (NHC) systems (entry 9–11, Table 2.1). With **NHC-9**[15] as a NHC–Cu complex precursor, **2.4** (S_N2' selective product) was the major component of the product mixture (S_N2': S_N2 = 69:31, entry 11, Table 2.1) but stereoselectivity remained very low (31:69 dr and 47:53 er, entry 9, Table 2.1). There was further important observation with the NHC-Cu complex derived from sulfonate-containing **NHC-6,**[16] which afforded **2.4** (S_N2' selective product) exclusively and in appreciable dr and er [13:87 dr and 80:20 er (for the major diastereomer), respectively]. Another unexpected observation was that the catalyst derived from **NHC-8,**[17] where the Mes unit (2,4,6- trimethylphenyl) is replaced by a 3,5-(2,4,6-triisopropoylphenyl) group, high S_N2':S_N2 ratio persisted (94:6) with stereoselectivity improving greatly as well (94:6 dr and er for major diastereomer of **2.4**). Interestingly, modification of the aryl group in the sulfonate-containing chiral NHC ligand can reverse diastereoselectivity although the chirality of the ligand was not changed (see the calculation in the Experimental section for further mechanistic study and discussion).

2.3.2 Optimal Base and Scope with Aryl-Substituted Electrophiles

A large number of different aryl-substituted allylic phosphates could be converted to homoallylic boronates, which were isolated as the corresponding alcohols after mild C–B bond oxidation (Scheme 2.4). Reactions were performed at ambient temperature with 5.5 mol % **NHC-8** and 5.0 mol % CuCl along with three equivalents of inexpensive

---

Buchwald, S. L. *J. Am. Chem. Soc.* **2014,** *136,* 15913–15916.

(15) Clavier, H.; Coutable, L.; Toupet, L.; Guillemin, J.-C.; Mauduit, M. *J. Organomet. Chem.* **2005,** *690,* 5237–5254.

(16) Brown, M. K.; May, T. L.; Baxter, C. A.; Hoveyda, A. H. *Angew. Chem. Int. Ed.* **2007,** *46,* 1097–1100.

(17) Jung, B.; Hoveyda, A. H. *J. Am. Chem. Soc.* **2012,** *134,* 1490 –1493.

PMHS and with LiO*t*-Bu which was identified as an optimal base with further base screening (entry 3, Table 2.2). Only a small excess of vinyl-B(pin) sufficed (1.1 equiv.)

Table 2.2. Examination of Different Bases[a]

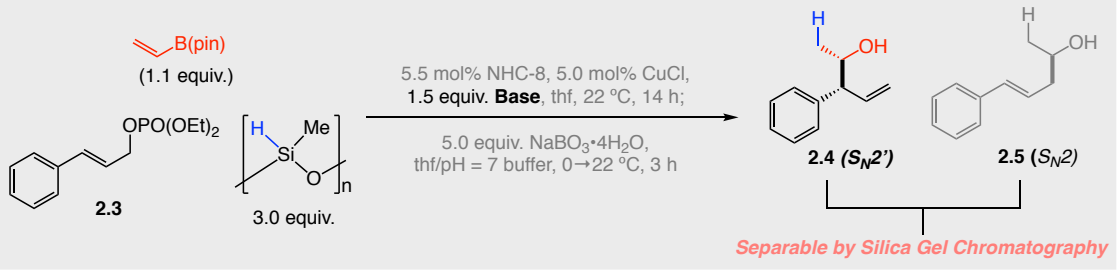

Entry	Base	Conv. (%)§	Yield (%)§§	S_N2':S_N2 (%)†	er (S_N2)††	dr (S_N2')†	er (S_N2')††
1	**NaOMe**	35	9 (S_N2'), ND (S_N2)	71:29	ND	97:3	95:5 (major diast.)
2	**KOMe**	<2	NA (S_N2'), NA (S_N2)	NA	NA	NA	NA
3	**LiO*t*-Bu**	95	66 (S_N2'), ND (S_N2)	95:5	ND	96:4	95:5 (major diast.)
4	**NaO*t*-Bu**	83	59 (S_N2'), ND (S_N2)	94:6	ND	94:6	94:6 (major diast.)
5	**KO*t*-Bu**	<2	NA (S_N2'), NA (S_N2)	NA	NA	NA	NA
6	**NaOPh**	9	ND (S_N2'), ND (S_N2)	ND	ND	ND	ND

a Reactions were perfomed under N_2 atmosphere. § Conversion (conv.) was based on the disappearance of the limiting reagent (2.3) and determined by analysis of the ^{1}H NMR spectra of the unpurified mixtures; the variance of values is estimated to be <±2%. §§ Yield of isolated and purified product; the variance of values is estimated to be <±5%. † S_N2'- and diastereoselectivity were determined by NMR analysis; the variance of values is estimated to be <±2%. †† Enantiomeric ratios were determined by HPLC analysis; the variance of values is estimated to be <±1%. See the Experimental section for details. ND, not determined; NA, not applicable; pin, pinacolato.

to get reasonable amount of desire products. Under the optimal condition, uniformly high S_N2' selectivity (S_N2':S_N2, 84:14 to >98:2, Scheme 2.4) was observed along with synthetically useful level of diastereo- and enantioselectivity for the formation of **2.6–2.16** (90:10 to 96:4 dr, 94:6 to 98:2 er, Scheme 2.4). Pure **2.6–2.16** were obtained in 60–84% yield after simple silica gel chromatography. Transformations proceeded with similarly high efficiency and selectivity regardless of whether the aryl group within the allylic phosphate was sterically hindered (**2.7–2.10**), electron withdrawing (**2.15** and **2.16**) or electron donating (**2.8** and **2.12**). The lower S_N2' selectivity with **2.16** may be attributed to direct alkylation of the exceptionally electrophilic *p*-nitrophenyl-substituted allylphosphate (vs. Cu–alkene complexation and allyl transfer).

Scheme 2.4. Reactions with Aryl-Substituted Allylic Phosphates[a]

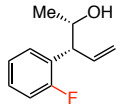

2.6
82% conv., 98:2 S_N2':S_N2,
60% yield (only S_N2'), 93:7 dr,
95:5 er (S_N2', major diast.)

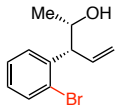

2.7
74% conv., >98:2 S_N2':S_N2,
62% yield (only S_N2'), 90:10 dr,
98:2 er (S_N2', major diast.)

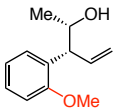

2.8
89% conv., >98:2 S_N2':S_N2,
67% yield (only S_N2'), 92:8 dr,
98:2 er (S_N2', major diast.)

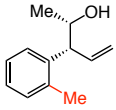

2.9
82% conv., >98:2 S_N2':S_N2,
75% yield (only S_N2'),90:10 dr,
97:3 er (S_N2', major diast.)

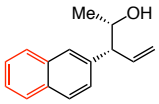

2.10
89% conv., >98:2 S_N2':S_N2,
81% yield (only S_N2'), 95:5 dr,
95:5 er (S_N2', major diast.)

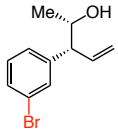

2.11
>98% conv., 94:6 S_N2':S_N2,
82% yield (only S_N2'), 94:6 dr,
96:4 er (S_N2', major diast.)

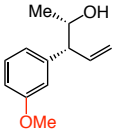

2.12
86% conv., 91:9 S_N2':S_N2,
65% yield (only S_N2'), 95:5 dr,
96:4 er (S_N2', major diast.)

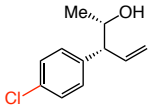

2.13
95% conv., 95:5 S_N2':S_N2,
68% yield (only S_N2'), 95:5 dr,
95:5 er (S_N2', major diast.)

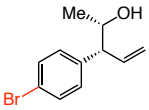

2.14
>98% conv., 95:5 S_N2':S_N2,
66% yield (only S_N2'), 95:5 dr,
94:6 er (S_N2', major diast.)

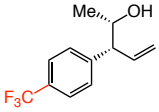

2.15
>98% conv., 94:6 S_N2':S_N2,
84% yield (only S_N2'), 95:5 dr,
96:4 er (S_N2', major diast.)

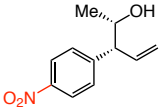

2.16
90% conv, 86:14 S_N2':S_N2,
64% yield (only S_N2'), dr = 93:7,
95:5 (S_N2', major diast.)

a Reactions were perfomed under N_2 atmosphere. Conversion (conv.) was based on the disappearance of the limiting reagent (allylic phosphate) and determined by analysis of the ^{1}H NMR spectra of the unpurified mixtures; the variance of values is estimated to be <±2%. Yield of isolated and purified product; the variance of values is estimated to be <±5%. S_N2'- and diastereoselectivity were determined by NMR analysis; the variance of values is estimated to be <±2%. Enantiomeric ratios were determined by HPLC analysis; the variance of values is estimated to be <±1%. See the Experimental section for details.

2.3.3 Wide Functional Group Tolerance

Allyl electrophiles containing a heteroaromatic cycle such as pyridyl or benzothiophene group can be used (**2.17** and **2.18**, Scheme 2.5). However, S_N2':S_N2 and diastereoselectivities were somewhat lower and the final product contained a small amount of impurities from the S_N2 addition with pyridinyl allyl electrohpile (**2.17**, Scheme 2.5). Similar results were obtained with a dienylphosphate (**2.19**, Scheme 2.5). The transformation with the corresponding enynylphosphate (**2.20**) was more S_N2'- (>98% vs 87% for **2.19**) and enantioselective (97:3 vs 92:8 er for **2.19**). In the case of **2.19**, none of the product from S_N2'' mode of reaction was detected, and the lower yield for **2.20** (46%) might be due to competitive Cu–H addition to the alkynyl group.[18]

(18) For examples of catalytic processes involving Cu–H addition to an alkyne, see: (a) Semba, K.;

Scheme 2.5. High Functional Group Compatibilities[a]

2.17[b]
>98% conv., 90:10 S_N2':S_N2,
55% yield (96% S_N2', 92:8 dr), 85:15 dr,
93:7 er (S_N2' major diast.)

2.18
82% conv., >98:2 S_N2':S_N2,
64% yield, 91:9 dr,
95:5 er (S_N2' major diast.)

2.19[b]
>98% conv., <2:87:13 S_N2'':S_N2':S_N2,
79% yield (only S_N2'), 90:10 dr,
92:8 er (S_N2' major diast.)

2.20
98% conv., >98:2 S_N2':S_N2,
46% yield, 84:16 dr,
97:3 er (S_N2' major diast.)

a Reactions were perfomed under N_2 atmosphere. Conversion (conv.) was based on the disappearance of the limiting reagent (allylic phosphate) and determined by analysis of the ^{1}H NMR spectra of the unpurified mixtures; the variance of values is estimated to be <±2%. Yield of isolated and purified product; the variance of values is estimated to be <±5%. S_N2'- and diastereoselectivity were determined by NMR analysis; the variance of values is estimated to be <±2%. Enantiomeric ratios were determined by HPLC analysis; the variance of values is estimated to be <±1%. b 7.0 mol% NHC–Cu complex was used. See the Experimental section for details.

2.3.4 Scope with Alkyl-Substituted Electrophiles and Utilities

Branched and linear alkyl-substituted allylic phosphates are also suitable substrates in the desired transformation (Scheme 2.6). As highlighted by synthesis of **2.21** and **2.22** (Scheme 2.6), while somewhat less enantioselective compared to when aryl-substituted allylic phosphates are utilized (Scheme 2.4), reaction with the larger cyclohexyl-substituted allylic phosphate was efficient with 7.0 mol % catalyst loading. In both cases, S_N2' selectivities were exceptional (>98%), and diastereoselectivities were high (92:8–93:7 dr) with high efficiencies (91% and 79% yield, respectively). Of special value are the transformations involving Me-substituted allylic phosphate **2.23**, which, when performed on 5.0 mmol scale and with 2.0 mol % catalyst loading, afforded **2.24** in 55% yield (volatile compound), >98:2 S_N2':S_N2, 92:8 dr, and 93:7 er after purification (Scheme 2.6). This is a valuable fragment that has been used in a total synthesis of a biologically active analog of natural product chondramide C **2.25**[19a] as well as complex polyketide **2.26** which was synthesized as a model complex for total synthesis of antitumor active natural products tedanolide **2.27** and 13-deoxytedanolide **2.28**.[19b]

Fujihara, T.; Xu, T.; Terao, J.; Tsuji, Y. *Adv. Synth. Catal.* **2012,** *354,* 1542–1550. (b) Shi, S.-L.; Buchwald, *S. L. Nat. Chem.* **2015,** *7,* 38–44. (c) Uehling, M. R.; Suess, A. M.; Lalic, G. *J. Am. Chem. Soc.* **2015,** *137,* 1424–1427.

(19) (a) Tannert, R.; Milroy, L.-G.; Ellinger, B.; Hu, T.-S.; Arndt, H.-D.; Waldmann, H. *J. Am. Chem. Soc.* **2010,** *132,* 3063–3077. (b) Hassfeld, J.; Eggert, U.; Kalesse, M. *Synthesis* **2005,** 1183–1199.

Scheme 2.6. Reactions with Alkyl-Substituted Allylic Phosphates and Utility[a]

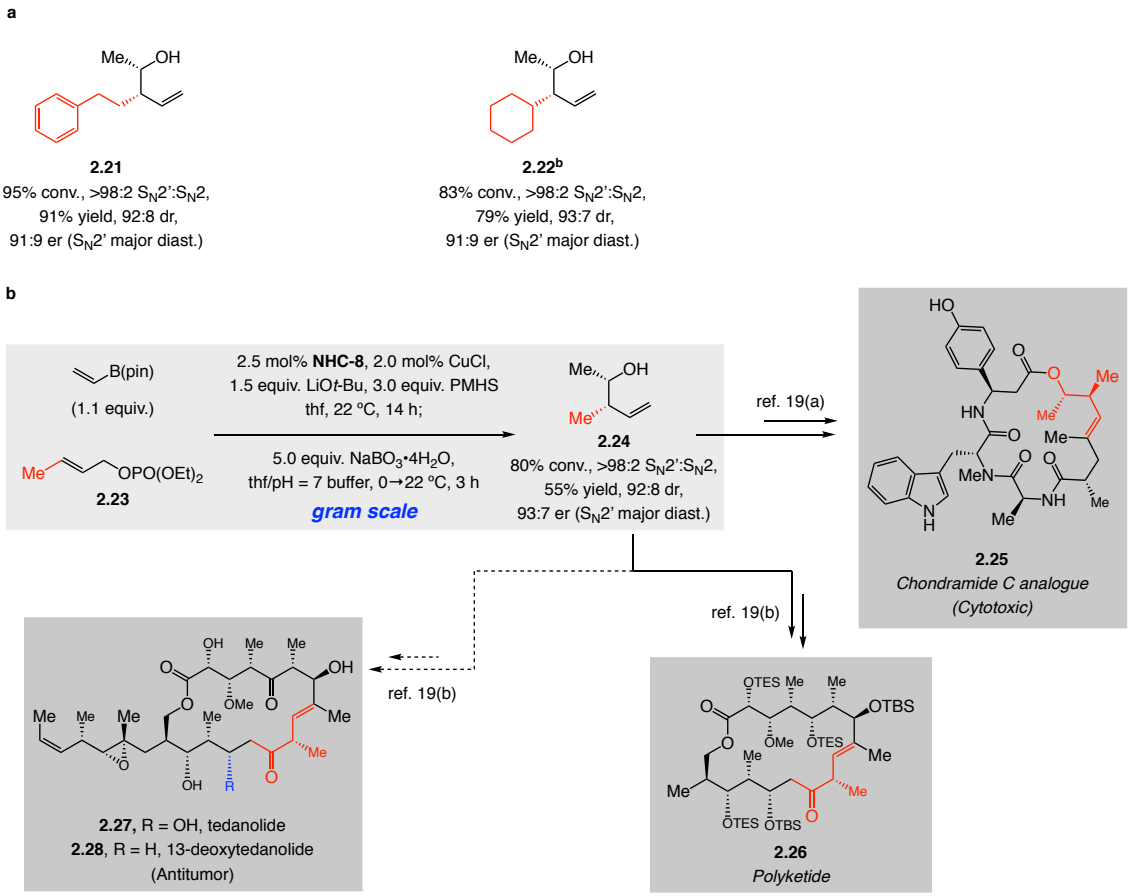

a Reactions were perfomed under N_2 atmosphere. Conversion (conv.) was based on the disappearance of the limiting reagent (allylic phosphate) and determined by analysis of the ^{1}H NMR spectra of the unpurified mixtures; the variance of values is estimated to be <±2%. Yield of isolated and purified product; the variance of values is estimated to be <±5%. S_N2'- and diastereoselectivity were determined by NMR analysis; the variance of values is estimated to be <±2%. Enantiomeric ratios were determined by HPLC analysis; the variance of values is estimated to be <±1%. b 7.0 mol% NHC–Cu complex was used. See the Experimental section for details. pin, pinacolato; PMHS, polymethylhydrosiloxane.

Previously, however, preparation of enantiomerically pure **2.24** entailed the use of Brown's chiral auxiliary,[20] necessitating somewhat forcing conditions along with the use of stoichiometric amounts of an exceptionally strong base (*n*BuLi/KO*t*-Bu to give *n*BuK, see Scheme 2.3b for the detailed reaction conditions). Another functionalization procedure entails conversion of the homoallylic boronate formed by the reaction of allylic phosphate **2.29** to the corresponding 2-furyl product **2.30** (Scheme 2.7).[21]

(20) (a) Brown, H. C.; Bhat, K. *J. Am. Chem. Soc.* **1986,** *108,* 5919–5923. For a more recent chiral auxiliary based approach, see: (b) Chen, J. L.-Y.; Scott, H. K.; Hesse, M. J.; Willis, C. L.; Aggarwal, V. K. *J. Am. Chem. Soc.* **2013,** *135,* 5316–5319.

(21) Bonet, A.; Odachowski, M.; Leonori, D.; Essafi, S.; Aggarwal, V. K. *Nat. Chem.* **2014,** *6,* 584–589.

Scheme 2.7. Functionalization of Secondary Boronic Ester

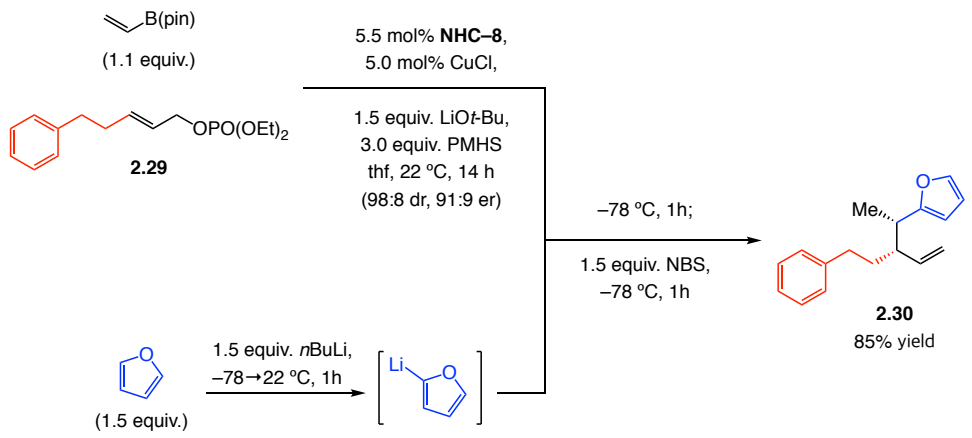

2.3.5 Unique Effectiveness of NHC–Copper Complex

For insights regarding the unique effectiveness of **NHC-8**-derived catalyst and the selectivity differences with **NHC-6** (Table 2.1), a series of DFT calculations were carried out. The studies indicate that the most favored mode of Cu–H addition to vinyl-B(pin) with **NHC-8** probably arises from coordination of pinacolato oxygen atom to the

Scheme 2.8. Enantioselective Cu–H Addition to Vinyl-B(pin)[a]

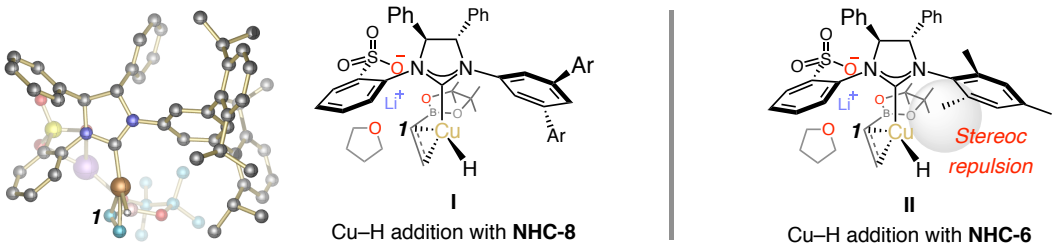

a Computations have been performed at the MN12SX/Def2TZVPP$_{thf(SMD)}$ level after geometry optimization performed with the ONIOM method M06L/Def2SVP:UFF$_{thf(PCM)}$. A r= 2,6-(iPr)$_2$C$_6$H$_3$. See the Experimental sections for details.

alkali metal counter-ion Li^+ (**I**, Scheme 2.8).[22] The corresponding mode of reaction with the NHC–Cu complex derived from **NHC-6** (Scheme 2.8) suffers from steric repulsion

(22) For representative reports where coordination of a Lewis acid to a B(pin) moiety has been suggested to play a key role, see: (a) Yamamoto, H.; Futatsugi, K. *Angew. Chem. Int. Ed.* **2005,** *44,* 1924–1942. (b) Rauniyar, V.; Zhai, H.; Hall, D. G. *J. Am. Chem. Soc.* **2008,** *130,* 8481–8490. (c) Barnett, D. S.; Moquist, P. N.; Schaus, S. E. *Angew. Chem. Int. Ed.* **2009,** *48,* 8679–8682. (d) Wang, H.; Jain, P.; Antilla, J. C.; Houk, K. N. *J. Org. Chem.* **2013,** *78,* 1208–1215. (e) van der Mei, F. W.; Miyamoto, H.; Silverio, D. L.; Hoveyda, A. H. *Angew. Chem. Int. Ed.* **2016,** *55,* 4701–4706. (f) For a detailed computational investigation of the role of the salt bridge on enantioselective Cu–H addition, see the Experimentals section.

between an *o*-methyl substituent of the ligand (**II**), resulting in diminished er. Allylic substitution with **NHC-8** is most favorable with the allyl electrophile approaching such that chelation with the more Lewis acidic Li cation is the most effective and there is less steric repulsion between its substituent (Ph from allylic phosphate) and the NHC's

Scheme 2.9. Diastereoselective Allylic Substitution[a]

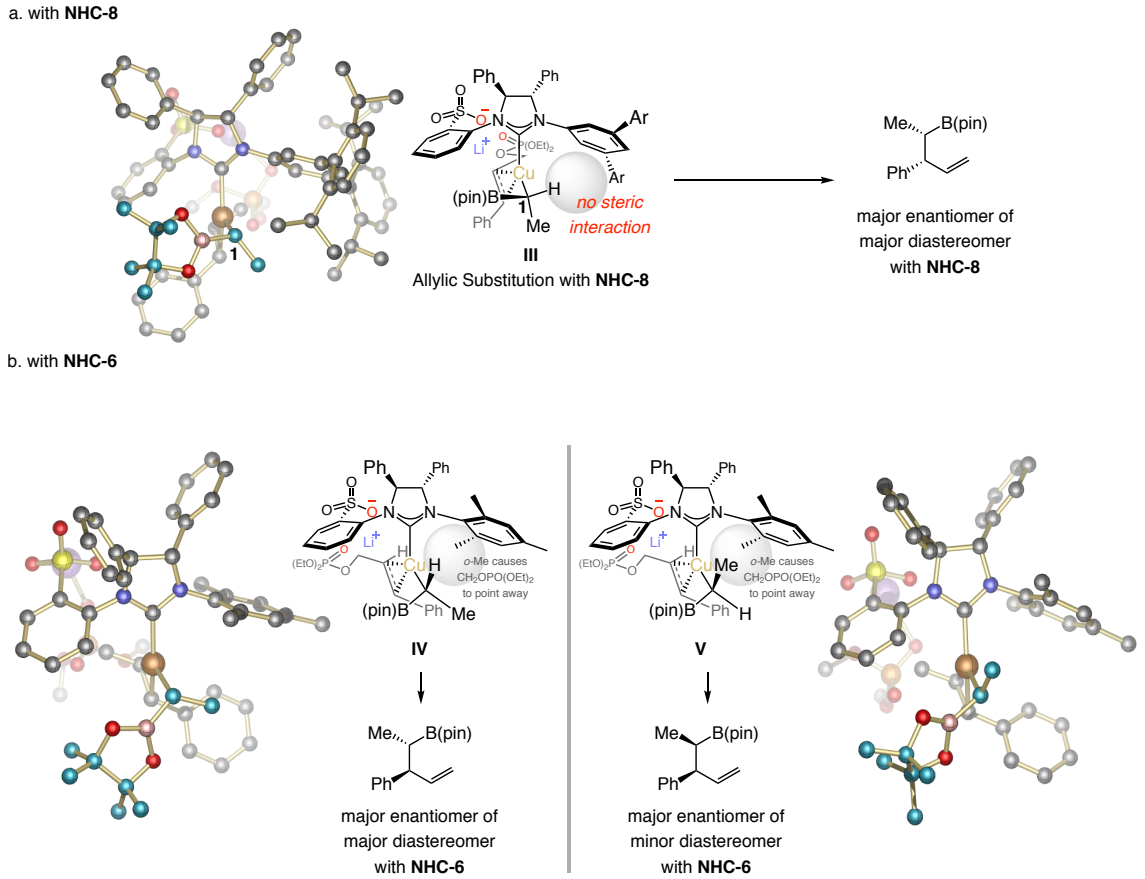

a Computations have been performed at the MN12SX/Def2TZVPP$_{thf(SMD)}$ level after geometry optimization performed with the ONIOM method M06L/Def2SVP:UFF$_{thf(PCM)}$. A r= 2,6-(iPr)$_2$C$_6$H$_3$. See the Experimental sections for details.

sizeable *N*-aryl moieties (**III**, Scheme 2.9).[23] Another consequence of the sulfonate/Li/phosphate chelation is the exceptional S_N2'-selectivity; otherwise, as is the case with the transformations involving phosphine ligands, the linear products are generated preferentially to minimize steric repulsions (**2.5**, Table 2.1). In **IV** and **V**,

(23) A similar mode of reaction was recently proposed (based on DFT calculations) for enantioselective allylic substitutions reactions involving propargylcopper intermediates and the same class of allylic phosphates. See: Shi, Y.; Jung, B.; Torker, S.; Hoveyda, A. H. *J. Am. Chem. Soc.* **2015,** *137,* 8948–8964.

arising from the **NHC-6**-based Cu complex (Scheme 2.9), the allyl electrophile is forced to coordinate with its $CH_2OPO(OEt)_2$ moiety pointing away from the large mesityl group[23] to generate different diastereomers from the product with **NHC-8**.

2.4 Conclusions

A highly chemo-, S_N2'-, diastereo-, and enantioselective multicomponent catalytic method that efficiently combines a silyl hydride, vinyl-B(pin), and (*E*)-1,2-disubstituted allylic phosphates is developed. The reaction is prompted by a Cu-based complex with a chiral sulfonate-containing *N*-heterocyclic carbene to access valuable homoallylic borons and alcohols which are typically obtained through challenging stereoselective crotyl-type additions to acetaldehyde. Aryl-, heteroaryl-, alkenyl-, alkynyl-, and alkyl-substituted allylic phosphates can be converted to the corresponding homoallylic boronates and then alcohols (after C–B bond oxidation) in 46–91% yield and in up to >98% $S_N2':S_N2$ ratio, 96:4 diastereomeric ratio, and 98:2 enantiomeric ratio. In addition, we provided further evidence regarding the importance of sulfonate-containing chiral NHC ligands to get high selectivities. These Cu-based complexes have formerly proven optimal in catalyzing enantioselective allylic substitution reactions[17,24] and conjugate addition processes[16,25] with C-based nucleophiles as well as Cu–B(pin) additions to alkenes[26] and allenes[27]. However, this is the first time that a member of the sulfonate-containing chiral NHC–Cu complex class has emerged as the most effective for enantioselective Cu–H additions to alkenes.

---

(24) Shi, Y.; Hoveyda, A. H. *Angew. Chem. Int. Ed.* **2016,** *55,* 3455–3458 and references therein.
(25) (a) Peese, K. M.; Gin, D. Y. *Chem. Eur. J.* **2008,** *14,* 1654–1665. (b) Slutskyy, Y.; Jamison, C. R.; Lackner, G. L.; Mgller, D. S.; Dieskau, A. P.; Untiedt, N. L.; Overman, L. E. J. *Org. Chem.* **2016,** *81,* 7029–7035.
(26) Meng, F.; Jang, H.; Hoveyda, A. H. *Chem. Eur. J.* **2013,** *19,* 3204–3214 and references therein.
(27) Jang, H.; Jung, B.; Hoveyda, A. H. *Org. Lett.* **2014,** *16,* 4658–4661.

2.5 Experimentals

2.5.1 General

Infrared (IR) spectra were recorded on a Bruker FT-IR Alpha (ATR mode) spectrophotometer, ν_{max} in cm^{-1}. Bands are characterized as broad (br), strong (s), medium (m), and weak (w). ^{1}H NMR spectra were recorded on Varian Unity INOVA 400 (400 MHz), 500 (500 MHz), or 600 (600 MHz) spectrometers. Chemical shifts are reported in ppm from tetramethylsilane with the solvent resonance as the internal standard ($CDCl_3$: δ 7.26 ppm). Data are reported as follows: chemical shift, integration, multiplicity (s = singlet, d = doublet, t = triplet, q = quartet, pent = pentet, m = multiplet, br = broad, app = apparent), and coupling constants (Hz). ^{13}C NMR spectra were recorded on Varian Unity INOVA 400 (100 MHz), 500 (125 MHz), or 600 (150 MHz) spectrometers with complete proton decoupling. Chemical shifts are reported in ppm from tetramethylsilane with the solvent resonance as the internal standard ($CDCl_3$: δ 77.16 ppm). High-resolution mass spectrometry was performed on a JEOL AccuTOF DART (positive mode) at the Mass Spectrometry Facility, Boston College. Enantiomeric ratios were determined by HPLC analysis (high-performance liquid chromatography) with a Shimadzu chromatograph [Chiral Technologies Chiralcel AZ-H (4.6 x 250 mm), Chiral Technologies Chiralcel OC-H (4.6 x 250 mm), Chiral Technologies Chiralcel OD-H (4.6 x 250 mm), Chiral Technologies Chiralcel OJ-H (4.6 x 250 mm), Chiral Technologies Chiralcel OZ-H (4.6 x 250 mm), or Chiral Technologies Chiralpak AD-H (4.6 x 250 mm)] in comparison with authentic racemic materials. Specific rotations were measured on a Rudolph Research Analytical Autopol IV Polarimeter. Melting points were measured on a Thomas Hoover capillary melting point apparatus and are

uncorrected.

Unless otherwise noted, reactions were carried out with distilled and degassed solvents under an atmosphere of dry N_2 in oven- (135 ºC) or flame-dried glassware with standard dry box or vacuum-line techniques. Dichloromethane was purified under a positive pressure of dry argon by a modified Innovative Technologies purification system through a copper oxide and alumina column. Tetrahydrofuran (Aldrich Chemical Co.) was purified by distillation from sodium benzophenone ketyl immediately prior to use. All work-up and purification procedures were carried out with reagent grade solvents (purchased from Fisher Scientific) under air.

2.5.2 Reagents

***N*-Bromosuccinimide (NBS):** purchased from Alfa Aesar and recrystallized from H_2O.

Buffer solution pH = 7.0 (20 ºC): purchased from Aldrich and used as received.

***n*-Butyllithium (1.6 M in hexanes):** purchased from Aldrich and used as received.

Chiral imidazolinium salt (NHC-6): prepared according to previously reported procedure.[28]

Chiral imidazolinium salt (NHC-8): prepared according to previously reported procedure.[29]

Chiral imidazolinium salt (NHC-9): prepared according to previously reported procedure.[30]

Chiral phosphine ligand (L2, L3b, L5–L10): purchased from Strem and used as

---

(28)Brown, M. K.; May, T. L.; Baxter, C. A.; Hoveyda, A. H. *Angew. Chem. Int. Ed.* **2007**, *119*, 1115–1118.
(29) B. Jung, A. H. Hoveyda, *J. Am. Chem. Soc*. **2012,** *134,* 1490–1493.
(30) X. Li, F. Meng, S. Torker, Y. Shi, A. H. Hoveyda, *Angew. Chem. Int. Ed.* **2016**, *55*, 9997–10002.

received.

Copper(I) chloride: purchased from Strem and used as received.

Furan: purchased from Aldrich and purified by washing with aqueous 5% KOH, dried with Na_2SO_4, then distilled over KOH under reduced pressure prior to use.

Lithium *tert*-butoxide: purchased from Strem and used as received.

Poly(methylhydrosiloxane) (PMHS): purchased from Alfa Aesar and used as received.

Sodium *tert*-butoxide: purchased from Strem and used as received.

Sodium perborate tetrahydrate ($NaBO_3$•$4H_2O$): purchased from Aldrich and used as received.

4,4,5,5-Tetramethyl-2-vinyl-1,3,2-dioxaborolane: purchased from Combi-blocks and distilled over CaH_2 under reduced pressure prior to use.

Triethylamine (Et_3N): purchased from Aldrich and used as received.

■ **Preparation of Allylic Phosphates:** Allylic alcohols were synthesized from the corresponding ester by a two-step Horner-Wadsworth-Emmons olefin synthesis/dibal–H reduction sequence. Subsequently, allylic alcohols were converted to the corresponding allylic phosphates based on established methods[31,32] The following substrates were prepared according to the above sequence. Characterization data matched those reported previously.

(*E*)-Diethyl 3-phenylprop-2-enyl phosphate (substrate for 2.4)[33]

(*E*)-Diethyl (3-(2-fluorophenyl)allyl) phosphate (substrate for 2.6)[30]

---

(31) Shi, Y.; Jung, B.; Torker, S.; Hoveyda, A. H. *J. Am. Chem. Soc*. **2015,** *137,* 8948–8964.
(32) Shi, Y.; Hoveyda, A. H. *Angew. Chem. Int. Ed.* **2016**, *55*, 3455–3458.
(33) Murahashi, S.;Y. Taniguchi, Y. Imada, Y. Tanigawa, *J. Org. Chem.* **1989,** *54,* 3292–3303.

(*E*)-3-(2-Bromophenyl)allyl diethyl phosphate (substrate for 2.7)[30]

(*E*)-Diethyl (3-(2-methoxyphenyl)allyl) phosphate (substrate for 2.8)[34]

(*E*)-Diethyl (3-(*o*-tolyl)allyl) phosphate (substrate for 2.9)[34]

(*E*)-Diethyl (3-(naphthalen-2-yl)allyl) phosphate (substrate for 2.10)[35]

(*E*)-3-(3-Bromophenyl)allyl diethyl phosphate (substrate for 2.11)[34]

(*E*)-Diethyl (3-(3-methoxyphenyl)allyl) phosphate (substrate for 2.12)[36]

(*E*)-3-(4-Chlorophenyl)allyl diethyl phosphate (substrate for 2.13)[34]

(*E*)-3-(4-Bromophenyl)allyl diethyl phosphate (substrate for 2.14)[37]

(*E*)-Diethyl (3-(4-(trifluoromethyl)phenyl)allyl) phosphate (substrate for 2.15)[30]

(*E*)-Diethyl (3-(4-nitrophenyl)allyl) phosphate (substrate for 2.16)[38]

(*E*)-Diethyl (3-(pyridin-3-yl)allyl) phosphate (substrate for 2.17)[31]

(*E*)-Diethyl (5-phenylpent-2-en-1-yl) phosphate (substrate for 2.21)[34]

(*E*)-3-Cyclohexylallyl diethyl phosphate (substrate for 2.22)[34]

(*E*)-But-2-en-1-yl diethyl phosphate (2.23)[39]

(*E*)-3-(Benzo[*b*]thiophen-3-yl)allyl diethyl phosphate (substrate for 2.18): IR (neat): 2983 (w), 1655 (w), 1510 (w), 1259 (s), 1164 (w), 1002 (s), 957 (s), 851 (m), 756 (s), 729 (s), 669 (w), 523 (m), 421 (m) cm^{-1}; ^1H NMR ($CDCl_3$, 400 MHz): δ 7.91 (1H, d, J = 8.0 Hz), 7.87 (1H, d, J = 8.0 Hz), 7.48 (1H, s), 7.44–7.38 (2H, m), 6.96 (1H, d, J = 15.2 Hz),

---

(34) Akiyama, K.; Gao, F.; Hoveyda, A. H. *Angew. Chem. Int. Ed.* **2010**, *49,* 429–433.
(35) Kacprzynski, M. A.; Hoveyda, A. H. *J. Am. Chem. Soc*. **2004,** *126,* 10676–10681.
(36) Delvos, L. B.; Vyas, D. J.; Oestreich, M. *Angew. Chem. Int. Ed.* **2013**, *52,* 4650–4653.
(37) Zhang, Z.-Q.; Zhang, B.; Lu, X.; Liu, J.-H.; Lu, X.-Y.; Xiao, B.; Fu, Y. *Org. Lett.* **2016,** *18,* 952–955.
(38) Luchaco-Cullis, C. A.; Mizutani, H.; Murphy, K. E.; Hoveyda, A. H. *Angew. Chem. Int. Ed.* **2001**, *40,* 1456–1460.
(39) Hojo, M.; Sakuragi, R.; Okabe, S.; Hosomi, A. *Chem. Commun.* **2001,** *4,* 357–358.

6.44–6.36 (1H, m), 4.77 (1H, dd, J = 7.6, 1.6 Hz), 4.75 (1H, dd, J = 8.4, 1.2 Hz), 4.16 (4H, m), 1.36 (6H, t, J = 6.8 Hz); ^{13}C NMR (100 MHz, $CDCl_3$): δ 140.5 137.6, 132.9, 126.2, 125.3 (d, J_{CP} = 6.8 Hz), 124.7, 124.5, 123.4, 123.0, 122.0, 68.1 (d, J_{CP} = 5.3 Hz), 64.0 (d, J_{CP} = 5.3 Hz), 16.3(d, J_{CP} = 6.8 Hz); HRMS (DART): Calcd for $C_{15}H_{19}O_4PS$ $[M]^+$: 326.0742; Found: 326.0747.

Diethyl ((2*E*,4*E*)-5-phenylpenta-2,4-dien-1-yl) phosphate (substrate for 2.19): IR (neat): 2983 (w), 1976 (w), 1449 (w), 1260 (m), 1165 (w), 1017 (s), 965 (s), 851 (m), 749 (m), 693 (m), 507 (m) cm^{-1}; ^{1}H NMR (400 MHz, $CDCl_3$): δ 7.41–7.39 (2H, m), 7.34–7.30 (2H, m), 7.25–7.22 (1H, m), 6.77 (1H, dd, J = 15.6, 10.8 Hz), 6.60 (1H, d, J = 15.6 Hz), 6.48 (1H, dd, J = 15.2, 10.4 Hz), 5.90 (1H, dt, J = 15.2, 6.4 Hz), 4.64 (1H, dd, J = 6.4, 1.2 Hz), 4.62 (1H, dd, J = 6.8, 1.2 Hz), 4.13 (4H, m), 1.35 (6H, td, J = 7.2, 0.8 Hz); ^{13}C NMR ($CDCl_3$, 100 MHz): δ 137.0, 134.4, 134.3, 128.8, 128.0, 127.6, 127.3 (d, J_{CP} = 6.1 Hz), 126.7, 67.8 (d, J_{CP} = 5.3 Hz), 63.9 (d, J_{CP} = 6.1 Hz), 16.3 (d, J_{CP} = 6.8 Hz).

(*E*)-Diethyl (5-phenylpent-2-en-4-yn-1-yl) phosphate (substrate for 2.20): IR (neat): 2983 (w), 1490 (w), 1443 (w), 1262 (s), 1004 (s), 950 (s), 846 (m), 800 (m), 755 (s), 690 (s), 582 (w), 527 (m) cm^{-1}; ^{1}H NMR (400 MHz, $CDCl_3$): δ 7.44–7.42 (2H, m), 7.32– 7.31 (3H, m), 6.26 (1H, dt, J = 15.6, 5.6 Hz), 6.02 (1H, dt, J = 15.6, 1.6 Hz), 4.63 (1H, dd, J = 6.0, 1.6 Hz), 4.61 (1H, dd, J = 6.0, 1.6 Hz), 4.17–4.10 (4H, m), 1.35 (6H, t, J = 6.8); ^{13}C NMR (100 MHz, $CDCl_3$): δ 136.6, 136.56, 131.7, 128.5 (d, J_{CP} = 11.4 Hz), 123.1, 113.3, 91.3, 86.8, 66.9 (d, J_{CP} = 5.3 Hz), 64.1 (d, J_{CP} = 6.0 Hz), 16.3 (d, J_{CP} = 6.1 Hz); HRMS (DART): Calcd for $C_{15}H_{20}O_4P$ $[M+H]^+$: 295.1099; Found: 295.1098

2.5.3 Representative Procedure and Products

In an N_2-filled glove box, an oven-dried 2-dram vial with magnetic stir bar was

charged with CuCl (0.5 mg, 0.005 mmol), **NHC-8** (4.70 mg, 0.0055 mmol), LiO*t*Bu (12 mg, 0.15 mmol), and freshly distilled tetrahydrofuran (thf, 0.5 mL). The mixture was premixed for 1 h before PMHS (18 mg, 0.30 mmol) and additional thf (0.5 mL) were added. The solution immediately turned dark red. After 1 min, vinyl boronic acid pinacol ester (17 mg, 0.11 mmol), allylic phosphate (27 mg, 0.10 mmol), and thf (0.5 mL) were added. The vial was sealed with electrical tape before removal from the glove box, and the resulting mixture was allowed to stir at 22 °C for 14 h. The mixture was passed through a short plug of basified silica gel (4 cm x 1 cm, 1% of triethylamine) and eluted with Et_2O. Removal of the volatiles *in vacuo* afforded bright yellow oil. To the oil was added thf (1.0 mL), pH = 7.0 buffer solution (1.0 mL), and $NaBO_3$•$4H_2O$ (77 mg, 0.50 mmol) at 0 ºC. The mixture was then allowed to stir at 22 ºC for 3 h after which it was washed with Et_2O (3 x 1.0 mL) and the combined organic layers were passed through a short plug of $MgSO_4$, concentrated and purified by silica gel chromatography (hexanes:Et_2O = 10:5, R_f = 0.2) to afford the desired product as colorless oil (10.7 mg, 0066 mmol, 66% yield). The racemic sample was prepared by the same procedure except through the use of 10 mol % ***rac*-NHC** and CuCl.

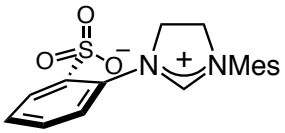

***rac*-NHC**

(2*S*,3*R*)-3-Phenylpent-4-en-2-ol (2.4): IR (neat): 3407 (br s) 2972 (w), 2924 (w), 1638 (w), 1493 (w), 1268 (w), 1116 (m), 1056 (m), 993 (m), 757 (m), 700 (s), 672 (m), 530 (m) cm^{-1}; ^1H NMR (400 MHz, $CDCl_3$): δ 7.40–7.33 (2H, m), 7.27–7.24 (3H, m), 6.09–6.00 (1H, m), 5.16–5.11 (2H, m), 4.07–4.03 (1H, m), 3.25 (1H, t, *J* = 8.2 Hz), 1.47 (1H,

br), 1.24 (3H, dd, J = 6.0, 0.8 Hz); ^{13}C NMR (100 MHz, $CDCl_3$): δ 141.0, 138.5, 129.0, 128.6, 127.1, 117.1, 70.6, 59.1, 20.9; HRMS (DART): Calcd for $C_{11}H_{13}$ $[M+H–H_2O]^+$: 145.1017; Found: 145.1013; Specific rotation: $[\alpha]_D^{20}$ –65.02 (c 0.61, $CHCl_3$) for a >98% S_N2', 96:4 dr, and 95:5 er sample. Enantiomeric purity of **2.4** was determined by HPLC analysis in comparison with authentic racemic material (95:5 er shown; chiralcel OD–H column, 99:1 hexanes:*i*PrOH, 0.3 mL/min, 220 nm).

Enantiomeric purity of the major diastereomers

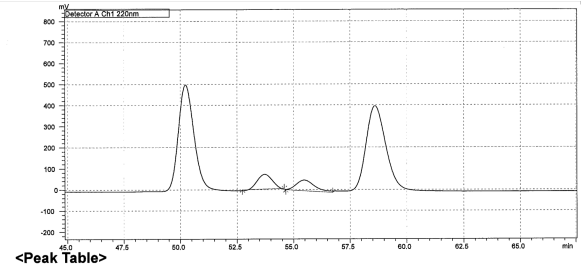

<Peak Table>

Detector A Channel 1 220nm

Peak#	Ret. Time	Area	Height	Conc.	Area%
1	53.727	3131031	70113	52.036	52.036
2	55.463	2885998	50642	47.964	47.964
Total		6017029	120754		100.000

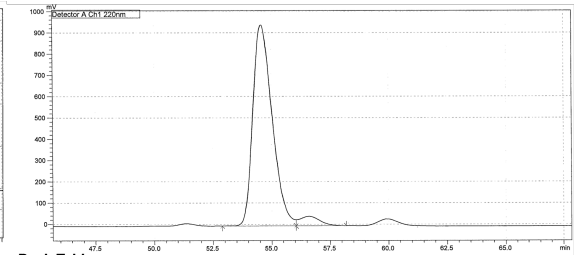

<Peak Table>

Detector A Channel 1 220nm

Peak#	Ret. Time	Area	Height	Conc.	Area%
1	54.566	54311349	944211	95.350	95.350
2	56.592	2648786	44444	4.650	4.650
Total		56960135	988655		100.000

Enantiomeric purity of the minor diastereomers

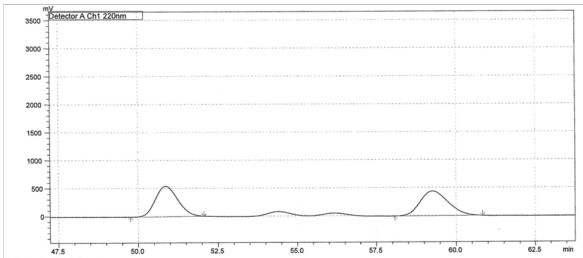

<Peak Table>

Detector A Channel 1 220nm

Peak#	Ret. Time	Area	Height	Conc.	Area%
1	50.857	26544874	543782	49.680	49.680
2	59.264	26886458	440794	50.320	50.320
Total		53431332	984577		100.000

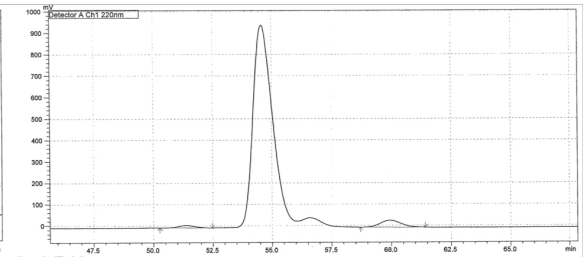

<Peak Table>

Detector A Channel 1 220nm

Peak#	Ret. Time	Area	Height	Conc.	Area%
1	51.364	537462	11547	21.438	21.438
2	59.938	1969576	32703	78.562	78.562
Total		2507037	44251		100.000

Peak #	Retention time	Area	Area %	Peak #	Retention time	Area	Area %
1	53.727	3131031	52.036	1	54.566	54311349	95.350
2	55.463	2885998	47.964	2	56.592	2648786	4.650
1	50.857	26544874	49.680	1	51.364	537462	21.438
2	59.264	26886458	50.320	2	59.938	1969576	78.562

(2*S*,3*R*)-3-(2-Fluorophenyl)pent-4-en-2-ol (2.6): IR (CH_2Cl_2): 3209 (br s), 2925 (m), 1638 (w), 1490 (m), 1454 (m), 1375 (m), 1119 (s), 1058 (s), 800 (w), 753 (s), 603 (w), 401 (m) cm^{-1}; ^1H NMR (400 MHz, $CDCl_3$): δ 7.34–7.29 (1H, m), 7.25–7.20 (1H, m), 7.15–7.11 (1H, m), 7.08–7.03 (1H, m), 6.11–6.02 (1H, m), 5.18–5.14 (2H, m), 4.18–4.12 (1H, m), 3.62 (1H, t, J = 8.4 Hz), 1.45 (1H, d, J = 4.4 Hz), 1.24 (3H, d, J = 6.4 Hz); ^{13}C NMR (100 MHz, $CDCl_3$): δ 161.1 (d, J_{CF} = 244.4 Hz), 137.3, 129.9 (d, J_{CF} = 4.6 Hz), 128.4 (d, J_{CF} = 8.4 Hz), 127.9 (d, J_{CF} = 14.4 Hz), 124.4 (d, J_{CF} = 3.0 Hz), 117.6, 115.9 (d, J_{CF} = 22.8 Hz), 69.8, 51.9, 21.2; HRMS (DART): Calcd for $C_{11}H_{12}F$ $[M+H–H_2O]^+$: 163.0929; Found: 163.0923; Specific rotation: $[\alpha]_D^{20}$ –44.30 (*c* 0.46, $CHCl_3$) for a >98% S_N2', 93:7 dr, and 95:5 er sample. Enantiomeric purity of **2.6** was determined by HPLC analysis in comparison with authentic racemic material (95:5 er shown; chiralcel AD–H column, 99:1 hexanes:*i*PrOH, 0.3 mL/min, 220 nm).

Enantiomeric purity of the major diastereomers

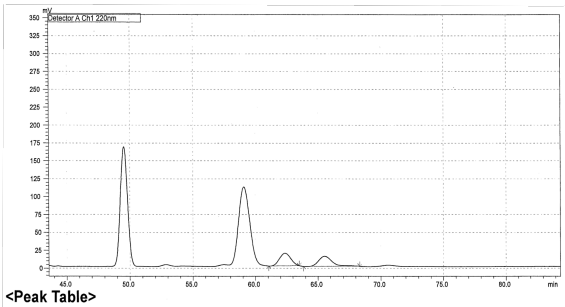

<Peak Table>

Detector A Channel 1 220nm

Peak#	Ret. Time	Area	Height	Conc.	Area%
1	62.348	1098734	17525	51.093	51.093
2	65.523	1051722	14048	48.907	48.907
Total		2150456	31573		100.000

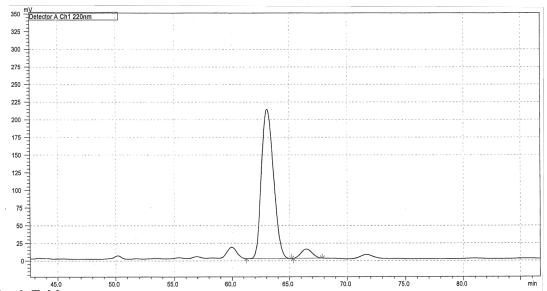

<Peak Table>

Detector A Channel 1 220nm

Peak#	Ret. Time	Area	Height	Conc.	Area%
1	63.066	15535438	211889	94.606	94.606
2	66.463	885722	13001	5.394	5.394
Total		16421161	224890		100.000

Enantiomeric purity of the minor diastereomers

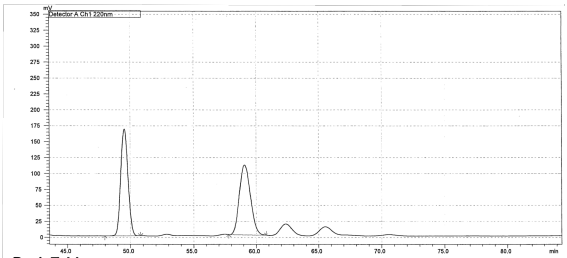

<Peak Table>

Detector A Channel 1 220nm

Peak#	Ret. Time	Area	Height	Conc.	Area%
1	49.520	6685853	167293	49.674	49.674
2	59.073	6773530	109558	50.326	50.326
Total		13459383	276851		100.000

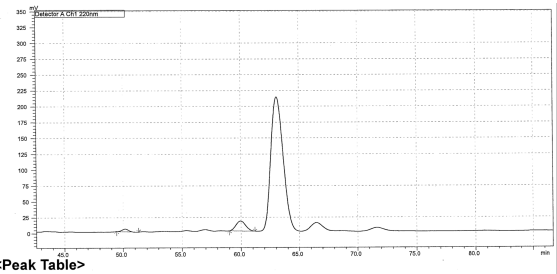

<Peak Table>

Detector A Channel 1 220nm

Peak#	Ret. Time	Area	Height	Conc.	Area%
1	50.158	153821	4256	14.670	14.670
2	59.953	894747	15541	85.330	85.330
Total		1048568	19797		100.000

Peak #	Retention time	Area	Area %	Peak #	Retention time	Area	Area %
1	62.348	1098734	51.093	1	63.066	15535438	94.606
2	65.523	1051722	48.907	2	66.463	885722	5.394
1	49.520	6685853	49.674	1	50.158	153821	14.670
2	59.073	6773530	50.326	2	59.953	894747	85.330

(2*S*,3*R*)-3-(2-Bromophenyl)pent-4-en-2-ol (2.7): IR (CH_2Cl_2): 3419 (br s), 2974 (w), 1637 (w), 1437 (m), 1266 (m), 1107 (s), 1020 (s), 993 (m), 816 (w), 422 (m) cm^{-1}; ^1H NMR (400 MHz, $CDCl_3$): δ 7.59 (1H, dd, *J* = 7.6, 0.8 Hz), 7.38 (1H, dd, *J* = 7.6, 1.6 Hz), 7.33–7.29 (1H, m), 7.12–7.01 (1H, m), 6.03–5.94 (1H, m), 5.19–5.14 (2H, m), 4.21–4.13 (1H, m), 3.95 (1H, t, *J* = 7.6 Hz), 1.46 (1H, d, *J* = 4.4 Hz), 1.27 (3H, d, *J* = 6.4 Hz); ^{13}C NMR (100 MHz, $CDCl_3$): δ 140.1, 137.5, 133.5, 129.2, 128.3, 127.8, 126.0, 117.9, 70.2, 56.4, 21.0; HRMS (DART): Calcd for $C_{11}H_{12}Br$ $[M+H–H_2O]^+$: 223.0122; Found: 223.0122; Specific rotation: $[\alpha]_D^{20}$ –20.07 (*c* 1.12, $CHCl_3$) for a >98% S_N2', 90:10 dr, and 98:2 er sample. Enantiomeric purity of **2.7** was determined by HPLC analysis in comparison with authentic racemic material (98:2 er shown; chiralcel OD–H column, 99:1 hexanes:*i*PrOH, 0.3 mL/min, 220 nm).

Enantiomeric purity of the major diastereomers

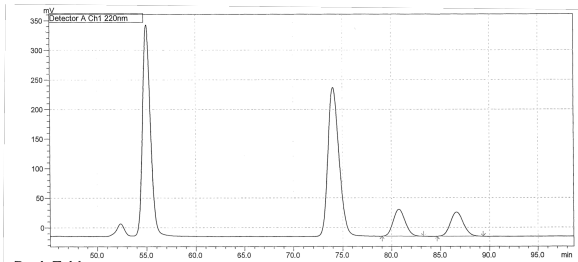

<Peak Table>

Detector A Channel 1 220nm

Peak#	Ret. Time	Area	Height	Conc.	Area%
1	80.743	3892381	45554	50.593	50.593
2	86.625	3801200	40914	49.407	49.407
Total		7693582	86469		100.000

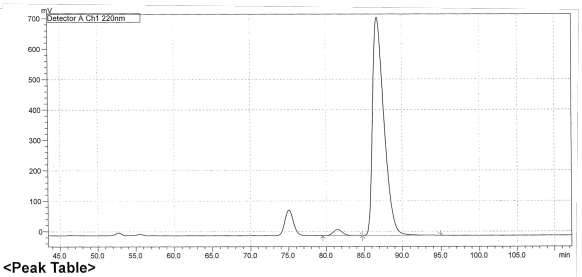

<Peak Table>

Detector A Channel 1 220nm

Peak#	Ret. Time	Area	Height	Conc.	Area%
1	81.459	1735145	20275	2.279	2.279
2	86.755	74391917	718863	97.721	97.721
Total		76127062	739137		100.000

Enantiomeric purity of the minor diastereomers

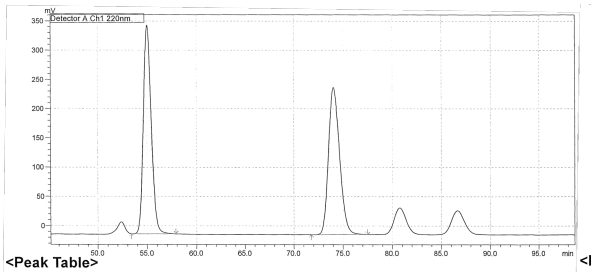

<Peak Table>

Detector A Channel 1 220nm

Peak#	Ret. Time	Area	Height	Conc.	Area%
1	55.004	19766804	356754	49.918	49.918
2	74.047	19832077	251709	50.082	50.082
Total		39598882	608463		100.000

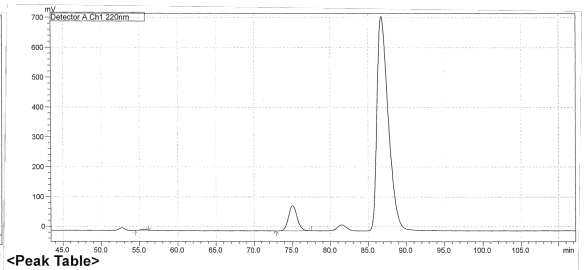

<Peak Table>

Detector A Channel 1 220nm

Peak#	Ret. Time	Area	Height	Conc.	Area%
1	55.505	188295	4070	2.759	2.759
2	75.029	6637342	84243	97.241	97.241
Total		6825637	88313		100.000

Peak #	Retention time	Area	Area %	Peak #	Retention time	Area	Area %
1	80.743	3892381	50.593	1	81.459	1735145	2.279
2	86.625	3801200	49.407	2	86.755	74391917	97.721
1	55.004	19766804	49.918	1	55.505	188295	2.759
2	74.047	19832077	50.082	2	75.029	6637342	97.241

(2*S*,3*R*)-3-(2-Methoxyphenyl)pent-4-en-2-ol (2.8): IR (CH_2Cl_2): 3423 (br s), 2926 (w), 1637 (w), 1491 (m), 1463 (m), 1170 (s), 1120 (m), 1026 (s), 915 (m), 879 (w), 579 (m), 400 (m) cm^{-1}; ^1H NMR (400 MHz, $CDCl_3$): δ 7.26–7.21 (2H, m), 6.98–6.94 (1H, m), 6.09 (1H, d, J = 8.4 Hz), 6.15–6.06 (1H, m), 5.15–5.08 (1H, m), 4.19–4.11 (1H, m), 3.83 (3H, s), 3.74 (1H, t, J = 8.0 Hz), 1.70 (1H, d, J = 4.4 Hz), 1.22 (3H, d, J = 6.4 Hz); ^{13}C NMR (100 MHz, $CDCl_3$): δ 1.57.5, 138.2, 129.2, 128.0, 121.1, 116.8, 111.2, 69.8, 55.6,

52.5, 21.1; HRMS (DART): Calcd for $C_{12}H_{15}O$ $[M+H–H_2O]^+$: 175.1123; Found: 175.1123; Specific rotation: $[\alpha]_D^{20}$ –36.14 (*c* 1.16, $CHCl_3$) for a >98% S_N2', 92:8 dr, and 98:2 er sample. Enantiomeric purity of **2.8** was determined by HPLC analysis in comparison with authentic racemic material (98:2 er shown; chiralcel OD–H column, 98:2 hexanes:*i*PrOH, 0.3 mL/min, 220 nm).

Enantiomeric purity of the major diastereomers

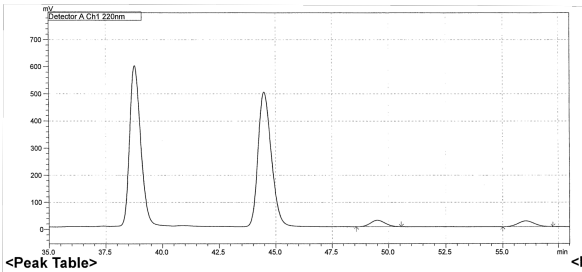

<Peak Table>
Detector A Channel 1 220nm

Peak#	Ret. Time	Area	Height	Conc.	Area%
1	49.501	1076980	23844	49.410	49.410
2	56.029	1102695	21125	50.590	50.590
Total		2179675	44969		100.000

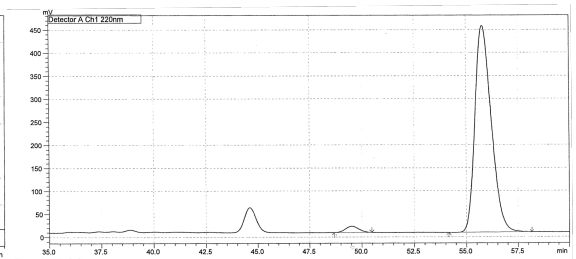

<Peak Table>
Detector A Channel 1 220nm

Peak#	Ret. Time	Area	Height	Conc.	Area%
1	49.523	604502	13609	2.394	2.394
2	55.777	24650974	448868	97.606	97.606
Total		25255476	462477		100.000

Enantiomeric purity of the minor diastereomers

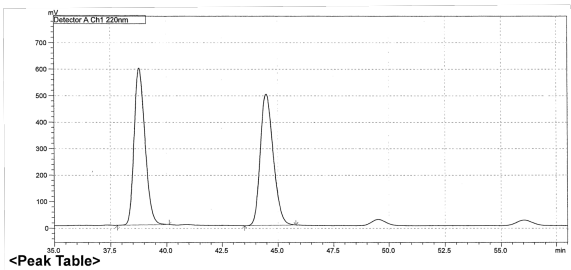

<Peak Table>
Detector A Channel 1 220nm

Peak#	Ret. Time	Area	Height	Conc.	Area%
1	38.789	20061008	591772	49.921	49.921
2	44.487	20124475	495872	50.079	50.079
Total		40185484	1087645		100.000

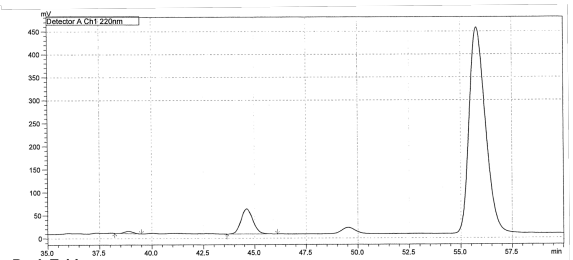

<Peak Table>
Detector A Channel 1 220nm

Peak#	Ret. Time	Area	Height	Conc.	Area%
1	38.871	135564	4644	5.796	5.796
2	44.608	2203203	54500	94.204	94.204
Total		2338767	59145		100.000

Peak #	Retention time	Area	Area %	Peak #	Retention time	Area	Area %
1	49.501	1076980	49.410	1	49.523	604502	2.394
2	56.029	1102695	50.590	2	55.777	24650974	97.606
1	38.789	20061008	49.921	1	38.871	135564	5.796
2	44.487	20124475	50.079	2	44.608	2203203	94.204

(2*S*,3*R*)-3-(*o*-Tolyl)pent-4-en-2-ol (2.9): IR (CH_2Cl_2): 3424 (br s), 2955 (m), 2854 (m),

1636 (w), 1490 (m), 1460 (m), 1118 (s), 1057 (s), 992 (m), 914 (s), 880 (m), 753 (s), 633 (m), 547 (m), 408 (m) cm^{-1}; ^{1}H NMR (400 MHz, $CDCl_3$): δ 7.30–7.12 (4H, m), 5.97–5.88 (1H, m), 5.10–5.05 (2H, m), 4.12 (1H, pent, *J* = 6.7 Hz), 3.55 (1H, t, *J* = 8.6 Hz), 2.36 (3H, s), 1.56 (1H, br), 1.30 (3H, d, J = 6.4 Hz); ^{13}C NMR (100 MHz, $CDCl_3$): δ 139.6, 138.5, 137.4, 137.1, 131.1, 126.7, 126.7, 116.8, 70.3, 54.3, 20.9, 20.0; HRMS (DART): Calcd for $C_{12}H_{15}$ $[M+H–H_2O]^+$: 159.1174; Found: 159.1172; Specific rotation: $[\alpha]_D^{20}$ –44.38 (*c* 0.73, $CHCl_3$) for a >98% S_N2', 90:10 dr, and 97:3 er sample. Enantiomeric purity of **2.9** was determined by HPLC analysis in comparison with authentic racemic material (97:3 er shown; chiralcel OD–H column, 99:1 hexanes:*i*PrOH, 0.3 mL/min, 220 nm).

Enantiomeric purity of the major diastereomers

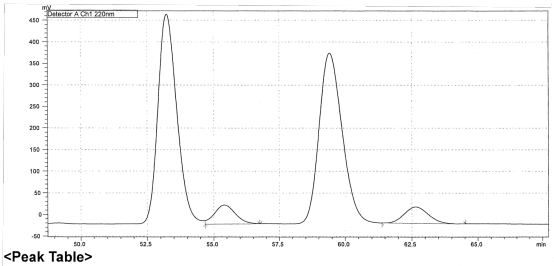

<Peak Table>

Detector A Channel 1 220nm

Peak#	Ret. Time	Area	Height	Conc.	Area%
1	55.405	2454587	44017	50.940	50.940
2	62.644	2364037	37886	49.060	49.060
Total		4818624	81902		100.000

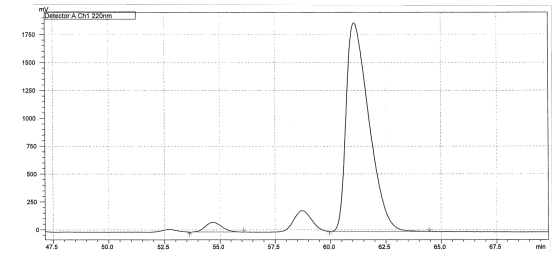

<Peak Table>

Detector A Channel 1 220nm

Peak#	Ret. Time	Area	Height	Conc.	Area%
1	54.676	4534962	86504	3.287	3.287
2	61.089	133439314	1866785	96.713	96.713
Total		137974276	1953288		100.000

Enantiomeric purity of the minor diastereomers

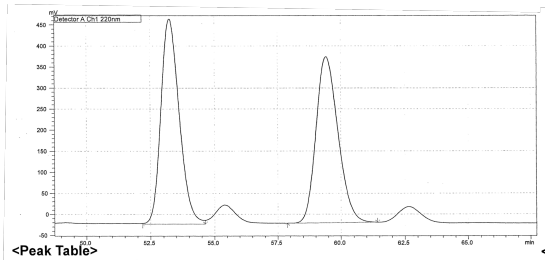

<Peak Table>

Detector A Channel 1 220nm

Peak#	Ret. Time	Area	Height	Conc.	Area%
1	53.235	24253929	487018	50.354	50.354
2	59.415	23912636	394898	49.646	49.646
Total		48166565	881916		100.000

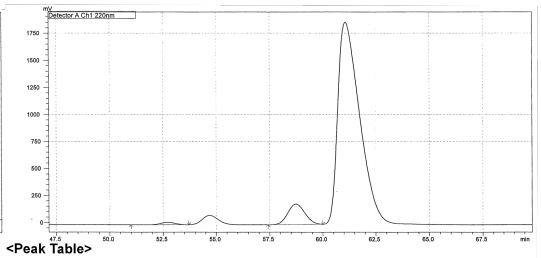

<Peak Table>

Detector A Channel 1 220nm

Peak#	Ret. Time	Area	Height	Conc.	Area%
1	52.708	1038401	22865	8.963	8.963
2	58.731	10546819	188976	91.037	91.037
Total		11585221	211841		100.000

Peak #	Retention time	Area	Area %	Peak #	Retention time	Area	Area %
1	55.405	2454587	50.940	1	54.676	4534962	3.287
2	62.644	2364037	49.060	2	61.089	133439314	96.713
1	53.235	24253929	50.354	1	52.708	22865	8.963
2	59.415	23912636	49.646	2	58.731	188976	91.037

(2*S*,3*R*)-3-(Naphthalen-2-yl)pent-4-en-2-ol (2.10): IR (CH_2Cl_2): 3423 (br s), 2971 (w), 1634 (w), 1599 (w), 1507 (w), 1370 (m), 1113 (s), 1056 (m), 1018 (m), 916 (s), 855 (m), 815 (s), 685 (m), 476 (s) cm^{-1}; ^1H NMR (400 MHz, $CDCl_3$): δ 7.85–7.81 (3H, m), 7.72 (1H, s), 7.51–7.44 (2H, m), 7.41 (1H, dd, *J* = 8.4, 1.6 Hz), 6.18–6.09 (1H, m), 5.20–5.16 (2H, m), 4.21–4.14 (1H, m), 3.43 (1H, t, *J* = 8.0 Hz), 1.52 (1H, d, *J* = 3.6 Hz), 1.29 (3H, d, *J* = 6.4 Hz); ^{13}C NMR (100 MHz, $CDCl_3$): δ 138. 5, 138.4, 133.7, 132.7, 128.7, 127.8, 127.79, 127.4, 126.6, 126.3, 125.9, 117.3, 70.5, 59.2, 20.9; HRMS (DART): Calcd for $C_{15}H_{15}$ $[M+H–H_2O]^+$: 195.1174; Found: 195.1174; Specific rotation: $[\alpha]_D^{20}$ –73.27 (*c* 1.35, $CHCl_3$) for a >98% S_N2', 95:5 dr, and 95:5 er sample. Enantiomeric purity of **2.10** was determined by HPLC analysis in comparison with authentic racemic material (95:5 er shown; chiralcel AD–H column, 99:1 hexanes:*i*PrOH, 0.3 mL/min, 220 nm).

Enantiomeric purity of the major diastereomers

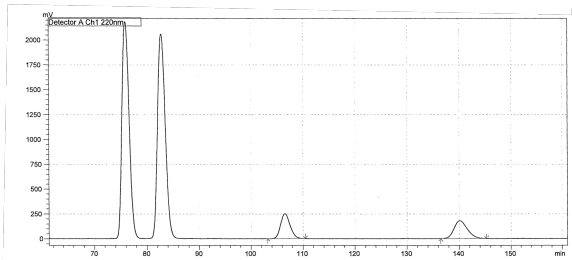

<Peak Table>

Detector A Channel 1 220nm

Peak#	Ret. Time	Area	Height	Conc.	Area%
1	106.504	31890262	250665	50.004	50.004
2	140.112	31884760	179534	49.996	49.996
Total		63775022	430199		100.000

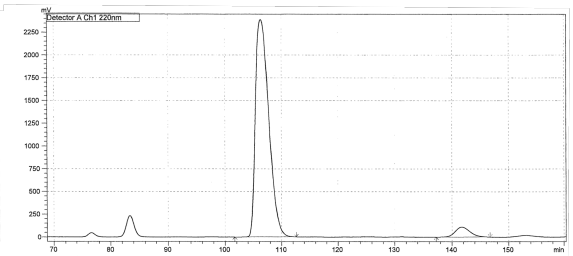

<Peak Table>

Detector A Channel 1 220nm

Peak#	Ret. Time	Area	Height	Conc.	Area%
1	106.315	392512518	2388461	95.218	95.218
2	141.696	19714745	109509	4.782	4.782
Total		412227263	2497969		100.000

Enantiomeric purity of the minor diastereomers

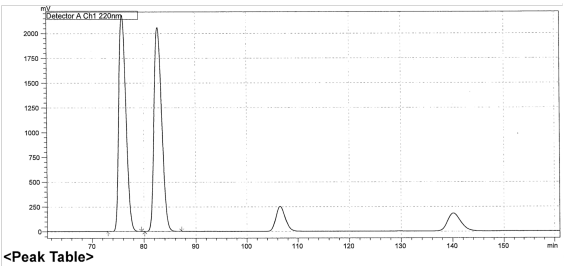

<Peak Table>
Detector A Channel 1 220nm

Peak#	Ret. Time	Area	Height	Conc.	Area%
1	75.906	208858929	2181643	49.489	49.489
2	82.734	213168273	2056619	50.511	50.511
Total		422027201	4238262		100.000

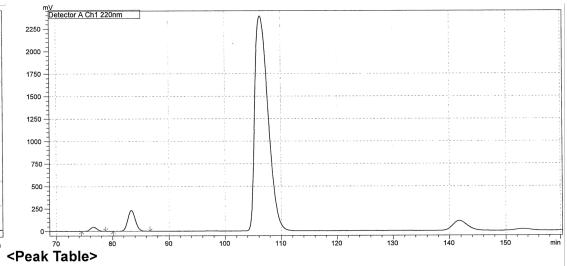

<Peak Table>
Detector A Channel 1 220nm

Peak#	Ret. Time	Area	Height	Conc.	Area%
1	76.574	3771038	44981	14.834	14.834
2	83.358	21650989	231891	85.166	85.166
Total		25422028	276872		100.000

Peak #	Retention time	Area	Area %	Peak #	Retention time	Area	Area %
1	106.504	31890262	50.004	1	106.315	392512518	95.218
2	140.112	31884760	49.996	2	141.696	19714745	4.782
1	75.906	208858929	49.489	1	76.574	3771038	14.834
2	82.734	213168273	50.511	2	83.358	21650989	85.166

(2*S*,3*R*)-3-(3-Bromophenyl)pent-4-en-2-ol (2.11): IR (CH_2Cl_2): 3386 (br s), 2924 (m), 1638 (w), 1592 (m), 1566 (m), 1474 (m), 1427 (w), 1193 (s), 1072 (s), 919 (s), 779 (s), 438 (m) cm^{-1}; ^1H NMR (400 MHz, $CDCl_3$): δ 7.42–7.36 (2H, m), 7.24–7.18 (2H, m), 5.99 (1H, ddd J = 17.2, 10.8, 8.8 Hz), 5.18–5.11 (2H, m), 4.09–4.01 (1H, m), 3.22 (1H, t, J = 8.0 Hz), 1.47 (1H, br), 1.23 (3H, d, J = 6.0 Hz); ^{13}C NMR ($CDCl_3$, 100 MHz): δ 143.5, 137.9, 131.6, 130.4, 130.2, 127.3, 123.0, 117.6, 70.5, 58.6, 21.0; HRMS (DART): Calcd for $C_{11}H_{12}Br$ $[M+H–H_2O]^+$: 223.0122; Found: 223.0128; Specific rotation: $[\alpha]_D^{20}$ – 52.90 (*c* 2.60, $CHCl_3$) for a >98% S_N2', 94:6 dr, and 96:4 er sample. Enantiomeric purity of **2.11** was determined by HPLC analysis in comparison with authentic racemic material (96:4 er shown; chiralcel OD–H column, 99:1 hexanes:*i*PrOH, 0.3 mL/min, 220 nm).

Enantiomeric purity of the major diastereomers

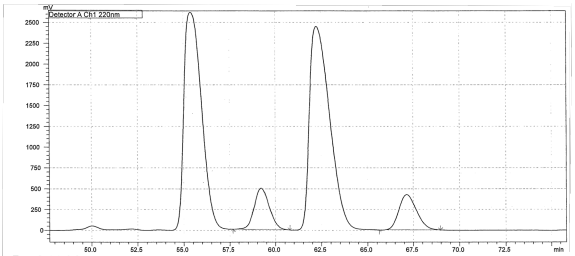

<Peak Table>

Detector A Channel 1 220nm

Peak#	Ret. Time	Area	Height	Conc.	Area%
1	59.216	28585068	497140	50.207	50.207
2	67.137	28349434	424212	49.793	49.793
Total		56934502	921352		100.000

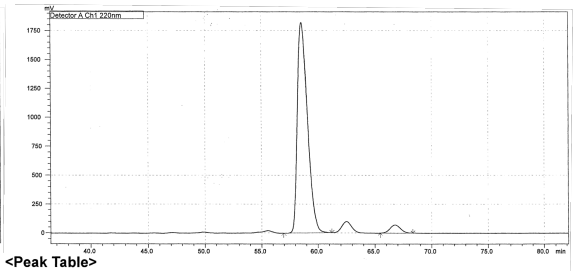

<Peak Table>

Detector A Channel 1 220nm

Peak#	Ret. Time	Area	Height	Conc.	Area%
1	58.548	113799806	1821184	96.114	96.114
2	66.753	4601431	71624	3.886	3.886
Total		118401237	1892807		100.000

Enantiomeric purity of the minor diastereomers

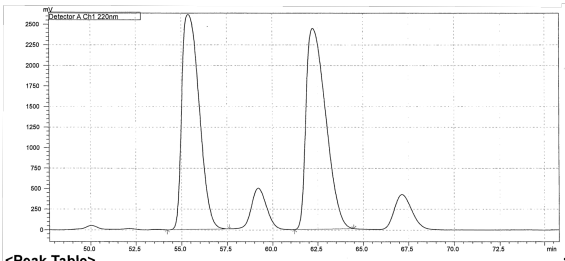

<Peak Table>

Detector A Channel 1 220nm

Peak#	Ret. Time	Area	Height	Conc.	Area%
1	55.386	173778455	2615989	48.515	48.515
2	62.237	184419515	2443110	51.485	51.485
Total		358197971	5059099		100.000

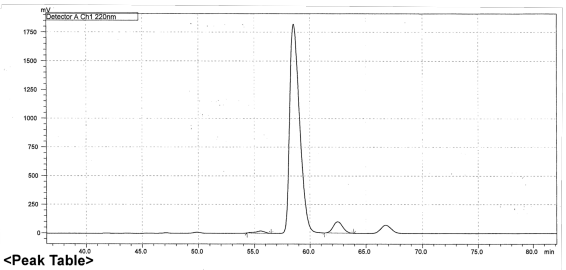

<Peak Table>

Detector A Channel 1 220nm

Peak#	Ret. Time	Area	Height	Conc.	Area%
1	55.561	1127634	19211	16.066	16.066
2	62.491	5891298	98233	83.934	83.934
Total		7018932	117444		100.000

Peak #	Retention time	Area	Area %	Peak #	Retention time	Area	Area %
1	59.216	28585068	50.207	1	58.548	113799806	96.114
2	67.137	28349434	49.793	2	66.753	4601431	3.886
1	55.386	173778455	48.515	1	55.561	1127634	16.066
2	62.237	184419515	51.485	2	62.491	5891298	83.934

(2*S*,3*R*)-3-(3-Methoxyphenyl)pent-4-en-2-ol (2.12): IR (CH_2Cl_2): 3402 (br s), 2974 (w), 1599 (m), 1488 (m), 1155 (m), 1118 (s), 1043 (s), 995 (m), 916 (m), 849 (w), 594 (m), 410 (m) cm^{-1}; ^1H NMR (400 MHz, $CDCl_3$): δ 7.29–7.25 (1H, m), 6.89–6.84 (1H, m), 6.81–6.78 (2H, m), 6.01 (1H, ddd, J = 17.2, 10.4, 8.4 Hz), 5.16–5.11 (2H, m), 4.08–3.99 (1H, m), 3.81 (3H, s), 3.21 (1H, t, J = 8.4 Hz), 1.50 (1H, d, J = 3.6 Hz), 1.24 (3H, d, J = 6.4 Hz); ^{13}C NMR (100 MHz, $CDCl_3$): δ 160.1, 142.7, 138.4, 130.0, 120.7, 117.1, 114.4,

112.3, 70.6, 59.3, 55.3, 20.8; HRMS (DART): Calcd for $C_{12}H_{15}O$ $[M+H–H_2O]^+$: 175.1123; Found: 175.1129; Specific rotation: $[\alpha]_D^{20}$ –47.84 (*c* 1.30, $CHCl_3$) for a >98% S_N2', 95:5 dr, and 96:4 er sample. Enantiomeric purity of **2.12** was determined by HPLC analysis in comparison with authentic racemic material (96:4 er shown; chiralcel AD–H column, 98:2 hexanes:*i*PrOH, 0.3 mL/min, 220 nm).

Enantiomeric purity of the major diastereomers

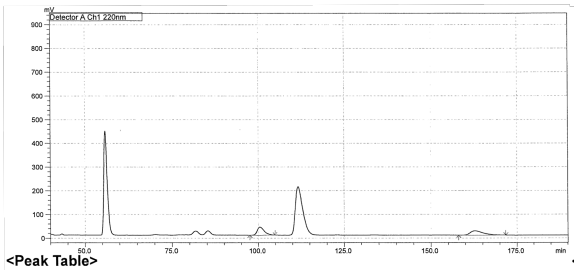

<Peak Table>

Detector A Channel 1 220nm

Peak#	Ret. Time	Area	Height	Conc.	Area%
1	100.366	4735579	33805	49.828	49.828
2	162.668	4768358	18136	50.172	50.172
Total		9503937	51940		100.000

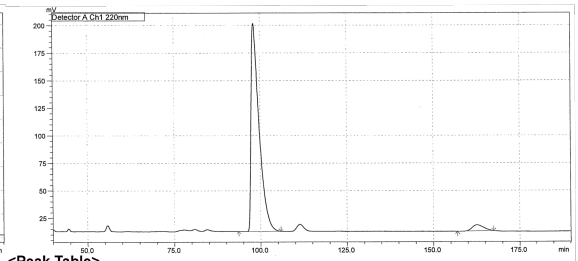

<Peak Table>

Detector A Channel 1 220nm

Peak#	Ret. Time	Area	Height	Conc.	Area%
1	98.096	30598073	188770	96.031	96.031
2	162.526	1264504	5485	3.969	3.969
Total		31862577	194255		100.000

Enantiomeric purity of the minor diastereomers

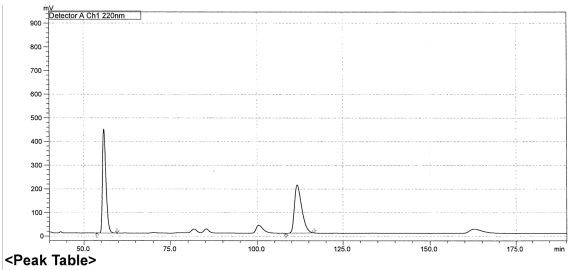

<Peak Table>

Detector A Channel 1 220nm

Peak#	Ret. Time	Area	Height	Conc.	Area%
1	55.854	30827488	439133	50.306	50.306
2	111.656	30452064	203900	49.694	49.694
Total		61279552	643033		100.000

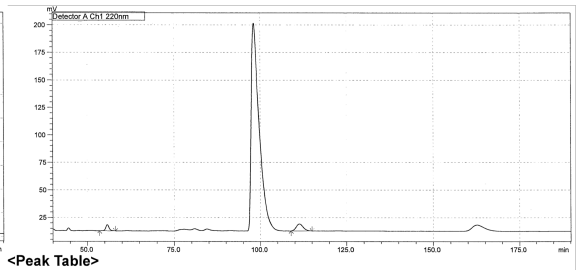

<Peak Table>

Detector A Channel 1 220nm

Peak#	Ret. Time	Area	Height	Conc.	Area%
1	55.718	374425	5598	29.247	29.247
2	111.289	905812	6416	70.753	70.753
Total		1280238	12015		100.000

Peak #	Retention time	Area	Area %	Peak #	Retention time	Area	Area %
1	100.366	4735579	49.828	1	98.096	30598073	96.031
2	162.668	4768358	50.172	2	162.526	1264504	3.969
1	55.854	30827488	50.306	1	55.718	374425	29.247
2	111.656	30452064	49.694	2	111.289	905812	70.753

(2*S*,3*R*)-3-(4-Chlorophenyl)pent-4-en-2-ol (2.13): IR (CH_2Cl_2): 3399 (br s), 2973 (w),

1637 (w), 1490 (s), 1374 (m), 1090 (s), 992 (s), 918 (s), 818 (s), 626 (m),530 (s), 412 (m) cm^{-1}; ^{1}H NMR (400 MHz, $CDCl_3$): δ 7.33–7.26 (2H, m), 7.21–7.19 (2H, m), 6.0 (1H, ddd, *J* = 16.8, 10.4, 8.4 Hz), 5.16–5.09 (2H, m), 4.08–4.00 (1H, m), 3.24 (1H, t, *J* = 8.0 Hz), 1.42 (1H, d, *J* = 4.0 Hz), 1.22 (3H, d, *J* = 6.4 Hz); ^{13}C NMR (100 MHz, $CDCl_3$): δ 139.5, 138.1, 132.8, 130.0, 129.0, 117.4, 70.5, 58.2, 21.0; HRMS (DART): Calcd for $C_{11}H_{12}Cl$ $[M+H–H_2O]^+$: 179.0628; Found: 179.0634; Specific rotation: $[\alpha]_D^{20}$ –70.10 (*c* 1.73, $CHCl_3$) for a >98% S_N2', 95:5 dr, and 95:5 er sample. Enantiomeric purity of **2.13** was determined by HPLC analysis in comparison with authentic racemic material (95:5 er shown; chiralcel AD–H column, 99:1 hexanes:*i*PrOH, 0.3 mL/min, 220 nm).

Enantiomeric purity of the major diastereomers

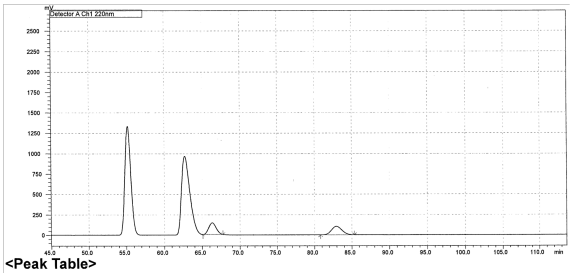

<Peak Table>
Detector A Channel 1 220nm

Peak#	Ret. Time	Area	Height	Conc.	Area%
1	66.314	9872369	143671	49.031	49.031
2	82.923	10262737	104993	50.969	50.969
Total		20135107	248663		100.000

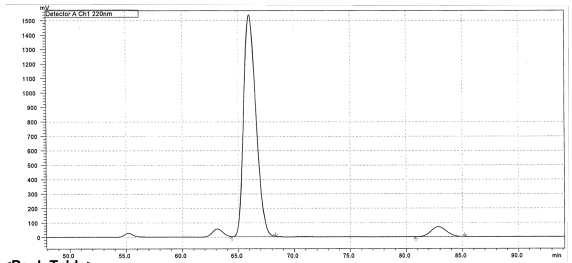

<Peak Table>
Detector A Channel 1 220nm

Peak#	Ret. Time	Area	Height	Conc.	Area%
1	66.013	118099130	1536940	94.662	94.662
2	82.842	6659696	68479	5.338	5.338
Total		124758826	1605419		100.000

Enantiomeric purity of the minor diastereomers

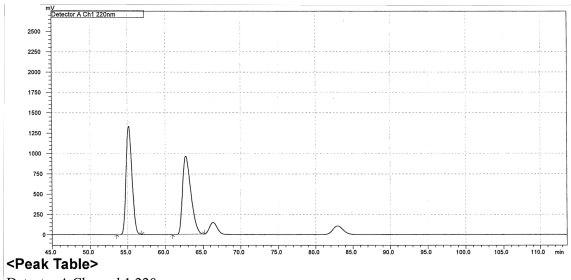

<Peak Table>
Detector A Channel 1 220nm

Peak#	Ret. Time	Area	Height	Conc.	Area%
1	55.172	73774818	1333613	49.960	49.960
2	62.715	73893875	961741	50.040	50.040
Total		147668693	2295355		100.000

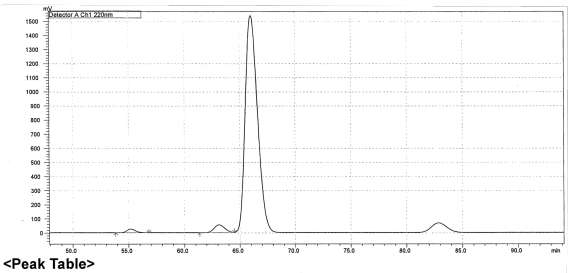

<Peak Table>
Detector A Channel 1 220nm

Peak#	Ret. Time	Area	Height	Conc.	Area%
1	55.190	1416072	26035	28.658	28.658
2	63.106	3525151	54019	71.342	71.342
Total		4941222	80054		100.000

Peak #	Retention time	Area	Area %	Peak #	Retention time	Area	Area %
1	66.314	9872369	49.031	1	66.013	118099130	94.662
2	82.923	10262737	50.969	2	82.842	6659696	5.338
1	55.172	73774818	49.960	1	55.190	1416072	28.658
2	62.715	73893875	50.040	2	63.106	3525151	71.342

(2*S*,3*R*)-3-(4-Bromophenyl)pent-4-en-2-ol (2.14): White solid; m.p. = 46–47 ºC; IR (CH_2Cl_2): 3400 (br s), 3078 (w), 2973 (w), 1637 (w), 1590 (s), 1487 (m), 1193 (s), 1117 (s), 1072 (s), 1010 (m), 918 (s), 617 (m), 527 (s), 412 (m) cm^{-1}; ^1H NMR (600 MHz, $CDCl_3$): δ 7.47 (2H, d, *J* = 7.8 Hz), 7.14 (2H, d, *J* = 8.4 Hz), 5.99 (1H, ddd, *J* = 16.8, 10.8, 9.0 Hz), 5.16–5.10 (2H, m), 4.06–4.01 (1H, m), 3.22 (1H, t, *J* = 8.4 Hz), 1.42 (1H, d, *J* = 3.6 Hz), 1.22 (3H, d, *J* = 6.6 Hz); ^{13}C NMR (100 MHz, $CDCl_3$): δ 140.1, 138.0, 132.0, 130.4, 120.9, 117.5, 70.5, 58.2, 21.0; HRMS (DART): Calcd for $C_{11}H_{12}Br$ $[M+H-H_2O]^+$: 223.0122; Found: 223.0123; Specific rotation: $[\alpha]_D^{20}$ –64.88 (*c* 1.55, $CHCl_3$) for a >98% S_N2', 95:5 dr, and 94:6 er sample. Enantiomeric purity of **2.14** was determined by HPLC analysis in comparison with authentic racemic material (94:6 er shown; chiralcel AZ–H column, 99:1 hexanes:*i*PrOH, 0.3 mL/min, 220 nm).

Enantiomeric purity of the major diastereomers

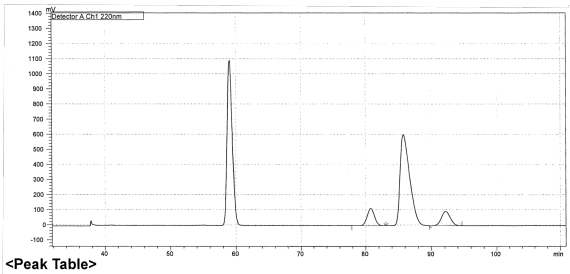

<Peak Table>
Detector A Channel 1 220nm

Peak#	Ret. Time	Area	Height	Conc.	Area%
1	80.759	8854887	113441	50.089	50.089
2	92.126	8823248	93743	49.911	49.911
Total		17678134	207184		100.000

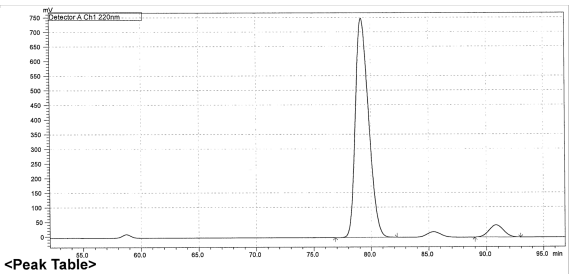

<Peak Table>
Detector A Channel 1 220nm

Peak#	Ret. Time	Area	Height	Conc.	Area%
1	79.170	60676341	751506	94.227	94.227
2	90.810	3717768	41897	5.773	5.773
Total		64394109	793403		100.000

Enantiomeric purity of the minor diastereomers

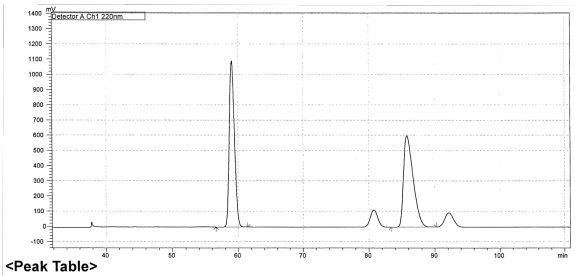

<Peak Table>
Detector A Channel 1 220nm

Peak#	Ret. Time	Area	Height	Conc.	Area%
1	59.035	60559246	1091897	49.947	49.947
2	85.783	60688317	601347	50.053	50.053
Total		121247563	1693245		100.000

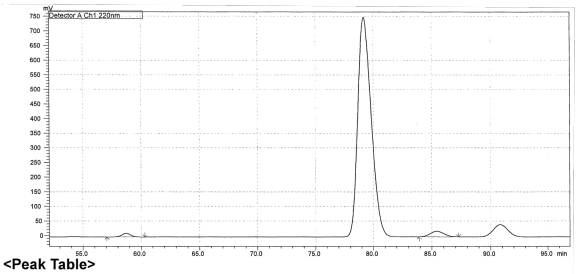

<Peak Table>
Detector A Channel 1 220nm

Peak#	Ret. Time	Area	Height	Conc.	Area%
1	58.705	628103	12051	28.749	28.749
2	85.418	1556716	18968	71.251	71.251
Total		2184819	31018		100.000

Peak #	Retention time	Area	Area %	Peak #	Retention time	Area	Area %
1	80.759	8854887	50.089	1	79.170	60676341	94.227
2	92.126	8823248	49.911	2	90.810	41897	5.773
1	59.035	60559246	49.947	1	58.705	628103	28.749
2	87.783	60688317	50.053	2	85.418	1556716	71.251

(2*S*,3*R*)-3-(4-(Trifluoromethyl)phenyl)pent-4-en-2-ol (2.15): IR (CH_2Cl_2): 3412 (br, s), 2977 (w), 1638 (w), 1323 (s), 1162 (m), 1118 (s), 1066 (s), 1018 (m), 921 (m), 835 (m), 405 (m) cm^{-1}; ^1H NMR (400 MHz, $CDCl_3$): δ 7.60 (2H, d, J = 8.0 Hz), 7.39 (2H, d, J = 8.8 Hz), 6.04 (1H, ddd, J = 16.8, 10.4, 8.8 Hz), 5.19–5.12 (2H, m), 4.14–4.07 (1H, m), 3.34 (1H, t, J = 8.0 Hz), 1.42 (1H, br), 1.24 (3H, d, J = 6.0 Hz); ^{13}C NMR (100 MHz, $CDCl_3$): δ 145.3, 137.8, 129.1 (q, J_{CF} = 31.9 Hz), 129.0, 125.7 (q, J_{CF} = 3.8 Hz), 124.3 (q, J_{CF} = 270.2 Hz), 117.8, 70.5, 58.6, 21.2; HRMS (DART): Calcd for $C_{12}H_{12}F_3$ $[M+H–H_2O]^+$: 213.0891; Found: 213.0900; Specific rotation: $[\alpha]_D^{20}$ –50.53 (*c* 1.67, $CHCl_3$) for a >98% S_N2', 95:5 dr, and 96:4 er sample. Enantiomeric purity of **2.15** was determined by HPLC analysis in comparison with authentic racemic material (96:4 er shown; chiralcel AD–H column, 99:1 hexanes:*i*PrOH, 0.3 mL/min, 220 nm).

Enantiomeric purity of the major diastereomers

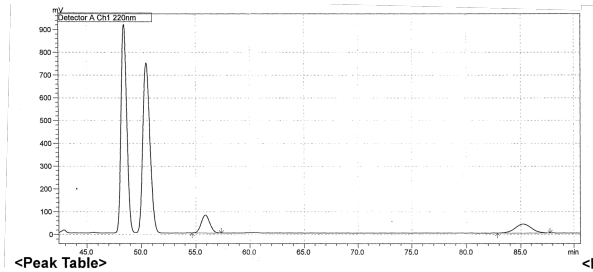

<Peak Table>

Detector A Channel 1 220nm

Peak#	Ret. Time	Area	Height	Conc.	Area%
1	55.882	4306390	78757	50.641	50.641
2	85.208	4197368	39471	49.359	49.359
Total		8503758	118228		100.000

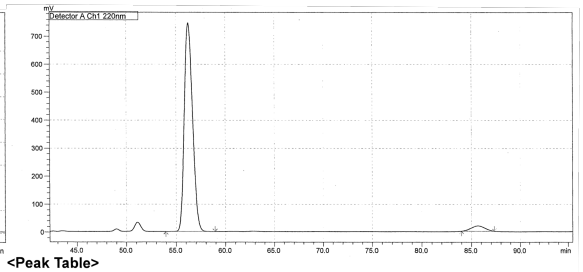

<Peak Table>

Detector A Channel 1 220nm

Peak#	Ret. Time	Area	Height	Conc.	Area%
1	56.241	43337839	745578	95.817	95.817
2	85.646	1892198	19245	4.183	4.183
Total		45230037	764823		100.000

Enantiomeric purity of the minor diastereomers

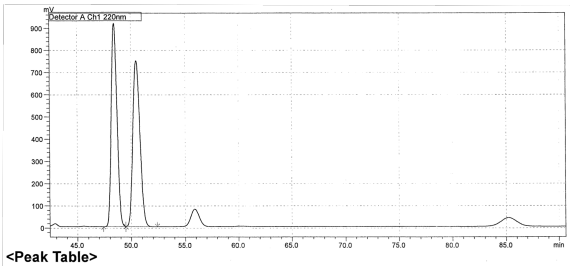

<Peak Table>

Detector A Channel 1 220nm

Peak#	Ret. Time	Area	Height	Conc.	Area%
1	48.426	33828664	915978	49.672	49.672
2	50.475	34275705	746951	50.328	50.328
Total		68104370	1662929		100.000

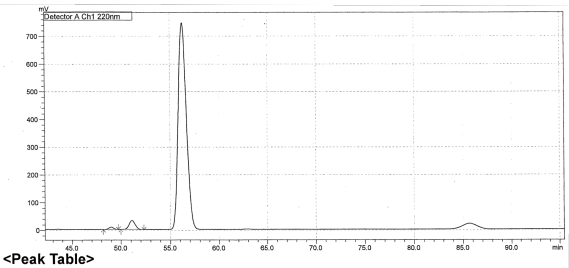

<Peak Table>

Detector A Channel 1 220nm

Peak#	Ret. Time	Area	Height	Conc.	Area%
1	48.976	297865	8638	17.357	17.357
2	51.105	1418264	32384	82.643	82.643
Total		1716129	41022		100.000

Peak #	Retention time	Area	Area %	Peak #	Retention time	Area	Area %
1	55.882	4306390	50.641	1	56.241	43337839	95.817
2	85.208	4197368	49.359	2	85.646	1892198	4.183
1	48.426	33828664	49.672	1	48.976	297865	17.357
2	50.275	34275705	50.328	2	51.105	1418264	82.643

(2*S*,3*R*)-3-(4-Nitrophenyl)pent-4-en-2-ol (2.16): IR (CH_2Cl_2): 3431 (br s), 2924 (w),1638 (m), 1517 (s), 1457 (w), 1343 (s), 1108 (s), 1055 (s), 922 (m), 846 (m), 661 (m), 522 (m), 402 (m) cm^{-1}; ^1H NMR (400 MHz, $CDCl_3$): δ 8.20 (2H, d, *J* = 8.8 Hz), 7.45 (2H, d, *J* = 8.8 Hz), 6.03 (1H, ddd, *J* = 16.8, 10.8, 8.8 Hz), 5.23–5.12 (2H, m), 4.14 (1H, pent, *J* = 6.0 Hz), 3.40 (1H, t, *J* = 8.0 Hz), 1.23 (1H, br), 1.24 (3H, d, *J* = 6.0 Hz); ^{13}C NMR (100 MHz, $CDCl_3$): δ 149.0, 147.0, 137.3, 129.6, 123.9, 118.3, 70.5, 58.4,

21.4; HRMS (DART): Calcd for $C_{11}H_{14}NO_3$ $[M+H]^+$: 208.0974; Found: 208.0973; Specific rotation: $[\alpha]_D^{20}$ –48.57 (*c* 1.97, $CHCl_3$) for a >98% S_N2', 93:7 dr, and 95:5 er sample. Enantiomeric purity of **2.16** was determined by HPLC analysis in comparison with authentic racemic material (95:5 er shown; chiralcel AD–H column, 98:2 hexanes:*i*PrOH, 0.3 mL/min, 220 nm).

Enantiomeric purity of the major diastereomers

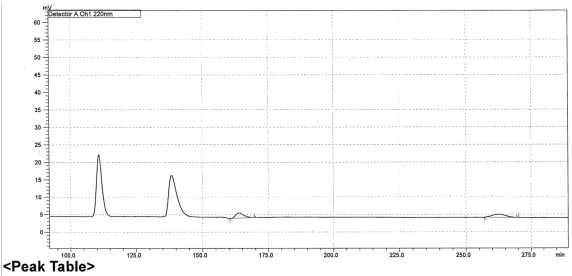

<Peak Table>
Detector A Channel 1 220nm

Peak#	Ret. Time	Area	Height	Conc.	Area%
1	163.790	318540	1479	50.220	50.220
2	262.444	315751	907	49.780	49.780
Total		634291	2386		100.000

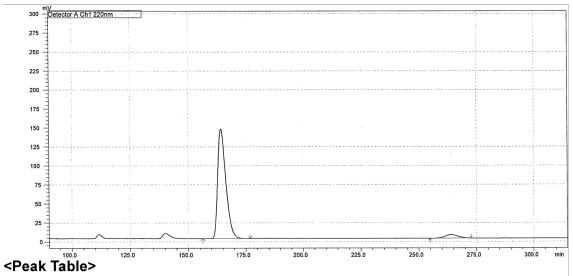

<Peak Table>
Detector A Channel 1 220nm

Peak#	Ret. Time	Area	Height	Conc.	Area%
1	164.250	35426562	144444	95.017	95.017
2	263.980	1857942	4773	4.983	4.983
Total		37284504	149217		100.000

Enantiomeric purity of the minor diastereomers

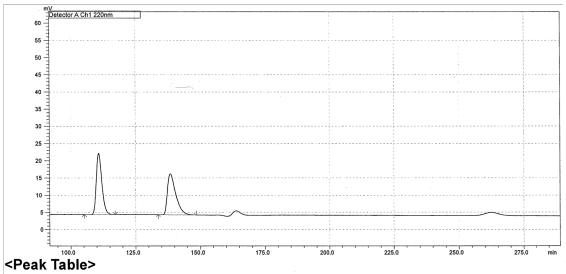

<Peak Table>
Detector A Channel 1 220nm

Peak#	Ret. Time	Area	Height	Conc.	Area%
1	110.793	2640525	17737	49.848	49.848
2	138.390	2656616	11908	50.152	50.152
Total		5297141	29645		100.000

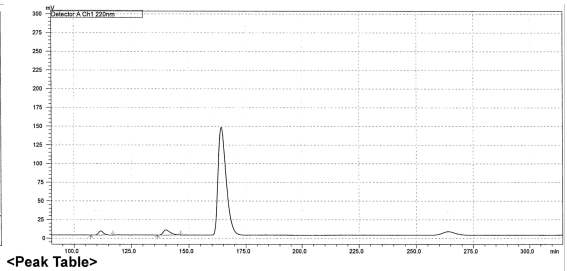

<Peak Table>
Detector A Channel 1 220nm

Peak#	Ret. Time	Area	Height	Conc.	Area%
1	111.597	809379	5466	35.568	35.568
2	140.009	1466230	6879	64.432	64.432
Total		2275609	12344		100.000

Peak #	Retention time	Area	Area %	Peak #	Retention time	Area	Area %
1	163.790	318540	50.220	1	164.250	35426562	95.017
2	262.444	315751	49.780	2	263.980	1857942	4.983
1	110.793	2640525	49.848	1	111.597	809379	35.568
2	138.390	2656616	50.152	2	140.009	1466230	64.432

(2*S*,3*R*)-3-(Pyridin-3-yl)pent-4-en-2-ol (2.17): Following the representative procedure

except 7.5 mol % **NHC-8** and 7.0 mol % CuCl were used. IR (CH_2Cl_2): 3232 (br s), 2923 (m), 1577 (w), 1427 (m), 1373 (m), 1312 (w), 1119 (s), 1029 (m), 918 (s), 802 (m), 714 (s), 402 (m) cm^{-1}; ^1H NMR (400 MHz, $CDCl_3$): δ 8.51–8.48 (2H, m), 7.61 (1H, dt, *J* = 7.6, 2.0 Hz), 7.28–7.25 (2H, m), 6.06 (1H, ddd, *J* = 16.8, 10.4, 8.4 Hz), 5.21–5.12 (2H, m), 4.11 (1H, pent, *J* = 6.8 Hz), 3.30 (1H, t, *J* = 7.6 Hz), 1.63 (1H, br), 1.22 (3H, d, *J* = 6.0 Hz); ^{13}C NMR (100 MHz, $CDCl_3$): δ 150.4, 148.4, 137.7, 136.5, 136.2, 123.6, 118.0, 70.4, 55.8, 21.3; HRMS (DART): Calcd for $C_{10}H_{14}NO$ $[M+H]^+$: 164.1075; Found: 164.1073; Specific rotation: $[\alpha]_D^{20}$ –43.32 (*c* 0.42, $CHCl_3$) for a 96% S_N2', 92:8 dr, and 93:7 er sample. Enantiomeric purity of **2.17** was determined by HPLC analysis in comparison with authentic racemic material (93:7 er shown; chiralcel OZ–H column, 97:3 hexanes:*i*PrOH, 0.3 mL/min, 254 nm).

Enantiomeric purity of the major diastereomers

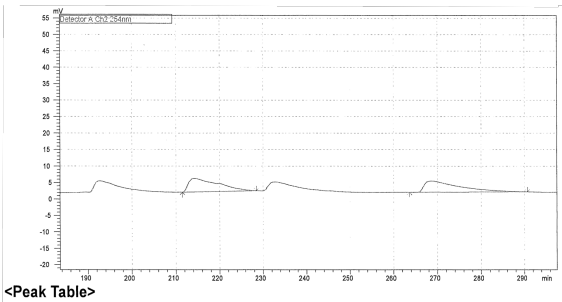

<Peak Table>

Detector A Channel 2 254nm

Peak#	Ret. Time	Area	Height	Conc.	Area%
1	214.158	1921177	4097	50.393	50.393
2	268.479	1891182	3393	49.607	49.607
Total		3812358	7490		100.000

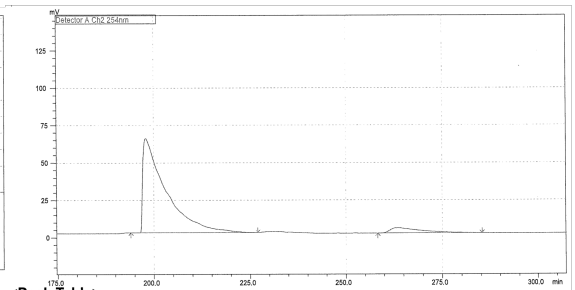

<Peak Table>

Detector A Channel 2 254nm

Peak#	Ret. Time	Area	Height	Conc.	Area%
1	197.925	25868140	62908	93.180	93.180
2	263.432	1893233	3423	6.820	6.820
Total		27761373	66331		100.000

Peak #	Retention time	Area	Area %	Peak #	Retention time	Area	Area %
1	214.158	1921177	50.393	1	197.925	25868140	93.180
2	268.479	1891182	49.607	2	263.432	1893233	6.820

(2*S*,3*R*)-3-(Benzo[*b*]thiophen-3-yl)pent-4-en-2-ol (2.18): IR (CH_2Cl_2): 3429 (br s), 2974 (w), 1637 (w), 1426 (m), 1392 (w), 1116 (m), 1063 (m), 871 (m), 760 (s), 599 (w), 425 (m) cm^{-1}; ^1H NMR (400 MHz, $CDCl_3$): δ 7.89–7.87 (1H, m), 7.82 (1H, dd, *J* = 6.4,

1.2 Hz), 7.14–7.34 (2H, m), 7.33 (1H, s), 7.26 (1H, s), 6.15–6.06 (1H, m), 5.21–5.17 (2H, m), 4.26 (1H, pent, J = 6.4 Hz), 3.81 (1H, t, J = 7.6 Hz), 1.71 (1H, br), 1.28 (3H, d, J = 6.0 Hz); ^{13}C NMR (100 MHz, $CDCl_3$): δ 140.7, 138.9, 137.2, 135.3, 124.6, 124.2, 123.1, 122.7, 122.2, 117.7, 70.0, 52.0, 20.9; HRMS (DART): Calcd for $C_{13}H_{13}S$ $[M+H–H_2O]^+$: 201.0738; Found: 201.0738; Specific rotation: $[\alpha]_D^{20}$ –20.61 (c 1.82, $CHCl_3$) for a >98% S_N2', 91:9 dr, and 95:5 er sample. Enantiomeric purity of **2.18** was determined by HPLC analysis in comparison with authentic racemic material (95:5 er shown; chiralcel AD–H column, 99:1 hexanes:*i*PrOH, 0.3 mL/min, 220 nm).

Enantiomeric purity of the major diastereomers

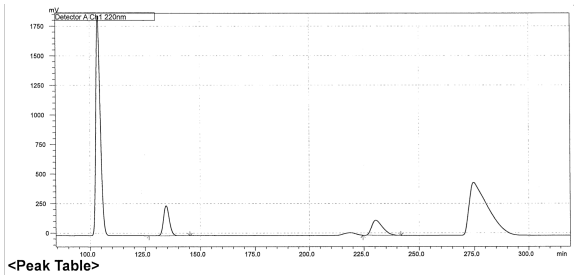

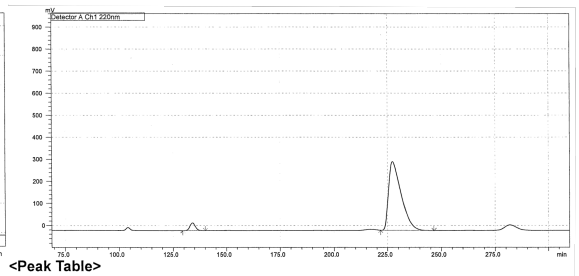

<Peak Table>

Detector A Channel 1 220nm

Peak#	Ret. Time	Area	Height	Conc.	Area%
1	134.537	46490882	253966	50.812	50.812
2	230.390	45004239	128962	49.188	49.188
Total		91495121	382928		100.000

<Peak Table>

Detector A Channel 1 220nm

Peak#	Ret. Time	Area	Height	Conc.	Area%
1	133.993	6142996	34919	4.597	4.597
2	227.344	127481162	311851	95.403	95.403
Total		133624158	346770		100.000

Enantiomeric purity of the minor diastereomers

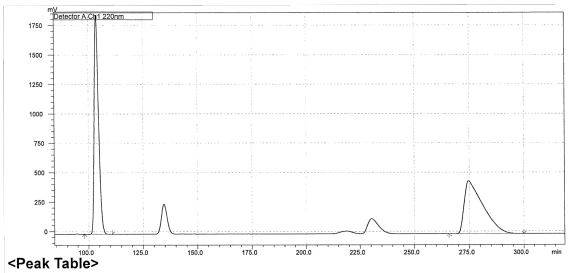

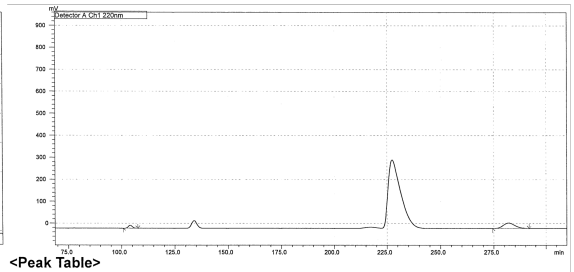

<Peak Table>

Detector A Channel 1 220nm

Peak#	Ret. Time	Area	Height	Conc.	Area%
1	103.675	267438465	1857474	49.975	49.975
2	274.662	267701211	448953	50.025	50.025
Total		535139676	2306427		100.000

<Peak Table>

Detector A Channel 1 220nm

Peak#	Ret. Time	Area	Height	Conc.	Area%
1	103.999	1728472	13379	15.230	15.230
2	281.890	9620797	24958	84.770	84.770
Total		11349269	38337		100.000

Peak #	Retention time	Area	Area %	Peak #	Retention time	Area	Area %
1	134.537	46490882	50.812	1	133.993	6142996	4.597
2	230.390	45004239	49.188	2	227.344	127481162	95.403
1	103.675	267438465	49.975	1	103.999	1728472	15.230
2	274.662	267701211	50.025	2	281.890	9620797	84.770

(2*S*,3*R*,*E*)-5-Phenyl-3-vinylpent-4-en-2-ol (2.19): Following the representative procedure except 7.5 mol % **NHC-8** and 7.0 mol % CuCl were used. IR (CH_2Cl_2): 3377 (br s), 2972 (w), 1636 (w), 1599 (w), 1449 (m), 1373 (w), 1119 (s), 1072 (s), 996 (s), 915 (s), 865 (m), 607 (m), 517 (m) cm^{-1}; ^1H NMR (500 MHz, $CDCl_3$): δ 7.40–7.37 (2H, m), 7.32 (2H, t, *J* = 7.0 Hz), 7.23 (1H, t, *J* = 7.0 Hz), 6.50 (1H, d, *J* = 16.0 Hz), 6.21 (1H, dd, *J* = 16.0, 8.5 Hz), 5.88 (1H, ddd, *J* = 17.5, 10.5, 8.0 Hz), 5.20–5.17 (2H, m), 3.83 (1H, pent, *J* = 6.0 Hz), 2.91 (1H, q, *J* = 8.0 Hz), 1.73 (1H, br), 1.23 (3H, d, *J* = 6.0 Hz);^{13}C NMR (100 MHz, $CDCl_3$): δ 137.6, 137.2, 133.0, 128.7, 128.5, 127.6, 126.4, 117.3, 69.9, 55.8, 20.5; HRMS (DART): Calcd for $C_{13}H_{15}$ $[M+H–H_2O]^+$: 171.1174; Found: 171.1183; Specific rotation: $[\alpha]_D^{20}$ –60.33 (*c* 1.15, $CHCl_3$) for a >98:2 S_N2', 90:10 dr, and 92:8 er sample. Enantiomeric purity of **2.19** was determined by HPLC analysis in comparison with authentic racemic material (92:8 er shown; chiralcel OD–H column, 99:1 hexanes:*i*PrOH, 0.3 mL/min, 254 nm).

Enantiomeric purity of the major diastereomers

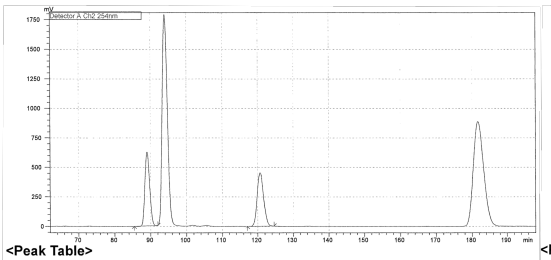

<Peak Table>
Detector A Channel 2 254nm

Peak#	Ret. Time	Area	Height	Conc.	Area%
1	89.082	55911504	625821	49.674	49.674
2	120.692	56644252	452282	50.326	50.326
Total		112555757	1078103		100.000

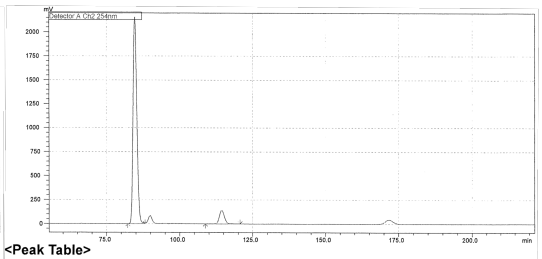

<Peak Table>
Detector A Channel 2 254nm

Peak#	Ret. Time	Area	Height	Conc.	Area%
1	84.609	195678063	2154765	92.103	92.103
2	114.405	16777727	140555	7.897	7.897
Total		212455790	2295320		100.000

Enantiomeric purity of the minor diastereomers

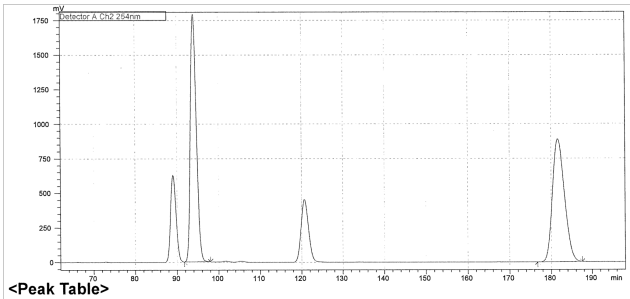

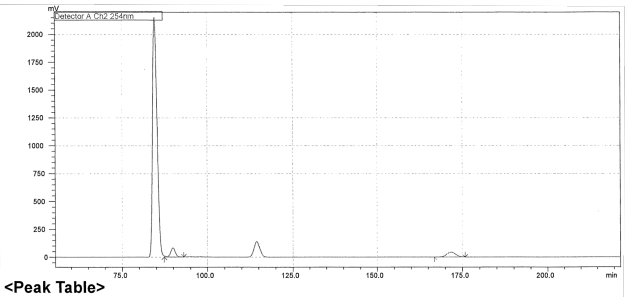

<Peak Table>

Detector A Channel 2 254nm

Peak#	Ret. Time	Area	Height	Conc.	Area%
1	93.997	178674606	1790176	49.880	49.880
2	181.639	179532462	886824	50.120	50.120
Total		358207068	2677000		100.000

<Peak Table>

Detector A Channel 2 254nm

Peak#	Ret. Time	Area	Height	Conc.	Area%
1	89.829	7853360	81506	49.388	49.388
2	171.676	8047969	44063	50.612	50.612
Total		15901329	125568		100.000

Peak #	Retention time	Area	Area %	Peak #	Retention time	Area	Area %
1	89.082	55911504	49.674	1	84.609	195678063	92.103
2	120.692	56644252	50.326	2	114.405	16777727	7.897
1	93.997	178674606	49.880	1	89.829	7853360	49.388
2	181.639	179532462	50.120	2	171.676	8047969	50.612

(2*S*,3*R*)-3-(Phenylethynyl)pent-4-en-2-ol (2.20): IR (CH_2Cl_2): 3399 (br s), 2975 (w), 1639 (w), 1598 (w), 1490 (m), 1443 (m), 1115 (s), 1070 (s), 921 (s), 825 (m), 597 (m), 469 (m) cm^{-1}; ^1H NMR (400 MHz, $CDCl_3$): δ 7.47–7.43 (2H, m), 7.33–7.30 (3H, m), 5.91 (1H, ddd, *J* = 20.8, 10, 6.4 Hz), 5.43–5.47 (1H, m), 5.31–5.28 (1H, m), 3.93–3.88 (1H, m), 3.38–3.35 (1H, m), 1.99 (1H, d, *J* = 2.0 Hz), 1.34 (3H, d, *J* = 6.0 Hz); ^{13}C NMR (100 MHz, $CDCl_3$): δ 134.5, 131.9, 128.4, 128.3, 123.2, 118.2, 86.7, 86.2, 69.9, 45.4, 20.7; HRMS (DART): Calcd for $C_{11}H_{15}O$ $[M+H]^+$: 187.1123; Found: 187.1131; Specific rotation: $[\alpha]_D^{20}$ –82.21 (*c* 0.85, $CHCl_3$) for a >98% S_N2', 93:7 dr, and 91:9 er sample. Enantiomeric purity of **2.20** was determined by HPLC analysis in comparison with authentic racemic material (97:3 er shown; chiralcel AZ–H column, 99:1 hexanes:*i*PrOH,

0.3 mL/min, 254 nm).

Enantiomeric purity of the major diastereomers

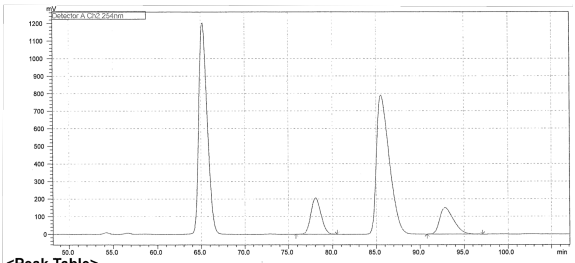

<Peak Table>

Detector A Channel 2 254nm

Peak#	Ret. Time	Area	Height	Conc.	Area%
1	78.052	16615430	206893	50.119	50.119
2	92.829	16536389	150750	49.881	49.881
Total		33151819	357643		100.000

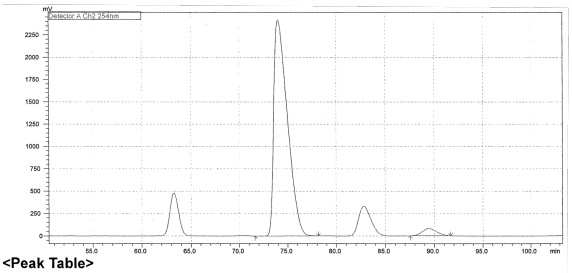

<Peak Table>

Detector A Channel 2 254nm

Peak#	Ret. Time	Area	Height	Conc.	Area%
1	74.007	235964984	2414322	96.619	96.619
2	89.420	8256356	80432	3.381	3.381
Total		244221340	2494754		100.000

Enantiomeric purity of the minor diastereomers

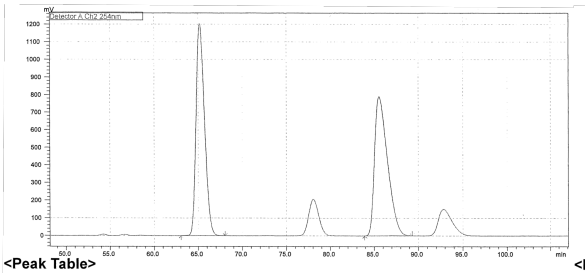

<Peak Table>

Detector A Channel 2 254nm

Peak#	Ret. Time	Area	Height	Conc.	Area%
1	65.189	80801160	1203861	49.993	49.993
2	85.567	80822719	790731	50.007	50.007
Total		161623879	1994592		100.000

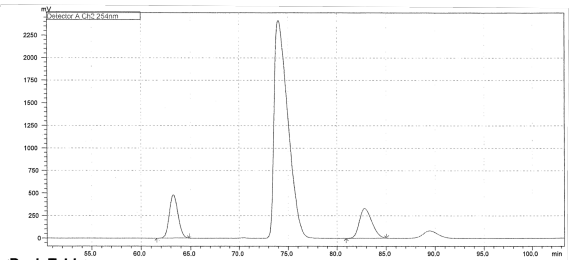

<Peak Table>

Detector A Channel 2 254nm

Peak#	Ret. Time	Area	Height	Conc.	Area%
1	63.246	29463954	480871	50.300	50.300
2	82.812	29112280	329933	49.700	49.700
Total		58576234	810805		100.000

Peak #	Retention time	Area	Area %	Peak #	Retention time	Area	Area %
1	78.052	16615430	50.119	1	74.007	235964984	96.619
2	92.829	16536389	49.881	2	89.420	8256356	3.381
1	65.189	80801160	49.993	1	63.246	480871	50.300
2	85.567	80822719	50.007	2	82.812	329933	49.700

(2*S*,3*S*)-3-Phenethylpent-4-en-2-ol (2.21): IR (CH_2Cl_2): 3358 (br s), 2923 (w), 1639 (w), 1496 (m), 1374 (w), 1122 (s), 1053 (m), 998 (m), 913 (s), 697 (s), 413 (m) cm^{-1}; ^1H NMR (400 MHz, $CDCl_3$): δ 7.30–7.27 (2H, m), 7.20–7.16 (3H, m), 5.66 (1H, ddd, *J* = 17.2, 10.4, 9.2 Hz), 5.23 (1H, dd, *J* = 10.0, 2.0 Hz), 5.15 (1H, ddd, *J* = 17.2, 2.0, 0.8 Hz), 3.75–3.67 (1H, m), 2.71 (1H, ddd, *J* = 14.0, 10.0, 4.4 Hz), 2.51 (1H, ddd, *J* = 13.6, 10.0,

7.2 Hz), 2.17–2.10 (1H, m), 1.92–1.84 (1H, m), 1.62–1.52 (1H, m), 1.45 (1H, d, J = 7.6 Hz), 1.15 (3H, d, J = 6.0 Hz); ^{13}C NMR (100 MHz, $CDCl_3$): δ 142.5, 138.4, 128.6, 128.5, 125.9, 118.4, 70.3, 51.4, 33.7, 32.4, 20.2; HRMS (DART): Calcd for $C_{13}H_{17}$ $[M+H–H_2O]^+$: 173.1330; Found: 173.1329; Specific rotation: $[\alpha]_D^{20}$ –6.29 (c 2.50, $CHCl_3$) for a >98% S_N2', 92:8 dr, and 91:9 er sample. Enantiomeric purity of **2.21** was determined by HPLC analysis in comparison with authentic racemic material (91:9 er shown; chiralcel AD–H column, 99:1 hexanes:*i*PrOH, 0.3 mL/min, 254 nm).

Enantiomeric purity of the major diastereomers

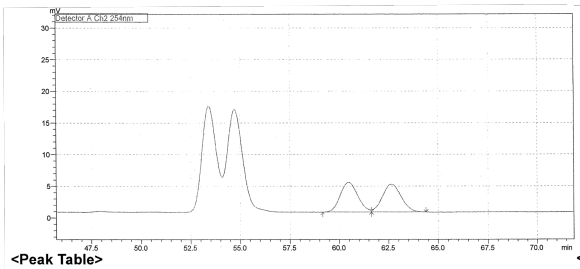

<Peak Table>

Detector A Channel 2 254nm

Peak#	Ret. Time	Area	Height	Conc.	Area%
1	60.459	292381	4701	50.242	50.242
2	62.663	289564	4403	49.758	49.758
Total		581945	9104		100.000

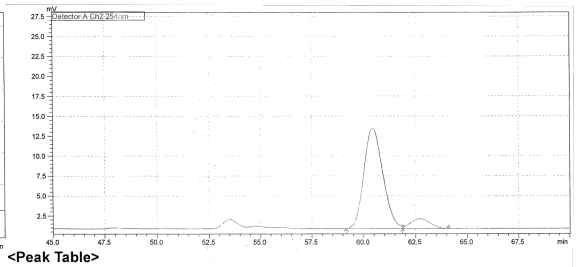

<Peak Table>

Detector A Channel 2 254nm

Peak#	Ret. Time	Area	Height	Conc.	Area%
1	60.443	803668	12613	90.809	90.809
2	62.693	81343	1253	9.191	9.191
Total		885012	13866		100.000

Enantiomeric purity of the minor diastereomers

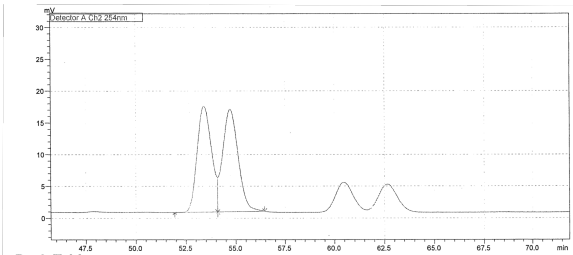

<Peak Table>

Detector A Channel 2 254nm

Peak#	Ret. Time	Area	Height	Conc.	Area%
1	53.416	834260	16669	48.791	48.791
2	54.720	875598	16122	51.209	51.209
Total		1709858	32792		100.000

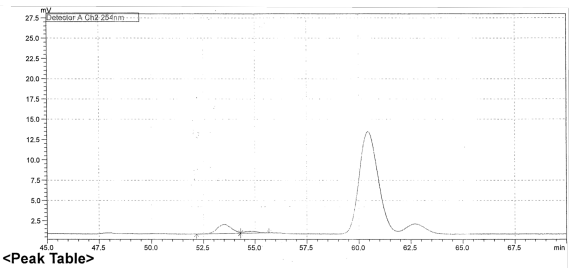

<Peak Table>

Detector A Channel 2 254nm

Peak#	Ret. Time	Area	Height	Conc.	Area%
1	53.476	53606	1108	84.024	84.024
2	54.788	10193	226	15.976	15.976
Total		63799	1334		100.000

Peak #	Retention time	Area	Area %	Peak #	Retention time	Area	Area %
1	60.459	292381	50.242	1	60.443	803668	90.809
2	62.663	289564	49.758	2	62.693	81343	9.191
1	53.416	834260	48.791	1	53.476	53606	84.024
2	54.720	875598	51.209	2	54.788	10193	15.976

(2*S*,3*R*)-3-Cyclohexylpent-4-en-2-ol (2.22): Following the representative procedure except 7.5 mol % **NHC-8** and 7.0 mol % CuCl were used. IR (CH_2Cl_2): 3377 (br s), 2967 (m), 2922 (s), 2852 (m), 1449 (m), 1420 (w), 1118 (s), 1057 (s), 1001 (m), 956 (w), 910 (s), 872 (w), 838 (w), 768 (s), 507 (w), 407 (m) cm^{-1}; ^1H NMR (400 MHz, $CDCl_3$): δ 5.56 (1H, dt, *J* = 16.8, 10.0 Hz), 5.17 (1H, dd, *J* = 10.0, 2.4 Hz), 5.06 (1H, dd, *J* = 16.8, 2.0 Hz), 3.92–3.87 (1H, m), 1.94–1.88 (1H, m), 1.74–1.71 (3H, m), 1.66–1.60 (2H, m), 1.50–1.41 (2H, m), 1.31–1.20 (3H, m), 1.10 (3H, d, *J* = 6.0 Hz), 0.99–0.84 (1H, m);^{13}C NMR (100 MHz, $CDCl_3$): δ 137.1, 118.8, 66.8, 57.9, 37.9m, 31.4, 30.3, 26.7, 26.6, 26.5, 20.0; HRMS (DART): Calcd for $C_{11}H_{19}$ $[M+H–H_2O]^+$: 151.1487; Found: 151.1491; Specific rotation: $[\alpha]_D^{20}$ –9.83 (*c* 0.55, $CHCl_3$) for a >98% S_N2', 93:7 dr, and 91:9 er sample. Enantiomeric purity of **2.22** was determined by HPLC analysis of the product from *p*-bromobenzoylation[13] in comparison with authentic racemic material (91:9 er shown; chiralcel AD–H column, 99:1 hexanes:*i*PrOH, 0.3 mL/min, 254 nm).

[13] W. Rao, M. J. Koh, P. Kothandaraman, P. W. H. Chan, *J. Am. Chem. Soc*. **2012,** *134,* 10811–10814.

Enantiomeric purity of the major diastereomers

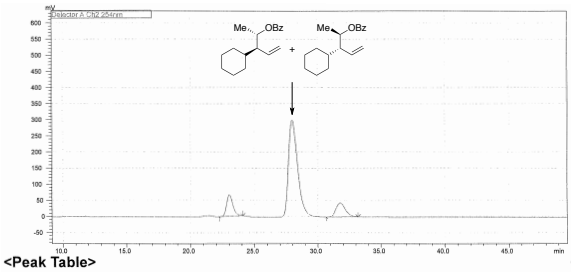

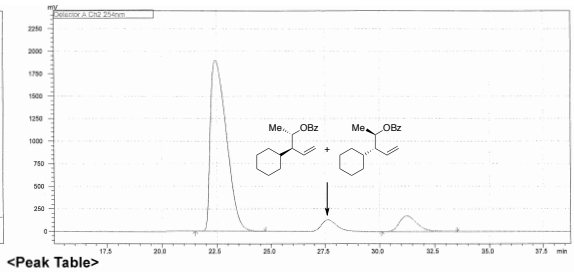

<Peak Table>

Detector A Channel 2 254nm

Peak#	Ret. Time	Area	Height	Conc.	Area%
1	23.031	2275091	65643	50.212	50.212
2	31.762	2255881	43492	49.788	49.788
Total		4530972	109135		100.000

<Peak Table>

Detector A Channel 2 254nm

Peak#	Ret. Time	Area	Height	Conc.	Area%
1	22.453	96662248	1899556	91.048	91.048
2	31.232	9503542	172352	8.952	8.952
Total		106165790	2071908		100.000

Peak #	Retention time	Area	Area %	Peak #	Retention time	Area	Area %
1	23.031	2275091	50.212	1	22.453	96662248	91.048
2	31.762	2255881	49.788	2	31.232	9503542	8.952

2.5.4 Gram Scale Reaction with (*E*)-But-2-en-1-yl diethyl phosphate

(2*S*,3*S*)-3-methylpent-4-en-2-ol (2.24): In a N_2-filled glove box, a flame-dried 100 mL round-bottom flask equipped with a stir bar was charged with CuCl (9.9 mg, 0.10 mmol), imidazolinium ligand (107.4 mg, 0.125 mmol), and LiO*t*Bu (600 mg, 7.50 mmol). The flask was sealed with a septum and electrical tape before removal from the glove box. Freshly distilled thf (10 mL) was added and the resulting solution was allowed to stir for 1 h under N_2 at 22 °C. A solution of PMHS (902.3 mg, 15.0 mmol) in thf (5 mL) was added to the mixture at 0 °C, causing the solution to turn yellow brown immediately. After 1 min, a solution of vinyl boronic acid pinacol ester (847mg, 5.50 mmol) and (*E*)-but-2-en-1-yl diethyl phosphate (1041 mg, 5.0 mmol) in thf (10 mL) was added by syringe. The resulting mixture was allowed to stir at 22 °C for 14 h after which the mixture was passed through a short plug of silica gel (4x4 cm, 1% of triethylamine) and eluted with Et_2O. Removal of the volatiles *in vacuo* afforded bright yellow oil. To the oil

was added thf (10 mL), pH 7.0 buffer solution (10 mL), and $NaBO_3 \bullet 4H_2O$ (3846 mg, 25.0 mmol) at 0 ºC. After complete addition, the mixture was allowed to stir at 22 ºC for 3 h. The mixture was washed with Et_2O (3 x 10 mL), and the combined organic layers were dried over $MgSO_4$. Carefully concentrated (product is volatile) mixture was purified by silica gel chromatography (hexanes:Et_2O = 10:5, R_f = 0.2) to afford the desired product as clear oil (275 mg, 2.746 mmol, 55% yield). Spectroscopic data match those reported previously.[40] ^{1}H NMR (400 MHz, $CDCl_3$): δ 5.83–5.74 (1H, m), 5.12–5.07 (2H, m), 3.73–3.64 (1H, m), 2.27–2.20 (1H, m), 1.50 (1H, br), 1.15 (3H, d, *J* = 6.4 Hz), 1.03 (3H, d, *J* = 6.8 Hz); Specific rotation: $[\alpha]_D^{20}$ –19.05 (c 4.43, $CHCl_3$) for a >98% S_N2', 92:8 dr, and 93:7 er sample. Based on reported optical rotation values $[\alpha]_D$ –35.2 (c 1.6, $CHCl_3$)[40] and $[\alpha]_D$ –19.56 (neat),[41] the absolute stereochemistry of the major enantiomer is assigned to be (2*S*,3*S*). The diastereoselectivity was determined by ^{1}H NMR spectra after *p*-methoxybenzylation of the alcohol.[42] ^{1}H NMR (400 MHz, $CDCl_3$): δ 7.27 (2H, d, *J* = 8.8 Hz), 6.87 (2H, d, *J* = 8.0 Hz), 5.82 (1H, ddd, *J* = 17.2, 10.0, 7.2 Hz), 5.05 (1H, d, *J* = 11.6 Hz), 5.01 (1H, d, *J* = 4.8 Hz), 4.52 (1H, d, *J* = 11.6 Hz), 4.40 (1H, d, *J* = 11.6 Hz), 3.80 (3H, s), 3.35 (1H, pent, *J* = 6.4 Hz), 2.41–2.33 (1H, m), 1.12 (3H, d, *J* = 6.4 Hz), 1.04 (3H, d, *J* = 7.2 Hz). Enantiomeric purity of **2.24** was determined by HPLC analysis of the corresponding *p*-methoxybenzyl ether[42] in comparison with authentic racemic material (93:7 er shown; chiralcel OJ–H column, 99:1 hexanes:*i*PrOH, 0.3 mL/min, 220 nm).

---

(40) Tannert, R.; Milroy, L.-G.; Ellinger, B.; Hu, T-S.; Arndt, H-D.; Waldmann, H. *J. Am. Chem. Soc.* **2010,** *132,* 3063–3077.
(41) Brown, H. C.; Bhat, K. S. *J. Am. Chem. Soc.* **1986,** *108,* 293–294.
(42) Eggert, U.; Diestel, R.; Sasse, F.; Jansen, R.; Kunze, B.; Kalesse, M. *Angew. Chem. Int. Ed.* **2008**, *47,* 6478–6482.

Enantiomeric purity of the major isomers

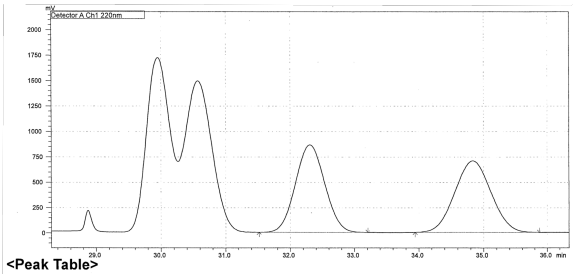

<Peak Table>

Detector A Channel 1 220nm

Peak#	Ret. Time	Area	Height	Conc.	Area%
1	32.306	27352504	861994	50.024	50.024
2	34.835	27326687	705214	49.976	49.976
Total		54679191	1567207		100.000

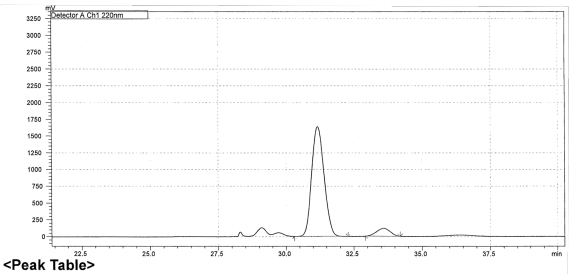

<Peak Table>

Detector A Channel 1 220nm

Peak#	Ret. Time	Area	Height	Conc.	Area%
1	31.169	52308708	1638017	92.774	92.774
2	33.586	4074216	117164	7.226	7.226
Total		56382924	1755181		100.000

Enantiomeric purity of the minor isomers

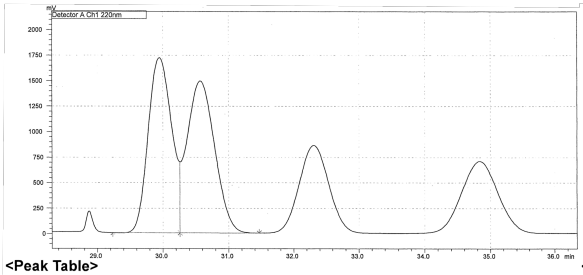

<Peak Table>

Detector A Channel 1 220nm

Peak#	Ret. Time	Area	Height	Conc.	Area%
1	29.948	42912130	1718245	49.685	49.685
2	30.569	43456870	1490743	50.315	50.315
Total		86368999	3208988		100.000

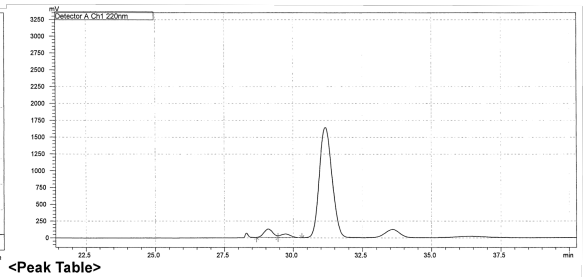

<Peak Table>

Detector A Channel 1 220nm

Peak#	Ret. Time	Area	Height	Conc.	Area%
1	29.090	2912130	126958	68.995	68.995
2	29.713	1308670	52532	31.005	31.005
Total		4220800	179490		100.000

Peak #	Retention time	Area	Area %	Peak #	Retention time	Area	Area %
1	32.306	27352504	50.024	1	31.169	52308798	92.774
2	34.835	27326687	49.976	2	33.586	4074216	7.226
1	29.948	42912130	49.685	1	29.090	2912130	68.995
2	30.569	43456870	50.315	2	29.713	1308670	31.005

2.5.5 C–B(pin) to C–furyl Conversion

2-((2*S*,3*S*)-3-Phenethylpent-4-en-2-yl)furan (2.30): The secondary boron compound

(0.35 mmol, precursor to alcohol **2.21**) was converted to **2.30** by a reported procedure[43] except 1.5 equiv. furan, 1.5 equiv. *n*-BuLi, and 1.5 equiv. NBS were used. IR (neat): 3026 (w), 2933 (w), 1640 (w), 1496 (m), 1454 (m), 1148 (m), 1117 (w), 1030 (s), 914 (s), 793 (m), 598 (m), 497 (m) cm^{-1}; ^{1}H NMR (400, MHz $CDCl_3$): δ 7.30–7.23 (3H, m), 7.18–7.16 (1H, m), 7.11 (2H, d, *J* = 7.6 Hz), 6.27 (1H, dd, *J* = 3.2, 2.0 Hz), 5.95 (1H, d, *J* = 2.8 Hz), 5.60 (1H, ddd, *J* = 16.8, 10.0, 9.2 Hz), 5.10 (1H, dd, *J* = 10.4, 2.0 Hz), 5.02–4.97 (2H, m), 2.81 (1H, pent, *J* = 6.8 Hz), 2.66 (1H, ddd, *J* = 13.6, 10.8, 5.2 Hz), 2.44 (1H, ddd, *J* = 14.0, 10.0, 6.4 Hz), 1.71–1.62 (1H, m), 1.51–1.44 (1H, m), 1.19 (3H, d, *J* = 6.8 Hz); ^{13}C NMR (100 MHz, $CDCl_3$): δ 159.3, 142.7, 140.7, 140.4, 128.5, 128.4, 125.7, 116.6, 110.0, 104.9, 48.7, 37.6, 34.1, 33.8, 16.4; HRMS $[M+H]^+$ Found for $C_{17}H_{21}O$: 241.1601; Specific rotation: $[\alpha]_D^{20}$ –2.31 (*c* 6.67, $CHCl_3$).

2.5.6 Assignment of Absolute Configuration of the Major Isomer from NHC-6

The absolute configuration of the major isomer from **NHC-6** was assigned by comparing the optical rotation of corresponding aldehyde **2.4-2** after homologation and oxidations.

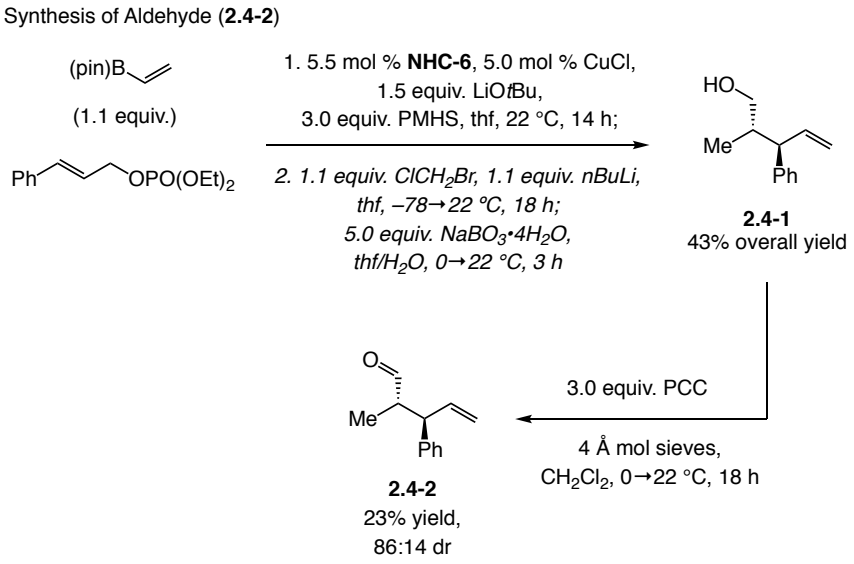

(43) Bonet, A.; Odachowski, M.; Leonori, D.; Essafi, S.; Aggarwal, V. K. *Nature Chem.* **2014,** *6,* 584–589.

2-Methyl-3-phenylpent-4-en-1-ol (2.4-1): The secondary boron compound was prepared from the representative procedure except **NHC-6** was used (0.3 mmol scale). After purification, the sample was homologated by the reported procedure[44] and oxidized to give the final product (43% overall yield after flash column chromatography). ^{1}H NMR data match those reported previously.[45] ^{1}H NMR (400, MHz $CDCl_3$): δ 7.32–7.17 (5H, m), 6.11–6.01 (1H, m), 5.14–5.04 (2H, m), 3.71–3.67 (1H, m), 3.60–3.56 (1H, m), 3.17 (1H, t, J = 9.6 Hz), 2.08–2.01 (1H, m), 1.51 (1H, br), 0.80 (3H, dd, J = 7.2, 1.2 Hz).

(2*S*,3*R*)-2-Methyl-3-phenylpent-4-enal (2.4-2): Prepared from **2.4-1** according to the reported procedure.[46] Spectroscopic data match those reported previously.[47] ^{1}H NMR (400, MHz $CDCl_3$): δ 9.71–9.69 (1H, m), 7.36–7.18 (5H, m), 6.08–5.98 (1H, m), 5.14–5.09 (2H, m), 3.53 (1H, t, J = 9.0 Hz), 2.83–2.75 (1H, m), 0.94–0.92 (3H, m); Specific rotation: $[\alpha]_D^{20}$ +22.79 (c 0.63, $CHCl_3$) for a >98% S_N2', 86:14 dr, and 87:13 er sample. Based on reported optical rotation values $[\alpha]_D^{26}$ +57.4 (c 1.0, $CHCl_3$),[47] the absolute stereochemistry of the major enantiomer is assigned to be (2*S*,3*R*).

2.5.7 Density Functional Theory (DFT)/ONIOM Calculations

(Please Note: In the following section, the term **imid-2** is synonymous with the term **NHC-6** used above, and the term **imid-3** is synonymous with the term **NHC-8** used above)

DFT/OMIOM computations[48] were performed with the Gaussian 09 suite of programs.[49]

---

(44) Ohmura, T.; Furukawa, H.; Suginome, M. *J. Am. Chem. Soc*. **2006,** *128,* 13366–13367.
(45) (a) Kwan, E. E.; Scheerer, J. R.; Evans, D. A. *J. Org. Chem.* **2013,** *78,* 175–203. (b) Kelly, B. D.; Allen, J. M.; Tundel, R. E.; Lambert, T. H. *Org. Lett.* **2009,** *11,* 1381–1383.
(46) Oh, C. H.; Hong, J. H. *Bull. Korean Chem. Soc.* **2005,** *26,* 1520–1524.
(47) Krautwald, S.; Schafroth, M. A.; Sarlah, D.; Carreira, E. M. *J. Am. Chem. Soc*. **2014,** *136,* 3020–3023.
(48) For reviews on the application of DFT calculations to transition metal chemistry see: (a) Cramer, C. J.; Truhlar, D. G. *Phys. Chem. Chem. Phys.* **2009,** *11,* 10757–10816. (b) Grimme, S.; Ehrlich, S.; Goerigk, L.

Geometries were optimized by the following ONIOM[50] method: M06L/Def2SVP:UFF (see Scheme S2 for definition of the boundaries; in cases where explicit thf molecules have been used in the simulations, only the oxygen atom has been modeled with the higher level). The effect of a polar reaction medium (tetrahydrofuran, THF) was approximated by means of an integral equation formalism variant of the polarizable continuum model (IEFPCM).[51] Stationary points were probed through vibrational analysis and Gibbs free energy corrections were performed under standard conditions (298.15 K, 1.0 atm). Intrinsic reaction coordinate (IRC) calculations have been performed starting from selected transition states (**ts**) employing the L(ocal) Q(uadratic) A(approximation) method, followed by subsequent optimization to obtain structures and energies for educt (**ed**) and product (**prod**) on either side of the transition state.[52] We furthermore probed the performance of various density functionals through single point energy calculations at the geometries optimized at the level described above by means of the SMD solvation model[53] with THF as solvent and the larger Def2TZVPP[54] basis set.

J. Comp. Chem. **2011,** *32,* 1456–1465. (c) Peverati, R.; Truhalr, D. G. *Phil. Trans. R. Soc.* **2014,** *A* 372:20120476.

(49) Frisch, M. J.; Trucks, G. W.; Schlegel, H. B.; Scuseria, G. E.; Robb, M. A.; Cheeseman, J. R.; Scalmani, G.; Barone, V.; Mennucci, B.; Petersson, G. A.; Nakatsuji, H.; Caricato, M.; Li, X.; Hratchian, H. P.; Izmaylov, A. F.; Bloino, J.; Zheng, G.; Sonnenberg, J. L.; Hada, M.; Ehara, M.; Toyota, K.; Fukuda, R.; Hasegawa, J.; Ishida, M.; Nakajima, T.; Honda, Y.; Kitao, O.; Nakai, H.; Vreven, T.; Montgomery Jr., J. A.; Peralta, J. E.; Ogliaro, F.; Bearpark, M.; Heyd, J. J.; Brothers, E.; Kudin, K. N.; Staroverov, V. N.; Kobayashi, R.; Normand, J.; Raghavachari, K.; Rendell, A.; Burant, J. C.; Iyengar, S. S.; Tomasi, J.; Cossi, M.; Rega, N.; Millam, J. M.; Klene, M.; Knox, J. E.; Cross, J. B.; Bakken, V.; Adamo, C.; Jaramillo, J.; Gomperts, R.; Stratmann, R. E.; Yazyev, O.; Austin, A. J.; Cammi, R.; Pomelli, C.; Ochterski, J. W.; Martin, R. L.; Morokuma, K.; Zakrzewski, V. G.; Voth, G. A.; Salvador, P.; Dannenberg, J. J.; Dapprich, S.; Daniels, A. D.; Farkas, Ö.; Foresman, J. B.; Ortiz, J. V.; Cioslowski, J.; Fox, D. J. *Gaussian 09, Revision **D.01**,* Gaussian, Inc., Wallingford CT, **2009**.

(50) Chung, L. W.; Sameera, W. M. C.; Ramozzi, R.; Page, A. J.; Hatanaka, M.; Petrova, G. P.; Harris, T. V.; Li, X.; Ke, Z.; Liu, F.; Li, H.-B.; Ding, L.; Morokuma, K. *Chem. Rev.* **2015,** *115,* 5678–5769.

(51) Scalmani, G.; Frisch, M. J. *Chem. Phys.* **2010***, 132,* 114110.

(52) (a) Page, M.; McIver Jr., J. W. *Phys.* **1988,** *88,* 922–935. (b) Page, M.; Doubleday Jr., C.; McIver Jr., J. W. *J. Chem. Phys.* **1990,** *93,* 5634–5642.

(53) Marenich, A. V.; Cramer, C. J.; Truhlar, D. G. *J. Phys. Chem. B.* **2009,** *113,* 6378–6396.

(54) Weigend, F.; Ahlrichs, R. *Phys. Chem. Chem. Phys.* **2005**, *7*, 3297–3305.

Since the correct density functional is not known we tested several state of the art approaches that have been developed over the past decade:[48, 55] ωB97XD,[56] M06,[57] MN12SX,[58] MN12L,[58] M06L,[57] BP86-D3BJ[48b,59] and PBE0-D3BJ[48b,60] (Figures S1–S9). Electronic and Gibbs free energies for Figures S4–S9 are provided on pages S53 to S76 in the original paper and the entries that have been used to construct Figures S1–S3 are highlighted with grey background. A file for convenient viewing of computed geometries with the program Mercury 3.3 is appended as separate "coordinates.xyz" file on pages S77 to S330 in the original paper.[61]

---

(55) For selected examples highlighting the importance of including treatment of dispersion interactions in modeling olefin metathesis reactions promoted by Ru carbene complexes see: (a) Torker, S.; Merki, D.; Chen, P. *J. Am. Chem. Soc.* **2008,** *130,* 4808–4814. (b) Minenkov, Y.; Occhipinti, G.; Singstad, A.; Jensen, V. R. *Dalton Trans.* **2012.** 41, 5526–5541. (c) Minenkov, Y.; Occhipinti, G.; Jensen, V. R. *Organometallics* **2013,** *32,* 2099–2111. (d) Torker, S.; Khan, R. K. M.; Hoveyda, A. H. *J. Am. Chem. Soc.* **2014,** *136,* 3439–3455. (e) Khan, R. K. M.; Torker, S.; Hoveyda, A. H. *J. Am. Chem. Soc.* **2014,** *136,* 14337–14340. (f) Torker, S.; Koh, M. J.; Khan, R. K. M.; Hoveyda, A. H. *Organometallics,* **2016,** *35,* 543–562. (g) Mikus, M. S.; Torker, S.; Hoveyda, A. H. *Angew. Chem., Int. Ed.* **2016,** *55,* 4997–5002; For modeling allyl addition to CF3-ketones see. (h) Lee, K.-A.; Silverio, D. L.; Torker, S.; Robbins, D. W.; Haeffner, F.; Hoveyda, A. H. *Nat. Chem.* **2016,** *8,* 768–777.

(56) Chai, J.-D.; Head-Gordon, M. *Phys. Chem. Chem. Phys.* **2008**, *10*, 6615–6620.

(57) Zhao, Y.; Truhlar, D. G. *Acc. Chem. Res.* **2008,** *41,* 157–167.

(58) Peverati, R.; Truhlar, D. G. *Phys. Chem. Chem. Phys.* **2012***, 14,* 16187–16191.

(59) (a) Becke, A. D. *Phys. Rev. A: At., Mol., Opt. Phys.* **1988,** *38,* 3098–3100. (b) Perdew, J. P.; Yue, W. *Phys. Rev. B* **1986,** *33,* 8800–8802

(60) Adamo, C.; Barone, V. *J. Chem. Phys.* **1999,** *110,* 6158–6169.

(61) Lichtenberger, D. L.; J. A. Gladysz, *Organometallics,* **2014,** *33,* 835−835. The "coordinates.xyz" file can be generated by copying all the coordinates on pages S77–S330 in the original paper (Lee, J,; Torker, S.; Hoveyda, A. H. *Angew. Chem., Int. Ed.* **2017,** *56,* 821–826.) into a text file without empty lines and changing the extension to ".xyz".

Scheme S1. ONIOM boundaries used in the simulations (two layers)

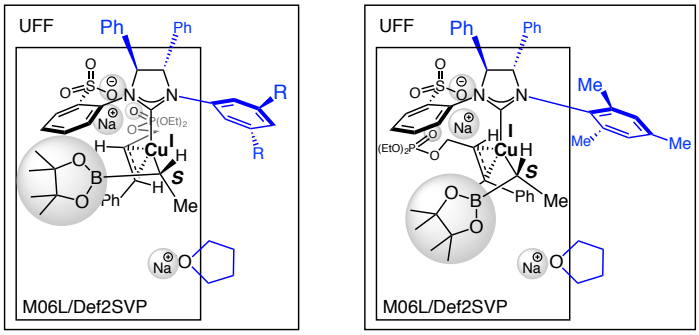

major product with ligand derived from **imid-3**

R = 2,6-(*i*-Pr)$_2$-C$_6$H$_3$

major product with ligand derived from **imid-2**

Nomenclature

The following modes for Cu-H addition with ligands derived from **imid-3** and **imid-2** have been investigated (Scheme S2). Modes **S1** and **S2** lead to the *S*-configuration at the carbon center that is directly bound to Cu after Cu-H addition, whereas modes **R1** and **R2** will generate the carbon stereogenic center with *R*-configuration. In modes **S1** and **R1** one of the oxygen atoms on the Bpin moiety, which is situated in the rear, is coordinated to the sodium counterion that is bound to the ligand's sulfonate group. In contrast, the Bpin group is facing towards the front in modes of addition **S2** and **R2**. The modes for Cu-H addition shown in Scheme 2a have further been reinvestigated with either two or three explicit thf molecules bound to the metal center in order to test the stability of the O^{Bpin}→Na coordination in presence of a coordinating solvent (tetrahydrofuran). See below for a detailed discussion.

Scheme S2. Investigated modes of Cu-H addition with ligands derived from **imid-3** (a) and **imid-2** (b)

a Cu-H addition with **imid-3**

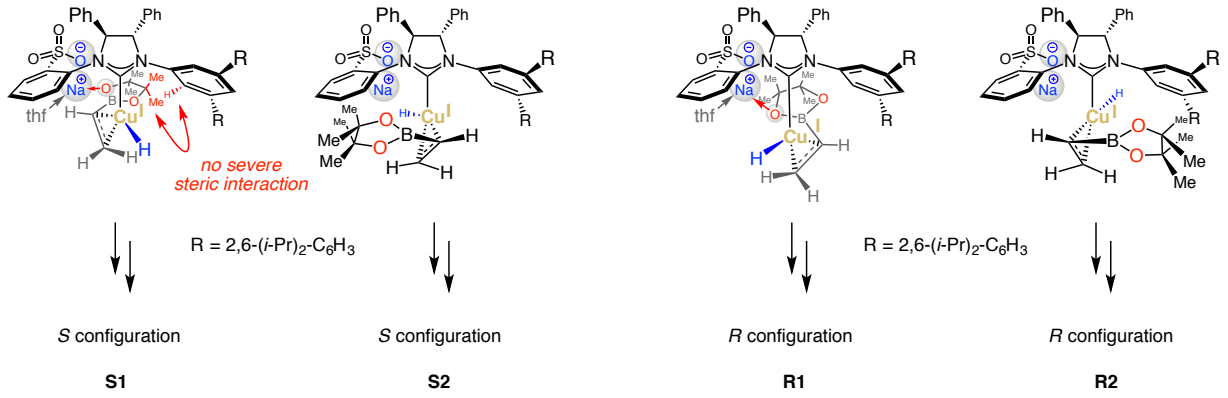

b Cu-H addition with **imid-2**

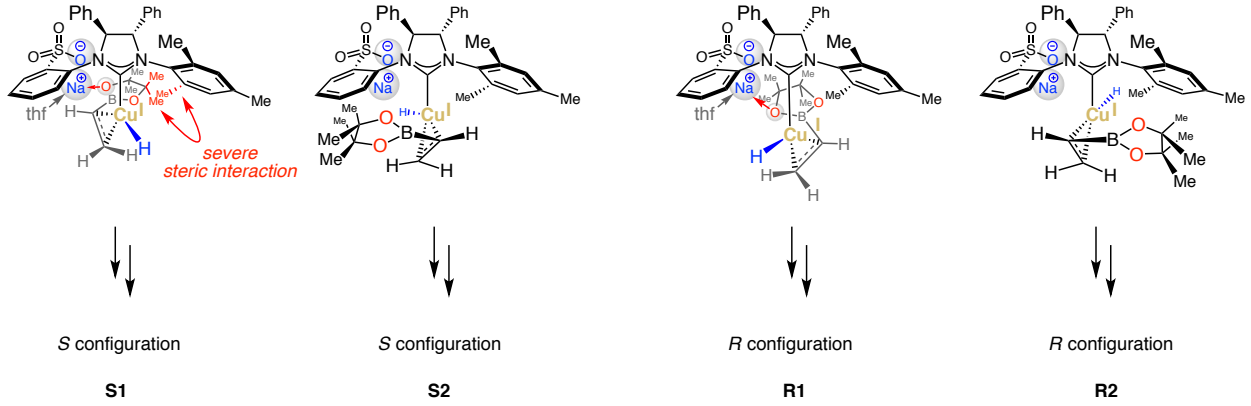

Additionally, all investigated modes for allylic substitution with ligands derived from **imid-3** and **imid-2** are displayed in Scheme S3. Here, **A** and **B** denote the pathways leading to the two enantiomers of the first diastereomer, whereas nomenclature **C** and **D** is used for the two enantiomers of the opposite diastereomer. Mode of allylic substitution **A** leads to the major product when the NHC ligand derived from **imid-3** is involved (Scheme S3c). Furthermore, mode **C** yields the major product when the reaction is performed with **imid-2** and mode **B** leads to the major enantiomer of the minor diastereomer under the same conditions (Scheme S3d).

Scheme S3. Investigated modes of allylic substitution (AS) with ligands derived from **imid-3** (c) and **imid-2** (d)

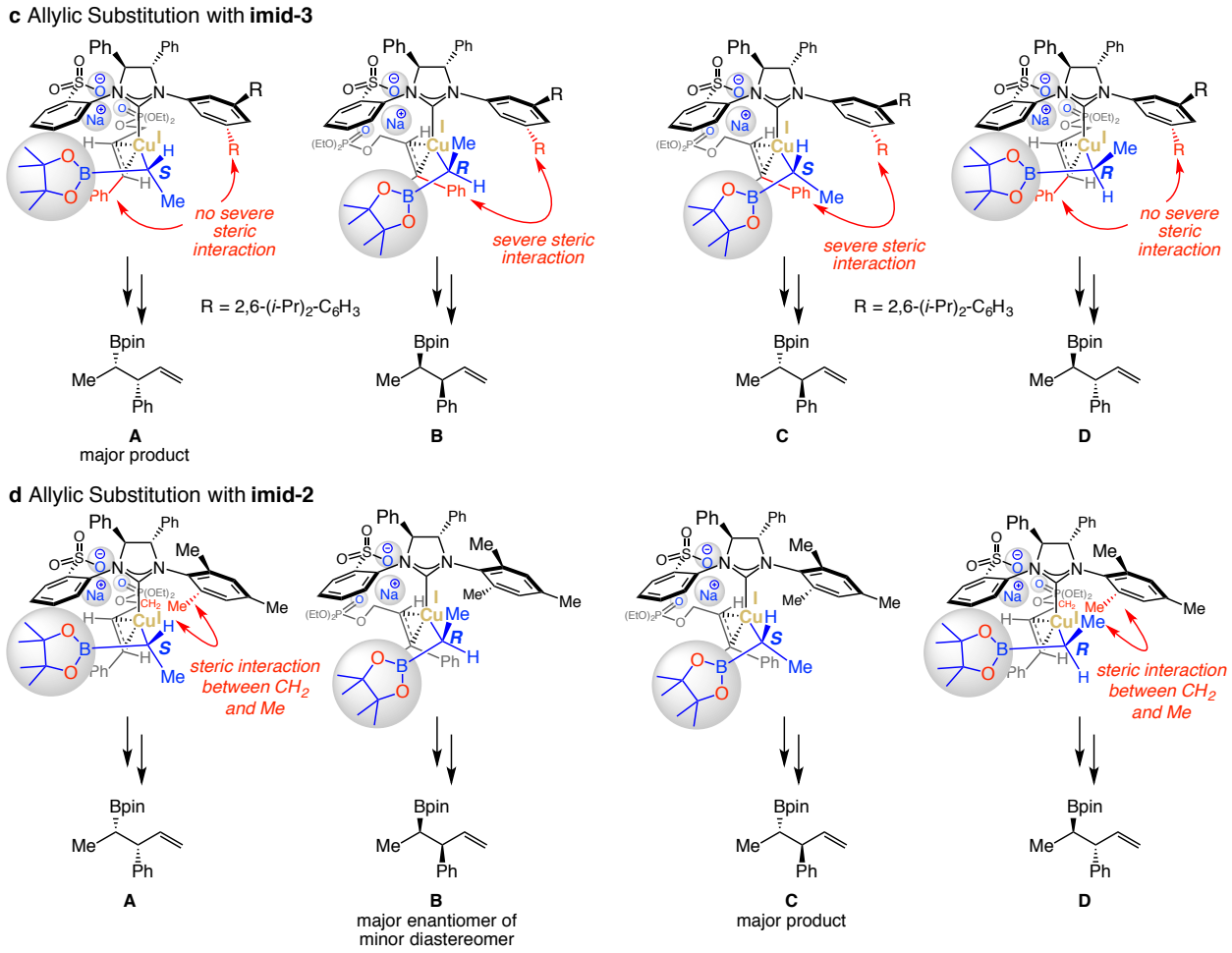

Stereochemical model with Cu–NHC complex derived from imid-3 (cf. Figure S1-1)

The pathways leading to the major (**A**) and minor enantiomer (**B**) of the major diastereomer at the MN12SX/Def2TZVPP$_{THF(SMD)}$//M06L/Def2SVP:UFF$_{THF}$ level are shown in Figure S1-1. For the corresponding free energy diagrams with other density functional, see Figure S1-2. For a complete picture containing all possible modes for Cu-H addition and allylic substitution (including investigation of several conformers), see Figures S4-1 and S7-1 or Figures S4-2 and S7-2, respectively. As seen in Figure S1-1,

mode of Cu-H addition **S1** (9.6 kcal/mol relative to the Cu-H species), wherein a coordination between the Bpin moiety and the Na counterion is established, is significantly more favored compared to the mode of addition **R2**, which leads to the opposite stereochemistry (*R*-configuration) while a O^{Bpin}→Na interaction is absent (20.0 kcal/mol). Such a large energy difference (10.4 kcal/mol) should preclude generation of even trace amounts of products that originate from the *R*-configured Cu-alkyl species and suggests that this model system represents a rather simplified version of the true mechanism (see below for further discussion of models with explicit thf molecules). Following Cu-H addition, the major product (**A**) is generated through the allylic substitution transition state to generate a π-allyl species (with a relative free energy of 6.5 kcal/mol).[62] In agreement with the experimental results Cu-H addition is likely irreversible as supported by the lower energy for allylic substitution (6.5 kcal/mol; Figure S1-1) compared to the transition state for Cu-H addition (9.6 kcal/mol; Figure S1-1). Further in agreement with the experimental results are the higher calculated free energies for allylic substitution that lead to minor products **B**, **C** and **D** (8.5–9.1 kcal/mol; cf. Figures S1-1 and S7-1). The herein proposed model for AS with the NHC ligand derived form **imid-3** supports a previous model for nucleophilic addition of propargyl groups to allyl electrophiles, and we refer here to this earlier work for a much more detailed mechanistic discussion.[63],[64]

---

(62) For general mechanistic considerations regarding nucleophilic reaction promoted by Cu(I) species see: Yoshikai, N.; Nakamura, E. *Chem. Rev.* **2012,** *112,* 2339–2372.

(63) Shi, Y.; Jung, B.; Torker, S.; Hoveyda, A. H. *J. Am. Chem. Soc.* **2015,** *137,* 8948–8964.

(64) For additional stereochemical models regarding 1,4- or 1,6-additions to enoates or dienoates that also suggest the involvement of an intramolecular coordination of the substrate to a metal counterion see: (a) Meng, F.; Li, X.; Torker, S.; Shi, Y.; Shen, X.; Hoveyda, A. H. *Nature,* **2016,** *537,* 387–393. (b) Li, X.; Meng, F.; Torker, S.; Shi, Y.; Hoveyda, A. H. *Angew. Chem., Int. Ed.* **2016,** *55,* 9997–10002.

Stereochemical model with Cu–NHC complex derived from imid-2 (cf. Figure S2-1)

The most critical pathways leading to the major product (**C**) and the major enantiomer of the minor diastereomer (**B**) at the MN12SX/Def2TZVPP$_{THF(SMD)}$//M06L/Def2SVP:UFF$_{THF}$ level are shown in Figure S2-1. For the corresponding free energy diagrams with other density functional, see Figure S2-2. For a complete picture containing all possible modes for Cu-H addition and allylic substitution (including investigation of several conformers), see Figures S8-1 and S9-1 or Figures S8-2 and S9-2, respectively. As seen in Figure S2-1, and similar to the reaction promoted by the NHC ligand derived from **imid-3**, mode of Cu-H addition **S1** (8.6 kcal/mol relative to the Cu-H species), wherein the a coordination between the Bpin moiety and the Na counterion is established, is significantly more favored compared to the mode of addition **R2**, which leads to the opposite stereochemistry (*R*-configuration), while a O^{Bpin}→Na interaction is absent (17.9 kcal/mol). Again, such a large energy difference (9.3 kcal/mol) should preclude generation of even trace amounts of products that originate from the *R*-configured Cu-alkyl species, which contradicts the experimental observation that significant amounts of allylic substitution product **B** are isolated. Nonetheless, the energy difference between modes of addition **S1** and **R2** (9.3 kcal/mol) is slightly smaller than in the case when imid-3 is involved (10.4 kcal/mol). This likely originates from a significant steric interaction between the Bpin moiety and the ortho methyl group on the mesityl group of the NHC (mode **S1** in Scheme S2b). Following Cu-H addition, the major product (**C**) is generated through allylic substitution transition state with a relative free energy of 1.5 kcal/mol (Figure S2-1). In agreement with the previous case (cf. Figure S1-1) as well as the experimental results, Cu-H addition is likely

irreversible as supported by the lower energy for allylic substitution (1.5 kcal/mol) compared to Cu-H addition (8.6 kcal/mol). Further in agreement with the experimental results are the higher calculated free energies for AS that lead to minor products **A**, **B** and **D** (4.4–6.7 kcal/mol; cf. Figures S2-1 and S9-1). The herein proposed model for AS with the NHC ligand derived from imid-2 supports a previous model for nucleophilic addition of vinyl groups to allyl electrophiles, and we refer here to this earlier work for a much more detailed mechanistic discussion.[63,64]

The effect of a coordinating reaction medium (thf) on the stability of intramolecular chelate interactions (cf. Figure S3-1)

Modeling reactions that involve charged species including counterions, etc. can be quite challenging and the use of solvation models such as PCM or SMD will face certain limitations. For example, relying solely on a continuum model will underestimate the distances between the metal center and the heteroatoms that are included in the simulation. The O^{Bpin}→Na distance in mode of addition **S1** without explicit thf molecules is 2.30 Å, whereas the same distance elongates to 2.59 Å when 3 thf molecules are added. Furthermore, one of the largest sources of error relates to the loss entropy that occurs when thf molecules are being bound to the Na counterion. The estimated gas phase corrections to the free energy (ΔG_{corr} ~15 kcal/mol which corresponds to dilute conditions at 1 atm or 0.05 M) will certainly be significantly overestimated for solvent molecules (as discussed below, 5–9 kcal/mol instead of 15 kcal/mol for ΔG_{corr} will be more realistic). It is also very unlikely that the simplified model without thf molecules is a true representation of the actual experiment since it precludes formation of products that arise from the *R*-configured Cu-alkyl species. To address the above issues, we have performed

the following additional calculations depicted in Figure S3-1. There, mode of addition **S1** with 0, 2 and 3 thf molecules is compared to mode of addition **R2** with also 0, 2 and 3 thf molecules. The top grey curve uses gas phase entropies for thf molecules, which renders binding of thf unfavorable. Additionally, we have included scenarios wherein the gas phase free energy correction per thf molecule (~15 kcal/mol) is overestimated by 4, 6 and 8 kcal/mol, respectively (black, blue and green curves). The same analysis has been performed with all other investigated functionals (cf. Figure S3-2). For the inclusion of 2 or 3 thf molecules in all other modes of Cu-H addition (**S2** and **R1**), see Figures S5 and S6, respectively.

The following analysis should severe as guidance to Figure S3-1: The gas phase free energies for Cu-H addition mode **S1** with 2 thf molecules and mode **R2** with 3 thf molecules are 18.9 and 33.9 kcal/mol, respectively (Figure S3-1). This corresponds to a difference of 15.0 kcal/mol. This means that in order to significantly disrupt the O^{Bpin}→Na interaction (i.e., favoring path **R2** with 3 thf molecules), the gas phase correction to the free energy has to be overestimated by more than 15 kcal/mol, otherwise binding of a third thf molecule will be entropically disfavored. In order to allow for some formation of the *R*-configured Cu-alkyl species through pathway **R2**, the gas phase entropy likely has to be overestimated by about 12 kcal/mol with functional MN12SX and to a lesser degree with functionals ωB97XD (ca. 8 kcal/mol), M06 (ca. 8 kcal/mol) or MN12L (ca. 6 kcal/mol). In other words: applying an overestimation of 12 kcal/mol per thf molecule to mode **S1** with 2 thf molecules leads to a free energy of –5.1 kcal/mol (= 18.9 – 2 x 12.0; cf. Figure S3-1). The same procedure applied to mode **R2** with 3 thf molecules yields a free energy of –2.1 kcal/mol (33.9 – 3 x 12.0; cf. Figure S3-1). Only

under these conditions, generation of the *R*-configured Cu-alkyl species can become competitive (ΔΔG between modes **S1** and **R2** will be close to 3 kcal/mol or below; = –2.1 – (–5.1) kcal/mol). Please note that the free energies after removal of the overestimated portion of the entropy are actually not negative, since additional thf molecules have not been included in the ground state Cu-H species, which would also experience a lowering in energy.

Figures of Free Energy Surfaces

Free Energy Surface for Cu-H Addition/Allylic Substitution with ligand derived from imid-3

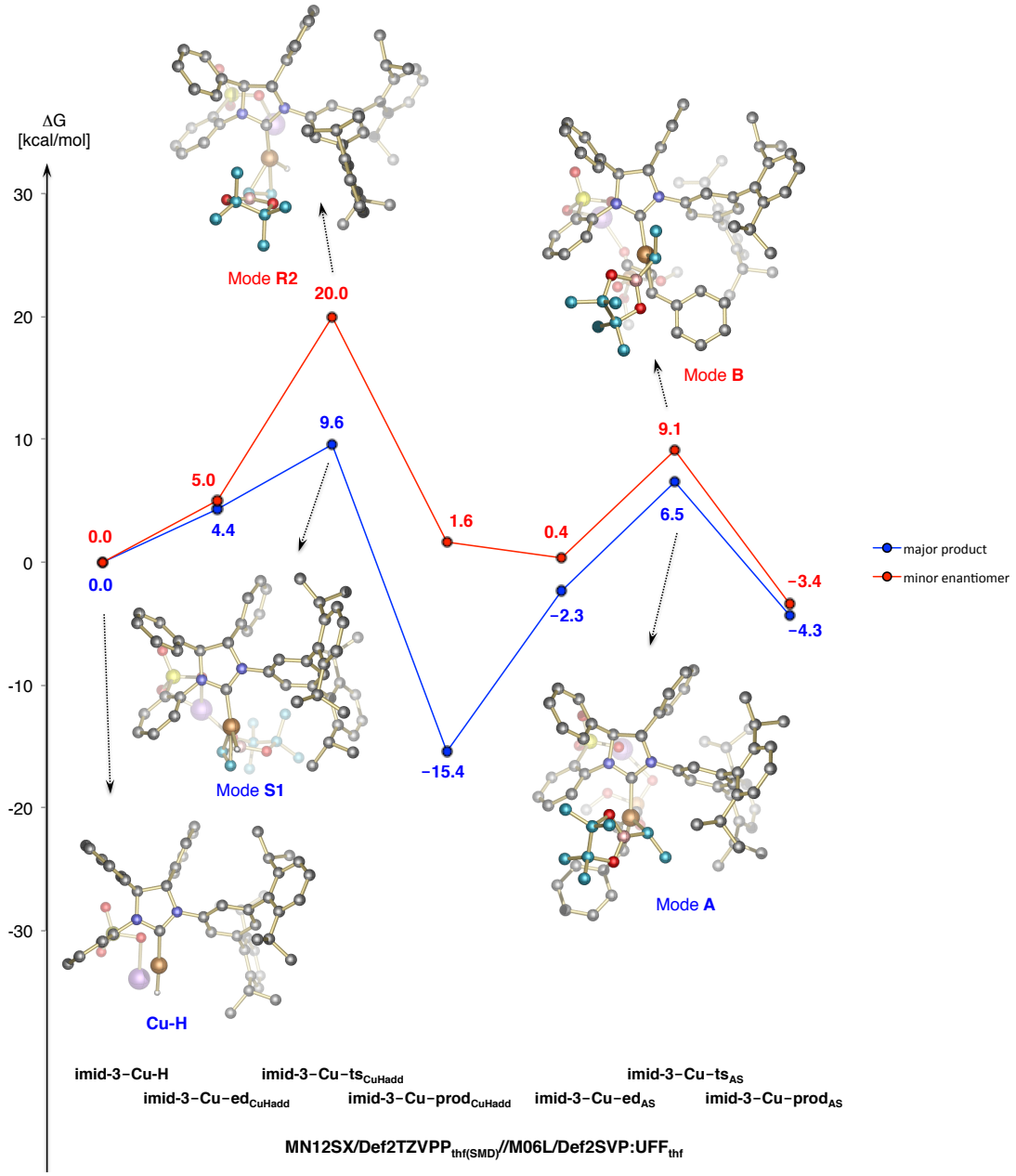

Figure S1-1. Free energy surfaces for Cu-H addition (CuHadd) and allylic substitution (AS) with NHC ligand derived from **imid-3** at the MN12SX/DefTZVPP$_{THF(SMD)}$//M06L/Def2SVP:UFF$_{THF}$ level (only lowest conformers for most critical pathways shown). For all other pathways including several conformers, see Figures S4-1 and S7-1.

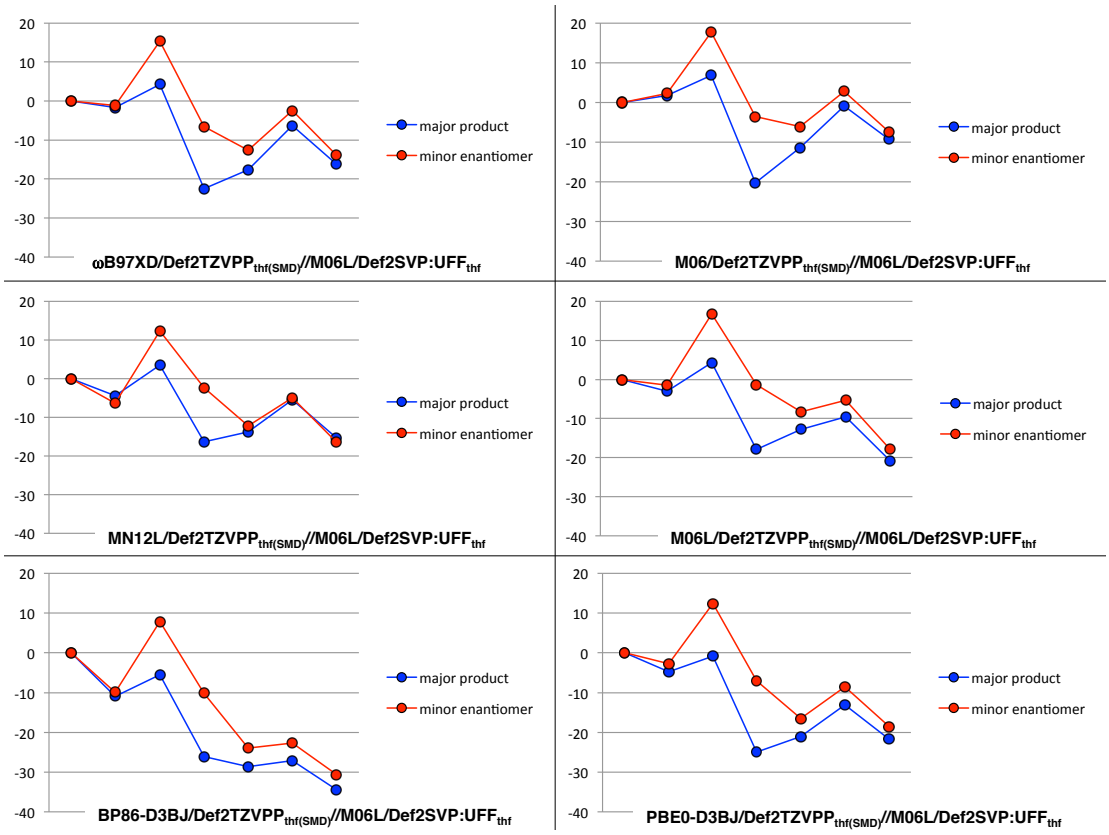

Figure S1-2. Free energy surfaces for Cu-H addition (CuHadd) and allylic substitution (AS) with NHC ligand derived from **imid-3** with various density functionals after optimization with M06L/Def2SVP:UFF$_{THF}$ (only lowest conformers for most critical pathways shown; cf. Figure S1-1). For all other pathways including several conformers, see Figures S4-2 and S7-2.

Free Energy Surface for Cu-H Addition/Allylic Substitution with ligand derived from imid-2

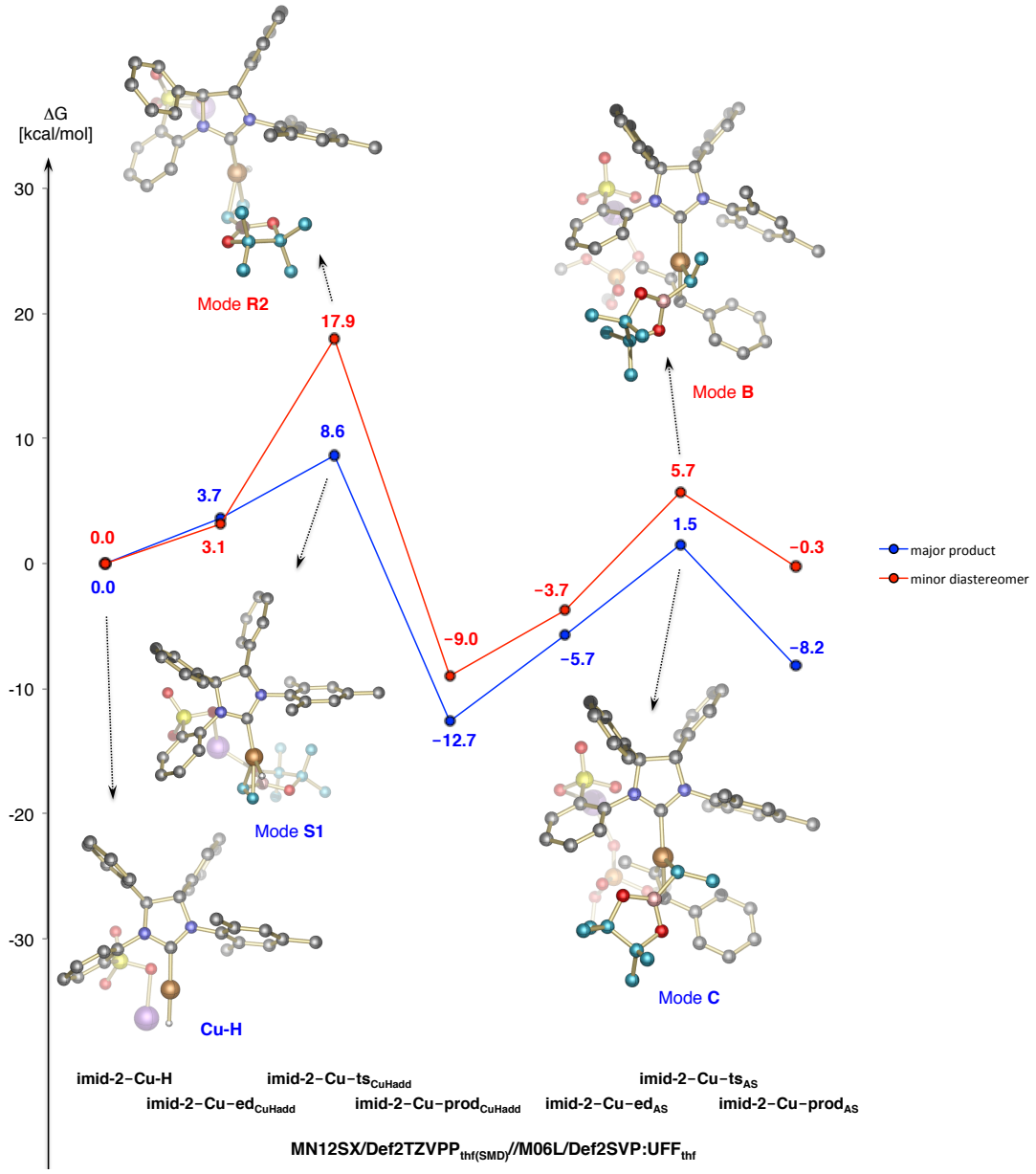

Figure S2-1. Free energy surfaces for Cu-H addition (CuHadd) and allylic substitution (AS) with NHC ligand derived from **imid-2** at the MN12SX/DefTZVPP$_{THF(SMD)}$//M06L/Def2SVP:UFF$_{THF}$ level (only lowest conformers for most critical pathways shown). For all other pathways including several conformers, see Figures S8-1 and S9-1.

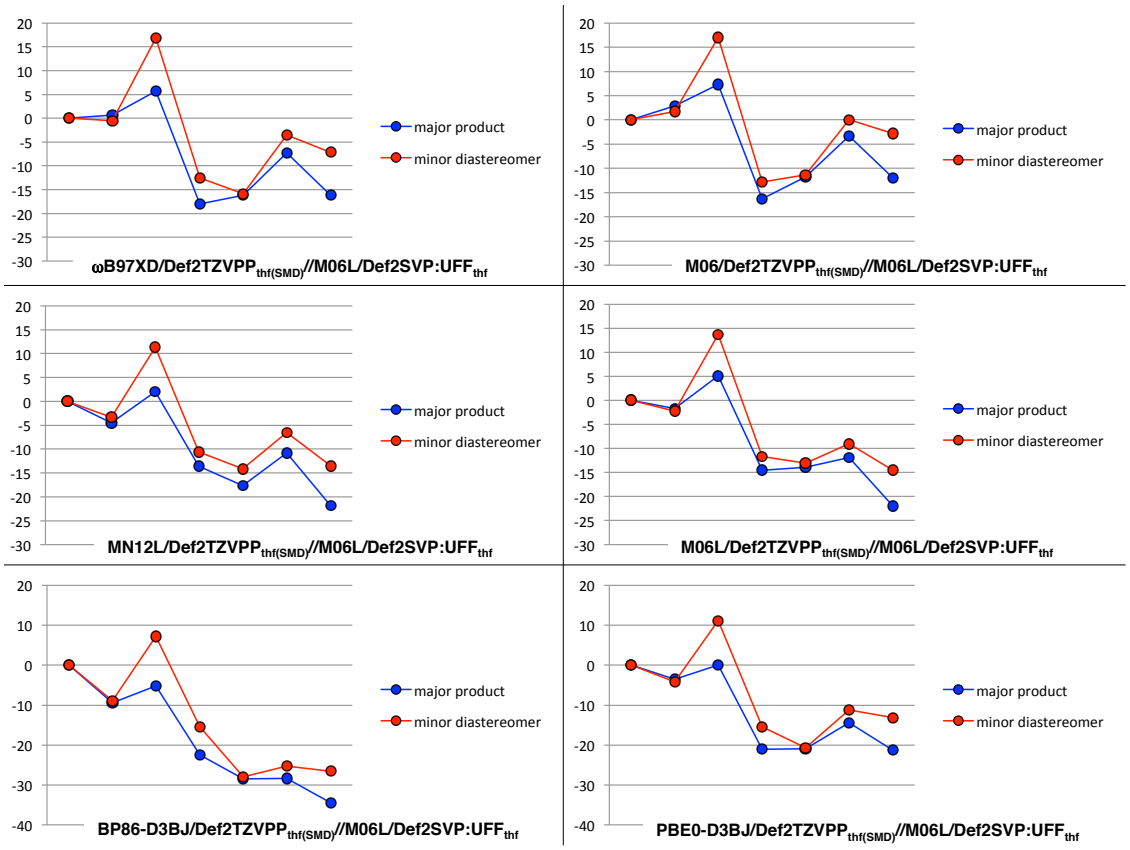

Figure S2-2. Free energy surfaces for Cu-H addition (CuHadd) and allylic substitution (AS) with NHC ligand derived from **imid-2** with various density functionals after optimization with M06L/Def2SVP:UFF$_{THF}$ (only lowest conformers for most critical pathways shown; cf. Figure S2-1). For all other pathways including several conformers, see Figures S8-2 and S9-2.

Detailed Investigation of the O^{Bpin}→Metal Coordination

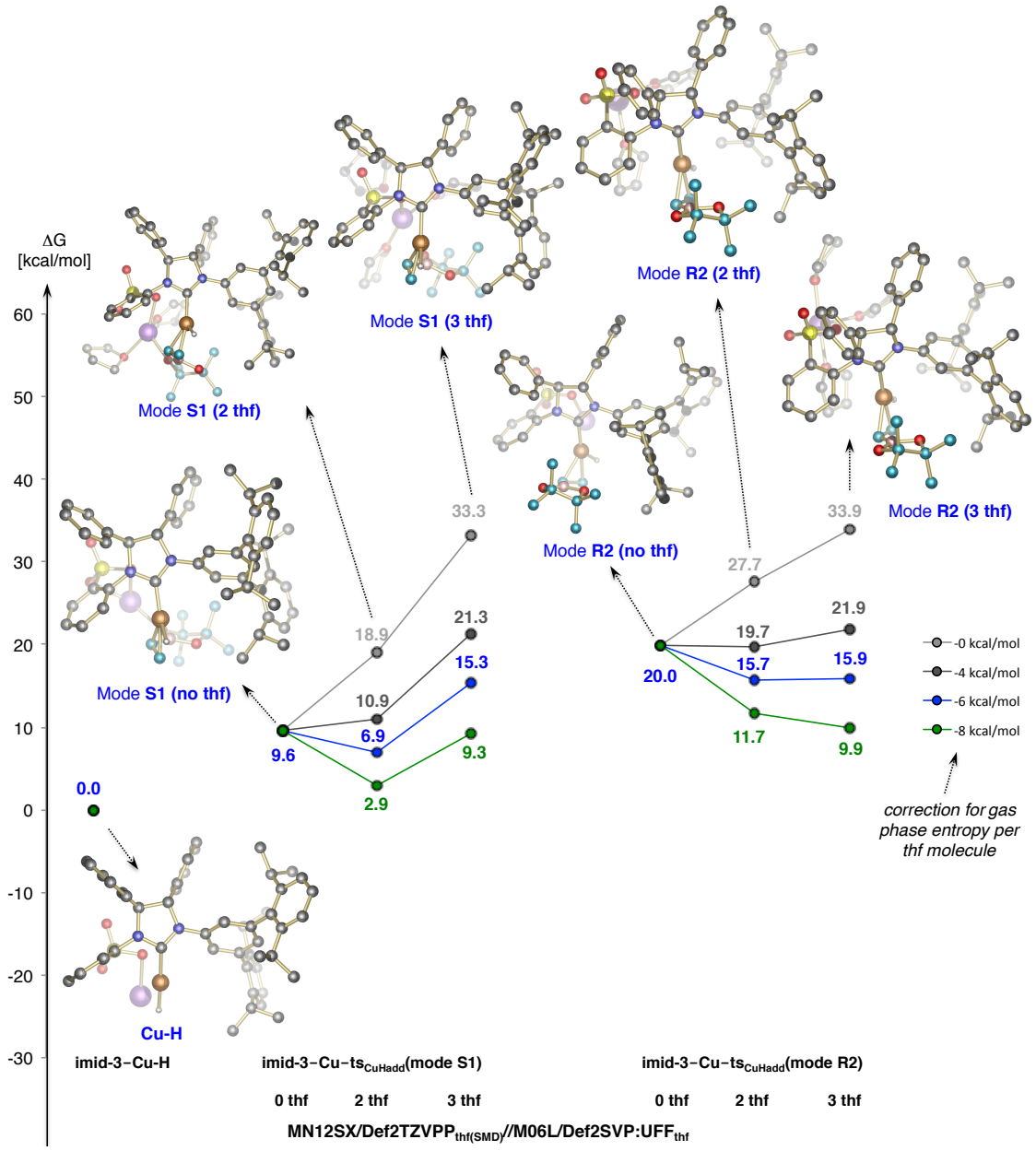

Figure S3-1. Free energies for Cu-H addition (CuHadd) with NHC ligand derived from **imid-3** at the MN12SX/DefTZVPP$_{THF(SMD)}$//M06L/Def2SVP:UFF$_{THF}$ level with varying number of thf molcules coordinated to the Na counterion (only lowest conformers for pathways **S1** and **R2** shown). For all other pathways including several conformers, see Figures S4-1, S5-1 and S6-1.

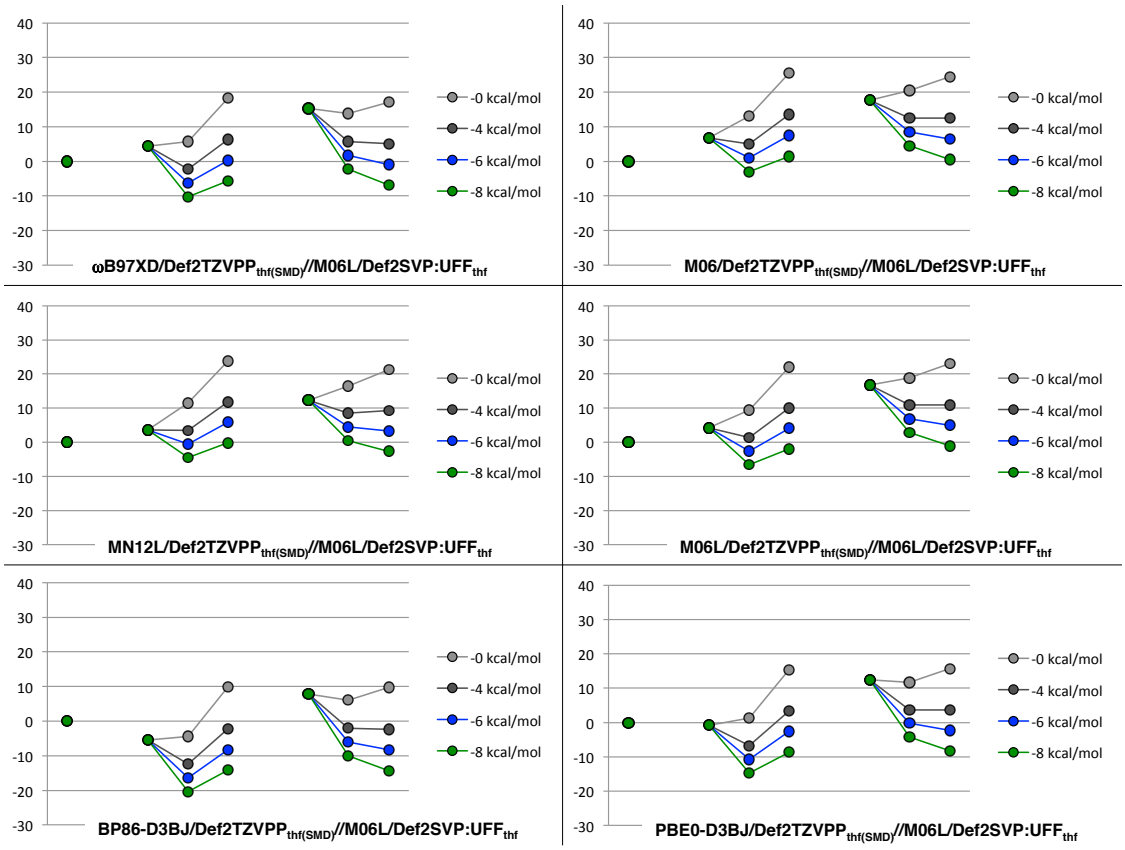

Figure S3-2. Free energies for Cu-H addition (CuHadd) with NHC ligand derived from **imid-3** with various density functionals after optimization with M06L/Def2SVP:UFF$_{THF}$ with varying number of thf molcules coordinated to the Na counterion (only lowest conformers for pathways **S1** and **R2** shown; cf. Figure S3-1). For all other pathways including several conformers, see Figures S4-2, S5-2 and S6-2.

Several Pathways and Conformers for Cu-H Addition (model without explicit thf molecules) with ligand derived from imid-3

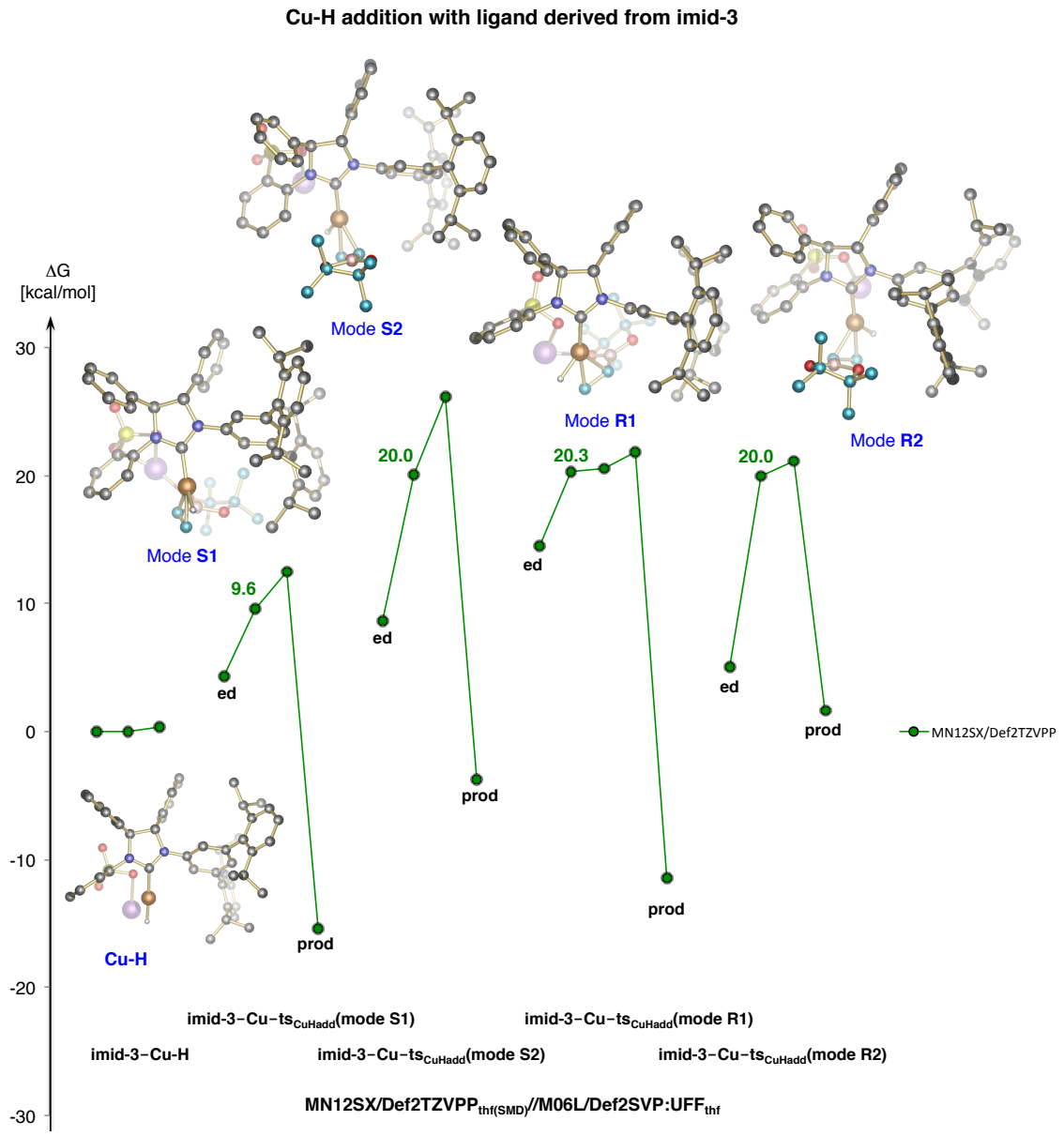

Figure S4-1. Free energy surfaces for Cu-H addition (CuHadd) with NHC ligand derived from **imid-3** at the MN12SX/DefTZVPP$_{THF(SMD)}$//M06L/Def2SVP:UFF$_{THF}$ level (all pathways **S1**, **S2**, **R1** and **R2** shown, including one **ed** and **prod** for each mode of addition).

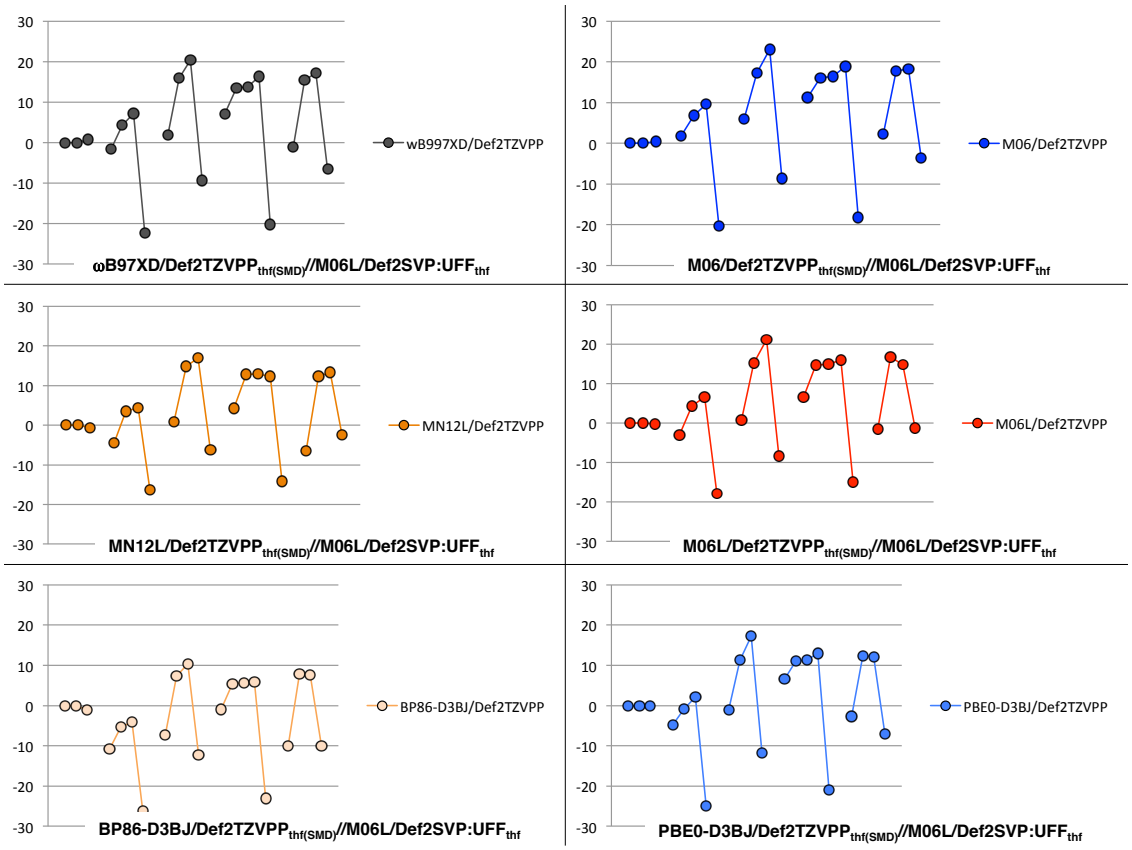

Figure S4-2. Free energy surfaces for Cu-H addition (CuHadd) with NHC ligand derived from **imid-3** with various density functionals after optimization with M06L/Def2SVP:UFF$_{THF}$ (all pathways **S1**, **S2**, **R1** and **R2** shown, including one **ed** and **prod** for each mode of addition; cf. Figure S4-1).

Several Pathways and Conformers for Cu-H Addition (model with 2 explicit thf molecules) with ligand derived from imid-3

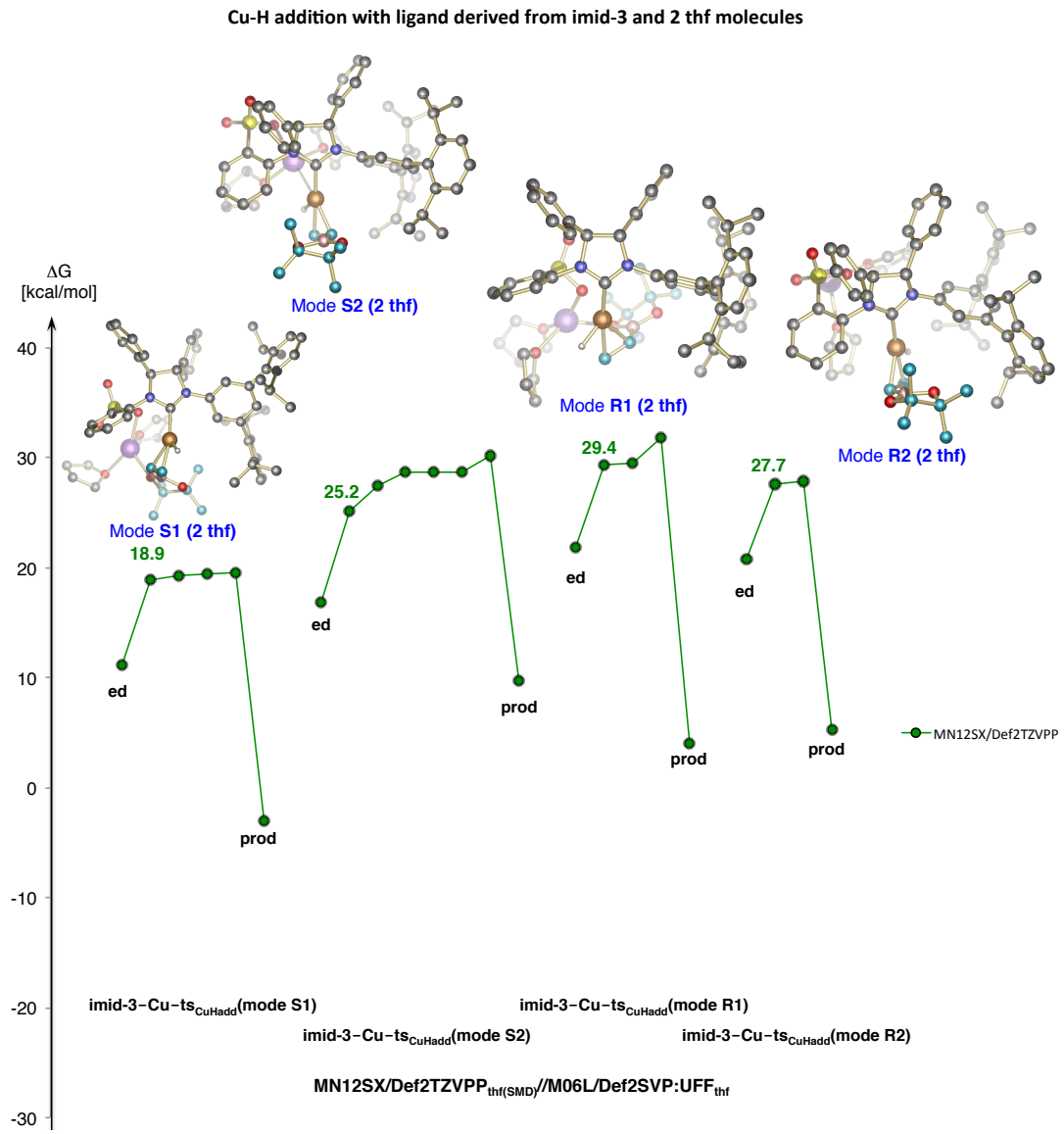

Figure S5-1. Free energy surfaces for Cu-H addition (CuHadd) with NHC ligand derived from **imid-3** with two explicit thf molecules coordinated to the Na counterion at the MN12SX/DefTZVPP$_{THF(SMD)}$//M06L/ Def2SVP:UFF$_{THF}$ level (all pathways **S1**, **S2**, **R1** and **R2** shown, including one **ed** and **prod** for each mode of addition).

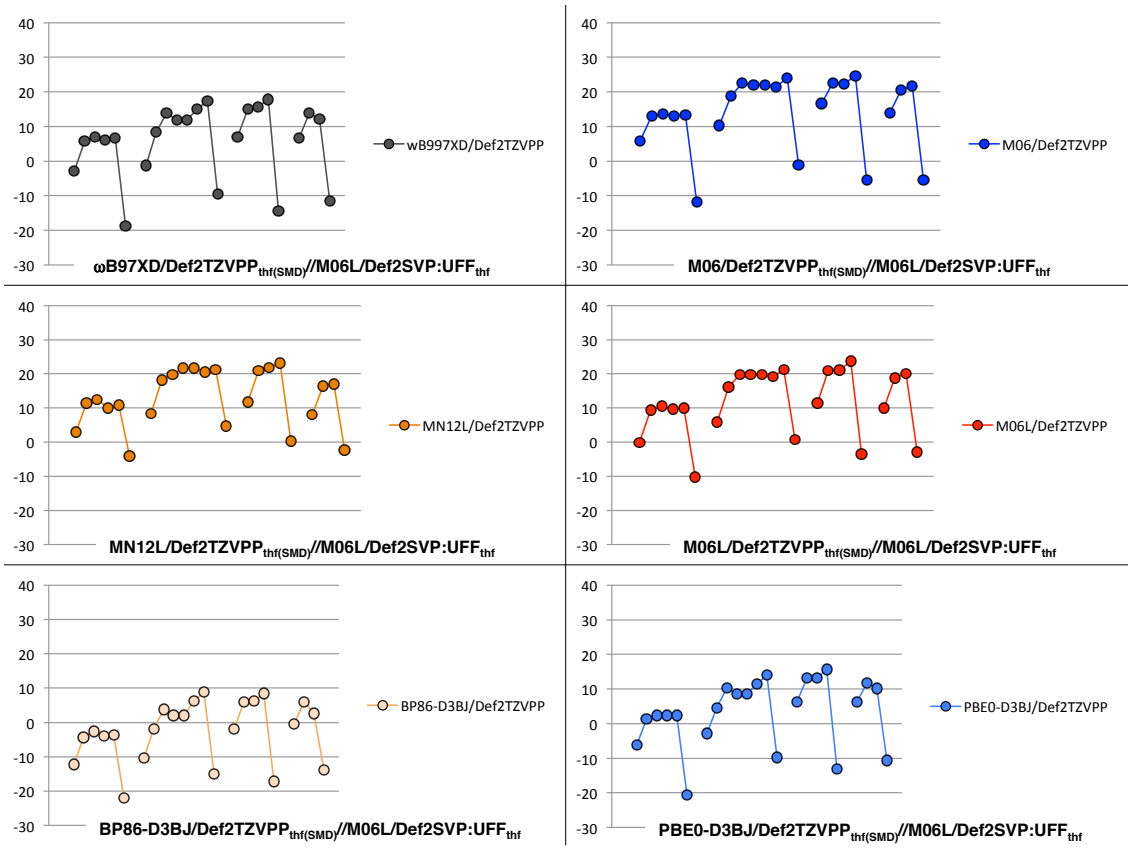

Figure S5-2. Free energy surfaces for Cu-H addition (CuHadd) with NHC ligand derived from **imid-3** with two explicit thf molecules coordinated to the Na counterion with various density functionals after optimization with M06L/Def2SVP:UFF$_{THF}$ (all pathways **S1**, **S2**, **R1** and **R2** shown, including one **ed** and **prod** for each mode of addition; cf. Figure S5-1).

Several Pathways and Conformers for Cu-H Addition (model with 3 explicit thf molecules) with ligand derived from imid-3

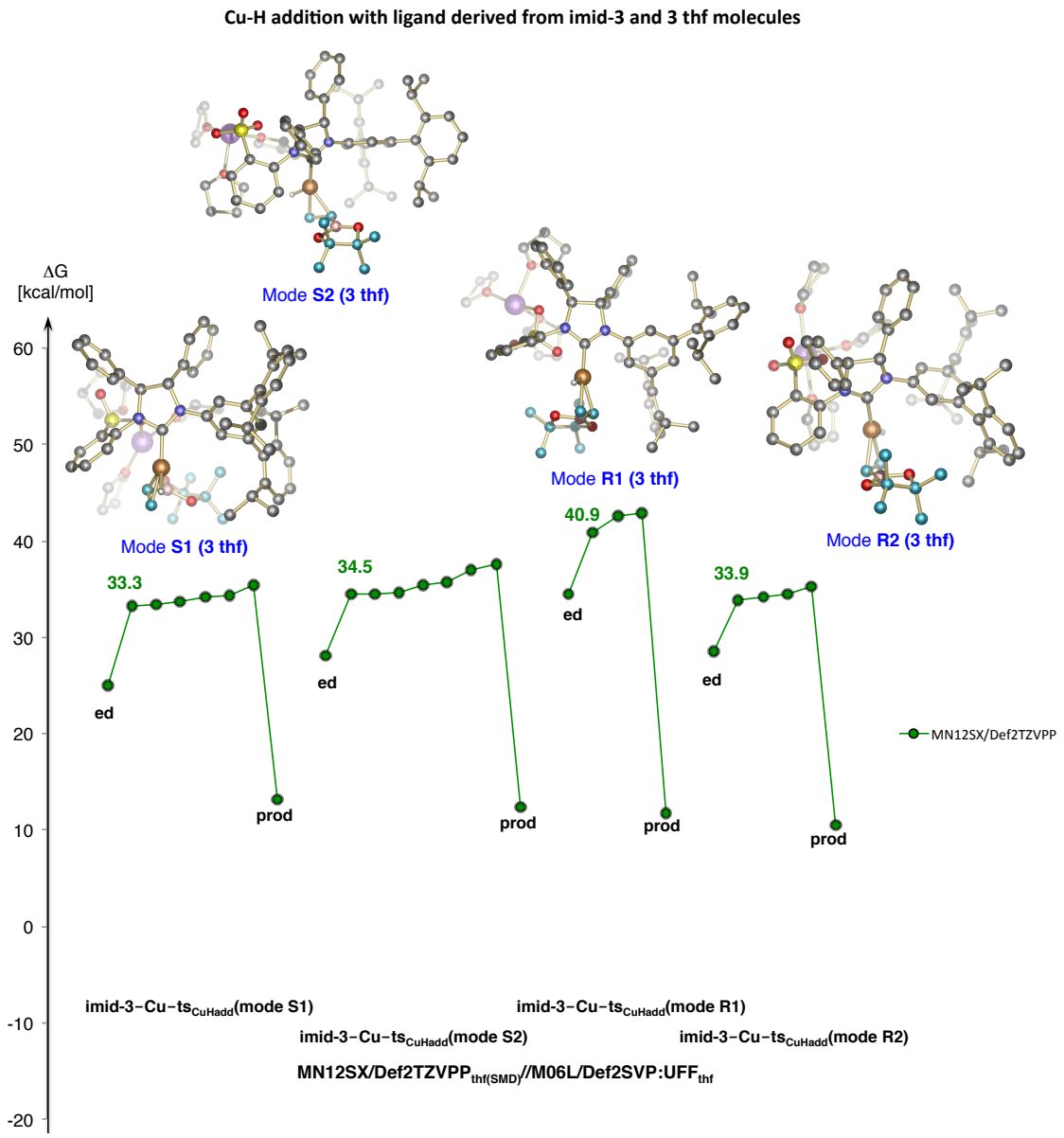

Figure S6-1. Free energy surfaces for Cu-H addition (CuHadd) with NHC ligand derived from **imid-3** with three explicit thf molecules coordinated to the Na counterion at the MN12SX/DefTZVPP$_{THF(SMD)}$//M06L/ Def2SVP:UFF$_{THF}$ level (all pathways **S1**, **S2**, **R1** and **R2** shown, including one **ed** and **prod** for each mode of addition).

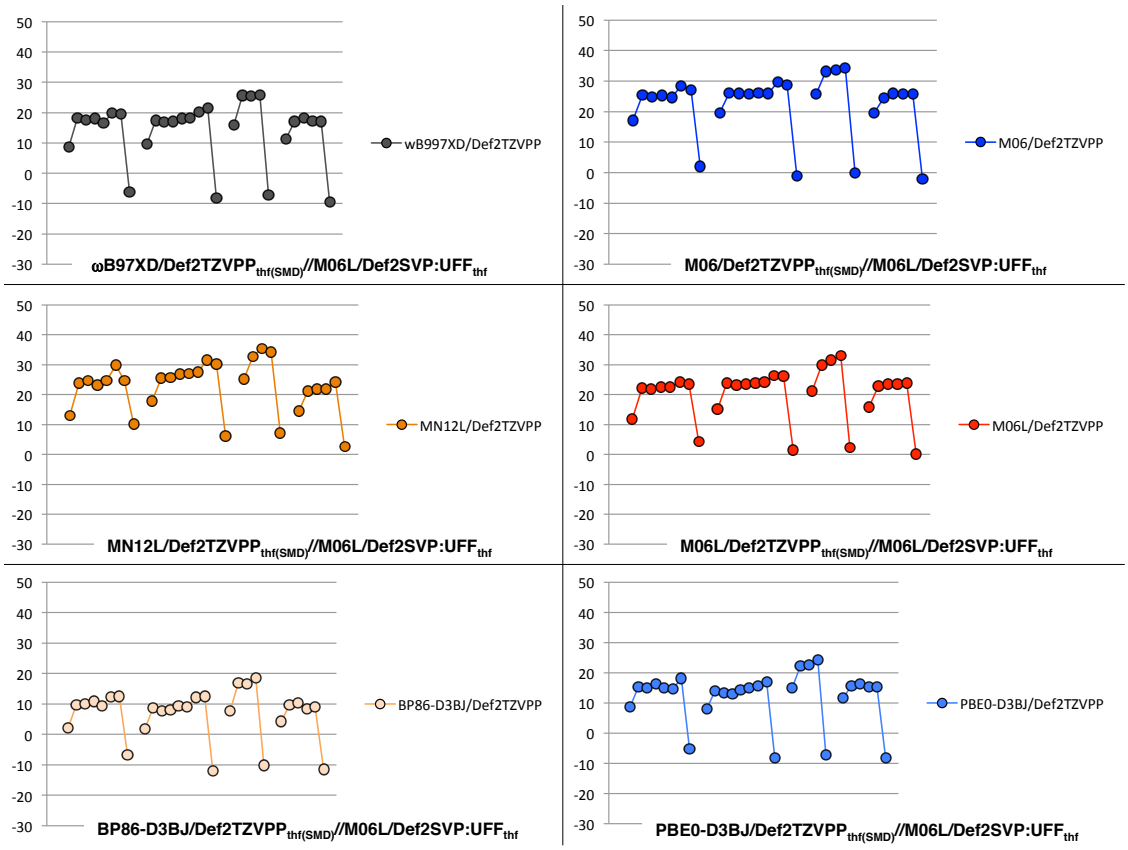

Figure S6-2. Free energy surfaces for Cu-H addition (CuHadd) with NHC ligand derived from **imid-3** with three explicit thf molecules coordinated to the Na counterion with various density functionals after optimization with M06L/Def2SVP:UFF$_{THF}$ (all pathways **S1**, **S2**, **R1** and **R2** shown, including one **ed** and **prod** for each mode of addition; cf. Figure S6-1).

Several Pathways and Conformers for Allylic Substitution with ligand derived from imid-3

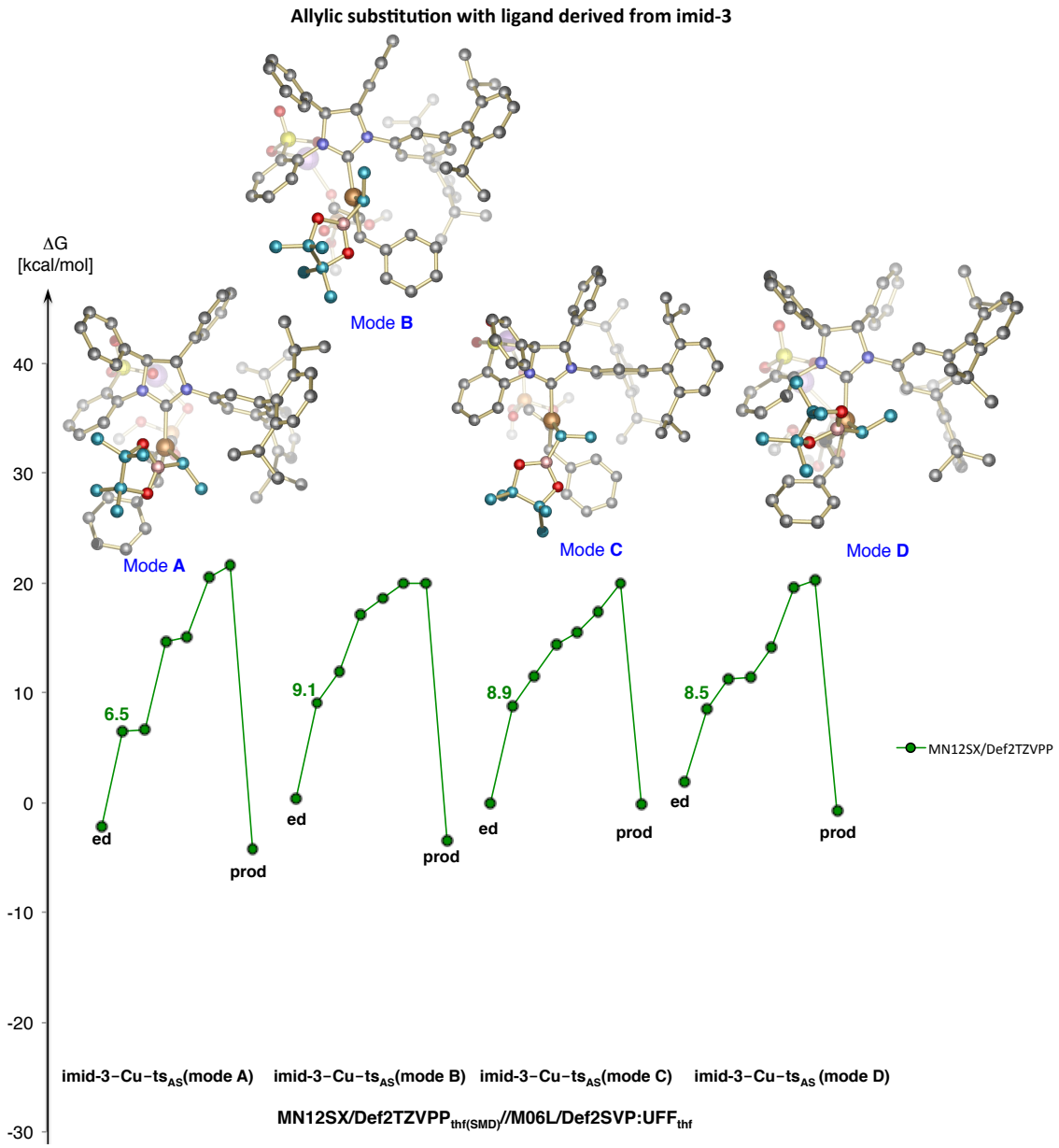

Figure S7-1. Free energy surfaces for allylic substitution (AS) with NHC ligand derived from **imid-3** at the MN12SX/DefTZVPP$_{THF(SMD)}$//M06L/Def2SVP:UFF$_{THF}$ level (all pathways **A**, **B**, **C** and **D** shown, including one **ed** and **prod** for each mode of addition).

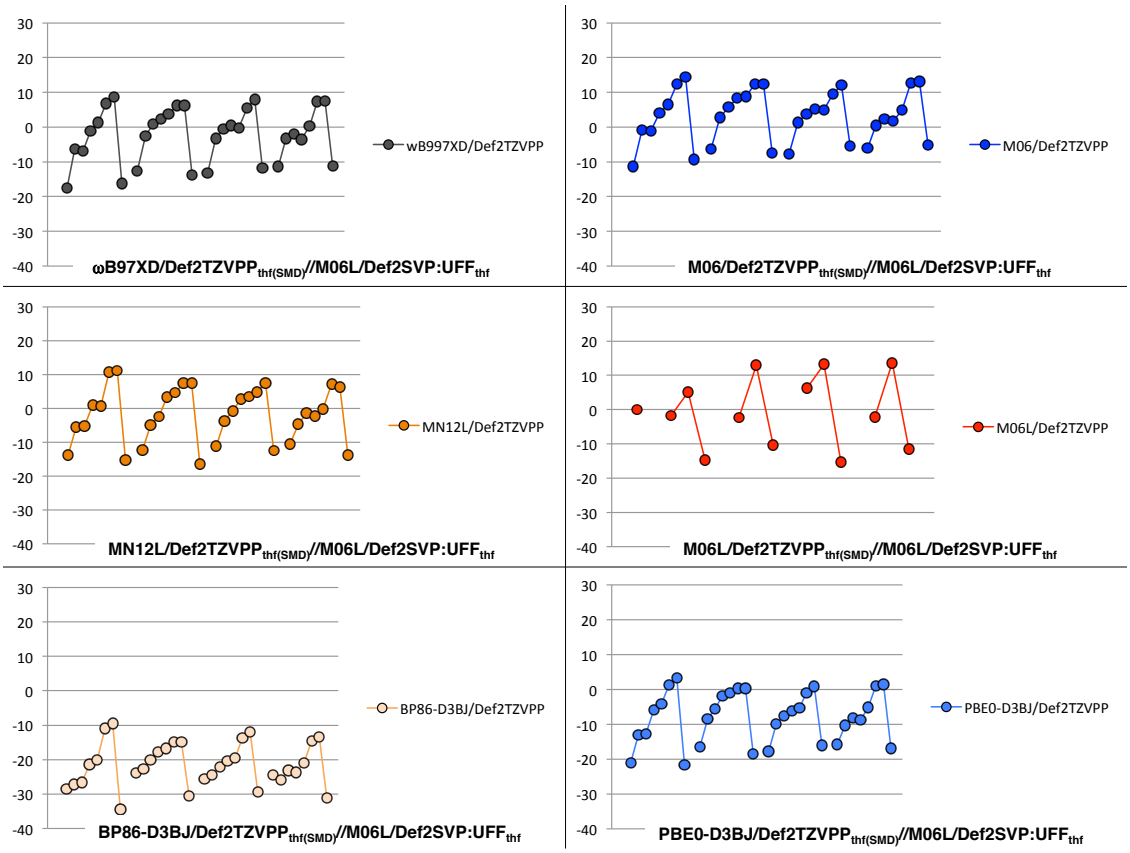

Figure S7-2. Free energy surfaces for allylic substitution (AS) with NHC ligand derived from **imid-3** with various density functionals after optimization with M06L/Def2SVP:UFF$_{THF}$ (all pathways **A**, **B**, **C** and **D** shown, including one **ed** and **prod** for each mode of addition; cf. Figure S7-1).

Several Pathways and Conformers for Cu-H Addition (model without explicit thf molecules) with ligand derived from imid-2

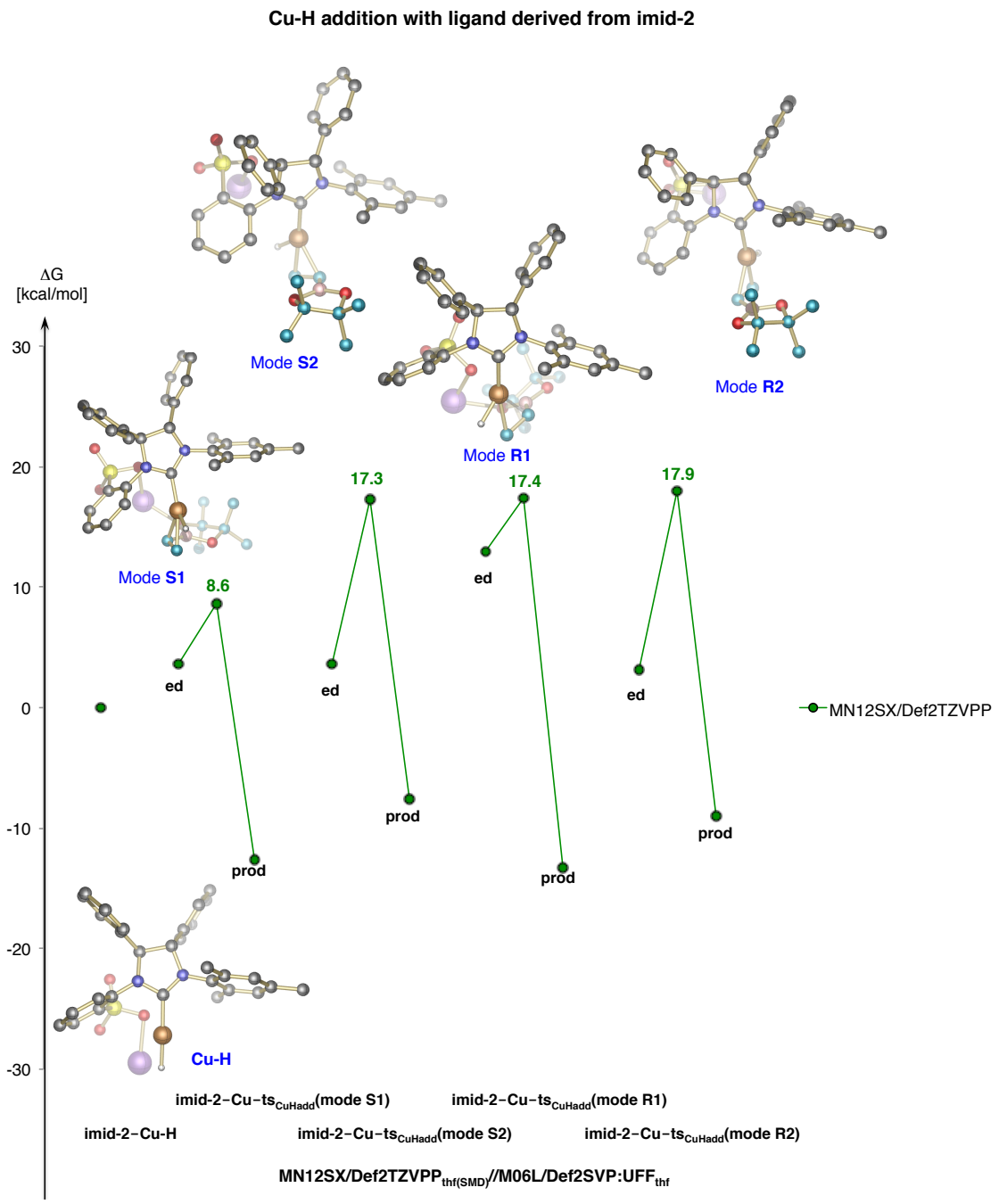

Figure S8-1. Free energy surfaces for Cu-H addition (CuHadd) with NHC ligand derived from **imid-2** at the MN12SX/DefTZVPP$_{THF(SMD)}$//M06L/Def2SVP:UFF$_{THF}$ level (all pathways **S1**, **S2**, **R1** and **R2** shown, including one **ed** and **prod** for each mode of addition).

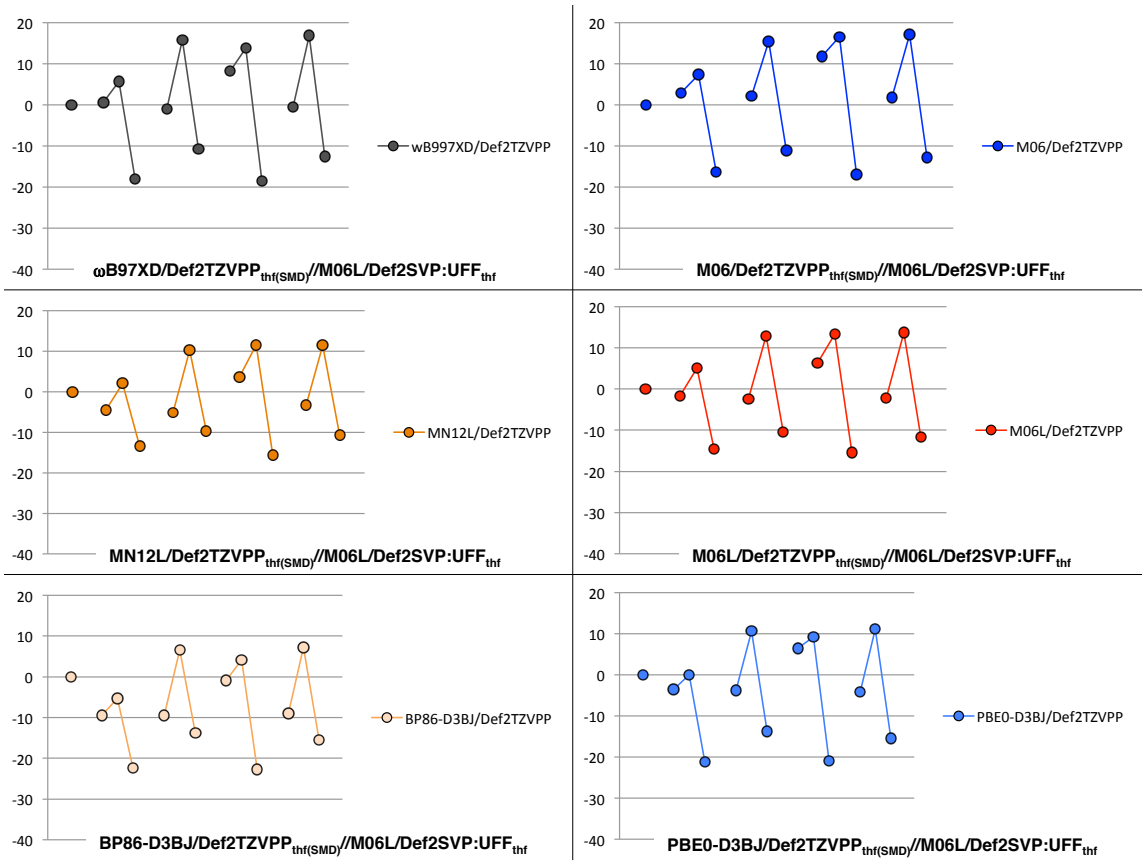

Figure S8-2. Free energy surfaces for Cu-H addition (CuHadd) with NHC ligand derived from **imid-2** with various density functionals after optimization with M06L/Def2SVP:UFF$_{THF}$ (all pathways **S1**, **S2**, **R1** and **R2** shown, including one **ed** and **prod** for each mode of addition; cf. Figure S8-1).

Several Pathways and Conformers for Allylic Substitution with ligand derived from imid-2

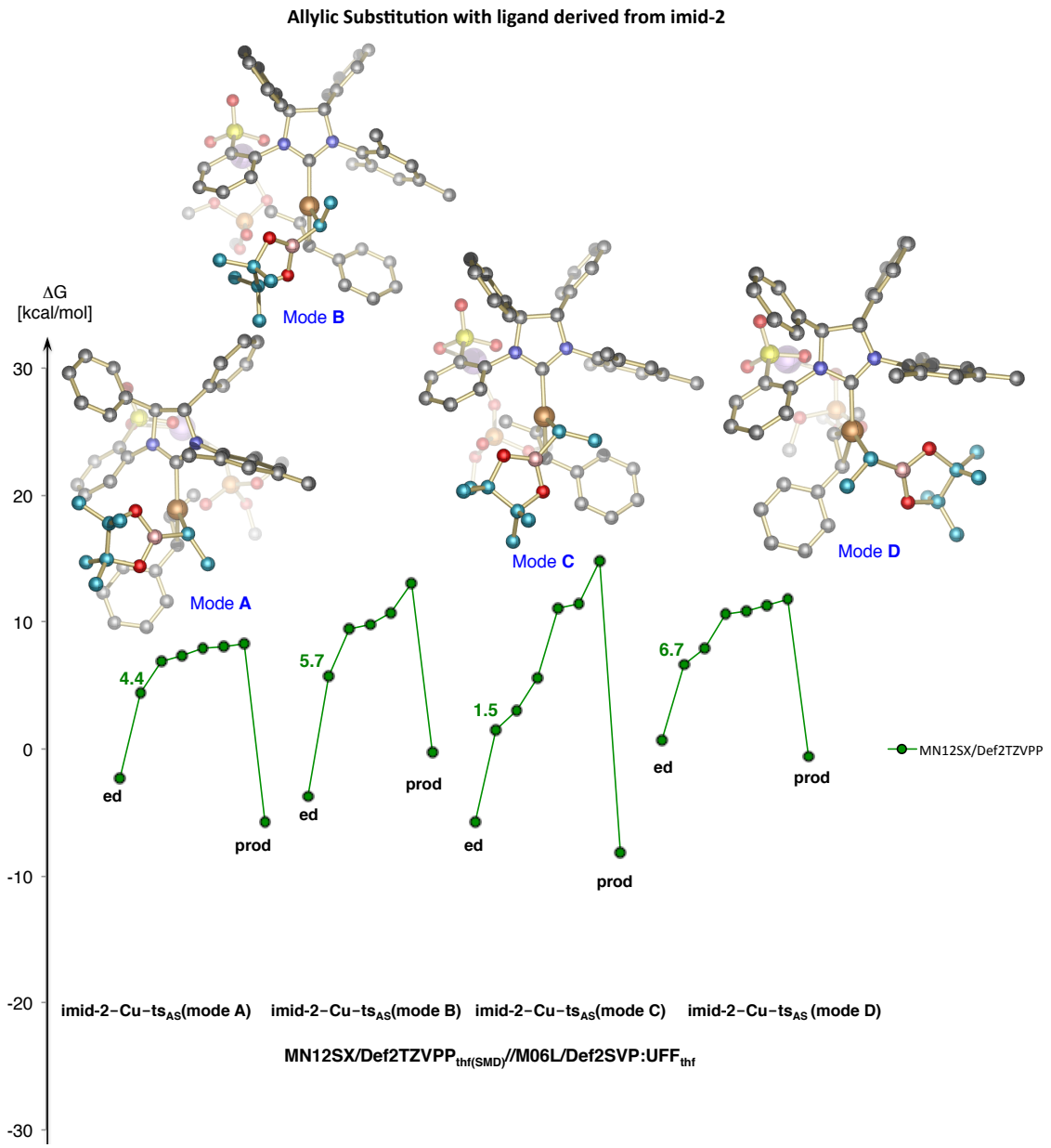

Figure S9-1. Free energy surfaces for allylic substitution (AS) with NHC ligand derived from **imid-2** at the MN12SX/DefTZVPP$_{THF(SMD)}$//M06L/Def2SVP:UFF$_{THF}$ level (all pathways **A**, **B**, **C** and **D** shown, including one **ed** and **prod** for each mode of addition).

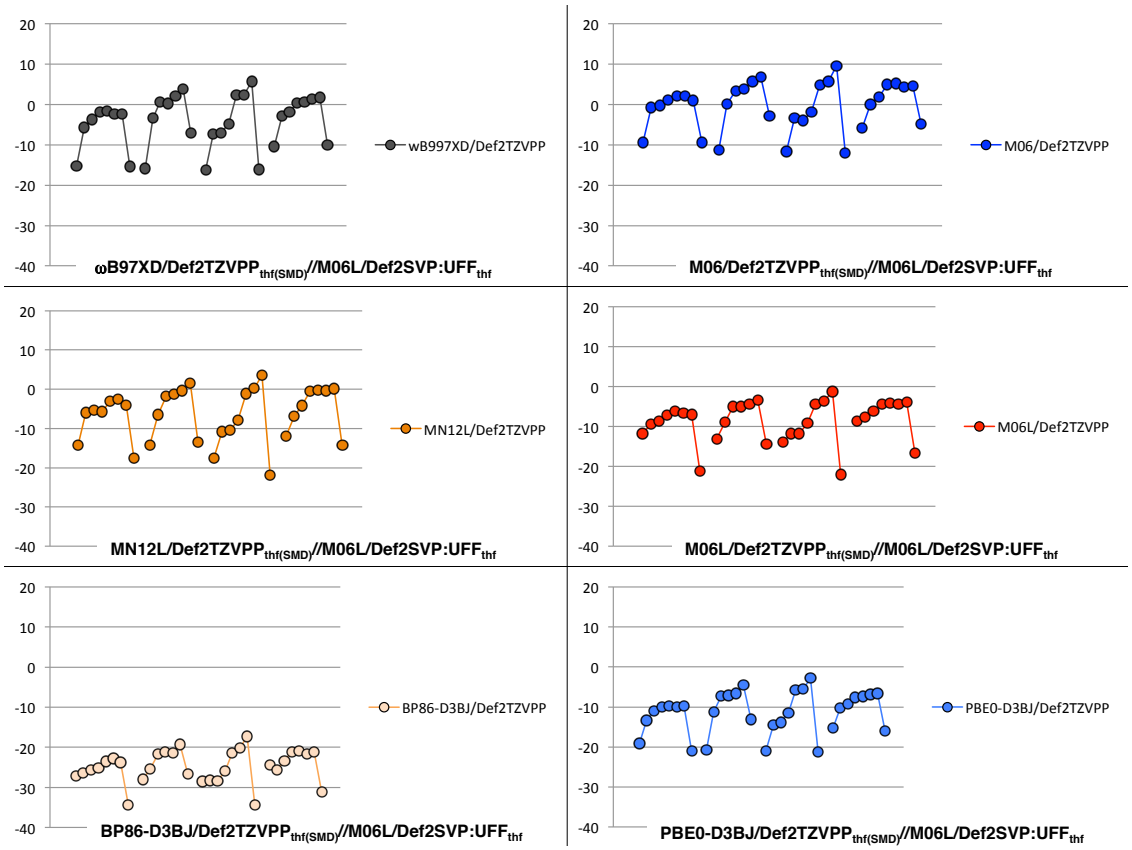

Figure S9-2. Free energy surfaces for allylic substitution (AS) with NHC ligand derived from **imid-2** with various density functionals after optimization with M06L/Def2SVP:UFF$_{THF}$ (all pathways **A**, **B**, **C** and **D** shown, including one **ed** and **prod** for each mode of addition; cf. Figure S9-1)

2.5.8 NMR Spectra

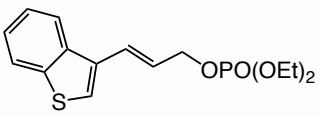

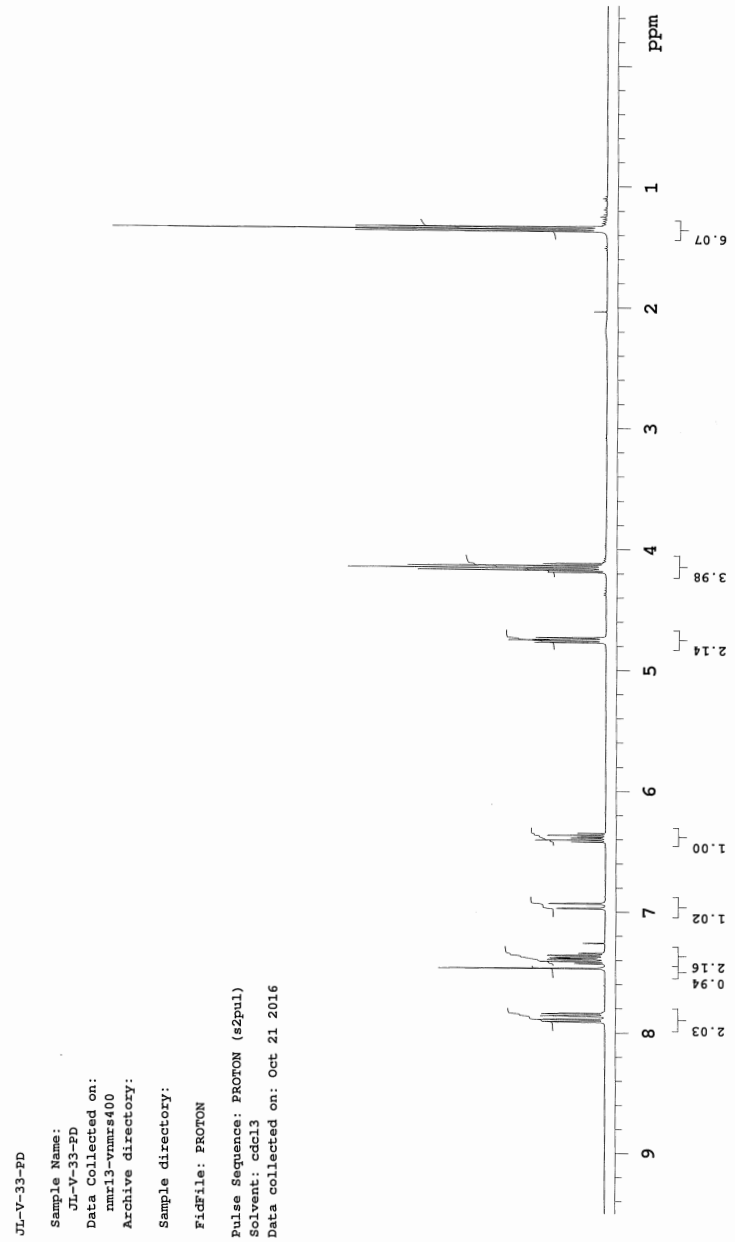

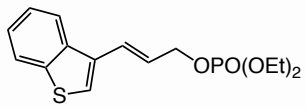
OPO(OEt)2
S

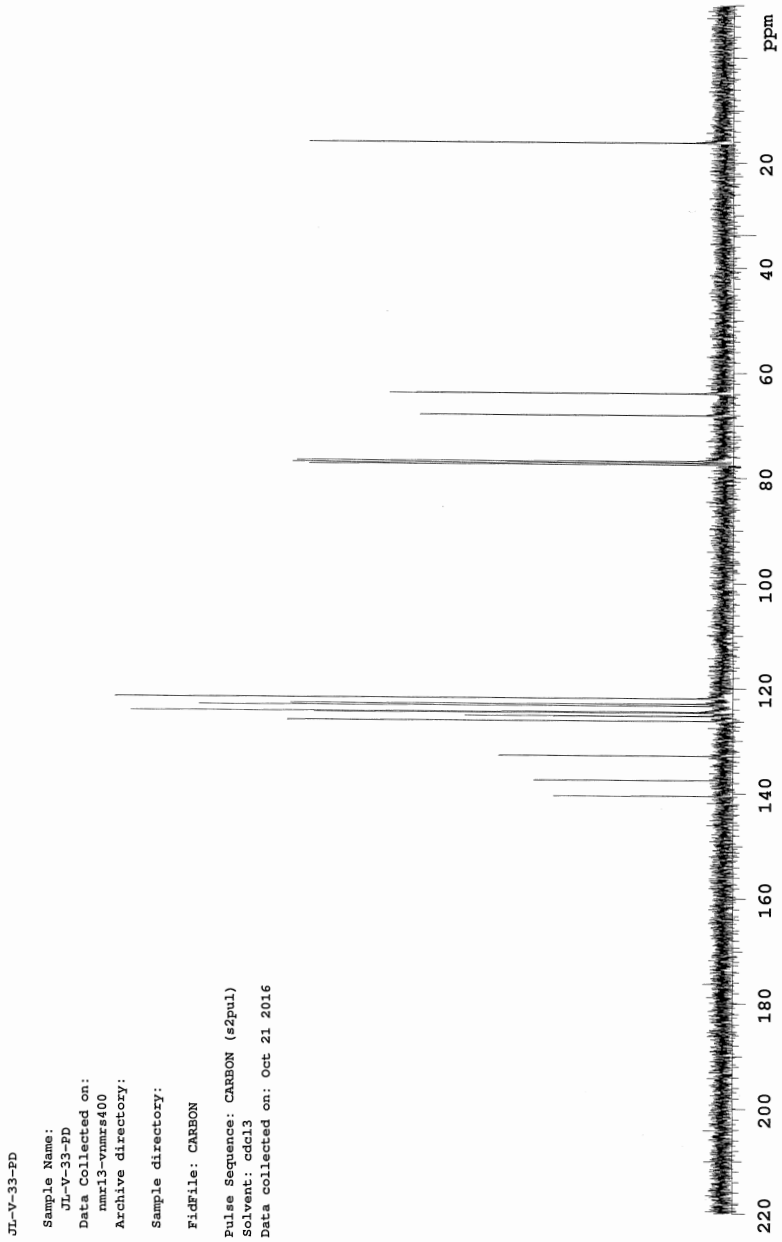
JL-V-33-PD
Sample Name:
JL-V-33-PD
Data Collected on:
nmr13-vnmrs400
Archive directory:
Sample directory:
FidFile: CARBON
Pulse Sequence: CARBON (s2pul)
Solvent: cdcl3
Data collected on: Oct 21 2016
ppm
220
200
180
160
140
120
100
80
60
40
20

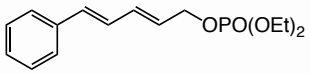
OPO(OEt)2

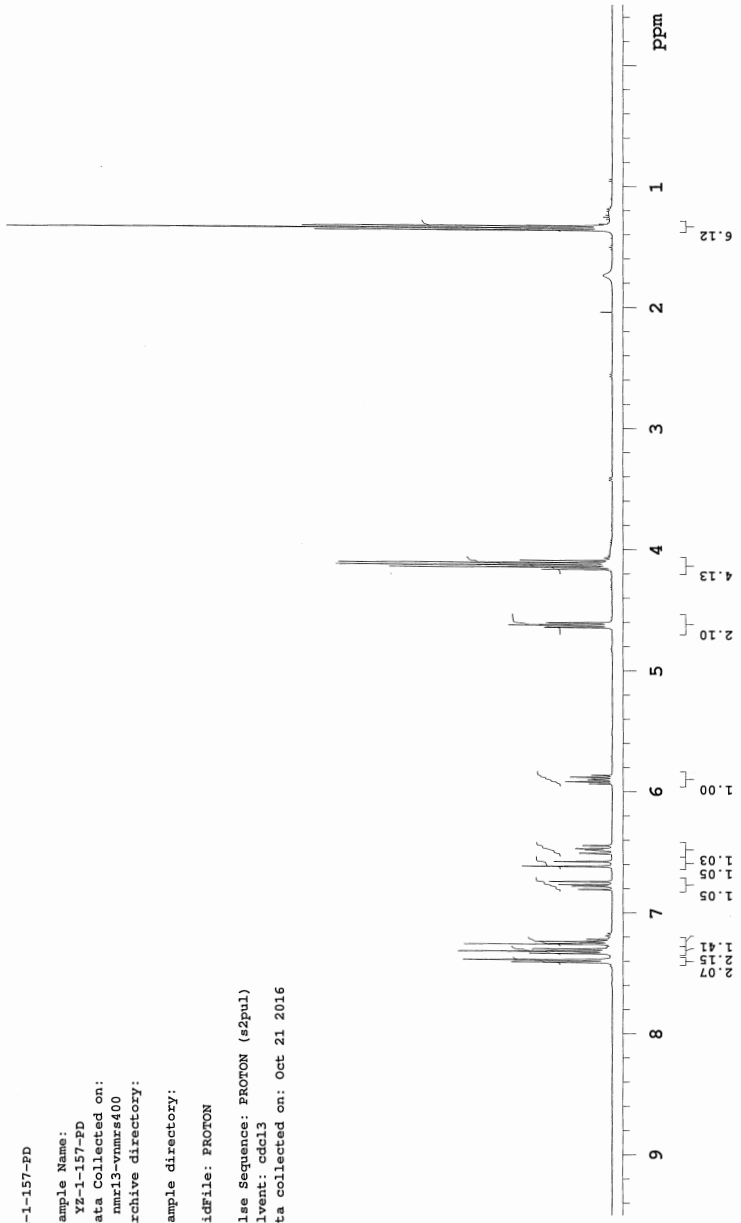
YZ-1-157-PD
Sample Name:
YZ-1-157-PD
Data Collected on:
nmr13-vnmrs400
Archive directory:
Sample directory:
FidFile: PROTON
Pulse Sequence: PROTON (s2pul)
Solvent: cdcl3
Data collected on: Oct 21 2016
ppm
9
8
7
6
5
4
3
2
1
2.07
2.15
1.41
1.05
1.05
1.03
1.00
2.10
4.13
6.12

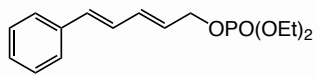
OPO(OEt)2

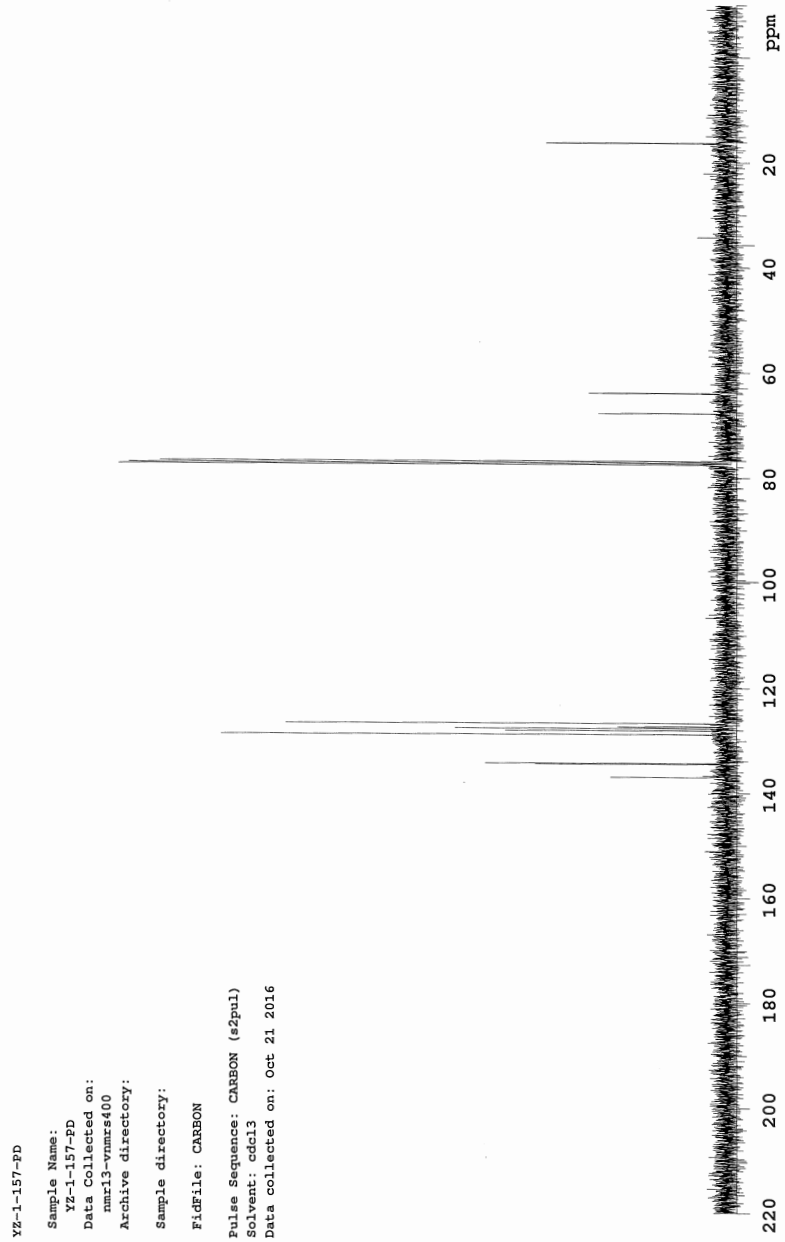
YZ-1-157-PD
Sample Name:
YZ-1-157-PD
Data Collected on:
nmr13-vnmrs400
Archive directory:
Sample directory:
FidFile: CARBON
Pulse Sequence: CARBON (s2pul)
Solvent: cdcl3
Data collected on: Oct 21 2016
220
200
180
160
140
120
100
80
60
40
20
ppm

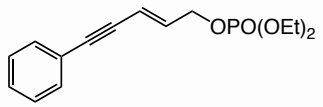
OPO(OEt)2

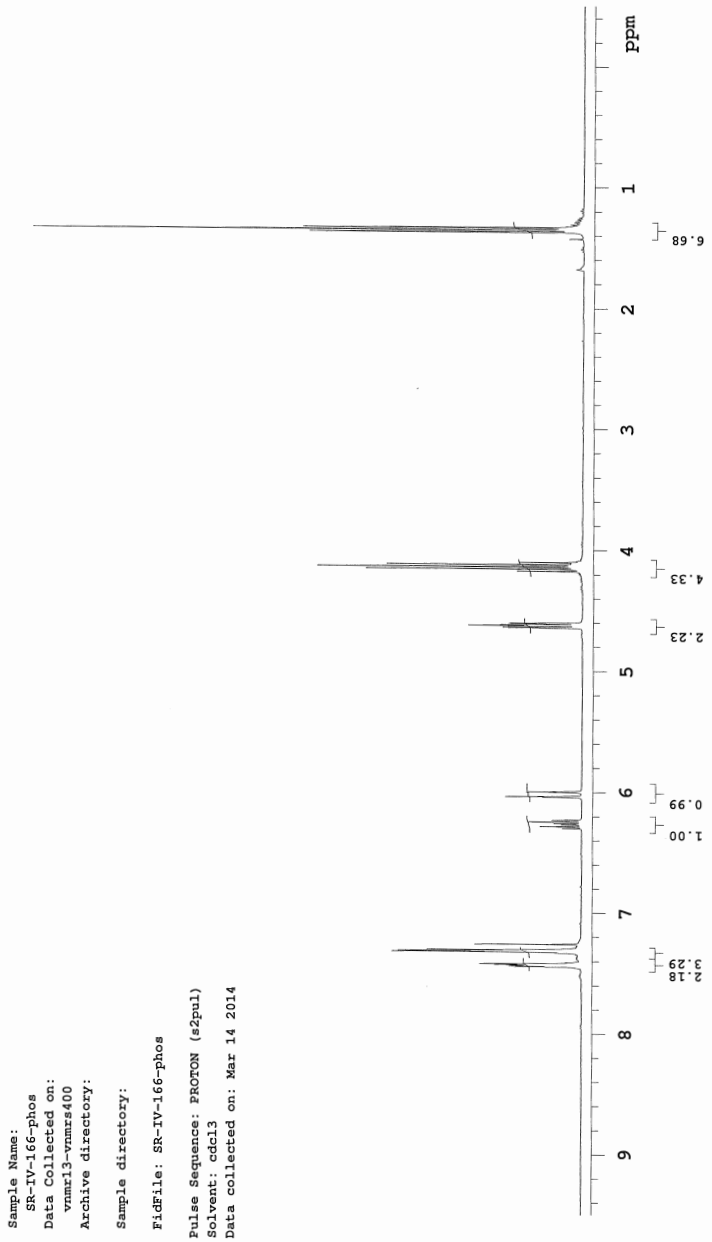
Sample Name:
SR-IV-166-phos
Data Collected on:
vnmr13-vnmrs400
Archive directory:
Sample directory:
FidFile: SR-IV-166-phos
Pulse Sequence: PROTON (s2pul)
Solvent: cdcl3
Data collected on: Mar 14 2014
ppm
1
2
3
4
5
6
7
8
9
6.68
4.33
2.23
0.99
1.00
2.18
3.29

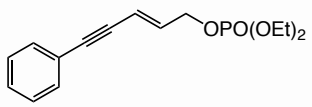
OPO(OEt)2

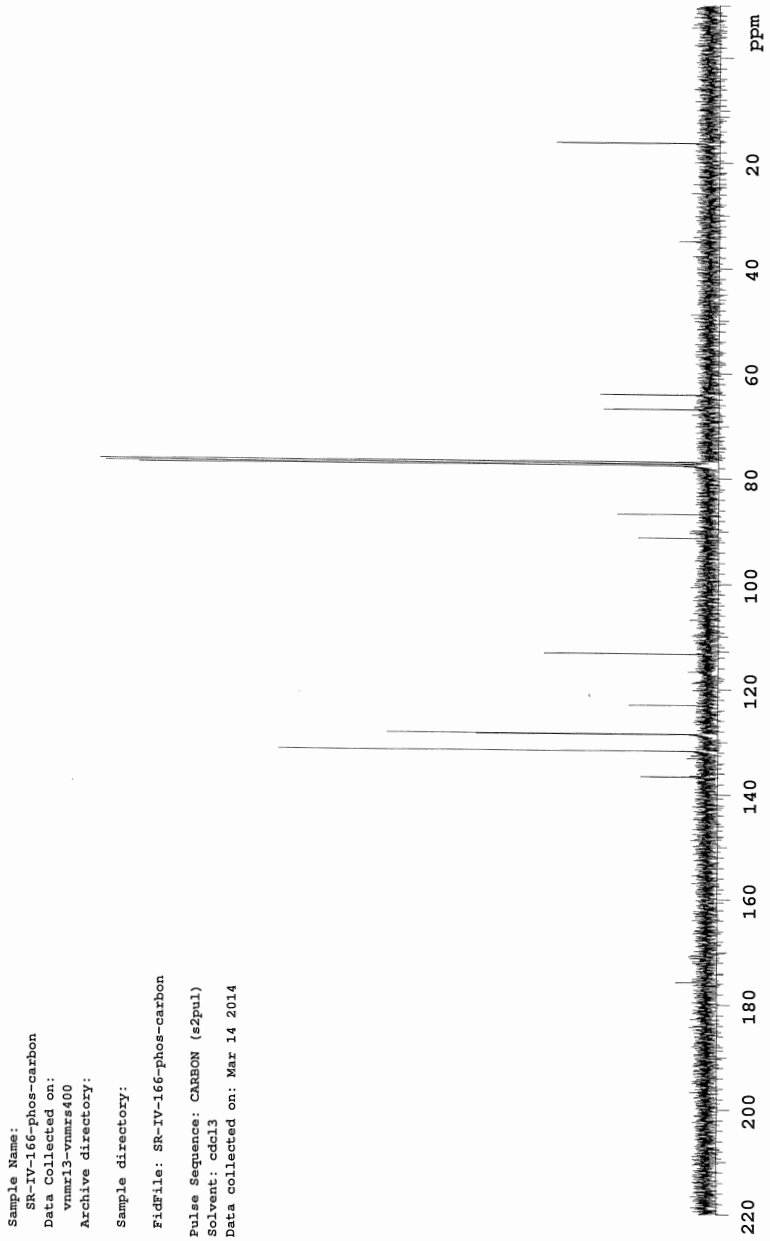
Sample Name:
SR-IV-166-phos-carbon
Data Collected on:
vnmr13-vnmrs400
Archive directory:
Sample directory:
FidFile: SR-IV-166-phos-carbon
Pulse Sequence: CARBON (s2pul)
Solvent: cdcl3
Data collected on: Mar 14 2014
220
200
180
160
140
120
100
80
60
40
20
ppm

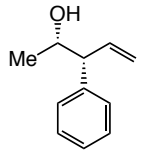

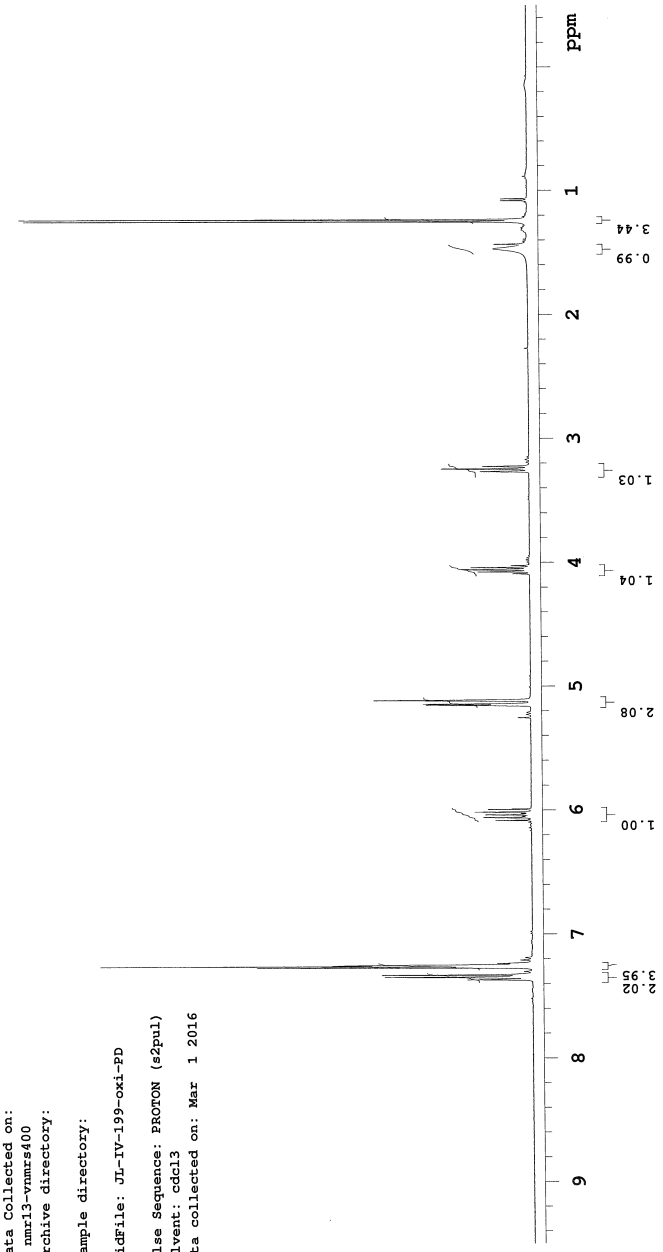

JL-IV-199-oxi-PD

Sample Name:
JL-IV-199-oxi-PD
Data Collected on:
nmrl3-vnmrs400
Archive directory:

Sample directory:

FidFile: JL-IV-199-oxi-PD

Pulse Sequence: PROTON (s2pul)
Solvent: cdcl3
Data collected on: Mar 1 2016

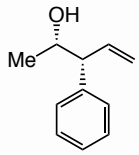
OH
Me

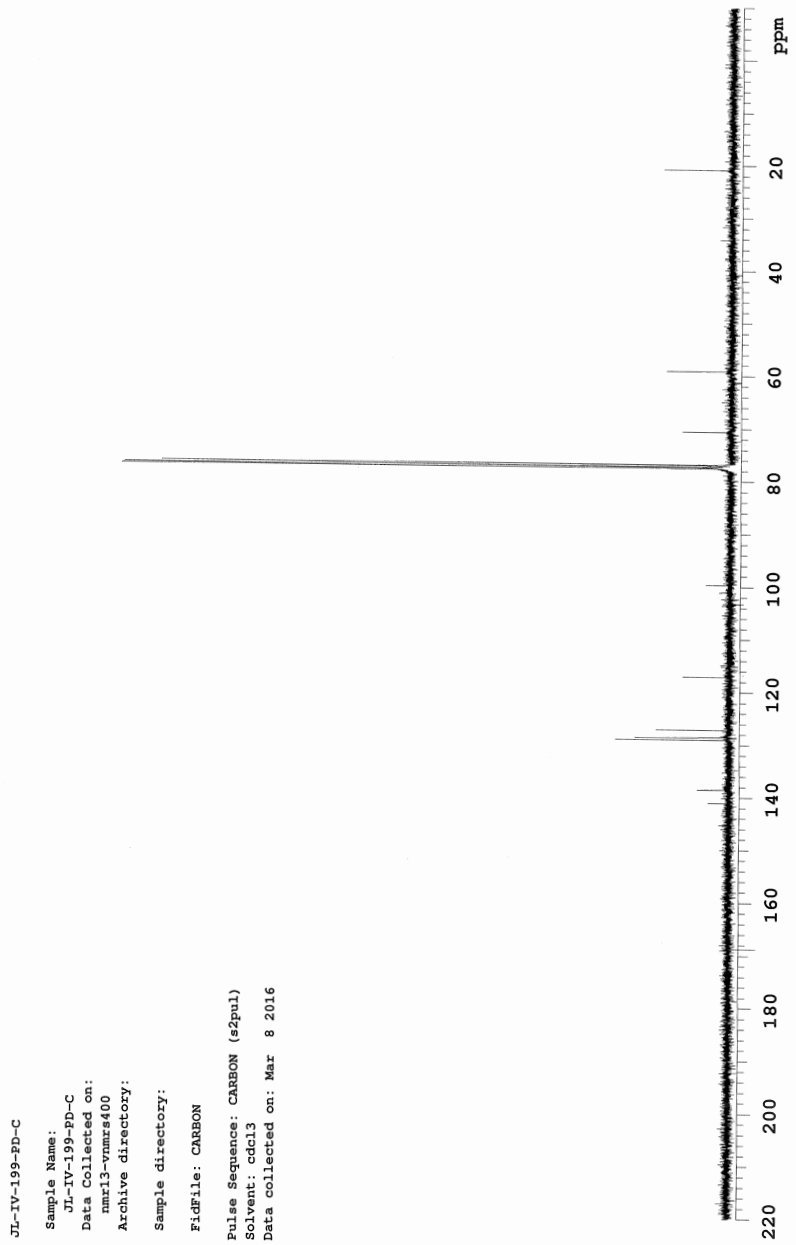
JL-IV-199-PD-C
Sample Name:
JL-IV-199-PD-C
Data Collected on:
nmr13-vnmrs400
Archive directory:
Sample directory:
FidFile: CARBON
Pulse Sequence: CARBON (s2pul)
Solvent: cdcl3
Data collected on: Mar 8 2016
220
200
180
160
140
120
100
80
60
40
20
ppm

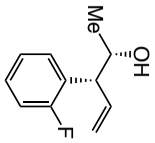

JL-IV-225-2-oxi-PD

Sample Name:
JL-IV-225-2-oxi-PD
Data Collected on:
nmr13-vnmrs400
Archive directory:

Sample directory:

FidFile: PROTON

Pulse Sequence: PROTON (s2pul)
Solvent: cdcl3
Data collected on: Mar 26 2016

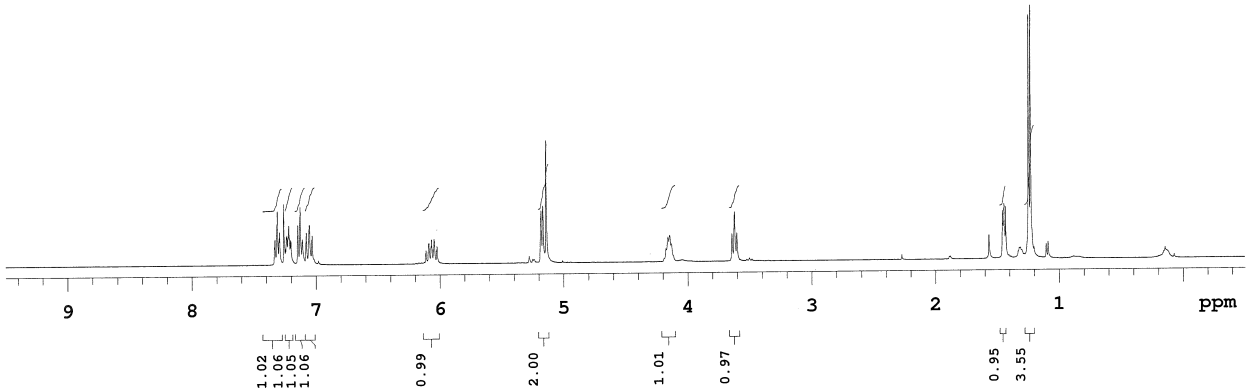

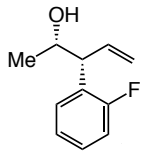
OH
Me
F

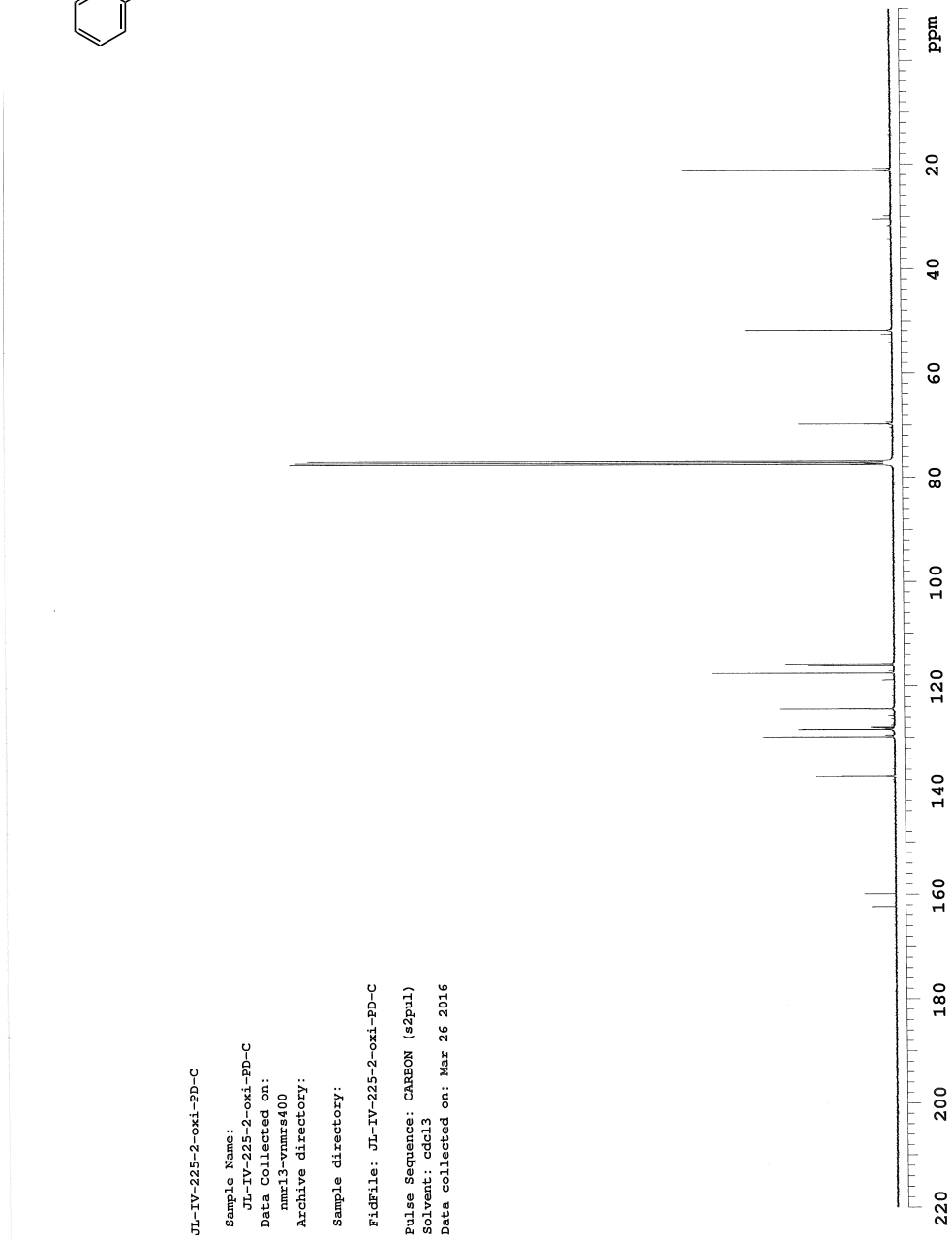
JL-IV-225-2-oxi-PD-C
Sample Name:
JL-IV-225-2-oxi-PD-C
Data Collected on:
nmr13-vnmrs400
Archive directory:
Sample directory:
FidFile: JL-IV-225-2-oxi-PD-C
Pulse Sequence: CARBON (s2pul)
Solvent: cdcl3
Data collected on: Mar 26 2016
ppm
220
200
180
160
140
120
100
80
60
40
20

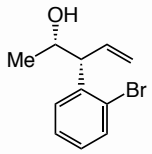

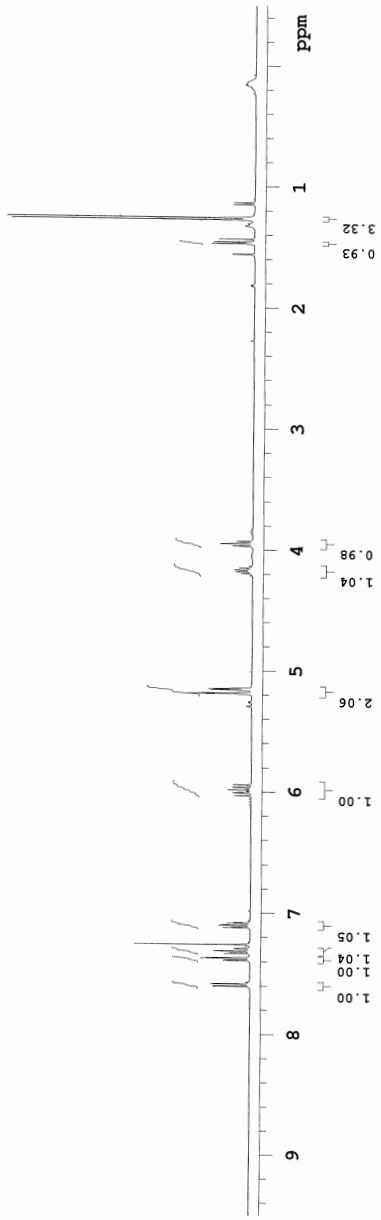

JL-IV-217-2-oxi-PD

Sample Name:
JL-IV-217-2-oxi-PD
Data Collected on:
nmr13-vnmrs400
Archive directory:

Sample directory:

FidFile: PROTON

Pulse Sequence: PROTON (s2pul)
Solvent: cdcl3
Data collected on: Mar 18 2016

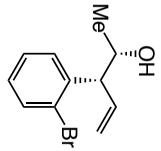

JL-IV-217-2-oxi-PD-C

Sample Name:
JL-IV-217-2-oxi-PD-C
Data Collected on:
nmr13-vnmrs400
Archive directory:

Sample directory:

FidFile: CARBON

Pulse Sequence: CARBON (s2pul)
Solvent: cdcl3
Data collected on: Mar 20 2016

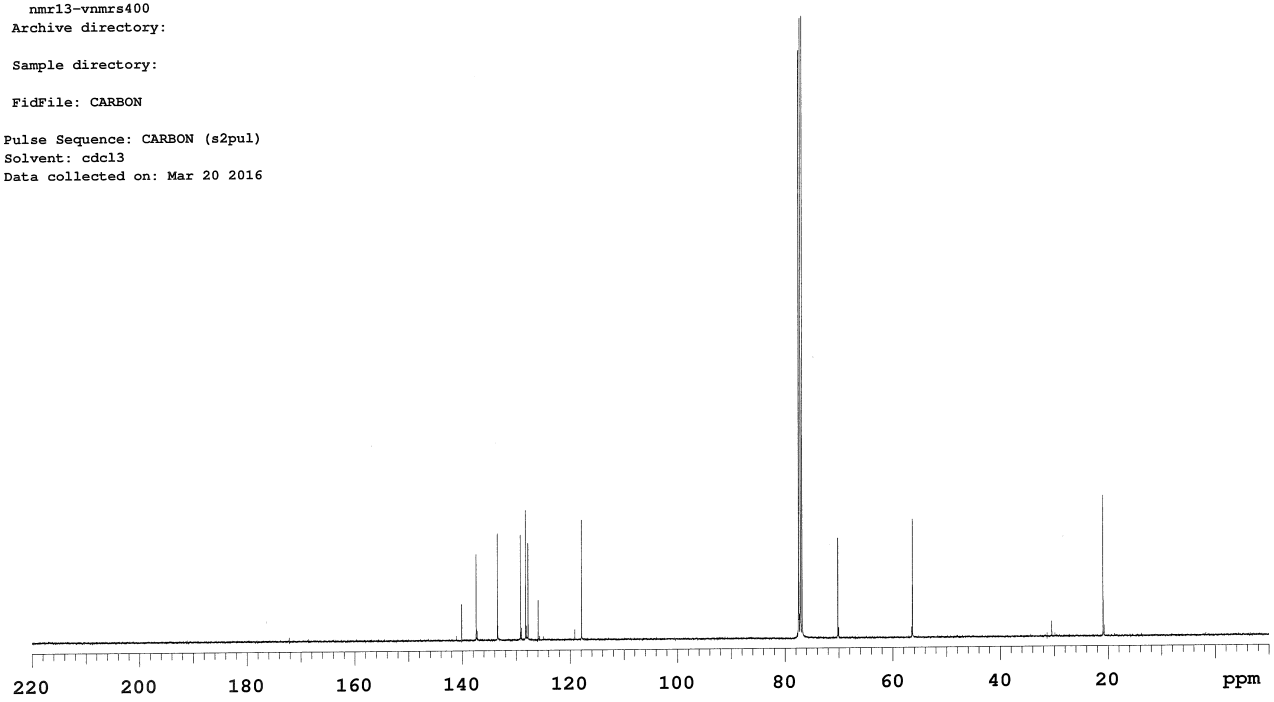

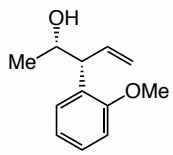
OH
Me
OMe

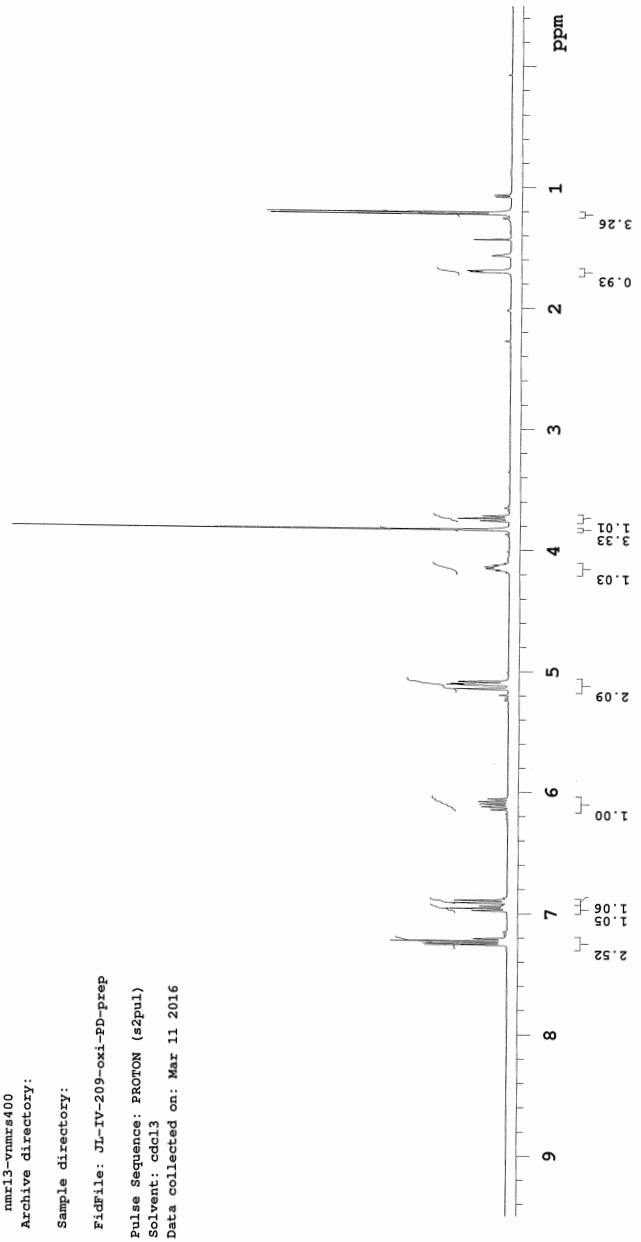
JL-IV-209-1-oxi-PD-prep
Sample Name:
JL-IV-209-1-oxi-PD-prep
Data Collected on:
nmr13-vnmrs400
Archive directory:
Sample directory:
FidFile: JL-IV-209-oxi-PD-prep
Pulse Sequence: PROTON (s2pul)
Solvent: cdcl3
Data collected on: Mar 11 2016
ppm
1
2
3
4
5
6
7
8
9
3.26
0.93
3.33
1.01
1.03
2.09
1.00
1.05
1.06
2.52

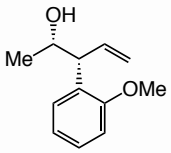

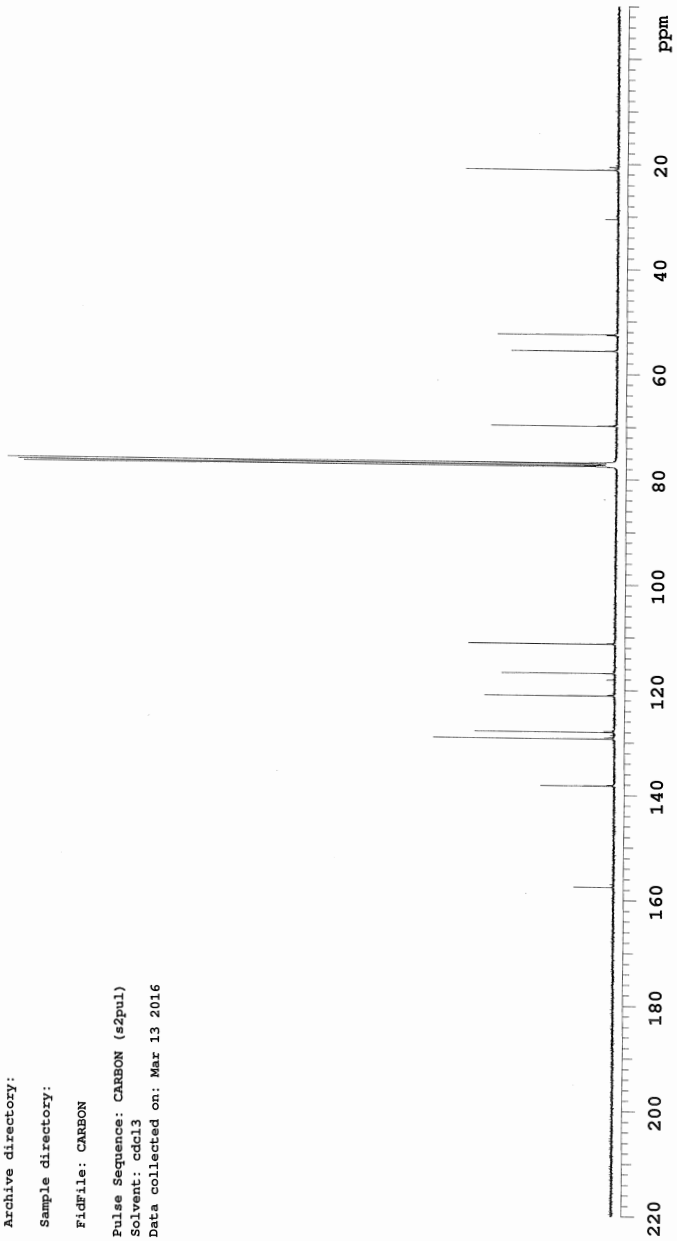

JL-IV-209-oxi-PD-C

Sample Name:
JL-IV-209-oxi-PD-C
Data Collected on:
nmr13-vnmrs400
Archive directory:

Sample directory:

FidFile: CARBON

Pulse Sequence: CARBON (s2pul)
Solvent: cdcl3
Data collected on: Mar 13 2016

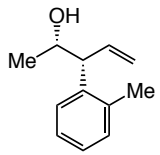

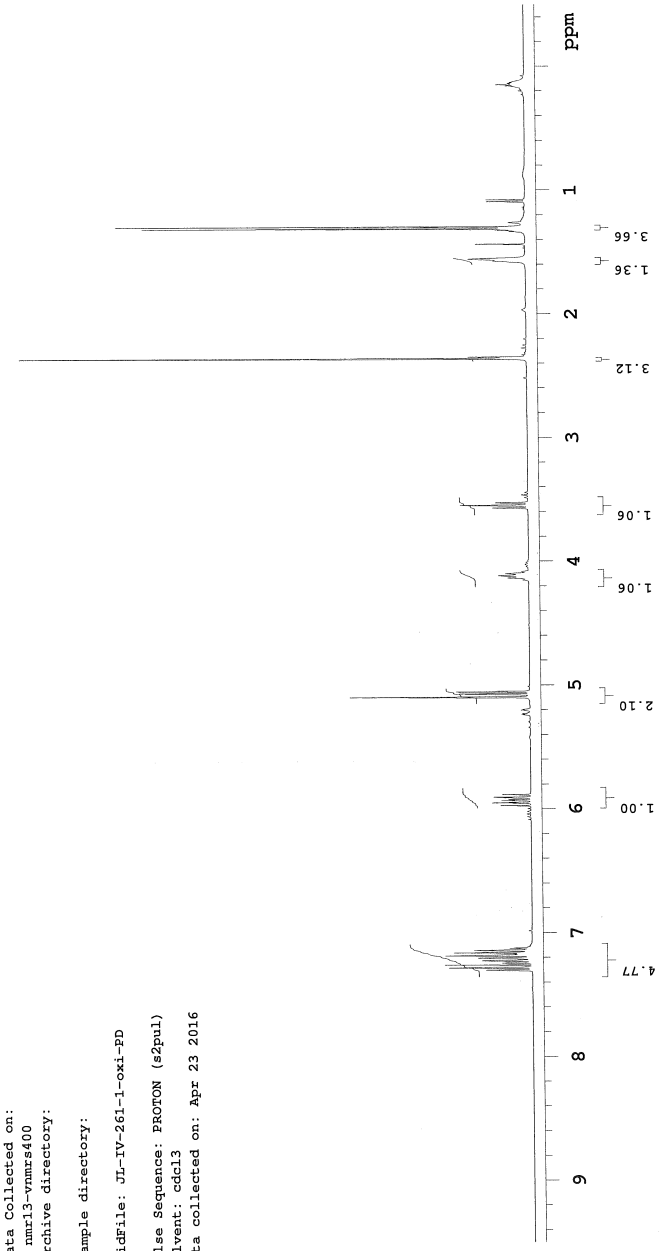

JL-IV-261-1-oxi-PD

Sample Name:
JL-IV-261-1-oxi-PD
Data Collected on:
nmr13-vnmrs400
Archive directory:

Sample directory:

FidFile: JL-IV-261-1-oxi-PD

Pulse Sequence: PROTON (s2pul)
Solvent: cdcl3
Data collected on: Apr 23 2016

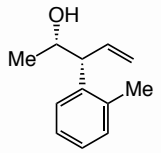
OH
Me
Me

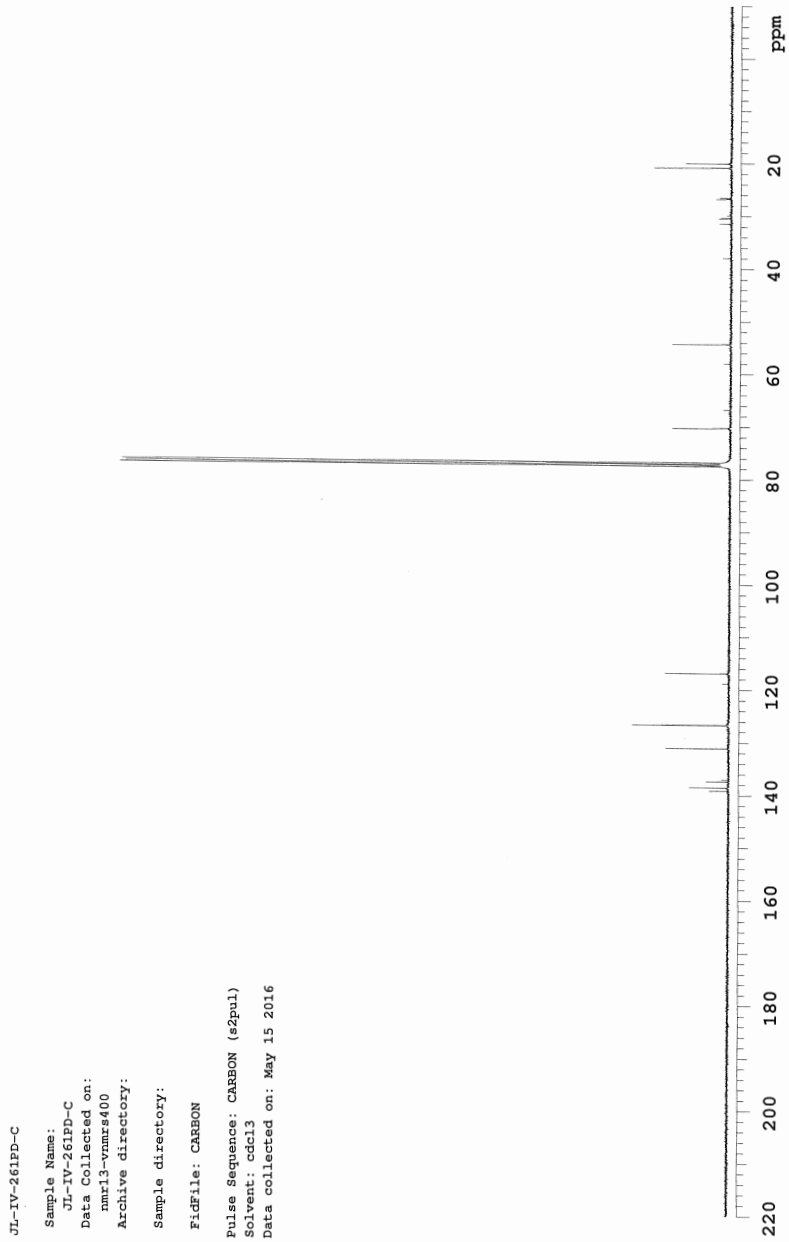
JL-IV-261PD-C
Sample Name:
JL-IV-261PD-C
Data Collected on:
nmr13-vnmrs400
Archive directory:
Sample directory:
FidFile: CARBON
Pulse Sequence: CARBON (s2pul)
Solvent: cdcl3
Data collected on: May 15 2016
220
200
180
160
140
120
100
80
60
40
20
ppm

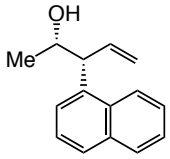

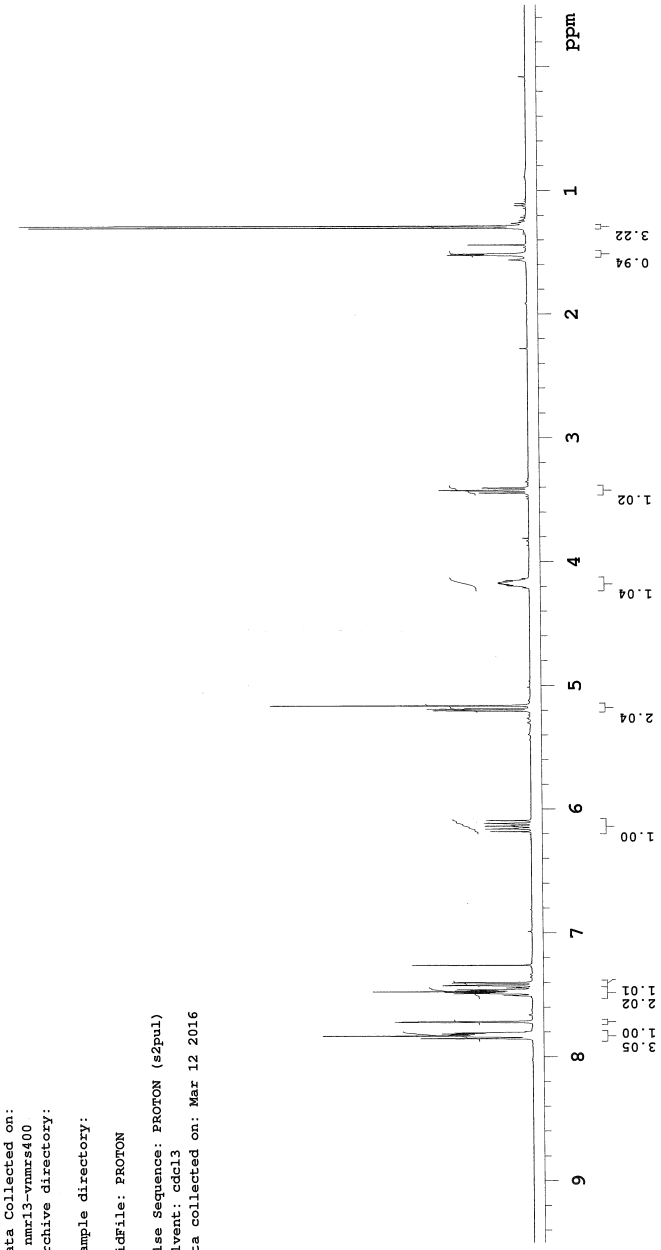

JL-IV-207-1-oxi-PD

Sample Name:
JL-IV-207-1-oxi-PD
Data Collected on:
nmr13-vnmrs400
Archive directory:

Sample directory:

FidFile: PROTON

Pulse Sequence: PROTON (s2pul)
Solvent: cdcl3
Data collected on: Mar 12 2016

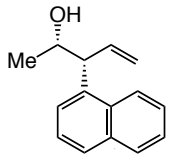
OH
Me

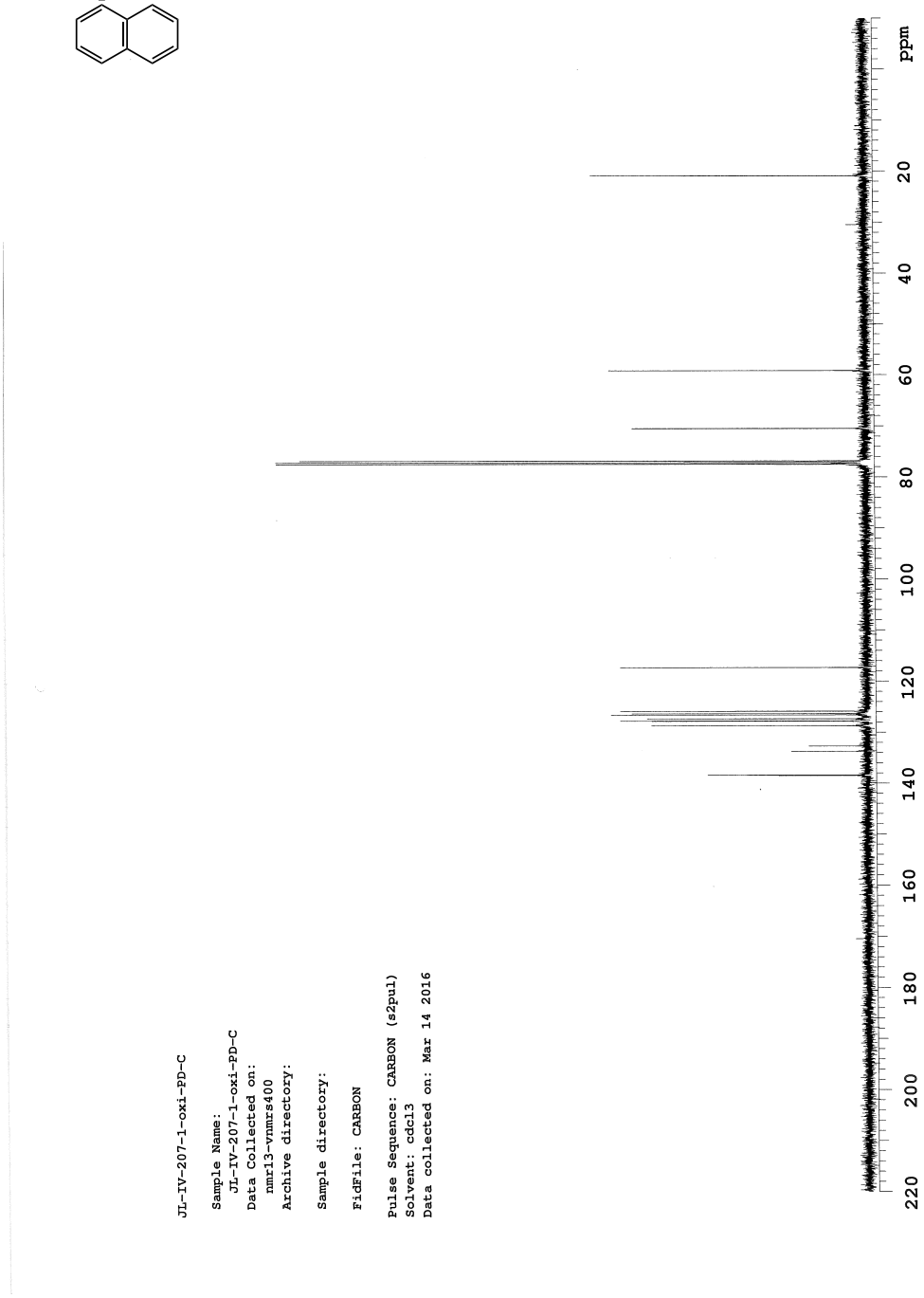
JL-IV-207-1-oxi-PD-C
Sample Name:
JL-IV-207-1-oxi-PD-C
Data Collected on:
nmr13-vnmrs400
Archive directory:
Sample directory:
FidFile: CARBON
Pulse Sequence: CARBON (s2pul)
Solvent: cdcl3
Data collected on: Mar 14 2016
ppm
220
200
180
160
140
120
100
80
60
40
20

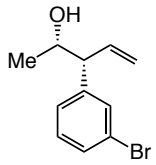
OH
Me
Br

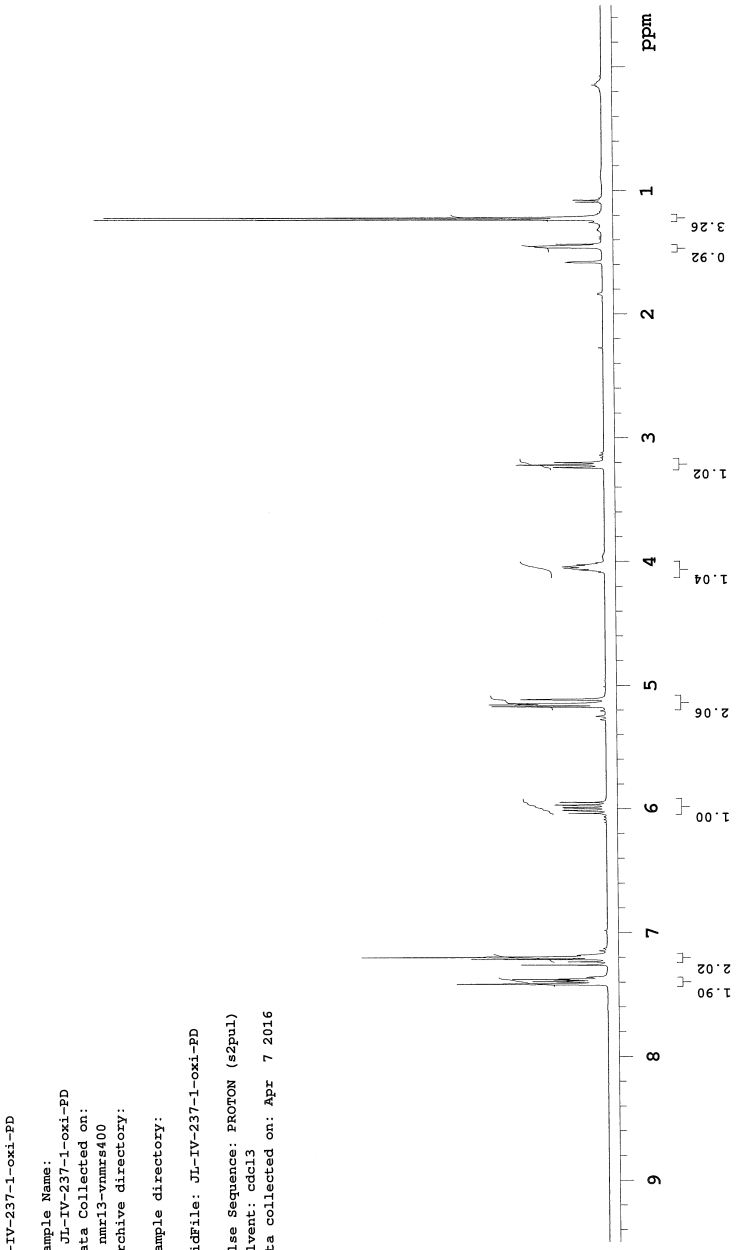
JL-IV-237-1-oxi-PD
Sample Name:
JL-IV-237-1-oxi-PD
Data Collected on:
nmr13-vnmrs400
Archive directory:
Sample directory:
FidFile: JL-IV-237-1-oxi-PD
Pulse Sequence: PROTON (s2pul)
Solvent: cdcl3
Data collected on: Apr 7 2016
ppm
1
2
3
4
5
6
7
8
9
3.26
0.92
1.02
1.04
2.06
1.00
2.02
1.90

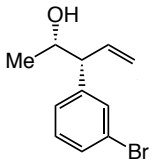
OH
Me
Br

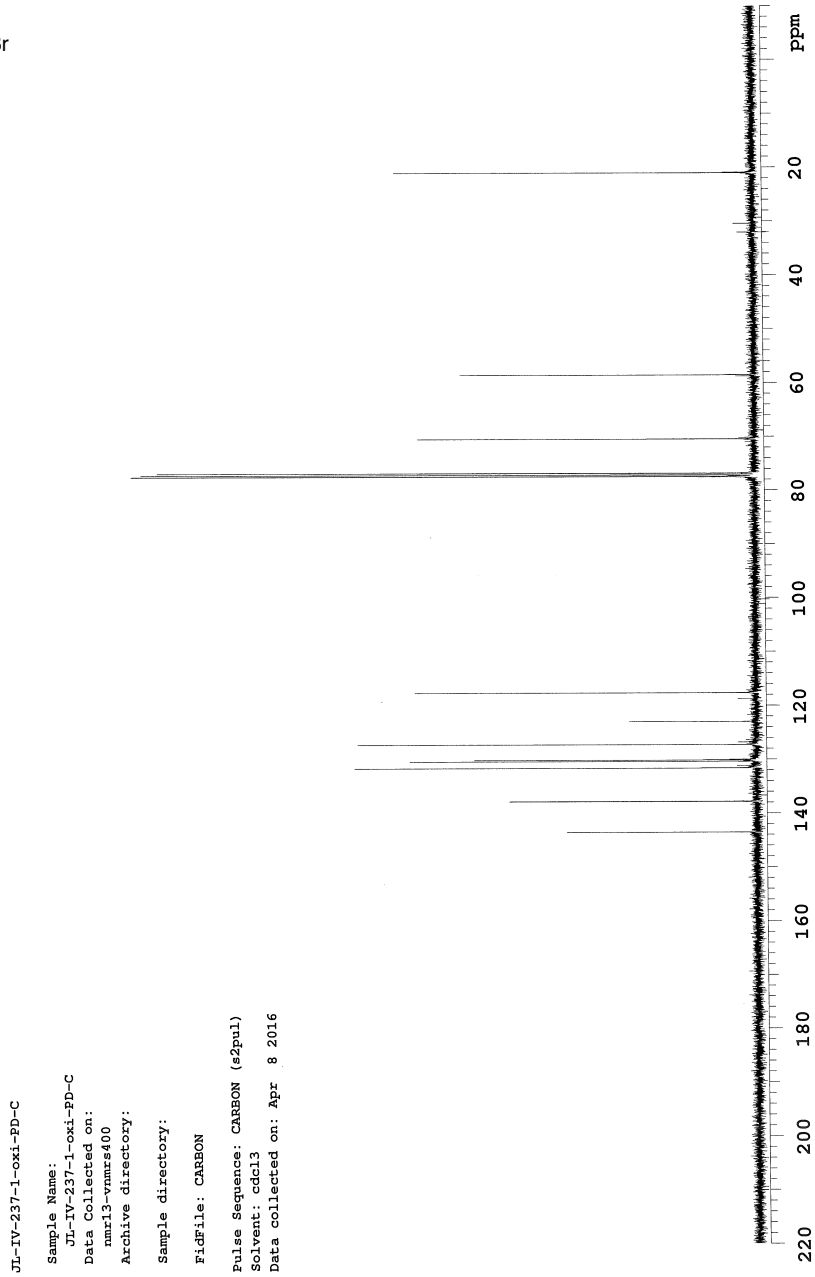
JL-IV-237-1-oxi-PD-C
Sample Name:
JL-IV-237-1-oxi-PD-C
Data Collected on:
nmr13-vnmrs400
Archive directory:
Sample directory:
FidFile: CARBON
Pulse Sequence: CARBON (s2pul)
Solvent: cdcl3
Data collected on: Apr 8 2016
ppm
220
200
180
160
140
120
100
80
60
40
20

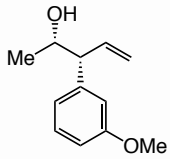
OH
Me
OMe

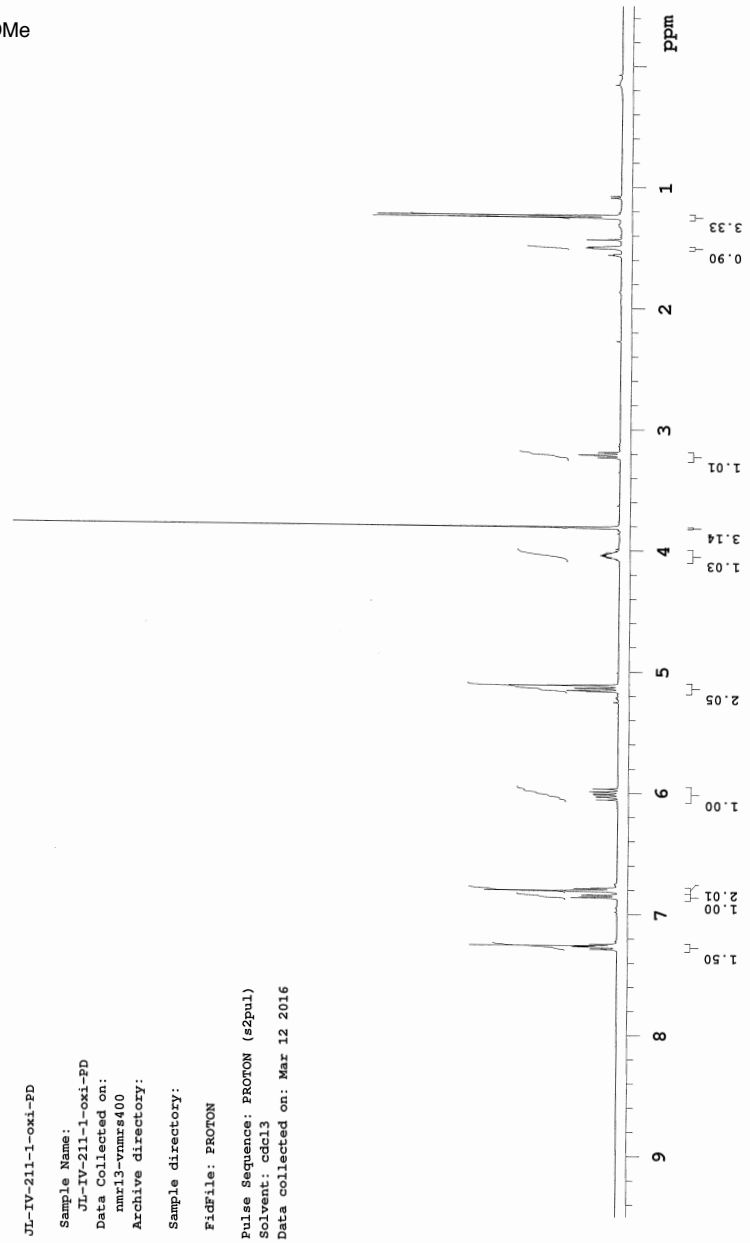
JL-IV-211-1-oxi-PD
Sample Name:
JL-IV-211-1-oxi-PD
Data Collected on:
nmr13-vnmrs400
Archive directory:
Sample directory:
FidFile: PROTON
Pulse Sequence: PROTON (s2pul)
Solvent: cdcl3
Data collected on: Mar 12 2016
ppm
1
2
3
4
5
6
7
8
9
3.33
0.90
1.01
3.14
1.03
2.05
1.00
2.01
1.00
1.50

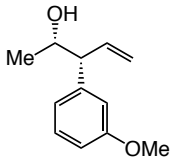

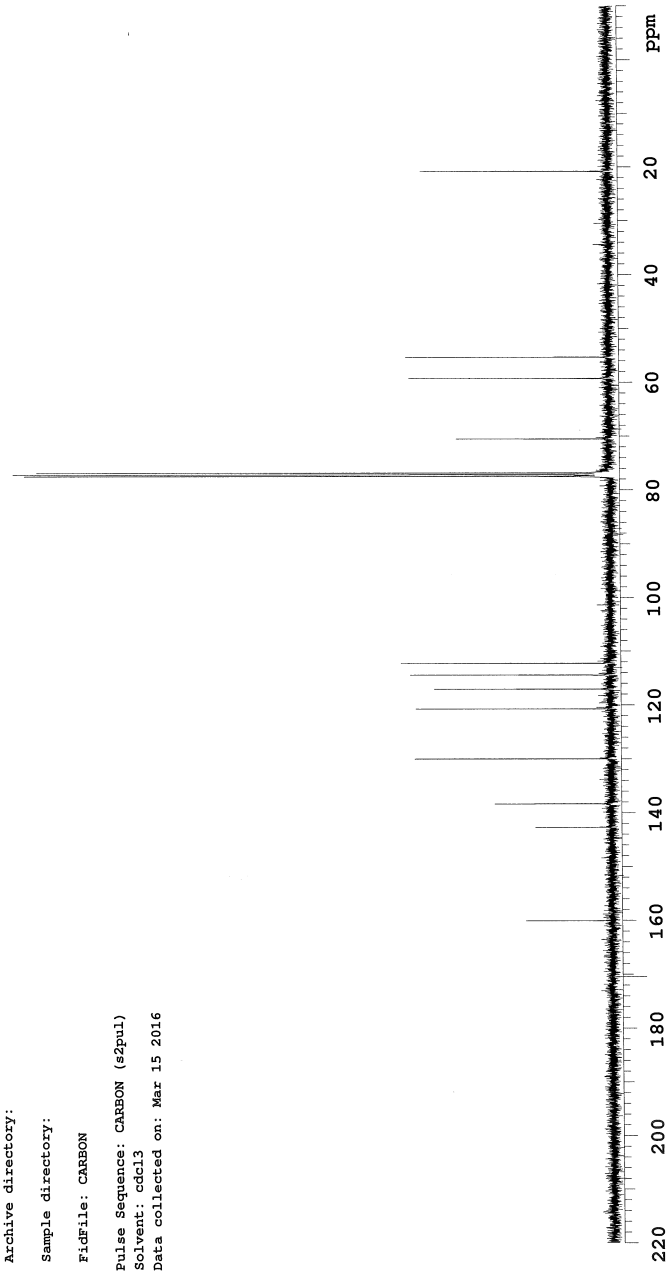

JL-IV-211-1-oxi-PD-C

Sample Name:
JL-IV-211-1-oxi-PD-C
Data Collected on:
nmr13-vnmrs400
Archive directory:

Sample directory:

FidFile: CARBON

Pulse Sequence: CARBON (s2pul)
Solvent: cdcl3
Data collected on: Mar 15 2016

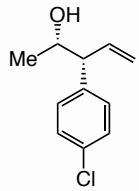

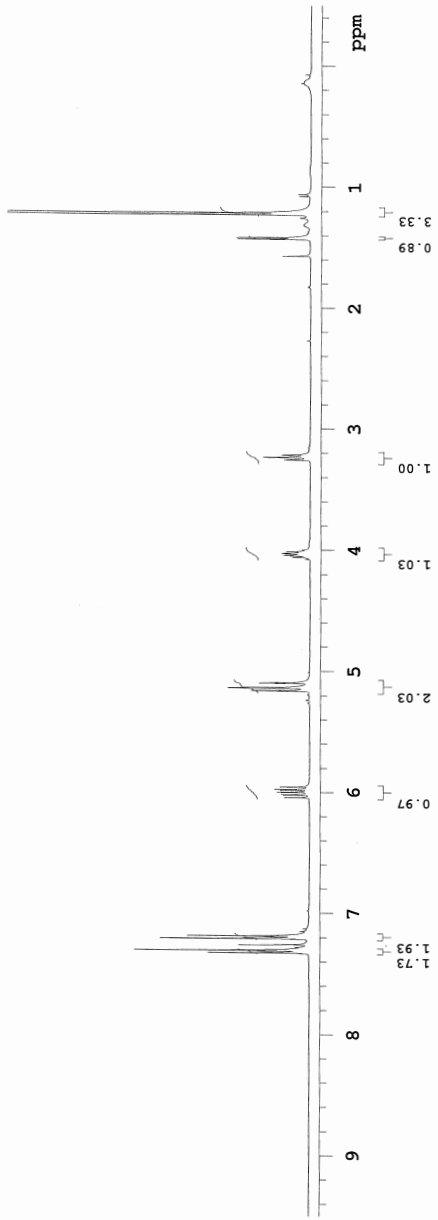

JL-IV-233-2-oxi-PD

Sample Name:
JL-IV-233-2-oxi-PD
Data Collected on:
nmr13-vnmrs400
Archive directory:

Sample directory:

FidFile: PROTON

Pulse Sequence: PROTON (s2pul)
Solvent: cdcl3
Data collected on: Apr 4 2016

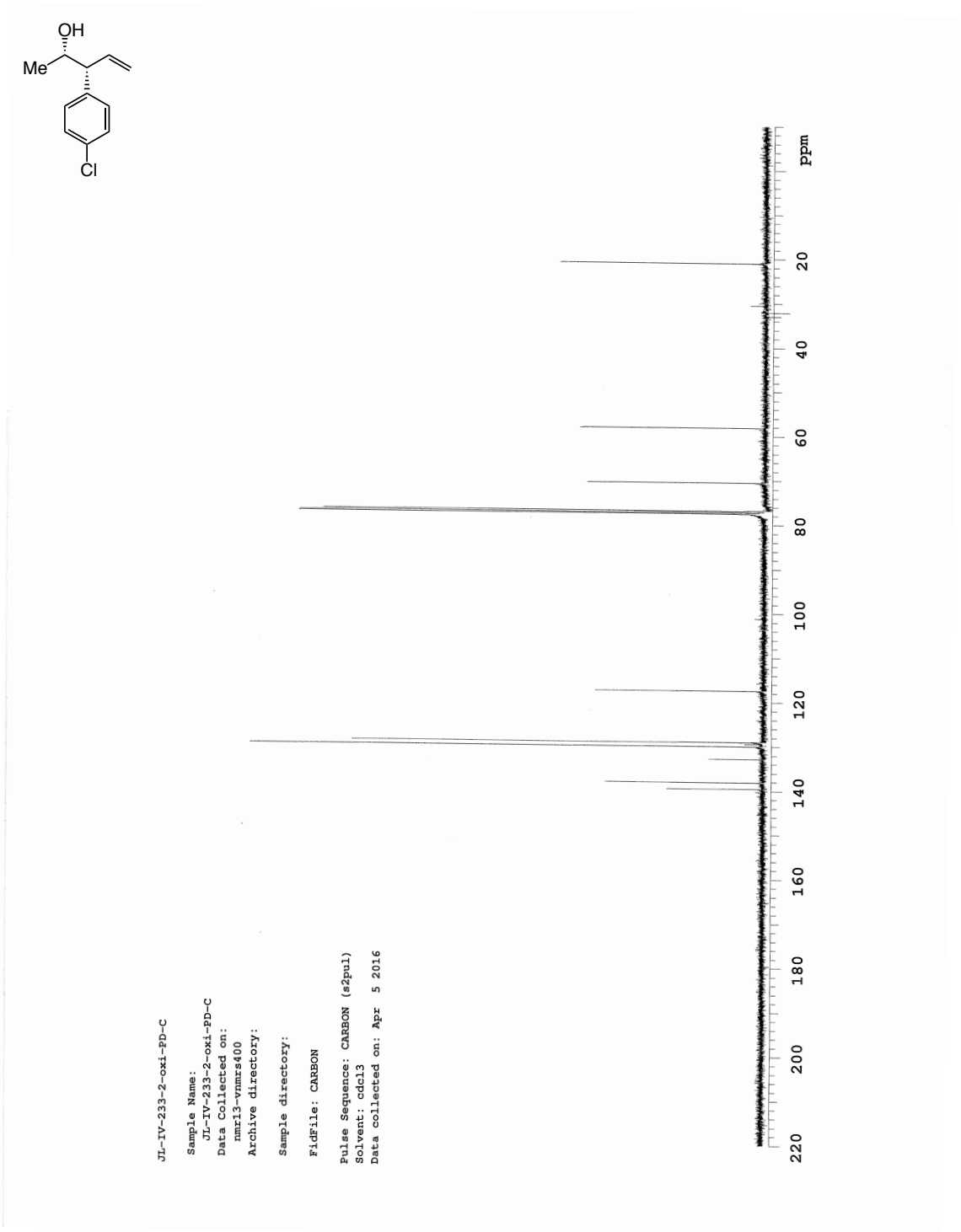
OH
Me
Cl
JL-IV-233-2-oxi-PD-C
Sample Name:
JL-IV-233-2-oxi-PD-C
Data Collected on:
nmr13-vnmrs400
Archive directory:
Sample directory:
FidFile: CARBON
Pulse Sequence: CARBON (s2pul)
Solvent: cdcl3
Data collected on: Apr 5 2016
ppm
220
200
180
160
140
120
100
80
60
40
20

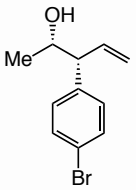

Agilent Technologies

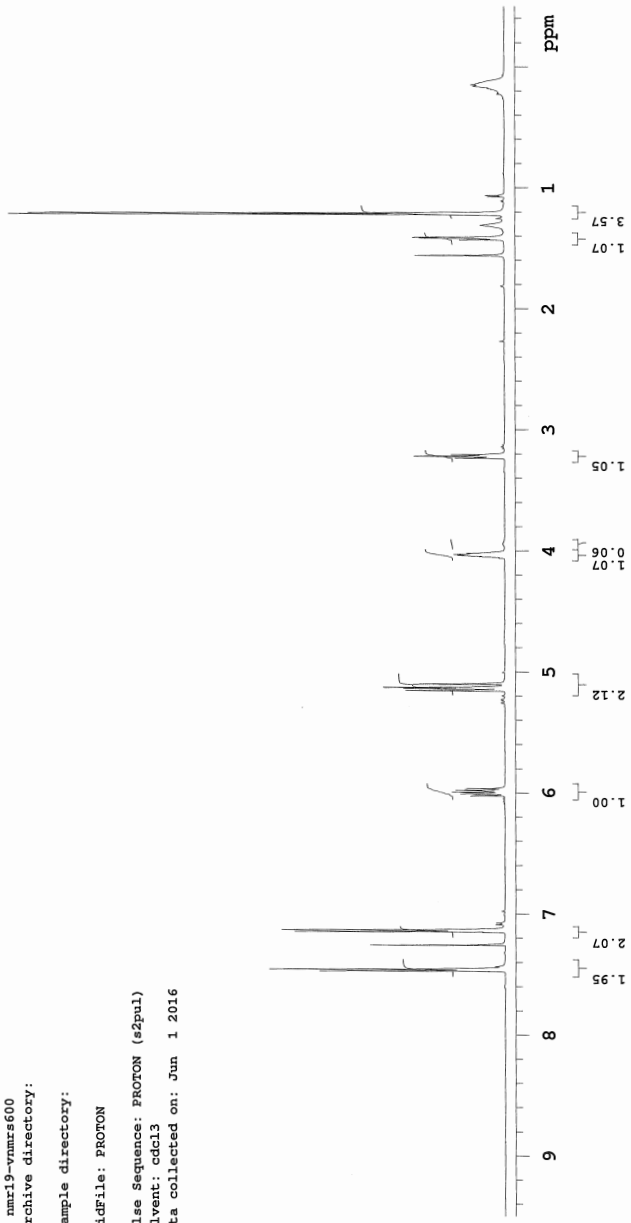

JL-V-6-1-oxi-PD

Sample Name:
JL-V-6-1-oxi-PD
Data Collected on:
nmr19-vnmrs600
Archive directory:

Sample directory:

FidFile: PROTON

Pulse Sequence: PROTON (s2pul)
Solvent: cdcl3
Data collected on: Jun 1 2016

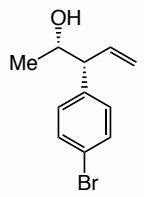

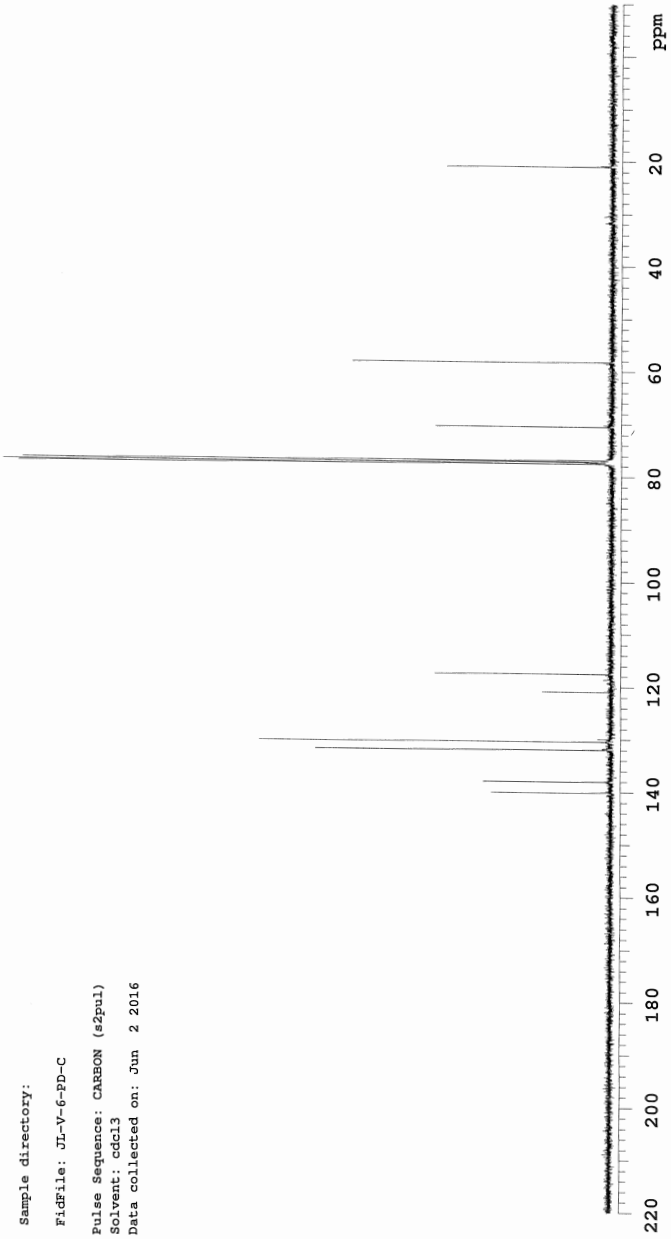

JL-V-6-PD-C

Sample Name:
JL-V-6-PD-C
Data Collected on:
nmr13-vnmrs400
Archive directory:

Sample directory:

FidFile: JL-V-6-PD-C

Pulse Sequence: CARBON (s2pul)
Solvent: cdcl3
Data collected on: Jun 2 2016

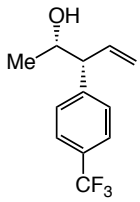

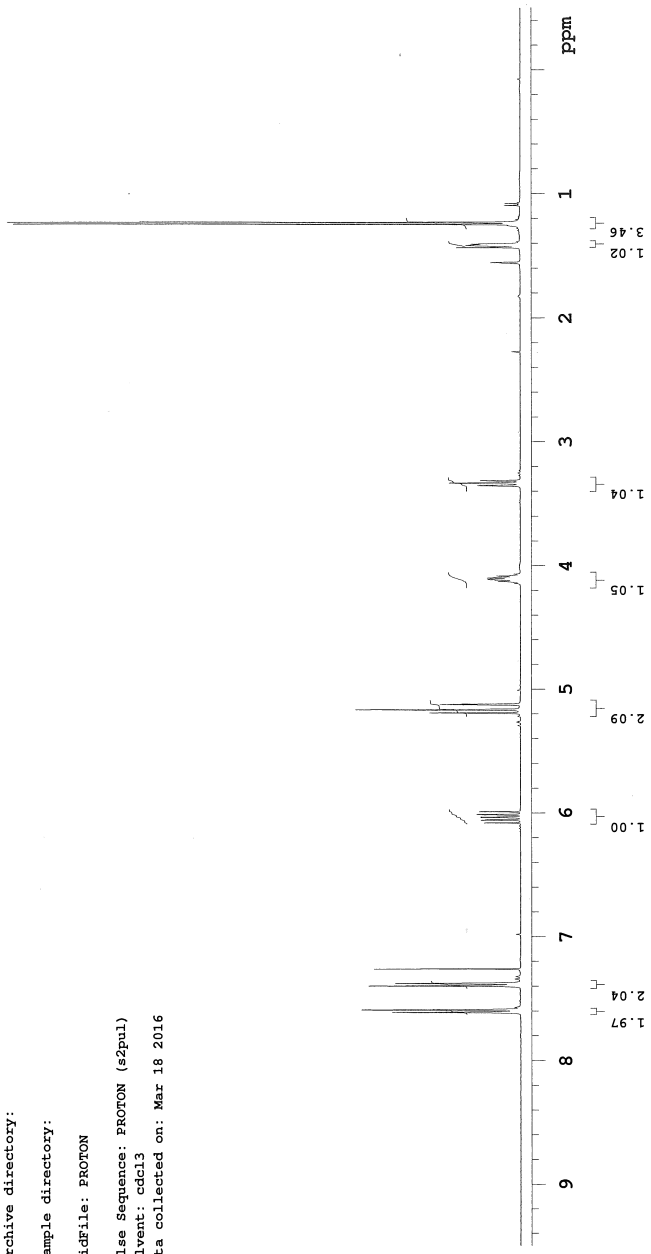


```
J1-IV-215-2-oxi-PD

  Sample Name:
     J1-IV-215-2-oxi-PD
  Data Collected on:
     nmr13-vnmrs400
  Archive directory:

  Sample directory:

  FidFile: PROTON

  Pulse Sequence: PROTON (s2pul)
  Solvent: cdcl3
  Data collected on: Mar 18 2016
```

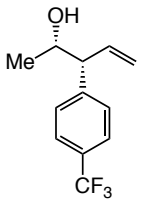
OH
Me
CF3

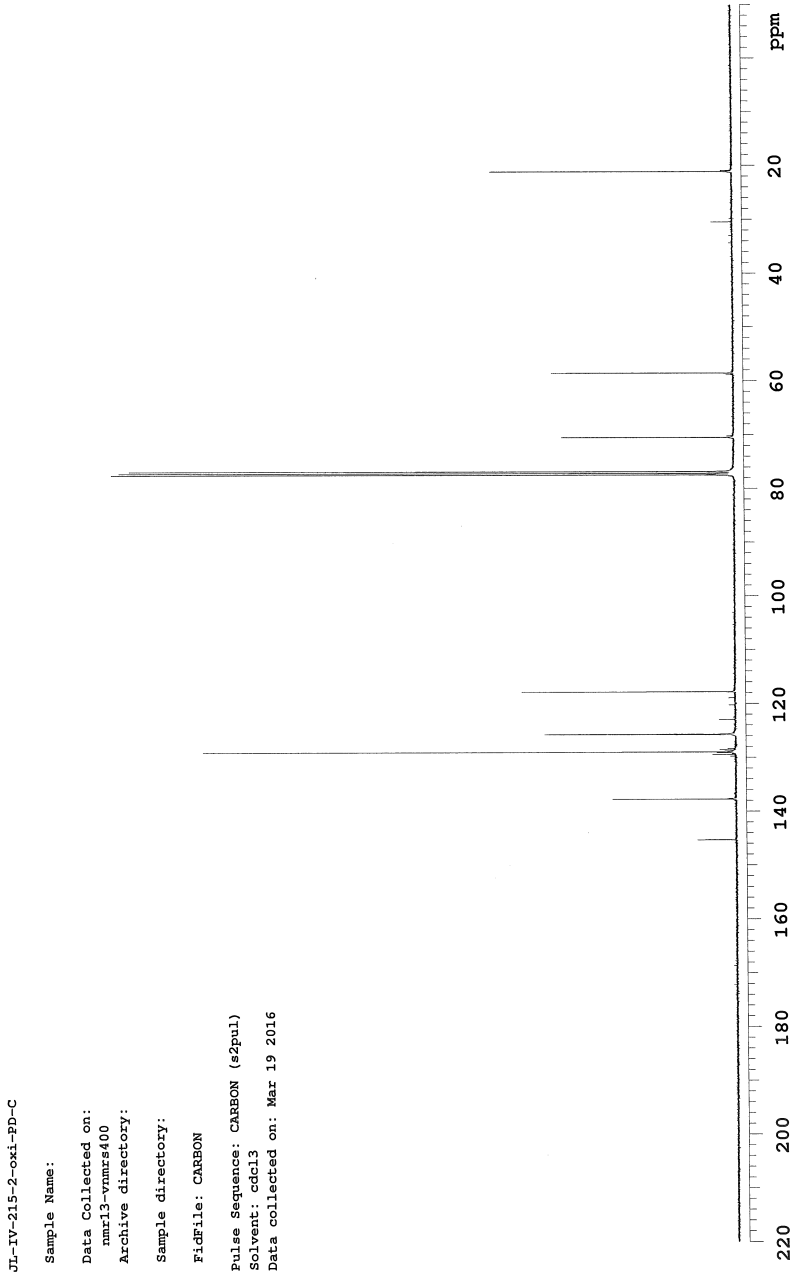
JL-IV-215-2-oxi-PD-C
Sample Name:
Data Collected on:
nmr13-vnmrs400
Archive directory:
Sample directory:
FidFile: CARBON
Pulse Sequence: CARBON (s2pul)
Solvent: cdcl3
Data collected on: Mar 19 2016
ppm
220
200
180
160
140
120
100
80
60
40
20

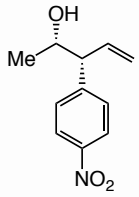

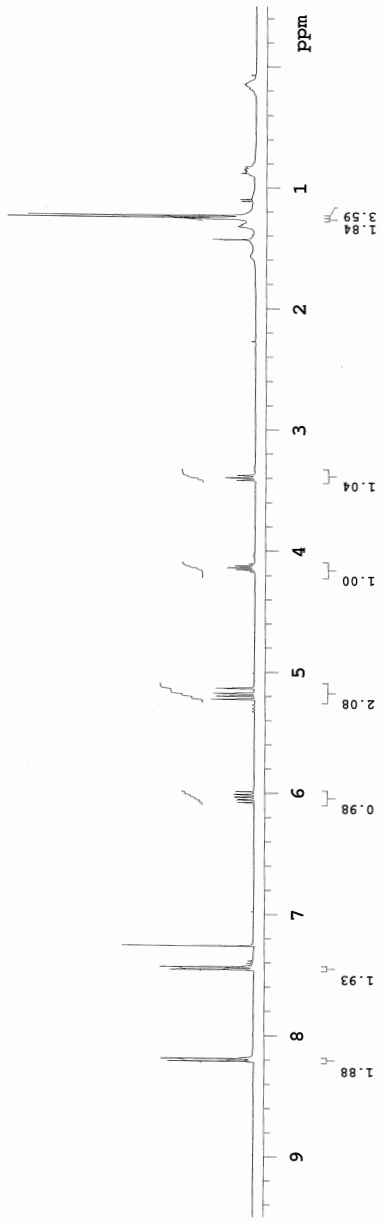

JL-IV-231-2-oxi-PD

Sample Name:
JL-IV-231-2-oxi-PD
Data Collected on:
nmr13-vnmrs400
Archive directory:

Sample directory:

FidFile: PROTON

Pulse Sequence: PROTON (s2pul)
Solvent: cdcl3
Data collected on: Apr 2 2016

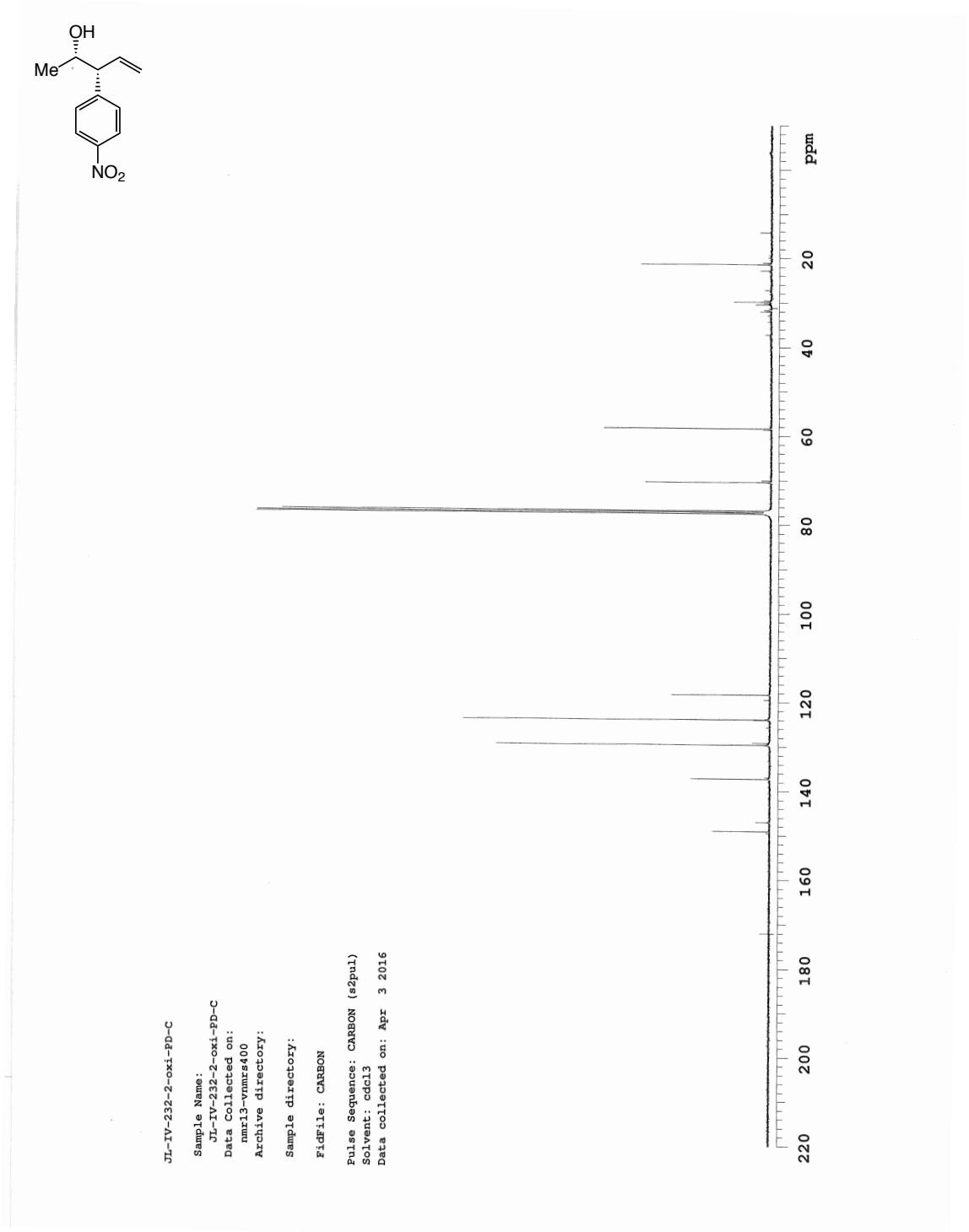
OH
Me
NO2
JL-IV-232-2-oxi-PD-C
Sample Name:
JL-IV-232-2-oxi-PD-C
Data Collected on:
nmr13-vnmrs400
Archive directory:
Sample directory:
FidFile: CARBON
Pulse Sequence: CARBON (s2pul)
Solvent: cdcl3
Data collected on: Apr 3 2016
220
200
180
160
140
120
100
80
60
40
20
ppm

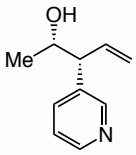

JL-V-86-2-oxi-PD

Sample Name:
JL-V-86-2-oxi-PD
Data Collected on:
nmr13-vnmrs400
Archive directory:

Sample directory:

FidFile: PROTON

Pulse Sequence: PROTON (s2pul)
Solvent: cdcl3
Data collected on: Aug 19 2016

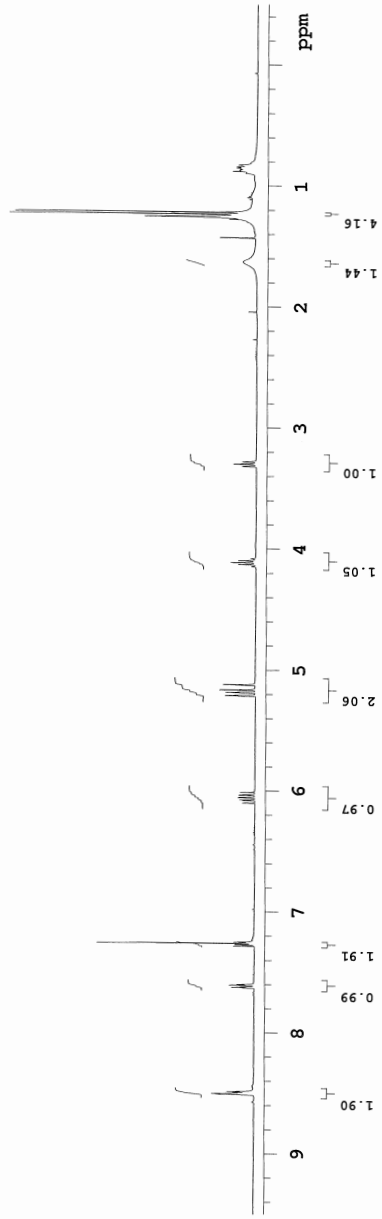

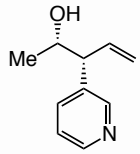

JL-V-86-2-oxi-PD-C

Sample Name:
JL-V-86-2-oxi-PD-C
Data Collected on:
nmr13-vnmrs400
Archive directory:

Sample directory:

FidFile: CARBON

Pulse Sequence: CARBON (s2pul)
Solvent: cdcl3
Data collected on: Aug 20 2016

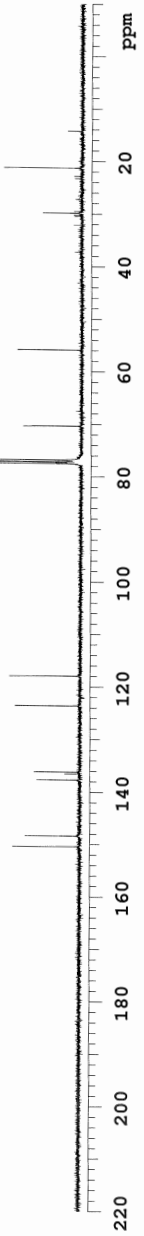

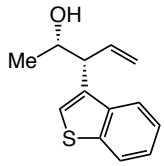

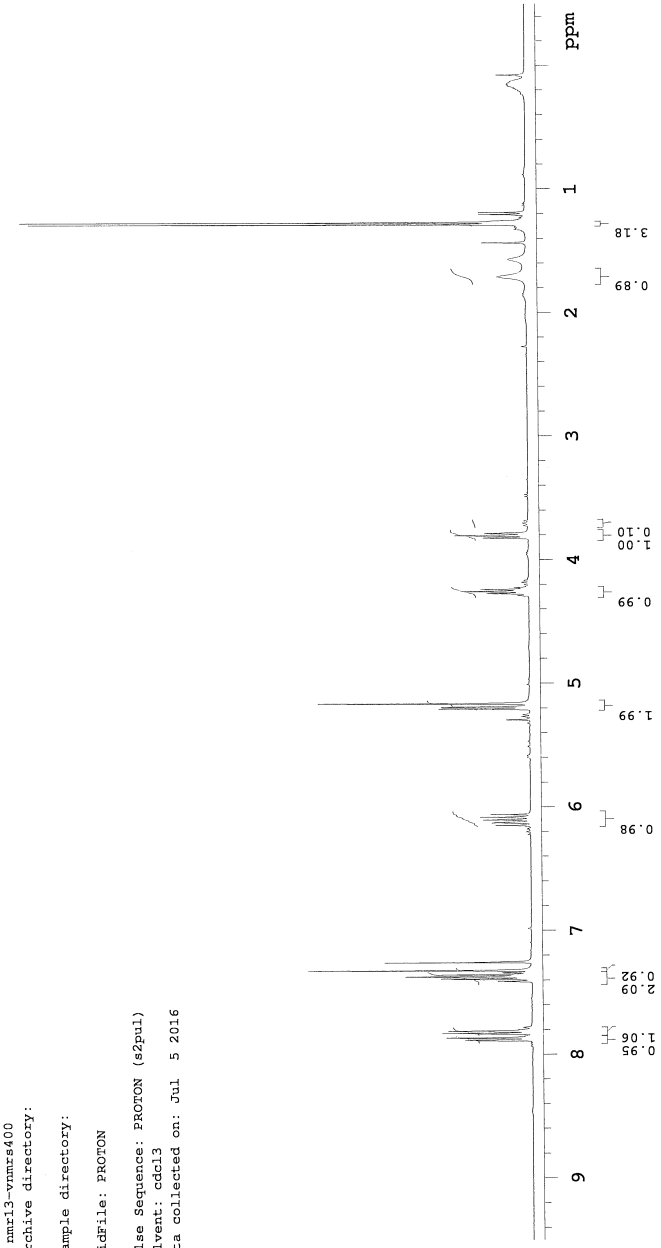

JL-V-38-2-oxi-PD

Sample Name:
JL-V-38-2-oxi-PD
Data Collected on:
nmr13-vnmrs400
Archive directory:

Sample directory:

FidFile: PROTON

Pulse Sequence: PROTON (s2pul)
Solvent: cdcl3
Data collected on: Jul 5 2016

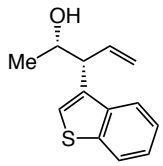
OH
Me
S

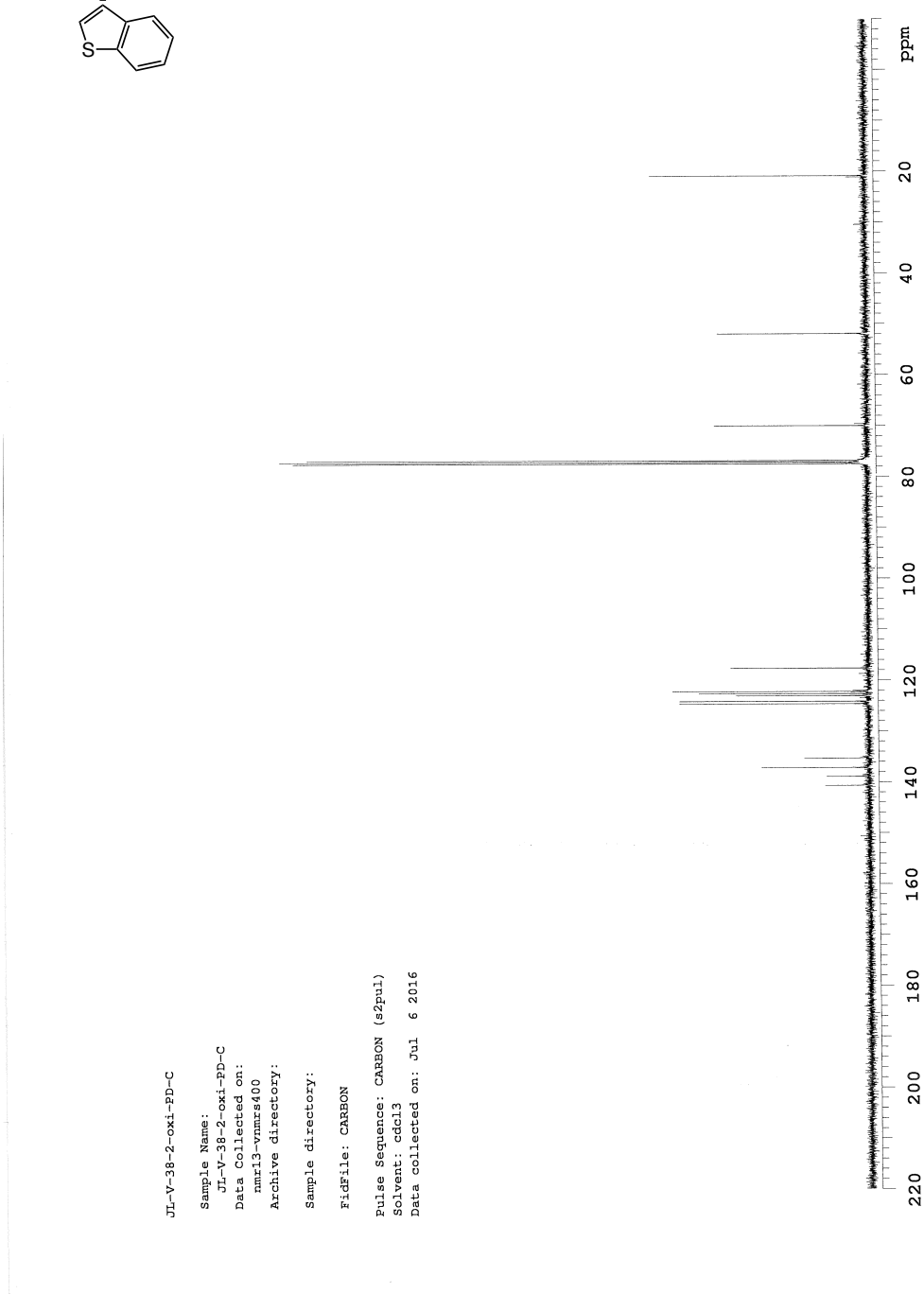
JL-V-38-2-oxi-PD-C
Sample Name:
JL-V-38-2-oxi-PD-C
Data Collected on:
nmr13-vnmrs400
Archive directory:
Sample directory:
FidFile: CARBON
Pulse Sequence: CARBON (s2pul)
Solvent: cdcl3
Data collected on: Jul 6 2016
ppm
220
200
180
160
140
120
100
80
60
40
20

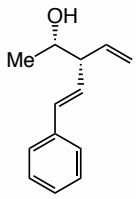

Agilent Technologies

JL-V-66PD

Sample Name:
JL-V-66PD
Data Collected on:
nmr18-vnmrs500
Archive directory:

Sample directory:

FidFile: PROTON

Pulse Sequence: PROTON (s2pul)
Solvent: cdcl3
Data collected on: Aug 4 2016

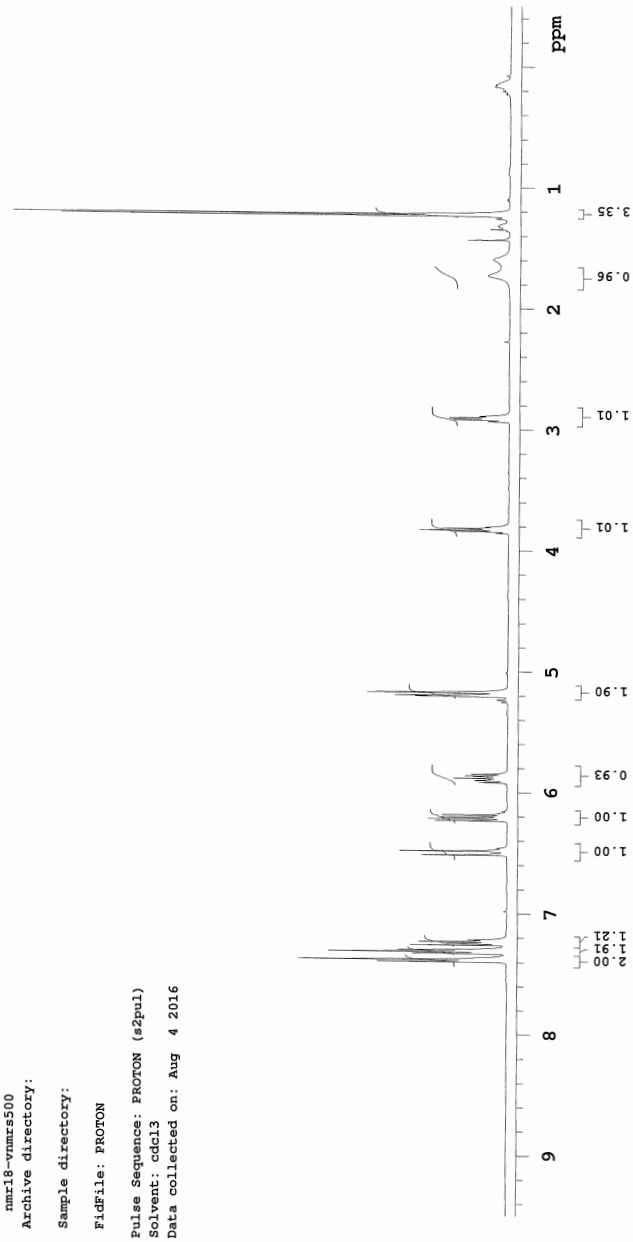

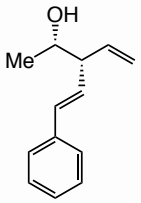
OH
Me

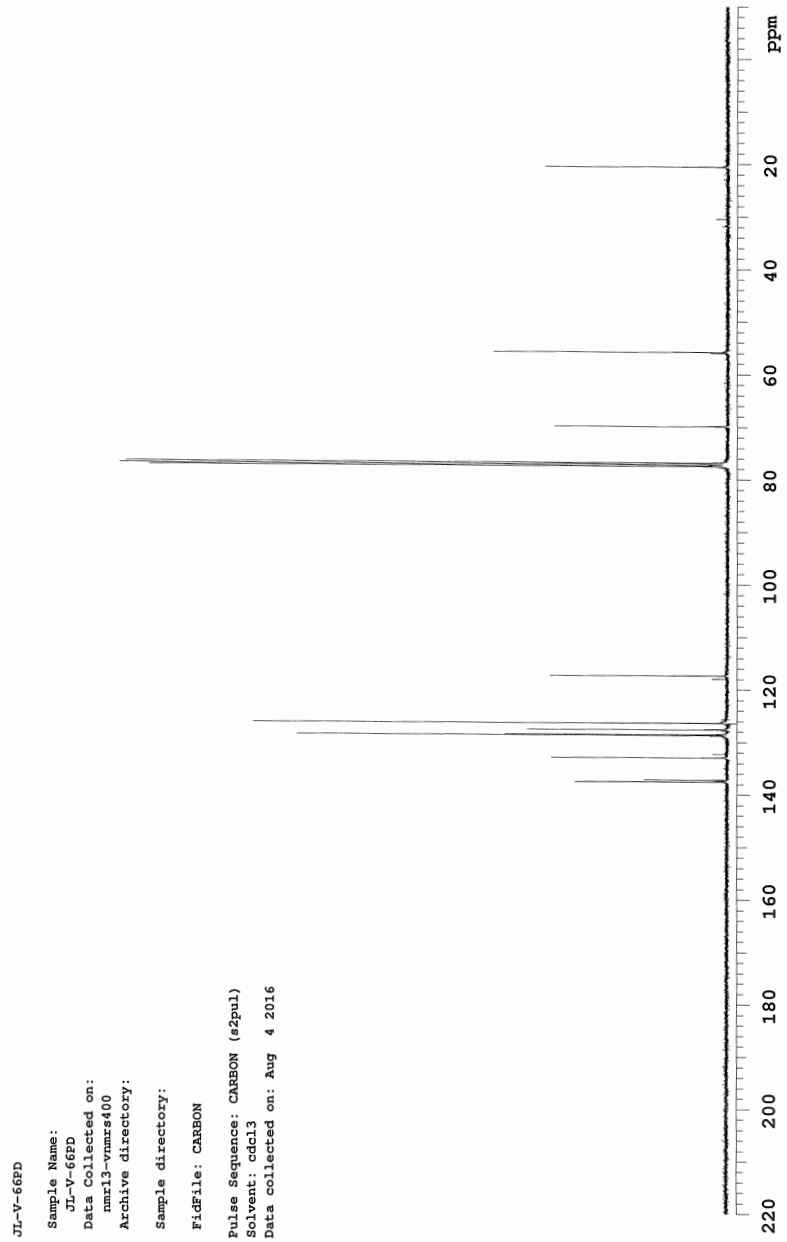
JL-V-66PD
Sample Name:
JL-V-66PD
Data Collected on:
nmr13-vnmrs400
Archive directory:
Sample directory:
FidFile: CARBON
Pulse Sequence: CARBON (s2pul)
Solvent: cdcl3
Data collected on: Aug 4 2016
ppm
220
200
180
160
140
120
100
80
60
40
20

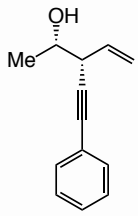

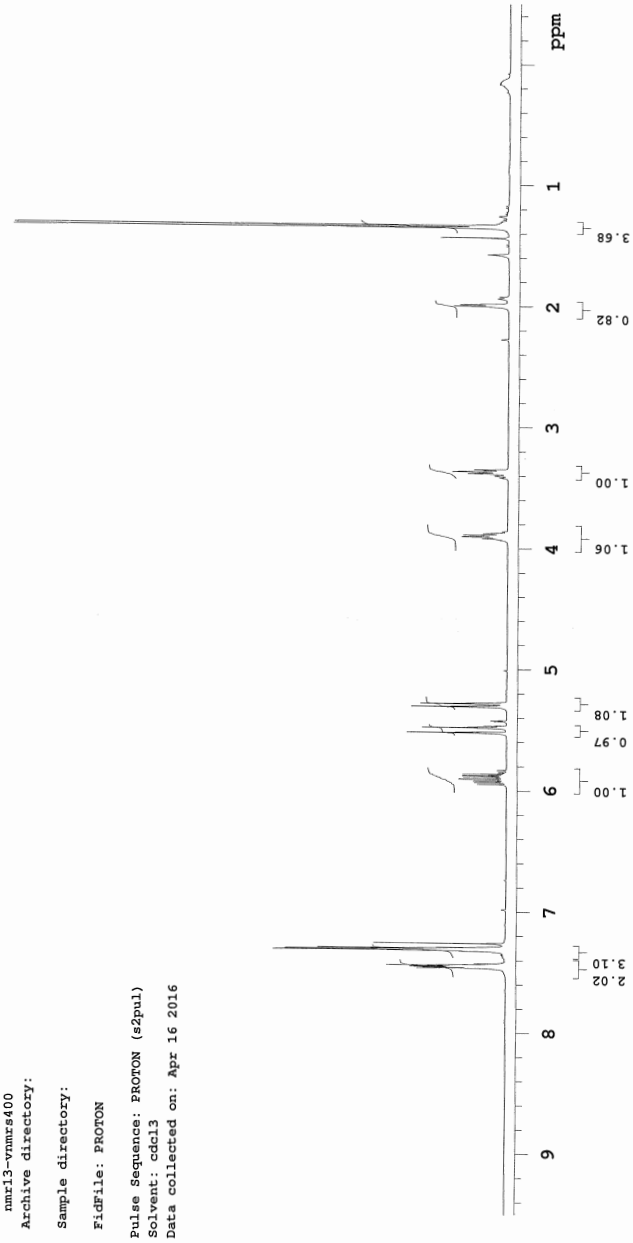

JL-IV-247-2-oxi-PD

Sample Name:
JL-IV-247-2-oxi-PD
Data Collected on:
nmr13-vnmrs400
Archive directory:

Sample directory:

FidFile: PROTON

Pulse Sequence: PROTON (s2pul)
Solvent: cdcl3
Data collected on: Apr 16 2016

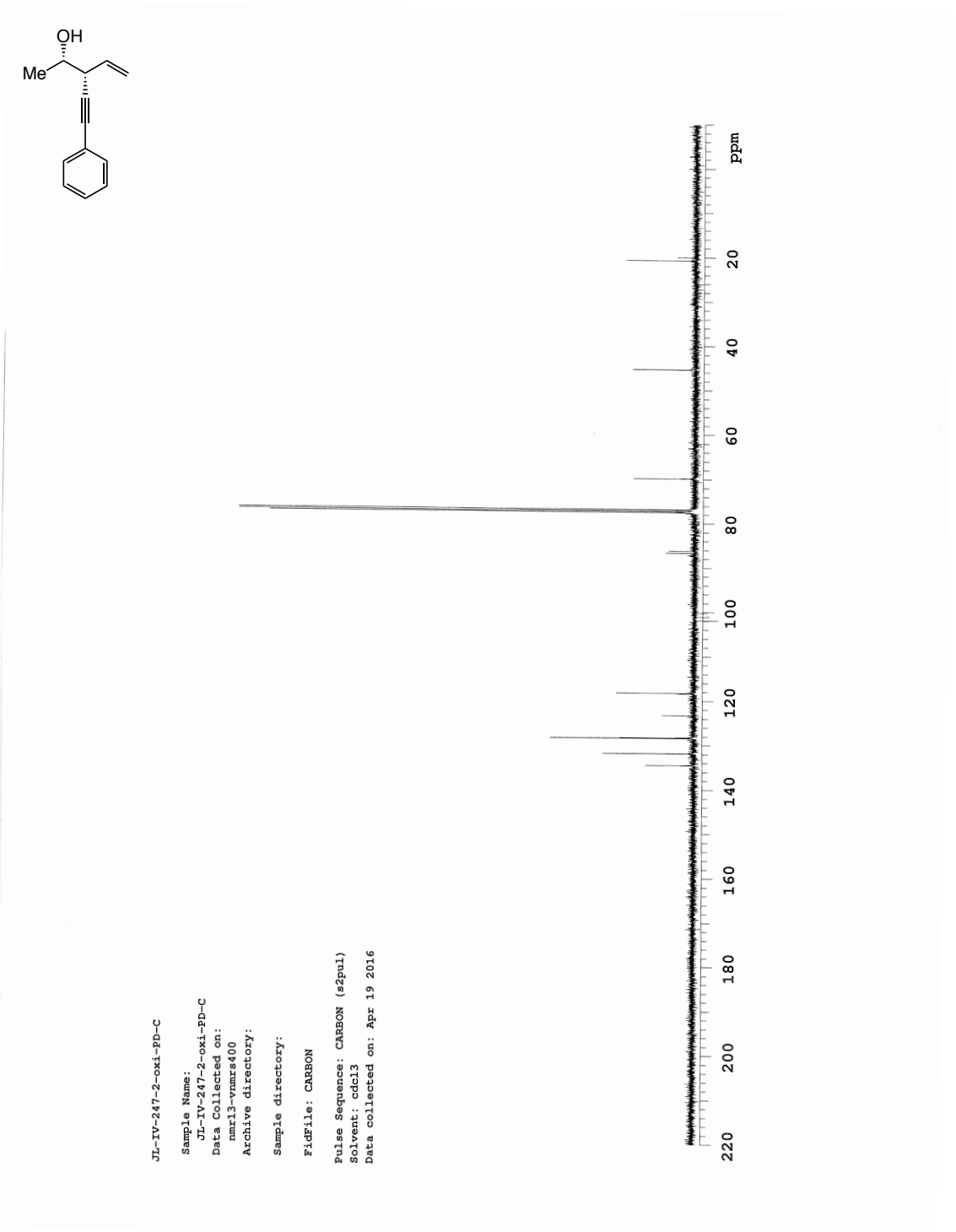
JL-IV-247-2-oxi-PD-C
Sample Name:
JL-IV-247-2-oxi-PD-C
Data Collected on:
nmr13-vnmrs400
Archive directory:
Sample directory:
FidFile: CARBON
Pulse Sequence: CARBON (s2pul)
Solvent: cdcl3
Data collected on: Apr 19 2016
OH
Me
ppm
220
200
180
160
140
120
100
80
60
40
20

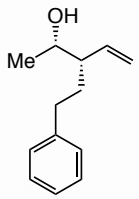

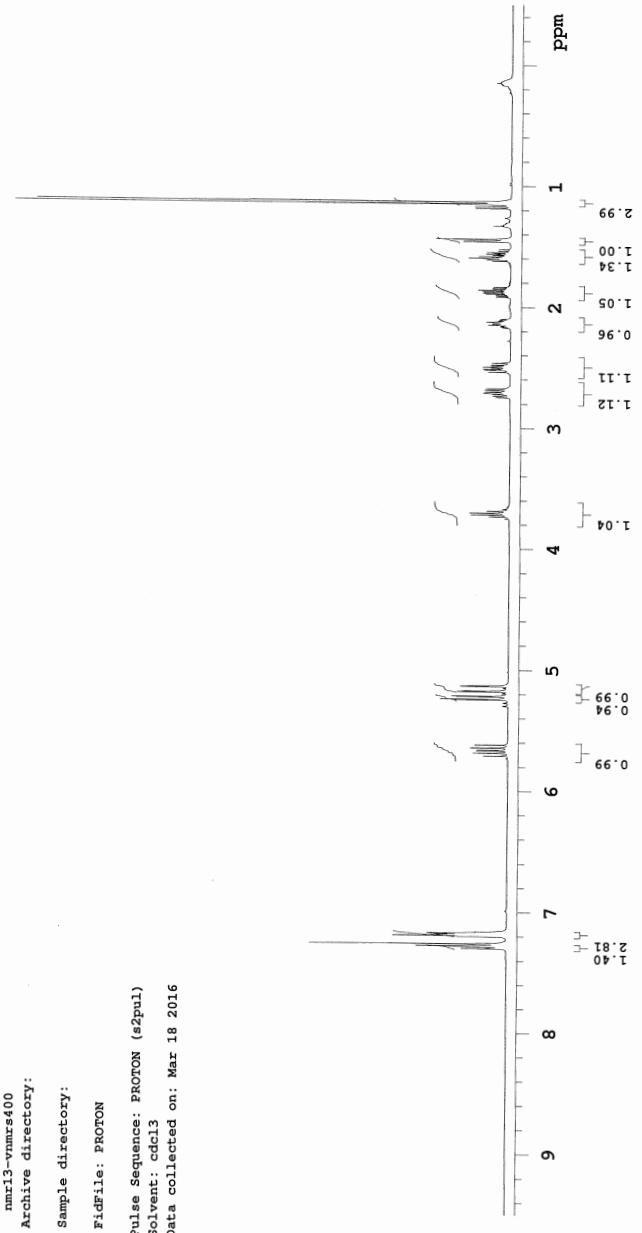

JL-IV-219-2-oxi-PD

Sample Name:
JL-IV-219-2-oxi-PD
Data Collected on:
nmr13-vnmrs400
Archive directory:

Sample directory:

FidFile: PROTON

Pulse Sequence: PROTON (s2pul)
Solvent: cdcl3
Data collected on: Mar 18 2016

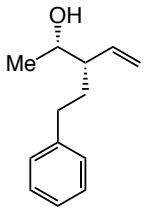
OH
Me

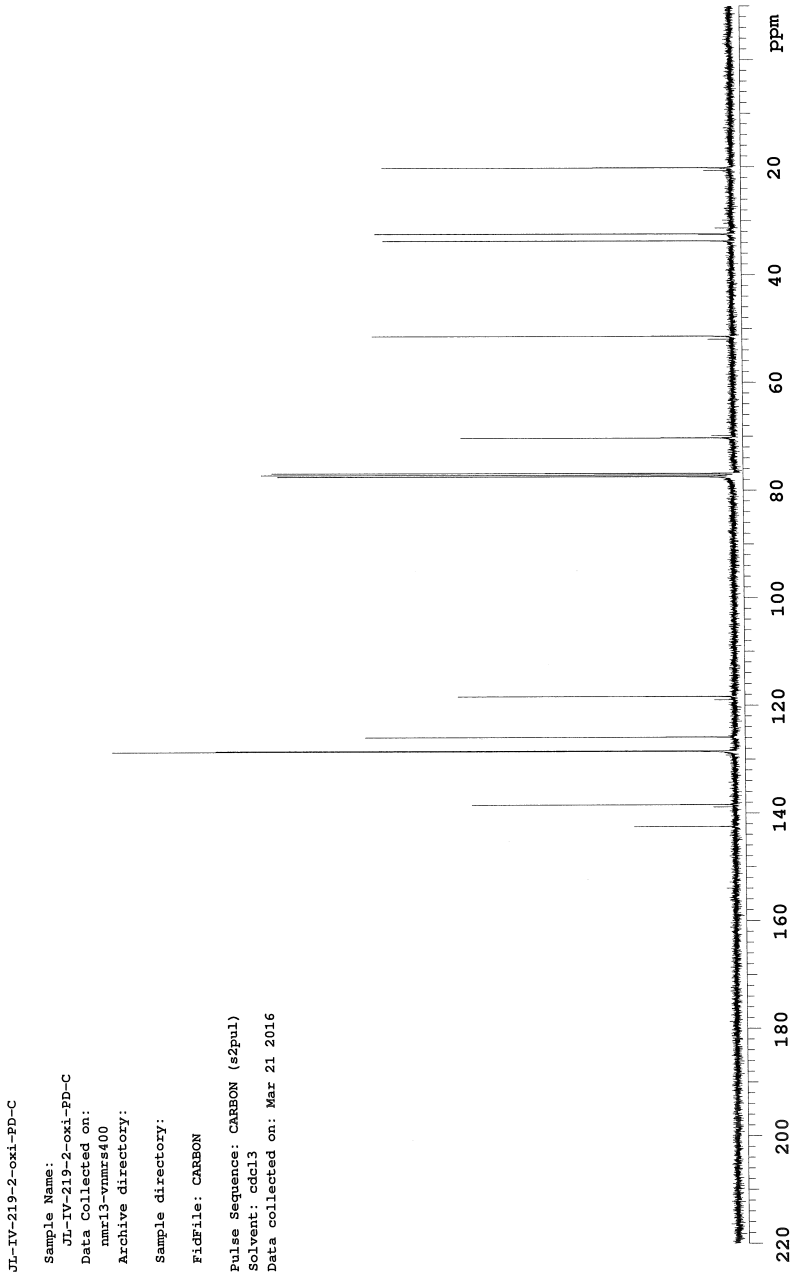
JL-IV-219-2-oxi-PD-C
Sample Name:
JL-IV-219-2-oxi-PD-C
Data Collected on:
nmr13-vnmrs400
Archive directory:
Sample directory:
FidFile: CARBON
Pulse Sequence: CARBON (s2pul)
Solvent: cdcl3
Data collected on: Mar 21 2016
ppm
220
200
180
160
140
120
100
80
60
40
20

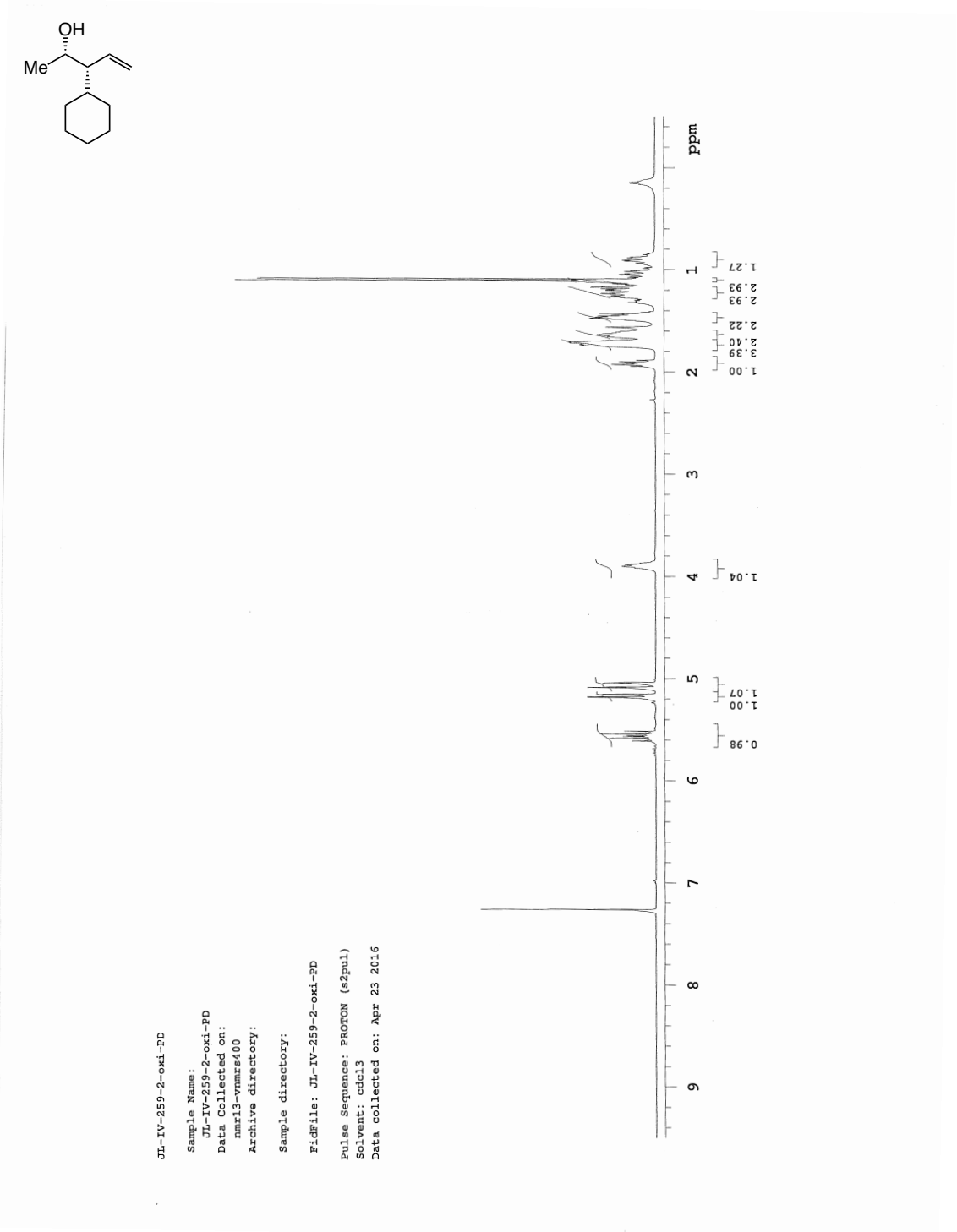
OH
Me
JL-IV-259-2-oxi-PD
Sample Name:
JL-IV-259-2-oxi-PD
Data Collected on:
nmr13-vnmrs400
Archive directory:
Sample directory:
FidFile: JL-IV-259-2-oxi-PD
Pulse Sequence: PROTON (s2pul)
Solvent: cdcl3
Data collected on: Apr 23 2016
ppm
9
8
7
6
5
4
3
2
1
0.98
1.00
1.07
1.04
1.00
3.39
2.40
2.22
2.93
2.93
1.27

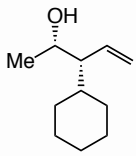
OH
Me

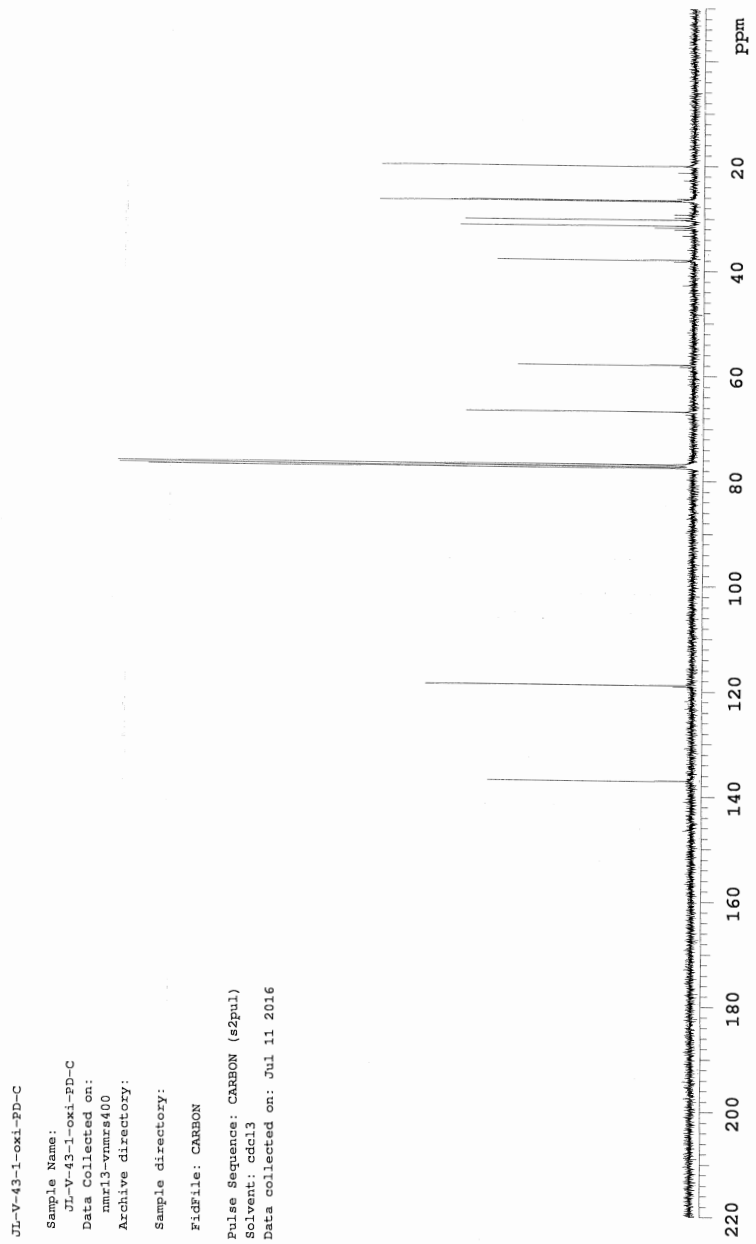
JL-V-43-1-oxi-PD-C
Sample Name:
JL-V-43-1-oxi-PD-C
Data Collected on:
nmr13-vnmrs400
Archive directory:
Sample directory:
FidFile: CARBON
Pulse Sequence: CARBON (s2pul)
Solvent: cdcl3
Data collected on: Jul 11 2016
ppm
220
200
180
160
140
120
100
80
60
40
20

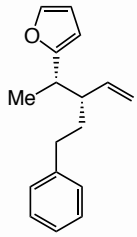

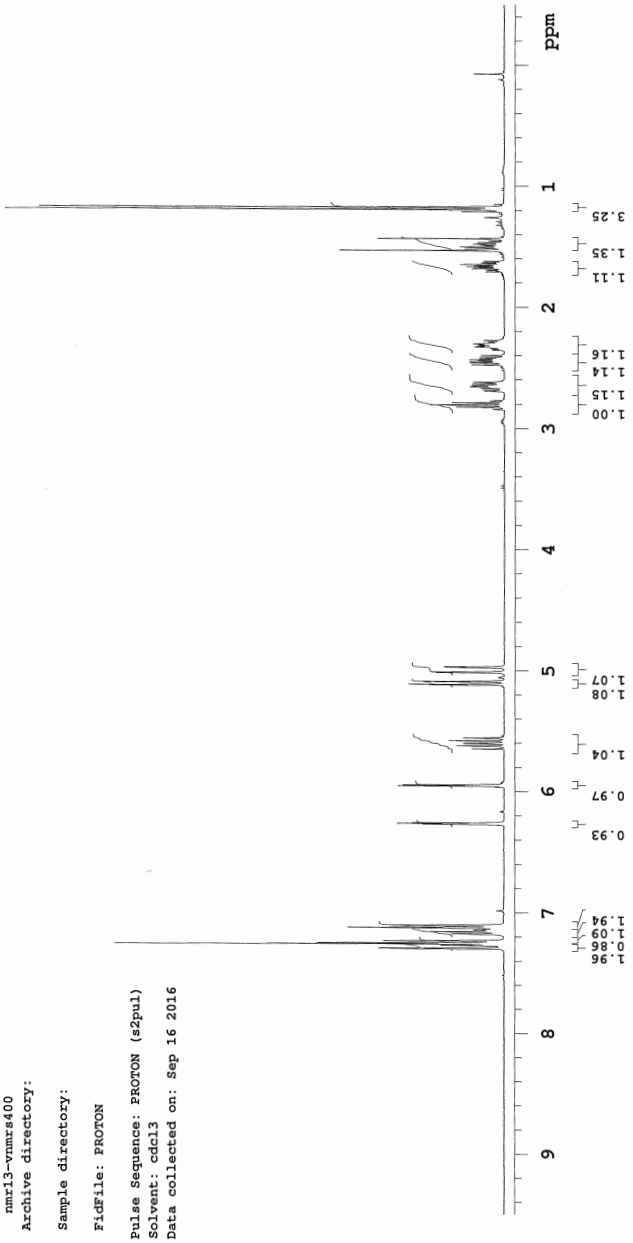

JL-V-109-2PD

Sample Name:
JL-V-109-2PD
Data Collected on:
nmr13-vnmrs400
Archive directory:

Sample directory:

FidFile: PROTON

Pulse Sequence: PROTON (s2pul)
Solvent: cdcl3
Data collected on: Sep 16 2016

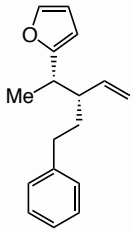
O
Me

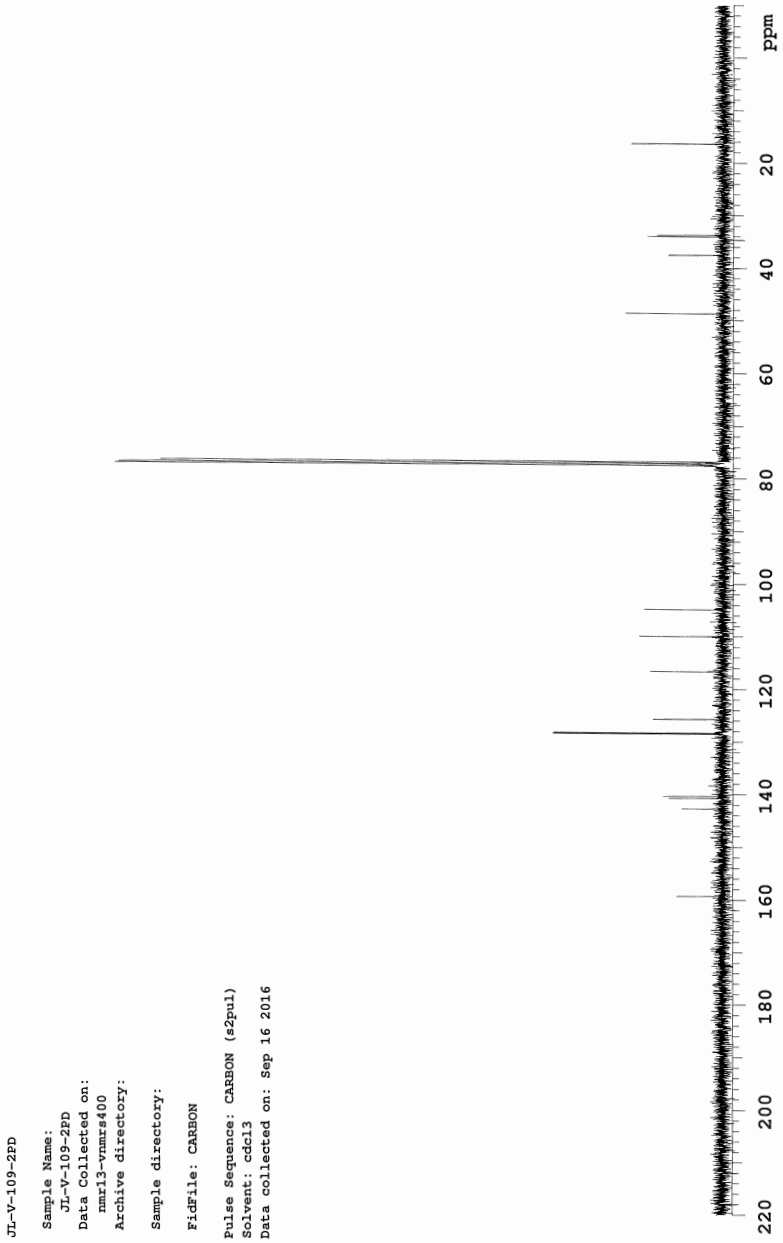
JL-V-109-2PD
Sample Name:
JL-V-109-2PD
Data Collected on:
nmr13-vnmrs400
Archive directory:
Sample directory:
FidFile: CARBON
Pulse Sequence: CARBON (s2pul)
Solvent: cdcl3
Data collected on: Sep 16 2016
220
200
180
160
140
120
100
80
60
40
20
ppm

CHAPTER 3

Enantioenriched Halogen-Substituted Alkenes through NHC–Cu-Catalyzed Borylation/Dehalogenation and Their Applications

3.1 Introduction

Because of their unique properties, mono- and difluoroalkenes have emerged as an important class of building blocks for fluorine-containing functional polymers[1] and biologically active molecules in medicine and agriculture.[2,3] In this respect, fluoro- and other halo-alkenyl compounds are of great interest in chemical synthesis. However, reported methods to prepare enantioenriched difluoroalkenes are scarce and often require the use of precious transition metals and very high/low temperatures.[3] To solve these challenges, we have developed a highly efficient, regio-, and enantioselective boron allylic substitution involving CF_3-alkenes and other halogen-substituted olefins by using an abundant copper-based catalyst under mild conditions.

---

(1) Souzy, B.; Ameduri, B.; Boutevin B. *Prog. Polym. Sci.* **2004,** *29*, 75–106.
(2) (a) Bobek, M.; Kavai, I.; Clercq, E. De. *J. Med. Chem.* **1987,** *30*, 1494–1497. (b) Moore, W. R.; Schatzman, G. L.; Jarvi, E. T.; Gross, R. S.; McCarthy, J. R. *J. Am. Chem. Soc.* **1992,** *114,* 360–361.
(3) Zhang, X.; Cao, S. *Tetrahedron Lett.* **2017,** *58*, 375–392.

3.2 Background

The application of 1,1-difluoroalkenes in the fields of fine chemicals, pharmaceuticals, pesticides, and materials science is very broad (Scheme 3.1a).[4] These difluorinated synthetic analogues usually process enhanced biological activities.[3] In addition, they are readily converted to various monofluoroalkenes and are widely used in medicine and organic chemistry (Scheme 3.1a and Scheme 3.1b).[3, 5] Traditionally,

Scheme 3.1. Bioactive Alkenyl Fluorides

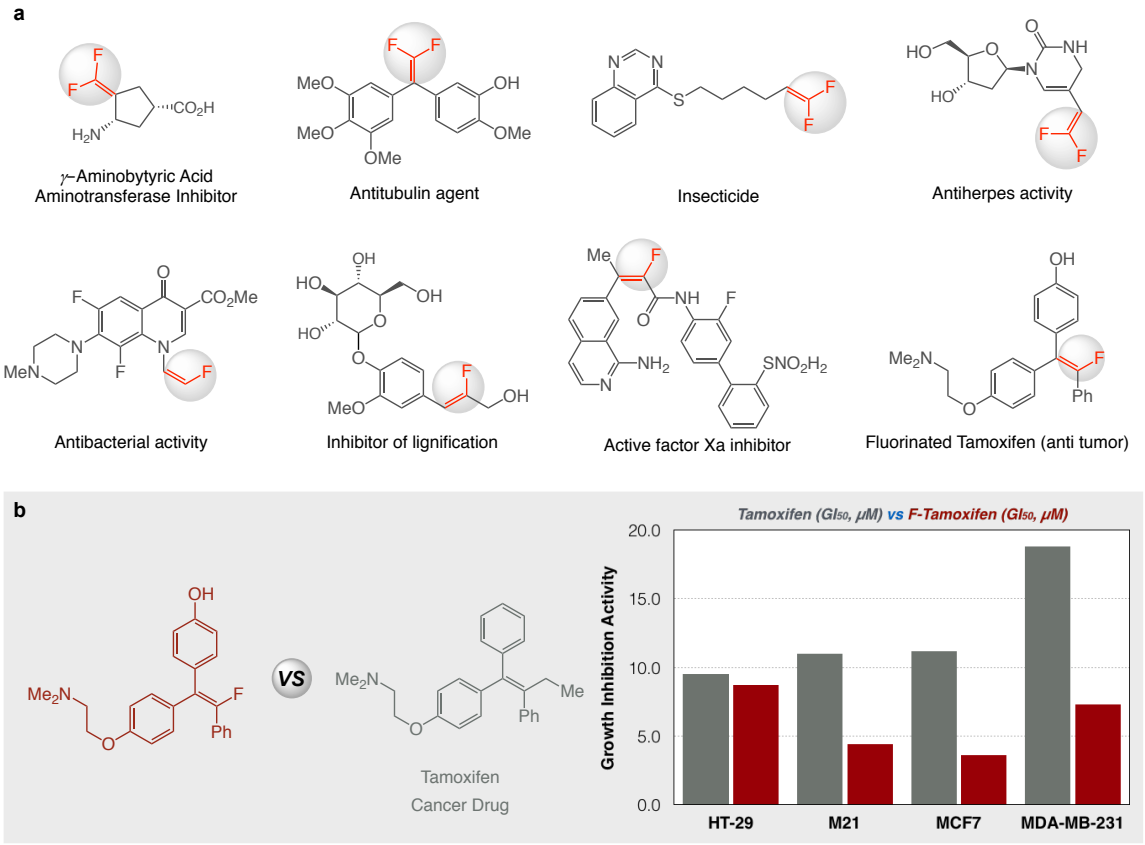

(4) (a) Pan, Y.; Qiu, J.; Silverman R. B. *J. Med. Chem.* **2003,** *46,* 5292–5293. (b) Messaoudi, S.; Tréguier, B.; Hamze, A.; Provot, O.; Peyrat, J. -F.; De Losada, J. R.; Liu, J. -M.; Bignon, J.; Wdzieczak-Bakala, J.; Thoret, S.; Dubois, J.; Brion, J. -D.; Alami, M. *J. Med. Chem.* **2009,** *52,* 4538–4542.

(5) (a) Malo-Forest, B.; Landelle, G.; Roy, J. -A.; Lacroix, J.; Gaudreault, R. C.; Paquin, J. -F. *Bioorg. Med. Chem. Lett.* **2013,** *23,* 1712–1715. (b) Eddarir, S.; Abdelhadi, Z.; Rolando, C. *Tetrahedron Lett.* **2001,** *42,* 9127–9130. (c) Song, Y.; Clizbe, L.; Bhakta, C.; Teng, W.; Li, W.; Wong, P.; Huang, B.; Sinha, U.; Park, G.; Reed, A.; Scarborough, R. M.; Zhu, B. -Y. *Bioorg. Med. Chem. Lett.* **2002,** *12,* 2043–2046. (d) Asahina, Y.; Iwase, K.; Iinuma, F.; Hosaka, M.; Ishizaki, T. *J. Med. Chem.* **2005,** *48,* 3194–3202.

fluoroalkenes were generated through Wittig,[6] Julia/Julia-Kocienski,[7] or Honer-Wadsworth-Emmons type difluoromethylenation[8] which suffered from a number of problems such as multi-step reagent synthesis, limited functional group tolerance and

Scheme 3.2. Classic Methods for Difluoromethylenation

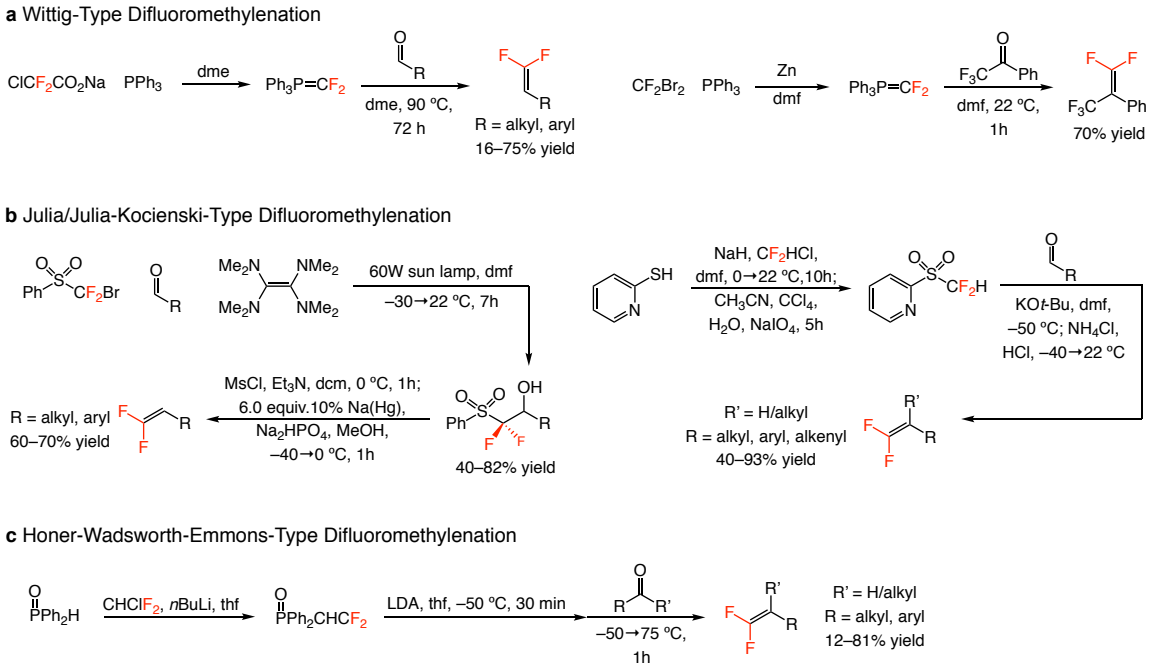

(6) (a) Fuqua, S. A.; Duncan, W. G.; Silverstein, R. M. *Tetrahedron Lett.* **1964,** *5,* 1461–1463. (b) Brahms, D. L. S.; Dailey, W. P. *Chem Rev.* **1996,** *96,* 1585–1632. (c) Ni, C.; Hu, J. *Synthesis.* **2014,** 842–863. (d) Fuqua, S. A.; Duncan, W. G.; Silverstein, R. M. *J. Org. Chem.* **1965,** *30,* 1027–1029. (e) Herkes, F. E.; Burton, D. J. *J. Org. Chem.* **1967,** *32,* 1311–1318. (f) Naae, D. G.; Burton, D. J. *J. Fluorine Chem.* **1971,** *72,* 123–125. (g) Zheng, J.; Cai, J.; Lin, J. -H.; Guo, Y.; Xiao, J. -C. *Chem. Commun.* **2013,** *49,* 7513–7515. (h) Li, Q.; Lin, J. -H.; Deng, Z. –Y.; Zheng, J.; Cai, J.; Xiao, J. -C. *J. Fluorine Chem.* **2014,** *163,* 38–41. (i) Loska, R.; Szachowicz, K.; Szydlik, D. *Org Lett.* **2013,** *15,* 5706–5709. (j) Naae, D. G.; Burton D. J. *Synth. Commun.* **1973,** *3,* 197–200. (k) Bhadury, P. S.; Palit, M.; Sharma, M.; Raza, S. K.; Jaiswal, D. K. *J. Fluorine Chem.* **2002,** *116,* 75–80. (l) Wheaton, G. A.; Burton, D. J. *J. Org. Chem.* **1983,** *48,* 917–927. (m) Speziale, A. J.; Ratts, K. W. *J. Am. Chem. Soc.* **1962,** *84,* 854–859. (n) Zheng, J.; Lin, J. -H.; Cai, J.; Xiao, J. -C. *Chem. Eur. J.* **2013,** *19,* 15261–15266. (o) Nowak, I.; Robins, M. J. *Org. Lett.* **2005,** *7,* 721–724. (p) Thomoson, C. S.; Martinez, H.; Dolbier, Jr W. R. *J. Fluorine Chem.* **2013,** *150,* 53–59. (q) Wang, F.; Li, L.; Ni, C.; Hu, J. *Beilstein J. Org. Chem.* **2014,** *10,* 344–351. (r) Aikawa, K.; Toya, W.; Nakamura, Y.; Mikami, K. *Org. Lett.* **2015,** *17,* 4996–4999.

(7) (a) Prakash, G. K. S.; Wang, Y.; Hu, J.; Olah, G. A. *J. Fluorine Chem.* **2005,** *126,* 1361–1367. (b) Zhao, Y.; Huang, W.; Zhu, L.; Hu, J. *Org Lett.* **2010,** *12,* 1444–1447. (c) Gao, B.; Zhao, Y.; Hu, M.; Ni, C.; Hu, J. *Chem. Eur. J.* **2014,** *20,* 7803–7810. (d) Gao, B.; Zhao, Y.; Hu, J.; Hu J. *Org. Chem. Front.* **2015,** *2,* 163–168. (e) Gao, B.; Hu, J.; Zhao, Y.; Hu, J. *Tetrahedron Lett.* **2015,** *56,* 4180–4183. (f) Wang, X. -P.; Lin, J. -H.; Xiao, J. -C.; Zheng, X. *Eur. J. Org. Chem.* **2014,** 928–932.

(8) (a) Obayashi, M.; Ito, E.; Matsui, K.; Kondo, K. *Tetrahedron Lett.* **1982,** *23,* 2323–2326. (b) Edwards, M. L.; Stemerick, D. M.; Jarvi, E. T.; Matthews, D. P.; McCarthy, J. R. *Tetrahedron Lett.* **1990,** *31,* 5571–5574. (c) Tsai, H. -J. *Phosphorus, Sulfur Silicon Relat. Elem.* 1997, 122, 247–259. (d) Piettre, S. R.; Cabanas, L. *Tetrahedron Lett.* **1996,** *37,* 5881–5884.

harsh reaction conditions (Scheme 3.2). However, introducing a new stereogenic center using the aforementioned methods is not possible. The development of catalytic enantioselective transformation to generate di- and monofluoroalkenes is extreme difficult, and there is only one study of involving arylation/defluorination of CF_3-alkenes that deliver enantioenriched 1,1-difluoroalkenes. However, the method entails the use of precious rhodium-based catalyst and is limited to aryl group additions (see section 3.2.2 for further discussions).[9]

3.2.1 Catalytic S_N2' Nucleophilic Addition to Trifluoromethyl Alkenes

In addition to the traditional protocols mentioned above, there are several alternative routes to prepare germinal difluoroalkenes. However, only a few catalytic strategies have been developed with limitations such as poor functional group compatibility and high/low temperature requirement. The first case of catalytic S_N2' selective nucleophilic addition to CF_3-alkenes were developed by Murakami and co-workers in 2008.[10] The reaction of trifluoromethyl alkenes with aryl–B(neo)

Scheme 3.3. Rodium-Catalyzed Arylation/Defluorination of Trifluoromethyl Alkenes

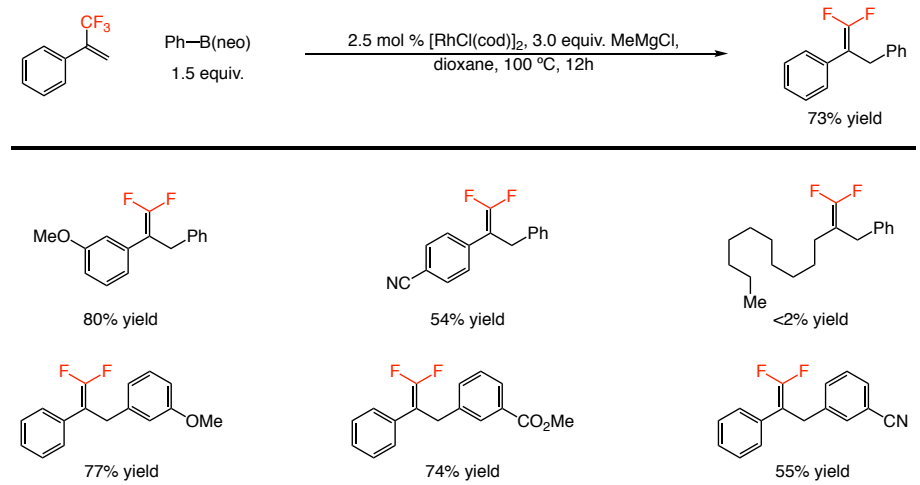

neo, neopentyl glycolato; cod, 1,5-cycloocadiene

(9) Huang, Y.; Hayashi, T. *J. Am. Chem. Soc.* **2016,** *138,* 12340–12343.
(10) Miura, T.; Ito, Y.; Murakami, M. *Chem. Lett.* **2008,** *37,* 1006–1007.

(neo, neopentyl glycolato) in the presence of a rhodium-based catalyst and excess amounts of additive (e.g., 3.0 equiv. of MeMgCl) under 100 ºC gave 1,1-difluoroalkenes in 54–80% yield although there was no reaction with alkyl substituted substrates (Scheme 3.3). In 2011, our group reported the first catalytic B(pin) allylic substitution with a CF_3-

Scheme 3.4. First Catalytic B(pin) Allylic Substitution with a CF_3-Alkene

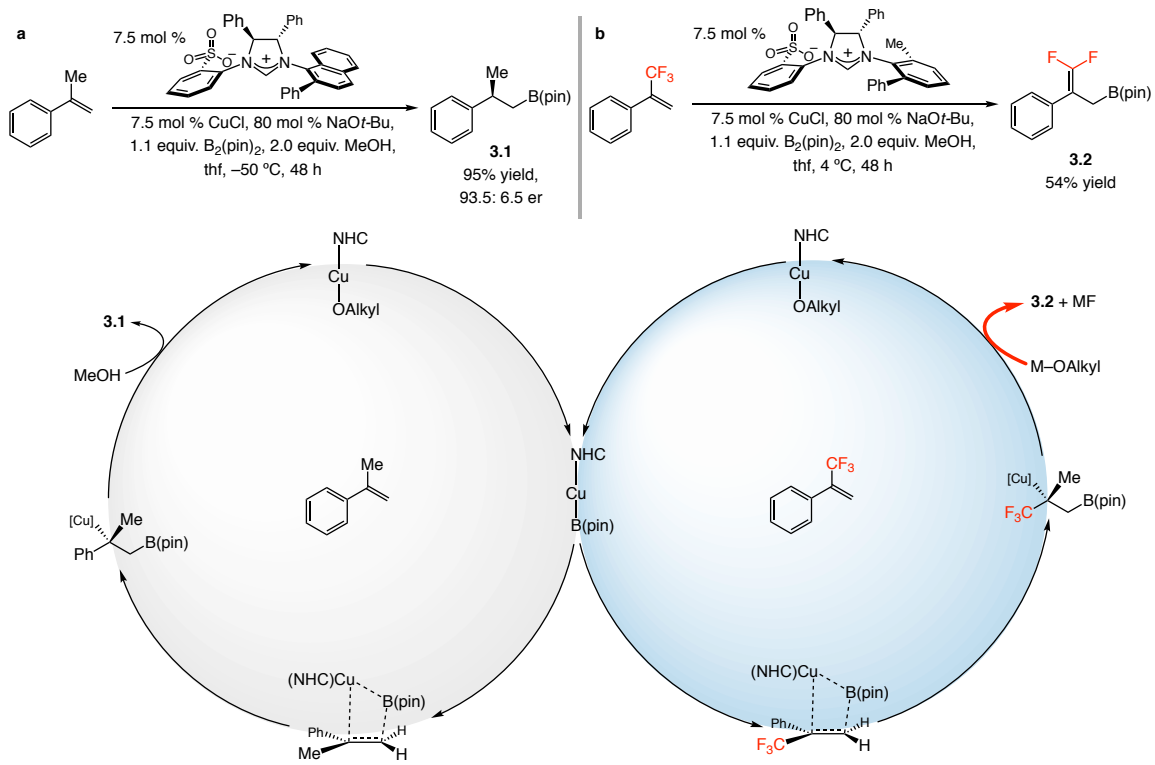

pin, pinacolato; NHC, *N*-heterocyclic carbene; M, metal

alkene (Scheme 3.4b) using a more abundant copper-based catalyst.[11] Under similar reaction conditions for enantioselective protoboration of 1,1-disubstituted aryl alkenes (Scheme 3.4a), the organocopper species generated from Cu–B(pin) addition to α-CF_3 styrene underwent metal fluoride elimination to form difluoroallylboronate compound **3.2** (Scheme 3.4b). Another example of catalytic boration/defluorination of trifluoromethyl alkenes was described recently.[12] Transformations were accomplished by 5.0–10 mol %

(11) Coberán, R.; Mszar, N. W.; Hoveyda, A. H. *Angew. Chem. Int, Ed.* **2011,** *50*, 7079–7082.
(12) Liu, Y.; Zhou, Y.; Zhao, Y.; Qu, J. *Org. Lett.* **2017,** *19,* 946–949.

of an iron-based catalyst and stoichiometric amounts of base at 65 ºC with somewhat larger functional group tolerance. However, cyano- and nitro-substituents were

Scheme 3.5. Iron-Catalyzed Boraton/Defluorination of Trifluoromethyl Alkenes

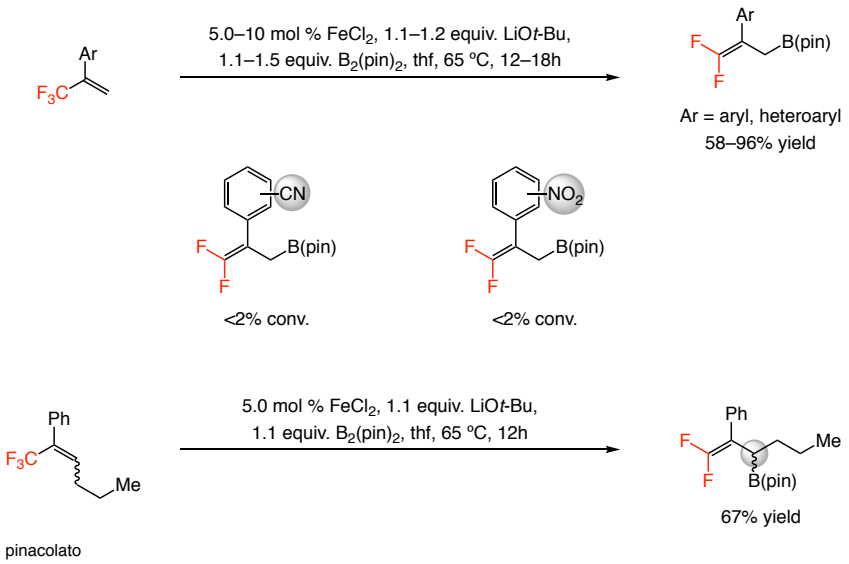

not compatible, and enantioselective allylic borylation still remains to be solved (Scheme 3.5).

3.2.2 Catalytic Enantioselective S_N2' Nucleophilic Addition to Trifluoromethyl Alkenes

The first catalytic enantioselective protocol where 1-(trifluoromethyl) alkenes were converted to enantiopure 1,1-difluoroalkenes was developed by Hayashi and Huang.[9] High efficiency and enantioselectivities were obtained (up to 99.5:0.5 er) in the presence of a chiral diene-rhodium catalyst **Rh-1** (Scheme 3.6). Although elaborate starting materials can be used to form the desired products in excellent yields and selectivities (Scheme 3.6), the method is restricted to aryl group additions to CF_3-alkenes which can limit further product functionalizations compared to boryl allylic substitution (Scheme 3.4 and Scheme 3.5). Moreover, excess amounts of nucleophilic reagent is

required [e.g., 3.0 equivalents of $(ArBO)_3$ or 4.0 equivalents of ArZnCl, Scheme 3.6] for high efficiency.

Scheme 3.6. Enantioselective Rhodium-Catalyzed Arylation/Defluorination of Trifluoromethyl Alkenes

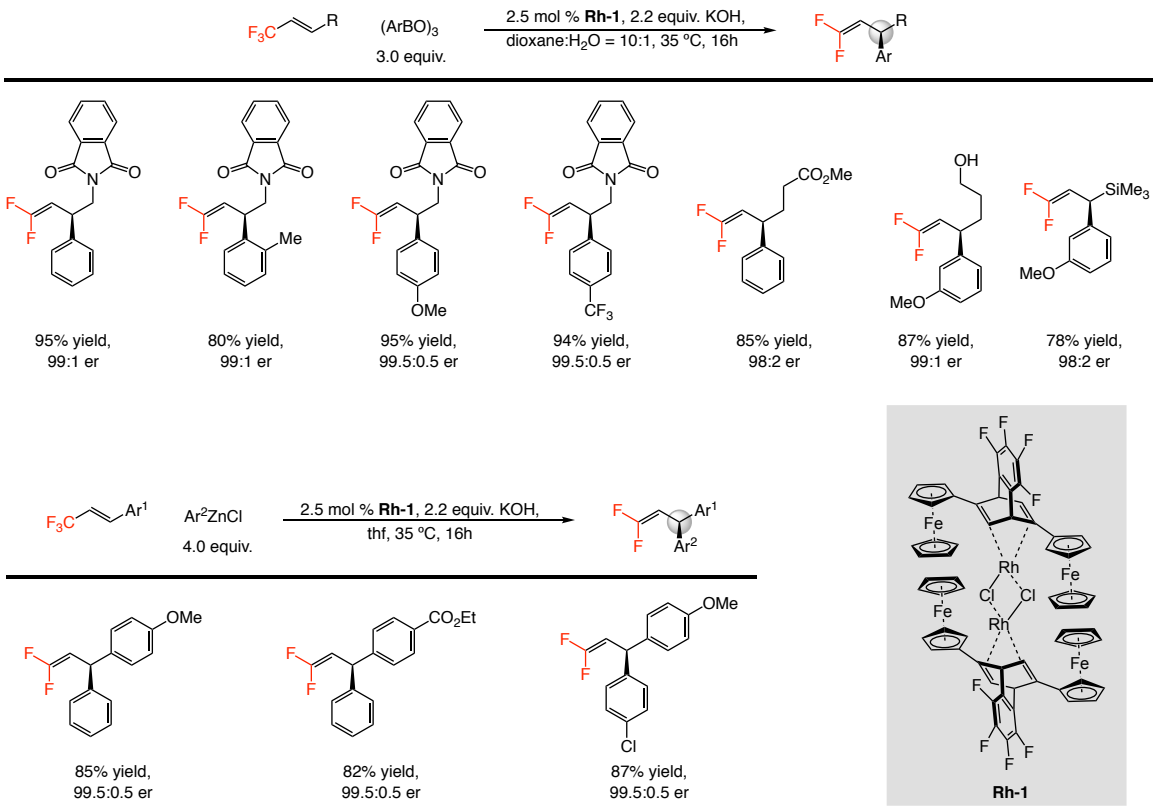

3.2.3 Reaction Design and Utility of Enantioenriched 1,1-Difluoroallyl Boronates

The blueprint of the reaction is generation of a boron-substituted stereogenic carboncenter through highly enantio-, *E*/*Z*-, and S_N2' selective boryl allylic substitution

Scheme 3.7. Design of Reactions that Afford Enantiopure Fluorinated Allylboronates

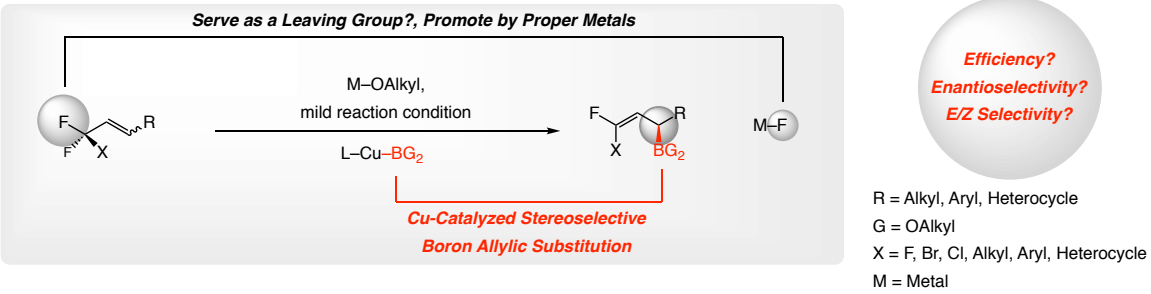

with an abundant and inexpensive copper-based catalyst (Scheme 3.7). Desired products

are particularly interesting because of their unique versatility; they can be converted to a

Scheme 3.8. Possible Functionalizations of Chiral 1,1-Difluoroallyl Boronates

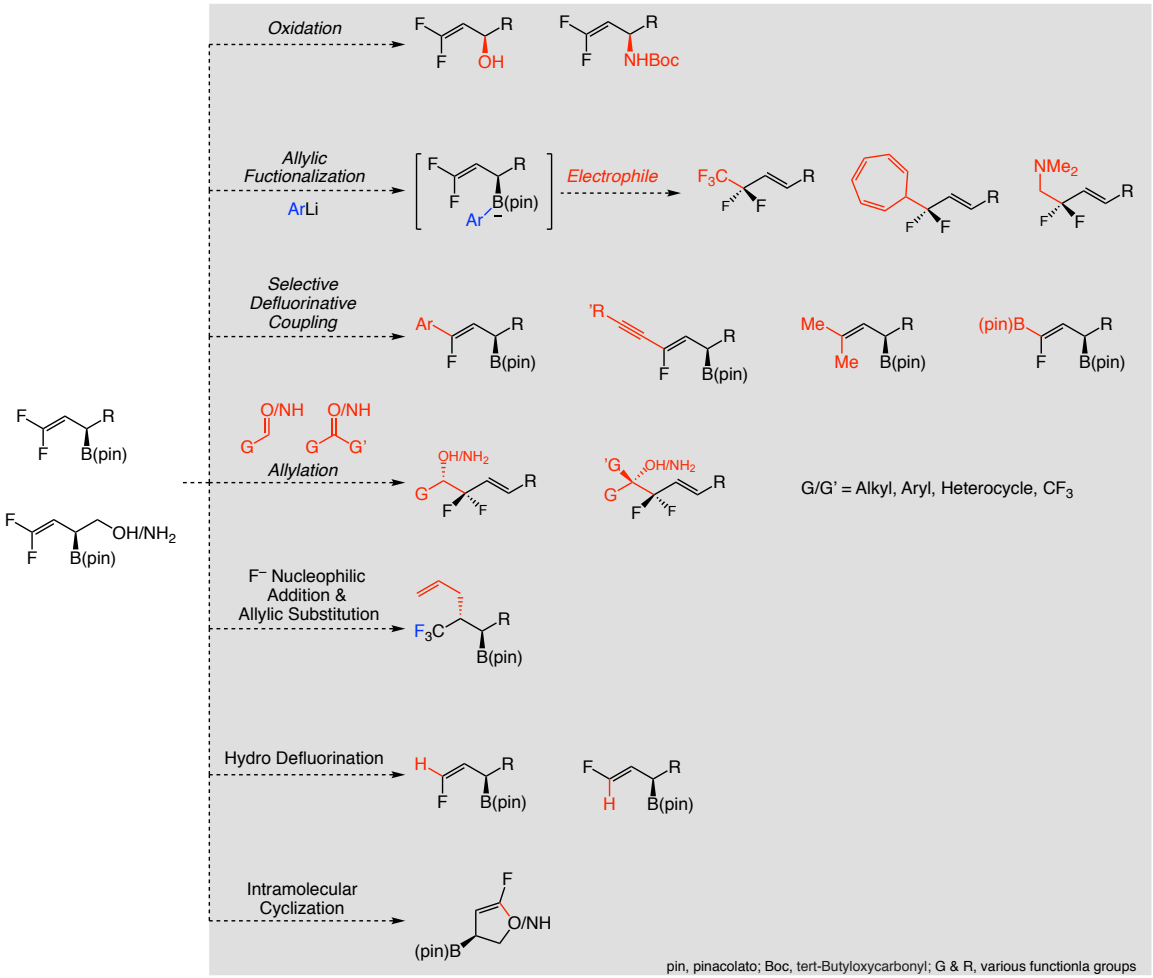

wide variety of desirable molecules through different transformations such as oxidation,[13] allylic functionalization,[14] selective defluorinative coupling,[9, 15] allylation,[16] multi-

(13) (a) Mlynarski, S. N.; Karns, A. S.; Morken, J. P. *J. Am. Chem. Soc.* **2012,** *134,* 16449–16451. (b) Lee, J.; Torker, S.; Hoveyda, A. H. *Angew. Chem. Int. Ed.* **2017,** *56,* 821–826.

(14) García-Ruiz, C.; Chen, J. L. -Y.; Sandford, C.; Feeney, K.; Lorenzo, P.; Berionni, G.; Mayr, H.; Aggarwal, V. K. *J. Am. Chem. Soc.* **2017,** *139,* 15324–15327.

(15) (a) Jin, G.; Zhang, J.; Wu, W.; Cao, S. *J. Fluorine Chem.* **2014,** *168,* 240–246. (b) Thornbury, R. T.; Toste, F. D. *Angew. Chem. Int. Ed.* **2016,** *55,* 11629–11632. (c) Zhang, J.; Dai, W.; Liu, Q.; Cao, S. *Org. Lett.* **2017,** *19,* 3283–3286.

(16) (a) Vieira, E. M.; Snapper, M. L.; Hoveyda,A. H. *J. Am. Chem. Soc.* **2011,** *133,* 3332–3335. (b) Lee, K.; Silverio, D. L.; Torker, S.; Haeffner, F.; Robbins, D. W.; van der Mei, F. W.; Hoveyda, A. H. *Nat. Chem.* **2016,** *8,* 768–777. (c) van der Mei, F. W.; Miyamoto, H.; Silverio, D. L.; Hoveyda, A. H. *Angew. Chem. Int. Ed.* **2016,** *55,* 4701–4706.

component reaction,[17] hydro defluorination,[18] and intramolecular cyclization[19] (Scheme 3.8).

3.3 Catalytic Enantioselective Borylation/Dehalogenation with NHC–Cu-Catalyst

3.3.1 Background Reactivity and Optimal Base

The previously disclosed Cu-catalyzed boryl allylic substitution employed excess amount of methanol (2.0 equivalent of MeOH, Scheme 3.4). However, it was found that

Scheme 3.9. Preliminary Result and Background Reactivity[a]

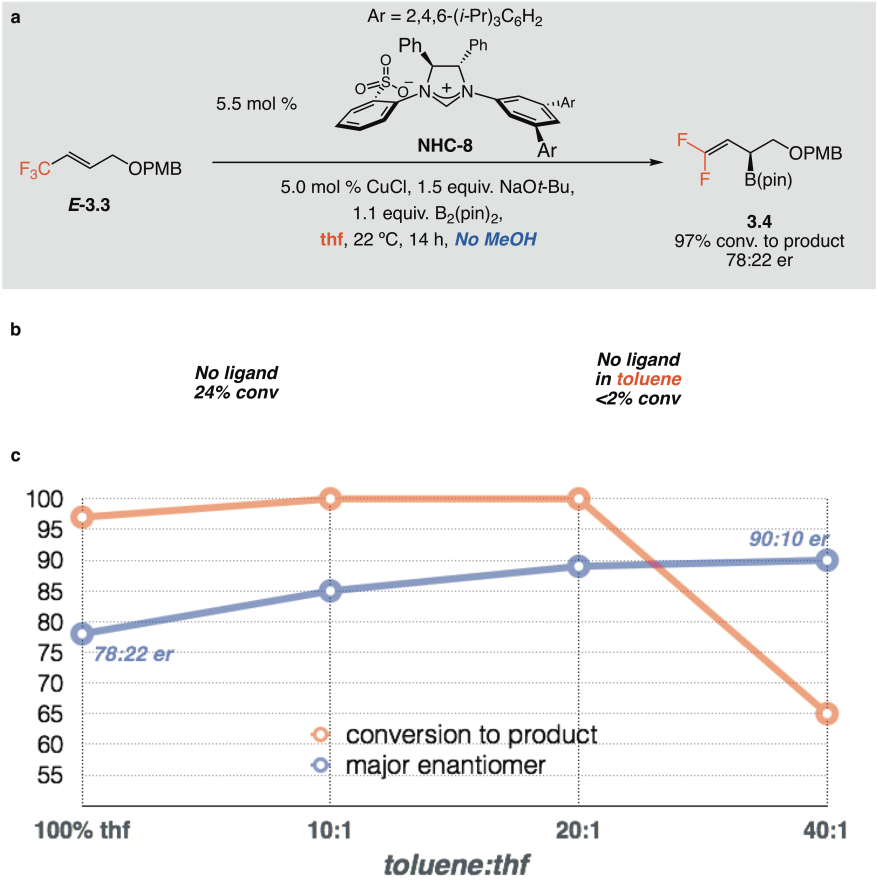

a Reactions were perfomed under N_2 atmosphere. Conversion (conv.) was based on the disappearance of the limiting reagent and determined by analysis of the ^{1}H NMR spectra of the unpurified mixtures; the variance of values is estimated to be <±2%. Enantiomeric ratios were determined by HPLC analysis; the variance of values is estimated to be <±1%. See the Experimental section for details. ND, not determined; NA, not applicable; pin, pinacolato; PMB, 4-methoxybenzyl ether.

(17) Tian, P.; Wang, C. -Q.; Cai, S. -H.; Song, S.; Ye, L.; Feng, C.; Loh, T. -P. *J. Am. Chem. Soc.* **2016,** *138,* 15869–15872.

(18) (a) Kojima, R.; Kubota, K.; Ito, H. *Chem. Commun.* **2017,** *53,* 10688-10691. (b) Hu, J.; Han, X.; Yuan, Y.; Shi, Z. *Angew. Chem. Int. Ed.* **2017,** *56,* 1–6.

(19) Ichikawa, J.; Wada, Y.; Okauchi, T.; Minami, T. *Chem. Commun.* **1997,** 1537–1538.

the proton source (MeOH) was not required in the catalytic transformation to generate allylic boronate **3.4**, and low temperature/prolonged reaction time (e.g., 4 ºC, 48 h, Scheme 3.4) were not necessary (scheme 3.9a). Through a systematic solvent study, we discovered that unbound copper–boron complex can also deliver racemic **3.4** in 100% thf, but there was no background reactivity in 100% toluene (Scheme 3.9b). Indeed, increasing the ratio of toluene:thf led to higher enantioselectivity (up to 90:10 er, Scheme 3.9c), but thf was still needed to dissolve the ligand and form the requisite NHC–Cu alkoxide species (100% toluene gave only 10% conversion to desired product). The

Table 3.1. Base Screening[a]

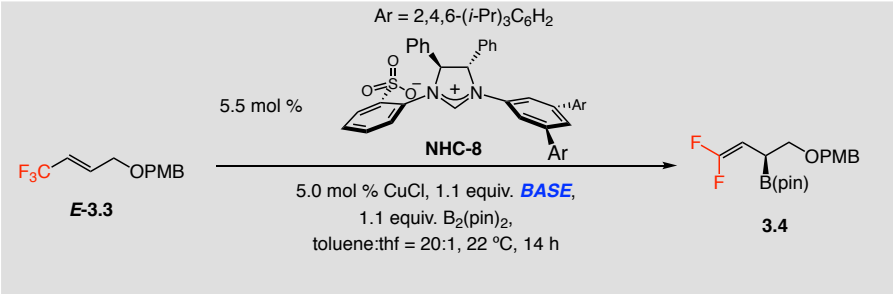

Entry	Base	Conv. (%)§	Yield (%)§§	er †
1	**NaOMe**	66	62	60:40
2	**KOMe**	68	50	52:48
3	**LiO*t*-Bu**	>98	82	95:5
4	**NaO*t*-Bu**	>98	80	89:11
5	**KO*t*-Bu**	>98	Complex Mixtures	ND
6	**NaOPh**	<2	NA	NA
7	**Mg(O*t*-Bu)$_2$**	<2	NA	NA

a Reactions were perfomed under N_2 atmosphere. § Conversion (conv.) was based on the disappearance of the limiting reagent and determined by analysis of the ^{1}H NMR spectra of the unpurified mixtures; the variance of values is estimated to be <±2%. §§ Yield of isolated and purified product; the variance of values is estimated to be <±5%. † Enantiomeric ratios were determined by HPLC analysis; the variance of values is estimated to be <±1%. See the Experimental section for details. ND, not determined; NA, not applicable; pin, pinacolato; PMB, 4-methoxybenzyl ether.

nature of cation is crucial to accelerate the desired reaction pathway through metal–fluoride elimination. High enantioselectivity and efficiency were obtained with LiO*t*-Bu as base (entry 3, Table 3.1) which presumably could facilitate fluoride elimination after Cu–B(pin) addition to alkene (Scheme 3.4b). Metal bases containing other cations such as sodium, potassium, or magnesium gave poor selectivity and/or efficiency.

3.3.2 Limited Substrate Scope with NHC-8

The same major enantiomer was obtained through NHC–Cu–B(pin) addition to ***Z*-3.3** indicates that the Cu-B(pin) complex reacted from the opposite face of the olefin when the *Z*-alkene was used (vs ***E*-3.3**, Shceme 3.10a). While high enantioselectivities were obtained using allylic PMB ether **3.3**, poor enantioselectivities were observed with aryl- and alkyl-substituted CF_3-olefins (64:36 er for **3.5** and 51:49 er for **3.6**, Scheme

Scheme 3.10. Substrate Scope[a]

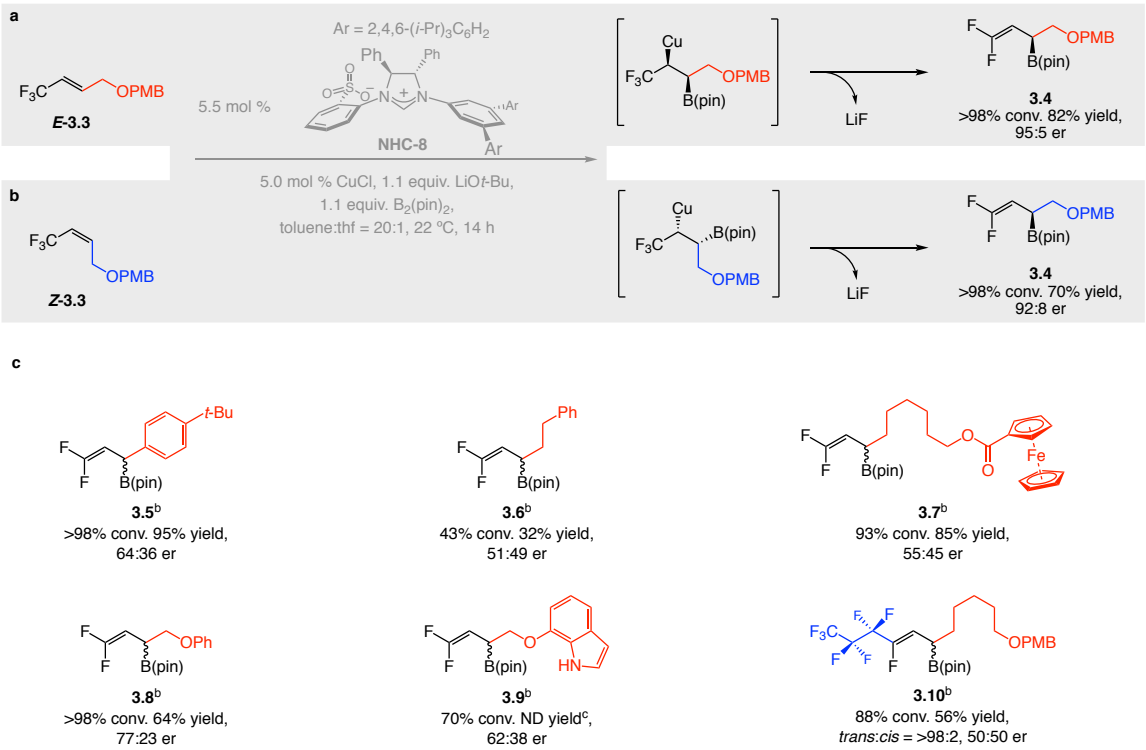

a Reactions were perfomed under N_2 atmosphere. Conversion (conv.) was based on the disappearance of the limiting reagent and determined by analysis of the ^{1}H NMR spectra of the unpurified mixtures; the variance of values is estimated to be <±2%. Enantiomeric ratios were determined by HPLC analysis; the variance of values is estimated to be <±1%. b the reaction was run for 18 h. c the product was inseparable from starting material. See the Experimental section for details. ND, not determined; pin, pinacolato; PMB, 4-methoxybenzyl ether.

3.10). Carboxylic esters could be tolerated, but the same trend of stereoselectivity was found as in the aryl and alkyl cases (55:45 er for **3.7**, Scheme 3.10). Interestingly, when the PMB protecting group was replaced with other aryl substituents, selectivity was significantly diminished (**3.8** and **3.9**, Scheme 3.10). Synthesis of **3.10** demonstrated that the methods is applicable to other class of perfluoroalkyl olefins (other than CF_3-alkenes).

3.3.3 Identification of an Effective and Broadly Applicable Catalyst

Table 3.2. Examination of Different Types of Cu Complexes[a]

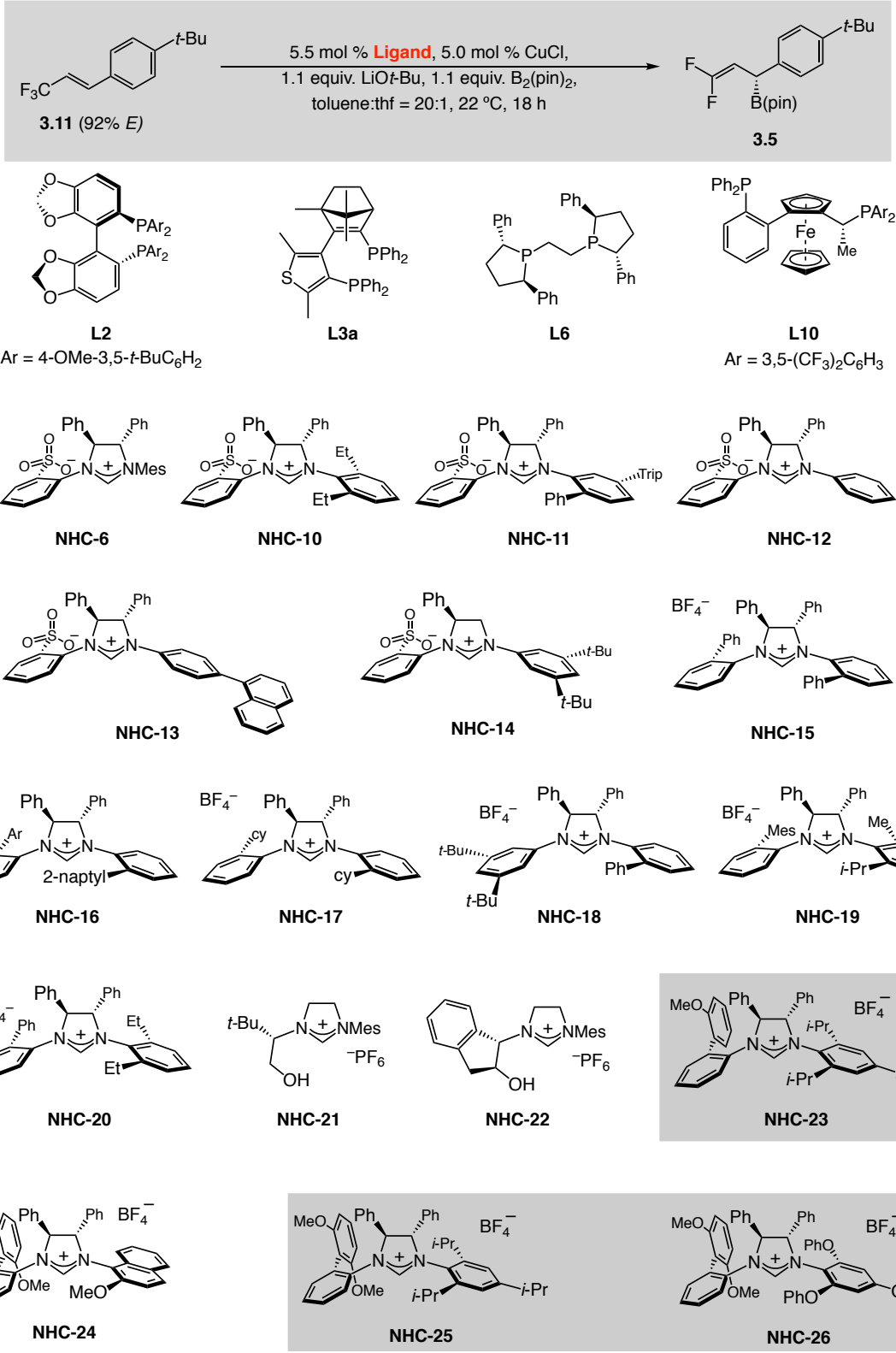

Entry	Ligand	Conv. (%)§	Yield (%)§§	er†
1	**L2**	<2	NA	NA
2	**L3a**	<2	NA	NA
3	**L6**	23	ND	56:44
4	**L10**	<2	NA	NA
5	**NHC-6**	93	93	73:27
6	**NHC-10**	95	54	79:21
7	**NHC-11**	83	27	40:60
8	**NHC-12**	>98	71	75:25
9	**NHC-13**	>98	63	77:23
10	**NHC-14**	95	93	74:26
11	**NHC-15**	68	64	68:32
12	**NHC-16**	64	63	70:30
13	**NHC-17**	49	43	57:43
14	**NHC-18**	98	98	68:32
15	**NHC-19**	>98	98	88:12
16	**NHC-20**	>98	88	85:12
17	**NHC-21**	61	60	32:68
18	**NHC-22**	>98	>98	51:48
19	**NHC-23**	85	84	92:8
20	**NHC-24**	80	75	81:19
21	**NHC-25**	>98	90	92:8
22	**NHC-26**	>98	98	92:8

a Reactions were perfomed under N_2 atmosphere. § Conversion (conv.) was based on the disappearance of the limiting reagent and determined by analysis of the ^{1}H NMR spectra of the unpurified mixtures; the variance of values is estimated to be <±2%. §§ Yield of isolated and purified product; the variance of values is estimated to be <±5%. † Enantiomeric ratios were determined by HPLC analysis; the variance of values is estimated to be <±1%. See the Experimental section for details. NA, not applicable; ND, not determined; Mes, 2,4,6-trimethylphenyl; pin, pinacolato; Trip, 2,4,6-(*i*-Pr)$_3$C$_6$H$_2$.

In the search for a broadly applicable catalyst, different copper-based complexes were examined under the optimized conditions with aryl CF_3-alkene substrate **3.11** to afford **3.5** (Table 3.2). Commercially available phosphine ligands were found to be ineffective (e.g., entries 1–4, Table 3.2) although they gave high efficiency and selectivity for other class of transformations involving Cu–X (X = boron or hydride) additions to alkenes.[20] Particularly high enantioselectivities were obtained with ligand

(20) For representative examples for **L-2** see: (a) Shi, S. -L.; Buchwald, S. L. *Nat. Chem.* **2015**, *7*, 38–44. (b) Yang, Y.; Shi, S. -L.; Niu, D.; Buchwald, S. L. *Science,* **2015,** *349,* 62–66. (c) Wang, Y. -M.; Bruno, N. C.; Placeres, Á. L.; Zhu, S.; Buchwald, S. L. *J. Am. Chem. Soc.* **2015**, *137*, 10524–10527. (d) Nishikawa, D.; Hirano, K.; Miura, M. *J. Am. Chem. Soc.* **2015**, *137*, 15620–15623. (e) Zhu, S.; Niljianskul, N.; Buchwald, S. L. *Nat. Chem.* **2016,** *8,* 144–150. (f) Shi, S. -L.; Wong, Z. L.; Buchwald, S. L. *Nature,* **2016,** *532,* 353–356. (g) Xi, Y.; Hartwig, J. F. *J. Am. Chem. Soc.* **2016**, *138*, 6703–6706. (h) Friis, S. D.; Pirnot, M. T.; Dupuis, L. N.; Buchwald, S. L. *Angew. Chem. Int. Ed.* **2017,** *56,* 7242–7246. (i) Wang, H.; Yang, J.

Scheme 3.11. NHC-26 as the Optimal Ligand for Enantioselective Allylic Borylation of CF_3-Alkenes[a]

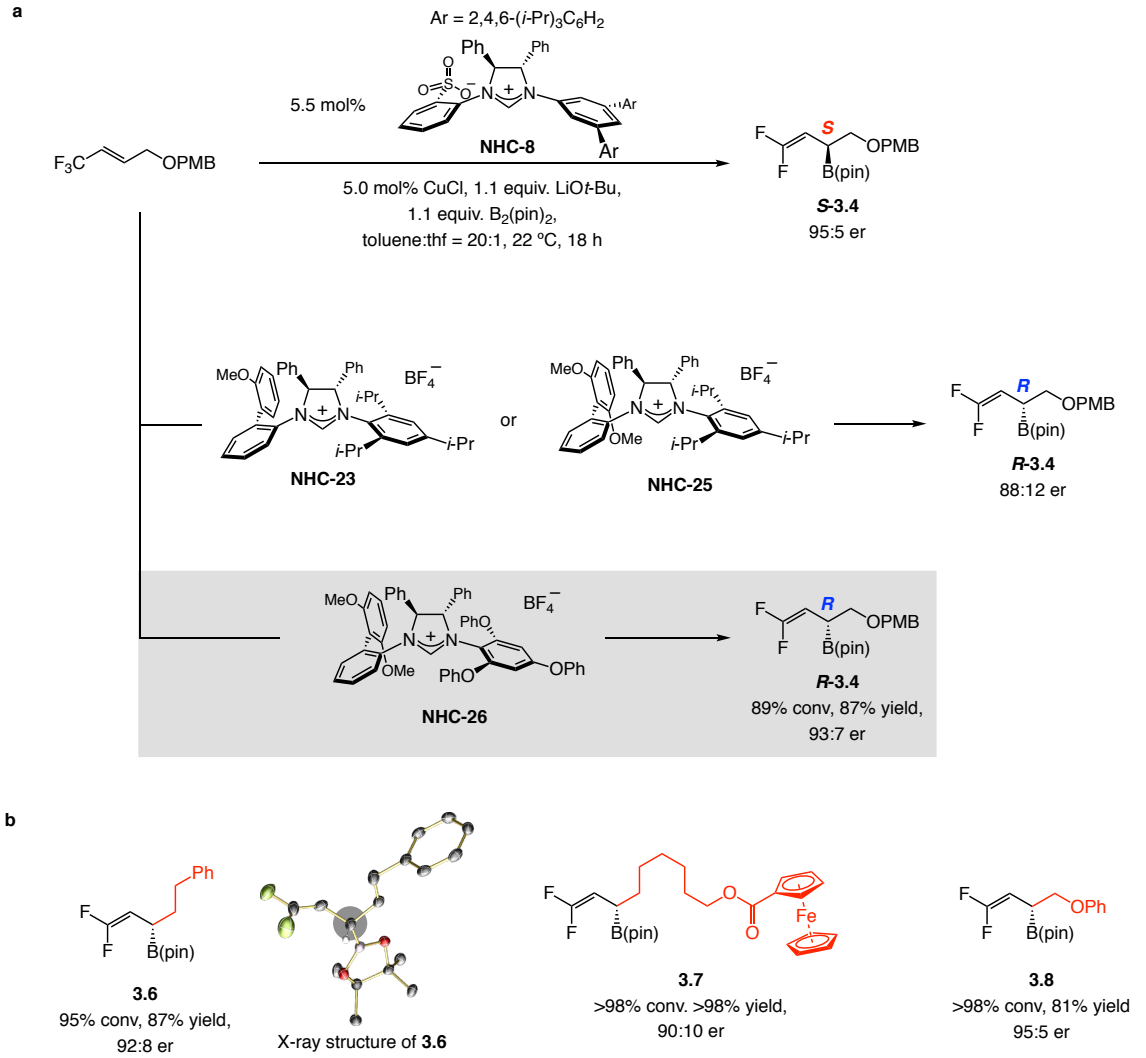

a Reactions were perfomed under N_2 atmosphere. Conversion (conv.) was based on the disappearance of the limiting reagent and determined by analysis of the ^{1}H NMR spectra of the unpurified mixtures; the variance of values is estimated to be <±2%. Enantiomeric ratios were determined by HPLC analysis; the variance of values is estimated to be <±1%. See the Experimental section for details. pin, pinacolato; PMB, 4-methoxybenzyl ether.

C.; Buchwald, S. L. J. *J. Am. Chem. Soc.* **2017**, *139*, 8428–8431. (j) Xi, Y.; Hartwig, J. F. *J. Am. Chem. Soc.* **2017**, *139,* 12758–12772. (k) Lu, G.; Liu, R. Y.; Yang, Y.; Fang, C.; Lambrecht, D. S.; Buchwald, S. L. *J. Am. Chem. Soc.* **2017**, *139,* 16548–16555. For representative examples for **L-3a** see: (l) Meng, F.; Haeffner, F.; Hoveyda, A. H. *J. Am. Chem. Soc.* **2014**, *136*, 11304–11307. (m) Lee, J.; Radomkit, S.; Torker, S.; del Pozo, J.; Hoveyda, A. H. *Nat. Chem.* **2018**, *10,* 99–108. For representative examples for **L-6** see: (n) Miki, Y.; Hirano, K.; Satoh, T.; Miura, M. *Angew. Chem. Int, Ed.* **2013**, *52*, 10830–10834. (o) Sakae, R.; Hirano, K.; Satoh, T.; Miura, M. *Angew. Chem. Int, Ed.* **2015**, *54*, 613–617. (p) Ascic, E.; Buchwald, S. L. *J. Am. Chem. Soc.* **2015**, *137*, 4666–4669. (q) Wang, Y. -M.; Buchwald, S. L. *J. Am. Chem. Soc.* **2016**, *138*, 5024–5027. (r) Bandar, J. S.; Ascic, E.; Buchwald, S. L. *J. Am. Chem. Soc.* **2016**, *138*, 5821–5824. (s) Yang, Y.; Perry, I. B.; Lu, G.; Liu, P. Buchwald, S. L. *Science,* **2016,** *353,* 144–150. (t) Yang, Y.; Perry, I. B.; Buchwald, S. L. *J. Am. Chem. Soc.* **2016**, *138*, 9787–9790. (u) Kato, K.; Hirano, K.; Miura, M. *Angew. Chem. Int, Ed.* **2016**, *55*, 14400–14404. (v) Gribble, Jr. M. W.; Pirnot, M. T.; Bandar, J. S.; Liu, R. Y.; Buchwald, S. L. *J. Am. Chem. Soc.* **2017**, *139*, 2192–2195. (w) Zhou, Y.; Bandar, J. S.; Buchwald, S. L. *J. Am. Chem. Soc.* **2017**, *139*, 8126–8129. For representative an example for **L-10** see: (x) Han, J. T.; Jang, W. J.; Kim, N.; Yun, J. *J. Am. Chem. Soc.* **2016**, *138*, 15146–15149.

NHC-23, **NHC-25**, and **NHC-26** which led to the formation of **3.5** in 92:8 er. The more electron-rich **NHC-26** also delivered **3.4** in high er in the opposite sense of enantioselectivity (vs with **NHC-8**, Scheme 3.11a). Moreover, broader applicability was observed with different starting materials to furnish of **3.6** (87% yield and 92:8 er, Scheme 3.11b), **3.7** (>98% yield and 90:10 er, Scheme 3.11b), and **3.8** (81% yield and 95:5 er, Scheme 3.11b). The X-ray structure secured for **3.6** (Scheme 3.11b) allowed us to establish the absolute stereochemical identity of the major product.

3.3.4 *trans*-Selective B(pin) Allylic Substitution and Application of Allyl B(pin)

High *trans*-selectivity was observed using fluoroalkyl terminal olefins (up to 94:6 *trans:cis* ratio, **3.12–3.15**, Scheme 3.12). In particular, despite the small atomic radius difference between F and H, reasonably high *trans*-selectivity was obtained for the

Scheme 3.12. B(pin) Allylic Subsitution with Terminal Olefins[a]

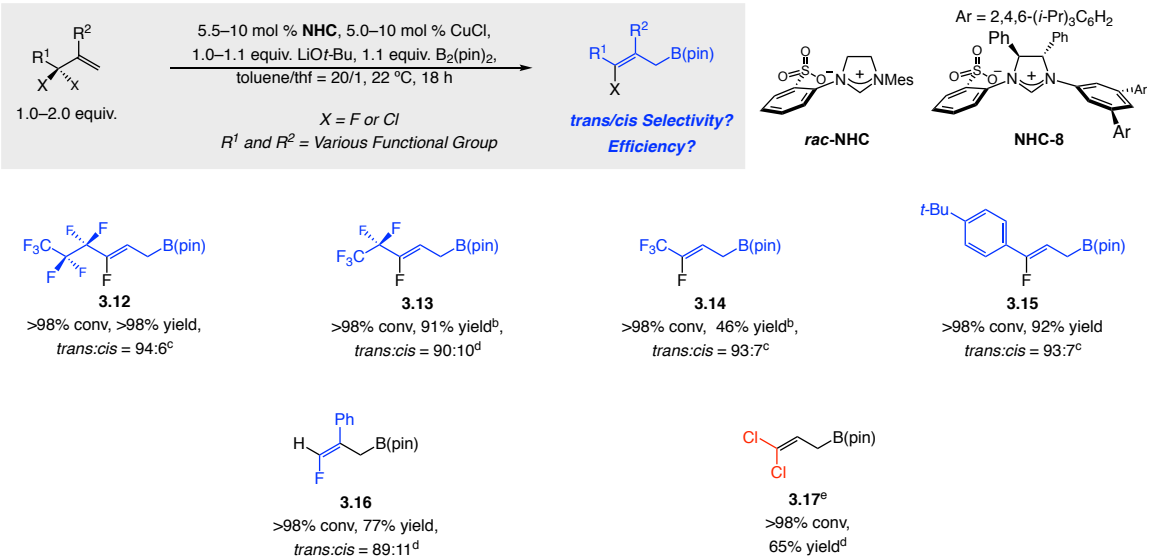

a Reactions were perfomed under N_2 atmosphere. Conversion (conv.) was based on the disappearance of the limiting reagent and determined by analysis of the ^{1}H NMR spectra of the unpurified mixtures; the variance of values is estimated to be <±2%. *Z:E* ratios were determined by NMR analysis; the variance of values is estimated to be <±2%. b 2.0 equiv. of starting materials were used. c NHC-8 was used. d. rac-NHC was used. e. 0.5 mmol of starting material was used with 10 mol% Cu-complex. pin, pinacolato.

transformation leading to **3.16** (89:11 *trans:cis*, Scheme 3.12). The preparation of **3.17** (from 3,3,3-tricloropropene) shows that the protocol can be extended to other useful halogenated allylboron reagents that could serve as important building blocks for the

synthesis of complex molecules. To showcase utility, fluotinated allyl–B(pin) **3.12** was employed as a reagent for allyl addition to benzaldehyde in the presence of an

Scheme 3.13. Representative Allylation with Halogenated Allyl B(pin)[a]

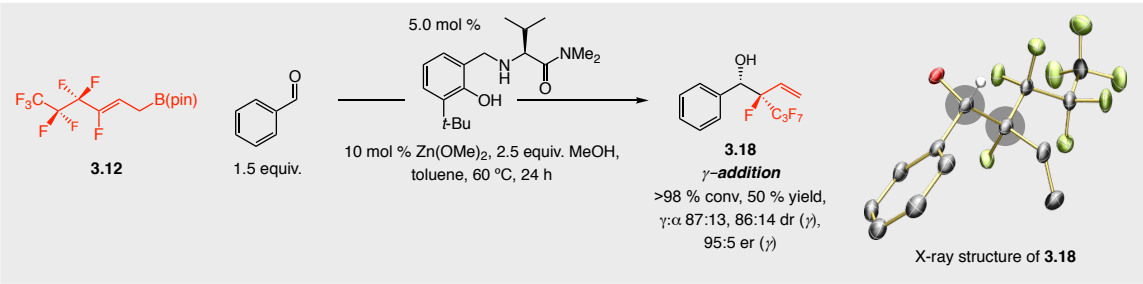

a Reactions were perfomed under N_2 atmosphere. Conversion (conv.) was based on the disappearance of the limiting reagent and determined by analysis of the ^{1}H NMR spectra of the unpurified mixtures; the variance of values is estimated to be <±2%. Enantiomeric ratios were determined by HPLC analysis; the variance of values is estimated to be <±1%. pin, pinacolato.

aminophenol-based catalyst[16] to furnish γ-selective product **3.18** in high diastereo- and enantioselectivity (86:14 dr and 95:5 er, Scheme 3.13). The crystal structure of **3.18** ascertained the absolute stereochemical identity of the major product (Scheme 3.13).

3.4 Conclusions

A highly stereoselective catalytic boryl allylic substitution protocol has been developed for the generation of valuable halogen-substituted allylboron reagents. The process is promoted by a chiral NHC–Cu-based complex and is applicable to a broad range of haloallkyl olefin substrates such as alkenyl-CF_3, -C_nF_{2n+1}, -CF_2Ar, -CF_2H, and CCl_3 to afford allyl–B(pin) products in high selectivity and efficiency (92:8 to 95:5 enantiomeric ratio, 89:11 to >98:2 *trans*:*cis* ratio, 46 to >98% yield, Scheme 3.11 and Scheme 3.12). Through our systematic studies, the background reactivity could be inhibited by adjustment of the solvent system, which led to an increase in enantioselectivity (Table 3.1). In addition, using a proper Lewis acid is crucial to accelerate metal–fluoride elimination,[21] necessary for high yield and selectivity.

(21) Kikushima, K.; Sakaguchi, H.; Saijo, H.; Ohashi, M.; Ogoshi, S. *Chem. Lett.* **2015,** *44,* 1019–1021.

Otherwise the in-situ generated alkyl-copper complex[22] could decompose, causing a loss of kinetic stereoselectivity[23] (see chapter 1 regarding the importance of keeping kinetic enantioselectivity). The resulting allyl–boron product may be used as a reagent for catalytic allylation to aldehydes using a simple aminophenol-derived catalyst (Scheme 3.13). Compared to the previously disclosed enantioselective allylic arylation of CF_3-alkenes using an expensive Rh-based catalyst, our developed allylic borylation methods presents a number of distinct advantages: (1) Inexpensive Cu-based catalyst is used for better sustainability. (2) Allylic boronate products are amenable to a wider range of transformations to afford coveted halogene-containing compounds. (3) Different classes of halloalkyl olefins may be utilized (other than CF_3-alkenes). To further demonstrate utility, studies to access **3.19**, an important building block for the preparation of

Scheme 3.14. Synthesis of Fluorinated Protease Inhibitors

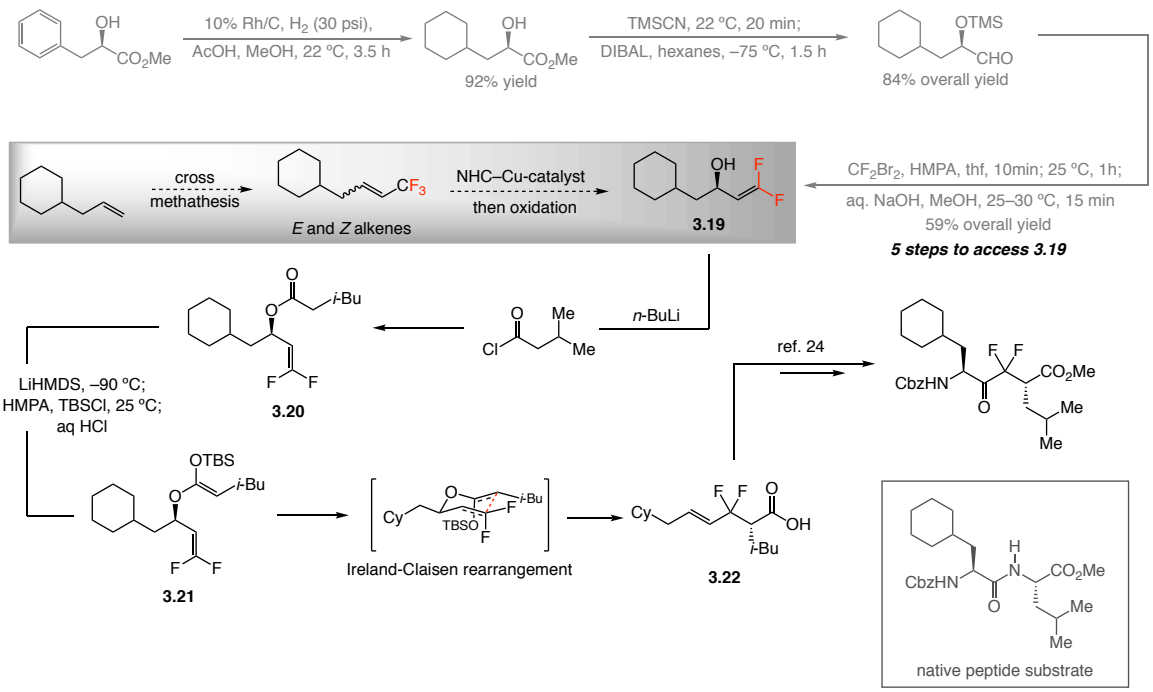

(22) For the crystal structure of difluoroalkylcopper complex see: Saijo, H.; Ohashi, M.; Ogoshi, S. *J. Am. Chem. Soc.* **2014,** *136,* 15158–15161.
(23) Lee, J.; Radomkit, S.; Torker, S.; del Pozo, J.; Hoveyda, A. H. *Nat. Chem.* **2018,** *10,* 99–108.

fluorinated enzyme inhibitors, are ongoing (Scheme 3.14).[24] This application offers an alternative way to generate **3.19** without resorting to conventional inefficient non-catalytic methods (2 steps vs 5 steps to access **3.19**, Scheme 3.14). Stereoretentive Ireland-Claisen rearrangement (**3.21** → **3.22**, Scheme 3.14) is a functionalization for enantioenriched allylic alcohols which can be readily accessed from the generated difluoroalkene (after one-step oxidation). In addition to the formation of fluorinated enzyme inhibitors (Scheme 3.14), difluoroinated analogs of anti-hepatitis B and anti-

Scheme 3.15. Synthesis of Fluorinated Anti-Hepatitis B and Anti-Cancer Reagents

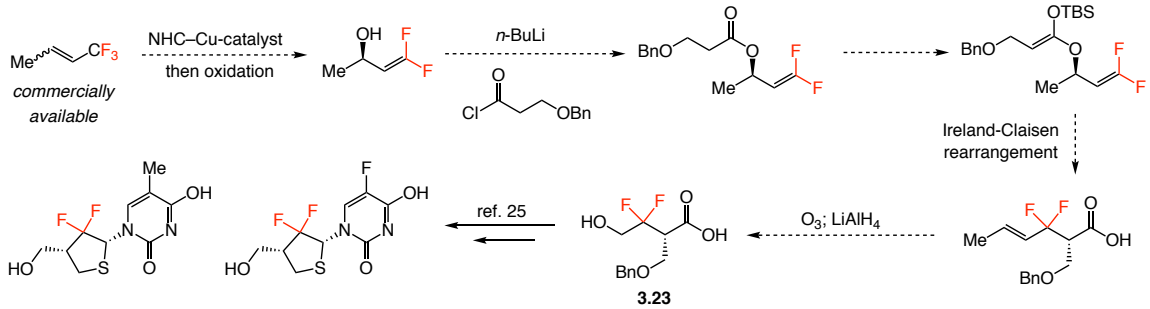

cancer agent[25] are going to be prepared (Scheme 3.15). The preliminary result for the formation of **3.17** (Scheme 3.12) means that dichloroalkene product may be potentially accessed. Future development of catalytic methods that generate enantioenriched

Scheme 3.16. Catalytic Enantioselective Boryl Allylic Substitution with CCl_3-Alkenes

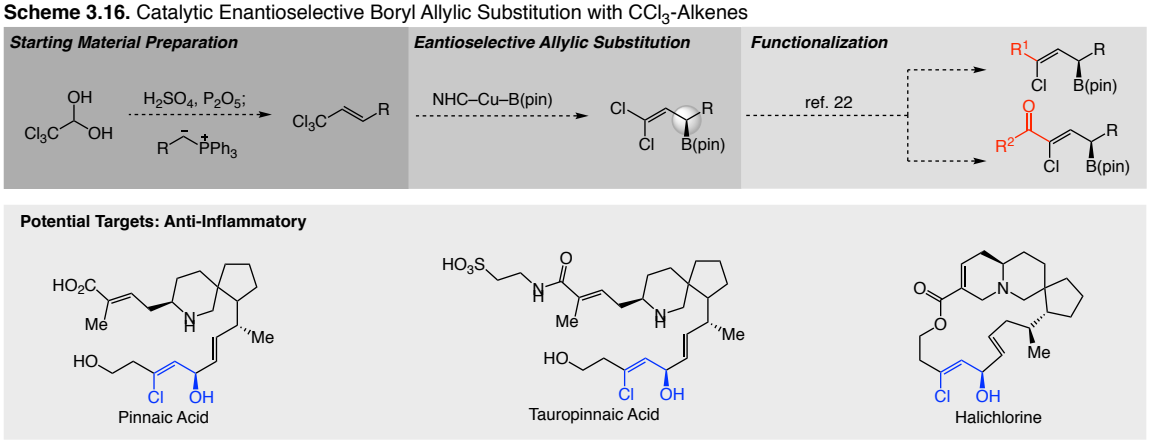

(24) Damon, D. B.; Hoover, D. J. *J. Am. Chem. Soc.* **1990**, *112*, 6439–6442.
(25) Zheng, F.; Zhang, X.; Qing, F.-L. *Chem. Commun.* **2009,** 1505–1507.

dichloro-allylic boronates for potential functionalization[26] an application in chlorinated natural product synthesis[27] (Scheme 3.16) is in the pipeline.

(26) Guinchard, X.; Roulland, E. *Synlett,* **2011,** *19,* 2779–2788.
(27) Clive, D. L. J.; Yu, M.; Wang, J.; Yeh, V. S. C.; Kang, S. *Chem. Rev.* **2005,** *105,* 4483–4514.

3.5 Experimentals

3.5.1 General

Infrared (IR) spectra were recorded on a Bruker FT-IR Alpha (ATR mode) spectrophotometer, ν_{max} in cm^{-1}. Bands are characterized as broad (br), strong (s), medium (m), and weak (w). ^{1}H NMR spectra were recorded on Varian Unity INOVA 400 (400 MHz), 500 (500 MHz), or 600 (600 MHz) spectrometers. Chemical shifts are reported in ppm from tetramethylsilane with the solvent resonance as the internal standard ($CDCl_3$: δ 7.26 ppm). Data are reported as follows: chemical shift, integration, multiplicity (s = singlet, d = doublet, t = triplet, q = quartet, pent = pentet, m = multiplet, br = broad, app = apparent), and coupling constants (Hz). ^{13}C NMR spectra were recorded on Varian Unity INOVA 400 (100 MHz), 500 (125 MHz), or 600 (150 MHz) spectrometers with complete proton decoupling. Chemical shifts are reported in ppm from tetramethylsilane with the solvent resonance as the internal standard ($CDCl_3$: δ 77.16 ppm). ^{19}F NMR spectra were recorded on a Varian Unity INOVA 400 (376 MHz). Chemical shifts are reported in ppm with trifluorotoluene as an external standard (trifluorotoluene: δ –63.72 ppm). Data are re

ported as follows: chemical shift, integration, multiplicity (s = singlet, d = doublet, t = triplet, q = quartet, pent = pentet, m = multiplet, br = broad, app = apparent), and coupling constants (Hz). High-resolution mass spectrometry was performed on a JEOL AccuTOF DART (positive mode) or an Advion Expression CMS (ESI+ or ESI-) at the Mass Spectrometry Facility, Boston College. Enantiomeric ratios were determined by HPLC analysis (high-performance liquid chromatography) with a Shimadzu chromatograph [Chiral Technologies Chiralcel AZ-H (4.6 x 250 mm), Chiral

Technologies Chiralcel OC-H (4.6 x 250 mm), Chiral Technologies Chiralcel OD-H (4.6 x 250 mm), Chiral Technologies Chiralcel OJ-H (4.6 x 250 mm), Chiral Technologies Chiralcel OZ-H (4.6 x 250 mm), or Chiral Technologies Chiralpak AD-H (4.6 x 250 mm)] in comparison with authentic racemic materials. Specific rotations were measured on a Rudolph Research Analytical Autopol IV Polarimeter. Melting points were measured on a Thomas Hoover capillary melting point apparatus and are uncorrected.

Unless otherwise noted, reactions were carried out with distilled and degassed solvents under an atmosphere of dry N_2 in oven- (135 ºC) or flame-dried glassware with standard dry box or vacuum-line techniques. Hexane, Toluene, and dichloromethane were purified under a positive pressure of dry argon by a modified Innovative Technologies purification system through a copper oxide and alumina column. Tetrahydrofuran (Aldrich Chemical Co.) was purified by distillation from sodium benzophenone ketyl immediately prior to use. All work-up and purification procedures were carried out with reagent grade solvents (purchased from Fisher Scientific) under air.

3.5.2 Regents

Bis(pinacolato)diboron [$B_2(pin)_2$]: purchased from Frontier Scientific, Inc., recrystallized from pentane and dried under vacuum prior to use.

Caesium Fluoride: purchased from Strem and used as received.

Copper(I) chloride: purchased from Strem and used as received.

***N,N*-Dimethylformamide:** purchased from Acros and used as received.

Lithium *tert*-butoxide: purchased from Strem and used as received.

Phosphine ligands (L2, 3a, 6 and 10): purchased from Strem and used as received.

Imidazolinium salt NHC-6: prepared according to a previously reported procedure.[24]

Imidazolinium salt NHC-7: prepared according to a previously reported procedure.[25]

Iodine: purchased from Alfa aesar and used as received.

(*E*)-Trimethyl-(3,3,3-trifluoroprop-1-enyl)silane: purchased from TCI America and used as received.

(*E*)-4,4,4-trifluorobut-2-en-1-ol: purchased from Oakwood chemicals and used as received.

Tris(2,4,6-trimethylphenyl)phosphine: purchased from Alfa aesar and used as received.

Tris(dibenzylideneacetone)dipalladium: purchased from Strem and used as received.

Trifluoromethyl(1,10-phenanthroline) copper(I): purchased from Strem and used as received.

1-(*tert*-butyl)-4-iodobenzene: purchased from Aldrich and used as received.

Preparation of starting materials:

β-trifluoromethylstyrene derivatives were synthesized by the Hiyama cross-coupling reaction of aryl iodides and (*E*)-Trimethyl-(3,3,3-trifluoroprop-1-enyl)silane.[26]

Alkyl alkenyl CF_3 reagents were synthesized from the corresponding iodines by a copper-mediated methods for trifluoromethylation.[27]

3.5.3 Representative Procedure and Products

In an N_2-filled glove box, an oven-dried 2 dram vial with magnetic stir bar was

---

(24) (a) Brown, M. K.; May, T. L.; Baxter, C. A.; Hoveyda, A. H. *Angew. Chem. Int. Ed.* **2007,** *46,* 1097–1100. (b) May, T. L.; Brown, M. K.; Hoveyda, A. H. *Angew. Chem. Int. Ed.* **2008,** *47,* 7468–7472.

(25) Clavier, H.; Coutable, L.; Toupet, L.; Guillemin, J.-C.; Mauduit, M. *J. Organomet. Chem.* **2005,** *690,* 5237–5254.

(26) Omote, M.; Tanaka, M.; Ikeda, A.; Nomura, S.; Tarui, A.; Sato, K.; Ando, A Org. Lett. **2012,** *14,* 2286–2289.

(27) Morimoto, H.; Tsubogo, T.; Litvinas, N. D.; Hartwig J. F. *Angew. Chem. Int. Ed.* **2011,** *50,* 3793–3798.

charged with CuCl (0.5 mg, 0.005 mmol), **NHC-8** (4.7 mg, 0.0055 mmol), LiO*t*-Bu (8.8 mg, 0.11 mmol), freshly distilled tetrahydrofuran (thf, 50 μL), and dried toluene (1.0 mL). The reaction mixture was premixed for 1 hour before $B_2(pin)_2$ (28 mg, 0.11 mmol) and alkenyl CF_3 reagent (24.6 mg, 0.1 mmol) were added. The vial was sealed with electrical tape before removal from the glove box, and the resulting mixture was allowed to stir at 22 °C for 14 hours. The mixture was passed through a short plug of silica gel and celite (4 cm x 1 cm) eluted with Et_2O. The organic layer was concentrated under reduced pressure and purified by silica gel chromatography (hexanes:Et_2O=10:1, R_f=0.2) to afford 29.2 mg of the desired product as a clear oil (0.0824 mmol, 82% yield). The racemic sample was prepared by the same procedure except through the use of 10 mol % ***rac*-NHC** and CuCl.

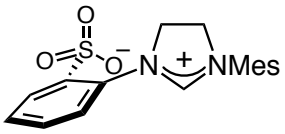

***rac*-NHC**

(*S*)-2-(4,4-difluoro-1-((4-methoxybenzyl)oxy)but-3-en-2-yl)-4,4,5,5-tetramethyl-1,3,2-dioxaborolane (3.4): IR (neat): 2979 (w), 2928 (w), 2855 (w), 1742 (m), 1613 (w), 1513 (m), 1465 (w), 1371 (s), 1325 (s), 1245 (s), 1142 (s), 1089 (s), 1036 (s), 819 (s), 677 (w), 515 (w) cm^{-1}; ^1H NMR ($CDCl_3$, 500 MHz): δ 7.25 (d, *J* = 8.5 Hz, 2H), 6.86 (d, *J* = 8.5 Hz, 2H), 4.43 (dt, *J* = 18.0, 12.0 Hz, 2H), 4.27 (ddd, *J* = 26.0, 9.5, 2.5 Hz, 1H), 3.80 (s, 3H), 3.53 (d, *J* = 6.5 Hz, 2H), 2.22 (q, *J* = 7.0 Hz, 1H), 1.23 (s, 12H); ^{13}C NMR ($CDCl_3$, 100 MHz): δ 159.2, 156.3 (dd, *J* = 283, 283.8 Hz), 130.7, 129.2, 113.8, 83.9, 77.0 (dd, *J* = 23.5, 20.5 Hz), 72.6, 71.0 (t, *J* = 3.0 Hz), 55.4, 24.9, 24.8; ^{19}F NMR (376 MHz, $CDCl_3$): δ –89.6 (d, *J* = 47.8, 1F), –91.5 (dd, *J* = 47.8, 25.9 Hz, 1F); HRMS $[M+NH_4]^+$ Found for

$C_{18}H_{29}BF_2O_4N$: 372.2178; specific rotation: $[\alpha]_D^{20}$ –1.18 (c = 2.13, $CHCl_3$) for an enantiomerically enriched sample of 95:5 er. Enantiomeric Purity of (*S*)-**3.4** was determined by HPLC analysis of the alcohol product after oxidation in comparison with authentic racemic material (95:5 er shown; AD–H column, 98:2 hexanes:*i*PrOH, 0.3 mL/min, 220 nm).

*Enantiomeric purity with E-alkene & **NHC-8***

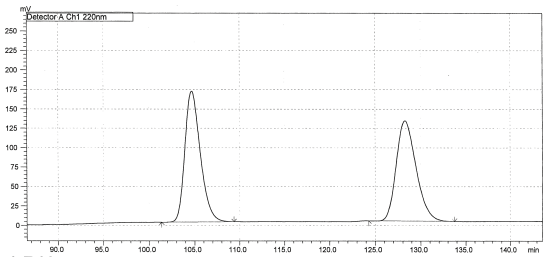

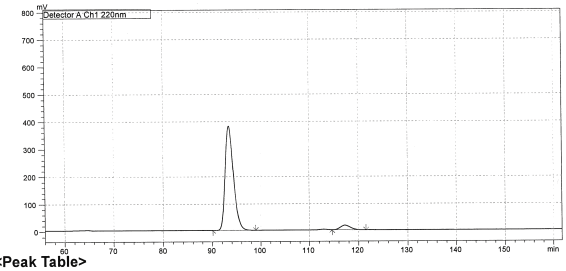

<Peak Table>

Detector A Channel 1 220nm

Peak#	Ret. Time	Area	Height	Conc.	Area%
1	104.693	19975305	168497	50.561	50.561
2	128.261	19532401	129084	49.439	49.439
Total		39507705	297581		100.000

<Peak Table>

Detector A Channel 1 220nm

Peak#	Ret. Time	Area	Height	Conc.	Area%
1	93.458	45426726	379688	94.976	94.976
2	117.216	2403010	16731	5.024	5.024
Total		47829736	396419		100.000

Peak #	Retention time	Area	Area %	Peak #	Retention time	Area	Area %
1	104.693	19975305	50.561	1	93.458	45429726	94.976
2	128.261	19532401	49.439	2	117.216	2403010	5.024

*Enantiomeric purity with Z-alkene & **NHC-8***

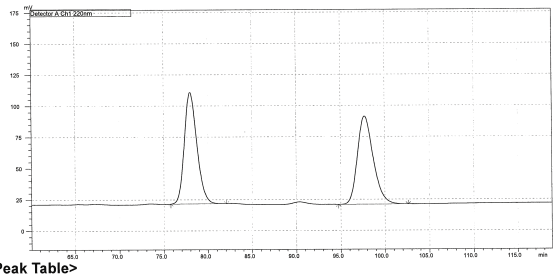

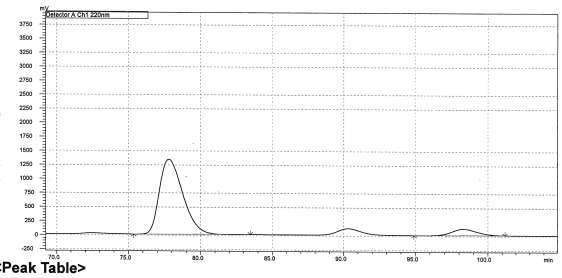

<Peak Table>

Detector A Channel 1 220nm

Peak#	Ret. Time	Area	Height	Conc.	Area%
1	78.009	8882676	89325	50.127	50.127
2	97.730	8837734	70653	49.873	49.873
Total		17720410	159978		100.000

<Peak Table>

Detector A Channel 1 220nm

Peak#	Ret. Time	Area	Height	Conc.	Area%
1	77.797	149651970	1330720	91.595	91.595
2	98.299	13733073	113180	8.405	8.405
Total		163385043	1443899		100.000

Peak #	Retention time	Area	Area %	Peak #	Retention time	Area	Area %
1	78.009	8882676	50.127	1	77.797	149651970	91.595
2	97.730	8837734	49.873	2	98.299	13733073	8.405

*Enantiomeric purity with E-alkene & **NHC-26***

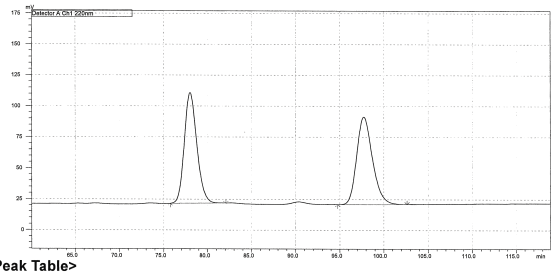

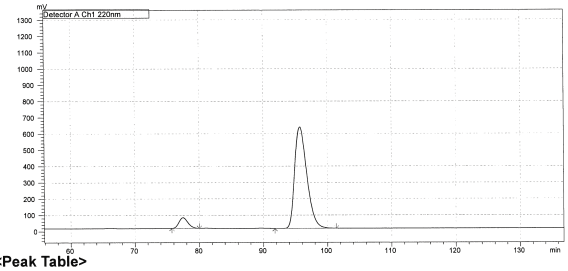

<Peak Table>
Detector A Channel 1 220nm

Peak#	Ret. Time	Area	Height	Conc.	Area%
1	78.009	8882676	89325	50.127	50.127
2	97.730	8837734	70653	49.873	49.873
Total		17720410	159978		100.000

<Peak Table>
Detector A Channel 1 220nm

Peak#	Ret. Time	Area	Height	Conc.	Area%
1	77.441	6342099	65412	7.153	7.153
2	95.703	82327235	622021	92.847	92.847
Total		88669334	687433		100.000

Peak #	Retention time	Area	Area %	Peak #	Retention time	Area	Area %
1	78.009	8882676	50.127	1	77.441	6342099	7.153
2	97.730	8837734	49.873	2	95.703	82327235	92.847

(*R*)-2-(1-(4-(*tert*-butyl)phenyl)-3,3-difluoroallyl)-4,4,5,5-tetramethyl-1,3,2-dioxaborolane (3.5): After the crude mixture was passed through a short plug of silica gel (4 cm x 1 cm) eluted with dried Et_2O, the organic layer was concentrated under reduced pressure and purified by using oven dried short silica gel (4 cm x 1 cm) with dried solvents. IR (CH_2Cl_2): 2965 (m), 1739 (s), 1510 (w), 1466 (w), 1363 (s), 1326 (s), 1292 (m), 1268 (m), 1256 (m), 1197 (s), 1108 (m), 914 (s), 571 (m), 521 (m) cm^{-1}; ^1H NMR ($CDCl_3$, 400 MHz): δ 7.30–7.29 (m, 2H), 7.15 (d, *J* = 8.0 Hz, 2H), 4.55 (ddd, *J* = 25.2, 10.0, 2.4 Hz, 1H), 3.23 (d, *J* = 10.4 Hz, 1H), 1.30 (s, 9H), 1.23 (d, *J* = 3.6 Hz, 12H); ^{13}C NMR ($CDCl_3$, 100 MHz): δ 156.0 (t, *J* = 285.4 Hz), 148.7, 137.7 (t, J = 2.3 Hz), 127.6, 125.7, 84.0, 79.4 (dd, J = 22.8, 20.5 Hz), 34.5, 31.5, 24.7; ^{19}F NMR (376 MHz, $CDCl_3$): δ –90.4 (d, *J* = 46.6, 1F), –92 (dd, *J* = 47.0, 25.9 Hz, 1F); HRMS was not determined due to instability of the product.; $[\alpha]_D^{20}$ –21.63 (*c* = 2.64, CH_2Cl_2) for an enantiomerically enriched sample of 92:8 er. Enantiomeric Purity of **3.5** was determined

by HPLC analysis in comparison with authentic racemic material (92:8 er shown; OZ–H column, 100% hexanes, 0.3 mL/min, 220 nm).

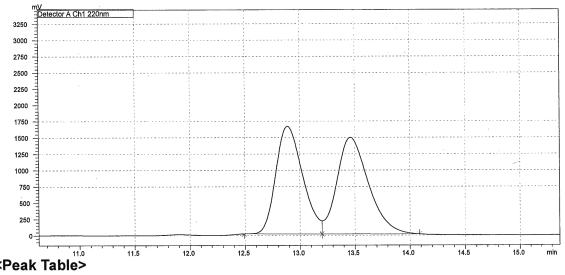

<Peak Table>
Detector A Channel 1 220nm

Peak#	Ret. Time	Area	Height	Conc.	Area%
1	12.889	27970221	1647683	48.680	48.680
2	13.463	29486726	1476699	51.320	51.320
Total		57456947	3124382		100.000

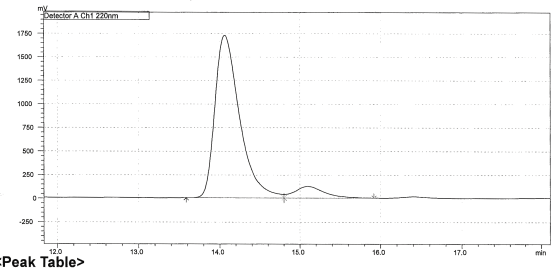

<Peak Table>
Detector A Channel 1 220nm

Peak#	Ret. Time	Area	Height	Conc.	Area%
1	14.062	36657832	1724881	92.137	92.137
2	15.096	3128387	122262	7.863	7.863
Total		39786219	1847143		100.000

Peak #	Retention time	Area	Area %	Peak #	Retention time	Area	Area %
1	12.889	27970221	48.680	1	14.062	36657832	92.137
2	13.463	29486726	51.320	2	15.096	3128387	7.863

(*S*)-2-(1,1-difluoro-5-phenylpent-1-en-3-yl)-4,4,5,5-tetramethyl-1,3,2-dioxaborolane (3.6): After the crude mixture was passed through a short plug of silica gel (4 cm x 1 cm) eluted with dried Et_2O, the organic layer was concentrated under reduced pressure and purified by using oven dried short silica gel (4 cm x 1 cm) with dried solvents. Melting point: 50–52 ºC; IR (CH_2Cl_2): 2977 (w), 2926 (w), 1738 (s), 1600 (w), 1454 (s), 1372 (s), 1363 (s), 1211 (s), 1156 (s), 1142 (s), 670 (m), 441 (s) cm^{-1}; ^1H NMR ($CDCl_3$, 400 MHz): δ 7.29–1.26 (m, 2H), 7.19–7.16 (m, 3H), 4.20 (ddd, *J* = 26.0, 10.4, 2.8 Hz), 2.71–2.64 (m, 1H), 2.57 (ddd, *J* = 13.7, 10.6, 5.8, 1H), 1.92–1.83 (m, 2H), 1.72–1.62 (m, 1H), 1.56 (s, 12H); ^{13}C NMR ($CDCl_3$, 100 MHz): δ 156.3 (t, *J* = 284.6 Hz), 142.3, 128.6, 128.5, 125.9, 83.7, 78.9 (*t*, J = 21.2 Hz), 35.3, 33.2, 24.9; ^{19}F NMR (376 MHz, $CDCl_3$): δ –90.0 (d, *J* = 48.9 Hz, 1F), –92.2 (dd, *J* = 48.9, 24.4 Hz, 1F); HRMS $[M+H]^+$ Found for $C_{17}H_{24}BF_2O_2$: 309.1823; $[\alpha]_D^{20}$ –1.20 (*c* = 2.07, CH_2Cl_2) for an enantiomerically enriched sample of 92:8 er. Enantiomeric Purity of **3.6** was determined by HPLC analysis in comparison

with authentic racemic material (92:8 er shown; OJ–H column, 100% hexanes, 0.3 mL/min, 220 nm).

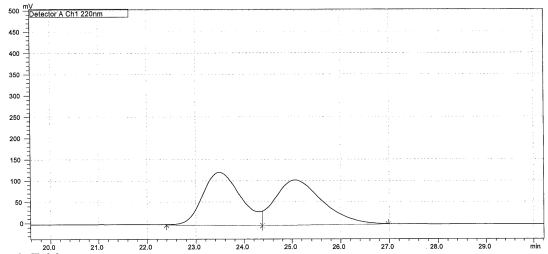

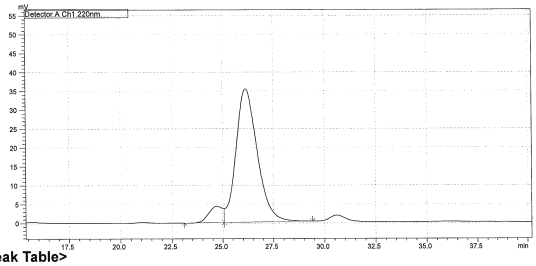

<Peak Table>
Detector A Channel 1 220nm

Peak#	Ret. Time	Area	Height	Conc.	Area%
1	23.482	6875659	124699	48.585	48.585
2	25.062	7276289	106234	51.415	51.415
Total		14151948	230932		100.000

<Peak Table>
Detector A Channel 1 220nm

Peak#	Ret. Time	Area	Height	Conc.	Area%
1	24.700	208449	4327	7.457	7.457
2	26.143	2586771	35297	92.543	92.543
Total		2795220	39624		100.000

Peak #	Retention time	Area	Area %	Peak #	Retention time	Area	Area %
1	23.482	6875659	48.585	1	24.700	208449	7.457
2	25.062	7276289	51.415	2	26.143	2586771	92.543

(*S*)-9,9-difluoro-7-(4,4,5,5-tetramethyl-1,3,2-dioxaborolan-2-yl)non-8-en-1-yl ferrocenecarboxylate (3.7): After the crude mixture was passed through a short plug of silica gel (4 cm x 1 cm) eluted with dried Et_2O, the organic layer was concentrated under reduced pressure and purified by using oven dried short silica gel (4 cm x 1 cm) with dried solvents. IR (CH_2Cl_2): 2986 (w), 2933 (w), 2879 (w), 1738 (m), 1712 (s), 1461 (m), 1372 (m), 1326 (m), 1274 (s), 1108 (s), 407 (s) cm^{-1}; ^1H NMR ($CDCl_3$, 400 MHz): δ 4.80 (t, *J* = 2.0 Hz, 2H), 4.38 (t, *J* = 2.0 Hz, 2H), 4.21–4.08 (m, 8H), 1.83 (app q, *J* = 8.4 Hz, 1H), 1.71 (app p, *J* = 6.4 Hz, 2H), 1.46–1.31 (m, 8 H), 1.23 (s, 12H); ^{13}C NMR ($CDCl_3$, 100 MHz): δ 171.9, 156.1 (t, *J* = 284.6 Hz), 83.6, 79.1 (t, *J* = 21.2 Hz), 71.7, 71.3, 70.2, 69.8, 64.4, 31.0 (t, *J* = 2.2 Hz), 29.3, 29.0, 28.8, 26.1, 25.2, 24.8; ^{19}F NMR (470 MHz, $CDCl_3$): δ –90.6 (d, *J* = 49.8 Hz, 1F), –92.9 (dd, *J* = 51.2, 26.3 Hz, 1F); HRMS $[M+H]^+$ Found for $C_{26}H_{36}BF_2FeO_4$: 517.2025; specific rotation: $[\alpha]_D^{20}$ –1.76 (*c* = 3.25, CH_2Cl_2) for an enantiomerically enriched sample of 90:10 er. Enantiomeric Purity of **3.7** was determined by HPLC analysis of the alcohol product after oxidation in comparison with

authentic racemic material (90:10 er shown; AD–H column, 98:2 hexanes:*i*PrOH, 0.3 mL/min, 220 nm).

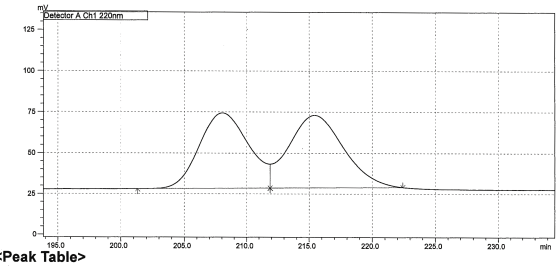

<Peak Table>

Detector A Channel 1 220nm

Peak#	Ret. Time	Area	Height	Conc.	Area%
1	208.040	12669915	46045	48.462	48.462
2	215.441	13474058	44369	51.538	51.538
Total		26143972	90413		100.000

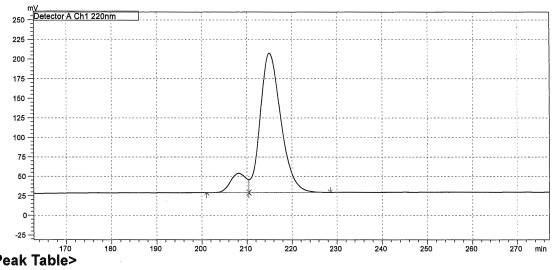

<Peak Table>

Detector A Channel 1 220nm

Peak#	Ret. Time	Area	Height	Conc.	Area%
1	208.189	5995527	24783	9.562	9.562
2	215.044	56702958	178295	90.438	90.438
Total		62698485	203078		100.000

Peak #	Retention time	Area	Area %	Peak #	Retention time	Area	Area %
1	208.040	12669915	48.462	1	208.189	5995527	9.562
2	215.441	13474058	51.538	2	215.044	56702958	90.438

(*R*)-2-(4,4-difluoro-1-phenoxybut-3-en-2-yl)-4,4,5,5-tetramethyl-1,3,2-dioxaborolane (3.8): After the crude mixture was passed through a short plug of silica gel (4 cm x 1 cm) eluted with dried Et_2O, the organic layer was concentrated under reduced pressure and purified by using oven dried short silica gel (4 cm x 1 cm) with dried solvents. IR (CH_2Cl_2): 2980 (m), 2935 (w), 1743 (s), 1600 (m), 1587 (w), 1382 (s), 1372 (s), 1329 (s), 1242 (s), 1170 (m), 1132 (s), 965 (w), 691 (m), 419 (w) cm^{-1}; ^1H NMR ($CDCl_3$, 400 MHz): δ 7.29–7.25 (m, 2H), 6.60–6.87 (m, 3H), 4.37 (ddd, *J* = 26.0, 10.4, 2.4 Hz, 1H), 4.05 (d, *J* = 6.0 Hz, 2H), 2.41–2.35 (m, 1H), 1.26 (s, 6H), 1.255 (s, 6H); ^{13}C NMR ($CDCl_3$, 100 MHz): δ 159.0, 156.5 (dd, *J* = 286.1, 284.6 Hz), 129.5, 120.9, 114.8, 84.1, 76.6 (dd, *J* = 23.6, 20.5 Hz), 69.1 (t, *J* = 2.3 Hz), 24.8, 24.79; ^{19}F NMR (376 MHz, $CDCl_3$): δ –89.1 (d, *J* = 46.2 Hz, 1F), 91.1 (dd, *J* = 46.6, 12.4 Hz, 1F); HRMS $[M+NH_4]^+$ Found for $C_{16}H_{25}BF_2O_3N$: 328.1910; $[\alpha]_D^{20}$ –11.27 (*c* = 1.72, CH_2Cl_2) for an enantiomerically enriched sample of 95:5 er. Enantiomeric Purity of **3.8** was determined by HPLC analysis

of the alcohol product after oxidation in comparison with authentic racemic material (95:5 er. shown; AD–H column, (99:1 hexanes:*i*PrOH,, 0.3 mL/min, 220 nm).

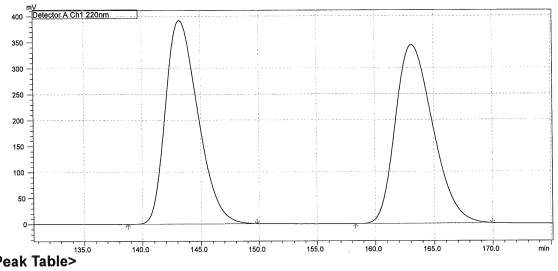

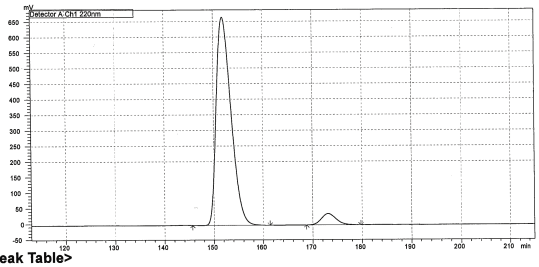

<Peak Table>
Detector A Channel 1 220nm

Peak#	Ret. Time	Area	Height	Conc.	Height%	Area%
1	143.226	75519136	391945	49.897	53.245	49.897
2	163.160	75830516	344167	50.103	46.755	50.103
Total		151349652	736111		100.000	100.000

<Peak Table>
Detector A Channel 1 220nm

Peak#	Ret. Time	Area	Height	Conc.	Area%
1	151.850	139802390	668089	94.834	94.834
2	173.128	7615666	36171	5.166	5.166
Total		147418057	704260		100.000

Peak #	Retention time	Area	Area %	Peak #	Retention time	Area	Area %
1	143.226	75519136	49.897	1	151.850	668089	94.834
2	163.160	75830516	50.103	2	173.128	36171	5.166

(*R*)-4,4-difluoro-2-(4,4,5,5-tetramethyl-1,3,2-dioxaborolan-2-yl)but-3-en-1-ol: After the crude mixture was passed through a short plug of silica gel (4 cm x 1 cm) eluted with dried Et_2O, the organic layer was concentrated under reduced pressure and purified by using oven dried short silica gel (4 cm x 1 cm) with dried solvents. IR (CH_2Cl_2): 2981 (w), 2885 (w), 1741 (s), 1470 (s), 1372 (s), 1239 (m), 1215 (m), 1141 (s), 1110 (m), 1052 (m), 487 (w) cm^{-1}; ^1H NMR ($CDCl_3$, 400 MHz): δ 4.24 (ddd, J = 26.4, 10.8, 2.8 Hz, 1H), 3.69 (t, J = 6.4 Hz, 2H), 2.15–2.09 (m, 1H), 1.91 (t, J = 6.0 Hz, 1H), 1.26 (s, 12 H); ^{13}C NMR ($CDCl_3$, 100 MHz): δ 159.7 (t, J = 286.2 Hz), 84.1, 76.0 (dd, J = 22.7, 20.5 Hz), 63.7 (t, J = 3.1 Hz), 24.9, 24.8; ^{19}F NMR (376 MHz, $CDCl_3$): δ –88.6 (d, J = 46.2 Hz, 1F), –90.8 (dd, J = 46.2, 25.9 Hz, 1F); HRMS $[M+H]^+$ Found for $C_{10}H_{18}BF_2O_3$: 235.1322; $[\alpha]_D^{20}$ –10.81 (c = 1.64, CH_2Cl_2) for an enantiomerically enriched sample of 83:17 er. Enantiomeric Purity of product was determined by HPLC analysis of the alcohol product after PMB protection and oxidation in comparison with authentic racemic material (83:17 er shown; AD–H column, (98:2 hexanes:*i*PrOH,, 0.3 mL/min, 220 nm).

*Enantiomeric purity with **NHC-26***

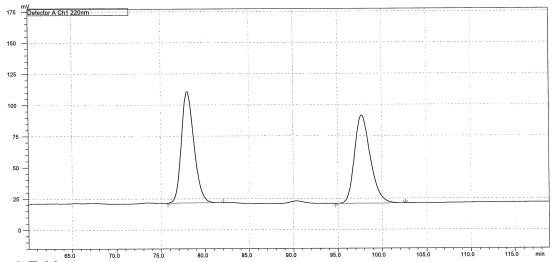

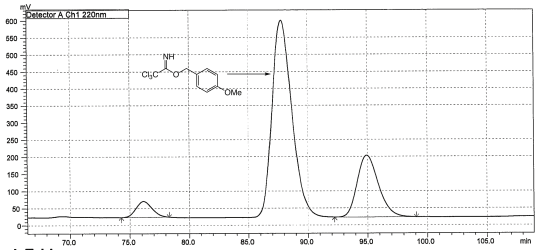

<Peak Table>

Detector A Channel 1 220nm

Peak#	Ret. Time	Area	Height	Conc.	Area%
1	78.009	8882676	89325	50.127	50.127
2	97.730	8837734	70653	49.873	49.873
Total		17720410	159978		100.000

<Peak Table>

Detector A Channel 1 220nm

Peak#	Ret. Time	Area	Height	Conc.	Area%
1	76.139	4404656	46624	16.577	16.577
2	94.942	22166609	180053	83.423	83.423
Total		26571265	226677		100.000

Peak #	Retention time	Area	Area %	Peak #	Retention time	Area	Area %
1	78.009	8882676	50.127	1	76.139	4404656	16.577
2	97.730	8837734	49.873	2	94.942	22166609	83.423

*Enantiomeric purity with **NHC-8***

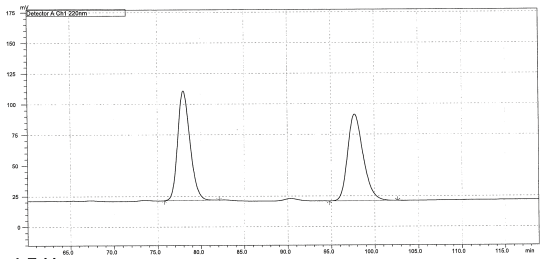

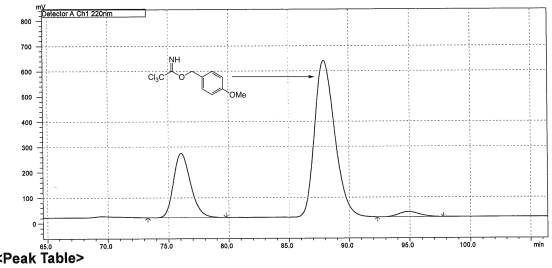

<Peak Table>

Detector A Channel 1 220nm

Peak#	Ret. Time	Area	Height	Conc.	Area%
1	78.009	8882676	89325	50.127	50.127
2	97.730	8837734	70653	49.873	49.873
Total		17720410	159978		100.000

<Peak Table>

Detector A Channel 1 220nm

Peak#	Ret. Time	Area	Height	Conc.	Area%
1	76.057	24830114	252921	91.210	91.210
2	94.862	2392829	20277	8.790	8.790
Total		27222943	273199		100.000

Peak #	Retention time	Area	Area %	Peak #	Retention time	Area	Area %
1	78.009	8882676	50.127	1	76.057	24830114	91.210
2	97.730	8837734	49.873	2	94.862	2392829	8.790

3.5.4 Data for X-ray Crystallography of 3.6

The absolute configuration of **3.6** was established by X-ray analysis, which was assigned to be (*R*) configuration. The absolute stereochemistry for other enantiomerically enriched products has been assigned by inference.

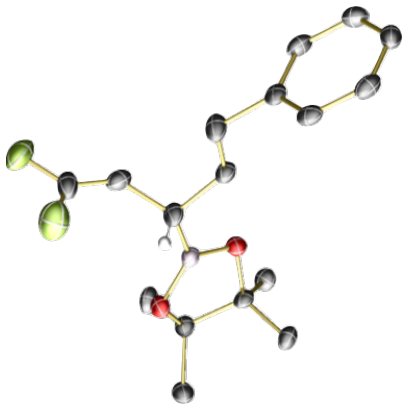

Table 3.3 Crystal data and structure refinement for $C_{17}H_{23}BF_2O_2$.

Identification code	C17H23BF2O2	
Empirical formula	C17 H23 B F2 O2	
Formula weight	308.16	
Temperature	100(2) K	
Wavelength	1.54178 ≈	
Crystal system	Triclinic	
Space group	P1	
Unit cell dimensions	a = 8.4140(4) ≈	α= 102.2931(18)∞.
	b = 8.8842(4) ≈	β= 95.7488(19)∞.
	c = 11.9257(6) ≈	γ = 104.3562(19)∞.
Volume	832.74(7) ≈^{3}	
Z	2	
Density (calculated)	1.229 Mg/m^3	
Absorption coefficient	0.766 mm^{-1}	
F(000)	328	
Crystal size	0.420 x 0.280 x 0.180 mm^3	

Theta range for data collection	5.303 to 70.308∞.
Index ranges	-10<=h<=10, -10<=k<=10, -14<=l<=14
Reflections collected	11546
Independent reflections	5804 [R(int) = 0.0350]
Completeness to theta = 67.679∞	99.3 %
Absorption correction	Semi-empirical from equivalents
Max. and min. transmission	0.7533 and 0.6486
Refinement method	Full-matrix least-squares on F^2
Data / restraints / parameters	5804 / 3 / 405
Goodness-of-fit on F^2	1.065
Final R indices [I>2sigma(I)]	R1 = 0.0556, wR2 = 0.1379
R indices (all data)	R1 = 0.0560, wR2 = 0.1384
Absolute structure parameter	-0.01(4)
Extinction coefficient	n/a
Largest diff. peak and hole	0.679 and -0.310 e.≈$^{-3}$

Table 3.4 Atomic coordinates (x 10^4) and equivalent isotropic displacement parameters (≈^{2}x 10^3) for $C_{17}H_{23}BF_2O_2$. U(eq) is defined as one third of the trace of the orthogonalized U^{ij} tensor.

	x	y	z	U(eq)
F(1)	6682(3)	8930(3)	5449(2)	41(1)
F(2)	4901(3)	6902(3)	5704(2)	45(1)
O(1)	8571(3)	4429(3)	8153(2)	23(1)
O(2)	9480(3)	5383(2)	6621(2)	22(1)
B(1)	8453(4)	5432(4)	7437(3)	22(1)
C(1)	6418(4)	7845(4)	6065(3)	28(1)
C(2)	7512(4)	7744(4)	6892(3)	24(1)
C(3)	7215(4)	6524(4)	7589(3)	24(1)
C(4)	7307(4)	7269(4)	8894(3)	24(1)
C(5)	6038(4)	8217(4)	9164(3)	28(1)
C(6)	6136(4)	8806(4)	10460(3)	25(1)
C(7)	7282(4)	10233(4)	11094(3)	26(1)
C(8)	7384(4)	10746(4)	12295(3)	29(1)
C(9)	6351(4)	9830(4)	12876(3)	31(1)
C(10)	5215(4)	8412(4)	12265(3)	31(1)
C(11)	5100(4)	7905(4)	11062(3)	28(1)
C(12)	9986(4)	3808(4)	7902(3)	22(1)
C(13)	10151(4)	4013(4)	6651(3)	22(1)
C(14)	11466(4)	4861(4)	8812(3)	26(1)

C(15)	9586(4)	2096(4)	8021(3)	28(1)
C(16)	11916(4)	4425(4)	6397(3)	28(1)
C(17)	9054(5)	2611(4)	5692(3)	30(1)
F(3)	2909(4)	1352(4)	4174(3)	60(1)
F(4)	5183(3)	3165(4)	4924(2)	56(1)
O(3)	1129(3)	5351(3)	1841(2)	27(1)
O(4)	307(3)	4596(3)	3453(2)	26(1)
B(2)	1196(4)	4370(4)	2567(3)	24(1)
C(18)	3869(5)	2681(5)	4086(3)	38(1)
C(19)	3642(4)	3510(4)	3315(3)	32(1)
C(20)	2168(4)	3043(4)	2380(3)	29(1)
C(21)	2578(4)	2731(4)	1144(3)	26(1)
C(22)	3460(5)	1425(5)	840(3)	33(1)
C(23)	3544(4)	1007(4)	-452(3)	25(1)
C(24)	2466(4)	-383(4)	-1177(3)	26(1)
C(25)	2478(4)	-755(4)	-2358(3)	28(1)
C(26)	3566(4)	247(4)	-2847(3)	28(1)
C(27)	4670(4)	1636(4)	-2133(3)	30(1)
C(28)	4644(4)	1999(4)	-946(3)	28(1)
C(29)	-186(4)	6119(4)	2131(3)	24(1)
C(30)	-246(4)	6032(4)	3417(3)	24(1)
C(31)	-1764(4)	5086(4)	1299(3)	29(1)
C(32)	298(5)	7796(4)	1936(3)	31(1)

C(33)	-1954(5)	5779(5)	3759(3)	34(1)
C(34)	996(5)	7426(4)	4295(3)	34(1)

Table 3.5 Bond lengths [≈] and angles [∞] for $C_{17}H_{23}BF_2O_2$.

F(1)-C(1)	1.322(4)
F(2)-C(1)	1.312(4)
O(1)-B(1)	1.372(4)
O(1)-C(12)	1.462(3)
O(2)-B(1)	1.365(4)
O(2)-C(13)	1.469(3)
B(1)-C(3)	1.589(4)
C(1)-C(2)	1.314(5)
C(2)-C(3)	1.489(4)
C(2)-H(2)	0.9500
C(3)-C(4)	1.542(4)
C(3)-H(3)	1.0000
C(4)-C(5)	1.534(4)
C(4)-H(4A)	0.9900
C(4)-H(4B)	0.9900
C(5)-C(6)	1.509(4)
C(5)-H(5A)	0.9900
C(5)-H(5B)	0.9900
C(6)-C(11)	1.393(5)
C(6)-C(7)	1.395(5)
C(7)-C(8)	1.394(5)
C(7)-H(7)	0.9500

C(8)-C(9)	1.381(5)
C(8)-H(8)	0.9500
C(9)-C(10)	1.380(5)
C(9)-H(9)	0.9500
C(10)-C(11)	1.394(5)
C(10)-H(10)	0.9500
C(11)-H(11)	0.9500
C(12)-C(15)	1.514(4)
C(12)-C(14)	1.524(4)
C(12)-C(13)	1.557(4)
C(13)-C(16)	1.516(5)
C(13)-C(17)	1.524(5)
C(14)-H(14A)	0.9800
C(14)-H(14B)	0.9800
C(14)-H(14C)	0.9800
C(15)-H(15A)	0.9800
C(15)-H(15B)	0.9800
C(15)-H(15C)	0.9800
C(16)-H(16A)	0.9800
C(16)-H(16B)	0.9800
C(16)-H(16C)	0.9800
C(17)-H(17A)	0.9800
C(17)-H(17B)	0.9800

C(17)-H(17C)	0.9800
F(3)-C(18)	1.286(6)
F(4)-C(18)	1.329(5)
O(3)-B(2)	1.359(4)
O(3)-C(29)	1.470(4)
O(4)-B(2)	1.364(4)
O(4)-C(30)	1.469(3)
B(2)-C(20)	1.585(4)
C(18)-C(19)	1.322(5)
C(19)-C(20)	1.491(5)
C(19)-H(19)	0.9500
C(20)-C(21)	1.531(4)
C(20)-H(20)	1.0000
C(21)-C(22)	1.526(4)
C(21)-H(21A)	0.9900
C(21)-H(21B)	0.9900
C(22)-C(23)	1.519(5)
C(22)-H(22A)	0.9900
C(22)-H(22B)	0.9900
C(23)-C(28)	1.381(5)
C(23)-C(24)	1.389(5)
C(24)-C(25)	1.378(5)
C(24)-H(24)	0.9500

C(25)-C(26)	1.376(5)
C(25)-H(25)	0.9500
C(26)-C(27)	1.392(5)
C(26)-H(26)	0.9500
C(27)-C(28)	1.387(5)
C(27)-H(27)	0.9500
C(28)-H(28)	0.9500
C(29)-C(32)	1.518(5)
C(29)-C(31)	1.527(5)
C(29)-C(30)	1.557(4)
C(30)-C(33)	1.510(5)
C(30)-C(34)	1.520(5)
C(31)-H(31A)	0.9800
C(31)-H(31B)	0.9800
C(31)-H(31C)	0.9800
C(32)-H(32A)	0.9800
C(32)-H(32B)	0.9800
C(32)-H(32C)	0.9800
C(33)-H(33A)	0.9800
C(33)-H(33B)	0.9800
C(33)-H(33C)	0.9800
C(34)-H(34A)	0.9800
C(34)-H(34B)	0.9800

C(34)-H(34C)	0.9800

B(1)-O(1)-C(12)	106.7(2)
B(1)-O(2)-C(13)	106.6(2)
O(2)-B(1)-O(1)	113.7(3)
O(2)-B(1)-C(3)	125.3(3)
O(1)-B(1)-C(3)	121.0(3)
F(2)-C(1)-C(2)	126.6(3)
F(2)-C(1)-F(1)	108.5(3)
C(2)-C(1)-F(1)	124.9(3)
C(1)-C(2)-C(3)	124.9(3)
C(1)-C(2)-H(2)	117.5
C(3)-C(2)-H(2)	117.5
C(2)-C(3)-C(4)	112.9(3)
C(2)-C(3)-B(1)	112.3(3)
C(4)-C(3)-B(1)	109.3(2)
C(2)-C(3)-H(3)	107.4
C(4)-C(3)-H(3)	107.4
B(1)-C(3)-H(3)	107.4
C(5)-C(4)-C(3)	114.3(2)
C(5)-C(4)-H(4A)	108.7
C(3)-C(4)-H(4A)	108.7
C(5)-C(4)-H(4B)	108.7

C(3)-C(4)-H(4B)	108.7
H(4A)-C(4)-H(4B)	107.6
C(6)-C(5)-C(4)	110.8(2)
C(6)-C(5)-H(5A)	109.5
C(4)-C(5)-H(5A)	109.5
C(6)-C(5)-H(5B)	109.5
C(4)-C(5)-H(5B)	109.5
H(5A)-C(5)-H(5B)	108.1
C(11)-C(6)-C(7)	118.1(3)
C(11)-C(6)-C(5)	120.3(3)
C(7)-C(6)-C(5)	121.6(3)
C(8)-C(7)-C(6)	121.0(3)
C(8)-C(7)-H(7)	119.5
C(6)-C(7)-H(7)	119.5
C(9)-C(8)-C(7)	120.0(3)
C(9)-C(8)-H(8)	120.0
C(7)-C(8)-H(8)	120.0
C(10)-C(9)-C(8)	119.9(3)
C(10)-C(9)-H(9)	120.1
C(8)-C(9)-H(9)	120.1
C(9)-C(10)-C(11)	120.2(3)
C(9)-C(10)-H(10)	119.9
C(11)-C(10)-H(10)	119.9

C(6)-C(11)-C(10)	120.8(3)
C(6)-C(11)-H(11)	119.6
C(10)-C(11)-H(11)	119.6
O(1)-C(12)-C(15)	108.2(3)
O(1)-C(12)-C(14)	106.4(2)
C(15)-C(12)-C(14)	110.3(3)
O(1)-C(12)-C(13)	102.5(2)
C(15)-C(12)-C(13)	115.3(3)
C(14)-C(12)-C(13)	113.3(3)
O(2)-C(13)-C(16)	108.6(3)
O(2)-C(13)-C(17)	106.4(2)
C(16)-C(13)-C(17)	109.9(3)
O(2)-C(13)-C(12)	102.2(2)
C(16)-C(13)-C(12)	115.0(3)
C(17)-C(13)-C(12)	113.9(3)
C(12)-C(14)-H(14A)	109.5
C(12)-C(14)-H(14B)	109.5
H(14A)-C(14)-H(14B)	109.5
C(12)-C(14)-H(14C)	109.5
H(14A)-C(14)-H(14C)	109.5
H(14B)-C(14)-H(14C)	109.5
C(12)-C(15)-H(15A)	109.5
C(12)-C(15)-H(15B)	109.5

H(15A)-C(15)-H(15B)	109.5
C(12)-C(15)-H(15C)	109.5
H(15A)-C(15)-H(15C)	109.5
H(15B)-C(15)-H(15C)	109.5
C(13)-C(16)-H(16A)	109.5
C(13)-C(16)-H(16B)	109.5
H(16A)-C(16)-H(16B)	109.5
C(13)-C(16)-H(16C)	109.5
H(16A)-C(16)-H(16C)	109.5
H(16B)-C(16)-H(16C)	109.5
C(13)-C(17)-H(17A)	109.5
C(13)-C(17)-H(17B)	109.5
H(17A)-C(17)-H(17B)	109.5
C(13)-C(17)-H(17C)	109.5
H(17A)-C(17)-H(17C)	109.5
H(17B)-C(17)-H(17C)	109.5
B(2)-O(3)-C(29)	106.7(2)
B(2)-O(4)-C(30)	106.8(2)
O(3)-B(2)-O(4)	113.9(3)
O(3)-B(2)-C(20)	123.2(3)
O(4)-B(2)-C(20)	122.9(3)
F(3)-C(18)-C(19)	127.8(4)
F(3)-C(18)-F(4)	109.6(3)

C(19)-C(18)-F(4)	122.6(4)
C(18)-C(19)-C(20)	124.7(4)
C(18)-C(19)-H(19)	117.7
C(20)-C(19)-H(19)	117.7
C(19)-C(20)-C(21)	114.3(3)
C(19)-C(20)-B(2)	109.5(3)
C(21)-C(20)-B(2)	110.3(2)
C(19)-C(20)-H(20)	107.5
C(21)-C(20)-H(20)	107.5
B(2)-C(20)-H(20)	107.5
C(22)-C(21)-C(20)	115.3(3)
C(22)-C(21)-H(21A)	108.5
C(20)-C(21)-H(21A)	108.5
C(22)-C(21)-H(21B)	108.5
C(20)-C(21)-H(21B)	108.5
H(21A)-C(21)-H(21B)	107.5
C(23)-C(22)-C(21)	111.2(3)
C(23)-C(22)-H(22A)	109.4
C(21)-C(22)-H(22A)	109.4
C(23)-C(22)-H(22B)	109.4
C(21)-C(22)-H(22B)	109.4
H(22A)-C(22)-H(22B)	108.0
C(28)-C(23)-C(24)	118.1(3)

C(28)-C(23)-C(22)	121.8(3)
C(24)-C(23)-C(22)	120.1(3)
C(25)-C(24)-C(23)	121.1(3)
C(25)-C(24)-H(24)	119.5
C(23)-C(24)-H(24)	119.5
C(26)-C(25)-C(24)	120.6(3)
C(26)-C(25)-H(25)	119.7
C(24)-C(25)-H(25)	119.7
C(25)-C(26)-C(27)	119.3(3)
C(25)-C(26)-H(26)	120.4
C(27)-C(26)-H(26)	120.4
C(28)-C(27)-C(26)	119.6(3)
C(28)-C(27)-H(27)	120.2
C(26)-C(27)-H(27)	120.2
C(23)-C(28)-C(27)	121.4(3)
C(23)-C(28)-H(28)	119.3
C(27)-C(28)-H(28)	119.3
O(3)-C(29)-C(32)	108.6(3)
O(3)-C(29)-C(31)	106.0(2)
C(32)-C(29)-C(31)	110.6(3)
O(3)-C(29)-C(30)	102.0(2)
C(32)-C(29)-C(30)	115.5(3)
C(31)-C(29)-C(30)	113.2(3)

O(4)-C(30)-C(33)	108.2(3)
O(4)-C(30)-C(34)	106.7(3)
C(33)-C(30)-C(34)	110.5(3)
O(4)-C(30)-C(29)	102.2(2)
C(33)-C(30)-C(29)	114.9(3)
C(34)-C(30)-C(29)	113.7(3)
C(29)-C(31)-H(31A)	109.5
C(29)-C(31)-H(31B)	109.5
H(31A)-C(31)-H(31B)	109.5
C(29)-C(31)-H(31C)	109.5
H(31A)-C(31)-H(31C)	109.5
H(31B)-C(31)-H(31C)	109.5
C(29)-C(32)-H(32A)	109.5
C(29)-C(32)-H(32B)	109.5
H(32A)-C(32)-H(32B)	109.5
C(29)-C(32)-H(32C)	109.5
H(32A)-C(32)-H(32C)	109.5
H(32B)-C(32)-H(32C)	109.5
C(30)-C(33)-H(33A)	109.5
C(30)-C(33)-H(33B)	109.5
H(33A)-C(33)-H(33B)	109.5
C(30)-C(33)-H(33C)	109.5
H(33A)-C(33)-H(33C)	109.5

H(33B)-C(33)-H(33C)	109.5
C(30)-C(34)-H(34A)	109.5
C(30)-C(34)-H(34B)	109.5
H(34A)-C(34)-H(34B)	109.5
C(30)-C(34)-H(34C)	109.5
H(34A)-C(34)-H(34C)	109.5
H(34B)-C(34)-H(34C)	109.5

Symmetry transformations used to generate equivalent atoms:

Table 3.6 Anisotropic displacement parameters (≈²x 10³) for $C_{17}H_{23}BF_2O_2$. The anisotropic displacement factor exponent takes the form: $-2\pi^2[h^2 a^{*2}U^{11} + ... + 2 h k a^* b^* U^{12}]$

	U^{11}	U^{22}	U^{33}	U^{23}	U^{13}	U^{12}
F(1)	51(1)	40(1)	42(1)	19(1)	10(1)	20(1)
F(2)	34(1)	44(1)	54(1)	19(1)	-9(1)	6(1)
O(1)	21(1)	28(1)	25(1)	9(1)	6(1)	14(1)
O(2)	23(1)	24(1)	23(1)	7(1)	4(1)	12(1)
B(1)	22(2)	23(2)	20(2)	3(1)	1(1)	10(1)
C(1)	31(2)	34(2)	26(2)	8(1)	5(1)	17(2)
C(2)	22(2)	24(1)	29(2)	6(1)	6(1)	11(1)
C(3)	23(2)	30(2)	23(2)	7(1)	2(1)	14(1)
C(4)	24(2)	28(2)	24(2)	6(1)	3(1)	16(1)
C(5)	27(2)	36(2)	26(2)	6(1)	2(1)	20(2)
C(6)	22(2)	30(2)	27(2)	5(1)	1(1)	19(1)
C(7)	25(2)	28(2)	32(2)	10(1)	8(1)	15(1)
C(8)	24(2)	29(2)	33(2)	2(1)	-2(1)	12(1)
C(9)	33(2)	38(2)	26(2)	5(1)	1(1)	21(2)
C(10)	28(2)	38(2)	34(2)	14(2)	9(1)	14(2)
C(11)	22(2)	29(2)	33(2)	4(1)	0(1)	10(1)
C(12)	20(2)	25(2)	24(2)	6(1)	4(1)	12(1)
C(13)	21(2)	26(2)	24(2)	5(1)	4(1)	15(1)
C(14)	24(2)	30(2)	24(2)	6(1)	0(1)	12(1)

C(15)	29(2)	26(2)	31(2)	7(1)	3(1)	12(1)
C(16)	25(2)	39(2)	28(2)	12(1)	10(1)	15(1)
C(17)	32(2)	30(2)	26(2)	2(1)	1(1)	14(1)
F(3)	67(2)	54(2)	60(2)	18(1)	0(1)	18(1)
F(4)	44(1)	76(2)	50(1)	8(1)	-4(1)	32(1)
O(3)	26(1)	36(1)	27(1)	10(1)	10(1)	19(1)
O(4)	31(1)	31(1)	25(1)	11(1)	8(1)	19(1)
B(2)	21(2)	30(2)	22(2)	5(1)	2(1)	12(2)
C(18)	47(2)	55(2)	26(2)	13(2)	9(2)	35(2)
C(19)	23(2)	37(2)	36(2)	4(1)	3(1)	12(1)
C(20)	34(2)	36(2)	27(2)	12(1)	6(1)	24(2)
C(21)	24(2)	31(2)	26(2)	6(1)	2(1)	15(1)
C(22)	42(2)	41(2)	26(2)	7(1)	5(1)	29(2)
C(23)	24(2)	31(2)	25(2)	6(1)	3(1)	20(1)
C(24)	21(2)	27(2)	37(2)	12(1)	7(1)	14(1)
C(25)	22(2)	25(2)	34(2)	1(1)	-2(1)	11(1)
C(26)	30(2)	37(2)	22(2)	5(1)	5(1)	19(2)
C(27)	23(2)	33(2)	39(2)	12(1)	10(1)	10(1)
C(28)	19(2)	26(2)	36(2)	0(1)	-2(1)	7(1)
C(29)	20(2)	29(2)	27(2)	5(1)	4(1)	15(1)
C(30)	27(2)	26(2)	26(2)	7(1)	5(1)	16(1)
C(31)	27(2)	33(2)	28(2)	5(1)	-3(1)	13(1)
C(32)	32(2)	32(2)	35(2)	14(1)	5(1)	16(2)

C(33)	31(2)	48(2)	32(2)	14(2)	12(1)	23(2)
C(34)	41(2)	33(2)	24(2)	1(1)	-3(1)	14(2)

Table 3.7 Hydrogen coordinates (x 10^4) and isotropic displacement parameters (≈^{2}x 10 ^{3}) for $C_{17}H_{23}BF_2O_2$.

	x	y	z	U(eq)
H(2)	8573	8506	7058	29
H(3)	6063	5806	7293	29
H(4A)	7133	6400	9307	29
H(4B)	8438	7992	9204	29
H(5A)	6258	9143	8809	34
H(5B)	4904	7523	8821	34
H(7)	8003	10864	10701	31
H(8)	8163	11725	12713	35
H(9)	6423	10176	13695	37
H(10)	4508	7779	12665	37
H(11)	4305	6933	10649	34
H(14A)	11723	5961	8719	38
H(14B)	12433	4447	8712	38
H(14C)	11195	4853	9592	38
H(15A)	9443	2081	8824	42
H(15B)	10498	1640	7821	42
H(15C)	8557	1459	7495	42
H(16A)	11900	4487	5586	43

H(16B)	12437	3592	6530	43
H(16C)	12553	5460	6913	43
H(17A)	7910	2367	5852	44
H(17B)	9470	1669	5664	44
H(17C)	9075	2896	4942	44
H(19)	4477	4472	3359	39
H(20)	1408	2026	2464	35
H(21A)	1530	2433	588	31
H(21B)	3287	3743	1035	31
H(22A)	4600	1798	1288	40
H(22B)	2857	454	1063	40
H(24)	1707	-1088	-854	32
H(25)	1730	-1711	-2839	34
H(26)	3562	-7	-3662	34
H(27)	5437	2333	-2457	36
H(28)	5400	2949	-463	34
H(31A)	-1578	5028	495	44
H(31B)	-2680	5562	1442	44
H(31C)	-2045	4004	1428	44
H(32A)	1373	8405	2416	46
H(32B)	-549	8338	2153	46
H(32C)	382	7728	1114	46
H(33A)	-2694	4772	3267	50

H(33B)	-2397	6671	3658	50
H(33C)	-1879	5730	4575	50
H(34A)	1091	7174	5055	50
H(34B)	614	8393	4356	50
H(34C)	2084	7611	4039	50

Table 3.8 Torsion angles [∞] for $C_{17}H_{23}BF_2O_2$.

C(13)-O(2)-B(1)-O(1)	10.7(3)
C(13)-O(2)-B(1)-C(3)	-169.5(3)
C(12)-O(1)-B(1)-O(2)	8.7(4)
C(12)-O(1)-B(1)-C(3)	-171.2(3)
F(2)-C(1)-C(2)-C(3)	-0.6(5)
F(1)-C(1)-C(2)-C(3)	179.8(3)
C(1)-C(2)-C(3)-C(4)	-116.7(3)
C(1)-C(2)-C(3)-B(1)	119.2(3)
O(2)-B(1)-C(3)-C(2)	-11.1(4)
O(1)-B(1)-C(3)-C(2)	168.7(3)
O(2)-B(1)-C(3)-C(4)	-137.2(3)
O(1)-B(1)-C(3)-C(4)	42.6(4)
C(2)-C(3)-C(4)-C(5)	60.1(4)
B(1)-C(3)-C(4)-C(5)	-174.1(3)
C(3)-C(4)-C(5)-C(6)	176.1(3)
C(4)-C(5)-C(6)-C(11)	-93.5(4)
C(4)-C(5)-C(6)-C(7)	84.8(4)
C(11)-C(6)-C(7)-C(8)	-0.2(4)
C(5)-C(6)-C(7)-C(8)	-178.6(3)
C(6)-C(7)-C(8)-C(9)	0.6(5)
C(7)-C(8)-C(9)-C(10)	-0.3(5)
C(8)-C(9)-C(10)-C(11)	-0.3(5)

C(7)-C(6)-C(11)-C(10)	-0.4(5)
C(5)-C(6)-C(11)-C(10)	178.0(3)
C(9)-C(10)-C(11)-C(6)	0.7(5)
B(1)-O(1)-C(12)-C(15)	-145.0(3)
B(1)-O(1)-C(12)-C(14)	96.5(3)
B(1)-O(1)-C(12)-C(13)	-22.7(3)
B(1)-O(2)-C(13)-C(16)	-145.8(3)
B(1)-O(2)-C(13)-C(17)	96.0(3)
B(1)-O(2)-C(13)-C(12)	-23.8(3)
O(1)-C(12)-C(13)-O(2)	28.0(3)
C(15)-C(12)-C(13)-O(2)	145.4(3)
C(14)-C(12)-C(13)-O(2)	-86.2(3)
O(1)-C(12)-C(13)-C(16)	145.5(3)
C(15)-C(12)-C(13)-C(16)	-97.2(3)
C(14)-C(12)-C(13)-C(16)	31.2(4)
O(1)-C(12)-C(13)-C(17)	-86.2(3)
C(15)-C(12)-C(13)-C(17)	31.1(4)
C(14)-C(12)-C(13)-C(17)	159.5(3)
C(29)-O(3)-B(2)-O(4)	-11.5(4)
C(29)-O(3)-B(2)-C(20)	166.6(3)
C(30)-O(4)-B(2)-O(3)	-8.2(4)
C(30)-O(4)-B(2)-C(20)	173.7(3)
F(3)-C(18)-C(19)-C(20)	0.6(6)

F(4)-C(18)-C(19)-C(20)	-178.2(3)
C(18)-C(19)-C(20)-C(21)	-118.2(4)
C(18)-C(19)-C(20)-B(2)	117.5(4)
O(3)-B(2)-C(20)-C(19)	111.3(4)
O(4)-B(2)-C(20)-C(19)	-70.8(4)
O(3)-B(2)-C(20)-C(21)	-15.3(5)
O(4)-B(2)-C(20)-C(21)	162.6(3)
C(19)-C(20)-C(21)-C(22)	58.3(4)
B(2)-C(20)-C(21)-C(22)	-177.8(3)
C(20)-C(21)-C(22)-C(23)	170.2(3)
C(21)-C(22)-C(23)-C(28)	75.4(4)
C(21)-C(22)-C(23)-C(24)	-102.7(4)
C(28)-C(23)-C(24)-C(25)	-0.7(4)
C(22)-C(23)-C(24)-C(25)	177.5(3)
C(23)-C(24)-C(25)-C(26)	0.0(5)
C(24)-C(25)-C(26)-C(27)	0.7(5)
C(25)-C(26)-C(27)-C(28)	-0.8(5)
C(24)-C(23)-C(28)-C(27)	0.7(5)
C(22)-C(23)-C(28)-C(27)	-177.6(3)
C(26)-C(27)-C(28)-C(23)	0.1(5)
B(2)-O(3)-C(29)-C(32)	147.0(3)
B(2)-O(3)-C(29)-C(31)	-94.1(3)
B(2)-O(3)-C(29)-C(30)	24.6(3)

B(2)-O(4)-C(30)-C(33)	144.4(3)
B(2)-O(4)-C(30)-C(34)	-96.8(3)
B(2)-O(4)-C(30)-C(29)	22.8(3)
O(3)-C(29)-C(30)-O(4)	-28.4(3)
C(32)-C(29)-C(30)-O(4)	-145.9(3)
C(31)-C(29)-C(30)-O(4)	85.0(3)
O(3)-C(29)-C(30)-C(33)	-145.2(3)
C(32)-C(29)-C(30)-C(33)	97.2(4)
C(31)-C(29)-C(30)-C(33)	-31.8(4)
O(3)-C(29)-C(30)-C(34)	86.1(3)
C(32)-C(29)-C(30)-C(34)	-31.4(4)
C(31)-C(29)-C(30)-C(34)	-160.4(3)

Symmetry transformations used to generate equivalent atoms:

3.5.5 NMR Spectra

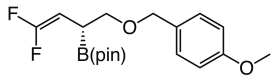

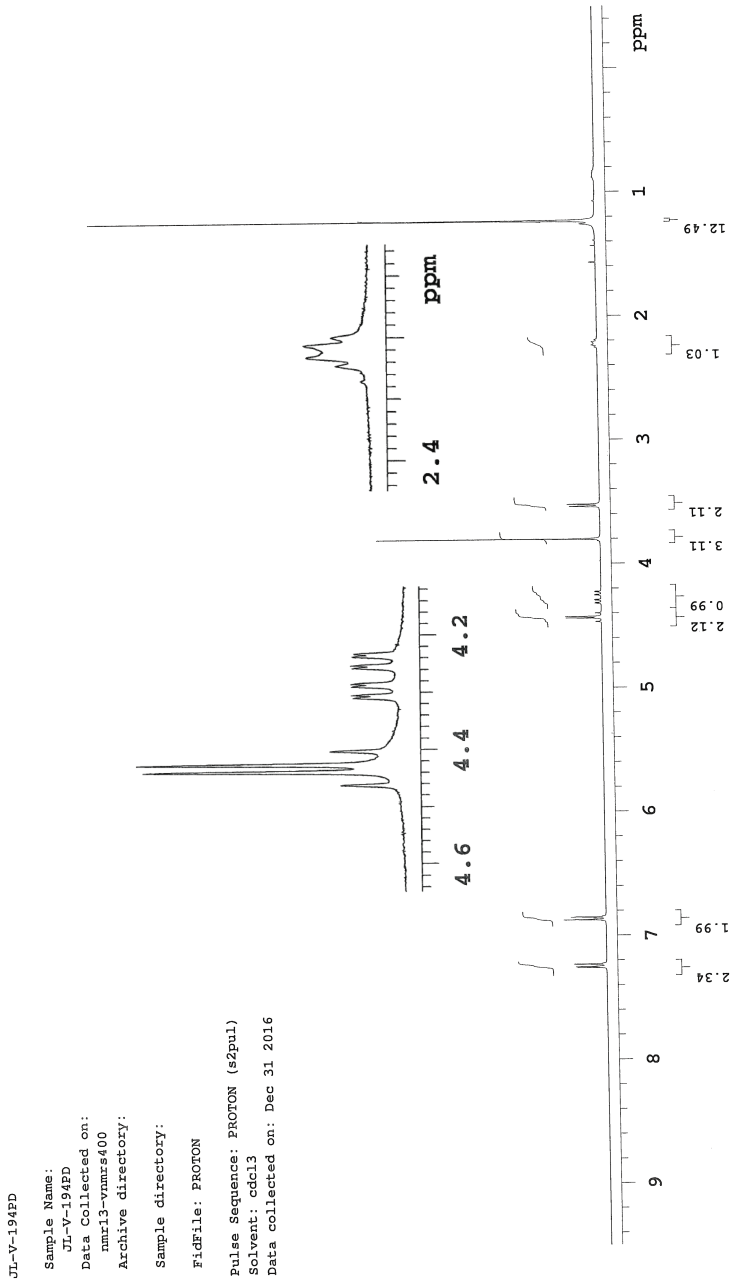

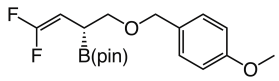
F
F
B(pin)
O
O

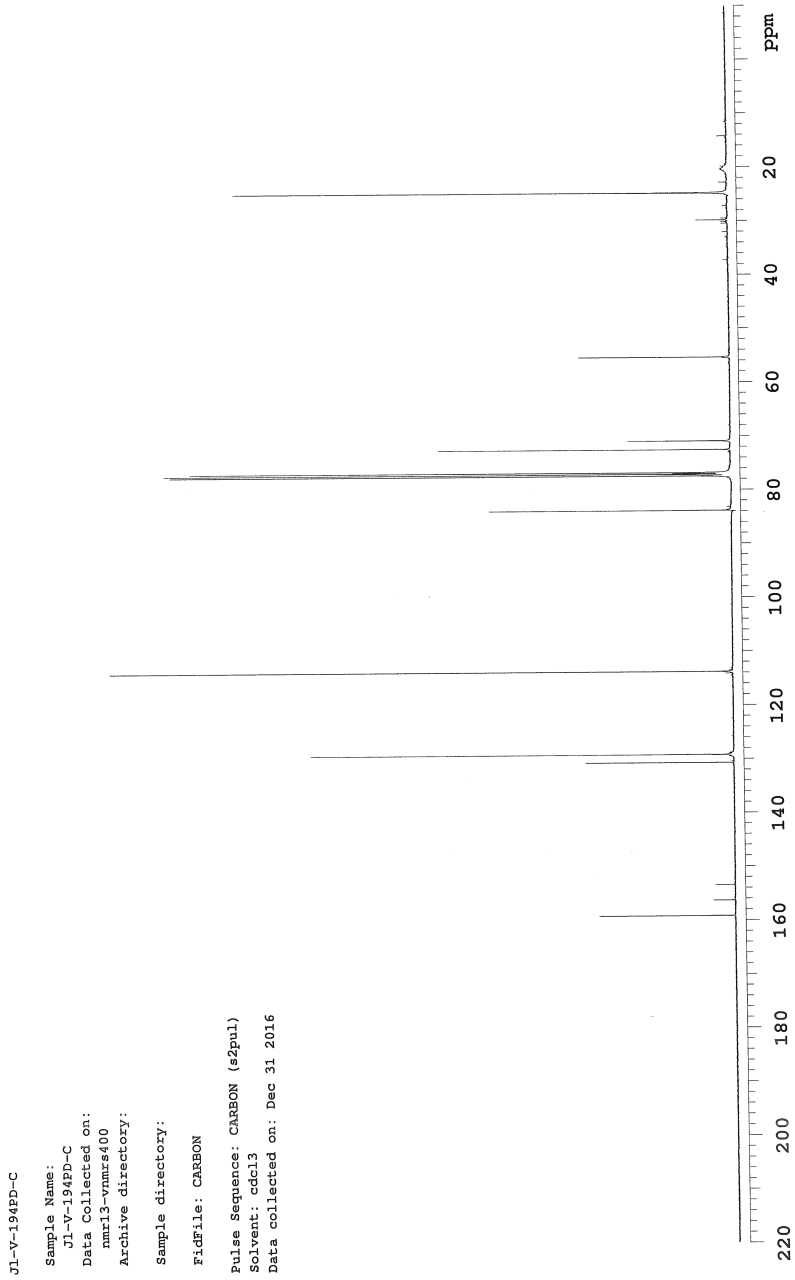
J1-V-194PD-C
Sample Name:
J1-V-194PD-C
Data Collected on:
nmr13-vnmrs400
Archive directory:
Sample directory:
FidFile: CARBON
Pulse Sequence: CARBON (s2pul)
Solvent: cdcl3
Data collected on: Dec 31 2016
ppm
220
200
180
160
140
120
100
80
60
40
20

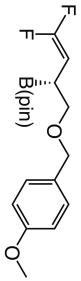

JL-V-182PD-F

Sample Name:
JL-V-182PD-F
Data Collected on:
nmr13-vnmrs400
Archive directory:

Sample directory:

FidFile: JL-V-182-PD-F

Pulse Sequence: FLUORINE (s2pul)
Solvent: cdcl3
Data collected on: Dec 21 2016

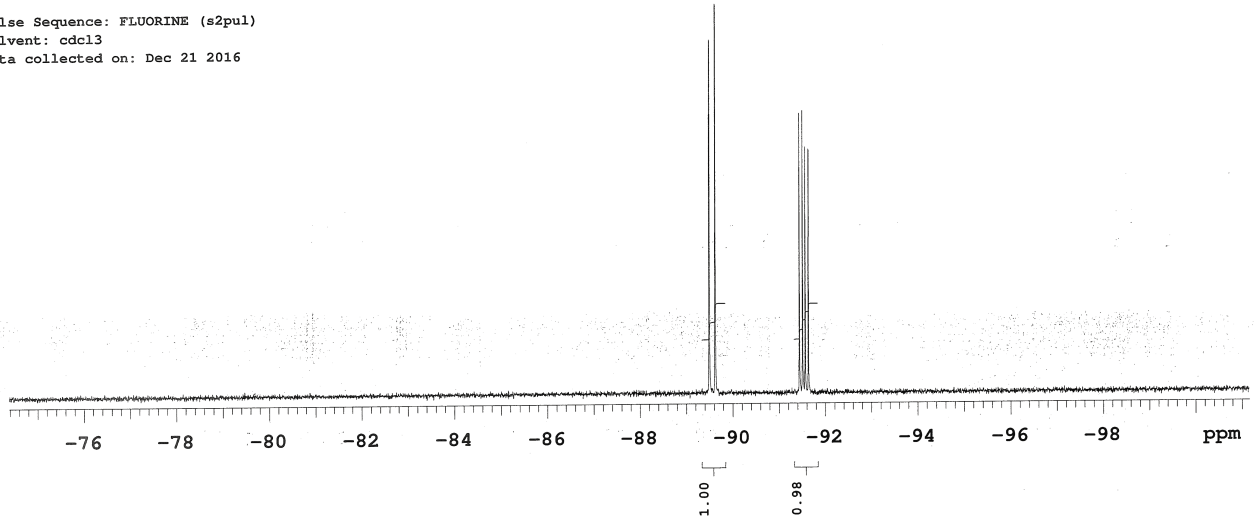

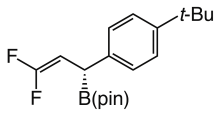
t-Bu
F
F
B(pin)

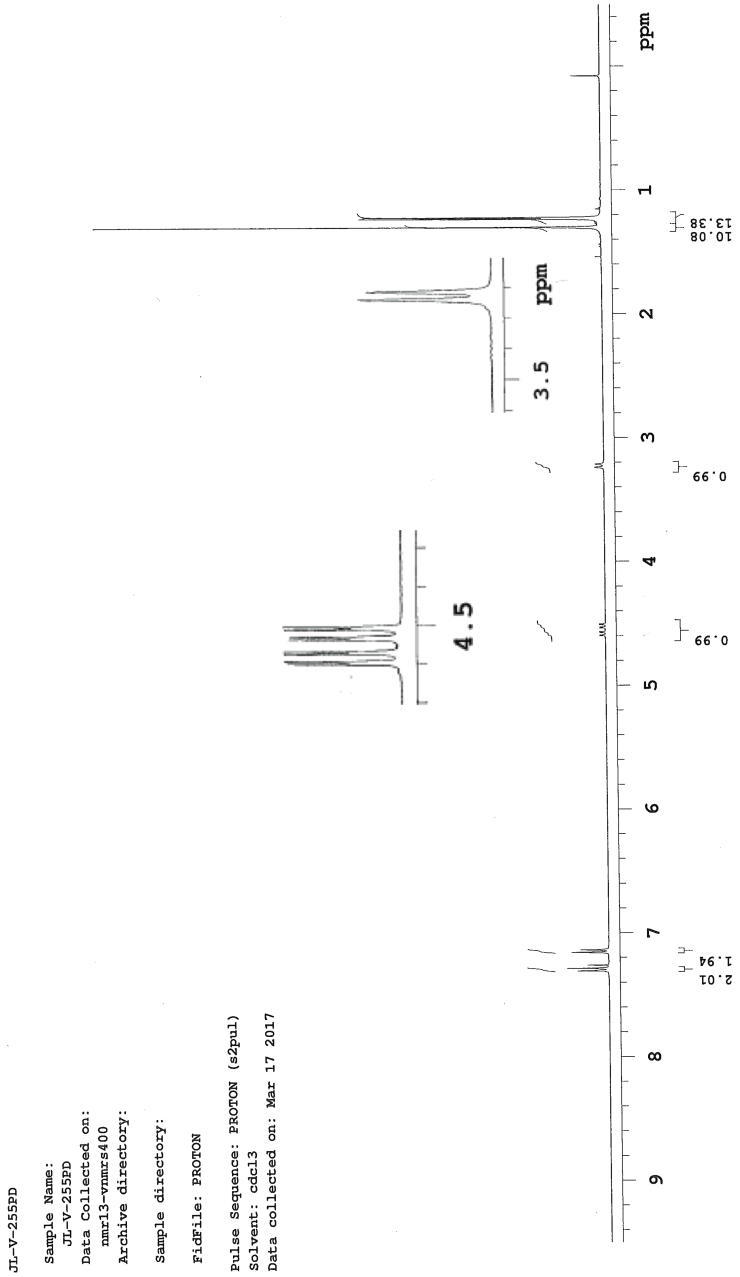
JL-V-255PD
Sample Name:
JL-V-255PD
Data Collected on:
nmr13-vnmrs400
Archive directory:
Sample directory:
FidFile: PROTON
Pulse Sequence: PROTON (s2pul)
Solvent: cdcl3
Data collected on: Mar 17 2017
4.5
3.5
ppm
ppm
10.08
13.38
0.99
0.99
2.01
1.94

JL-V-255PD-C

Sample Name:
JL-V-255PD-C
Data Collected on:
nmr13-vnmrs400
Archive directory:

Sample directory:

FidFile: CARBON

Pulse Sequence: CARBON (s2pul)
Solvent: cdcl3
Data collected on: Mar 17 2017

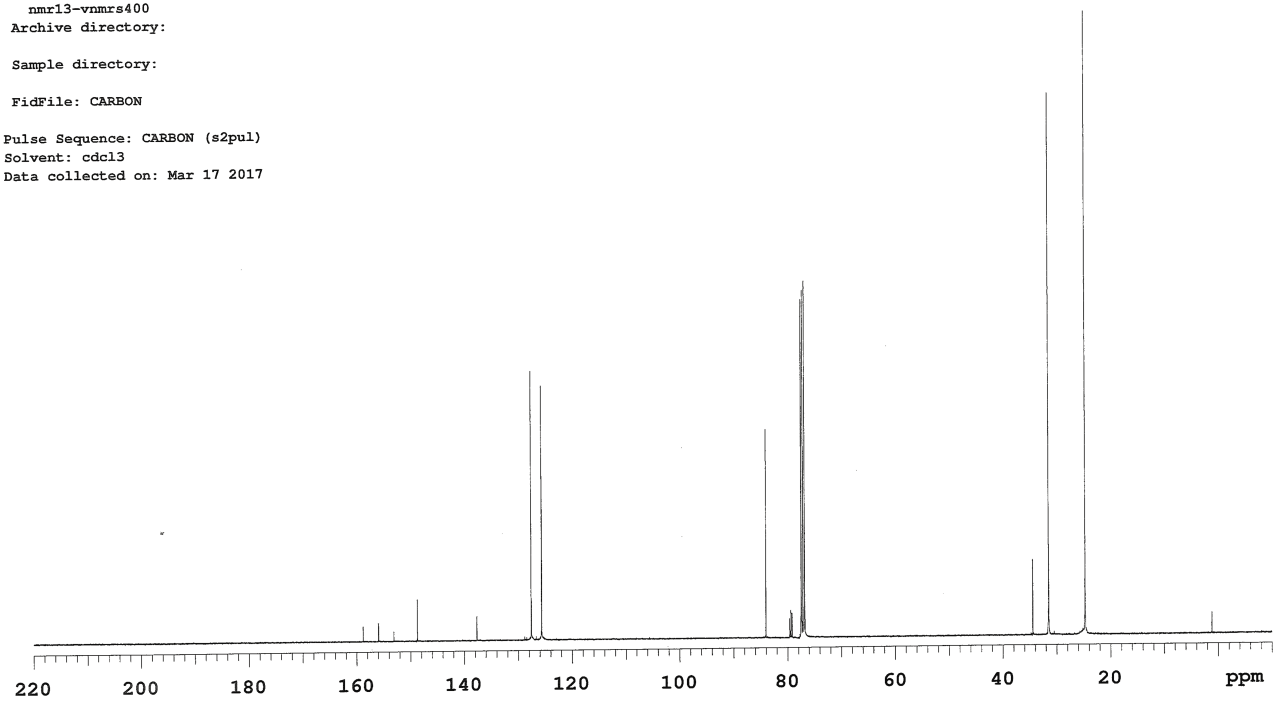

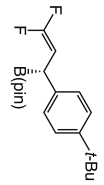

STANDARD FLUORINE PARAMETERS
JL-V-255PD-F

Sample Name:
JL-V-254PD-F
Data Collected on:
nmr13-vnmrs400
Archive directory:

Sample directory:

FidFile: FLUORINE

Pulse Sequence: FLUORINE (s2pul)
Solvent: cdcl3
Data collected on: Mar 17 2017

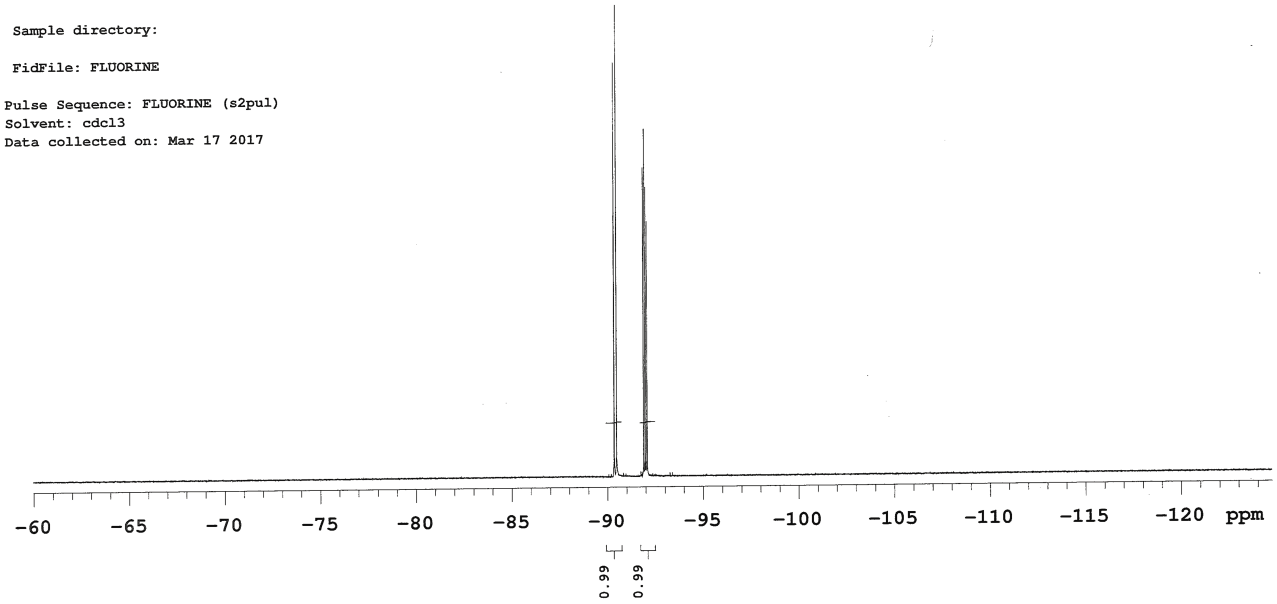

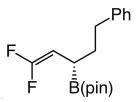
Ph
F
F
B(pin)

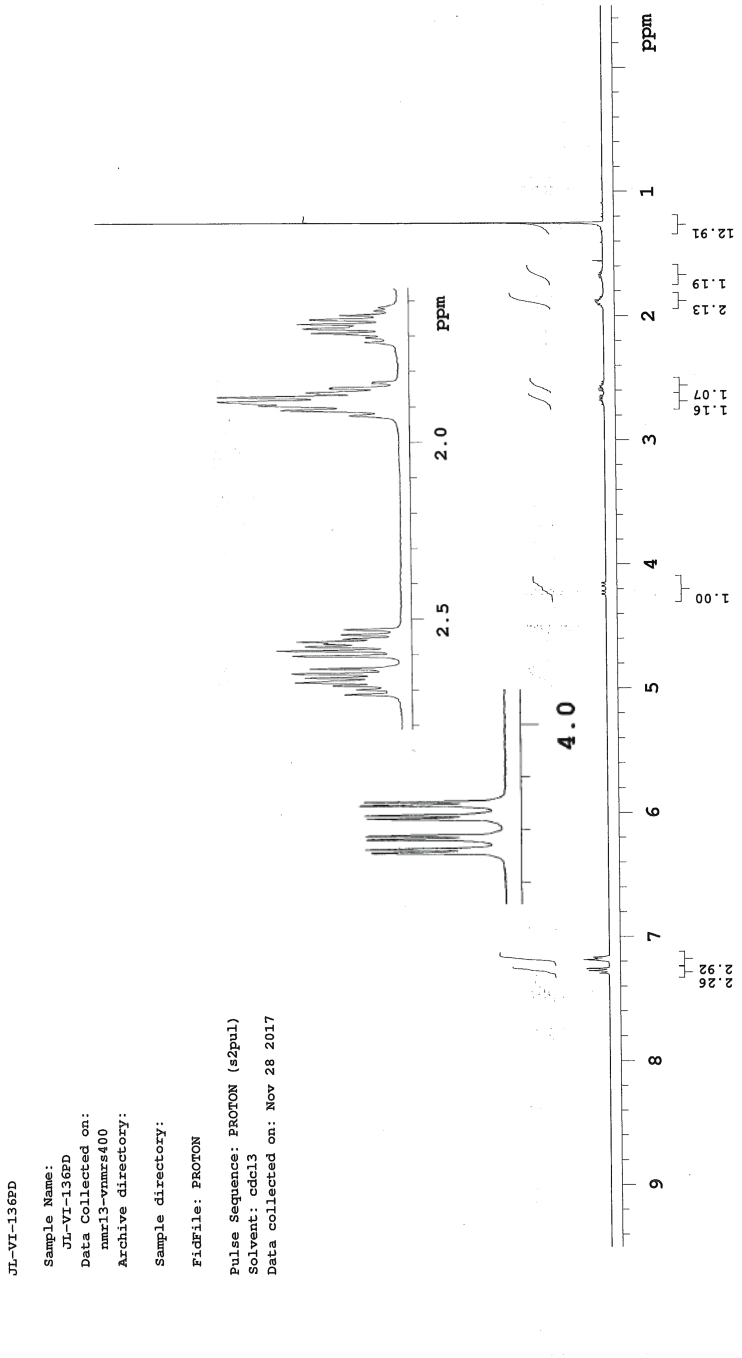
JL-VI-136PD
Sample Name:
JL-VI-136PD
Data Collected on:
nmr13-vnmrs400
Archive directory:
Sample directory:
FidFile: PROTON
Pulse Sequence: PROTON (s2pul)
Solvent: cdcl3
Data collected on: Nov 28 2017
ppm
2.5
2.0
4.0
12.91
1.19
2.13
1.16
1.07
1.00
2.26
2.92

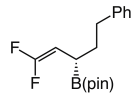
Ph
F
F
B(pin)

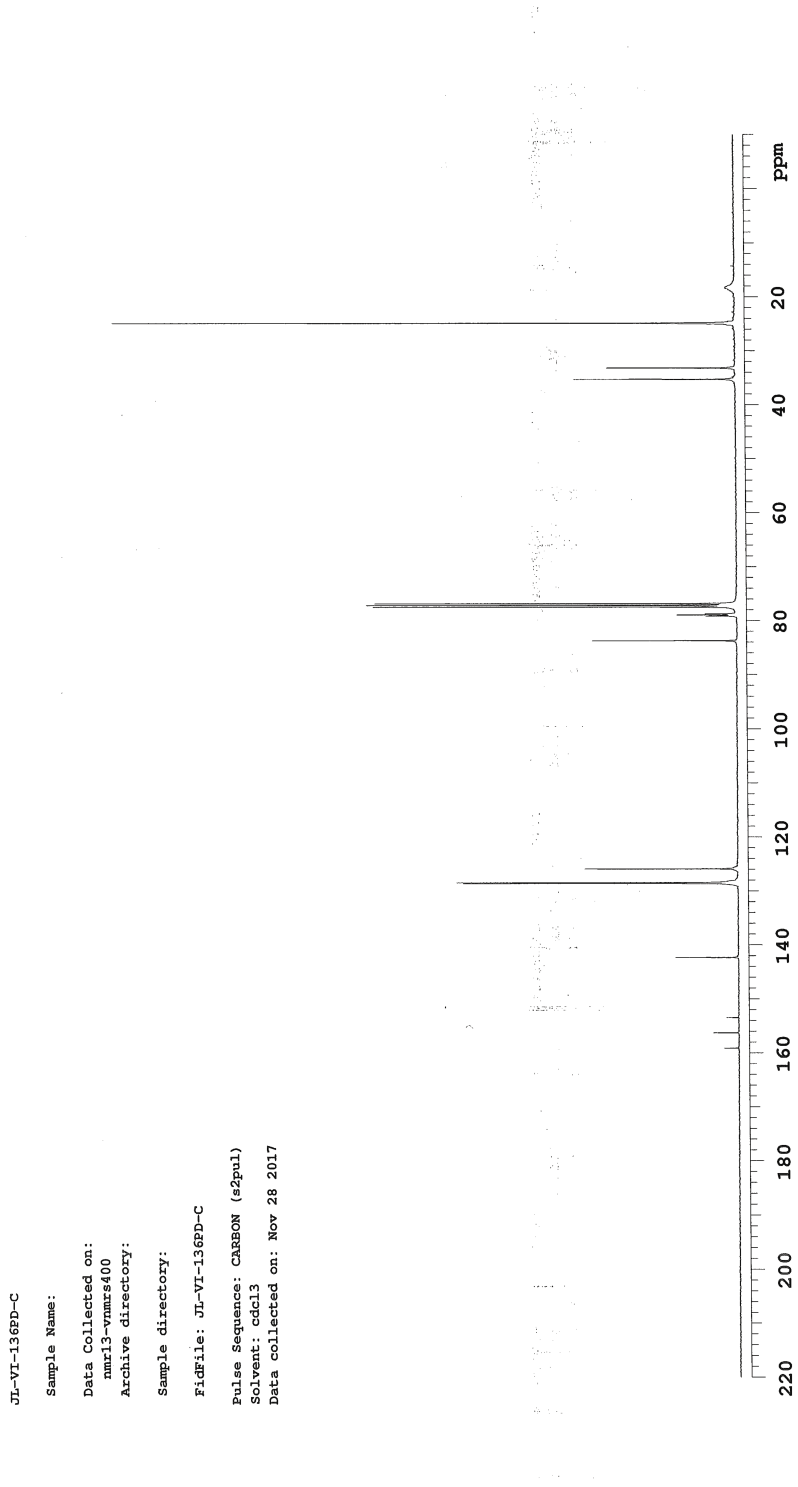
JL-VI-136PD-C
Sample Name:
Data Collected on:
nmr13-vnmrs400
Archive directory:
Sample directory:
FidFile: JL-VI-136PD-C
Pulse Sequence: CARBON (s2pul)
Solvent: cdcl3
Data collected on: Nov 28 2017
ppm
220
200
180
160
140
120
100
80
60
40
20

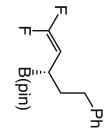

STANDARD FLUORINE PARAMETERS
JL-VI-107-F-2

Sample Name:
JL-VI-107-F-2
Data Collected on:
nmr13-vnmrs400
Archive directory:

Sample directory:

FidFile: FLUORINE

Pulse Sequence: FLUORINE (s2pul)
Solvent: cdcl3
Data collected on: Oct 11 2017

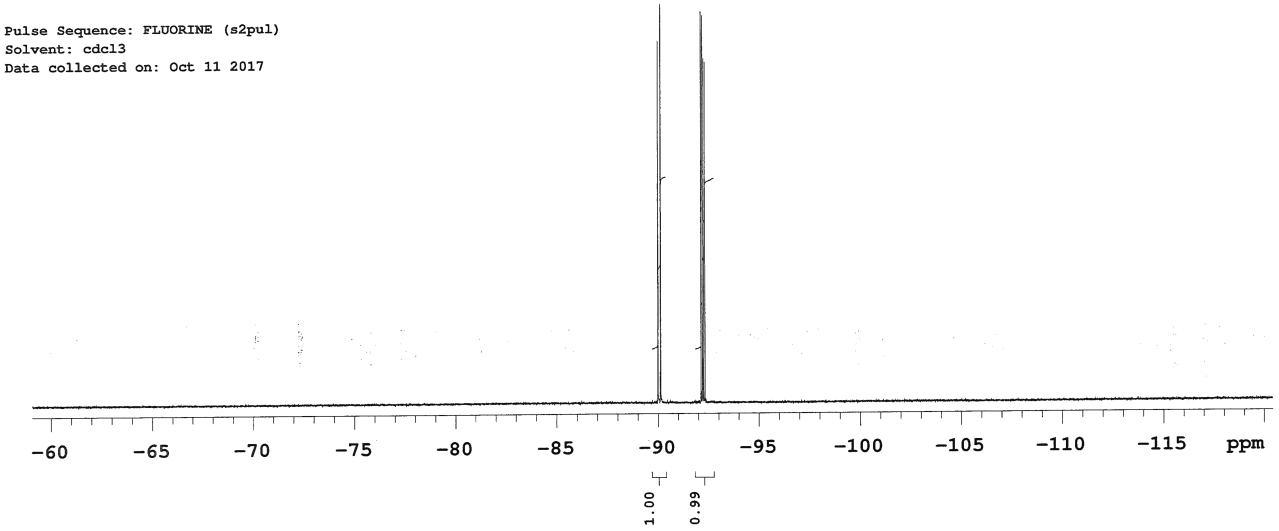

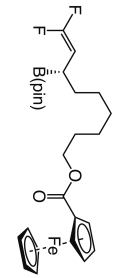

JL-VI-131PD

Sample Name:
JL-VI-131PD
Data Collected on:
nmr13-vnmrs400
Archive directory:

Sample directory:

FidFile: JL-VI-131PD

Pulse Sequence: PROTON (s2pul)
Solvent: cdcl3
Data collected on: Nov 17 2017

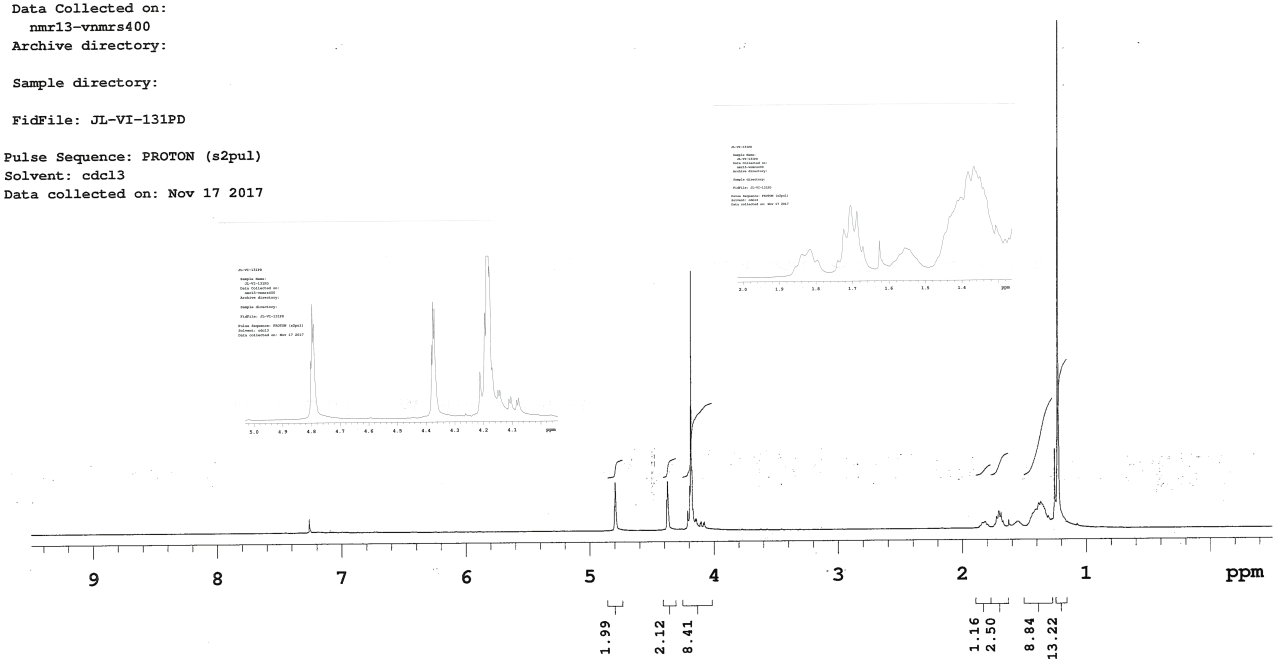

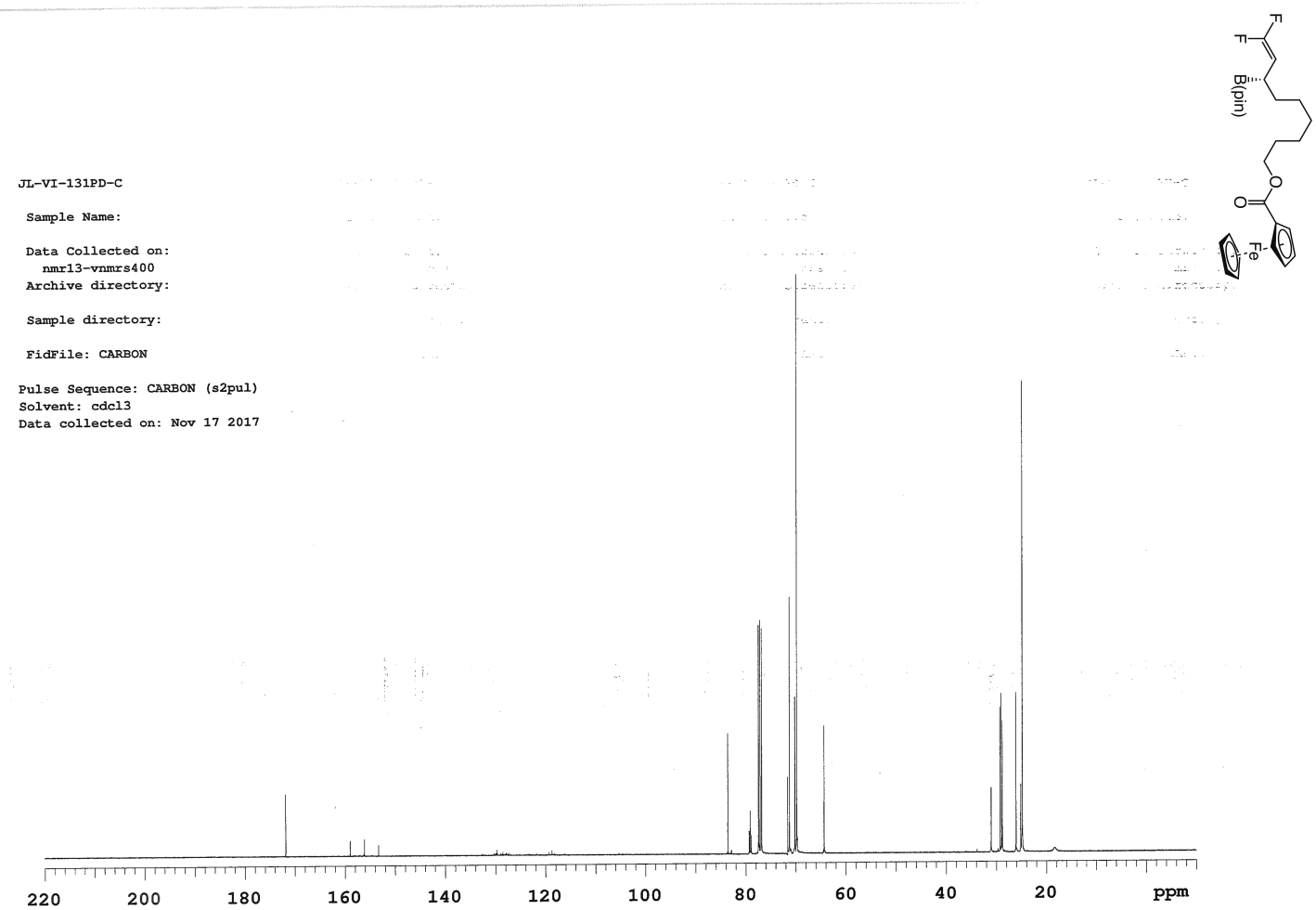
F
F
B(pin)
O
O
Fe
JL-VI-131PD-C
Sample Name:
Data Collected on:
nmr13-vnmrs400
Archive directory:
Sample directory:
FidFile: CARBON
Pulse Sequence: CARBON (s2pul)
Solvent: cdcl3
Data collected on: Nov 17 2017
220
200
180
160
140
120
100
80
60
40
20
ppm

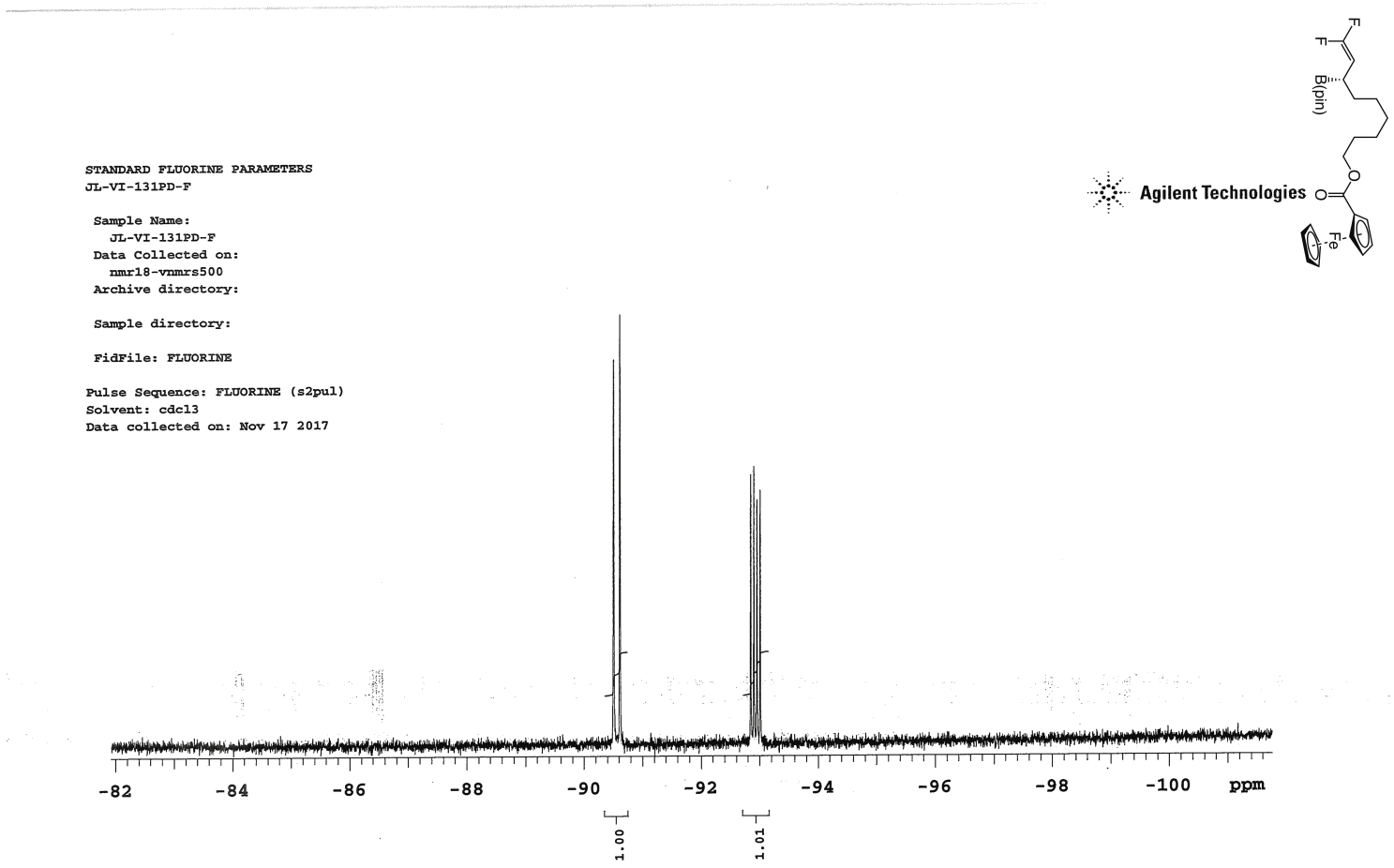
STANDARD FLUORINE PARAMETERS
JL-VI-131PD-F
Sample Name:
JL-VI-131PD-F
Data Collected on:
nmr18-vnmrs500
Archive directory:
Sample directory:
FidFile: FLUORINE
Pulse Sequence: FLUORINE (s2pul)
Solvent: cdcl3
Data collected on: Nov 17 2017
Agilent Technologies
F
F
B(pin)
O
O
Fe
-82
-84
-86
-88
-90
-92
-94
-96
-98
-100
ppm
1.00
1.01

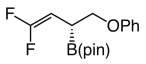
F
F
OPh
B(pin)

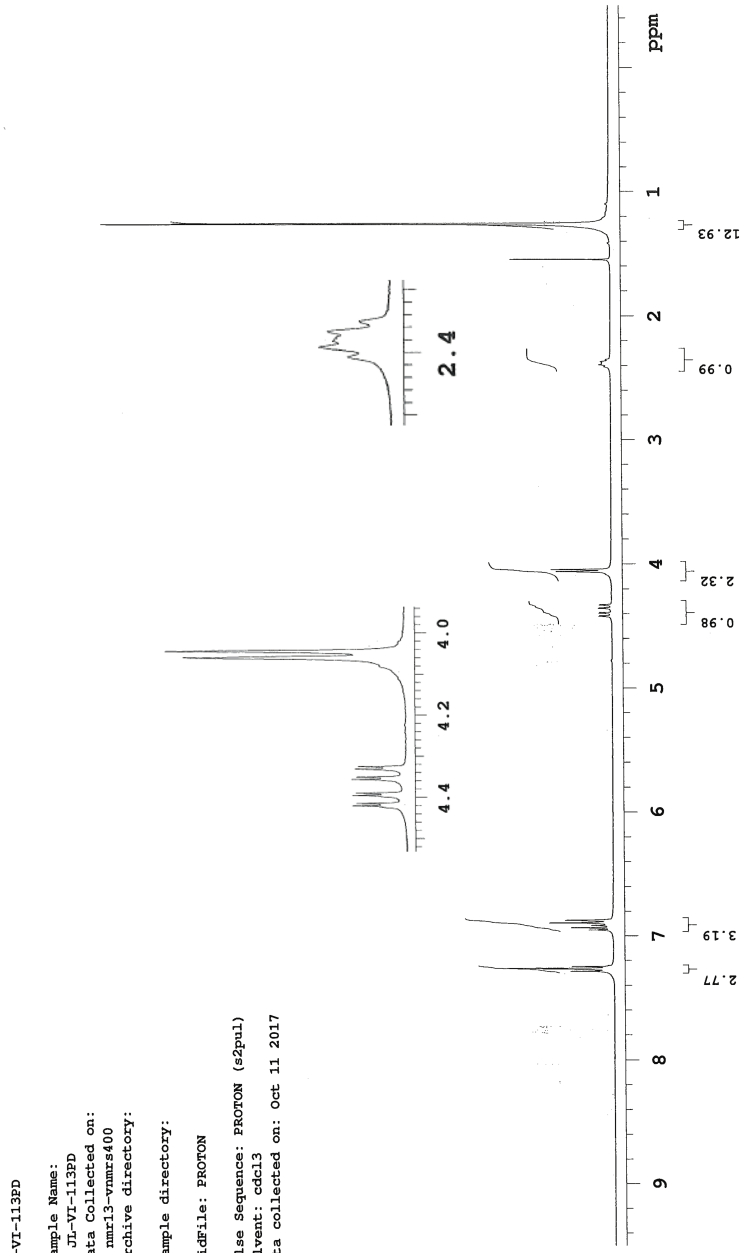
JL-VI-113PD
Sample Name:
JL-VI-113PD
Data Collected on:
nmr13-vnmrs400
Archive directory:
Sample directory:
FidFile: PROTON
Pulse Sequence: PROTON (s2pul)
Solvent: cdcl3
Data collected on: Oct 11 2017
ppm
12.93
0.99
2.32
0.98
3.19
2.77
2.4
4.4
4.2
4.0

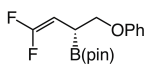
F
F
OPh
B(pin)

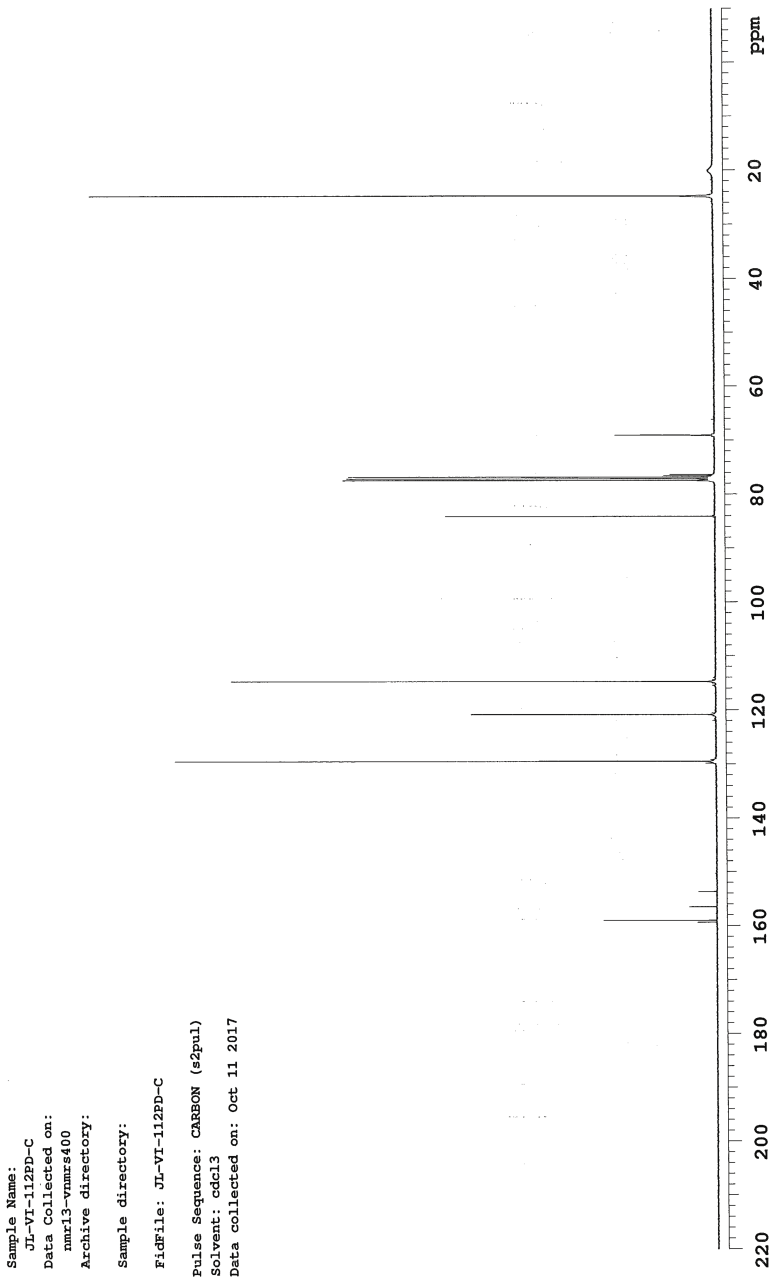
Sample Name:
JL-VI-112PD-C
Data Collected on:
nmr13-vnmrs400
Archive directory:
Sample directory:
FidFile: JL-VI-112PD-C
Pulse Sequence: CARBON (s2pul)
Solvent: cdcl3
Data collected on: Oct 11 2017
ppm
220
200
180
160
140
120
100
80
60
40
20

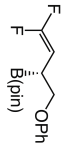

STANDARD FLUORINE PARAMETERS
JL-VI-113PD-F

Sample Name:
JL-VI-113PD-F
Data Collected on:
nmr13-vnmrs400
Archive directory:

Sample directory:

FidFile: FLUORINE

Pulse Sequence: FLUORINE (s2pul)
Solvent: cdcl3
Data collected on: Oct 11 2017

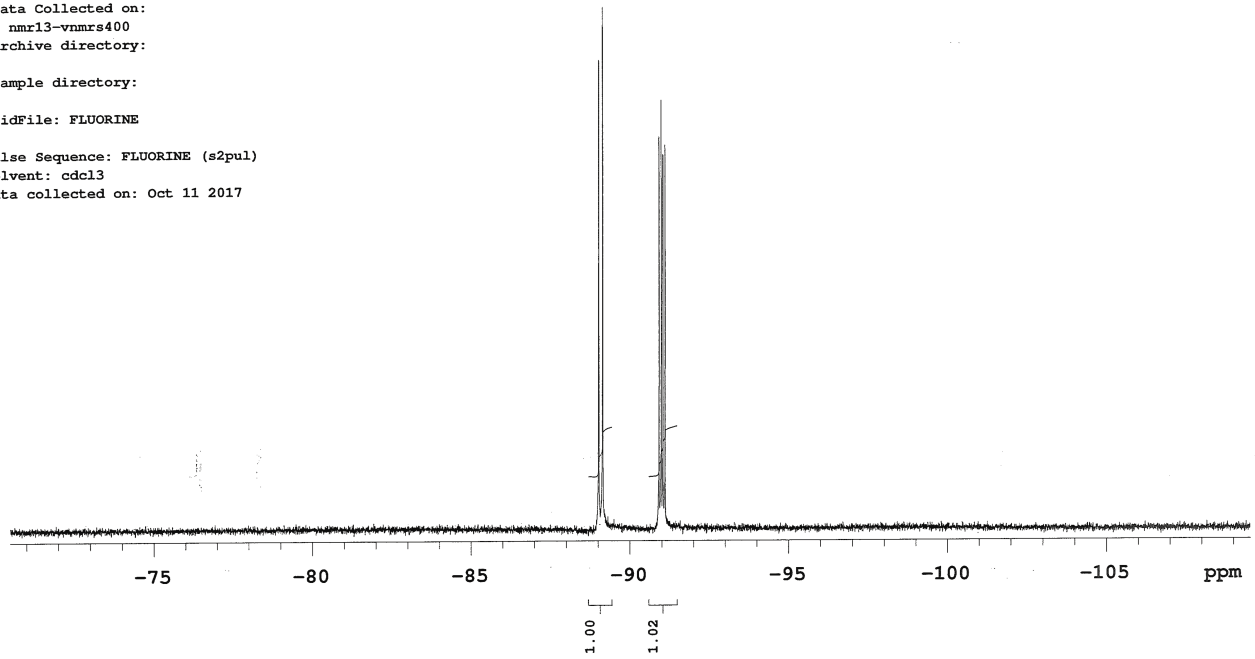

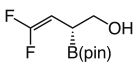
F
F
OH
B(pin)

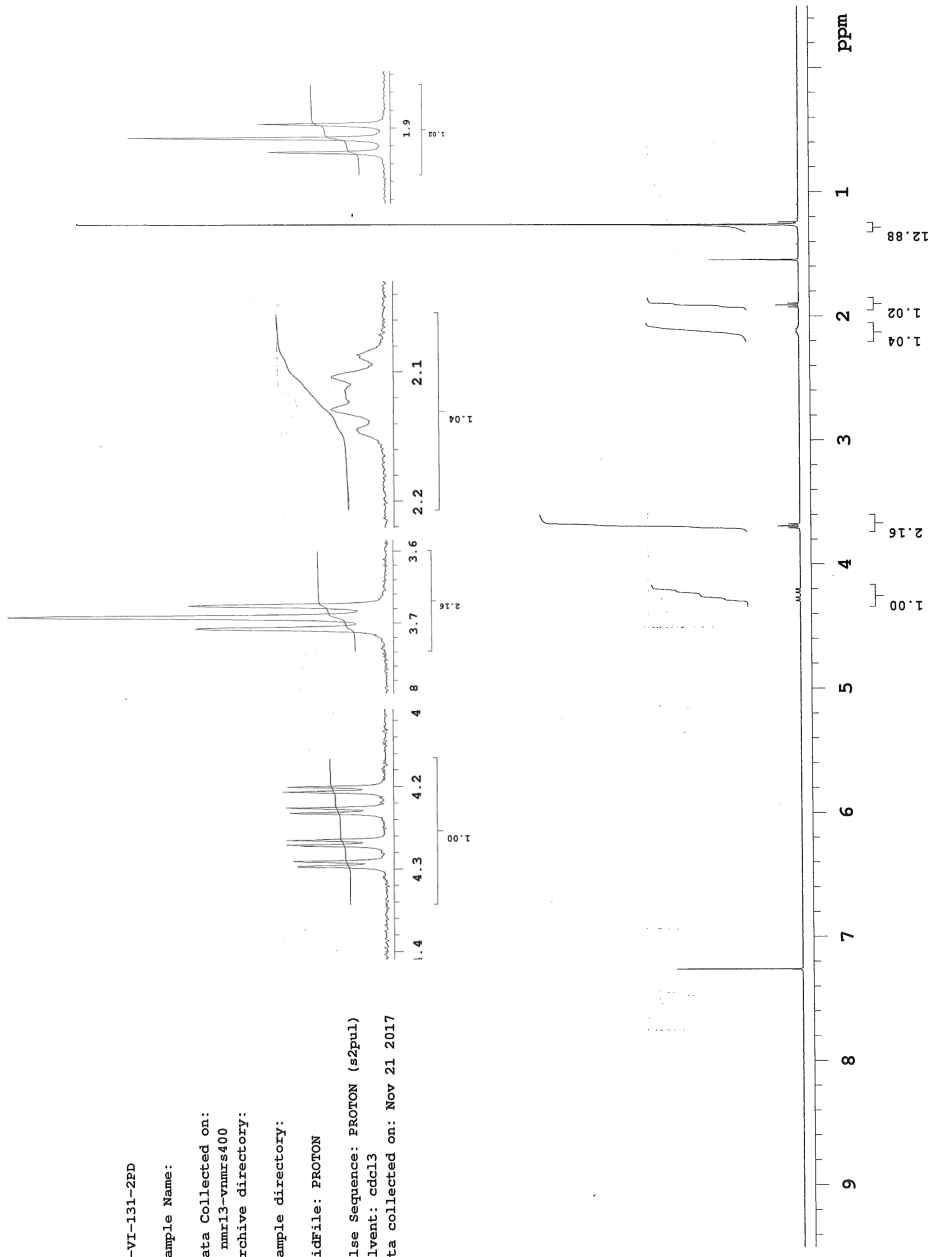
JL-VI-131-2PD
Sample Name:
Data Collected on:
nmr13-vnmrs400
Archive directory:
Sample directory:
FidFile: PROTON
Pulse Sequence: PROTON (s2pul)
Solvent: cdcl3
Data collected on: Nov 21 2017
ppm
12.88
1.02
1.04
2.16
1.00
1.02
1.9
2.1
2.2
1.04
3.6
3.7
2.16
4.2
4.3
1.00

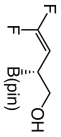

J1-VI-132-2-PD-C

Sample Name:
J1-VI-132-2-PD-C
Data Collected on:
nmr13-vnmrs400
Archive directory:

Sample directory:

FidFile: JL-VI-132-2PD-C

Pulse Sequence: CARBON (s2pul)
Solvent: cdcl3
Data collected on: Nov 21 2017

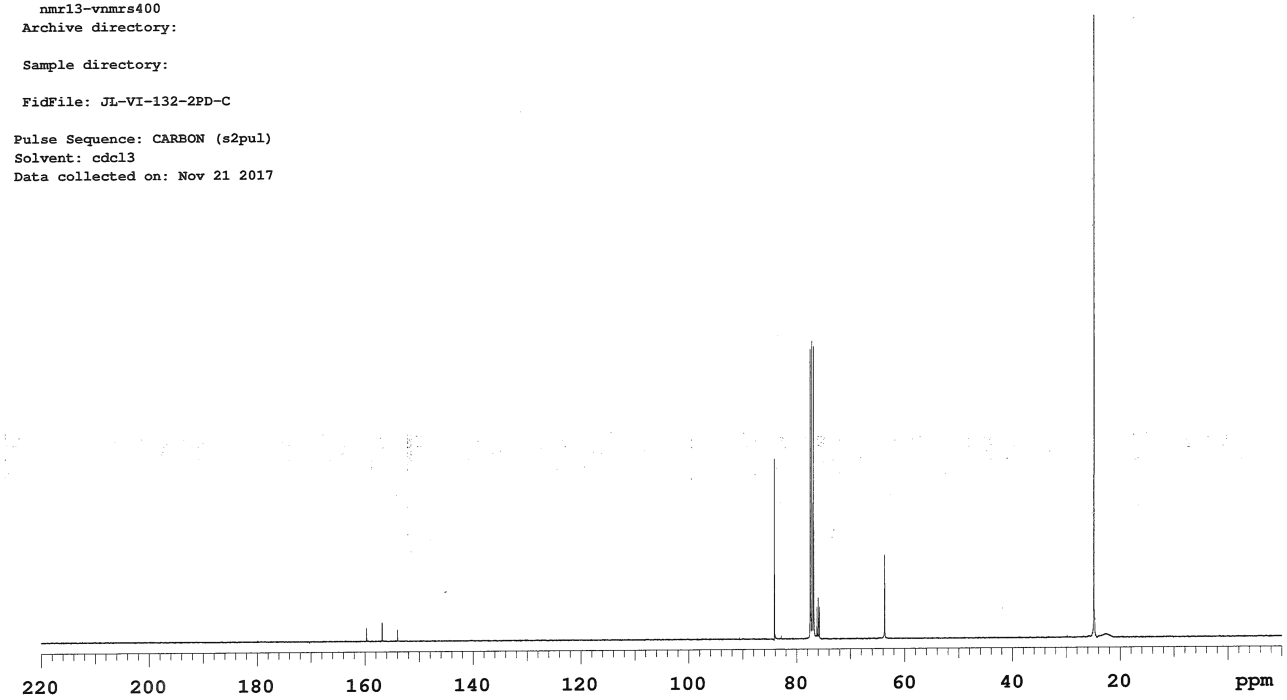

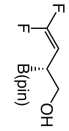

STANDARD FLUORINE PARAMETERS
JL-VI-132-2-F-PD

Sample Name:
JL-VI-132-2-F-PD
Data Collected on:
nmr13-vnmrs400
Archive directory:

Sample directory:

FidFile: FLUORINE

Pulse Sequence: FLUORINE (s2pul)
Solvent: cdcl3
Data collected on: Nov 21 2017